

Single-Particle Model

7-1 INTRODUCTION

One of the main objectives of the study of nuclear physics is understanding the *structure of nuclei*. This expression is used to include all aspects of the motion of intranuclear nucleons: their paths in space, their momenta, the correlations between them, the energies binding them to each other. Mathematically, the complete description of nuclear structure is contained in the correct total wave function of the nucleus. It is clear that there are formidable difficulties in the experimental or theoretical determination of the behavior of all the degrees of freedom of a dynamical system of such complexity as a moderately heavy nucleus. Even if these difficulties could be overcome, it would be necessary to look for some simplified description of nuclei in terms of a number of parameters sufficiently small to permit ready assimilation by the human mind. At the same time, the parameters should be sufficient to give a fairly complete picture of the most important features of a particular nucleus. The problem is an example of the search for a systematic description of nature, by which science has progressed. Both our present inadequate knowledge and the general need for systematization drive us to look for conceptual or mathematical models. From a nuclear model, it must be possible, in a systematic way and without prohibitively lengthy calculation, to predict various observable properties of the nuclides. The test of the usefulness or realism of any model is the extent to which its predictions are confirmed by experiment.

We made some use of certain simple models in the discussions of Part I. Although the agreement of the model with experiment is not precise, we saw

that some of the properties of nuclides, such as angular momenta and magnetic moments, suggest the usefulness of the single-particle model. In this model the individual nucleons are considered to move in stationary orbits and are paired off in such a way that the values of many nuclear parameters are determined solely by a single unpaired nucleon. The model contains no correlated or collective motion of several nucleons and no explicit reference to two-body forces between nucleons. These omissions, particularly the latter, suggest that the model must be of strictly limited applicability, and we found, for example, that its predictions of quadrupole moments are completely erroneous. To describe quadrupole moments within the framework of a model, we had recourse to the other extreme of regarding the nucleus as a distorted liquid drop, in which fairly large fractions of the fluid are moving together to produce a nonspherical shape. A simple liquid-drop model contains little reference to the numbers of nucleons present and can hardly predict the discontinuities associated with the "magic" numbers. It is clear that, to incorporate even the main features of nuclear structure, a model must be considerably more complicated than either of these extreme cases.

The more realistic models can be described as generalizations and extensions built on the single-particle model. Despite this model's sweeping simplifications and the neglect of internucleon interactions, it may well be that the single-particle orbits represent fairly well an average of the actual nucleon motions. Certain nuclear quantities are sensitive only to the average motion, but others are strongly affected by the details of the nuclear structure and, in particular, by particle correlations. From this viewpoint, the single-particle model makes a reasonable starting point to which more sophisticated models may be adduced. In this chapter we shall describe in detail the simplest form of shell model, the so-called single-particle model, and in later chapters of Part II we shall examine the embellishments that make it more realistic. In Chapter 8 we shall consider a basic question: "Why does the shell model work at all, even as a first approximation?" In attempting to answer this question, we shall be describing a nuclear theory as distinguished from a model, that is, an effort to build up the description of the nucleus from the fundamental facts concerning nuclear interactions and without introducing any ad hoc assumptions, however plausible they may appear.

7-2 SINGLE PARTICLE ORBITS

If each nucleon moves in a permanent orbit with fixed angular momentum, it is tempting to try to describe the effective force on each particle by means

of a central potential $V(r)$. In analogy with atomic electrons, where $V(r) = -Ze^2/r$, one might then expect to find a shell structure in nuclei. This hypothesis was suggested during the 1930's (e.g., ref. 1), but was not widely used because of the theoretical difficulties inherent in the assumption that the strong internucleon forces could average out in such a simple way, and also because of the paucity, at that time, of experimental data that suggested shell structure or quasi-single-particle behavior. However, by 1949, a large number of measurements of nuclear spins and magnetic moments had accumulated, and the discontinuities associated with the magic numbers were recognized. In that year, a description of a single-particle model, which systematically explained these data, was published. Like many other significant developments in physics, the nuclear-shell model was arrived at simultaneously but independently, in this case by Maria Goeppert Mayer [2, 3], acting on a suggestion by E. Fermi, and by O. Haxel, J. H. D. Jensen, and H. E. Suess [4, 5]. Their papers were devoted to describing the postulated single-particle force and showing that there was impressive agreement with experiment. No attention was given to the theoretical basis of the model, and in this book also such discussion is postponed to a later section.

As a starting point, we may confine ourselves to spherical nuclei and remark that the average force on a nucleon at the center is zero. Thus, if the force can be derived from a potential $V(r)$, this potential will be flat at $r = 0$. Moreover, since nuclear matter is of roughly uniform density throughout the nuclear volume, we can expect V to be fairly constant in the nuclear interior and to decrease steadily throughout the boundary region, where the density falls to zero. Indeed, it is reasonable to suppose that $V(r)$ is a function with much the same shape as $\rho(r)$, but with a rather larger range, since the potential will extend beyond the nucleons that produce it.

A difficulty is encountered in connection with the identity of the center of the potential well. The potential is an average over nucleon motions; as such its center has no fundamental physical significance, but coincides *on the average* with the mass center. In a model in which the center of the potential is fixed at the origin, there are oscillations of the mass center about the origin. The energy associated with this mass-center motion is, however, fictitious, since it is in reality the mass center itself that is fixed. This model may thus give rise to spurious states associated with the center-of-mass motion.

In a central potential, the orbital angular momentum of each nucleon is a constant of motion. For each quantum number l there is a series of energy levels, which we shall distinguish by the quantum number n , associated with

the number of nodes of the radial wave function. For example, the state of lowest energy with $l = 1$ is called the $0p$ -state; the fifth state with $l = 3$ is the $4f$ -state, etc.[†] The spacing of the energy levels depends on the form of the potential, but for $V(r)$'s of the general type discussed above, the order of levels is almost fixed. Two extreme cases for which analytic calculations can be made are the harmonic oscillator:

$$V = -V_0 + \frac{1}{2}M\omega^2r^2; \quad (7-1)$$

and the infinite square well:

$$\begin{aligned} V &= -V_0, \quad r < R, \\ &= \infty, \quad r > R. \end{aligned} \quad (7-2)$$

Numerical calculations for the finite square well (i.e., $V = 0, r > R$) and for $V(r)$ given by a Fermi distribution like Eq. 4-9 [6] yield level orders intermediate to those of the above two extremes. The levels of the harmonic oscillator are shown on the left of Fig. 7-1; they are evenly spaced and are highly degenerate, since all states with the same value of $2n + l$ have the same energy. On the right of Fig. 7-1 are the levels of the infinite square well. It will be observed that the degeneracies have been removed, the states of

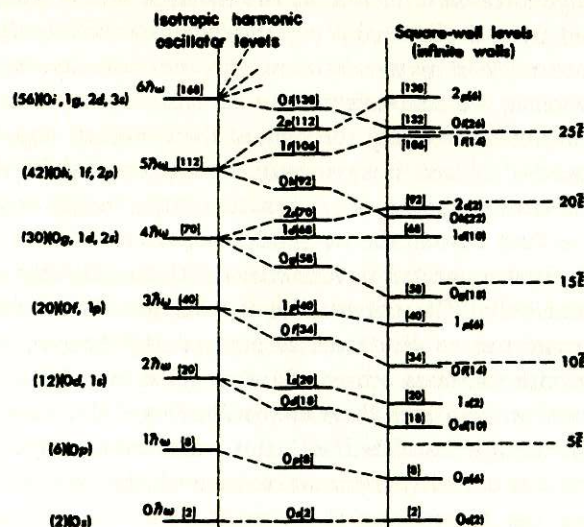


Fig. 7-1 The levels of an harmonic oscillator, a square well, and an intermediate potential shape. The energy units \tilde{E} and $\hbar\omega$ depend on the radii of the potentials.

[†] The spectroscopist's alphabet begins "s, p, d, f, g, h, i, j, . . ." Explicitly, n = number of nodes in the radial wave function, excluding the origin and infinity.

higher angular momentum moving to lower energy. For more realistic potentials intermediate to these extremes, we expect a level spacing like that arbitrarily interpolated in the center of the figure. It should be noted that, although the spacing is different, the order of levels is the same in the two extreme cases, with two exceptions in the range of levels shown, namely, the $0h$, $2s$ states and the $0i$, $2p$ states. In an intermediate potential these pairs of states may be expected to be rather close in energy.

The single-particle model describes a nuclear state by stating how many nucleons are in each of the orbits. For each level, there are $2l + 1$ degenerate substates corresponding to different orientations of the angular momentum (i.e., m_l -values), and in accordance with the exclusion principle each of these substates can contain at most two nucleons of each type. Thus a d -level, for example, can contain ten protons and ten neutrons. For the interpolated level sequence, Fig. 7-1 shows, for each level, the number of protons (or neutrons) which it can hold and also the total numbers which can be held in that level and all lower ones. Thus, if these levels were realistic, $^{13}_6C_7$ would have two protons and two neutrons in the $0s$ -level and four protons and five neutrons in the $0p$ -level. As another example, in $^{87}_{37}Rb_{50}$, all levels below the $1p$ -level would be completely filled, and this level itself would have its full complement of six neutrons. It would also have three protons, and there would be ten neutrons in the $0g$ -level.

In a single-particle model, wherever there is a large gap in the spacing of the energy levels, corresponding discontinuities appear in the nuclear properties, such as binding energy, capture cross section, and angular momentum, which mark the magic numbers. Consequently, the magic numbers indicated by Fig. 7-1 are 2, 8, 20, 40, 70, etc. Except for the first three, these are not the magic numbers occurring in the experimental data in Chapter 6. The feature of the shell model that produces energy gaps at the correct magic numbers in a quite natural way is the assumption of a spin-orbit force. Explicitly, it is assumed that, in addition to the static potential already discussed, each nucleon is subject to a potential:

$$V_{ls} = -V(r)\mathbf{l} \cdot \mathbf{s} = -V(r)(\mathbf{r} \times \mathbf{p}) \cdot \mathbf{s}, \quad (7-3)$$

where the vectors refer to the orbital angular momentum, spin, position, and momentum of the individual nucleon. Originally this potential was introduced in 1949 as an hypothesis to explain the magic numbers; but, as we shall see, there is now considerable evidence that it is real. A completely satisfactory theoretical explanation of its presence has not been provided. Its strength shows that it is due to nuclear forces, not to electromagnetic

phenomena or small relativistic effects; the tensor force does not seem to account for it wholly, but the two-nucleon $\mathbf{L} \cdot \mathbf{S}$ force may provide a source.

Unlike the tensor force, the spin-orbit force does not mix states of different l , since l^2 commutes with $\mathbf{l} \cdot \mathbf{s}$. However, the orientation of \mathbf{l} is not a constant of motion, and only \mathbf{j} has a fixed z -component. There are, of course, two possible j -values for a given l , namely, $j = l \pm \frac{1}{2}$. The factor $\mathbf{l} \cdot \mathbf{s}$ in the potential implies that the energy of a nucleon with parallel orbital and spin angular momenta will differ from that of a nucleon for which these vectors are anti-parallel. If $V(r)$ is taken as positive in Eq. 7-3, the potential is attractive when \mathbf{l} and \mathbf{s} are predominantly parallel. Hence each level of the sequence shown in Fig. 7-1 is split into two corresponding to the two j -values, with $j = l + \frac{1}{2}$ being the lower level. It is also clear that the magnitude of the splitting increases with l , and this can be shown to be proportional to $2l + 1$ if the radial dependence of the $\mathbf{l} \cdot \mathbf{s}$ potential is smooth. However, it may, in fact, be largely concentrated near the nuclear boundary, in which case the l -dependence of the splitting is somewhat modified.

With these facts in mind, let us examine Fig. 7-2. An s -state ($l = 0$) is of course not split, and the splitting of p -states is small. Thus the gaps at 2

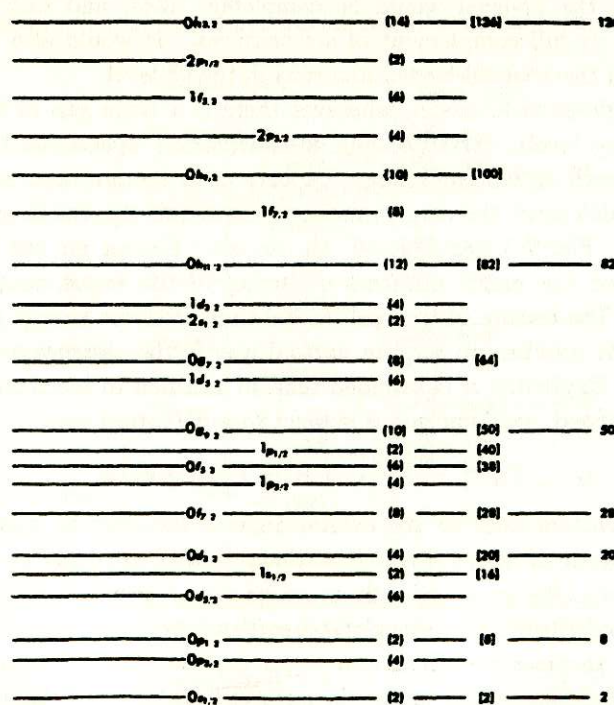


Fig. 7-2 The energy levels of the first 126 neutrons in the simple shell model.

and 8 persist. The $0d_{5/2}$ -state is lower and the $0d_{3/2}$ -state higher than the original $0d$ -state; whether or not they bracket the $1s$ -state depends on the magnitude of the $\mathbf{l} \cdot \mathbf{s}$ force, and experimental data indicate that it is sufficiently large to produce the order shown in the figure. Although the $0f_{7/2}$ -state is depressed and the $0d_{3/2}$ -state is raised by the $\mathbf{l} \cdot \mathbf{s}$ splitting, there is still a gap corresponding to the magic number at 20. On the other hand, the elevation of the $0f_{5/2}$ -state produces an energy gap at nucleon number 28.

The substitution of 50 for 40 as a magic number is achieved by the splitting of the $0g$ -level, whose l -value is sufficiently high so that a pronounced gap appears above the $0g_{9/2}$ -level (50 nucleons) which has been depressed so close to the $1p_{1/2}$ -state that there is no large gap at 40 nucleons. Similarly, the large splitting of the $0h$ -level has removed any large gaps at numbers 70 and 92 and introduced the correct magic number 82. The i -level splitting has introduced the magic number 126.

Within each shell the level order will depend on the specific properties of the potentials assumed. The level order in Fig. 7-2 is that which, for neutrons, is found to agree with experiment. For $Z > 50$, the proton level scheme is different in that higher angular momenta tend to have lower energies. The level order is $0g_{7/2}$, $1d_{5/2}$, $1d_{3/2}$, $2s_{1/2}$, and $0h_{11/2}$.

7-3 EXTREME SINGLE-PARTICLE MODEL AND SPIN

In general, the extent of the agreement of the various nuclear models with experiment will be discussed in later chapters, individually devoted to the different observable quantities. However, it is convenient to consider, in this part of the book, the predictions concerning nuclear spin, one of the simpler nuclear properties, which served as a fundamental guide in the development of the models. In the simplest form of the shell model, the extreme single-particle model, the nucleons are supposed, in the ground state, to have dynamically paired motions so that many of the nuclear properties are due only to the last unpaired nucleon. It is also assumed that the neutron and proton states fill independently, that is, that the state into which a given proton goes is independent of the number of neutrons in the nucleus, and vice versa. In such a system, every even-even nuclide has zero spin, every odd- A nuclide has the angular momentum of the unpaired particle, and the angular momentum of odd-odd nuclides cannot be predicted, since there is nothing to indicate which of the various possible resultants of the \mathbf{j} -vectors of the two unpaired particles has lowest energy. This is a very unsophisticated model, ignoring as it does all nucleon correlation. A more realistic approach would consider only the nucleons in closed shells to form an inert core and take into account the internucleon forces between particles in unfilled orbitals.

TABLE 7-1 Shell-Model Configurations for Odd-*A* Nuclides.(a) Odd-*N* Nuclides

Nuclide	<i>N</i>	<i>Z</i>	<i>J</i>	μ nm	<i>Q</i> barns	Configuration of Neutrons
8						
						$0s_{1/2}$ $0p_{3/2}$ $0p_{1/2}$
¹ n	1	0	1/2	- 1.9131		1
³ He	1	2	1/2	- 2.1276		1
⁷ Be	3	4	3/2			2 1
⁹ Be	5	4	3/2	- 1.1776	0.05	2 1
¹¹ C	5	6	3/2	± 1.03	0.031	2 3
¹³ C	7	6	1/2	0.7024		2 4 1
¹⁵ O	7	8	1/2	0.7189		2 4 1
10						
						$0d_{5/2}$ $1s_{1/2}$ $0d_{3/2}$
¹⁷ O	9	8	5/2	- 1.8937	- 0.026	1
¹⁹ Ne	9	10	1/2	- 1.887		0 1
¹⁹ O	11	8	5/2			3
²¹ Ne	11	10	3/2	- 0.6618	0.09	3
²³ Mg	11	12	3/2			3
²³ Ne	13	10	5/2	- 1.08	5	
²⁵ Mg	13	12	5/2	- 0.8551	0.22	5 deformed
²⁷ Si	13	14	5/2			5
²⁷ Mg	15	12	1/2			6 1
²⁹ Si	15	14	1/2	- 0.5553	$ Q < 10^{-4}$	6 1
³¹ S	15	16	1/2			6 1
³³ S	17	16	3/2	0.6433	- 0.055	6 2 1
³⁵ Ar	17	18	3/2	0.63		6 2 1
³⁵ S	19	16	3/2	$\begin{cases} +1.00 \text{ or} \\ -1.07 \end{cases}$	0.04	6 2 3
³⁷ Ar	19	18	3/2	0.95		6 2 3
³⁹ Ca	19	20	3/2			6 2 3
20						
						$0f_{7/2}$
³⁷ S	21	16	7/2			1
³⁹ Ar	21	18	7/2	- 1.3		1
⁴¹ Ca	21	20	7/2	- 1.595		1
⁴¹ Ar	23	18	7/2			3
⁴³ Ca	23	20	7/2	- 1.317		3
⁴⁵ Ti	23	22	7/2	0.095	0.015	3
⁴⁷ Ti	25	22	5/2	- 0.7881	0.29	5
⁴⁹ Cr	25	24	5/2	0.476		5
⁴⁹ Ti	27	22	7/2	- 1.1039	0.24	7
⁵¹ Cr	27	24	7/2	0.933		7
⁵³ Fe	27	26	7/2			7

7-3 | Extreme Single-Particle Model and Spin

Nuclide	<i>N</i>	<i>Z</i>	<i>J</i>	μ nm	<i>Q</i> barns	Configuration of Neutrons
28						
						$1p_{3/2}$ $0f_{5/2}$ $1p_{1/2}$ $0g_{9/2}$
⁵¹ Ti	29	22	3/2			1
⁵³ Cr	29	24	3/2	- 0.4744	0.026	1
⁵⁵ Fe	29	26	3/2			1
⁵⁷ Ni	29	28	3/2			1
⁵⁵ Cr	31	24	3/2			3
⁵⁷ Fe	31	26	1/2	0.0906		3
⁵⁹ Ni	31	28	3/2			3
⁶¹ Zn	31	30	3/2			3
⁵⁹ Fe	33	26	3/2			3 2
⁶¹ Ni	33	28	3/2	- 0.7487	0.128	3 2
⁶³ Zn	33	30	3/2	- 0.282	0.29	3 2
⁶³ Ni	35	28	3/2			3 4
⁶⁵ Zn	35	30	5/2	0.769	- 0.026	4 3
⁶⁵ Ni	37	28	5/2			4 5
⁶⁷ Zn	37	30	5/2	0.8754	0.17	4 5
⁶⁹ Ge	37	32	5/2	0.735	0.028	4 5
⁶⁹ Zn	39	30	1/2			4 6 1
⁷¹ Ge	39	32	1/2	0.546		4 6 1
⁷³ Ge	41	32	9/2	- 0.8792	- 0.173	4 6 2 1
⁷⁵ Se	41	34	5/2		1.0	
⁷⁷ Kr	41	36	5/2			
⁷⁵ Ge	43	32	1/2	0.508		4 6 1 4
⁷⁷ Se	43	34	1/2	0.534		4 6 1 4
⁷⁹ Kr	43	36	1/2			4 6 1 4
⁷⁹ Se	45	34	7/2	- 1.02	0.9	4 6 7?
⁸¹ Kr	45	36	7/2			4 6 7?
⁸¹ Se	47	34	1/2			4 6 1 8
⁸³ Kr	47	36	9/2	± 0.970	0.26	4 6 2 7
⁸³ Se	49	34	9/2			4 6 2 9
⁸⁵ Kr	49	36	9/2	± 1.005	0.43	4 6 2 9
⁸⁷ Sr	49	38	9/2	- 1.093	0.30	4 6 2 9
⁸⁹ Zr	49	40	9/2			4 6 2 9
50						
						$1d_{5/2}$ $0g_{7/2}$ $2s_{1/2}$ $1d_{3/2}$ $0h_{11/2}$
⁸⁷ Kr	51	36	7/2			0 1
⁸⁹ Sr	51	38	5/2			1
⁹¹ Zr	51	40	5/2	- 1.303		1
⁹³ Mo	51	42	5/2			1
⁹¹ Sr	53	38	5/2			3
⁹³ Zr	53	40	5/2			3

Nuclide	<i>N</i>	<i>Z</i>	<i>J</i>	μ nm	<i>Q</i> barns	Configuration of Neutrons				
						$1d_{5/2}$	$0g_{7/2}$	$2s_{1/2}$	$1d_{3/2}$	$0h_{11/2}$
^{95}Mo	53	42	5/2	- 0.9133	± 0.12	3				
^{97}Ru	53	44	5/2			3				
^{95}Zr	55	40	5/2			5				
^{97}Mo	55	42	5/2	- 0.9325	± 1.1	5				
^{99}Ru	55	44	5/2	0.623	≥ 0.05	5				
^{101}Pd	55	46	7/2			5				
^{97}Zr	57	40	1/2			6			1	
^{99}Mo	57	42	1/2			6			1	
^{101}Ru	57	44	5/2	- 0.69		5	2			
^{105}Cd	57	48	5/2	- 0.7385	0.43	5	2			
^{103}Ru	59	44	5/2			5	4			
^{105}Pd	59	46	5/2	- 0.6116	0.8	5	4			
^{107}Cd	59	48	5/2	- 0.6163	0.68	5	4			
^{109}Cd	61	48	5/2	- 0.8270	0.69	5	6			
^{109}Pd	63	46	5/2			5	8			
^{111}Cd	63	48	1/2	- 0.5943		6	6		1	
^{113}Sn	63	50	1/2	0.879		6	6		1	
^{113}Cd	65	48	1/2	- 0.6217		6	8		1	
^{115}Sn	65	50	1/2	- 0.918		6	8		1	
^{117}Te	65	52	1/2			6	8		1	
^{115}Cd	67	48	1/2	- 0.6484		6	8	1	0	2
^{117}Sn	67	50	1/2	- 1.00		6	8	1	0	2
^{119}Te	67	52	1/2	0.25		6	8	1	0	2
^{119}Sn	69	50	1/2	- 1.046		6	8	1	0	4
^{121}Sn	71	50	3/2	0.70	0.08	6	8	2	1	4
^{123}Te	71	52	1/2	- 0.7359		6	8	1	0	6
^{125}Te	73	52	1/2	- 0.8871		6	8	1	0	8
^{125}Sn	75	50	11/2			6	8	2	0	9
^{127}Te	75	52	3/2	0.66		6	8	2	1	8
^{129}Xe	75	54	1/2	- 0.7768		6	8	1	0	10
^{131}Ba	75	56	1/2			6	8	1	0	10
^{129}Te	77	52	3/2	0.67		6	8	2	1	10
^{131}Xe	77	54	3/2	0.6908	- 0.12	6	8	2	1	10
^{133}Ba	77	56	1/2			6	8	1	0	12
^{131}Te	79	52	3/2			6	8	2	1	12
^{133}Xe	79	54	3/2			6	8	2	1	12
^{135}Ba	79	56	3/2	0.8365	0.18	6	8	2	1	12
^{137}Ce	79	58	3/2	0.90		6	8	2	1	12
^{135}Xe	81	54	3/2			6	8	2	3	12
^{137}Ba	81	56	3/2	0.9357	0.28	6	8	2	3	12
^{139}Ce	81	58	3/2	0.90		6	8	2	3	12
^{141}Nd	81	60	3/2			6	8	2	3	12
^{143}Sm	81	62	3/2			6	8	2	3	12

7-3 | Extreme Single-Particle Model and Spin

(b) Odd-Z Nuclides

Nuclide	Z	N	J	μ nm	Q barns	Configuration of Protons
						$0s_{1/2}$ $0p_{3/2}$ $0p_{1/2}$
¹ H	1	0	1/2	2.7928		1
³ H	1	2	1/2	2.9789		1
⁷ Li	3	4	3/2	3.2564	- 0.04	2 1
¹¹ B	5	6	3/2	2.6885	0.04	2 3
¹³ B	5	8	3/2			2 3
¹⁵ N	7	6	1/2	- 0.3221		2 4 1
¹⁵ N	7	8	1/2	- 0.2831		2 4 1
	8					
						$0d_{5/2}$ $1s_{1/2}$ $0d_{3/2}$
¹⁷ F	9	8	5/2	4.7224		1
¹⁹ F	9	10	1/2	2.6288		0 1
²¹ Na	11	10	3/2	2.386		
²³ Na	11	12	3/2	2.2175	0.14	(3)
²⁵ Na	11	14	5/2			(3)
²⁷ Al	13	12	5/2			(5)
²⁷ Al	13	14	5/2	3.6414	0.15	(5)
²⁹ P	15	14	1/2	1.2349		6 1
³¹ P	15	16	1/2	1.1317		6 1
³³ Cl	17	16	3/2			6 2 1
³⁵ Cl	17	18	3/2	0.8218	- 0.079	6 2 1
³⁷ Cl	17	20	3/2	0.6841	- 0.062	6 2 1
³⁹ Cl	17	22	3/2			6 2 1
³⁷ K	19	18	3/2	0.203		6 2 3
³⁹ K	19	20	3/2	0.3914	0.057	6 2 3
⁴¹ K	19	22	3/2	0.2149	0.076	6 2 3
⁴³ K	19	24	3/2	0.163		6 2 3
⁴⁵ K	19	26	3/2	0.173		6 2 3
	20					
						$0f_{7/2}$
⁴¹ Sc	21	20	7/2	5.43		1
⁴³ Sc	21	22	7/2	4.62	- 0.26	1
⁴⁵ Sc	21	24	7/2	4.7564	- 0.22	1
⁴⁷ Sc	21	26	7/2	5.34	- 0.22	1
⁴⁹ Sc	21	28	7/2			1
⁴⁷ V	23	24	3/2			(3) ?
⁴⁹ V	23	26	7/2	4.5		3
⁵¹ V	23	28	7/2	5.149	- 0.05	3
⁵³ V	23	30	7/2			(3) deformed ?
⁵¹ Mn	25	26	5/2	3.583		(5) deformed ?

Nuclide	Z	N	J	μ nm	Q barns	Configuration of Protons
						$0f_{7/2}$
⁵³ Mn	25	28	7/2	5.046		5
⁵⁵ Mn	25	30	5/2	3.468	0.40	(5)
⁵⁵ Co	27	28	7/2	4.3		7
⁵⁷ Co	27	30	7/2	4.58		7
⁵⁹ Co	27	32	7/2	4.62	0.40	7
	28					
						$1p_{3/2}$ $0f_{5/2}$ $1p_{1/2}$ $0g_{9/2}$
⁶¹ Cu	29	32	3/2	2.13		1
⁶³ Cu	29	34	3/2	2.223	- 0.180	1
⁶⁵ Cu	29	36	3/2	2.382	- 0.195	1
⁶⁷ Cu	29	38	3/2			1
⁶⁷ Ga	31	36	3/2	1.850	0.22	3
⁶⁹ Ga	31	38	3/2	2.016	0.19	3
⁷¹ Ga	31	40	3/2	2.562	0.12	3
⁷¹ As	33	38	5/2			4 1
⁷³ As	33	40	3/2			3 2
⁷⁵ As	33	42	3/2	1.439	0.29	3 2
⁷⁷ Br	35	42	3/2			3 4
⁷⁹ Br	35	44	3/2	2.106	0.31	3 4
⁸¹ Br	35	46	3/2	2.270	0.26	3 4
⁸³ Br	35	48	3/2			3 4
⁸⁵ Br	35	50	3/2			3 4
⁸¹ Rb	37	44	3/2	2.05		3 6
⁸³ Rb	37	46	5/2	1.40		4 5
⁸⁵ Rb	37	48	5/2	1.3524	0.29	4 5
⁸⁷ Rb	37	50	3/2	2.7500	0.14	3 6
⁸⁹ Y	39	50	1/2	- 0.1373		4 6 1
⁹¹ Y	39	52	1/2	0.164		4 6 1
⁹³ Nb	41	52	9/2	6.167	- 0.22	4 6 2 1
⁹⁵ Nb	41	54	9/2	6.3		4 6 2 1
⁹⁹ Tc	43	56	9/2	5.68	0.3	4 6 2 3
¹⁰³ Rh	45	58	1/2	- 0.0883		4 6 1 6
¹⁰³ Ag	47	56	7/2	4.4		4 6 2 7?
¹⁰⁵ Ag	47	58	1/2	0.101		4 6 1 8
¹⁰⁷ Ag	47	60	1/2	- 0.1135		4 6 1 8
¹⁰⁹ Ag	47	62	1/2	- 0.1305		4 6 1 8
¹¹¹ Ag	47	64	1/2	- 0.145		4 6 1 8
¹¹³ Ag	47	66	1/2	0.159		4 6 1 8
¹⁰⁹ In	49	60	9/2	5.53	1.20	4 6 2 9
¹¹¹ In	49	62	9/2	5.53	1.18	4 6 2 9
¹¹³ In	49	64	9/2	5.523	1.14	4 6 2 9

Nuclide	Z	N	J	μ nm	Q barns	Configuration of Protons				
						$1p_{3/2}$	$0f_{5/2}$	$1p_{1/2}$	$0g_{9/2}$	
^{115}In	49	66	1/2	5.5357	1.16	4	6	1	10	
^{117}In	49	68	9/2			4	6	2	9	
50										
						$0g_{7/2}$	$1d_{5/2}$	$0h_{11/2}$	$1d_{3/2}$	$2s_{1/2}$
^{116}Sb	51	64	5/2	3.46	— 0.20	0	1			
^{117}Sb	51	66	5/2	2.67	— 0.30	0	1			
^{119}Sb	51	68	5/2	3.45	— 0.21	0	1			
^{121}Sb	51	70	5/2	3.359	— 0.26	0	1			
^{123}Sb	51	72	7/2	2.547	— 0.37	1				
^{125}Sb	51	74	7/2	2.6		1				
^{127}I	53	70	5/2			2	1			
^{125}I	53	72	5/2	3.0	— 0.89	2	1			
^{127}I	53	74	5/2	2.808	— 0.79	2	1			
^{129}I	53	76	7/2	2.617	— 0.55	3				
^{131}I	53	78	7/2	2.74	— 0.40	3				
^{133}I	53	80	7/2	2.84	— 0.26	3				
^{135}I	53	82	7/2			3				
^{125}Cs	55	70	1/2	1.41						
^{127}Cs	55	72	1/2	1.46						
^{129}Cs	55	74	1/2	1.479						
^{131}Cs	55	76	5/2	3.54	— 0.70	4	1			
^{133}Cs	55	78	7/2	2.578	— 0.003	5				
^{135}Cs	55	80	7/2	2.729	0.044	5				
^{137}Cs	55	82	7/2	2.838	0.045	5				
^{139}La	57	82	7/2	2.778	0.22	7				
^{141}Pr	59	82	5/2	4.3	— 0.07	8	1			
^{143}Pr	59	84	7/2			7	2			
^{143}Pm	61	82	7/2	3.9		7	2			
^{147}Pm	61	86	7/2	2.7	0.7	(7)	(2)			
^{149}Pm	61	88	7/2	3.3		(7)	(2)			
^{151}Pm	61	90	5/2	1.8	1.9	(8)	(1)			
$Z = 63\text{-}78$: Nonspherical Nuclei										
^{191}Au	79	112	3/2	0.137		8	6	12	3	
^{193}Au	79	114	3/2	0.139		8	6	12	3	
^{195}Au	79	116	3/2	0.147		8	6	12	3	
^{197}Au	79	118	3/2	0.1449	0.58	8	6	12	3	
^{199}Au	79	120	3/2	0.270		8	6	12	3	
^{195}Tl	81	114	1/2	1.56		8	6	12	4	1
^{197}Tl	81	116	1/2	1.55		8	6	12	4	1
^{199}Tl	81	118	1/2	1.59		8	6	12	4	1
^{201}Tl	81	120	1/2	1.60		8	6	12	4	1

Nuclide	Z	N	J	μ nm	Q barns	Configuration of Protons					
						$0g_{7/2}$	$1d_{5/2}$	$0h_{11/2}$	$1d_{3/2}$	$2s_{1/2}$	
^{203}Tl	81	122	1/2		1.611		8	6	12	4	1
^{205}Tl	81	124	1/2		1.627		8	6	12	4	1
82											
						$0h_{9/2}$	$1f_{7/2}$	$2p_{3/2}$	$1f_{5/2}$	$2p_{1/2}$	$0i_{13/2}$
^{199}Bi	83	116	9/2								1
^{201}Bi	83	118	9/2								1
^{203}Bi	83	120	9/2		4.59		— 0.64	1			
^{205}Bi	83	122	9/2		5.5			1			
^{209}Bi	83	126	9/2		4.24		— 0.35	1			
^{211}At	85	126	9/2								3
$Z > 86$: Nonspherical Nuclei											

We find that this more realistic single-particle model makes the same predictions about spin, that is, it predicts that the lowest state of an even number of neutrons or protons in the same j -shell is $J = 0$ and that the lowest state of an odd number is $J = j$. Consequently, the experimental values of J for odd- A nuclides should allow us to determine the level order of the shell model.

Table 7-1 shows the experimentally known spin values and the expected configurations of nucleons. It is seen that the successive states of the level sequence are filled in order until N or $Z = 33$ is reached. There is one exception, however, to this statement, namely, the ninth proton is in the $0d_{5/2}$ -level in ^{17}F , but is in a $1s_{1/2}$ -state in ^{19}F . The two levels are close together, and this behavior demonstrates that small variations in the effective central potential occur from nuclide to nuclide. In particular, the neutron number is observed to have some effect on the method of filling the proton shells, making it clear that the assumed independence of the neutron and proton shells is only approximate. Attention should also be directed to nucleon number 11 (^{21}Ne , ^{23}Na), in which three nucleons in $d_{5/2}$ -orbitals are believed to couple their angular momenta to a total J of $\frac{3}{2}$, and to number 25 (^{47}Ti , ^{55}Mn), in which $f_{7/2}$ -nucleons are coupled to $J = \frac{5}{2}$. These anomalous cases will be considered below.

At nucleon number 33 a new principle becomes evident. The $1p_{3/2}$ -shell is filled by the 32nd neutron or proton, and we would expect to find the 33rd in the $0f_{5/2}$ -state. However, the nuclides with 33 neutrons or protons have spin $\frac{3}{2}$, as do many of the nuclides with 35 or 37 nucleons of one kind. Similarly, we would expect the $1d_{5/2}$ -state to fill at $N = 56$, but in fact spins

of $\frac{1}{2}$ are still found for nuclides with 59 and 61 neutrons, and in ^{101}Ru , which has 57 neutrons. Evidently, the higher-angular-momentum states (e.g., the $0g_{7/2}$ -state in this case) fill in pairs, so that when the 59th neutron is added, it does not enter as the third $g_{7/2}$ -neutron; instead the closed $d_{5/2}$ -shell is broken up, and the configuration is $(1d_{5/2})^5(0g_{7/2})^4$.

The probable explanation of this behavior is the pairing energy. Consider a nuclide with an even number N of neutrons having binding energy $B(N)$. When two neutrons are added, it is found that $B(N+2) - B(N)$ is always greater than $2[B(N+1) - B(N)]$. In other words, there exists extra pairing energy between two neutrons in the same shell over and above the "individual" neutron binding energies. The same phenomenon is observed with protons. The source of this extra energy is not accounted for in the extreme single-particle model, but when we take internucleon interactions into consideration, we shall see that the pairing energy increases with the j -value of the particles (see Problem 7-5). Thus, although the $0g_{7/2}$ -level is above the $1d_{5/2}$ -level, binding energy can be gained by breaking the $d_{5/2}$ -shell and adding an extra pair in the $g_{7/2}$ -state. Allowing for this principle of the filling by pairs of the $0f_{5/2}$ -shells, the $0g_{9/2}$ -proton shell, the $0g_{7/2}$ -neutron shell, the $0h_{11/2}$ -shells, and the $0i_{13/2}$ -neutron shell, and remembering that certain levels (such as the $0g_{7/2}$ - and $1d_{5/2}$ -proton states) are very close in energy, we see that the single-particle model accounts in a very natural way for the J -values of almost all the odd- A nuclides. Except for two or three isolated cases such as ^{79}Se and ^{201}Hg , the exceptional J -values all occur for $155 \leq A \leq 180$ and $N \geq 140$. In these regions, the nuclei are considerably deformed from sphericity, and we cannot expect the level sequence of a spherical potential well to apply. There are also deformed nuclei in other parts of the periodic table, and the present level scheme cannot be applied in these cases; the correct scheme for such nuclides is discussed in Chapter 9.

The unforced prediction of such a large number of experimental J -values was historically one of the most important indications that the single-particle model might have a considerable range of validity. There were others, which we shall mention later, but we may also recall that the single-particle model predicts magnetic moments on the Schmidt lines. The nature of the experimental agreement is such that an underlying significance of the model is confirmed, while it is also made clear that refinements of the simple model are necessary. We shall refer to the model already described as the *extreme single-particle model*; when we allow for the interactions between particles in unfilled shells and consider filled shells to form an inert core, we shall say that we are using the *single-particle model*.

7-4 SINGLE-PARTICLE MODEL

In this model, we attribute all the low-energy properties of a nuclide to its "loose" particles outside closed shells. We assume that the interactions of these loose particles with each other do not perturb them appreciably from the single-particle orbits described by the quantum numbers (n, l, j) . This is equivalent to ignoring any correlations in the motion of the particles (such as formation of clusters); the model will not be expected to be any improvement over the extreme single-particle model for treating topics (such as total binding energy) for which correlations are important.

In the extreme single-particle model, all the different states that can be formed by k particles with the same (n, l, j) have the same energy. This degeneracy is removed by considering the interaction between the particles. The calculations on which the extended single-particle model is based require that the interaction be strong enough to remove the degeneracies but not so strong, compared with the spin-orbit force, that j ceases to be a good quantum number for each nucleon. This assumption is part of the single-particle model. It is sometimes possible to relax this approximation and, at the same time, maintain the language of the single-particle model by taking for the particle state a superposition of the wave functions of two or three (n, l, j) -states whose energies are close to one another; such a procedure is called *configuration mixing*.

It is not implied that the interaction potential v_{ij} between particles in a shell is the same as that in the two-particle system. A large part of the actual interaction is accounted for in the single-particle shell-model potential, which represents the average effect on one nucleon of all the other nucleons. The force that removes the degeneracy of shell-model states is consequently often referred to as a remanent effective interaction. Its exact form is hard to calculate; for many purposes, it is satisfactory to take simple analytic forms with adjustable parameters.

In a discussion of the light nuclei ($A \lesssim 50$), the i -spin plays an important role. We define the total i -spin of a nucleus as

$$\mathbf{T} = \sum_{i=1}^A \mathbf{t}_i, \quad (7-4)$$

where \mathbf{t}_i is the i -spin vector of the i th nucleon. For any nuclear state, $T_3 = \frac{1}{2}(Z - N)$ and is therefore a good quantum number. To the extent to which the internucleon forces are charge independent, T^2 is also a constant of motion. We have seen that the two-nucleon nuclear force is very probably charge

independent to quite a good approximation, but, of course, the Coulomb force is not. Hence, in the lighter nuclei where the Coulomb energy is a small part of the total, it is reasonable to treat $T^2 = T(T + 1)$ as a quantum number of the system, but, as the value of Z^2/A increases, this approximation breaks down.[†] The dividing line between the two regions is also characterized by increasing neutron excess and by the fact that, when T is no longer a good quantum number, the neutrons and protons fill different single-particle shells.

The exclusion principle requires that the wave function be antisymmetric under interchange of all coordinates of any pair of nucleons. If we are dealing with a shell containing only protons, say, this requirement means that the angular-momentum wave function must be antisymmetric in all pairs; if we are dealing with a shell containing both neutrons and protons and if T is a good quantum number, the angular-momentum function must be symmetric or antisymmetric for exchange of a given pair, depending on the symmetry of the i -spin function for the same exchange.

These stipulations imply certain restrictions on the states that can be formed. For example, it is not possible to construct an antisymmetric state with J odd from two particles with the same value of j , as can be seen by noting that the appropriate wave function for two (n, l, j) -particles combining to give angular momentum (J, M) is[‡]

$$u_n(r_1)u_n(r_2) \sum_m (jjm M - m|JM)\chi_j^m(1)\chi_j^{M-m}(2). \quad (7-5)$$

When particles 1 and 2 are interchanged, expression 7-5 becomes

$$u_n(r_1)u_n(r_2) \sum_m (jjm M - m'|JM)\chi_j^m(2)\chi_j^{M-m}(1);$$

or, changing the summation index by introducing $m' = M - m$, we have

$$\begin{aligned} & u_n(r_1)u_n(r_2) \sum_{m'} (jj M - m'm'|JM)\chi_j^m(1)\chi_j^{M-m'}(2) \\ &= u_n(r_1)u_n(r_2) \sum_{m'} (-)^{2j-J} (jjm' M - m'|JM)\chi_j^m(1)\chi_j^{M-m'}(2), \end{aligned} \quad (7-6)$$

where we have used the property

$$(j_1 j_2 m_1 m_2 | JM) = (-)^{j_1 + j_2 - J} (j_2 j_1 m_2 m_1 | JM).$$

Since j is half an odd integer, 7-6 and 7-5 differ only by the factor $(-)^{J+1}$, and we observe that antisymmetric functions exist only for even J .

[†] Formally, the Coulomb term in the Hamiltonian is $\sum (e^2/r_{ij})(\frac{1}{2} + t_{3,i})(\frac{1}{2} + t_{3,j})$. This operator does not commute with T^2 , and therefore T is not a good quantum number.

[‡] The Clebsch-Gordan symbols are defined in Appendix A.

There are similar restrictions for states of more than two particles. For example, it can be shown that the three-particle configuration $(n, l, j)^3$ has no state $J = \frac{1}{2}$ antisymmetric for exchange of all three pairs of nucleons. A discussion of these cases is considerably more complicated and may be found in Chapter XII of Rose [7] or in Edmonds and Flowers [8]. Table 7-2 shows the possible antisymmetric states for k particles, for values of $j \leq \frac{11}{2}$. The possible states for $2j + 1 - k$ particles, that is, k holes in a shell, are the same as for k particles.

TABLE 7-2 Possible Total Spins J for Various Configurations $(j)^k$. From Mayer and Jensen [9].

$j = \frac{3}{2}$	$j = \frac{5}{2}$	$j = \frac{7}{2}$
$k = 1: \frac{3}{2}$ = 2: 0, 2	$k = 1: \frac{5}{2}$ = 2: 0, 2, 4 = 3: $\frac{3}{2}, \frac{5}{2}, \frac{9}{2}$	$k = 1: \frac{7}{2}$ = 2: 0, 2, 4, 6 = 3: $\frac{3}{2}, \frac{5}{2}, \frac{7}{2}, \frac{9}{2}, \frac{11}{2}, \frac{15}{2}$ = 4: 0, 2 (twice), 4 (twice), 5, 6, 8
$j = \frac{9}{2}$		
$k = 1: \frac{9}{2}$ = 2: 0, 2, 4, 6, 8 = 3: $\frac{3}{2}, \frac{5}{2}, \frac{7}{2}, \frac{9}{2}$ (twice), $\frac{11}{2}, \frac{15}{2}, \frac{17}{2}, \frac{21}{2}$ = 4: 0 (twice), 2 (twice), 3, 4 (3 times), 5, 6 (3 times), 7, 8, 9, 10, 12 = 5: $\frac{1}{2}, \frac{3}{2}, \frac{5}{2}$ (twice), $\frac{7}{2}$ (twice), $\frac{9}{2}$ (3 times), $\frac{11}{2}$ (twice), $\frac{13}{2}$ (twice), $\frac{15}{2}$ (twice), $\frac{17}{2}$ (twice), $\frac{19}{2}, \frac{21}{2}, \frac{25}{2}$		
$j = \frac{11}{2}$		
$k = 1: \frac{11}{2}$ = 2: 0, 2, 4, 6, 8, 10 = 3: $\frac{3}{2}, \frac{5}{2}, \frac{7}{2}, \frac{9}{2}$ (twice), $\frac{11}{2}$ (twice), $\frac{13}{2}, \frac{15}{2}$ (twice), $\frac{17}{2}, \frac{19}{2}, \frac{21}{2}, \frac{23}{2}, \frac{27}{2}$ = 4: 0 (twice), 2 (3 times), 3, 4 (4 times), 5 (twice), 6 (4 times), 8 (4 times), 9 (twice), 10 (3 times), 11, 12 (twice), 13, 14, 16 = 5: $\frac{1}{2}, \frac{3}{2}$ (twice), $\frac{5}{2}$ (3 times), $\frac{7}{2}$ (4 times), $\frac{9}{2}$ (4 times), $\frac{11}{2}$ (5 times), $\frac{13}{2}$ (4 times), $\frac{15}{2}$ (5 times), $\frac{17}{2}$ (4 times), $\frac{19}{2}$ (4 times), $\frac{21}{2}$ (3 times), $\frac{23}{2}$ (3 times), $\frac{25}{2}$ (twice), $\frac{27}{2}$ (twice), $\frac{29}{2}, \frac{31}{2}, \frac{35}{2}$ = 6: 0 (3 times), 2 (4 times), 3 (3 times), 4 (6 times), 5 (3 times), 6 (7 times), 7 (4 times), 8 (6 times), 9 (4 times), 10 (5 times), 11 (twice), 12 (4 times), 13 (twice), 14 (twice), 15, 16, 18		

The quantum numbers J and T are not sufficient to fix the state of a system of k nucleons. In this case two other quantum numbers, the seniority, s , and the reduced i -spin, t , may be used. To define these we consider the symmetry of the system. Each particle has available only two i -spin states, and hence at most two particles can be in a given space state, with the

same (n, l, j, m) . Thus there may be space-symmetric pairs, which will automatically be antisymmetric in i -spin. In addition to particles that are so paired, there may be particles whose space states are different from those of all other particles, and which form space-exchange antisymmetric pairs with other nucleons. These pairs are i -spin symmetric, that is, $T = 1$. Of these space-antisymmetric pairs, some may have resultant $J = 0$. The seniority quantum number s is defined as the number of particles left in the shell after removal of any such antisymmetric pairs for which $T = 1, J = 0$. The reduced i -spin t is defined as the i -spin of these remaining s nucleons.[†]

If the interaction potential v_{ij} between two particles is sufficiently small compared with the single-particle forces, its contribution to the energy is simply the expectation value $\langle \sum_{i < j=1}^k v_{ij} \rangle$ evaluated for the single-particle state in question. If v_{ij} is a Wigner potential (i.e., a central, nonexchange force), it is possible to give a closed expression for the energy contribution in terms of J , T , s , t , and certain integrals of the radial function [8, 10]. However, the nuclear potential contains spin-exchange forces. In this case, a general formula for $\langle \sum v_{ij} \rangle$ can be given only under the further assumptions that (a) the force range is much less than the radius of the nucleus, and (b) all particles in the shell have the same charge. If these conditions are satisfied, only the singlet (antisymmetric) states contribute to v_{ij} . The result for a potential of form of Eq. 2-17 is

$$\langle \sum v_{ij} \rangle = (W + M - H - B)V_0(2j + 1)f_{nl} \left[k - \frac{2j + 3 - s}{2(j + 1)} s \right], \quad (7-7)$$

where

$$V_0 = 4\pi \int V_0(r)r^2 dr \dagger$$

and

$$f_{nl} = \frac{1}{4} \int [ru_{nl}(r)]^4 \frac{dr}{4\pi r^2}.$$

The expression $(W + M - H - B)V_0(r)$ is the potential in the ${}^1S(n, p)$ -system, which is attractive. Since s is necessarily less than $2j$ and f_{nl} is positive, we see that the lowest energy is obtained with the smallest value of s . From the definition of s , it is clear that, for an even number of nucleons, k , the smallest possible value of s is zero, whereas for odd k the lowest s is 1. But

[†] Further discussions of these concepts may be found in Elliott and Lane [10], Section 20, and Edmonds and Flowers [8].

[‡] Actually Assumption (a) is used in the calculation by taking $V_0(r) = V_0 \delta(r)$.

$s = 0$ means that all nucleons are coupled in pairs to $J = 0$, while $s = 1$ means that all but one nucleon are so coupled. Hence the ground-state spin of an odd number of like nucleons with the same (n, l, j) is $J = j$.

Before we can use the preceding results to predict the spin of a nucleus, we must make the further assumption that the effective interparticle forces between nucleons in different orbits l and l' are weak compared to those between two particles in the same orbit. A possible basis for such an assumption lies in the short-range nature of nuclear forces and in the small overlap of the l - and l' -wave functions. This simplification means that the angular-momentum coupling within a shell, whether filled or not, is not upset by internucleon interaction with other shells. Hence, in an even- Z , odd- N nucleus, the protons still couple to $J = 0$, and the neutrons to $J = j_n$, the j -value of the neutron shell which is filling. Then the resultant angular momentum of the whole nucleus is $J = j_n$. Similarly, in an odd- Z , even- N nucleus, $J = j_p$, and in an even-even nucleus, J remains zero. These results show why the simple shell model predicts correct angular-momentum values in spite of its complete disregard of specific internucleon forces in unfilled shells.

For odd-odd nuclides the ambiguity inherent in the extreme shell model is not removed. We still have a neutron shell $(n_n l_n j_n)^{k_n}$ with total angular momentum j_n , and a proton shell $(n_p l_p j_p)^{k_p}$ with angular momenta coupled to j_p . The resultant nuclear J may be any value from $|j_n - j_p|$ to $j_n + j_p$. To remove the degeneracy of these J -values, we must evaluate the energy of the forces between individual neutrons and protons in the two unfilled shells, assuming that these forces do not change the states calculated for the individual shells. In symbols we evaluate

$$\sum_{i=1}^{k_n} \sum_{j=1}^{k_p} \langle (j_n)_{j_n}^{k_n} (j_p)_{j_p}^{k_p}, J | V_{ij} | (j_n)_{j_n}^{k_n} (j_p)_{j_p}^{k_p}, J \rangle, \quad (7-8)$$

where $| (j_n)_{j_n}^{k_n} (j_p)_{j_p}^{k_p}, J \rangle$ is the wave function for the states in which the k_n neutrons are coupled to yield j_n , the k_p protons are coupled to give j_p , and then the two resulting states are coupled so that their vector sum $j_n + j_p$ has magnitude J . To evaluate expression 7-8 in a simple, general form, it is again necessary to assume very short-range forces, that is, to express the potential as a delta function, $V_0(r_{ij}) = V_0 \delta(r_{ij})$. In this limit, space exchange, P_x , is meaningless, and both Heisenberg and Bartlett forces are spin-exchange forces, while Majorana and Wigner forces have no exchange character. Thus we write:

$$v_{ij} = -(1 - \alpha + \alpha \sigma_i \cdot \sigma_j) V_0 \delta(r_{ij}), \quad (7-9)$$

where

$$\alpha = \frac{1}{2}(H + B) = \frac{1}{2}(1 - W - M).$$

Then the energy (Eq. 7-8) is found to be [11, 12]

$$\begin{aligned} E[(j_n)_{j_n}^{k_n}(j_p)_{j_p}^{k_p}, J] &= E_0(k_n, k_p) + E_\sigma \\ &= \lambda_n \lambda_p E_0(1, 1) + (k_n k_p - \lambda_n \lambda_p)(1 - \alpha) F_0(l_n, l_p) + E_\sigma, \end{aligned} \quad (7-10)$$

where

$$\lambda_n = \frac{2j_n + 1 - 2k_n}{2j_n - 1},$$

$$F_0(l_n, l_p) = \frac{V_0}{4\pi} \int (ru_{l_n})^2 (ru_{l_p})^2 \frac{1}{r^2} dr,$$

$$\begin{aligned} E_0(1, 1) &= \frac{1}{2}(1 - \alpha) F_0(l_n, l_p) (2j_n + 1)(2j_p + 1)(j_n j_p \frac{1}{2} - \frac{1}{2}|J|0)^2 \\ &\times (2J + 1)^{-1} \left\{ \frac{[(j_n + \frac{1}{2}) + (-)^{j_n+j_p+J}(j_p + \frac{1}{2})]^2}{J(J+1)} + 1 \right\}, \end{aligned}$$

$$\begin{aligned} E_\sigma &= \frac{1}{2}\alpha F_0(l_n, l_p) (2j_n + 1)(2j_p + 1)(j_n j_p \frac{1}{2} - \frac{1}{2}|J|0)^2 (2J + 1)^{-1} \\ &\times \left\{ \frac{[(j_n + \frac{1}{2}) + (-)^{j_n+j_p+J}(j_p + \frac{1}{2})]^2}{J(J+1)} - [1 + 2(-)^{j_n+j_p+J}] \right\}. \end{aligned}$$

The energy E_σ is due to the forces that involve exchange and is independent of the number of nucleons in the shells.

Even for a single neutron and proton in each shell, the energy, which is given by

$$E[(j_n)^1(j_p)^1, J] = E_0(1, 1) + E_\sigma,$$

is seen to be a complicated function of J . We can derive some insight into the situation by noting that the potential (Eq. 7-9) implies that the triplet interaction is V_0 and the singlet is $(1 - 4\alpha)V_0$. If the net spin-exchange force is attractive, α is positive and the triplet interaction is stronger than the singlet. Of course, this is the situation for two free nucleons. We therefore expect the orientation of the two nucleons to favor the triplet spin state, that is, σ_n and σ_p parallel. If $j_p - l_p$ and $j_n - l_n$, each of which is $\pm \frac{1}{2}$, are of opposite sign, parallel σ 's are obtained for opposite orientations of j_n and j_p . Thus, in this case, we expect $J = |j_n - j_p|$. On the other hand, if $j_p - l_p$ and $j_n - l_n$ are of the same sign, the tendency toward parallel spins makes $J = j_n + j_p$ the state of lowest energy. However, even the state with $J = |j_n - j_p|$ is not a pure triplet state but contains a singlet component; for a

numerical example, see Problem 7-3. Hence, for the above argument to hold, it is necessary that the preference for the triplet state be fairly pronounced. This means that α cannot be too small. De Shalit [11] and Brink [13] have shown that even for forces of finite range, provided $\alpha > \frac{1}{10}$, the state $J = |j_n - j_p|$ is energetically well below the other possible states if $j_p - l_p$ and $j_n - l_n$ are of opposite sign. When these quantities are of the same sign, the energy of the state $J = j_n + j_p$ is lowered, and if α is large enough, it may cross the state $|j_n - j_p|$. However, the spacing between the states is fairly small, so that reasonable perturbations of our idealized picture might well alter the order.

These results are summarized in *Nordheim's rules* [14], as modified by Brennan and Bernstein [15]. If we define Nordheim's number $N = j_p - l_p + j_n - l_n$, the spin J of an odd-odd nuclide is given by

$$\text{strong rule: } N = 0, \quad J = |j_n - j_p|;$$

$$\text{weak rule: } N = \pm 1, \quad J \text{ is either } |j_n - j_p| \text{ or } j_n + j_p.$$

The same rules hold for k_n and $k_p > 1$, with the understanding that j_n and j_p are replaced by J_n and J_p , the total angular momenta of the configurations $j_n^{k_n}$ and $j_p^{k_p}$ in neighboring odd- A nuclides. In exceptional cases, J_n and J_p may not be equal to j_n and j_p . These rules have been theoretically established by DeShalit and Walecka [16] on the basis of a spin-dependent residual interaction; they also clarify the nature of some of the effects which can invert the expected order of the closely spaced states when the weak rule applies.

When confronted with experimental data, Nordheim's rules are found to work quite well, most of the exceptions being for light nuclei. A number of examples are listed in Problem 7-4; an examination of the observed spins and parities will show that, when two orbits are close together in energy, an odd nucleon is not always in the same orbit in the odd-odd nuclide as in the corresponding odd- A one.

7-5 CONFIGURATION MIXING

As we have remarked before, it is strictly correct to consider particles to move in pure (n, l, j) -orbits only if there are no interparticle interactions in addition to the effective single-particle potential. But, in the absence of such interactions, all states of k particles in the same configuration will be degenerate; we have removed this degeneracy by introducing interactions and calculating the energy splitting between different states by first-order perturbation theory. However, although we have in this way taken account of the energy

effects of the interaction, we have assumed that it is not sufficiently strong to alter the wave functions of the states appreciably. This may well be a good approximation, but its validity should at least be investigated.

Let us consider a nucleus with the extreme single-particle wave function $\psi_0(JM)$, corresponding to the configuration

$$(n_1, l_1, l_1 + \frac{1}{2})^{k_1} (n_1, l_1, l_1 - \frac{1}{2})^{K_1} (n_2, l_2, l_2 + \frac{1}{2})^{k_2} (n_2, l_2, l_2 - \frac{1}{2})^{K_2} \dots \quad (7-11)$$

Usually only one or two of the shells will be unfilled, that is, the majority of the $k_i = 2l_i + 2$, and the majority of the $K_i = 2l_i$. The various ways of coupling the vectors j_i in the unfilled shells lead to various states of different J , and in the absence of nucleon-nucleon interactions all these states are degenerate with energy E_0 . The state $\psi_0(JM)$ is a particular one, which we have chosen to study. If we now introduce an internucleon potential v_{ij} , this state will alter its energy, to first order, by an amount $(\psi_0 | \sum_{i < j} v_{ij} | \psi_0)$, thus removing the degeneracy. But, at the same time, the wave function is altered by the interaction and, in first-order perturbation theory, can be represented as a sum of various states as follows:

$$\psi_{JM} = \psi_0(JM) + \sum_p \alpha_p \psi_p(JM) + \sum_q \alpha_q \psi_q(JM), \quad (7-12)$$

where

$$\alpha_p = \frac{(\psi_0 | \sum_{i < j} v_{ij} | \psi_p)}{E_0 - E_p}, \quad (7-13)$$

with a similar expression for α_q . The states p and q are single-particle states, with unperturbed energies E_p and E_q , and the sums include all such states of the same J and M for which α_p or α_q is nonzero. From the form of Eq. 7-13 it is seen that an admixed state p or q can differ from the unperturbed state ψ_0 by having at most two particles in different states. The states p are distinguished from the states q in that, in the states p , all nucleons have the same n - and l -values as in ψ_0 . Hence the configuration of a state ψ_p is

$$(n_1, l_1, l_1 + \frac{1}{2})^{k_1-a} (n_1, l_1, l_1 - \frac{1}{2})^{K_1+a} (n_2, l_2, l_2 + \frac{1}{2})^{k_2-a} (n_2, l_2, l_2 - \frac{1}{2})^{K_2+a} \dots \quad (7-14)$$

with $a_i = -2, -1, 0, 1$, or 2 and $\sum_i |a_i| = 1$ or 2 .

A typical state of type q has the configuration

$$(n_1, l_1, l_1 + \frac{1}{2})^{k_1+b} (n_1, l_1, l_1 - \frac{1}{2})^{K_1+b} (n_2, l_2, l_2 + \frac{1}{2})^{k_2+b} (n_2, l_2, l_2 - \frac{1}{2})^{K_2+b} \dots \quad (7-15)$$

with b_i and $\beta_i = -2, -1, 0, 1$, or 2 , $\sum_i (|b_i| + |\beta_i|) = 2$ or 4 , and $b_i + \beta_i \neq 0$ for at least one value of i . This ensures that in a state q at least one nucleon has changed its n and/or l .

It will be observed that, if states of type p only were admixed, each nucleon could still be assigned a specific l -value, although j would no longer be a good quantum number, but that for states of type q neither l nor j is, in general, a constant of motion. Note also that in both types of admixture we envisage exciting to unfilled levels nucleons initially in both filled and unfilled shells.

The coefficients α_p and α_q measure the amount of admixture. For first-order perturbation theory to hold and, *a fortiori*, to ignore configuration mixing, it is necessary that all the $|\alpha|^2 \ll 1$. Usually only a few states are appreciably mixed into the wave function, and Eq. 7-13 shows that these will be the states whose unperturbed energies E_p or E_q are near E_0 or those for which the matrix element $(\psi_0 | v_{ij} | \psi_p)$ is extraordinarily large. Generally speaking, the single-particle states that are quite close in energy have different l -values (see Fig. 7-2). This fact seems to suggest that certain states of type q may be important in configuration mixing. On the other hand, two nucleons with the same n and l have very similar wave functions, so that the matrix element may be large, even though the energy difference is not particularly small. Thus states of type p are also important.

A reasonable amount of configuration mixing does not change the conclusions that we have reached about the energies of the various states, since our calculations have allowed already for the first-order energy correction. Thus none of the conclusions about ground-state spins will be changed, although we can perhaps appreciate more clearly now how the order of neighboring states is occasionally inverted because of higher-order effects—for example, the inversions that make Nordheim's weak rule a tendency rather than a precise result. However, other properties of nuclides may be more strongly modified. For example, magnetic moments may be substantially changed by the admixture of a state with an appreciably different single-particle moment. We shall study such effects in later chapters.

REFERENCES

1. W. Elsasser, *J. Phys. Rad.* 5, 625 (1934).
2. M. G. Mayer, *Phys. Rev.* 75, 1969 (1949).
3. M. G. Mayer, *Phys. Rev.* 78, 16 (1950).
4. O. Haxel, J. H. D. Jensen, and H. E. Suess, *Phys. Rev.* 75, 1766 (1949).
5. O. Haxel, J. H. D. Jensen, and H. E. Suess, *Z. Physik* 128, 295 (1950).

6. A. Ross, R. D. Lawson, and H. Mark, *Phys. Rev.* **102**, 1613; **104**, 401 (1956).
7. M. E. Rose, *Elementary Theory of Angular Momentum*, John Wiley, New York, 1957.
8. A. R. Edmonds and B. H. Flowers, *Proc. Roy. Soc. (London)* **A214**, 515 (1952).
9. M. G. Mayer and J. H. D. Jensen, *Elementary Theory of Nuclear Shell Structure*, John Wiley, New York, 1955.
10. J. P. Elliott and A. M. Lane, "The Nuclear Shell Model," *Encyclopedia of Physics*, Vol. XXXIX, Springer-Verlag, Berlin, 1957.
11. A. De Shalit, *Phys. Rev.* **91**, 1479 (1953).
12. C. Schwartz, *Phys. Rev.* **94**, 95 (1954).
13. D. M. Brink, *Proc. Phys. Soc.* **A67**, 757 (1954).
14. L. Nordheim, *Phys. Rev.* **78**, 294 (1950).
15. M. H. Brennan and A. M. Bernstein, *Phys. Rev.* **120**, 927 (1960).
16. A. De Shalit and J. D. Walecka, *Nucl. Phys.* **22**, 184 (1961).

PROBLEMS

7-1. Show that $(E_{l-1/2} - E_{l+1/2}) \propto (2l + 1)$ if $V(r)$ in V_{ls} is constant. How does this formula change if $V(r)$ has a maximum near the nuclear surface?

7-2. It has been suggested that the Coulomb field may be responsible for the different level orders for neutrons and protons for N or $Z > 50$. Calculate the difference in electrostatic energy between a $0g_{7/2}^-$ and a $1d_{5/2}$ -proton, assuming that the potential is that of a uniform, spherically symmetric charge distribution and using harmonic-oscillator wave functions. For a numerical estimate, use a suitable typical nucleus.

7-3. Show that the wave function $\langle (d_{5/2})^1 (\phi_{1/2})^1, 2 |$ with $M = 2$ can be written as

$$\begin{aligned} \frac{1}{3\sqrt{5}} \{ {}^3(\sigma)_1 [\sqrt{2} Y_2^1(1) Y_1^0(2) - 5 Y_2^2(1) Y_1^{-1}(2)] - {}^3(\sigma)_{-1} Y_2^2(1) Y_1^1(2) \\ + {}^3(\sigma)_0 [- \sqrt{2} Y_2^1(1) Y_1^1(2) + 3 Y_2^2(1) Y_1^0(2)] \\ + {}^1(\sigma)_0 [- \sqrt{2} Y_2^1(1) Y_1^1(2) + 2 Y_2^2(1) Y_1^0(2)] \}. \end{aligned}$$

and show that this wave function is $\frac{2}{13}$ singlet state and $\frac{11}{13}$ triplet. Similarly, demonstrate that $\langle (d_{5/2})^1 (\phi_{1/2})^1, 3 |$ is $\frac{1}{3}$ singlet and $\frac{2}{3}$ triplet. Does this confirm Nordheim's rule?

7-4. For the following nuclides, the most likely experimental ground-state spins and parities are given in parentheses. State the probable single-particle configurations in each case and comment on any unusual circumstances:

- ${}^3\text{He}(\frac{1}{2}^+)$, ${}^9\text{Be}(\frac{3}{2}^-)$, ${}^{14}\text{N}(1^+)$, ${}^{15}\text{N}(\frac{1}{2}^-)$, ${}^{17}\text{F}(\frac{5}{2}^+)$, ${}^{21}\text{Ne}(\frac{3}{2}^+)$, ${}^{27}\text{Al}(\frac{5}{2}^+)$, ${}^{30}\text{P}(1^+)$, ${}^{33}\text{S}(\frac{3}{2}^+)$,
- ${}^{34}\text{Cl}(0^+)$, ${}^{35}\text{Cl}(\frac{3}{2}^+)$, ${}^{38}\text{K}(3^+)$, ${}^{40}\text{K}(4^-)$, ${}^{42}\text{K}(2^-)$, ${}^{43}\text{Ca}(\frac{7}{2}^-)$, ${}^{50}\text{V}(6^+)$, ${}^{53}\text{Mn}(\frac{7}{2}^-)$,
- ${}^{53}\text{Cr}(\frac{3}{2}^-)$, ${}^{54}\text{Mn}(2^+)$, ${}^{65}\text{Cu}(\frac{3}{2}^-)$, ${}^{66}\text{Cu}(1^+)$, ${}^{66}\text{Ga}(1^+)$, ${}^{69}\text{Ga}(\frac{3}{2}^-)$, ${}^{97}\text{Mo}(\frac{5}{2}^+)$, ${}^{99}\text{Tc}(\frac{9}{2}^+)$,
- ${}^{103}\text{Rh}(\frac{1}{2}^-)$, ${}^{105}\text{Pd}(\frac{5}{2}^+)$, ${}^{106}\text{Rh}(1^+)$, ${}^{121}\text{Sb}(\frac{5}{2}^+)$, ${}^{122}\text{Sb}(2^-)$, ${}^{123}\text{Sb}(\frac{7}{2}^+)$, ${}^{123}\text{Te}(\frac{1}{2}^+)$,

Problems

- ${}^{130}\text{Cs}(1^+)$, ${}^{131}\text{Cs}(\frac{5}{2}^+)$, ${}^{133}\text{Cs}(\frac{7}{2}^+)$, ${}^{131}\text{Xe}(\frac{3}{2}^+)$, ${}^{134}\text{Cs}(4^+)$, ${}^{138}\text{La}(5^+)$, ${}^{199}\text{Hg}(\frac{1}{2}^-)$, ${}^{203}\text{Tl}(\frac{1}{2}^+)$, ${}^{206}\text{Tl}(0^-)$, ${}^{209}\text{Bi}(\frac{9}{2}^-)$, ${}^{210}\text{Bi}(1^-)$.

7-5. (a) From formula 7-7, calculate the pairing energy $v = [B(N+2) - B(N)] - 2[B(N+1) - B(N)]$, when N is even and is the number of particles in a given shell (n, l, j) , and B is the binding energy of the ground state. Show that v increases with j , provided f_{nl} does not decrease as l increases.

(b) If an (n, l, j) -nucleon is bound by an energy E in the effective single-particle potential $V_c + V_{ls}$, compare the binding energy of the lowest state with $2j(n, l, j)$ -nucleons and $N(n', l', j')$ -nucleons with that of the lowest state with $(2j+1)(n, l, j)$ -nucleons and $(N-1)(n', l', j')$ -nucleons, and thus explain the filling in pairs of high-angular-momentum states in the single-particle model.

(c) Give qualitative arguments to show that f_{nl} tends to increase with l .

7-6. Show that, if Nordheim's rules were strictly true, there would be no odd-odd nuclides with ground state 0^+ or 1^- . Find some exceptions to these results.

7-7. Show that the mean-square radius of a particle in the oscillator state with quantum numbers n, l, m is

$$\alpha^{-2}(2n+l+\frac{3}{2}),$$

where $\alpha = (m\omega/\hbar)^{1/2}$.

Find the mean-square radius of the whole nucleus for ${}^{40}\text{Ca}$, ${}^{41}\text{K}$, and ${}^{60}\text{Ni}$.

Chapter 8

Correlations in Nuclear Matter

8-1 INTRODUCTION

In Chapter 7 we saw how satisfactorily the shell model "explains" a substantial number of nuclear properties. And yet at first sight one might not expect a shell model to be at all appropriate for nuclei. After all, it implies that each nucleon moves in a single-particle orbital and, therefore, that the wave function of a nucleon and hence its behavior at a given position are independent of whether or not another nucleon is close to it. Since there is a strong short-range nucleon-nucleon force, this approximation would seem to be unreasonable. The explanation lies to a great extent in the operation of the Pauli exclusion principle, which modifies the classical behavior of interacting fermions, as well as in certain properties of the interaction between nucleons. In this chapter we shall examine the derivation of properties of nuclei, starting from known interactions between nucleons *in vacuo*, that is, free nucleons.

In order to understand the main features, it is useful to introduce the concept of *nuclear matter*. Nuclear matter is a medium of infinite extent, of uniform density, consisting of equal numbers of neutrons and protons, and in which the Coulomb force between protons is ignored. In such a system, each particle moves with constant momentum except when it interacts with another. This plane-wave motion is the analog of the closed orbital of a nucleon in the shell model of a finite nucleus. In each case the nucleon "feels" an average field of some kind, which we shall seek to understand. In the finite case the geometry is such that the average field permits a set of discrete bound states; in the infinite case the geometrical symmetry

insists that uncorrelated states be states of constant momentum, but the average field will alter the relationship between the momentum p and the energy e_p of a particle so that $p^2 \neq 2Me_p$.

It is important to realize some of the consequences of a momentum-dependent "potential." A potential in this sense is defined as the difference between the total energy of the particle and its kinetic energy, $p^2/2M$. In infinite, uniform nuclear matter, the properties are the same at all points of space, since the system is translationally invariant. Thus the energy of a particle cannot depend on its location but may depend on its momentum. Alternatively, it may be said that the energy of a particle can depend on the location of other particles in its vicinity, but that this local structure cannot be at variance with the homogeneity of nuclear matter; this is possible since the particles are not, in fact, localized and the overall density is constant. Although in the neighborhood of a particle center there may be considerable fluctuations in the density of other particles, the distribution of these centers can be considered to be uniform and continuous, leading to a homogeneous density distribution.

On the other hand, in a finite nucleus, density is a function of position, there is no translational invariance, and the energy of a particle may depend not only on the correlation of other particles in its immediate position, but also on its position with respect to the center of the nucleus. It could also be said that the potential energy can depend on both momentum and position.

We shall now demonstrate the equivalence of the concepts of a nonlocal potential and a momentum-dependent one. If the vectors \mathbf{r} are measured from a fixed center, the energy at a point \mathbf{r} can depend, in the infinite homogeneous medium, only on vectors $\mathbf{r}' - \mathbf{r}$ connecting the point with other points in its immediate vicinity, and the resultant total density cannot depend on \mathbf{r} . In a finite nucleus, not only is there this possibility but also the potential may depend directly on \mathbf{r} . Thus, in general, the Schrödinger equation becomes

$$-\frac{\hbar^2}{2M} \nabla_{\mathbf{r}}^2 \psi(\mathbf{r}) + \int d\mathbf{r}' U(\mathbf{r}, \mathbf{r}' - \mathbf{r}) \psi(\mathbf{r}') = e\psi(\mathbf{r}). \quad (8-1)$$

This form of energy operator (which is not diagonal in coordinate space) can be understood as reflecting correlations, whereby the presence of a particle at position \mathbf{r} influences the probability of finding another at a point \mathbf{r}' , and this in turn affects the energy of the particle at \mathbf{r} and leads to a potential energy in the form of the integral shown.

If the wave functions are plane waves of constant momentum, appropriate as the first approximation for an infinite medium in which U does not depend

on its first argument \mathbf{r} , Eq. 8-1 becomes

$$\epsilon_p = \frac{p^2}{2M} + \int d\mathbf{r}' U(\mathbf{r}' - \mathbf{r}) \exp\left[\frac{i\mathbf{p} \cdot (\mathbf{r}' - \mathbf{r})}{\hbar}\right].$$

The integral is not a function of \mathbf{r} but depends only on \mathbf{p} , being, in fact, the Fourier transform of $U(\mathbf{r}' - \mathbf{r})$. If we call this $U(\mathbf{p})$, we see that

$$\epsilon_p = \frac{p^2}{2M} + U(\mathbf{p}). \quad (8-2)$$

This demonstrates the equivalence between the nonlocal and momentum-dependent formalisms. It is readily generalized to the case in which the wave functions are not plane waves. Two cases will interest us, the correlated wave functions of nuclear matter and those of finite nuclei, but in any case the wave function can be written as a superposition of plane waves, namely,

$$\psi(\mathbf{r}) = \int \phi(\mathbf{p}) \exp(i\mathbf{p} \cdot \mathbf{r}/\hbar) d\mathbf{p}.$$

The potential term in Eq. 8-1 becomes

$$\begin{aligned} & \int d\mathbf{r}' U(\mathbf{r}, \mathbf{r}' - \mathbf{r}) \psi(\mathbf{r}') \\ &= \iint d\mathbf{r}' \phi(\mathbf{p}) U(\mathbf{r}, \mathbf{r}' - \mathbf{r}) \exp(i\mathbf{p} \cdot \mathbf{r}'/\hbar) d\mathbf{p} \\ &= \int \exp(i\mathbf{p} \cdot \mathbf{r}/\hbar) d\mathbf{p} \phi(\mathbf{p}) \int d\mathbf{r}' U(\mathbf{r}, \mathbf{r}' - \mathbf{r}) \exp\left[\frac{i\mathbf{p} \cdot (\mathbf{r}' - \mathbf{r})}{\hbar}\right] \\ &= \int \exp(i\mathbf{p} \cdot \mathbf{r}/\hbar) d\mathbf{p} \phi(\mathbf{p}) U(\mathbf{r}, \mathbf{p}) \\ &= \int d\mathbf{p} U(\mathbf{r}, \mathbf{p}) \phi(\mathbf{p}) \exp(i\mathbf{p} \cdot \mathbf{r}/\hbar) \\ &= U(\mathbf{r}, \mathbf{p}_{0p}) \int d\mathbf{p} \phi(\mathbf{p}) \exp(i\mathbf{p} \cdot \mathbf{r}/\hbar) \\ &= U(\mathbf{r}, \mathbf{p}_{0p}) \psi(\mathbf{r}) \end{aligned} \quad (8-3)$$

where $\mathbf{p}_{0p} = -i\hbar\nabla_r$. Of course, in the infinite case U does not depend on \mathbf{r} .

To some approximation, nuclear matter is an idealization of the constant-density central region of a large nucleus, where the nucleons may be "unaware" of the boundaries of the nucleus. Since, in fact, neither the average inter-

nucleon distance in real nuclei nor the nuclear force range is exceedingly small compared with the dimensions of even large nuclei, it is more accurate to say that the nuclear-matter idealization needs to be corrected for surface effects, effects of neutron excess, and Coulomb effects in order to make comparisons with experiment. However, the semiempirical mass formula contains precisely such terms, and it is reasonable, therefore, to demand that the calculations of nuclear matter predict correctly a density equal to that in the region of constant density of heavy nuclei and a binding energy per particle equal to the volume term of the semiempirical formula. These quantities are [1, 2]

$$\rho_0 = 0.170 \text{ nucleons fm}^{-3} \quad (8-4a)$$

and

$$E/A = -15.68 \text{ MeV per particle.} \quad (8-4b)$$

It might be thought that the actual central density would be less than the value appropriate for hypothetical nuclear matter, since real protons are repelled by electrostatic force; however, Brandow [3] found that the surface tension compensates for this Coulomb pressure.

For fermions, only one particle may occupy a given quantum state, and, as we saw in Section 6-2, a good first approximation to nuclear matter is a zero-temperature gas enclosed in a large volume and with all states occupied up to the Fermi momentum $p_F = \hbar k_F$. If the volume is denoted by Ω , the wave function of a particle with momentum[†] \mathbf{k}_α , normalized to one particle in the volume, is

$$\phi_\alpha \equiv \phi(\mathbf{k}_\alpha) = \Omega^{-1/2} \exp(i\mathbf{k}_\alpha \cdot \mathbf{r}). \quad (8-5)$$

Similarly, a finite system will have its n lowest energy levels occupied, if there are n particles.

The density (in particles per unit volume) is given, in either finite or infinite systems, by summing the square of the wave function over all occupied states, that is,

$$\rho = \sum_\alpha |\phi_\alpha|^2. \quad (8-6a)$$

For the infinite system, this expression becomes

[†] We shall frequently speak of "momentum" k , even though k is, of course, actually the associated wave number. Note also, as indicated in Section 6-2, that $\sum_\alpha \rightarrow \Omega \int d^3k/(2\pi)^3$ for one particle per state.

$$\rho = \frac{k_F^3}{6\pi^2}. \quad (8-6b)$$

Of course, in nuclear matter there are four particles per momentum state, and, as in Eq. 6-2,

$$\rho_0 = \frac{2}{3\pi^2} k_F^3 \quad (8-7)$$

with $k_F = 1.36 \text{ fm}^{-1}$.

8-2 EXCLUSION PRINCIPLE CORRELATIONS

In the first paragraph of this chapter, we noted that it is difficult to believe that interacting particles can move in an approximately uncorrelated way, because we have the classical picture that for noninteracting uncorrelated particles the probability of finding a particle in a prescribed volume element is independent of the location of a second particle and, therefore, the particles have reasonable likelihood of being close together, a situation which the actual repulsive nuclear force would prevent. In fact, the probability of finding a particle at \mathbf{r}_1 and one at \mathbf{r}_2 is, classically,

$$P_{cl} d\mathbf{r}_1 d\mathbf{r}_2 = \rho(1)\rho(2) d\mathbf{r}_1 d\mathbf{r}_2 = \sum_m |\phi_m(1)|^2 d\mathbf{r}_1 \sum_n |\phi_n(2)|^2 d\mathbf{r}_2, \quad (8-8)$$

where $\rho(1)$ represents the density at \mathbf{r}_1 , and the sums on m and n extend over all the occupied states. We shall consistently use this summation convention.

However, quantum statistics alter this situation drastically, and for identical fermions, that is, those with the same charge and spin state, the probability of finding two particles, one at \mathbf{r}_1 and one at \mathbf{r}_2 , one in state α and one in state β , is

$$\frac{1}{2} |\phi_\alpha(1)\phi_\beta(2) - \phi_\alpha(2)\phi_\beta(1)|^2 d\mathbf{r}_1 d\mathbf{r}_2.$$

We note immediately the well-known fact that two identical fermions cannot be at the same point, but we can be more precise than this. The probability of finding one such fermion of the system at \mathbf{r}_1 and another at \mathbf{r}_2 is clearly the sum of the above expression over occupied states, namely,

$$P_F d\mathbf{r}_1 d\mathbf{r}_2 = \frac{1}{2} \sum_m \sum_n |\phi_m(1)\phi_n(2) - \phi_m(2)\phi_n(1)|^2 d\mathbf{r}_1 d\mathbf{r}_2,$$

$$P_F = \sum_m \sum_n |\phi_m(1)|^2 |\phi_n(2)|^2 - \operatorname{Re} \sum_m \sum_n \phi_m(1)\phi_n(2)\phi_m^*(2)\phi_n^*(1). \quad (8-9a)$$

The first term of P_F is simply $\rho(1)\rho(2)$, and we see that the fermion and classical probability densities differ by the correlation

$$P_F - P_{cl} = -C^2(1, 2) = -\operatorname{Re} \sum_m \sum_n \phi_m(1)\phi_n^*(1)\phi_m^*(2)\phi_n(2) \\ = -|\sum_m \phi_m(1)\phi_m^*(2)|^2. \quad (8-9b)$$

For the infinite medium, we note that, where $\mathbf{r} = \mathbf{r}_1 - \mathbf{r}_2$,

$$\sum_m \phi_m(1)\phi_m^*(2) = \frac{4\pi}{(2\pi)^3} \int_0^{k_F} j_0(kr) k^2 dk \\ = \frac{1}{2\pi^2} k_F^3 \frac{j_1(k_F r)}{k_F r}.$$

The first line follows simply from Eq. 8-5 and the partial wave expansion of a plane wave. The result is

$$C^2(1, 2) = \rho^2 \left[\frac{3j_1(k_F r)}{k_F r} \right]^2 = P_{cl} F_1(k_F r), \quad (8-10a)$$

where we have introduced a correlation function F_1 . In this case $P_{cl} = \rho^2$, and, using Eq. 8-9, we note that

$$P_F(1, 2) = \rho^2 [1 - F_1(k_F r)]. \quad (8-10b)$$

The quantity $F_1(x)$ is plotted in Fig. 8-1. It has the value unity at $x = 0$, remains large up to $x \sim 2$, and is small (less than 0.1) for $x > 3$. With $k_F = 1.36 \text{ fm}^{-1}$ corresponding to nuclear-matter density, these two values of x correspond to $r = 1.5$ and 2.2 fm . The short-range part of the two-nucleon force between identical nucleons will therefore be suppressed because

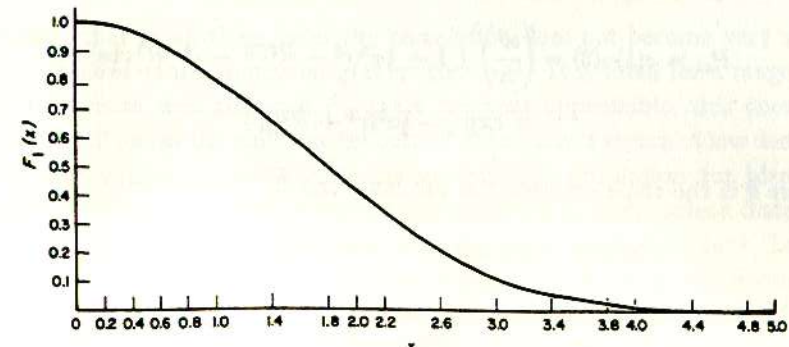


Fig. 8-1 The Pauli correlation function F_1 for an infinite medium.

$P_F(1, 2)$ is small where the force is large. It is apparent that the exclusion principle alone accounts for the possibility of using an effective force in nuclear matter, much weaker than the free nucleon-nucleon force, for collisions between pairs of identical particles. Such states are spin triplet and have odd angular momentum. The exclusion principle creates a "wound" or "hole" in the wave function for other states as well, including neutron-proton pairs, but this phenomenon occurs only when a force is acting to scatter the particles. We discuss this in the next section.

It is instructive to perform the same calculation for a finite nucleus. Consider ^{16}O with the $1s$ - and $1p$ -states filled in accordance with the shell model, and assume that the states can be described by harmonic oscillator functions. These are the uncorrelated states ϕ_m . To evaluate the correlation, it is convenient to take it as $\text{Re} \sum_{m,n} \phi_m(1)\phi_n^*(2)\phi_m(2)\phi_n(1)$, to use the expressions in Problem 4-10 for the wave functions, together with the spherical harmonic addition theorem (Eq. A-70), and to replace \mathbf{r}_1 and \mathbf{r}_2 by relative and center-of-mass coordinates. The result is found to be

$$C^2(\mathbf{r}, \tilde{\mathbf{R}}) = \left(\frac{\alpha^2}{\pi}\right)^3 [1 + \frac{1}{2}\alpha^2(\tilde{\mathbf{R}}^2 - \mathbf{r}^2)]^2 \exp[-\frac{1}{2}\alpha^2(\mathbf{r}^2 + \tilde{\mathbf{R}}^2)], \quad (8-11)$$

where α is the oscillator constant $(M\omega/\hbar)^{1/2}$, $\tilde{\mathbf{R}} = \mathbf{r}_1 + \mathbf{r}_2$, and $\mathbf{r} = \mathbf{r}_1 - \mathbf{r}_2$. This is the correlation in the probability of finding two identical nucleons, for example, neutrons with spin up, one at \mathbf{r}_1 and the other at \mathbf{r}_2 . The density is

$$\rho(1) = \sum_m |\phi_m(1)|^2 = \left(\frac{\alpha^2}{\pi}\right)^{3/2} (1 + 2\alpha^2 r_1^2) \exp(-\alpha^2 r_1^2). \quad (8-12)$$

(Of course, the nuclear density is four times this value.) The classical joint probability is found to be

$$\begin{aligned} P_{cl} = \rho(1)\rho(2) &= \left(\frac{\alpha^2}{\pi}\right)^3 \{[1 + \frac{1}{2}\alpha^2(r^2 + \tilde{\mathbf{R}}^2)]^2 - \alpha^4 r^2 \tilde{\mathbf{R}}^2 \cos^2 \theta\} \\ &\times \exp[-\frac{1}{2}\alpha^2(r^2 + \tilde{\mathbf{R}}^2)], \end{aligned}$$

where θ is the angle between the vectors \mathbf{r} and $\tilde{\mathbf{R}}$. Consequently

$$P_F(1, 2) = \rho(1)\rho(2)[1 - F_2(\mathbf{r}, \tilde{\mathbf{R}})]$$

with

$$F_2(\mathbf{r}, \tilde{\mathbf{R}}) = \frac{[1 + \frac{1}{2}\alpha^2(\tilde{\mathbf{R}}^2 - \mathbf{r}^2)]^2}{[1 + \frac{1}{2}\alpha^2(r^2 + \tilde{\mathbf{R}}^2)]^2 - \alpha^4 r^2 \tilde{\mathbf{R}}^2 \cos^2 \theta}. \quad (8-13)$$

The function F_2 is shown in Fig. 8-2 for three special cases:

1. The center of mass of the two particles is at the center of the nucleus ($\tilde{\mathbf{R}} = 0$).
2. The center of mass is at the position of maximum density ($\tilde{\mathbf{R}} = \sqrt{2}/\alpha$) and \mathbf{r} is parallel to $\tilde{\mathbf{R}}$, that is, the particles lie on the same nuclear diameter and at points of different density.
3. The mass center is at $\tilde{\mathbf{R}} = \sqrt{2}/\alpha$ but \mathbf{r} is perpendicular to $\tilde{\mathbf{R}}$, that is, the particles are at points of equal density.

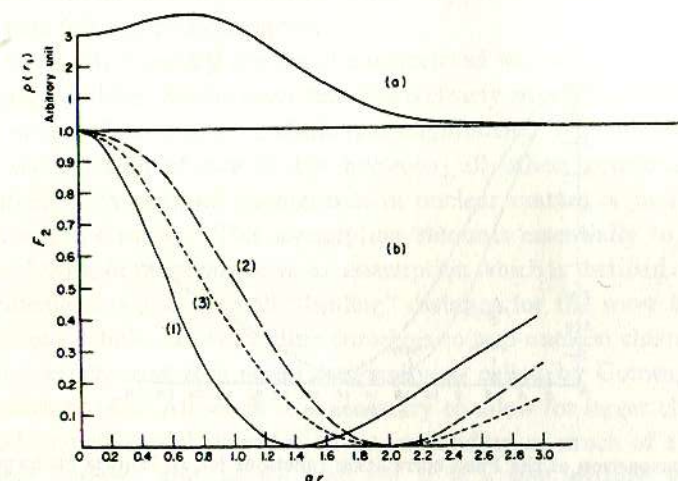


Fig. 8-2 (a) The density of ^{16}O in the harmonic-oscillator shell model. (b) The correlation function F_2 defined in Eq. 8-13 for three cases described in the text.

It is seen that in all these cases the correlation does not become very small until r reaches values somewhat greater than α^{-1} . It is small for a range of r near this value, and although F_2 again becomes appreciable, this does not happen until one of the particles (or both of them) is in a region of low density. Thus we see that for ^{16}O the exclusion principle correlation for identical fermions will suppress the effects of the interaction at internucleon distances up to about α^{-1} and also to some extent at distances larger than $2\alpha^{-1}$. In this model, the rms radius of ^{16}O happens to be $1.5\alpha^{-1}$; it is 2.6 fm. Consequently the force is reduced for $r \lesssim 1.6$ fm, and there may be a good possibility of understanding the real nucleus in terms of small perturbations of the shell model.

Although the applicability of the nuclear-matter approximation to any part of a nucleus as small as ^{16}O might be questioned, it is tempting nevertheless to compare the correlation calculated for the finite case with that obtained for nuclear matter of the same density. Combining Eqs. 8-6b and 8-12 and using the above value for α , we find that the density at the center of ^{16}O corresponds to $k_F = 1.26 \text{ fm}^{-1}$ and that the maximum density (at $r_1 = 1/\alpha\sqrt{2}$) corresponds to $k_F = 1.34 \text{ fm}^{-1}$. Hence in Fig. 8-3 we show the nuclear-matter correlation $F_1(k_F r)$ for $k_F = 1.30 \text{ fm}^{-1}$ and compare it with $F_2(r, 0)$,

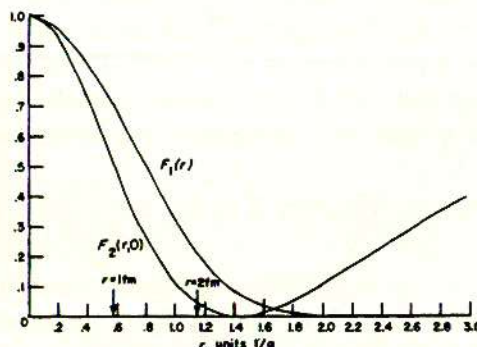


Fig. 8-3 Comparison of the Pauli correlation functions for an infinite medium and for like particles in ^{16}O .

which is the function for two particles with mass center at the center of the nucleus, and each a distance $r/2$ from the center. It is seen that, at least as far as estimates of the Pauli correlation effect are concerned, calculations with the infinite medium would give a very good approximation to the finite case. Of course, the questions of what value of k_F to use, and of how to take account of angular dependence, become more acute for particles that are not equidistant from the origin.

8-3 BETHE-GOLDSTONE EQUATION AND G-MATRIX

There is a further reason why the wave function of two nucleons is small at distances of close approach—the repulsive core of the nucleon-nucleon potential v . Although this core may be quite strong, the product $v\psi$ of the

core potential multiplied by the true wave function is finite. Of course, if v is infinite, ψ is zero. We might, therefore, consider it useful to write

$$G\phi = v\psi,$$

where ϕ is the model two-body wave function (e.g., oscillator or plane wave), and the equation defines G . In this way we replace the actual potential v by a quantity G so that G acting on the model function is the same as v applied to the actual wave function; it might be that for many purposes G could serve as an effective potential. Moreover, G might be reasonably smooth compared with the actual potential. These suggestions are confirmed by the theory that follows in this chapter.

We have still to justify the use of uncorrelated waves to describe strongly interacting particles. Such a wave function is clearly wrong within the distance around each nucleon where correlations are significant. We shall assume that, during the collision of two of the nucleons, all others continue to move undisturbed with constant momentum in nuclear matter or in shell-model orbitals in finite nuclei. This assumption amounts essentially to neglect of clusters of three or more nucleons, an assumption which is justified *a posteriori* if the calculations give a small “healing” distance for the wave function of the two that collide. If we confine ourselves to two-nucleon clusters, we are using the *independent-pair model* (originally so called by Gomes, Walecka, and Weisskopf [4]). Although it is necessary to allow for larger clusters, the independent-pair model provides an understanding of much of the physics of nuclear matter; and, as we shall see, it is a well-justified low-density approximation.

Let the model wave functions be denoted by $\phi_\alpha(\mathbf{r})$. We shall consider A particles and denote their coordinates by $\mathbf{r}_1, \mathbf{r}_2, \dots, \mathbf{r}_A$ with respect to a fixed center. We shall suppress spin and i -spin coordinates for the moment. Suppose that the two particles moving freely in states k and l collide and that all other particles in states m, \dots, n continue undisturbed. The wave function of the colliding particles is modified; let us call it ψ_{kl} . The wave function of the whole system must be antisymmetric in coordinates of all the nucleons, and it is, therefore,

$$\Psi_{kl} = \mathcal{A}\{\psi_{kl}(\mathbf{r}_1, \mathbf{r}_2)\phi_m(\mathbf{r}_3) \cdots \phi_n(\mathbf{r}_A)\}, \quad (8-14)$$

where the \mathcal{A} indicates that all terms formed by antisymmetric exchange of $\mathbf{r}_1, \dots, \mathbf{r}_A$ are to be taken.

The wave functions $\phi_\alpha(\mathbf{r})$ are eigenfunctions of a single-particle Hamiltonian. For nuclear matter, they are plane waves, each with its momentum \mathbf{p}_α ; for

finite nuclei, they are some sort of orbitals. Thus

$$H_0(i)\phi_\alpha(r_i) \equiv [T(i) + U(i)]\phi_\alpha(i) = e_\alpha\phi_\alpha(i). \quad (8-15)$$

In nuclear matter the single-particle field U is a function of momentum only; in the finite nucleus it depends on position (e.g., oscillator or Woods-Saxon potential) but can also be momentum dependent. Temporarily we shall not specify $U(i)$ further.

The colliding pair feel the same overall potential as do all the particles and in addition experience the free nucleon-nucleon potential; this is the essence of the independent-pair approximation. Hence the Schrödinger equation is

$$[H_0(1) + H_0(2) + v_{12}]\psi_{kl}(1, 2) = e_{kl}\psi_{kl}(1, 2). \quad (8-16)$$

The energy e_{kl} is not the unperturbed energy $e_k + e_l$. We shall examine the physical significance of this later.

The antisymmetry demanded in the wave function (Eq. 8-14) of the whole system and the assumption that each state, m, \dots, n , contains precisely one nucleon mean that ψ_{kl} is orthogonal to all the filled states, except of course states k and l . In other words, if ψ_{kl} is expanded in eigenfunctions of H_0 , it contains no component of states m, \dots, n , since these are filled by other nucleons. With the normalization usual in the literature,

$$\begin{aligned} \psi_{kl}(1, 2) &= \phi_k(1)\phi_l(2) + \sum_{a,b} a_{ab}\phi_a(1)\phi_b(2) \\ &\quad + \sum_a a_{ka}\phi_k(1)\phi_a(2) + \sum_a a_{al}\phi_a(1)\phi_l(2). \end{aligned} \quad (8-17)$$

We use a, b, c, \dots for states unoccupied in the ground state and k, l, m, \dots for filled states. Note that

$$\langle \phi_k \phi_l | \psi_{kl} \rangle = 1. \quad (8-18)$$

We can write Eq. 8-16 as

$$(e_k + e_l)\phi_k(1)\phi_l(2) + \sum'_{\alpha, \beta} a_{\alpha\beta}(e_\alpha + e_\beta)\phi_\alpha(1)\phi_\beta(2) + v_{12}\psi_{kl} = e_{kl}\psi_{kl},$$

where the summation \sum' over the single-particle states α, β is such that $\alpha = k, a, b, c, \dots$; $\beta = l, a, b, c, \dots$; $\alpha \neq \beta$; and $(\alpha, \beta) \neq (k, l)$. If we take the scalar product of the above expression with $\langle \phi_\alpha(1)\phi_\beta(2) |$, we obtain

$$\begin{aligned} a_{\alpha\beta}(e_{kl} - e_\alpha - e_\beta) &= \langle \phi_\alpha(1)\phi_\beta(2) | v_{12} | \psi_{kl}(1, 2) \rangle \\ &= \langle \alpha\beta | v | \psi_{kl} \rangle. \end{aligned} \quad (8-19)$$

We shall usually abbreviate $\langle \phi_\alpha(1)\phi_\beta(2) |$ to the form $\langle \alpha\beta |$. Substitution of Eq. 8-19 into 8-17 yields

$$|\psi_{kl}(1, 2) \rangle = |\phi_k(1)\phi_l(2) \rangle + \sum'_{\alpha, \beta} \frac{\langle \alpha\beta | v | \psi_{kl} \rangle}{e_{kl} - e_\alpha - e_\beta} |\phi_\alpha(1)\phi_\beta(2) \rangle,$$

which may be written as

$$|\psi_{kl}(1, 2) \rangle = |\phi_k(1)\phi_l(2) \rangle + \sum'_{\alpha, \beta} \frac{1}{e_{kl} - H_0} |\alpha\beta\rangle \langle \alpha\beta | v | \psi_{kl} \rangle, \quad (8-20)$$

where $H_0 = H_0(1) + H_0(2)$. It is usual to introduce the projection operator Q , that takes care of the Pauli principle:

$$Q_{kl} = \sum_{ab} |ab\rangle \langle ab| + \sum_a |ka\rangle \langle ka| + \sum_b |bl\rangle \langle bl|. \quad (8-21)$$

Then Eq. 8-20 may be rewritten as

$$|\psi_{kl} \rangle = |\phi_k \phi_l \rangle + \frac{Q_{kl}}{e_{kl} - H_0} v |\psi_{kl} \rangle. \quad (8-22)$$

This is the form of the Bethe-Goldstone equation [5], and a number of important results follow from it.

Equation 8-22 suggests a perturbation procedure obtained by continually substituting expression 8-22 itself for ψ whenever it appears at the end of the equation, that is,

$$\begin{aligned} |\psi_{kl} \rangle &= |\phi_k \phi_l \rangle + \sum'_{\alpha, \beta} \frac{|\alpha\beta\rangle}{e_{kl} - (e_\alpha + e_\beta)} \langle \alpha\beta | v | kl \rangle \\ &\quad + \sum'_{\alpha, \beta} \sum'_{\gamma, \delta} \frac{|\alpha\beta\rangle}{e_{kl} - (e_\alpha + e_\beta)} \langle \alpha\beta | v | \gamma\delta \rangle \frac{1}{e_{kl} - (e_\gamma + e_\delta)} \langle \gamma\delta | v | kl \rangle \\ &\quad + \dots, \end{aligned} \quad (8-23)$$

where, as before, the Pauli principle restricts the intermediate states. This expression is of little value for computation unless it converges rapidly, and, unfortunately, nuclear potentials do not produce rapid convergence since the repulsive core, even when finite, contributes largely to the matrix elements $\langle \alpha\beta | v | \gamma\delta \rangle$ between uncorrelated states.

Expansion 8-23 provides the formal justification for the arguments concerning intermediate states in Section 6-2. For nuclear matter, $|\alpha\beta\rangle$ are states in which the total momentum $P = p_\alpha + p_\beta$ is a constant of motion. Moreover, the nuclear potential conserves momentum. Hence $\langle \alpha\beta | v | kl \rangle$

vanishes, unless $\mathbf{p}_\alpha + \mathbf{p}_\beta = \mathbf{p}_k + \mathbf{p}_l$. Consequently, no matter to how high an order we go in the series of Eq. 8-23, all the intermediate states $|\alpha\beta\rangle$, $|\gamma\delta\rangle, \dots$ have the same total momentum. Furthermore, k and l are inside the Fermi sea, and momentum conservation does not allow only one of the particles to be scattered above the Fermi sea. This implies that in this case there are no components of ψ_{kl} like the last two in Eq. 8-17, where only one of the particles is excited. Consequently the operator Q_{kl} may be written in nuclear matter as

$$Q = \sum_{ab} |ab\rangle\langle ab|. \quad (8-24)$$

Clearly this simplification does not apply to the finite nucleus. The result is valid only in the independent-pair approximation; once we consider the interaction of three particles, we can conserve momentum in the chain $|klm\rangle \rightarrow |abm\rangle \rightarrow |kbc\rangle$ and the last of these is an intermediate state (in the second-order term) where one of the particles is in a level below k_F .

One of the major consequences of the Bethe-Goldstone equation is the "healing" of the wave function, that is, the fact that correlations which constitute a "wound" in the model wave function $\phi_k\phi_l$ are confined to short relative distances. Note that the Bethe-Goldstone equation 8-22 is very similar in structure to the Lipmann-Schwinger equation 5-49 for two-nucleon scattering in free space. In the latter case, however, there is a singularity in the energy denominator, and a term $+i\varepsilon$ is required for an outgoing wave of the same momentum, as in Eq. 5-51. This singularity introduces a phase shift in the scattered wave that modifies the asymptotic form. In the Bethe-Goldstone equation 8-22, on the other hand, the operator Q_{kl} ensures that no singularity is present in the energy denominator and the wound contains no asymptotic modification of $\phi_k\phi_l$. Consequently there is no real scattering in nuclear matter, and the wave function ψ_{kl} must heal to $\phi_k\phi_l$ for large relative distances. That there is no real scattering in nuclear matter is physically understandable, since the Pauli principle allows only scatterings that defy the conservation of energy. These virtual scatterings above the Fermi sea serve to distort the relative wave function at short distances. A more detailed discussion of healing will be found in ref. [6].

It is useful to define a defect wave function

$$\zeta_{kl} = \phi_k\phi_l - \psi_{kl}, \quad (8-25)$$

which tends to zero for large values of $|\mathbf{r}_1 - \mathbf{r}_2|$ as the wave function heals. Indeed, the integral

$$\kappa_{kl} = \int |\zeta_{kl}|^2 d\mathbf{r}_1 d\mathbf{r}_2 \quad (8-26)$$

is often called the "wound" in the wave function. It is easy to see from Eq. 8-17 that

$$\kappa_{kl} = \sum_{ab} |a_{ab}|^2 + \sum_a [|a_{ka}|^2 + |a_{al}|^2]; \quad (8-27)$$

in words, κ_{kl} is the probability of finding the actual system excited out of the noninteracting Fermi sea, relative to the probability of finding it in the state $|kl\rangle$.

As we have seen, the wound ζ contains as Fourier components no states below the Fermi level. Hence the range of ζ is restricted to distances of the order of k_F^{-1} or shorter, that is, less than about 1.5 fm. In other words, the exclusion principle has the effect of restricting the correlations between particles to short distances. In Section 8-2 we considered noninteracting identical fermions and saw that the exclusion principle introduced correlations on the length scale of k_F^{-1} . We now have seen that, even when there is interaction, and even when a pair of nonidentical fermions in nuclear matter is considered, the fact that all the low-momentum fermion states are filled means that only short-range correlations are possible. This is the basis for our earlier statement that the operation of the exclusion principle is one of the reasons why shell-model wave functions are valid first approximations for many purposes: they are modified only at relatively short distances. Of course, the nature of the modification does depend on the potential v or, more specifically, on the matrix elements $\langle ab|v|kl\rangle$.

We may also introduce a quantity G , mentioned earlier as an effective interaction in the sense that

$$G\phi_k\phi_l = v\psi_{kl}. \quad (8-28)$$

Multiplying Eq. 8-22 by v and using this definition G , we obtain

$$G\phi_k\phi_l = v\phi_k\phi_l + v \frac{Q_{kl}}{e_{kl} - H_0} G\phi_k\phi_l$$

or

$$G = v + v \frac{Q_{kl}}{e_{kl} - H_0} G. \quad (8-29a)$$

Now in this equation for the infinite medium the only reference to states k and l is in the energy e_{kl} , and therefore it is usual to define $G(\omega)$ as

$$G(\omega) = v + v \frac{Q}{\omega - H_0} G, \quad (8-29b)$$

with Q from Eq. 8-24. The quantity G is also a function of the Fermi level k_F , through Q , and of course it depends on the assumed Hamiltonian H_0 .

Let us now consider once again the complete system of A particles. Its Hamiltonian is

$$H = \sum_{i=1}^A T(i) + \frac{1}{2} \sum_{i,j=1}^A v(i,j), \quad (8-30)$$

and its ground state corresponds to the lowest eigenvalue of

$$(H - E)\Psi = 0. \quad (8-31)$$

We also consider the Hamiltonian for the single-particle model where particles are in the states k, l, m, \dots . This is

$$H_0 = \sum_{i=1}^A H_0(i), \quad (8-32)$$

and it defines an orthogonal set of states Φ_i of the A -particle system by

$$(H_0 - W_i)\Phi_i = 0. \quad (8-33)$$

The lowest model state Φ_0 is that in which all levels are filled up to the Fermi level; its energy is

$$W_0 = \sum_k e_k,$$

using the notation of Eq. 8-15. The wave function Φ_0 is simply the Slater determinant of the occupied states ϕ_k .

To obtain a Bethe-Goldstone equation for the A -body system we may generalize the techniques already used. We first write

$$H = H_0 + V, \quad (8-34)$$

where $V = \frac{1}{2} \sum v(i,j) - \sum U(i)$. Then, by writing

$$\Psi = \Phi_0 + \sum a_i \Phi_i$$

and noting that

$$(H_0 - E)(\Phi_0 + \sum a_i \Phi_i) + V\Psi = 0,$$

it is easy to see, taking the scalar product with Φ_0 , that

$$E = W_0 + (\Phi_0|V|\Psi). \quad (8-35)$$

Also, generalizing the method used to obtain Eq. 8-22, we find

$$\Psi = \Phi_0 + \frac{Q'}{E - H_0} V\Psi, \quad (8-36a)$$

$$G'\Phi_0 = V\Psi, \quad (8-36b)$$

$$G' = V + V \frac{Q'}{E - H_0} G', \quad (8-36c)$$

and

$$Q' = 1 - |\Phi_0\rangle\langle\Phi_0|. \quad (8-36d)$$

These equations form the basis for a rigorous approach to the many-body problem. Primes are used to emphasize the many-body nature of G' and Q' .

For the moment we wish to use only the equation for the energy of the system, E (Eq. 8-35). We work within the independent-pair approximation, so that Ψ is of the form

$$\Psi = N \sum_{kl} \Psi_{kl},$$

where Ψ_{kl} , as given in Eq. 8-14, represents a state in which only the $k-l$ pair interacts and N is a normalization constant $2/A(A-1)$.

Of the terms in $(\Phi_0|V|\Psi)$, we first consider $(\Phi_0|\sum_i U(i)|\Psi_{kl})$. Since $U(i)$ is a single-particle operator, it cannot link states in which more than one particle changes state; and since the filled states other than k, l all remain filled in Ψ_{kl} , only diagonal terms survive for these other filled states. Thus the expression is

$$\sum_{m \neq k,l} \langle m|U|m \rangle + \frac{1}{2} \langle \phi_k(1)\phi_l(2) - \phi_l(1)\phi_k(2) | U(1) + U(2) | \psi_{kl}(1,2) - \psi_{kl}(2,1) \rangle,$$

where the factor $\frac{1}{2}$ comes from the antisymmetric normalization of Ψ_{kl} .

In finite nuclei the terms in ψ_{kl} that have a single-particle excitation cause an extra complication, but for nuclear matter the single-particle potentials U link the term $\phi_k\phi_l$ only to the term $\phi_k\phi_l$ in ψ_{kl} , and the result for the above expression is simply $\sum \langle m|U|m \rangle$ summed over all occupied states m , including k and l .

For the two-particle potential in V , we have

$$\begin{aligned} \langle \Phi_0 | \sum v(i,j) | \Psi \rangle &= \langle \Phi_0 | v(1,2) | \sum_{kl} \Psi_{kl} \rangle \\ &= \sum_{kl} \frac{1}{2} \langle \phi_k(1)\phi_l(2) - \phi_l(1)\phi_k(2) | v(1,2) | \psi_{kl}(1,2) - \psi_{kl}(2,1) \rangle \end{aligned}$$

$$= \sum_{kl} [\langle kl|v|\psi_{kl}(1, 2) \rangle - \langle kl|v|\psi_{kl}(2, 1) \rangle],$$

where we have used the facts that $v(1, 2)$ is symmetric and that $\psi_{kl}(2, 1) = \psi_{lk}(1, 2)$.

Hence in nuclear matter Eq. 8-35 becomes

$$E = W_0 + \frac{1}{2} \sum_{kl} (\langle kl|G|kl \rangle - \langle kl|G|lk \rangle) - \sum_m \langle m|U|m \rangle, \quad (8-37a)$$

$$= \sum_m \langle m|T|m \rangle + \frac{1}{2} \sum_{kl} (\langle kl|G|kl \rangle - \langle kl|G|lk \rangle). \quad (8-37b)$$

Equation 8-37b demonstrates one reason for thinking of G as an effective interaction, for its matrix elements between uncorrelated states appear in the total energy precisely where one would see the matrix elements of the potential energy between actual wave functions.

For the finite nucleus it is necessary to add other terms to account for the permissible one-particle excitations, namely, the terms

$$\frac{1}{2}N \sum_{kla} (a_{al}\langle \phi_k|U|\phi_a \rangle + a_{ka}\langle \phi_l|U|\phi_a \rangle),$$

which, by Eq. 8-19, can be reduced to

$$N \sum_{kla} \frac{\langle ka|G|kl \rangle}{e_{kl} - e_a - e_k} \langle l|U|a \rangle. \quad (8-38)$$

Although this sum runs over an infinity of unoccupied states a , convergence arises from the energy denominator as e_a increases, and also because reasonable U and G give small matrix elements between occupied states and highly excited states.

The results 8-37 and 8-38 are important in that they show how to compute the energy of the system within the limitations of the independent-pair approximation. One postulates any convenient single-particle Hamiltonian H_0 , finds its states ϕ_α , uses Eq. 8-29 to calculate $G(e_{kl})$, and substitutes the result in Eqs. 8-37 and 8-38. It will be seen that there appears to be nothing unique about the choice of the single-particle potential U , except that the independent-pair approximation will presumably not be valid unless the occupied eigenstates ϕ_m bear a reasonable resemblance to the actual wave functions outside the region of correlation. This is necessary not only because of the basic idea of the independent-pair approximation, but also because the treatment of the exclusion principle would be incorrect if the occupied ϕ_m 's did not span the space of the real occupied states. We shall say more later about the choice of U , and we shall see that for a certain choice the term 8-38 will be canceled by terms from clusters of more than two particles.

With this choice of potential, Eq. 8-37 applies to both finite and infinite cases, and we note that to determine the energy of the system we need only the diagonal matrix elements of G for occupied states although of course both the direct and the exchange elements are required. But one gap remains before we can carry out the prescription of the last paragraph in order to find E , namely, before we can indicate methods of solution for the G -matrix in Eq. 8-29 we need a value for e_{kl} .

Let us examine e_{kl} . We take the scalar product of Eq. 8-16 with $\langle \phi_k \phi_l \rangle$ to obtain

$$\langle kl|H_0(1) + H_0(2)|\psi_{kl} \rangle + \langle kl|v|\psi_{kl} \rangle = e_{kl}\langle kl|\psi_{kl} \rangle$$

and use Eqs. 8-15 and 8-18 to get

$$\epsilon_{kl} = e_{kl} - e_k - e_l = \langle kl|v|\psi_{kl} \rangle = \langle kl|G(e_{kl})|kl \rangle. \quad (8-39)$$

This suggests a self-consistency technique, in that we could assume a value for e_{kl} , calculate G , use Eq. 8-39 to find a new value for e_{kl} , and continue such cycles until convergence was reached. However, this is not necessary for nuclear matter, because in that case ϵ_{kl} is infinitesimal.

This is perhaps best seen by noting that v conserves total momentum and depends only on the relative coordinate of the two interacting particles. We have already noticed that all the terms of ψ have the same total momentum. For plane waves

$$\phi_\alpha(\mathbf{r}_1)\phi_\beta(\mathbf{r}_2) = \frac{1}{\Omega} \exp[i(\mathbf{p}_\alpha \cdot \mathbf{r}_1 + \mathbf{p}_\beta \cdot \mathbf{r}_2)] = \frac{1}{\Omega} \exp[i(\mathbf{p}_{\alpha\beta} \cdot \mathbf{r} + \mathbf{P}_{\alpha\beta} \cdot \mathbf{R})]$$

with

$$\mathbf{p}_{\alpha\beta} = \frac{1}{2}(\mathbf{p}_\alpha - \mathbf{p}_\beta), \quad \mathbf{r} = \mathbf{r}_2 - \mathbf{r}_1;$$

$$\mathbf{P}_{\alpha\beta} = \mathbf{p}_\alpha + \mathbf{p}_\beta, \quad \mathbf{R} = \frac{1}{2}(\mathbf{r}_1 + \mathbf{r}_2).$$

Consider the matrix element $\langle \alpha\beta|v|\psi_{kl} \rangle$, where α and β are any two momentum states above or below k_F . We write

$$\psi_{kl} = |kl\rangle + \sum ab |ab\rangle, \quad (8-40)$$

where, as in Eq. 8-19,

$$a_{ab} = \langle ab|v|\psi_{kl} \rangle (e_{kl} - e_a - e_b)^{-1}. \quad (8-41)$$

We expand the potential in its Fourier components:

$$v(\mathbf{r}) = \frac{1}{(2\pi)^3} \int v(\mathbf{k}) \exp(i\mathbf{k} \cdot \mathbf{r}) d^3 k. \quad (8-42)$$

Then

$$\begin{aligned}\langle \alpha\beta|v|\psi_{kl}\rangle &= \frac{1}{\Omega^2} \int d\mathbf{r} d\mathbf{R} d\mathbf{k} \exp(-i\mathbf{p}_{\alpha\beta} \cdot \mathbf{r} - i\mathbf{P}_{\alpha\beta} \cdot \mathbf{R}) \\ &\quad \times \frac{1}{(2\pi)^3} v(\mathbf{k}) \exp(i\mathbf{k} \cdot \mathbf{r}) \{\exp(i\mathbf{p}_{kl} \cdot \mathbf{r} + i\mathbf{P}_{kl} \cdot \mathbf{R}) \\ &\quad + \int da a_{ab} \exp(i\mathbf{p}_{ab} \cdot \mathbf{r} + i\mathbf{P}_{ab} \cdot \mathbf{R})\}.\end{aligned}$$

The last term is written as a single sum because b is determined when a is given, since $\mathbf{P}_{kl} = \mathbf{P}_{ab} = \mathbf{p}_a + \mathbf{p}_b$. Since $\mathbf{P}_{\alpha\beta}$ is also the same as \mathbf{P}_{kl} , the integrand is independent of \mathbf{R} and the integral over \mathbf{R} yields the volume Ω . Hence, performing integrations on \mathbf{r} also, we obtain

$$\begin{aligned}\langle \alpha\beta|v|\psi_{kl}\rangle &= \frac{1}{\Omega} \int d\mathbf{k} v(\mathbf{k}) \left[\delta^{(3)}(\mathbf{k} - \mathbf{p}_{\alpha\beta} + \mathbf{p}_{kl}) + \int da a_{ab} \delta^{(3)}(\mathbf{k} - \mathbf{p}_{\alpha\beta} + \mathbf{p}_{ab}) \right] \\ &= \frac{1}{\Omega} \left[v(\mathbf{p}_{\alpha\beta} - \mathbf{p}_{kl}) + \int da a_{ab} v(\mathbf{p}_{\alpha\beta} - \mathbf{p}_{ab}) \right] \\ &= \frac{1}{\Omega} \left[v(\mathbf{p}_\alpha - \mathbf{p}_k) + \int da a_{ab} v(\mathbf{p}_\alpha - \mathbf{p}_a) \right].\end{aligned}\quad (8-43)$$

In the last step we used again the fact that the total momentum is conserved.

Let us now consider $\epsilon_{kl} = \langle kl|v|\psi_{kl}\rangle$. We see that

$$\epsilon_{kl} = \frac{1}{\Omega} \left[v(0) + \int da a_{ab} v(\mathbf{p}_k - \mathbf{p}_a) \right].$$

The first term $v(0)$ is the zero-frequency Fourier transform of the potential. For a potential of finite range, this is finite, and since it is divided by the large volume Ω , this contribution to ϵ_{kl} is infinitesimal. Can the second term give a finite contribution to ϵ_{kl} ? It could do so only if the integral were to be very large, and this in turn could happen only if a_{ab} became large. We see from Eq. 8-41 that this can happen if e_{kl} is near $e_a + e_b$, which is, in turn, a possibility if k and l are just below the Fermi surface and a and b just above it, with e_{kl} being near $e_k + e_l$. Moreover, since the energy spacing of momentum states is inversely related to the size of the enclosure, this is just the right kind of behavior to compensate for the $1/\Omega$ factor. But the precise result depends also on the nature of the potential. If we trace back through the derivation, we see that the integral in ϵ_{kl} is essentially the Fourier transform of $v\zeta$, where

ζ is the defect wave function.[†] We have already seen that ζ is of very short range, and hence all these Fourier components within the Fermi sea also are finite. Thus for nuclear matter ϵ_{kl} is infinitesimal.

We note that this conclusion does not follow if the force is of longer range, or if the spectrum is discrete as in finite nuclei. We remark in passing that, when there is a finite value of ϵ_{kl} for k and l near the Fermi level, the extra binding arises for like particle pairs, and we find the phenomenon of superconductivity both in the electron gas in metals and in real nuclei (as opposed to nuclear matter), in the first case because the electromagnetic force is of long range and in the second case because the bound states have discrete spectra.

The solution of the Bethe-Goldstone equations (Eqs. 8-36) of the general many-body problem is an extensive topic in theoretical physics, about which a great deal of literature exists. We do not intend to describe the subject in this book, but we shall find it convenient to quote some results. We have already suggested that the independent-pair approximation is valid only if the density is sufficiently low so that clusters of larger numbers of particles can be ignored. Particles are in interaction only when their relative wave function is correlated; if we write c for an average healing distance of the wave-function defect, the probability that the motion of one particle is correlated with that of some one other particle is of order $(c/r_0)^3$, where r_0 is the radius of the sphere containing, on the average, one particle, that is, its volume is $1/r_0^3$. But if κ is the probability that the motion of one particle is correlated with that of another, the probability that a particle has two other particles within correlation distance is κ^2 . Hence, if we write \bar{v} for an average interaction energy for two correlated particles, we would expect the contributions to the binding energy per particle from two-, three-, and four-particle clusters to be, respectively, of order $(1/2!)\kappa\bar{v}$, $(3/3!)\kappa^2\bar{v}$, and $(6/4!)\kappa^3\bar{v}$, that is, $\frac{1}{2}\kappa\bar{v}$, $\frac{1}{2}\kappa^2\bar{v}$, and $\frac{1}{4}\kappa^3\bar{v}$.

Estimation of κ requires knowledge of the wave-function defect, and it is possible to be rather more accurate than simply to replace κ by $(c/r_0)^3$. In fact, if one particle is interacting with another, its motion is modified, that is, it is excited out of the Fermi sea. Hence the probability of interaction for a particle

[†] Explicitly,

$$\begin{aligned}\int dr \exp(-i\mathbf{p}_{kl} \cdot \mathbf{r}) v(r) \zeta_{kl}(r) &= \int dr \sum_a \exp(-i\mathbf{p}_{kl} \cdot \mathbf{r}) v(r) a_{ab} \exp(i\mathbf{p}_{ab} \cdot \mathbf{r}) \\ &= (2\pi)^{3/2} \sum_a a_{ab} v(\mathbf{p}_k - \mathbf{p}_a),\end{aligned}$$

where b is fixed by $\mathbf{p}_{ab} = \mathbf{p}_{kl}$.

is the same as the probability of excitation, and this is simply related to the wound κ_{kl} , defined in Eq. 8-26. In fact, the probability per particle of such excitation is

$$\kappa = \frac{1}{A} \sum_{k < l} \kappa_{kl} = \frac{1}{A} \sum_{k < l} \langle \zeta_{kl} | \zeta_{kl} \rangle = \frac{A}{2} \langle \zeta | \zeta \rangle_{av}, \quad (8-44)$$

where the average is over all pairs $k-l$. For nuclear matter, if we write

$$\phi_{kl} = \left(\frac{1}{\Omega} \right) \exp(i\mathbf{k}_1 \cdot \mathbf{r}_1) \exp(i\mathbf{k}_2 \cdot \mathbf{r}_2) |SM_S\rangle |TM_T\rangle$$

and

$$\begin{aligned} \zeta_{kl} = & \left(\frac{1}{\Omega} \right) \exp(i\mathbf{P} \cdot \mathbf{R}) \sum_{JLM} 4\pi(i)^L \zeta_{JLS}(kr) \\ & \times (LSM_L M_S | JM) Y_L^M L(\mathbf{r}) Y_L^{M*}(\mathbf{k}) |SM_S\rangle |TM_T\rangle, \end{aligned} \quad (8-45)$$

we find

$$\kappa = \frac{1}{8} \rho \sum_{JLS} (2J+1)(2T+1) \langle \zeta_{JLS} | \zeta_{JLS} \rangle_{av(k)}, \quad (8-46)$$

where, as indicated, the average is taken over the relative momentum k . We see that, if the defect wave function ζ is nonzero in a sphere of radius c where it has an average value θ/Ω , κ is indeed of order $\theta^2(c/r_0)^3$, as our qualitative reasoning suggested.

We shall see below that for nuclear matter κ is of the order 0.15; its exact value depends, of course, on density and on the internucleon force. Now the average kinetic energy per particle ($0.6e_F$) is 23 MeV at $k_F = 1.36 \text{ fm}^{-1}$. Therefore, to give the observed binding of 16 MeV, taking two-, three-, and four-body clusters into account, we must have

$$\frac{1}{2}\kappa\bar{v}(1 + \kappa + \frac{1}{2}\kappa^2) = 39 \text{ MeV}.$$

Taking $\kappa = 0.15$, we find that the two-body clusters contribute about 33.6 MeV to the binding energy, while the three- and four-body clusters give 5.0 and 0.4 MeV, respectively.

We should note that the small parameter of the expansion is κ , the wound, and not G , the interaction.

The three-body clusters are contributing about 5 MeV of the binding energy (although only one-eighth of the potential energy) and hence can hardly be ignored. If the many-body Bethe-Goldstone equations 8-36 are treated analogously to the two-body equations 8-16 to 8-20, a series for the

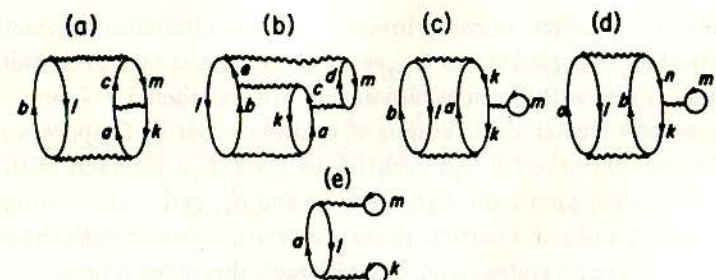


Fig. 8-4 Three-body cluster diagrams. Downward-pointing arrows refer to states in the Fermi sea; upward-pointing ones, to states above the sea. Arrows pointing into a vertex indicate the states occupied before the interaction; arrows pointing away from a vertex, the states occupied afterward. For example, the bottom wavy line of diagram (a) indicates the interaction in which the states k and l ($e_k, e_l < e_F$) scatter to states a and b , and the next wavy line refers to the interaction in which particles in states a and m scatter to states k and c . Diagrams of this kind are extensively used for actual calculation in many-body theory, but we do not give the details here. Each diagram represents a term in the total energy. Summation on all state labels is implied.

ground-state energy can be obtained. When only two-nucleon forces are taken, all the expressions are related to a succession of virtual excitations involving only two particles and all can be given in terms of the *two-body* G -matrix. We have described a two-body cluster as a correlation ζ_{kl} in the wave function, which we have pictured as a collision causing the virtual excitation of two particles above the Fermi sea, immediately followed by a second interaction refilling their original states in the Fermi sea. A three-body cluster involves simultaneous interaction of three particles, which, with a two-body force, must be pictured as a collision of two particles, producing excitation out of the Fermi sea, a subsequent interaction of one of these with a third particle, exciting it out of the Fermi sea, and then interactions refilling the three original states. The expressions for the energies of three-body clusters are of third or higher order in the G -matrix. For example, a third-order term is

$$-(ml|G|bc)(ck|G|am)(ab|G|kl)(e_a + e_b - e_{kl})^{-1}(e_c + e_d - e_m + e_k - e_{kl})^{-1}.$$

This may be described as due to the interaction of particles in states k and l which go to states a and b , with the particle so placed in state a interacting with the particle in state m to reoccupy state k and place a particle in state c , where it interacts with the particle in state b to re-establish the undisturbed Fermi sea. As an aid to visualizing this term, we show the appropriate Goldstone diagram in Fig. 8-4a. This term is an energy properly attributed

to a three-body cluster since it involves the simultaneous interaction of particles in three occupied states k, l, m . The diagram is said to contain three "hole lines," those with downward-pointing arrows labeled k, l, m .

A three-body cluster contribution of a higher order in G appears in Fig. 8-4b. We see that states k and l scatter to a and b , a interacts with m to produce two states above the Fermi sea (c and d), and c and b interact to reoccupy state k and put a particle in state e , which interacts with the particle in state d to reoccupy states l and m . Although this gives a term

$$-\frac{(ml|G|de)(ke|G|cb)(cd|G|am)(ab|G|kl)}{(e_a + e_b - e_{kl})(e_b + e_c + e_a - e_m - e_{kl})(e_a + e_e - e_m + e_k - e_{kl})}$$

of fourth order in G , it is part of the three-body-cluster energy since only three hole states appear. Because the small parameter for a series expansion is κ , not G , it is important to sum all the terms, of whatever order, which constitute the three-body cluster. Bethe [7] showed how to perform this sum, using the methods developed by Faddeev [7] for the three-body problem.

There is an important class of three-body-cluster terms which require separate treatment. These are the ones that contain a diagonal matrix element $\langle mn|G|mn\rangle$ involving two hole states. Such factors are said to produce the "hole self-energy," since they describe the change in energy of a particle in an occupied state due to its interaction with the other particles of the system. The simplest of these diagrams appears in Fig. 8-4c; its contribution to the energy is

$$\langle kl|G|ab\rangle\langle ab|G|kl\rangle\langle km|G|km\rangle(e_a + e_b - e_{kl})^{-2}.$$

It will be recalled (Eq. 8-34) that the perturbation to H_0 in the exact theory is the nucleon-nucleon potential minus the assumed single-particle U , and hence that there are terms in the energy expansion which involve U . We saw in Eq. 8-37 how U contributes in the independent-pair approximation. The next terms to involve U are of the type illustrated by Fig. 8-5a. This diagram represents an energy

$$-\langle kl|G|ab\rangle\langle ab|G|kl\rangle\langle k|U|k\rangle(e_a + e_b - e_{kl})^{-2}.$$

We see that, if we choose U so that

$$\langle k|U|k\rangle = \sum_m \langle km|G|km\rangle,$$

all the terms represented by Fig. 8-4c would cancel those represented by Fig. 8-5a. But there are also exchange diagrams giving the same contributions as Fig. 8-4c except that $\langle km|G|km\rangle$ is replaced by $-\langle km|G|mk\rangle$. It is a

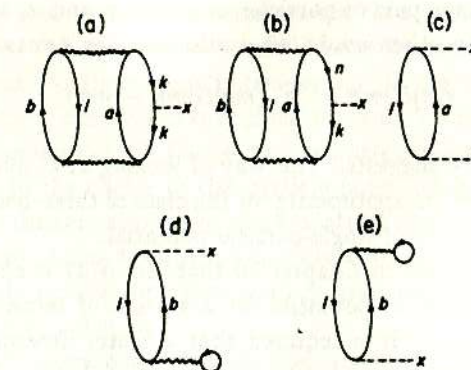


Fig. 8-5 Some diagrams involving U . The single-particle potential U is indicated by a dashed line with a cross at the end. Diagram (a) represents an energy contribution $\langle kl|G|ab\rangle\langle ab|G|kl\rangle\langle k|U|k\rangle(e_a + e_b - e_{kl})^{-2}$.

very important and nontrivial result of the general theory that all self-energy terms to all orders cancel against the terms involving U , provided U satisfies

$$\langle k|U|k\rangle = \sum_m \langle km|G|km\rangle(km - mk), \quad (8-47)$$

where $|km - mk\rangle = |k(1)m(2)\rangle - |m(1)k(2)\rangle$, and we have explicitly shown the starting energy $\omega = e_k + e_m$, for which G is to be evaluated (see Eq. 8-29b). This result is referred to as the BBP theorem after the initials of its authors: Bethe, Brandow, and Petschek [8].

It will be recalled that the selection of a single-particle Hamiltonian H_0 has until now been arbitrary. The choice of Eq. 8-47 for the potential energy of occupied states simplifies the calculation of three-particle clusters and gives more rapid convergence to the cluster expansion. Although this property is its rigorous justification, the choice is also suggested by intuitive reasoning. We have noted that, if the independent-pair approximation is to be valid (in the sense that we can ignore clusters of more than two particles), the eigenfunctions ϕ_k of H_0 must be good approximations to the actual wave functions outside the correlation region. In other words, U should reflect the "average" or "background" effect that a particle experiences from being embedded in the real medium. Since G is in a very real sense the effective interaction between particles in the medium, and since the potential energy of any particle is simply due to its interaction with the other particles, we would

reason that the potential energy for a particle in a state m would be the interaction energy of a pair of particles in states m and n , summed over all occupied states n . In other words, we would consider it reasonable to choose

$$\langle m|U|m\rangle = \sum_n \langle mn|G|mn - nm\rangle, \quad (8-47)$$

just as the full theory suggests. This way of looking at U makes it clear why the term "self-energy" is appropriate for the class of three-body contributions subsumed by this choice of single-particle potential.

We shall demonstrate in Chapter 10 that Eq. 8-47 is also the condition defining the single-particle potential for a system of fermions with a two-particle interaction G , if it is required that a Slater determinant of single-particle states $\phi_i(\mathbf{r}_i)$ give as accurate a value as possible for the total energy. This is the Hartree-Fock condition.

This condition does not completely define U , since it specifies only its diagonal matrix elements between hole states. Because of momentum conservation these are the only matrix elements that arise in the case of a uniform medium. In finite nuclei, however, if there is a hole k , a nucleon in another normally occupied state n may fill state k by interacting with a nucleon in state m ; this is portrayed in Fig. 8-4d. Also nucleons in states k and l may interact, leaving one nucleon in state k and the other in a particle state a ; a filling of state l may then occur by interaction with any occupied state (Fig. 8-4e). But analogous processes may also occur through the intermediary of the single-particle interaction, as indicated in Figs. 8-5b to 8-5e. The general theory also shows that all such terms cancel if

$$\langle k|U|l\rangle = \sum_m \langle km|\frac{1}{2}[G(e_k + e_m) + G(e_l + e_m)]|lm - ml\rangle, \quad (8-48a)$$

$$\langle k|U|a\rangle = \sum_m \langle km|G(e_k + e_m)|am - ma\rangle. \quad (8-48b)$$

Notice that the term 8-38 in the independent-pair energy corresponds to Fig. 8-5d, and is removed by this choice of U .

The convergence of the cluster expansion for the energy depends on the value of U . If the independent-pair approximation is to be valid, higher cluster contributions must be small. We see that many of them are canceled if U is chosen so that Eqs. 8-48 hold. This, then, we must do. The specification is not complete, since we have not listed a condition for the value of U in normally unoccupied states $\langle a|U|a\rangle$. It might be hoped that this could be chosen so that some other higher clusters were canceled, as well as the self-energy terms. To do this, however, proves much more difficult, and in

most calculations up to 1972 the particle energies e_α have been taken arbitrarily. If third- and fourth-order clusters are then small, we have made a reasonable choice. Alternatively, we could test the sensitivity of the independent-pair result to the values taken for e_α ; if the sensitivity is great, higher-order clusters are important, since the sum of the cluster series to all orders is independent of U . The results for nuclear matter have been found to be insensitive to the choice of the particle potential, provided it is small, and higher-order clusters also make small contributions in this case. Hence, for nuclear matter, it has been usual to take $\langle a|U|a\rangle = 0$. At the time of writing an equally satisfactory treatment of the particle spectrum has not been found for finite nuclei.

For the "real" three-body clusters (i.e., for terms that do not involve self-energies) and for realistic internucleon forces, the contribution to the binding energy per particle in nuclear matter is found to be about 2 MeV attraction [9]. This is less than the approximate value of 5 MeV obtained above for $\frac{1}{2}\kappa^2\bar{v}$, but the result is reasonable, because κ^2 is the estimated probability of all three-body clusters, including those producing self-energy contributions, whereas the latter have been included in the calculated two-body contribution by the correct choice of U .

The contribution of four-body correlations has been estimated by Day [10]. There are about 100 different terms, and the computation is rather uncertain; it seems reasonable to quote a potential energy of -1.1 ± 0.5 MeV. To this can be compared the order-of-magnitude estimate $\frac{1}{4}\kappa^3\bar{v}$, which is 0.4 MeV.

It seems completely reasonable to expect the energy due to five-body correlations to be quite small, of the order of $\frac{1}{8}\kappa^4\bar{v}$ or 0.02 MeV. It may be even less, because two particles have only a small probability of being as close together as the healing distance unless they are in a relative S -state, and it is impossible to put more than four nucleons simultaneously in relative S -states.

The following equations summarize the calculation of the binding energy of nuclear matter or of a finite nucleus in the independent-pair approximation:

$$H_0 = T + U, \quad (8-49a)$$

$$H_0\phi_\alpha = e_\alpha\phi_\alpha, \quad (8-49b)$$

$$G(\omega) = v + v \frac{Q}{\omega - H_0} G(\omega), \quad (8-49c)$$

$$Q = \sum_{ab} |ab\rangle\langle ab| + \sum_a |ka\rangle\langle ka| + \sum_b |bl\rangle\langle bl|, \quad (8-49d)$$

$$E = \sum_k \langle k|T|k\rangle + \frac{1}{2} \sum_{kl} \langle kl|G(e_k + e_l)|kl - lk\rangle, \quad (8-49e)$$

$$\langle k|U|k\rangle = \sum_l \langle kl|G(e_k + e_l)|kl - lk\rangle, \quad (8-49f)$$

$$E_k = \langle k|T|k\rangle + \langle k|U|k\rangle, \quad (8-49g)$$

$$e_a = ?, \quad (8-49h)$$

$$\langle k|U|a\rangle = \sum_m \langle km|G(e_k + e_m)|am - ma\rangle, \quad (8-49i)$$

$$\langle k|U|l\rangle = \sum_m \langle km|\frac{1}{2}[G(e_k + e_m) + G(e_l + e_m)]|lm - ml\rangle, \quad (8-49j)$$

$$\langle a|U|b\rangle = ? \quad (8-49k)$$

The choice of U is restricted by Eqs. 8-49i and 8-49j so as to ensure reasonable convergence of the cluster expansion. The spectrum of the unoccupied states and the matrix elements of U between these states are not similarly indicated by the considerations already mentioned, and this fact is indicated by the question marks in Eqs. 8-49h and 8-49k; these values remain arbitrary.

This set of equations can be dealt with only by an iterative approach. The process for nuclear matter is indicated in Fig. 8-6. Since the model wave functions are plane waves, a given value of density determines the Pauli operator Q from Eq. 8-49d, and one can also compute $\langle kl|v|\alpha\beta\rangle$. One assumes a spectrum, that is, the values $e_\alpha = e(k_\alpha)$. These three elements— Q , $\langle kl|v|\alpha\beta\rangle$, $\{e_\alpha\}$ —permit the calculation of G -matrix elements from Eq. 8-49c. Equations 8-49f and 8-49g are then used to find $\langle k|U|k\rangle$ and e_k for various

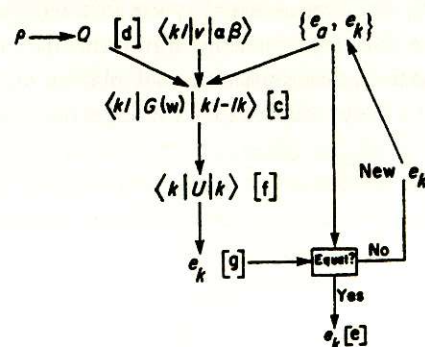


Fig. 8-6 Brueckner self-consistency for nuclear matter.

values of k . If the values found for the energies e_k of the occupied levels are not equal to the starting values, one replaces the old values with the new and repeats the cycle until convergence is obtained. When the input and output values of e_k do agree to within some prescribed limit, one then calculates E , the binding energy of the system, using Eq. 8-49e. By following this procedure, one is said to have established "Brueckner self-consistency," since this is the method of solution of the infinite-medium problem developed by Brueckner in his pioneering work on nuclear matter [11]. Note that the unoccupied-state spectrum, e_a , is not found self-consistently but is fixed arbitrarily.

In dealing with a finite nucleus, there is a second self-consistency problem, which arises because the single-particle wave functions ϕ_α are not known *a priori*. As Fig. 8-7 indicates, one starts with an assumed potential U which generates a set $\{\phi_\alpha\}$ and the corresponding energies e_α . Together with the mass and charge numbers A and Z of the nucleus being studied, the set $\{\phi_\alpha\}$ determines Q through Eq. 8-49d. If $N \neq Z$, there are two different Fermi levels, or, in other language, Q is a function of i -spin. Next, G is determined by Eq. 8-49c, and the Brueckner self-consistency cycle is followed, as shown by the double lines in Fig. 8-7. When self-consistency is reached on e_k , Eqs. 8-49i and 8-49j are used to compute $\langle k|U|\alpha\rangle$. One adds these quantities to the matrix elements of kinetic energy formed from the original wave functions $\{\phi_\alpha\}$ in order to obtain $\langle k|H_0|\alpha\rangle$. If the initial assumption for U were the self-consistent value, this last quantity would be diagonal; when it is not, one diagonalizes the matrix found and obtains new eigenfunctions

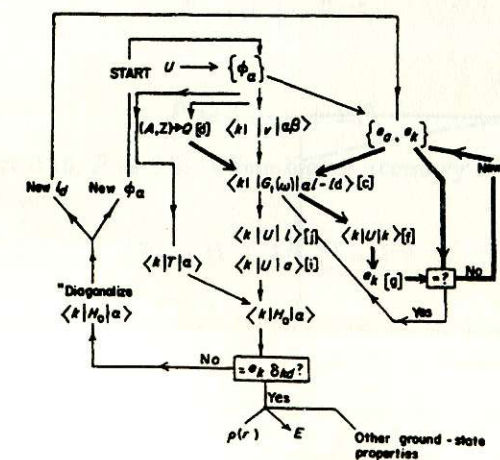


Fig. 8-7 Brueckner-Hartree-Fock self-consistency for a finite nucleus.

$\{\phi_\alpha\}$ and new energies e_α . In principle, this process is repeated until convergence is obtained. One then may calculate the energy of the nucleus and various other properties.

In practice, this is a very complicated procedure. The finding of a self-consistent single-particle U , even one permitted to be nonlocal, is at best an approximate process. Indeed, what we are doing is attempting to find the best single-particle description of the nucleus. This in itself is a matter to which we devote a later chapter. It is the Hartree-Fock problem, and the statement that "one diagonalizes" a trial $\langle k|H_0|\alpha\rangle$ must be regarded as a schematic description of one of a number of possible approximations to obtain good $\{\phi_\alpha\}$. Although it would be beyond the scope of this book to discuss the details of methods of solution, we shall quote below some results for finite nuclei.

There is another practical difficulty, connected with the Pauli operator. As Fig. 8-7 emphasizes, each successive set of functions $\{\phi_\alpha\}$ implies a different Q . Even worse, Q is defined in terms of single-particle wave functions. But so long as there exist correlations, this is only an approximation of the Pauli principle. We have remarked that the wound integral κ_{kl} is a measure of the depletion of the state $|kl\rangle$. The independent-pair model ignores this effect for all states but those of the two interacting particles. In fact, however, all the "occupied" states are somewhat depleted, and some of the "unoccupied" states are partially filled. We sometimes say that the Fermi level is not sharp,

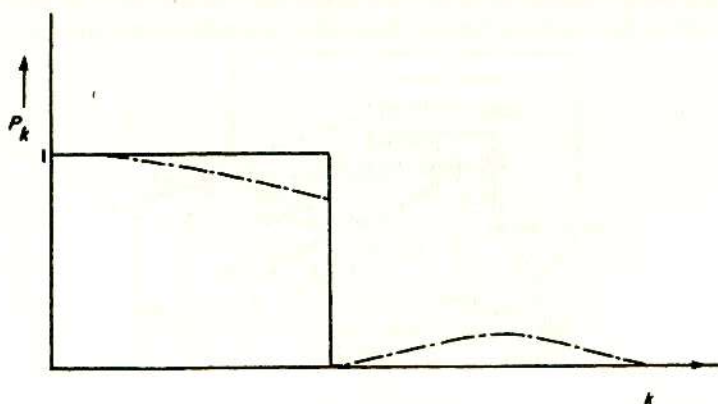


Fig. 8-8 A schematic representation of the state occupation number. The solid line is a sharp Fermi surface, $P_k = 1$, $k < k_F$, and zero otherwise. The dot-dash line shows the effect of correlations in particle occupancy. The shape of this curve depends on the nature of the two-body interaction. For $k > k_F$, P_k will be largest when k is near the maximum of the Fourier transform of $v(r)\zeta(r)$, as can be deduced from Eq. 8-41.

even though, as Fig. 8-8 suggests, the probability of occupation is discontinuous.

To be precise, Eq. 8-27 shows that κ_{kl} is the relative probability of the excitation out of the Fermi sea of the pair of particles that are asymptotically in states k and l , with the probability normalized so that there is one particle in each of these model states. Now let us write P_k for the actual occupation of each state k . Then, when the particle which asymptotically is in state ϕ_k is interacting with that in state ϕ_l , the normalization of the joint occupation is $P_k P_l$, and $\kappa_{kl} P_k P_l$ is the probability that the interaction of a particle in state k with one in state l will lift particles out of the Fermi sea. Hence $\frac{1}{2} \sum_l \kappa_{kl} P_k P_l$ is the probability that a particle asymptotically in state k will leave the Fermi sea due to all its interactions. The factor $\frac{1}{2}$ arises because half of the particles excited in the interaction of k with l can be considered to come from each of the states. But the particle in state k either leaves the sea or remains in state k , and therefore

$$P_k + \frac{1}{2} \sum_l \kappa_{kl} P_k P_l = 1, \quad (8-50)$$

that is,

$$P_k = (1 + \frac{1}{2} \sum_l \kappa_{kl} P_l)^{-1}.$$

To orient ourselves concerning the values of P_k , we might assume them all to be equal to an average value \bar{P} . Then, recalling Eq. 8-44, we see that, if we also take an average for κ_{kl} , we have

$$\bar{P} = (1 + \kappa \bar{P})^{-1},$$

which implies

$$\bar{P} \approx 1 - \kappa + 2\kappa^2. \quad (8-51)$$

Since κ is about 0.15, $\bar{P} \approx 0.9$. When higher accuracy is required, one finds individual P_k 's from

$$P_k = (1 + \frac{1}{2}\bar{P} \sum_l \kappa_{kl})^{-1} \quad (8-52)$$

and could then iterate again with these values of P_k .

The significant point is that the occupation probabilities are very near unity. Nevertheless, it is more accurate to "renormalize" the energy and the potential by taking

$$\langle k|U|k\rangle = \sum_l \langle kl|G(e_k + e_l)|kl - lk\rangle P_l, \quad (8-53a)$$

$$e_k = \langle k|T|k \rangle + \langle k|U|k \rangle, \quad (8-53b)$$

$$E = \sum_k \langle k|T|k \rangle + \frac{1}{2} \sum_{kl} \langle kl|G|kl - lk \rangle P_k P_l + \sum_k (1 - P_k) \langle k|U|k \rangle \quad (8-53c)$$

$$= \sum_k e_k - \frac{1}{2} \sum_k \langle k|U|k \rangle P_k. \quad (8-53d)$$

Of course, with $P_k = 1$ these equations reduce to our previous results.

The equations can be given some plausibility. If we think of $\langle k|U|k \rangle$ as the potential on a particle in state k due to its interaction with other occupied states, Eq. 8-53a can be seen as allowing for the fact that the other states are occupied only partially. Rigorous theory, in fact, shows that these expressions are the correct ones to allow for this effect [12, 13].

In terms of computation, it will be realized that in principle P_k can be evaluated once $G(\omega)$ is known (see Problem 8-5), and the Brueckner self-consistency cycle can then be suitably modified.

In practice, the introduction of occupation probabilities is important for the value of e_k , but not for the calculation of the total energy. If one puts $P_k = 1$, expression 8-53b for e_k will not be close to the actual removal energy of a particle from state k ; if one uses the renormalized expression, the result is near the observed separation energy. From Eq. 8-53a it is evident that the effect is to reduce the attractive potential in each state by about 10%; since the kinetic and potential energies in e_k are both large and of opposite sign, the change is appreciable.

But in the total energy E this loss of attraction is compensated for by the attraction from the correlated parts of the wave functions—in other words, by the interaction between particles excited out of the Fermi sea. It is the last term of Eq. 8-53c that represents this contribution.

We can see these facts explicitly as follows. In Eq. 8-53a, the renormalized value for $\langle k|U|k \rangle$ differs from its unrenormalized value because $P_l \neq 1$ and because the matrix element of G is evaluated at a different energy since $e_k + e_l$ has changed. But the derivative of G with respect to starting energy, $\partial G / \partial \omega$, is of the order of the wound κ_{kl} (see Problem 8-5), and since the change in e_k is also of this order, the change in $G = (\partial G / \partial \omega)(\delta e_k + \delta e_l)$ is of second order. Hence, if we write $P_k = 1 - d_k$, we have for the changes due to renormalization to second order (where A indicates “antisymmetrized”)

$$\begin{aligned} \delta e_k &= \delta \langle k|U|k \rangle \\ &= - \sum_l \langle kl|G|kl \rangle_A d_l - 2 \sum_{lm} \left(\frac{\partial G}{\partial \omega} \right)_{kl,A} \langle km|G|km \rangle_A d_m. \end{aligned}$$

$$\begin{aligned} \delta E &= \sum_k \delta e_k - \frac{1}{2} \sum_k [(\langle k|V|k \rangle + \delta e_k)(1 - d_k) - \langle k|V|k \rangle] \\ &= \frac{1}{2} \sum_k \delta e_k (1 + d_k) + \frac{1}{2} \sum_k d_k \langle k|U|k \rangle \\ &= \frac{1}{2} \sum_{kl} \langle kl|G|kl \rangle_A (d_k - d_l - d_l d_k) - \sum_{klm} \left(\frac{\partial G}{\partial \omega} \right)_{kl,A} \langle km|G|km \rangle_A d_m. \end{aligned}$$

Since all the d_k are roughly equal to κ , $\delta e_k \approx -\kappa \langle k|U|k \rangle$. On the other hand, each term of δE is of order $\kappa^2 G$; and, since the sum $\sum_{kl} G$ is the total potential energy of pairs (i.e., $\kappa \bar{v}$), $\delta E \approx \kappa^3 \bar{v}$, which is of the order of magnitude of the energy of four-body clusters: about 1 MeV per particle.

Indeed, it is not necessary to renormalize in a nuclear-matter calculation, since the effect will arise as a four-body contribution and the single-particle potential U is not compared directly with experiment. It is vital to do so, however, for a finite nucleus in order to have a realistic evaluation of the measurable energies of the discrete single-particle states.

8-4 RESULTS IN NUCLEAR MATTER AND FINITE NUCLEI

It will be apparent to the reader that the crucial step in finding G is the solution of the Bethe-Goldstone equation. There are basically two approaches to this: one is a matrix inversion, and the other involves the solution of an integrodifferential equation. In either case it is necessary to deal with the fact that our basic states are single-particle states best suited to expression in terms of the coordinates of the separate particles, whereas the interaction is a function of relative coordinates. Fortunately, this is not a particularly difficult problem for plane-wave states. Indeed, as is apparent from Eq. 8-43, the matrix elements of v are independent of the total momentum P and are

$$\begin{aligned} \langle \phi_\alpha \phi_\beta | v | \phi_\gamma \phi_\delta \rangle &= (2\pi)^3 \delta^{(3)}(\mathbf{P}_{\alpha\beta} - \mathbf{P}_{\gamma\delta}) Q^{-1} v(\mathbf{p}_{\alpha\beta} - \mathbf{p}_{\gamma\delta}), \\ v(\mathbf{k}) &= \int v(\mathbf{r}) \exp(-i\mathbf{k} \cdot \mathbf{r}) d^3 r. \end{aligned} \quad (8-54)$$

In the equation

$$G = v - v \frac{Q}{H_0 - e_{kl}} G$$

the energy denominator will, in general, depend on P . It is true, of course, that P cancels from the kinetic-energy parts of H_0 and of $e_k + e_l$, but the potential is a function of momentum. We have remarked that the unoccupied

states are usually taken to have zero potential energy, but even so the hole states have e_k as a function of \mathbf{p}_k . If e_k is a function of p_k^2 , then e_{kl} will be a function of $p_k^2 + p_l^2 = \frac{1}{2}P^2 + 2p_{kl}^2$, and the dependence of G on P may be quite simple in this respect.

However, the projection operator Q is a function of P , for it is easy to describe the exclusion of the Fermi sea in terms of \mathbf{p}_a and \mathbf{p}_b but not so simple in terms of \mathbf{P}_{ab} and \mathbf{p}_{ab} . The condition, of course, is that $|\frac{1}{2}\mathbf{P} \pm \mathbf{p}| \geq k_F$. Both inequalities are satisfied if $p \geq k_F + \frac{1}{2}P$, and both fail if $p^2 < k_F^2 - \frac{1}{4}P^2$. (Of course $\frac{1}{2}P \leq k_F$.) When p lies between these two limits, the two momenta \mathbf{p}_a and \mathbf{p}_b both are outside k_F , provided $\pm \mathbf{P} \cdot \mathbf{p} \geq k_F^2 - \frac{1}{4}P^2 - p^2$. In other words, in the expression $Q|\mathbf{P}, \mathbf{p}\rangle$,

$$\begin{aligned} Q &= 0 \quad \text{if } p^2 < k_F^2 - \frac{1}{4}P^2, \\ Q &= 1 \quad \text{if } p \geq k_F + \frac{1}{2}P, \\ Q &= 1 \quad \text{if } k_F^2 - \frac{1}{4}P^2 < p^2 \leq (k_F + \frac{1}{2}P)^2, \end{aligned} \quad (8-55)$$

and

$$|\cos \theta| \leq \frac{\frac{1}{4}P^2 + p^2 - k_F^2}{Pp},$$

where θ is the angle between \mathbf{p} and \mathbf{P} .

The states of fixed p are distributed in angle with a density proportional to solid angle $d\Omega$, that is, $d\phi|d \cos \theta|$. Consequently, the average value of Q for a given value of p in the third case is

$$Q_{av} = \frac{\frac{1}{4}P^2 + p^2 - k_F^2}{Pp} \quad (8-56)$$

in the sense that

$$\langle \mathbf{P}', \mathbf{p}' | \mathfrak{D}Q | \mathbf{P}, \mathbf{p} \rangle = Q_{av} \langle \mathbf{P}', \mathbf{p}' | \mathfrak{D} | \mathbf{P}, \mathbf{p} \rangle, \quad (8-57)$$

which is exact if the matrix element of the operator \mathfrak{D} does not depend on the angle between \mathbf{P} and \mathbf{p} , but otherwise is an approximation. Of the matrix elements entering the Bethe-Goldstone equation, those of v depend on the angle between \mathbf{p}' and \mathbf{p} (Eq. 8-54) and those of $H_0 - e_{kl}$ do not depend on $\mathbf{P} \cdot \mathbf{p}$ until we consider terms of the order p_k^4 . Consequently, the use of the angle-average Q in Eq. 8-56 is quite accurate in nuclear-matter calculations.

Therefore, although the nuclear-matter G -matrix is diagonal in \mathbf{P} , it does depend on it parametrically through Q and H_0 . We can replace $\langle \alpha\beta | G | kl \rangle$ with $\langle \mathbf{p}_{\alpha\beta} | G(\mathbf{P}) | \mathbf{p}_{kl} \rangle$, where only relative coordinates now occur in the wave

functions. A further step is usually taken before any computation is done. Since the nucleon-nucleon potential is different in different spin-isospin states, it is desirable to expand the plane waves in angular-momentum components. It is usual to write \mathbf{k} instead of $\mathbf{p}_{\alpha\beta}$. A complete set of quantum numbers specifying a two-nucleon collision consists of the momenta, spin components, and charges or, equivalently, \mathbf{P} , \mathbf{k} , M_S , and M_T . To expand such a state we write

$$|\mathbf{P}, \mathbf{k}, M_S, M_T \rangle = \sum_{JLMS} c_{JLMS} |\mathbf{P}, \mathbf{k}, J, L, M, S, M_S, (T), M_T \rangle. \quad (8-58)$$

The total i -spin T is shown in parentheses since its value is determined when L and S are fixed. Explicitly, the well-known expansion for a plane wave in spherical harmonics can be rewritten to yield

$$\begin{aligned} |\alpha\beta - \beta\alpha \rangle &= \phi_A(\mathbf{p}_\alpha, \mathbf{p}_\beta, M_S, M_T) \\ &= \Omega^{-1} \exp(i\mathbf{P} \cdot \mathbf{R}) \sum_{JLMS} 4\pi i^L (LSM_L M_S | JM) \\ &\quad \times Y_L^{M_L}(\hat{\mathbf{k}}) j_L(kr) |JLMS(T)M_T \rangle. \end{aligned} \quad (8-59a)$$

Similarly, we write

$$\begin{aligned} |\psi_{\alpha\beta} - \psi_{\beta\alpha} \rangle &= \psi_A(\mathbf{p}_\alpha, \mathbf{p}_\beta, M_S, M_T) \\ &= \Omega^{-1} \exp(i\mathbf{P} \cdot \mathbf{R}) \sum_{JLMS} 4\pi i^L (LSM_L M_S | JM) Y_L^{M_L}(\hat{\mathbf{k}})(kr)^{-1} \\ &\quad \times u_{JLS}^M(r) |JLMS(T)M_T \rangle, \end{aligned} \quad (8-59b)$$

$$\begin{aligned} &= \Omega^{-1} \exp(i\mathbf{P} \cdot \mathbf{R}) \sum_{JLMS} 4\pi i^L (LSM_L M_S | JM) \sum_{L'} Y_L^{M_L}(\hat{\mathbf{k}})(kr)^{-1} \\ &\quad \times u_{L'L}^{IS}(r) |JL'MS(T)M_T \rangle, \end{aligned} \quad (8-59c)$$

where

$$|JLMS(T)M_T \rangle = \sum_m (LSm M_S | JM) Y_L^m(\hat{\mathbf{r}}) |SM - m\rangle |TM_T \rangle$$

and $M_L = M - M_S$. The equations are somewhat simplified when one can choose the z -axis in the direction of the relative momentum, for then $M_L = 0$, the spherical harmonic becomes $\sqrt{(2L+1)/4\pi}$, and the sum over M reduces to one term, $M = M_S$. Since each term of these sums is a state of specified parity, spin, and i -spin, one can readily form matrix elements of v between states expanded in this way.

Equation 8-59b for ψ is a general expression for the wave function of two nucleons and is written in this way since it goes asymptotically to the free

motion ϕ if the radial function u_{JLS}^M approaches $krj_L(kr)$. It is helpful also to write the defect function $\zeta = \phi - \psi$ in a similar expansion, replacing u by a radial defect function $\chi(r)$, so that

$$\chi_{JLS}^M = krj_L(kr) - u_{JLS}^M, \quad (8-60a)$$

$$\chi_{L'L}^{JS} = \delta_{LL'}krj_L(kr) - u_{L'L}^{JS}. \quad (8-60b)$$

The two forms of ψ need some explanation. They differ in the radial functions u , a difference which arises only in the presence of tensor forces. Let us first explain why the radial function in Eq. 8-59b depends on M . If the axis is taken as the direction of \mathbf{k} , M is simply the spin component along \mathbf{k} . But the tensor force contains the term proportional to $\sigma_1 \cdot \hat{\mathbf{r}} \sigma_2 \cdot \hat{\mathbf{r}}$, which depends on the spin orientations. If $M = 1$, both spins are along \mathbf{k} ; if $M = 0$, the resultant is perpendicular. Hence the effective force is different in states of different M when L is fixed. [For example, $\langle JLM|v(r)\sigma_1 \cdot \hat{\mathbf{r}} \sigma_2 \cdot \hat{\mathbf{r}}|JLM\rangle$ is $(11/210)v(r)$ for $J = 1, L = 2, M = 1$ and is $(4/21)v(r)$ for $J = 1, L = 2, M = 0$.] This dependence of the radial function on M is inconvenient; and, as we already know from the chapters on the deuteron and nucleon scattering, it is desirable to adopt a different description, using states in which L is not a constant of motion, but in which both values, $L = J \pm 1$, are present. There are two orthogonal states, in each of which one of these L values is dominant (i.e., is the incoming wave in a scattering experiment). In our notation $u_{L'L}^J$, L is the dominant value specifying which solution is being used and L' is the angular momentum actually present with amplitude u . It is only in coupled triplet states that we shall employ two suffixes on the radial functions; otherwise one will do, and L' is put equal to L in Eq. 8-59c.

At this point we wish to define a G -matrix for each angular-momentum state. The basic idea of the G -matrix is that when the G -operator acts on the unperturbed state it reproduces the effect of the actual potential applied to the actual state. Now, for each uncoupled angular-momentum state defined by JLS , there is a potential function $v_L^{JS}(r) = \langle JLS|v|JLS\rangle$, and we define

$$G_L^{JS}krj_L(kr) = v_L^{JS}u_L^{JS}(r; k). \quad (8-61a)$$

When there are coupled states, we have to recall that we are dealing with a true wave function of the form

$$\psi = \sum_{L''} u_{L''L}^{JS}(r)\Phi(JL''S),$$

where Φ stands for the angular-momentum part of ψ , and that v couples two states so that

$$v\Phi(JLS) = \sum_{L'} v_{L'L}^{JS}(r)\Phi(JL'S).$$

Hence

$$v\psi = \sum_{L'L''} v_{L'L}^{JS}u_{L''L}^{JS}\Phi(JL'S),$$

and we require that G applied to the free wave give this result. Therefore, we define angular-momentum components of G by

$$G|k, JLS\rangle = \sum_{L'} G_{L'L}^{JS}|k, JL'S\rangle = v\psi.$$

It follows that

$$G_{L'L}^{JS}krj_L(kr) = \sum_{L''} v_{L'L''}^{JS}u_{L''L}^{JS}. \quad (8-61b)$$

The G -matrix also depends on P and ω , and for uncoupled states it satisfies the equation

$$(k|G_L^{JS}|k_0) = (k|v_L^{JS}|k_0) - \sum_{k'} \frac{(k|v_L^{JS}|k') (k'|G_L^{JS}|k_0)}{e(\frac{1}{2}\mathbf{P} + \mathbf{k}') + e(\frac{1}{2}\mathbf{P} - \mathbf{k}') - \omega} Q(k', P), \quad (8-62)$$

where $(k|v_L^{JS}|k_0)$ and $(k|G_L^{JS}|k_0)$ are Bessel transforms, namely,

$$(k|v_L^{JS}|k_0) = \int j_L(kr)v_L^{JS}(r)j_L(k_0 r)r^2 dr,$$

and where $Q(k', P)$ is given by Eqs. 8-55 and 8-56. Equation 8-62 may be solved by matrix inversion, for if we suppress the various suffixes and write

$$(k|A|k') = \frac{(k|v|k')Q(k', P)}{e(\frac{1}{2}\mathbf{P} + \mathbf{k}') + e(\frac{1}{2}\mathbf{P} - \mathbf{k}') - \omega},$$

we have

$$(k|G|k_0) = (k|v|k_0) - \sum_{k'} (k|A|k')(k'|G|k_0). \quad (8-63)$$

For a numerical computation, we replace the continuous variable k by a set of selected values k_s . These need not be distributed uniformly, but should be chosen so that they are more closely packed in regions where the matrix elements are large. Then Eq. 8-63 is simply

$$\sum_i (\delta_{rs} + A_{rs})G_{is} = v_{rs}, \quad (8-64)$$

which is solved by inverting the matrix $I + A$. In practice, this operation

is readily handled by modern computers and the number of k -values needed is not excessive [14].

In dealing with coupled states, the principle is the same but the two matrices G_{LL}^{IS} and $G_{L'L'}^{IS}$ satisfy coupled equations, namely,

$$(k|G_{LL}|k_0) = (k|v_{LL}|k_0) - \sum_{k'} [(k|A_{LL}|k')(k'|G_{LL}|k_0) + (k|A_{LL'}|k')(k'|G_{L'L}|k_0)],$$

$$(k|G_{L'L}|k_0) = (k|v_{L'L}|k_0) - \sum_{k'} [(k|A_{L'L}|k')(k'|G_{LL}|k_0) + (k|A_{L'L'}|k')(k'|G_{L'L}|k_0)],$$

where

$$(k_1|v_{L_1 L_2}|k_2) = (k_1 L_1 JS|v|h_2 L_2 JS),$$

with a similar definition for A . In matrix notation analogous to Eq. 8-64, these two equations are

$$\begin{aligned} (1 + A_{LL})G_{LL} + A_{LL'}G_{L'L} &= v_{LL}, \\ A_{L'L}G_{LL} + (1 + A_{L'L'})G_{L'L} &= v_{L'L}, \end{aligned} \quad (8-65)$$

which give

$$\begin{aligned} [1 + A_{LL} - A_{LL'}(1 + A_{L'L'})^{-1}A_{L'L}]G_{LL} &= v_{LL} - A_{LL'}(1 + A_{L'L'})^{-1}v_{L'L}, \\ [1 + A_{L'L'} - A_{L'L}(1 + A_{LL})^{-1}A_{LL'}]G_{L'L} &= v_{L'L} - A_{L'L}(1 + A_{LL})^{-1}v_{LL}. \end{aligned} \quad (8-66)$$

This technique is in many ways the most straightforward and useful procedure for finding G and hence the energy of the system and the wave functions ψ . It will not work if v has an infinite hard core, for then the matrix elements of v are infinite. However, it works with the realistic potentials with finite repulsion, even though v reaches quite high values in some cases.

The differential-equation technique arises from writing Eq. 8-22 in terms of the wave-function defect as

$$|\zeta_{kl}\rangle = \frac{Q_{kl}}{H_0 - e_{kl}} v |\psi_{kl}\rangle$$

or

$$(H_0 - e_{kl})\zeta_{kl} = Q_{kl}v(\phi_k\phi_l - \zeta_{kl}). \quad (8-67)$$

By writing Q_{kl} in the angle-average approximation (Eq. 8-56), it becomes a straightforward but tedious matter to rewrite this equation in terms of the relative coordinate r for each state of the angular-momentum decomposition. The Hamiltonian H_0 acts on ζ_{kl} , which contains only momenta above the Fermi sea. Hence, in order to reduce the equation to one in the radial coordinate, some assumption is needed about the effect of the operator H_0 on states above the Fermi level. Of course, this is also true in the matrix-inversion method, since the two methods are identical in physical assumptions. Equation 8-62 contains these energies, $e(\frac{1}{2}\mathbf{P} \pm k')$; the advantage of the matrix-inversion method is that the form of e can be taken arbitrarily. In differential equations, on the other hand, the potential-energy function $U(\mathbf{p})$ in H_0 would introduce several difficulties if it were more complicated than a quadratic. When it is quadratic, H_0 (acting on states with $p > p_F$) can be written as

$$H_0(i) = A + \frac{p_i^2}{2Mm^*},$$

where A is a constant and m^* is an "effective mass." If $m^* = 1$, the potential energy of particle states is constant and the last term of H_0 is just the kinetic energy. With this assumption,

$$\begin{aligned} H_0 - e_{kl} &= -\left(\frac{\hbar^2}{Mm^*}\right)\nabla^2 + \frac{P^2}{4Mm^*} + 2A - e_{kl} \\ &= \frac{\hbar^2}{Mm^*}(-\nabla^2 + \gamma^2), \end{aligned} \quad (8-68)$$

where the quantity γ^2 is positive, since, if the system is bound, $e_{kl} < 0$.

For numerical work, it is more convenient to use a projection operator $R = 1 - Q$, since it spans a finite region of momentum space, namely, the Fermi sphere. We may write Eq. 8-67 as

$$\frac{\hbar^2}{Mm^*}(-\nabla^2 + \gamma^2)\zeta = v\psi - Rv\psi. \quad (8-69)$$

The projection operator is

$$R = \int d^3k' d^3P' |\mathbf{k}', \mathbf{P}'\rangle \langle \mathbf{k}', \mathbf{P}'|,$$

where \mathbf{k}' and \mathbf{P}' define vectors \mathbf{p}_1 and \mathbf{p}_2 inside the Fermi sea. Using the angle-average approximation, we can make the angular-momentum reduction and find

$$\begin{aligned} & \left[-\frac{d^2}{dr^2} + \frac{L'(L'+1)}{r^2} + \gamma^2 \right] \chi_{L'L}^{JS}(r) \\ &= \frac{Mm^*}{\hbar^2} \sum_{L''} \left[v_{L'L''}^{JS}(r) u_{L''L}^{JS}(r) - r j_{L'}(kr) \frac{2}{\pi} \int_0^\infty k'^2 dk' \int_0^\infty r' dr' R_0(k', P) \right. \\ &\quad \left. \times r' j_{L'}(k'r') v_{L'L''}^{JS}(r') u_{L''L}^{JS}(r') \right] \end{aligned} \quad (8-70)$$

where

$$R_0(k', P) = \begin{cases} 1 & \text{if } k'^2 < k_F^2 - \frac{1}{2}P^2, \\ 0 & \text{if } k' \geq k_F + \frac{1}{2}P, \\ \frac{k_F^2 - (\frac{1}{2}P - k')^2}{Pk'} & \text{otherwise.} \end{cases}$$

This set of integrodifferential equations has been solved by a number of techniques of approximation. One of particular interest is to ignore the Pauli principle in the first approximation, that is, to put $R_0 = 0$. Then the equation is simply a differential equation. The G -matrix so obtained is corrected for the Pauli principle by a perturbation procedure. This is an essential step in the "reference spectrum method" [8].

The reader may also notice that Eq. 8-70 makes explicit the healing of the wound in the wave function. At distances of separation where the potential has vanished, the equation is just

$$\left[-\frac{d^2}{dr^2} + \frac{L'(L'+1)}{r^2} + \gamma^2 \right] \chi = 0,$$

the solution to which is a Hankel function with the exponential decay factor $\exp(-\gamma r)$. The expression given for γ^2 in Eq. 8-68 directly connects the size of the wound with the energies involved—those of the interacting particles, e_{kl} , and those of two particles of the same total momentum but above the Fermi sea.

We have given this detail of the methods of solution because a discussion of the physics of the results of calculations relies heavily on the different behaviors of the several angular-momentum states. Many calculations of the properties of nuclear matter have been made since the pioneering work of Brueckner and his collaborators [11] in 1955. During the same years knowledge of the free two-nucleon force also improved steadily, and, naturally, successive nuclear-matter calculations were carried out with the contemporary forces. It was never entirely clear, however, which features of the results

were attributable to the force used and which to improvements in calculating techniques. We shall discuss a variety of illustrative results in the literature, with a variety of forces.

In principle, if one has good control of the accuracy of the calculation, the resulting binding energy and density can be used as criteria for choice among different postulated nucleon-nucleon forces, all of which fit the two-nucleon data. The free nucleon-nucleon scattering involves matrix elements of the potential only between states of the same energy; but, as a glance at almost any of the equations of Section 8-3 (e.g., Eq. 8-20) makes clear, a calculation in a many body system involves matrix elements between two-nucleon states of different energy. Hence it is the "off-energy-shell" behavior that distinguishes which of a class of otherwise identical potentials are physically acceptable (see Section 5-9).

As long as at least one other entity is involved and can absorb some energy, a process will involve off-shell matrix elements. For example, the properties of the triton and of nucleon-deuteron reactions depend on off-shell behavior, and so do proton-proton bremsstrahlung ($p + p \rightarrow p + p + \gamma$) and inelastic electron scattering from the deuteron. However, at reasonable energies these processes are not sensitive tests, since most potentials that have the same two-body phase shifts do not differ much for relatively small departures from the energy shell.

The matrix elements of G —and hence the properties of nuclear matter—can in a good approximation be related directly to the wave-function defect. The approximation is to ignore the Pauli operator ($R_0 = 0$) in Eq. 8-70 for $\chi(r)$. We then can start with the definition of $G_{L'L}^{JS}$ in Eq. 8-61b and write

$$\begin{aligned} \langle k' | G_{L'L}^{JS} | k \rangle &= \int r^2 dr j_{L'}(k'r) G_{L'L}^{JS} j_L(kr) \\ &= \int r dr j_{L'}(k'r) k^{-1} \sum_{L''} v_{L'L''}^{JS} u_{L''L}^{JS} \\ &= \int r dr j_{L'}(k'r) \frac{\hbar^2}{Mm^*k} \left[-\frac{d^2}{dr^2} + \frac{L'(L'+1)}{r^2} + \gamma^2 \right] \chi_{L'L}^{JS} \end{aligned}$$

using Eq. 8-70. We then apply the differential operator to the Bessel function to get

$$\langle k' | G_{L'L}^{JS} | k \rangle = \frac{\hbar^2}{Mm^*kk'} (k'^2 + \gamma^2) \int k' r j_{L'}(k'r) \chi_{L'L}^{JS}(r) dr. \quad (8-71)$$

The important result is that, except for Pauli corrections, the off-shell G -

matrix elements are essentially Bessel transforms of the wave defect. This implies that two potentials will have similar nuclear-matter properties only if they have similar defects (i.e., similar short-range correlations) [15].

We may also note that, although G and χ are functions of P , the total momentum of the colliding pair, their dependence on P is quite weak. Whereas the effective interaction of two particles is a sensitive function of their relative momentum, just as their free interaction is, the dependence on P arises only through the energy denominator and the Pauli operator Q . In both these factors, the process of averaging over the angle between k and P reduces markedly the extent of the dependence on the total momentum. Table 8-1 shows the 1S_0 G-matrix for various values of P and k and makes clear that for many purposes it is possible to ignore the dependence on P and merely evaluate G for an average P . This is done in most calculations, and we shall not refer to P in most of the remaining discussion.

TABLE 8-1 1S_0 G-Matrix Elements (MeV fm³) for Reid Soft-Core Potential for $k_F = 1.4$ fm⁻¹. From Siemens [16].

k/k_F	P/k_F			
	0.1	0.35	0.65	0.9
0.1	- 884	- 885	- 891	- 903
0.35	- 634	- 636	- 642	
0.65	- 322	- 324	- 329	
0.9	- 121	- 123		

The matrix elements important for the properties of nuclear matter and of reasonably heavy finite nuclei involve the scattering of two particles within the Fermi sea to states with relative momenta two or three times k_F ; this corresponds to moving about 200 MeV off shell. Unfortunately, there are only a limited number of experimentally determined numbers for nuclear matter, and in finite nuclei, where more parameters may be compared, the calculations are not yet quite so well under control. There is another regime in which some checks are now available, namely, neutron stars. The best approach for improving understanding seems to be the development of greater accuracy in calculations of medium-mass nuclei.

Turning to the results for nuclear matter, let us first consider some typical wave functions. Figure 8-9 shows the defect function $\chi_{L'L}^{JS}(r)$ for several partial waves and for a typical value of the relative momentum k of the colliding

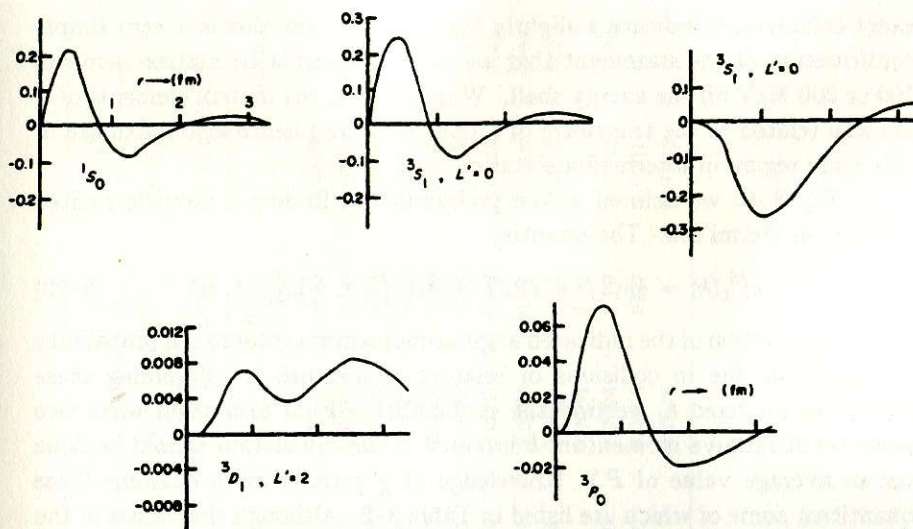


Fig. 8-9 The defect function χ for some typical partial waves. The potential is the Reid soft core, $k_F = 1.36$ fm⁻¹, $k = 0.91$ fm⁻¹, and an appropriate average value of P is used.

nucleons: $0.65k_F$. These calculations of Siemens [16] are for normal nuclear density $k_F = 1.36$ fm⁻¹ and for the Reid soft-core potential, described in Chapter 5 (Fig. 5-14). Since this is a “realistic” potential, the results are physically instructive. It is seen at once that the wave function heals rapidly, and that the wound is most pronounced in the S -states. The defect χ is a measure of how the true wave function u differs from the free wave function, which is $krj_L(kr)$. Asymptotically, the free wave function is a sine wave of amplitude unity. Of course, the free wave function for $L' = 2$ is zero for a collision asymptotically in the triplet S -channel, as is also the $L' = 0$ function for a collision asymptotically in the triplet D -state. We see that the tensor force introduces quite an appreciable component of $L = 2$ into the short-range correlation of a pair of nucleons otherwise interacting in the triplet S -state.

We noted in Section 8-3 (Fig. 8-8) that the most highly populated states above the Fermi sea are those for which the Fourier transform of $v\zeta$ is a maximum. It can be seen that for the $L' = 0$ states ζ is mostly inside about 0.8 fm; and if one multiplies in the Reid soft-core potential of Fig. 5-14, one sees that $v\zeta$ also lies mostly inside this distance. Consequently, the Fourier transform will maximize for relative momenta about $\pi/(0.8 \text{ fm}) \approx 4 \text{ fm}^{-1} \approx 3k_F$. This corresponds to kinetic energy of relative motion of about 300 MeV. More

exact calculations indicate a slightly lower energy, but this is a very simple confirmation of the statement that we are concerned with matrix elements 100 or 200 MeV off the energy shell. What is more, the matrix elements of G are also related to the transform of ζ (Eq. 8-71) and hence also maximize in this same region of intermediate states.

In Eq. 8-46 we defined κ , the probability of finding a particle excited outside the Fermi sea. The quantity

$$\kappa_{L'L}^{JS}(k) = \frac{1}{8}\rho(2J+1)(2T+1)\langle\zeta_{L'L}^{JS}(\mathbf{r}, k)|\zeta_{L'L}^{JS}(\mathbf{r}, k)\rangle \quad (8-72)$$

is the contribution of the indicated angular-momentum state to the probability of excitation due to collisions of relative momentum k . Summing these quantities for fixed k , we find the probability $\kappa(k)$ of excitation when two particles of relative momentum k interact. (The calculation should be done for an average value of P .) Knowledge of χ permits us to examine these quantities, some of which are listed in Table 8-2. Although the values in the table do not make possible a precise comparison of the values for different k , the values for the S -states are not, in fact, very sensitive to the relative momentum [16]. The table shows the dependence on density for a given force, the Reid soft-core potential. It will be seen that, as the density increases, the effective interaction in states of higher angular momentum also increases, although even for twice normal nuclear density ($k_F = 1.7 \text{ fm}^{-1}$) the incident S -states still account for 83% of the excitation. For the two $L' = 0$ states the defect lies mostly in the region of the repulsive core (Fig. 8-9), and it is therefore not surprising that, while the amount of the wounds in these states increases with density, the relative contribution to the total wound changes only slowly. On the other hand, the "defect" in the $L' = 2$ component of the incident 3S_1 -state is the whole wave function generated in this substate by the tensor force and therefore is of much longer range. Notice that the fractional contribution of this state to the total wound decreases rapidly with increasing density.

This difference can be understood when it is realized that the shorter-range χ 's contain mainly states of relatively large k , that is, the correlations are admixtures into the unperturbed ϕ of intermediate states substantially above the Fermi sea. On the other hand, a defect of longer range, about 3 or 4 fm, contains a significant amount of excitation of small k , and hence of states not far from the Fermi sea.

In Fig. 8-10, particles with momenta m, n inside the Fermi sphere interact. If their virtual excitation involves fairly large relative momenta such as k' , the intermediate-state points are a and b . As the sphere grows, there is no

TABLE 8-2 Excitation Probabilities from Wound Integrals

	OBEP					
	Reid Potential			OBEP		
	$k_F = 1.0 \text{ fm}^{-1} \text{ a}$	$k_F = 1.4 \text{ fm}^{-1} \text{ a}$	$k_F = 1.5 \text{ fm}^{-1} \text{ b}$	$k_F = 1.7 \text{ fm}^{-1} \text{ a}$	$k_F = 0.65k_F$	$k_F = 1.5 \text{ fm}^{-1} \text{ b}$
$k = 0.65k_F$	0.0573	0.0644	0.0699	0.0735	0.36	0.0370
$= 0.65 \text{ fm}^{-1}$	0.0188	0.0321	0.0388	0.0542	0.27	0.0282
	0.0126	0.013	0.0237	0.0285	0.18	0.0265
3S_1	κ_{20}^{11}	0.58	0.45	0.46	0.0396	0.20
3S_1	κ_{80}^{11}	0.19	0.23	0.25	0.1673	0.83
1S_0	κ_{10}^{11}	0.0126	0.13	0.17	0.0038	0.04
All S states	κ_{887}^{11}	0.90	0.1202	0.85	0.0051	0.037
3P_0	κ_{10}^{21}	0.0009	0.01	0.0036	0.0086	0.04
3P_1	κ_{10}^{21}	0.0028	0.03	0.0056	0.03	0.048
3P_2	κ_{10}^{21}	0.0017	0.02	0.0028	0.02	0.0025
3D_1	κ_{10}^{21}	0.0020	0.02	0.0024	0.01	0.0018
3D_2	κ_{10}^{21}	0.0001	0.00	0.0002	0.04	0.0013
Total $\kappa(k)$	0.0983	0.1413	0.1569	0.2019	0.1062	0.0001

^a Ref. 16.^b Ref. 17.

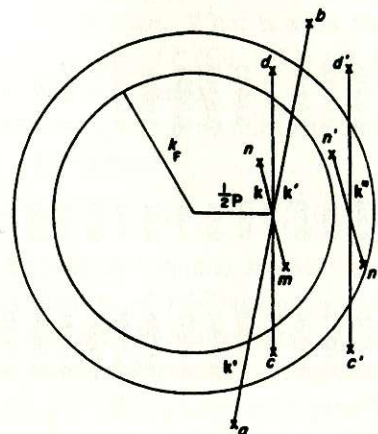


Fig. 8-10 Momentum-space diagram showing some intermediate-state vectors and Fermi spheres for two densities.

change in the number of such states a and b , but the amount of excitation of this kind will increase because there are more states (e.g., m' and n') that can have the same relative momentum k and the same excitation k' . In contrast, if there is a relatively small relative momentum (k'') in the intermediate state, the nucleons in that state have momenta such as c and d . When the density is increased, contributions to the correlation from states c and d are removed, since they are now within the Fermi sea. It is true that the relative momentum k' is still available from scattering to c' and d' from states m' and n' , but as the size of the sphere increases the relative importance of the smaller components decreases. Thus, although all the wounds increase with density, the relative importance of a wound due to a long-range force decreases.

This behavior of the wound due to the tensor force is one of the two main reasons for the so-called saturation of nuclear binding energy, the fact that, as more nucleons are added to a nucleus, the binding energy per particle remains roughly constant. With ordinary attractive forces the potential energy per particle would increase steadily with the density, and since the system would seek the state of lowest energy, stable nuclei would be indefinitely dense and tightly bound. Real nuclear matter saturates, implying minimum energy per particle for the actual density ρ_0 and increasing energy if the

density varies from ρ_0 . Consequently, there must be some parts of the effective internucleon force which become less attractive as the density increases. The long-range and strong tensor force plays this role for densities near values appropriate to nuclei.

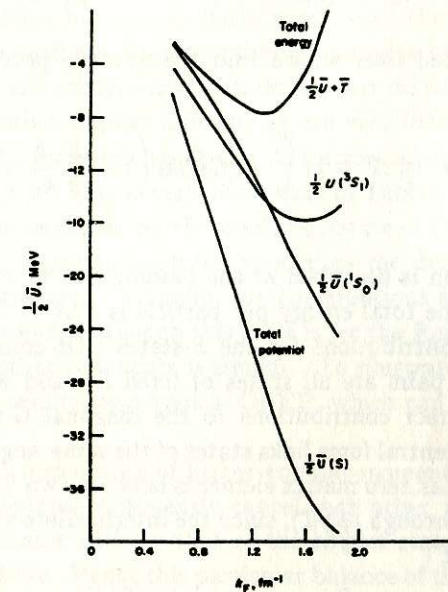


Fig. 8-11 Certain contributions to binding at various densities; \bar{U} is the average potential energy per particle due to pair interactions in the indicated states. Also shown on the same scale is the sum of the potential total and the kinetic energy per particle. (Data from [18] and D. W. L. Sprung as quoted in [1].) The potential is Reid soft core.

This is illustrated in Fig. 8-11, which shows the binding due to the 1S -, 3S -, and 3D_1 -states. The potential in a state m is given by

$$\begin{aligned} U(m) &= \sum_n \langle mn|G|mn - nm \rangle \\ &= \frac{8\pi\hbar^2}{M} \sum_{JSL} (2J+1)(2T+1) \int_0^{k_{\max}} (k|G_{LL}^{JS}|k) F(k) k^2 dk, \quad (8-73) \end{aligned}$$

where $k_{\max} = \frac{1}{2}(k_F + k_m)$ and is the largest value of relative momentum k possible for m fixed and n extending over all occupied states. Strictly speaking, G should be evaluated at each P and the permitted range of P should be summed over, but it is adequate to evaluate G at an average value of P , as

this formula suggests. The quantity $F(k)$ takes account of the effect of the exclusion principle on the angular integration and is

$$F(k) = 1, \quad 0 < k < \frac{1}{2}(k_F - k_m)$$

$$= \frac{1}{2k_m k} (\frac{1}{4}k_F^2 + k_m k - \frac{1}{4}k_m^2 - k^2), \quad \frac{1}{2}(k_F - k_m) < k < \frac{1}{2}(k_F + k_m).$$

If this is now summed over m , we find the average potential energy per particle as

$$U = \frac{8\pi^2}{M} \sum_{JSL} (2J+1)(2T+1) \int_0^{k_F} (k|G_{LL}^{JS}|k) \left(1 - \frac{3}{2} \frac{k}{k_F} + \frac{1}{2} \frac{k^3}{k_F^3}\right) k^2 dk. \quad (8-74)$$

Each term in this sum is described as the binding due to a specific angular-momentum state. The total energy per particle is $E/A = T + \frac{1}{2}U$. In Fig. 8-11 we show the contributions for the S -states. Of course, the "initial" states ϕ of colliding pairs are all states of fixed L ; and when the force is central, there are direct contributions to the diagonal G -matrix from the term $(\phi|v|\phi)$, since a central force links states of the same angular momentum. But the tensor force has zero matrix elements between two S -states and hence can contribute only through $(\phi|v|\zeta)$, since the intermediate states in ζ contain D -states. Recall that

$$|\zeta\rangle = \frac{Q}{e} G|\phi\rangle = \sum_a \frac{|a\rangle\langle a|G|\phi\rangle}{e}.$$

When G contains a tensor operator, and $|\phi\rangle$ is a 3S -state, some of the states $|a\rangle$ will be 3D_1 . This means that the tensor force can contribute only through excitations outside the Fermi sphere and that the considerations associated with Fig. 8-10 are important. Of course, the central force contributes also in this way, but since there is a direct contribution as well, the central-force contribution to the G -matrix does not fall off with increasing density. Thus G_0^{00} is monotonic, but G_0^{11} results from an interplay of central and tensor contributions and behaves as shown by the curve labeled 3S_1 in Fig. 8-11. For low density, where the exclusion principle is not as important, the triplet state has greater binding than the singlet, as we know from the free two-body scattering at low energies. But as the tensor force is progressively more inhibited, the effective singlet strength becomes greater. In the figure the sum of the two potential-energy contributions is shown, and so is the result of adding the average kinetic energy. It is seen that this total energy has a minimum at k_F of about 1.3 fm^{-1} and an energy per particle of -7.8 MeV .

These numbers are surprisingly close to the experimental results (1.36 fm^{-1} , -15.7 MeV), considering that we have ignored interactions in all states with $L > 0$.

This brings us to the second main cause of saturation: the exchange character of the nuclear force, which, as we saw in Sections 5-6 and 5-7, keeps the interaction in P -states fairly weak, with the 3P_2 -force attractive, the 3P_1 repulsive, and the 3P_0 attractive for energies below about 200 MeV. At low densities, the relative momenta in nuclear matter are of course small and states of positive angular momentum are very little affected; however, as the value of k_F increases, so do the distortions in the wave functions of states having $L \geq 1$. This is very noticeable in Table 8-2. Consequently, if it were not for the weak and partly repulsive nature of the P -states, we would expect increasing negative potential energy as the density rose, and there would be no saturation.[†] Actually, the contributions for various states are as shown in Table 8-3. Although this table is for the Reid soft-core potential, the behavior of other potentials is similar. To illustrate this fact, the table also shows some results for a typical OBEP, which can be compared at two densities.

The increasing importance of higher-angular-momentum states is evident, but the triplet P -states consistently cancel each other, so that the whole P -contribution is almost entirely that of the singlet state, which is relatively weak and is repulsive. Hence this particular balance of the $\sigma_1 \cdot \sigma_2$, $\tau_1 \cdot \tau_2$, and $L \cdot S$ forces is very important for saturation. The D -states do not exhibit such cancellation and their contribution has reached 6 MeV in the region of nuclear density; if there were no cancellations in the P -states, the latter would contribute an attraction somewhere between that of the S - and that of the D -states, perhaps 15 MeV, and saturation would not be in sight.

Of course, at still higher densities the states with $L \geq 2$ will be increasingly important and might well override the effects in the S - and P -states which have produced the minimum in the energy curve. This might then be a local minimum, and there might be states of much lower energy at much higher density. This is prevented by a third fact: the repulsive core plays an important role when the average separation of nucleons is of the order of twice the core radius, or about eight times the normal nuclear density. Calculations are not reliable for densities higher than about $3\rho_0$, or k_F much greater than 2 fm^{-1} , because we do not know the details of the force at short distances. It is possible to prescribe necessary conditions on analytic expres-

[†] Recall that, although the tensor force would be somewhat inhibited, it has nonzero direct matrix elements in all triplet states except the S -state.

TABLE 8-3 Contributions to the Energy of Nuclear Matter of Various States Taking Two-Body Clusters Only. The calculations are by D. W. L. Sprung as quoted in ref. 1 except for those labeled with superscript *a*, which are by P. Grangé. The OBEP force is that described in ref. 17. The contributions of higher states are estimated in different ways: those labeled *b* are estimated by Sprung using the phase-shift approximation, and those labeled *c* are based on the "OBEPEP + σ " model and include only $J = 3, 4, 5$ (see ref. 19).

k_F , fm $^{-1}$	1.0	1.0 (OBEP) ^a	1.2	1.4	1.5 ^a	1.5 (OBEP) ^a	1.6	1.7
ρ , fm $^{-3}$	0.068	0.068	0.117	0.185	0.228	0.228	0.276	0.332
3S_1	-10.15	-11.46	-13.08	-15.19	-15.77	-19.96	-15.89	-15.67
1S_0	-8.36	-8.54	-12.24	-16.35	-18.43	-18.68	-20.30	-22.10
3P_0	-1.34	-1.34	-2.36	-3.56	-4.18	-4.17	-4.77	-6.54
3P_1	3.02	3.03	6.15	11.08	14.40	14.42	18.30	22.90
3P_2	-1.93	-1.93	-4.21	-7.91	-10.38	-10.37	-13.36	-16.84
1P_1	0.55	1.37	1.30	2.76	3.90	5.43	5.34	7.17
3D_1	0.40	0.36	0.87	1.62	2.12	1.97	2.67	3.31
3D_2	-1.17	-1.09	-2.58	-4.85	-6.36	-6.02	-8.13	-10.19
1D_2	-0.65	-0.69	-1.48	-2.89	-3.88	-4.15	-5.08	-6.54
3F_2	-0.11	-0.11	-0.30	-0.64	-0.88	-0.89	-1.20	-1.58
$J \geq 3$	0.11 ^b	0.30 ^c	0.22 ^b	0.33 ^b	1.15 ^c	0.88 ^c	0.35 ^b	0.26 ^b
Sum	-19.63	-20.08	-27.71	-35.58	-38.33	-41.42	-42.05	-44.50
Kinetic	12.44	12.44	17.92	24.38	28.00	28.00	31.85	35.95
E/A	-7.19	-7.64	-9.79	-11.20	-10.34 ^c	-13.43	-10.20	-8.55
ΣS	-18.61	-20.00	-25.32	-31.54	-34.20	-38.54	-36.19	-37.77
ΣP	0.30	1.13	0.88	2.37	3.74	5.31	5.51	6.69
ΣD	-1.42	-1.53	-3.19	-6.12	-8.12	-8.20	-10.54	-13.42

sions for nuclear forces to ensure that there is not a regime of collapsed nuclei of very high density and binding [20]. Most of the current forces do not satisfy the conditions, but since the expressions for the forces are not to be taken seriously for relative momenta greater than, say, 5 fm $^{-1}$, corresponding to a kinetic energy of several hundred MeV, there is no problem. We are, of course, required to assume that strong repulsion arises at higher momenta, but it is also true that in a high-density regime excited nucleon states will be present, both Δ 's and N 's and the strange baryons Λ 's and Σ 's.

Having seen the mechanism of saturation, we may now ask how well the quantitative results agree with experiment. Table 8-3 shows that for a given density two potentials, both acceptable on the energy shell, may give binding energies differing by 2 or 3 MeV. Comparison of the Reid soft core and the OBEP at $k_F = 1.5$ fm $^{-1}$ shows two main differences, the 3S_1 - and 1P_1 -states.

The OBEP singlet P -potential is that predicted by the OBEP theory; it gives 1P_1 -phase shifts noticeably different from those of the Reid potential, both above 200 MeV (where it yields the better agreement with experiment) and below 50 MeV. In the latter region there is need for improved experimental information, since current data have been subject to considerable uncertainty; some accurate 1P_1 -phase shifts would probably distinguish between the more and the less repulsive forces now possible.

The different results for the 3S_1 -state can be attributed to the different values of the ratio of central force to tensor force in the two potentials. With the OBEP more of the binding is due to the central force, and although the

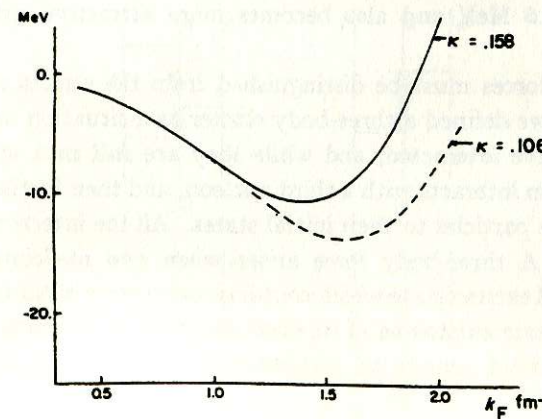


Fig. 8-12 Binding energy of nuclear matter as a function of Fermi momentum. Upper curve: Reid soft core, lower curve: OBEP of Grangé and Preston [17]. Two-body correlations only. The quantity κ is the wound at $k_F = 1.5$ fm $^{-1}$, $\kappa = 0.86$ fm $^{-1}$.

quadrupole moment of the deuteron is fitted, the percentage of D -state is lower. This is reflected in a lower value of the scattering parameter ϵ_1 , as discussed in Chapter 5, but one which nevertheless may lie in the experimentally determined range. The result in nuclear matter is that the Pauli-effect inhibition of the tensor force is not quite so effective in preventing the growth of the 3S_1 -contribution. A considerable range of central-tensor mixtures is permitted by the two-nucleon data [21], and rather different results ensue for nuclear matter throughout the range, as has been shown by Afnan, Clement, and Serduke [22]. Since the tensor suppression mechanism is relatively less significant for OBEP, one would expect that the density at which the energy saturates would be higher. This is borne out by computation, and Fig. 8-12 gives the results. The Reid potential[†] saturates at $k_F = 1.42 \text{ fm}^{-1}$ with $E/A = -10.59 \text{ MeV}$, and the OBEP at $k_F = 1.58 \text{ fm}^{-1}$ with $E/A = -13.58 \text{ MeV}$.

Both results are at densities greater than the experimental number $k_F = 1.36 \text{ fm}^{-1}$, but so far we have considered only two-body clusters. We must now consider additional effects. We shall discuss three- and four-body clusters and relativistic kinematics.

We have already indicated that the work of Dahlblom [9] gives an attractive contribution of three-body clusters of about 2 MeV. A more precise calculation by Grangé for the Reid soft-core potential gives a value of -1.59 MeV at $k_F = 1.36 \text{ fm}^{-1}$. The three-body contribution becomes less attractive at high density. These numbers are uncertain by $\pm 0.5 \text{ MeV}$. Also we have already given the result of a calculation of the four-body-cluster energy; it is $-1.1 \pm 0.5 \text{ MeV}$ and also becomes more attractive with increasing density.

Three-body forces must be distinguished from the effects of three-body clusters. We have defined a three-body cluster as a situation in which, after two nucleons have interacted, and while they are still in a virtual excited state, one of them interacts with a third nucleon, and then further interaction returns the three particles to their initial states. All the interactions are two-nucleon ones. A three-body force arises when two nucleons interact to produce a virtual excited state which contains some entity other than nucleons, and while this state exists one of its constituent parts interacts with a third nucleon. The effect cannot be attributed to a succession of two-nucleon interactions.

[†] This result differs slightly from Sprung's [2], quoted as $k_F = 1.44 \text{ fm}^{-1}$, $E/A = -11.25 \text{ MeV}$. The discrepancy is due chiefly to the different treatments of the states with $J > 2$.

Some diagrams may help to make the difference clear. Figure 8-13a represents a typical three-body cluster. Nucleons in states k and l interact and are excited to momenta a and b , a and m interact and receive momenta c and k , and c and b interact, returning to momenta l and m . This is a three-body cluster and, in fact, is the same as the cluster represented in Fig. 8-4a. The wavy lines represent the complete two-nucleon interaction due to all possible exchanges of pions and other bosons with appropriate intermediate states. For example, if we use a dotted line to represent a pion exchange and a heavy line to represent a $\Delta(1236)$, diagram (a) would contain diagrams (b) and (c) and a host of others. In diagram (b) we deal only with a succession of single-pion exchanges; this is a portion of what occurs in a three-body cluster. In diagram (c) we show another portion, where the result of the first pion exchange is a virtual state containing a nucleon and a $\Delta(1236)$, which then exchange a second pion, resulting in a state with two nucleons in states a and b above the Fermi sea. Then a interchanges two pions with m before c

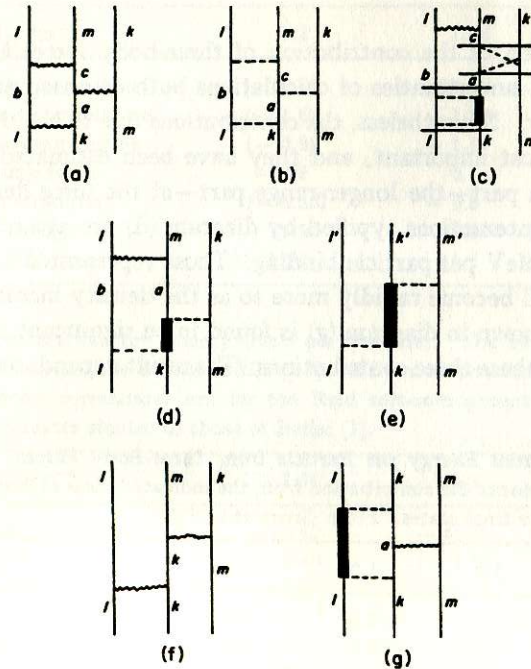


Fig. 8-13 Diagrams to illustrate three-body forces in nuclear matter.

and k result. But all processes between states l, k and a, b and between a, m and c, k are just parts of the two-nucleon interaction. In contrast, the bottom part of diagram (d) represents a portion of the three-body forces, because the virtual state with which the third nucleon interacts is not a nucleonic state; there is no way in which this process reduces to a succession of applications of the two-nucleon force. Diagram (d) then is a three-body contribution to the energy of nuclear matter, involving a three-body force followed by a two-nucleon force.

The diagonal three-body force can also contribute to nuclear matter. It is represented by diagram (e), in which k', l', m' are any permutation of k, l, m . Note that diagram (f), on the other hand, does not represent even a three-body cluster. It merely represents two completely distinct two-body clusters (the states that we would describe as ψ_{kl} and ψ_{km}), and it reminds us to include in the binding energy the quantities $(\phi_{kl}|v|\psi_{kl})$ and $(\phi_{km}|v|\psi_{mk})$. This remark should delineate clearly the nature of the three-body force: the interaction in nuclei is not the superposition of the free interaction for all nucleon pairs; rather, the virtual meson and baryon fields are modified by the presence of the other nucleons, as we already noticed in discussing magnetic moments.

The calculation of the contribution of three-body forces entails all the complexities and uncertainties of calculations both of boson exchanges and of nuclear matter. Nevertheless, the contributions due to the $\Delta(1236)$ should be by far the most important, and they have been estimated [23, 24, 25]. They represent a part—the longer-range part—of the force due to two-pion exchange. The interactions typified by diagram (d) are attractive and contribute about 2 MeV per particle binding. Those represented by diagram (e) are repulsive and become rapidly more so as the density increases. Finally, a third process shown in diagram (g) is found to be significant, though small. Table 8-4 shows these three contributions. The result depends on the cancella-

TABLE 8-4 Potential Energy per Particle from Three-Body Forces. Each number is in MeV and represents the contribution from the indicated class of diagram, including exchange among the final states. From Green et al. [23].

$k_F, \text{ fm}^{-1}$:	1.2	1.3	1.4	1.5	1.6	1.7
Fig. 8-13d	-1.6	-1.9	-2.3	-2.7	-3.2	-3.8
Fig. 8-13e	1.0	1.7	2.6	4.0	5.8	8.4
Fig. 8-13g	-0.3	-0.1	0.1	0.3	0.5	0.6
Total	-0.9	-0.3	0.4	1.6	3.1	5.2

tion between the two larger terms, each of which is sensitive to some assumptions in a lengthy calculation; in particular, the two-nucleon correlation is important. The repulsion of diagram (e) may be substantially overestimated.

It will be realized that all calculations have used nonrelativistic quantum mechanics. This can be changed only when a fully relativistic many-body theory, including the meson fields, is developed. However, it is desirable to make allowance for the most simple relativistic effect, the altered relationship between energy and momentum. This "minimal" allowance for relativity has been estimated by Brown, Jackson, and Kuo [26] and results in additional binding of about 0.5 MeV at normal density.

The various components of the binding energy are collected in Tables 8-5 and 8-6. Since the four-nucleon correlations and some of the three-nucleon correlations have been calculated only for $k_F = 1.36 \text{ fm}^{-1}$, their dependence on k_F has to be estimated. It is difficult, therefore, to be very precise about

TABLE 8-5 Nuclear-Matter Energy (MeV per Particle). The first three contributions are based on the Reid soft-core potential. The bracketed numbers are estimates by Bethe [1].

$k_F, \text{ fm}^{-1}$:	1.2	1.36	1.6
Two-body correlation	-27.71	-34.02	-42.05
Three-body correlation	(-1.6)	-1.59	(-1.1)
Four-body correlation	(-0.9)	-1.1	(-1.5)
Three-body forces	-0.9	0.1	3.1(?)
Minimal relativity	(-0.35)	-0.5	(-0.7)
Kinetic energy	17.92	22.97	31.85
Total E/A	-13.5	-14.1	-10.4

TABLE 8-6 Nuclear-Matter Energy (MeV per Particle). The two-body and part of the three-body correlations are for OBEP [17]; the rest of the three-body correlations and the four-body correlations are for the Reid soft-core potential. The bracketed numbers are estimates similar to those of Bethe [1].

$k_F, \text{ fm}^{-1}$:	1.36	1.5	1.7
Two-body correlation	-35.42	-41.43	-49.14
Three-body correlation	-1.49	(-1.9)	(-2.6)
Four-body correlation	-1.09	(-1.4)	(-1.8)
Three-body forces	0.1	1.6	5.2
Minimal relativity	-0.5	(-0.6)	(-0.8)
Kinetic energy	22.97	28.00	35.95
Total E/A	-15.4	-15.7	-13.2

the saturation density and energy. The values of Table 8-5 suggest $k_F = 1.32 \text{ fm}^{-1}$ and $E/A = -14.2 \text{ MeV}$ per particle for the Reid soft-core potential, whereas those of Table 8-6 give $k_F = 1.46 \text{ fm}^{-1}$ and $E/A = -15.8 \text{ MeV}$ per particle for the OBEP. Since some components of the energy are in doubt by as much as 0.5 MeV, both results are consistent with the experimental binding energy. Also, the equilibrium density is very sensitive to the k_F -dependence of the higher-order corrections, even though these may be relatively small near equilibrium. In other words, the energy-density curve for pair correlations alone is quite flat in the region of nuclear densities, and the small higher-order terms have a marked effect on the curvature and the minimum of the total energy-density function.

Since the two forces that we have considered are typical of realistic nucleon-nucleon forces, we may conclude that the energy and the density of nuclear matter are understood and are consistent with the properties of the actual forces. It should be stressed, however, that this result depends on the inclusion of the higher-order terms. We have already noted that the equilibrium values for pair correlations only occur at excessively high densities and at binding energies 2–4 MeV too small. Other potentials with equivalent phase shifts can be devised which will alter these numbers, but a potential that would account for the total binding by the two-body correlation alone should probably be ruled out on the grounds that the higher-order terms do contribute a few MeV.

Nuclear matter, being in its lowest energy state, is at zero temperature. Hence the connection between the pressure, the density, and the energy per particle is

$$P = -\frac{d(E/A)}{dv} = \rho^2 \frac{d(E/A)}{d\rho}, \quad (8-75)$$

where $v = 1/\rho$ is the volume per particle. In other words, the pressure is the rate at which the energy per particle decreases as the volume per particle increases. At equilibrium the pressure is zero. If, because of external agencies, the system is in a region of positive pressure, it remains stable in the sense that in losing energy it expands, decreasing in density and reaching equilibrium, where it can exist in isolation. If, however, the pressure is negative, the system breaks up since it loses energy by forming isolated lumps of matter at equilibrium density. In the case of nuclear matter, the pressure is of course negative for $\rho < \rho_0$, and therefore an isolated uniform assembly of protons and neutrons at $\rho < \rho_0$ will coalesce into regions of normal density ρ_0 with “empty” space between them. Of course, there can be a stable

situation with $\rho < \rho_0$ in completely different geometries such as a surface layer on a finite nucleus.

It is important to know whether nuclei are compressible. If they are readily so, a common form of excitation of a nucleus would be density oscillations, or the so-called breathing mode, in which the nucleus would alternately contract and expand without change in shape. A measure of the energy needed to produce a change from the equilibrium density ρ_0 is clearly the value of the second derivative of E/A at equilibrium. In fact, it is usual to define the “incompressibility” as

$$K = k_F^2 \left[\frac{d^2(E/A)}{dk_F^2} \right]_0 = 9\rho_0^2 \left[\frac{d^2(E/A)}{d\rho^2} \right]_0. \quad (8-76)$$

Excited states corresponding to density changes are not observed, at least in the low-lying regions of nuclear spectra. We deduce that K must be appreciable, and a value of at least 120 MeV is indicated. (See Problem 8-8.) The value of K is of course sensitive to the higher-order corrections, since these affect the shape of the energy-density curve. For the calculations in Tables 8-5 and 8-6 the results are, respectively, 170 and 180 MeV. The two-body correlation alone provides only 130 and 120 MeV for the same two potentials.

Nuclear-matter calculations can be made with unequal numbers of neutrons and protons. There are two distinct Fermi momenta, and some additional complications arise both in handling the two exclusion-principle operators Q which now arise and in weighting the various spin-isospin states. Nevertheless the computations are feasible. For small neutron excess, it is possible in this way to find the coefficient of the symmetry-energy term in the semiempirical mass formula. We write

$$\frac{E(\rho, \alpha)}{A} = \frac{E(\rho, 0)}{A} + \varepsilon_1(\rho)\alpha^2 + \varepsilon_2(\rho)\alpha^4 + \dots, \quad (8-77)$$

where

$$\rho = \rho_n + \rho_p, \quad \alpha = \frac{\rho_n - \rho_p}{\rho} = \frac{N - Z}{A}.$$

The quantity $\varepsilon_1(\rho_0)$ should be the coefficient $-a_{\text{sym}}$ of formulas 6-21 and 6-24. The results are satisfactory [16], giving

$$\varepsilon_1(\rho) = 32 \left(\frac{\rho}{\rho_0} \right)^{2/3} \text{ MeV}.$$

It may be noticed that with the number of protons fixed the binding of the whole system increases with each neutron added by an amount $[\partial E(A, Z)/\partial A]_Z$. Using the constants of the semiempirical formula, one finds that this derivative vanishes for Z/A about $\frac{1}{3}$. Hence, when there are twice as many neutrons as protons, any additional neutrons are unbound. In other words, a system with α greater than about $\frac{1}{3}$ is unstable in isolation. But of course it could exist if additional attraction, other than nuclear forces, could hold the neutrons. Such an attraction is the force of gravity, and there is little doubt that there are dense stars which consist primarily of neutrons with a few protons and other charged baryons accompanied by electrons and negative muons. The structure of such stars is a fascinating subject for study, ranging from the low-density regime where there are nuclear clusters, that is, very large "nuclei," with free neutrons and electrons in the relatively empty space between them [27], through the regime of neutron matter, which is nuclear matter with α quite close to unity (a few protons) [28, 29, 30], and then into the very-high-density regime [31, 32]. Unfortunately, however, this topic is somewhat outside the scope of this book.

At the end of Section 8-3 we described the procedure for a renormalized Brueckner-Hartree-Fock calculation (RBHF) for a finite nucleus and stressed its extreme complication. One of the computational problems is the necessity to calculate matrix elements like $\langle kl|v|\alpha\beta\rangle$, where the single-particle wave functions are determined self-consistently by the Hartree-Fock process and are functions of the coordinates of the nucleons, while v depends on the relative coordinate. We saw that in nuclear matter there are two simplifications: the wave functions must be plane waves, and plane waves can easily be expressed in relative and center-of-mass coordinates. There is a set of finite range functions such that $\phi_\alpha(\mathbf{r}_1)\phi_\beta(\mathbf{r}_2)$ can be written as a finite sum of terms $\phi_\alpha(\mathbf{r})\phi_\beta(\mathbf{R})$; these are the harmonic-oscillator functions. (See Problem 8-11.) But no other set has this property, and, of course, the self-consistent potential U does not turn out to be an harmonic oscillator. The only practical approach to the computation of matrix elements is to express the actual wave functions in terms of a complete set of oscillator functions. If the actual functions are fairly close to oscillator functions, only a few terms are needed in such a series. Fortunately this is often the case; indeed, for many purposes it is not an entirely misleading approximation to take the wave function of a deeply bound nucleon to be a single oscillator function.

The second major technical task is to deal with the exclusion principle. The operator Q must span the complete Hilbert space except for the A occupied states, which are the self-consistent $\{\phi_\alpha\}$. Since the solution of the

Bethe-Goldstone equation requires that terms like $\langle 1|v|i\rangle\langle i|G|2\rangle(E_i - \omega)^{-1}$ be summed over unoccupied states i , there must be a convenient expression also for the states outside the Fermi sea.

A third, more basic problem is to decide on the spectrum E_i for unoccupied states. As was emphasized in Section 8-3, the results are quite sensitive to this choice, unless one proceeds to calculate three- and four-body clusters. Otherwise, one should choose the excited-state spectrum to cancel important higher-order terms. In nuclear matter, sufficient work has been done on three-body clusters to suggest a reasonable excited-state spectrum; there $U = \text{constant}$ is reasonable for states above the Fermi level. But there are no calculations of three-body clusters in finite nuclei. Consequently, in a RBHF calculation one should study the effects of different assumptions concerning the excited spectrum.

In these circumstances, the early calculations were not complete. Some did not obtain a self-consistent set $\{\phi_\alpha\}$, some applied Q only to the states of the oscillator basis, not to the "real" states, some assumed the excited states to be plane waves, some took them as oscillators, some took the excited states to have zero potential energy, some assumed oscillator spectra or modifications of these.

It is most important to "renormalize," that is, to allow for the partial occupation of states in the Fermi sea. In some papers, this is done by means of a "saturation potential" or "rearrangement energy," introduced into Eq. 10-13. There are now much improved calculations, but it remains true that in 1973 it was not clear to what extent the inadequacies of the results obtained were to be attributed to approximations in the calculations and to what extent they were due to the assumed properties of the nucleon-nucleon force.

The most complete calculations have difficulty principally with the spectrum of the unoccupied states. Two prescriptions have been commonly used. One is to take $(a|U|a) = 0$, since in nuclear matter this leads to small higher-order cluster contributions. This argument is not particularly strong, since higher-order clusters have not been calculated in finite nuclei. Also in nuclear matter the results for pair correlations are insensitive to $(a|U|a)$ as long as it is small, whereas, as we shall see, the results for finite nuclei are sensitive. This prescription means that the energy of such states is the kinetic energy only. The Hamiltonian is written as QTQ ; this is not the free-particle Hamiltonian, since the projection operators prevent it from having matrix elements between particle states and hole states, that is, the occupied and unoccupied states remain orthogonal.

The other common approach is to take the spectrum to be that of a harmonic oscillator, but shifted by an arbitrary amount:

$$e_a = \hbar\omega(2n_a + l_a + \frac{3}{2}) - C - B_0\theta_a, \quad (8-78)$$

where ω is the oscillator frequency used for the basis states, C and B_0 are arbitrary constants, and θ_a is unity if a is a state in a certain arbitrarily chosen set near the Fermi level and is zero for states above that set. If $B_0 = 0$ and $C \neq 0$ the whole spectrum is lowered in energy, whereas if $C = 0$ and $B_0 \neq 0$ only a certain number of states have their energies lowered. It is argued that the lowest unoccupied single-particle level of a finite nucleus may be a bound state and therefore should have negative energy, or it may be unbound by a small amount. In any case its energy should be near zero; this is achieved by putting

$$C + B_0 = \hbar\omega(2n' + l' + \frac{3}{2}), \quad (8-79)$$

where n' and l' are the quantum numbers of the first unoccupied state. For example, if one is studying ^{16}O , the relevant states are the $1s$ and $0d$, which give $C + B_0 = 7\hbar\omega/2$. Alternatively, to come close to the free-particle prescription, one could take $C + B_0$ at half the above value, since then the energy of the lowest state would be just its kinetic energy; or, by using a somewhat greater value, one could subtract the average potential energy of the first few low-lying unoccupied states.

Tables 8-7 and 8-8 display some results for ^{16}O and ^{40}Ca . The first point to note is that columns A, B, and C in Table 8-7 show that the results are insensitive to the oscillator frequency of the basis states. They should, in principle, be independent of ω since the oscillator states serve only as a complete set in which the Hartree-Fock states are expanded for computational purposes. The actual dependence reflects the fact that the calculations are not completely self-consistent [34]. Next we examine the sensitivity to the intermediate-state energies by comparing columns B and D of Table 8-7. In column B, the lowest intermediate-state energy is zero and the two-particle intermediate states are reduced in energy by $7\hbar\omega$, provided that

$$2n_\alpha + l_\alpha + 2n_\beta + l_\beta \leq \bar{N} - 4 \quad (8-80)$$

with $\bar{N} = 18$. This is a substantial number of shifted states. In column D, all states are shifted but the energy of the two-particle intermediate states falls by only $2\hbar\omega$. It will be seen that the differences in the energies and the occupation probabilities are very marked. This can be understood as follows. Lowering the intermediate-state spectrum reduces the denominators in the

TABLE 8-7 Renormalized Brueckner-Hartree-Fock Calculations for ^{16}O . A: $\hbar\omega = 12.5$, $B_0/\hbar\omega = 3.5$, $C = 0$, $\bar{N} = 18$; B: $\hbar\omega = 14.0$, $B_0/\hbar\omega = 3.5$, $C = 0$, $\bar{N} = 18$; C: $\hbar\omega = 15.5$, $B_0/\hbar\omega = 3.5$, $C = 0$, $\bar{N} = 18$; D: $\hbar\omega = 14.0$, $B_0 = 0$, $C = \hbar\omega$. A, B, C, D: Reid soft-core potential; E: OBEP potential, neutron and proton states not distinguished, $\hbar\omega = 13.3$, for spectrum see text. The total energy E includes Coulomb energy. Energies are in MeV, the mean-square mass and charge radii are in fm.

	Experiment ^a	A ^b	B ^b	C ^b	D ^c	E ^d
Neutrons						
$e(0s_{1/2})$	-40 ± 8	-36.9	-37.0	-37.4	-38.4	-40.8
$e(0p_{3/2})$	-21.8	-18.3	-18.2	-18.3	-17.0	-19.9
$e(0p_{1/2})$	-15.7	-15.3	-15.2	-15.1	-13.3	-16.5
$e(0d_{5/2})$	-4.14					-2.59
$e(1s_{1/2})$	-3.27					-0.15
$P(0s_{1/2})$		0.82	0.82	0.82	0.88	
$P(0p_{3/2})$		0.78	0.78	0.78	0.90	
$P(0p_{1/2})$		0.78	0.78	0.78	0.90	
Protons						
$e(0s_{1/2})$		-34.2	-34.3	-34.7	-35.2	
$e(0p_{3/2})$		-15.8	-15.7	-15.7	-14.0	
$e(0p_{1/2})$		-12.9	-12.7	-12.6	-10.4	
$P(0s_{1/2})$		0.81	0.82	0.82	0.88	
$P(0p_{3/2})$		0.78	0.78	0.78	0.90	
$P(0p_{1/2})$		0.79	0.77	0.78	0.90	
$-E/A$	7.98	6.57	6.49	6.47	4.19	7.57
r_{mass}		2.44	2.43	2.41		2.64
r_c	2.73	2.57	2.57	2.55	2.61	

^a As quoted in ref. 33.

^b Ref. 34.

^c Ref. 35.

^d Ref. 33.

Bethe-Goldstone equation and makes the G -matrix more attractive. This, in turn, gives more binding, both in single-particle states and overall. The shifts in the occupied state are smaller than those in the intermediate states which caused them, and therefore the energy gap is reduced self-consistently. Moreover, this implies more excitation, that is, a larger wound κ , and a smaller occupation probability P . These effects are also apparent in comparing columns A and C of Table 8-8.

The effect of lowering more states can be seen in columns C, D, and E of Table 8-8. In each case the states are lowered by $4.5\hbar\omega$, but the number

TABLE 8-8 Renormalized Brueckner-Hartree-Fock Calculations for ^{40}Ca . Proton states are not tabulated, but are included in the energy E . A: $\hbar\omega = 12.5$, $B_0/\hbar\omega = 4$, $C = 0$, $\bar{N} = 20$; B: same as A, but not renormalized; C: $\hbar\omega = 12.5$, $B_0/\hbar\omega = 4.5$, $C = 0$, $\bar{N} = 20$; D: $\hbar\omega = 12.5$, $B_0/\hbar\omega = 4.5$, $C = 0$, $\bar{N} = 26$; E: $\hbar\omega = 12.5$, $B_0 = 0$, $C/\hbar\omega = 4.5$. A, B, C, D, E: Reid soft-core potential; F: OBEP, neutron and proton states not distinguished, $\hbar\omega = 15$ MeV, spectrum described in text. Energies are in MeV, radii in fm.

Experiment ^a	A ^b	B ^b	C ^b	D ^b	E ^b	F ^c
Neutrons						
$e(0s_{1/2})$	-50 ± 11	-54.8	-68.2	-54.7	-58.2	-70.7
$e(0p_{3/2})$	-34 ± 6	-35.1	-45.3	-34.9	-37.5	-46.6
$e(0p_{1/2})$		-32.4	-41.4	-32.2	-34.5	-42.6
$e(0d_{5/2})$			-17.5	-24.7	-18.0	-19.7
$e(1s_{1/2})$	-18.1	-15.8	-21.8	-16.4	-17.9	-23.0
$e(0d_{3/2})$	-15.6	-13.4	-18.8	-14.1	-15.5	-20.1
$e(0f_{7/2})$	-8.36	3.1	0.54			-6.6
$e(1p_{3/2})$	-6.2	1.9	1.1			0.1
$P(0s_{1/2})$	0.83	1	0.82	0.81	0.80	
$P(0p_{3/2})$	0.84	1	0.81	0.80	0.80	
$P(0p_{1/2})$	0.83	1	0.81	0.79	0.79	
$P(0d_{5/2})$	0.84	1	0.79	0.77	0.73	
$P(1s_{1/2})$	0.84	1	0.79	0.77	0.72	
$P(0d_{3/2})$	0.83	1	0.78	0.76	0.71	
$-E/A$	8.55	4.99	4.21	5.83	6.98	10.7
r_{mass}						3.38
r_c	3.49	3.19	3.05	3.14	3.06	2.85

^a As quoted in ref. 33.

^b Ref. 34.

^c Ref. 33.

of states progressively increases, \bar{N} being 20, 26, and infinity. It is seen that this has a marked effect of the kind just described, since more states are at energies capable of participating in the correlation wound. The multiplicity of states of higher spin helps in this process.

A comparison of columns A and B of Table 8-8 demonstrates the importance of renormalization. As we pointed out at the end of Section 8-3, the single-particle energies are very sensitive to renormalization, but the total energy is affected less drastically.

It has been suggested that the intermediate spectrum should be chosen to give a good fit to the observed single-particle bound-state energies. It is safer, however, to consider the choice an open question.

The columns so far discussed are for the Reid soft-core potential. The last column of each table reports a calculation with the same OBEP as we used for nuclear-matter comparisons. In this case the intermediate-state spectrum was taken as discrete through a "valence" band—a few low-lying unoccupied states—and as continuous and free above a specified cutoff energy. This appears to be a good way to treat the Pauli principle. The discrete states were shifted by the average potential energy in the valence band; this would be similar to a B_0 of about $2\hbar\omega$ for ^{16}O and perhaps $3\hbar\omega$ for ^{40}Ca .

It will be observed that with the Reid soft-core potential a substantial spectral shift is required to produce total binding near the experimental value, and that, when this is made, the nuclear radius decreases to values substantially lower than experimental ones. Indeed, when the calculation is adjusted to give radii near experiment, the binding energy is considerably too small. The OBEP, on the other hand, does better at fitting both quantities simultaneously. We should be cautious, however, about what this means physically. The OBEP gives more binding in nuclear matter also, but in nuclear matter we know that there is 3 MeV or so of binding per particle from many-body clusters, many-body forces, and relativistic effects. All of these will occur in finite nuclei but have not been calculated. It is difficult, therefore, to know what answer to desire for a calculation (such as RBHF) based on the independent-pair approximation.

Because of this uncertainty, and also because of increased simplicity in computational aspects and perhaps also greater richness in physical insight, another approach to finite nuclei has also been pursued. This approach emphasizes the idea of thinking of G as an effective interaction to be used with the wave functions ϕ , instead of using v with the real wave functions ψ , and then it exploits the fact that outside a relatively short distance ψ heals to ϕ . Since $G\phi = v\psi$, it follows that, if G is expressed as an interaction in coordinate space, it is identical to v for separations greater than the healing distance. The correlations ζ are of short range compared to the radii of nuclei. Nuclei, except in a relatively small surface region, have slowly changing density. In a nucleus the states ϕ are finite in range; but just as the plane waves of nuclear matter with $k < k_F$ change slowly within a distance of the order of the healing distance, so also do the ϕ 's of the finite nucleus. Would it not then seem reasonable that the correlation ζ in a two-nucleon collision taking place in the central region of a nucleus should be very similar to the correlation in nuclear matter of the same density? Since two colliding nucleons have their interaction effectively modified only by others nearby, is it not reasonable to expect to obtain good results for finite nuclei simply by

taking G over from nuclear matter and using it as the nucleon-nucleon interaction in finite nuclei? In this way, the short-range correlations are built into the interaction and the wave functions themselves can be the simple single-particle ϕ 's of a shell model or of a Hartree-Fock calculation.

Of course, G depends on density, and therefore we adopt a local density approximation. It is assumed that the effective interaction of two nucleons in a finite nucleus is equal to their effective interaction in nuclear matter with constant density equal to the density in the region where the nucleons interact, that is, at a density which is some mean value of the densities at nucleon 1 and nucleon 2. Both arithmetic and geometric means have been used in actual calculations. This basic approach was taken first by Brueckner, Gammel, and Weitzner [36]. In their work, they preserved the nonlocal character of the G -matrix. It was later suggested by Brandow that the theory would be not only simpler, but also more amenable to the use of physical insight, if a local effective interaction could be substituted without much loss of accuracy. This suggestion has been the basis of a considerable amount of more recent work.

We shall write $V_{L'L}^{JS}(r)$ for the effective two-nucleon interaction. At a given density in nuclear matter, this quantity is, in fact, the G -matrix. Using Eq. 8-61b, we can write

$$V_{L'L}^{JS}(r, k, P, k_F; v) = \sum_{L''} \frac{v_{L'L''}^{JS} u_{L''L}^{JS}(r)}{kr j_L(kr)}. \quad (8-81)$$

The basic requirement of an effective interaction is that its matrix elements $\langle k' | V | k \rangle$ be as close as possible to those of G . The V defined in Eq. 8-81 of course satisfies this exactly if u is taken as the result of a self-consistent Brueckner nuclear-matter calculation. There will still be some freedom in regard to the value of V , because of some arbitrariness in the choice of the energy spectrum of the intermediate states in the calculation. The various arguments attached to V emphasize that it depends on the free nucleon-nucleon interaction v , on the density or k_F , and on k and P . We can immediately assume that an average value of P has been used for each k . But the dependence on k is inescapable, and it is this momentum dependence which makes the interaction nonlocal. (The reader may recall Eq. 8-3.)

In order to simplify this expression and obtain a local effective interaction, one may average appropriately over k . A natural thing to do is simply to weight the contribution for each k by the probability of finding relative momentum k in matter having Fermi momentum k_F [37]. The quantities that enter into a calculation of binding energy are the *diagonal* matrix elements

of the effective interaction for $k < k_F$. These, then, are the quantities averaged, leading to

$$V_{L'L}^{JS}(k, k_F) = \frac{\int_0^{k_F} \omega(k) j_{L'}(kr) V_{L'L}^{JS}(r, k, k_F) j_L(kr) dk}{\int_0^{k_F} \omega(k) j_{L'}(kr) j_L(kr) dk}, \quad (8-82)$$

where

$$\omega(k) = 12k^2(k_F - k)^2(k + 2k_F).$$

The result is that, on the average, the diagonal matrix elements of V are the same as those of G , but no particular matrix element $\langle k' | V | k \rangle$ necessarily agrees with $\langle k' | G | k \rangle$.

Once one has fixed a local potential, one has fixed both its diagonal and its off-diagonal matrix elements. Conversely, once one has fixed the diagonal elements *for all* k , one has fixed the potential. The off-diagonal elements are important in that they give the excitation of intermediate states, and they do play a role in Hartree-Fock calculations. The use of the nuclear-matter G , averaged in this way, should lead to reasonable off-diagonal elements.

Sprung [38] suggested that it would be more reasonable to use an effective interaction which reproduces exactly the diagonal elements for $k < k_F$, and which also has the same general appearance as the averaged V when regarded as a function of r . This latter criterion should ensure reasonable behavior for the matrix elements not fixed by Sprung's first requirement. To do this, it is of course necessary to resort to phenomenology. Sprung and Banerjee obtain a satisfactory effective interaction which is a sum of five Gaussian functions of r with appropriate constants.

Of course, if one fixes the interaction for all states J, S, L', L , one can then express the effective potential as a linear combination of central, tensor, $L \cdot S$, L^2 , and exchange forces. Since the L^2 -force is rather awkward, Negele [37] in his work simplified V further by averaging V_{LL}^{JS} over J and L for a given S and T to obtain an effective central force.

When $N \neq Z$, it is desirable to have a different effective interaction for each kind of nucleon. It is customary to use the local proton density for proton-proton interactions, the local neutron density for neutron-neutron collisions, and an average of the two densities for neutron-proton interactions.

It must be emphasized that the density dependence of the effective interaction is a vital feature. As will be seen in Chapter 10, the rearrangement energy due to this is an essential component of any understanding of nuclear energies. Equally important for explaining other effects is the change in the single-particle wave function that follows from the density dependence.

If the reader recalls that the density dependence of the total binding energy of nuclear matter is quite different from that of the contribution from two-body clusters, he may well question the usefulness of using the two-body G as the effective interaction in the finite case. There is also the fact that the two-body clusters alone underbind nuclear matter by several MeV per particle and give an incorrect equilibrium density. There is no reason to expect significantly less from higher-order effects in finite nuclei, although they would be very difficult to compute. Yet the goal of Hartree-Fock calculations with effective interactions is to study the nucleus in terms of effective two-body correlations. Consequently, it is important to use an effective interaction that gives the right binding energy at actual nuclear densities. To achieve this, the workers in this field [39] arbitrarily increase the strength of the attractive interaction at short range. It is desirable to use the actual strength for $r \gtrsim 2$ fm, however, since the purpose of the increased attraction is to allow for higher-order effects, which are mostly of short range. Of course, this adjustment does not necessarily produce the right density dependence, and one might think of adjusting the effective interaction to improve this aspect. But the more one adjusts, the more phenomenological the interaction becomes.

In order to give some notion of the nature of the effective interaction, Figure 8-14 shows the tensor components of V plotted against the Reid soft-core potential from which they were derived. The remarkable smoothing and weakening of the potential at distances less than 1 fm are apparent, as is the agreement of V and v at larger distances.

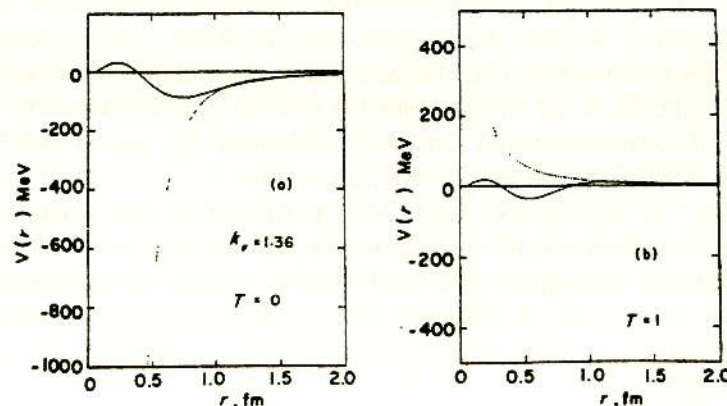


Fig. 8-14 Tensor components of the effective interaction at $k_F = 1.36 \text{ fm}^{-1}$ for $T = 0$ and 1. For comparison, we also show, as a dotted curve, corresponding components of the free potential, from which the effective interaction was derived. (From ref. 38.)

We have not discussed to any extent the changes in the theory that arise if energy levels are degenerate and are not completely filled. This situation occurs in any nucleus where some shell-model states are not fully occupied, that is, in all but magic nuclei. The basic theory of such "valence shells" has been supplied by Brandow [40], but most calculations have been performed by assuming effective interactions. Some cases are discussed in Chapter 10.

Just as an effective interaction is required if ϕ 's are used instead of ψ 's, so one needs effective operators for other observables such as electromagnetic moments. The following schematic equation is required:

$$\langle \phi_{mn} | \theta_{\text{eff}} | \phi_{kl} \rangle = \langle \psi_{mn} | \theta | \psi_{kl} \rangle. \quad (8-83)$$

One can write

$$\psi = \Omega \phi, \quad (8-84)$$

where Ω , sometimes called the "wave operator," is clearly a formal way of representing the correlations. In this notation

$$\theta_{\text{eff}} = \Omega \theta \Omega^{-1}. \quad (8-85)$$

This rather formal approach leads to complicated calculations, and more phenomenological approaches, such as "effective charges," are usually employed. However, the above presentation shows that such quantities can, in principle, be computed.

8-5 PAIRING CORRELATIONS AND THE GROUND STATE

In the preceding sections of this chapter we considered a theory of nuclear structure, potentially of very considerable accuracy, but based on the underlying picture of particles moving freely except for short-range correlations arising during the transient existence of clusters of two or more particles. This picture was shown to be possible because of the exclusion principle and the specific nature of the two-nucleon force; nevertheless the model is essentially that of a gas of fermions with very-short-range spatial correlations. These remarks apply to the main features of both nuclear matter and of real nuclei.

The question arises whether or not this quasi-gas state, which we call the *normal* state, is the nuclear ground state. To be more specific, we are asking this question: "Are there other types of states with long-range spatial correlations with lower energy?" In respect to correlations, such states would resemble liquids rather than gases, with wave functions so different that they would not be obtainable from a perturbative calculation starting with

quasi-gas wave functions. A similar situation arises in the superconductivity of metals. Following Cooper [41], let us first consider the simple situation of a pair of nucleons outside a quiescent Fermi sphere and interacting with an attractive force. It will be shown that under these circumstances the pair would form a bound state with a ground-state energy lower than that in the quasi-gas model, and the wave function of the pair would extend over a relatively large spatial distance. Furthermore, on considering the density of the two-nucleon states, we would find an energy gap between the ground state and the excited states. This bound pair, which is formed as long as the interaction between the two nucleons is attractive, no matter how weak, is popularly called the Cooper pair.

In this model, we emphasize that the Fermi sea in the presence of which the two nucleons are interacting is considered quiescent, that is, the nucleons inside the sea are inert and are not influenced in any way; the only effect they have is to block all momentum states up to k_F . Consider two identical nucleons of momenta $\mathbf{k}_1, \mathbf{k}_2$ ($k_1, k_2 > k_F$), with center-of-mass momentum $\mathbf{K} = \mathbf{k}_1 + \mathbf{k}_2$. Since the interaction potential V_{12} is a function of relative coordinates only, \mathbf{K} must be conserved. Furthermore, since we are interested in the ground state, it is reasonable to take the two identical nucleons to be of opposite spins. For a complete set of two-nucleon wave functions we take the plane-wave product $(1/\Omega) \exp[i(\mathbf{k}_1 \cdot \mathbf{r}_1 + \mathbf{k}_2 \cdot \mathbf{r}_2)]$, which in relative coordinates is $(1/\Omega) \exp[i(\mathbf{k} \cdot \mathbf{r} + \mathbf{K} \cdot \mathbf{R})]$, where $\mathbf{k} = \frac{1}{2}(\mathbf{k}_1 - \mathbf{k}_2)$, $\mathbf{R} = \frac{1}{2}(\mathbf{r}_1 + \mathbf{r}_2)$, and $\mathbf{r} = \mathbf{r}_1 - \mathbf{r}_2$. For a given \mathbf{K} , the center-of-mass wave function of the pair remains unaffected by the interactions and is simply $(1/\sqrt{\Omega}) \exp(i\mathbf{K} \cdot \mathbf{R})$. For the relative wave function, we can attempt to take a linear combination of plane-wave states to minimize the energy. Thus we write the pair wave function as

$$\psi_{\mathbf{K}}(\mathbf{R}, \mathbf{r}) = \frac{1}{\sqrt{\Omega}} \exp(i\mathbf{K} \cdot \mathbf{R}) \sum_{\mathbf{k}} c_{\mathbf{k}} \frac{1}{\sqrt{\Omega}} \exp(i\mathbf{k} \cdot \mathbf{r}). \quad (8-66)$$

Substituting this in the two-nucleon Schrödinger equation

$$\left[-\frac{\hbar^2}{2M} (\nabla_1^2 + \nabla_2^2) + V_{12} \right] \Psi_{\mathbf{K}} = E \Psi_{\mathbf{K}},$$

we obtain

$$(e_{k_1} + e_{k_2} - E)c_{\mathbf{k}} + \sum_{\mathbf{k}'} c_{\mathbf{k}'} \langle \mathbf{k} | V_{12} | \mathbf{k}' \rangle = 0, \quad (8-67)$$

where $e_{k_i} = (\hbar^2/2M)k_i^2$; $\mathbf{k}_i = (\mathbf{K}/2) \pm \mathbf{k}$, with \mathbf{k} a variable; and

$$\langle \mathbf{k} | V_{12} | \mathbf{k}' \rangle = \frac{1}{\Omega} \int d^3r \exp[i(\mathbf{k}' - \mathbf{k}) \cdot \mathbf{r}] V_{12}(r).$$

In Eq. 8-67, it is understood that only pairs with fixed center-of-mass momentum \mathbf{K} are being considered. Note from Eq. 8-67 that, in the absence of V_{12} , $E = e_{k_1} + e_{k_2}$, whose lowest limit is simply $2e_F$, e_F being the Fermi energy.

In order to solve Eq. 8-67 analytically, we now make some simplifying assumptions about the matrix elements $\langle \mathbf{k} | V_{12} | \mathbf{k}' \rangle$. We assume that

$$\begin{aligned} \langle \mathbf{k} | V_{12} | \mathbf{k}' \rangle &= -G, & k_F < k_i, k'_i &\leq k_F + \delta k_F, \\ &= 0, & \text{otherwise,} \end{aligned}$$

where G is a positive constant.[†] We shall discuss the rationale of this approximation later. With this V_{12} , it follows from Eq. 8-67 that, when \mathbf{k} is such that \mathbf{k}_1 and \mathbf{k}_2 lie in the region where G is nonzero,

$$c_{\mathbf{k}} = \frac{CG}{\epsilon_K + e_{\mathbf{k}} - E},$$

where $C = \sum_{\mathbf{k}'} c_{\mathbf{k}'}$, the sum in \mathbf{k}' is over the allowed region where V_{12} is finite, and

$$\epsilon_K + e_{\mathbf{k}} = \frac{\hbar^2}{M} \left(\frac{K^2}{4} + k^2 \right) = \frac{\hbar^2}{2M} (k_1^2 + k_2^2).$$

A little algebraic manipulation now yields the eigenvalue equation

$$\frac{1}{G} = \sum_{\mathbf{k}} \frac{1}{\epsilon_K + e_{\mathbf{k}} - E}. \quad (8-68)$$

The graphical solutions of this equation are easily found from Fig. 8-15, where the right-hand side of Eq. 8-68 is plotted as a function of E . The unperturbed energies of the pair, for a given center-of-mass energy ϵ_K , are shown by the dotted vertical lines. The actual eigensolutions are shown by crosses where the right-hand side equals $1/G$. It will be seen from this figure that only the lowest eigenvalue is shifted appreciably downward in energy from its unperturbed value of $2e_F$, the others remaining almost unaffected. In the case that we are considering, the unperturbed spectrum actually forms a continuum; nevertheless our analysis shows that the lowest-energy state of the pair will

[†] Not, of course, the G -Matrix.

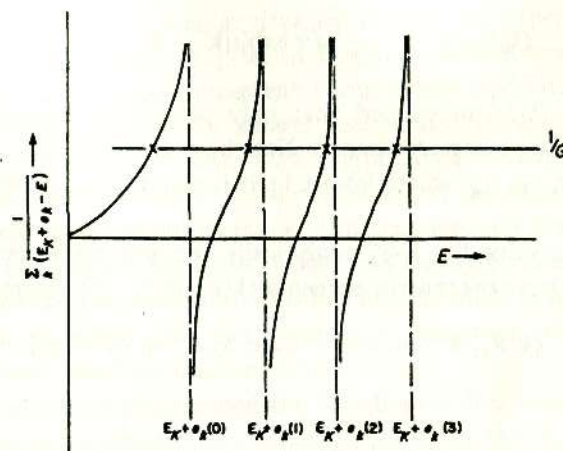


Fig. 8-15 The graphical solutions of Eq. 8-88 are denoted by crosses, showing that the lowest eigenvalue, designated by the cross at the extreme left, is lowered appreciably from the unperturbed position, whereas the others are little affected.

be shifted downward from the other states, giving rise to an energy gap in the spectrum.

The binding energy of the ground state of the pair may be found analytically by rewriting Eq. 8-88 as

$$\frac{1}{G} = \int_{e(0)}^{e(\max)} \frac{N(K, e) de}{e_K + e - E},$$

where we have replaced the sum over \mathbf{k} by an integration, $N(K, e)$ being the unperturbed density of two-nucleon states of total momentum K and energy $e = (\hbar^2/M)k^2$. The energy limits $e(0)$ and $e(\max)$ arise from the restriction $k_F < k_1, k_2 \leq k_F + \delta k_F$. Replacing $N(K, e)$ over this narrow range of e by the density of states at the Fermi surface, $N[K, e(0)]$, we can take N out of the integral sign and perform the integration analytically. A little algebra shows that the lowest eigenvalue E_0 of the pair is given by

$$E_0 = e(0) + \epsilon_K - E_B, \quad (8-89a)$$

where E_B is the binding energy of the pair:

$$E_B = \frac{e(\max) - e(0)}{\exp \left\{ \frac{1}{N[K, e(0)] \cdot G} \right\} - 1}. \quad (8-89b)$$

Note that E_B is strongly dependent on the product $N[K, e(0)] \cdot G$. The quantity $N(K, e)$ in turn is strongly dependent on K , being maximum for $K = 0$ and going rapidly to zero. Thus Eq. 8-89b shows that E_B will be largest for $K = 0$, that is, for two nucleons of momentum, spin (k_i, \uparrow) and $(-k_i, \downarrow)$. It is also possible to show that the bound-state pair wave function has considerable spatial extent [41].

In this idealized model, some important physical points have emerged. The inert Fermi sea plays a crucial role in providing a large number of nearly degenerate states at the Fermi surface, without which the bound pair cannot be formed. Essentially, the wave function of the pair is formed by a coherent superposition of these nearly degenerate states, at practically no cost in kinetic energy, to take maximum advantage of the *attractive* two-nucleon potential. It is essential to keep in mind that the interaction must be attractive for two nucleons colliding head on ($K = 0$) at the Fermi surface to form the bound pair. For nuclear matter this corresponds to a single nucleon of energy $(\hbar^2/2M)(2k_F)^2 \approx 160$ MeV colliding with a nucleon at rest. As we know, the two-nucleon interaction in the S-state becomes progressively less attractive at higher energies, turning repulsive at about $E_{\text{lab}} \approx 200$ MeV. Thus, at nuclear-matter density, the S-state interaction at the Fermi surface is weak but still attractive, giving rise to a small gap. For finite nuclei, the local Fermi momentum is much smaller in the surface region, and consequently a larger gap is formed [42].

Although the idealized model of the Cooper pair is very instructive, it is not very realistic, since in the many-body problem we expect a large number of such pairs to be present, with strong spatial overlap between the wave functions of the different pairs and numerous pair-pair collisions [43]. The basic many-body problem here is to construct a superconducting ground state $|\Psi_0\rangle$, formed as a coherent superposition of normal (quasi-gas) configurations $|\Phi_n\rangle$,

$$|\Psi_0\rangle = \sum_n c_n |\Phi_n\rangle, \quad (8-90)$$

so that the energy will be as low as possible and lower than in the normal ground state. In terms of the Hamiltonian H (which we will presently specify), the energy of the superconducting ground state is

$$E_0 = \langle \Psi_0 | H | \Psi_0 \rangle = \sum_{n,n'} c_n c_n^* \langle \Phi_{n'} | H | \Phi_n \rangle. \quad (8-91)$$

A straightforward diagonalization procedure would be very complicated and not too instructive. In the following discussion, we shall isolate, for a simplified

interaction, the configurations $|\Phi_n\rangle$ whose superposition may lead to a value of E_0 lower than that of the lowest lying "shell-model" state $|\Phi_n\rangle$.

Obviously, if H is such that all its off-diagonal matrix elements are negative, then, with the proper choice of c_n 's, all the terms in the sum of Eq. 8-90 can be in phase, yielding a low E_0 . Generally, however, the matrix elements $\langle\Phi_n|H|\Phi_n\rangle$ are expected to vary randomly in sign with random variations of normal-state configurations. This random behavior cannot be corrected by adjusting the signs of the coefficients c_n (say N in number), since there are N^2 matrix elements with random signs. Note that the normal configurations $|\Phi_n\rangle$ are determinantal states, although the superconducting state $|\Psi_0\rangle$ is not. If H contains only one- and two-body operators, $\langle\Phi_n|H|\Phi_n\rangle$ is just a sum of one- and two-body matrix elements. Let us restrict the sum in Eq. 8-90 by choosing nonzero c_n 's for only those normal-state configurations $|\Phi_n\rangle$ in which the single-particle orbitals are filled pairwise; that is, if an orbital (\mathbf{k}_i, \uparrow) is occupied, its time-reversed state $(-\mathbf{k}_i, \downarrow)$ is also occupied. The total momentum for each of these $|\Phi_n\rangle$'s is thus zero.

The two-body matrix elements arising from $\langle\Phi_n|H|\Phi_n\rangle$ will be of the form $\langle\mathbf{k}_i(1), -\mathbf{k}_i(2)|V_{12}|\mathbf{k}'_i(1), -\mathbf{k}'_i(2)\rangle$, where we have suppressed the spin indices. If the interaction is local and of very short range, all these matrix elements will have the same sign. To see this, observe that we can write, using the notation developed earlier in this section,

$$\langle\mathbf{k}_i(1), -\mathbf{k}_i(2)|V_{12}|\mathbf{k}'_i(1), -\mathbf{k}'_i(2)\rangle = \frac{1}{Q} \int \exp(i\mathbf{q} \cdot \mathbf{r}) V_{12}(\mathbf{r}) d^3r,$$

where $\mathbf{q} = \mathbf{k}'_i - \mathbf{k}_i$ and $\mathbf{r} = \mathbf{r}_1 - \mathbf{r}_2$. If we take for $V_{12}(\mathbf{r})$ the extreme example of a delta function,

$$V_{12}(\mathbf{r}) = -GQ \delta(\mathbf{r}), \quad (8-92)$$

we obtain the simple result

$$\langle\mathbf{k}_i(1), -\mathbf{k}_i(2)|V_{12}|\mathbf{k}'_i(1), -\mathbf{k}'_i(2)\rangle = -G. \quad (8-93)$$

Such a simplified pairing potential, effective in a narrow band about the Fermi surface, should give rise to a superconducting solution with energy less than that of the normal ground state. It may be verified that for nuclei, where the single-particle wave functions are not plane waves, the corresponding pairing matrix elements (Eq. 8-93) are not quite equivalent to a delta-function potential, although strong similarities remain.

Before considering the details of the superconducting wave function, we inquire whether any part of the two-nucleon interaction may be effectively

regarded as a delta-function potential of type 8-92. It is true that the free two-nucleon potential is of short range compared to the dimensions of a heavy nucleus, but we also know that the extreme-short-range part of the potential is repulsive rather than attractive. We must remember, however, that the pairing matrix elements 8-93 are taken in a narrow band of momenta near the Fermi surface, which, for nuclear-matter density, corresponds to $E_{\text{lab}} \approx 160$ MeV, as we have already discussed. At such energies, the *effective* two-nucleon interaction (i.e., the G -matrix) is still weakly attractive. What we want to see is whether a part of this effective two-nucleon interaction, operative on the nucleons near the Fermi surface, may have some characteristics of a delta-function type of potential. Assuming, for simplicity, the effective interaction V_{12} to be local, we may decompose it in the following convenient manner:

$$V_{12}(|\mathbf{r}_1 - \mathbf{r}_2|) = \sum_i \frac{2l+1}{4\pi} v_i(\mathbf{r}_1, \mathbf{r}_2) P_l(\cos \theta_{12}), \quad (8-94a)$$

where θ_{12} is the angle between the vectors \mathbf{r}_1 and \mathbf{r}_2 . Using Eq. A-70, we may rewrite Eq. 8-94a in the form

$$V_{12}(|\mathbf{r}_1 - \mathbf{r}_2|) = \sum_{l,m} v_i(\mathbf{r}_1, \mathbf{r}_2) Y_l^m(\mathbf{r}_1) Y_l^{m*}(\mathbf{r}_2), \quad (8-94b)$$

where a little algebra will show that

$$v_i(\mathbf{r}_1, \mathbf{r}_2) = \frac{2}{\pi} \int V(q) j_i(q\mathbf{r}_1) j_i(q\mathbf{r}_2) q^2 dq,$$

with

$$V(q) = \int \exp(i\mathbf{q} \cdot \mathbf{r}) V_{12}(\mathbf{r}) d^3r.$$

It should be realized, from Eq. 8-47, that the effective two-nucleon interaction gives rise to a self-consistent one-body average potential U , which, neglecting exchange, may be written in terms of the single-particle density ρ as

$$\begin{aligned} U(\mathbf{r}_1) &= \int \rho(\mathbf{r}_2) V_{12}(|\mathbf{r}_1 - \mathbf{r}_2|) d^3r_2 \\ &= \sum_{l,m} Y_l^m(\mathbf{r}_1) \int v_i(\mathbf{r}_1, \mathbf{r}_2) \rho(\mathbf{r}_2) Y_l^{m*}(\mathbf{r}_2) d^3r_2 \\ &\equiv \sum_{l,m} Y_l^m(\mathbf{r}_1) U_{lm}(\mathbf{r}_1). \end{aligned} \quad (8-95)$$

In phenomenological nuclear calculations, the one-body potential U is taken to consist of a spherically symmetric part U_0 and a quadrupole part U_2 , which provides the deformed field (see Sections 9-6 and 9-8). The dipole $l = 1$ term can connect only states of opposite parity (belonging thus in different major shells), and as such is not important. Occasionally, even some higher multipole terms like $l = 4$ are included in the deformed field U (see Eq. 9-170). Even then, it is clear that the average deformed one-body potential U does not take any account of the higher multipoles of the effective interaction $V(|\mathbf{r}_1 - \mathbf{r}_2|)$ in Eq. 8-94, which are thus left as part of a residual interaction rich in high-multipole components. Now a delta function is also rich in high multipoles, as can be seen from the expansion

$$\delta(\mathbf{r}_{12}) = \sum_l \frac{2l+1}{4\pi r_{12}^2} \delta(r_1 - r_2) P_l(\cos \theta_{12}). \quad (8-96)$$

Because of this common property, the residual interaction containing the higher multipoles may be thought of as a delta-function-like potential with an attractive strength, thus giving rise to pairing. It should be emphasized that the short-range repulsive part of the free two-body interaction has already been accounted for in the wound of the relative wave function and has nothing to do with pairing. It is the residual attractive effective interaction, which is rich in high multipoles and in this respect is analogous to a delta-function type of potential, which gives rise to pairing.

In a many-body problem with the schematic residual interaction 8-93 responsible for pairing, we may write the Hamiltonian as

$$H = \sum_v e_v a_v^+ a_v - G \sum_{\mu, \nu > 0} a_\mu^+ a_\mu^- + a_\nu^+ a_\nu^- \quad (8-97)$$

in the second-quantized notation; here the e_v 's are the single-particle energies of the nucleons in an average potential U , and the two-body residual interaction term containing G acts in a narrow band of states around the Fermi surface. In nuclear matter, μ stands for the state (\mathbf{k}_i, \uparrow) and $\bar{\mu}$ for its conjugate $(-\mathbf{k}_i, \downarrow)$. In calculations of practical concern, however, we deal with finite nuclei; in a spherical-potential well μ stands for the quantum numbers n, l, j, m , with $\mu > 0$ meaning[†] $m > 0$. For convenience, we suppress the quantum numbers n and l , and examine under what approximations a general Hamiltonian of the form (see Eq. C-29)

[†] For the quantum numbers in a deformed well, see Eq. 9-162; in this case $\mu > 0$ means $\Omega > 0$.

$$H = \sum_{j,m} e_j a_{jm}^+ a_{jm} + \frac{1}{2} \sum_{j_1, j_2, j'_1, j'_2, m_1, m_2} \langle j_1 m_1, j_2 m_2 | V_{12} | j'_1 m'_1, j'_2 m'_2 \rangle a_{j_1 m_1}^+ a_{j_2 m_2}^+ a_{j'_1 m'_1} a_{j'_2 m'_2} \quad (8-98)$$

reduces to the schematic form 8-97. We can write, using Eq. A-33,

$$|j_1' m_1', j_2' m_2'\rangle = \sum_J (j_1' j_2' m_1' m_2' | JM) |(j_1' j_2') JM\rangle.$$

We saw that in nuclear matter pairing is important for nucleons coupled to $K = 0$; we now assume that in finite nuclei the pairing matrix elements are finite only for nucleons coupled to $J = 0$. The experimental evidence for this will be discussed presently. Thus, taking only the $J = 0$ term in the above sum, we obtain

$$\langle j_1' m_1', j_2' m_2' \rangle_{J=0} = \frac{(-)^{j'-m'}}{\sqrt{2j'+1}} \delta_{j_1' j_2'} \delta_{m_1' -m_2'} |(j' j') 00\rangle.$$

Making a similar decomposition for $\langle j_1 m_1, j_2 m_2 |$, we may write for Eq. 8-98

$$H = \sum_j e_j a_{jm}^+ a_{jm} + \frac{1}{2} \sum_{j, j', m} \frac{\langle (jj) 00 | V_{12} | (j' j') 00 \rangle}{\sqrt{(2j+1)(2j'+1)}} \\ \cdot a_{jm}^+ (-)^{j-m} a_{j-m}^+ (-)^{j-m'} a_{j'-m'} a_{j'-m'}^+$$

If we now put

$$-G = \frac{\langle (jj) 00 | V_{12} | (j' j') 00 \rangle}{\sqrt{(j+\frac{1}{2})(j'+\frac{1}{2})}}, \quad (8-99)$$

$$a_u^+ \equiv a_{jm}^+, \quad a_{\bar{\mu}}^+ \equiv (-)^{j-m} a_{j-m}^+, \\ a_v \equiv a_{j'm'}^+, \quad a_{\bar{\nu}} \equiv (-)^{j'-m'} a_{j'-m'}^+,$$

we obtain Eq. 8-97, where $\mu, \nu > 0$ indicates that the sum over m and m' are taken over positive values only. It is clear from Eq. 8-99 that actually G should depend on the orbitals j, j' ; for simplicity in calculation, however, an average constant value of G over a band of states near the Fermi surface is chosen, so that it may be taken outside the summation sign. Note that the Hamiltonian 8-97 is a schematic representation of a residual interaction which is rich in high multipoles and is rather weak; it therefore can scatter nucleon pairs only in a narrow band around the unperturbed Fermi sea. Thus the sum over the states μ and ν in Eq. 8-97 includes only a limited number of states over the Fermi sea for which G is nonzero. In typical calculations, the value of G is adjusted to restrict the sum over an energy

band of about $1.5 \hbar\omega$ on either side of the Fermi energy, where $\hbar\omega$ is the shell spacing.

We shall now try to construct a trial wave function for the superconducting ground state $|\Psi_0\rangle$ of the schematic Hamiltonian 8-97. Note that the residual interaction is such as to cause scattering of pairs (v, \bar{v}) coupled to $K = 0$ (or $J = 0$ in finite geometry) to other conjugate states $(\mu, \bar{\mu})$. Consequently, we should not use a trial wave function as one in which each pair state is definitely occupied or definitely empty, since the pairs could not scatter and lower the energy in that case. Rather, we should introduce an amplitude, say V_μ , that the orbitals $(\mu, \bar{\mu})$ are occupied in $|\Psi_0\rangle$, and consequently an amplitude $U_\mu = (1 - V_\mu^2)^{1/2}$ that the orbitals $(\mu, \bar{\mu})$ are empty. Since a large number of scatterings in and out of a given pair state $(\mu, \bar{\mu})$ are taking place, the amplitudes V_μ and U_μ describe the average rather than the instantaneous behavior.

Consider the state $(U_\mu + V_\mu a_\mu^+ a_{\bar{\mu}}^-)|0\rangle$, where $|0\rangle$ denotes the vacuum containing no nucleons. This describes the situation in which the pair state $(\mu, \bar{\mu})$ is occupied with probability V_μ^2 , and is empty with probability U_μ^2 . Bardeen, Cooper, and Schrieffer [44] approximated the ground state $|\Psi_0\rangle$ by a trial wave function $|\text{BCS}\rangle$, in which they assumed that the occupancies of the different pair states are uncorrelated, that is,

$$|\text{BCS}\rangle = \prod_{\mu>0} (U_\mu + V_\mu a_\mu^+ a_{\bar{\mu}}^-)|0\rangle. \quad (8-100)$$

In order to find the lowest-energy state with this form of wave function, we must take U_μ and V_μ to minimize $\langle \text{BCS}|H|\text{BCS}\rangle$. But note that the wave function $|\text{BCS}\rangle$ does not describe a state with a fixed number of nucleons; rather it is an admixture of states with different numbers of nucleons, a price that must be paid for its simplicity. We should therefore find the energy minimum subject to the condition that the mean particle number has the desired value N , that is, $\langle \text{BCS}|\hat{N}|\text{BCS}\rangle = N$, where $\hat{N} = \sum_v a_v^+ a_v$. This means that we must introduce a Lagrange multiplier λ and adjust the coefficients U_μ and V_μ in the trial wave function (Eq. 8-100) to minimize the expectation value of $\langle \text{BCS}|H'|\text{BCS}\rangle$, where

$$H' = \sum_v (e_v - \lambda) a_v^+ a_v - G \sum_{\mu, v>0} a_\mu^+ a_{\bar{\mu}}^- a_v^+ a_v. \quad (8-101)$$

In order to evaluate this expectation value, it is most convenient to introduce the so-called Bogolyubov-Valatin transformation [45, 46]:

$$a_\mu^+ = U_\mu a_\mu^+ - V_\mu a_{\bar{\mu}}^-, \quad a_\mu = U_\mu a_\mu - V_\mu a_{\bar{\mu}}^+. \quad (8-102a)$$

These are unitary transformations, so that the anticommutation relations between the new operators a_μ, a_v^+ are the same as those of fermions (not that $U_\mu^2 + V_\mu^2 = 1$),

$$\{a_\mu, a_v^+\} = \delta_{\mu\nu}, \quad \{a_\mu, a_v\} = \{a_\mu^+, a_v^+\} = 0.$$

Note that it follows from Eq. 8-102a that

$$a_\mu^+ = U_\mu a_\mu^+ + V_\mu a_\mu, \quad a_{\bar{\mu}}^- = U_\mu a_{\bar{\mu}}^- + V_\mu a_\mu^+, \quad (8-102b)$$

as may be easily verified in the spherical representation, where $a_\mu \equiv a_{j,m}$, $a_{\bar{\mu}}^- \equiv (-)^{j-m} a_{j,-m}$. It is much simpler to work with the transformed creation and annihilation operators a_μ^+, a_μ (called quasiparticle operators), since the trial wave function $|\text{BCS}\rangle$ is a quasiparticle vacuum, that is,

$$a_\mu |\text{BCS}\rangle = 0 \quad \text{for all } \mu. \quad (8-103)$$

It is clear in Appendix C (see Eq. C-33) that in the independent-particle model the sharp Fermi surface behaves like a vacuum to particle and hole operators; from Eq. 8-103 we note that this simplicity of the independent-particle model is regained by working with quasi-particle operators a_μ on the state $|\text{BCS}\rangle$, although this is not a determinantal state. Obviously, the wave function $a_\mu^+ |\text{BCS}\rangle$ represents a state with a single quasiparticle in orbital μ . Such a quasiparticle, quite literally, is a mixture of a particle state μ , with amplitude U_μ , and a hole state $\bar{\mu}$, with amplitude V_μ . It follows that, deep inside the Fermi sphere, a quasiparticle is simply a hole, while far above the Fermi surface it is a particle.

In order to work out explicitly the expectation value $\langle \text{BCS}|H'|\text{BCS}\rangle$, we need the inverse relations of Eq. 8-102a, which are

$$a_\mu = U_\mu a_\mu + V_\mu a_{\bar{\mu}}^+, \quad a_{\bar{\mu}}^- = U_\mu a_{\bar{\mu}}^- - V_\mu a_\mu^+, \quad (8-102c)$$

and the corresponding Hermitian relations for the creation operators $a_\mu^+, a_{\bar{\mu}}^+$. Using Eqs. 8-102 and 8-103, we can now easily calculate the expectation value of the first term in H' , that is,

$$\begin{aligned} \langle \text{BCS} | \sum_v (e_v - \lambda) a_v^+ a_v | \text{BCS} \rangle &= \sum_{v>0} (e_v - \lambda) \langle \text{BCS} | a_v^+ a_v + a_{\bar{v}}^+ a_{\bar{v}}^+ | \text{BCS} \rangle \\ &= 2 \sum_{v>0} (e_v - \lambda) V_v^2. \end{aligned} \quad (8-104)$$

In evaluating the expectation value of the two-body interaction term in H' with respect to $|\text{BCS}\rangle$, we can use Wick's theorem (Appendix C), which states that in such a case only the fully contracted terms may contribute to the expectation value. Thus

$$\begin{aligned} & \sum_{\mu, \nu > 0} \langle \text{BCS} | a_\mu^+ a_\mu^- + a_\nu^+ a_\nu^- | \text{BCS} \rangle \\ &= \sum_{\mu, \nu > 0} \{ \langle a_\mu^+ a_\mu^- \rangle \langle a_\nu^+ a_\nu^- \rangle + \langle a_\mu^+ a_\nu^- \rangle \langle a_\mu^- a_\nu^+ \rangle - \langle a_\mu^+ a_\nu^- \rangle \langle a_\mu^- a_\nu^+ \rangle \}, \quad (8-105) \end{aligned}$$

where the $\langle \rangle$ denote the expectation value with respect to the state $|\text{BCS}\rangle$. A little algebra, making use of Eq. 8-103 and the anticommutation relations, would show that the last term on the right-hand side of Eq. 8-105 vanishes, and that

$$\sum_{\mu, \nu > 0} \langle \text{BCS} | a_\mu^+ a_\mu^- + a_\nu^+ a_\nu^- | \text{BCS} \rangle = (\sum_{\nu > 0} U_\nu V_\nu)^2 + \sum_{\nu > 0} V_\nu^4.$$

Combining this result with Eq. 8-104, we finally obtain

$$\langle \text{BCS} | H' | \text{BCS} \rangle = \sum_{\nu > 0} [2(e_\nu - \lambda)V_\nu^2 - GV_\nu^4] - G(\sum_{\nu > 0} U_\nu V_\nu)^2. \quad (8-106)$$

We now impose the condition

$$\frac{\partial}{\partial V_\nu} \langle \text{BCS} | H' | \text{BCS} \rangle = 0,$$

which immediately yields

$$4(e_\nu - \lambda)V_\nu - 4GV_\nu^3 - 2G(\sum_{\mu > 0} U_\mu V_\mu) \left(U_\nu + V_\nu \frac{\partial U_\nu}{\partial V_\nu} \right) = 0.$$

Noting, from the normalization condition $U_\nu^2 + V_\nu^2 = 1$, that $V_\nu(\partial U_\nu / \partial V_\nu) = -V_\nu^2/U_\nu$, and simplifying, we obtain the equation

$$2(e_\nu - \lambda)U_\nu V_\nu = \Delta(U_\nu^2 - V_\nu^2), \quad (8-107)$$

where

$$e'_\nu = e_\nu - GV_\nu^2, \quad \Delta = G \sum_{\mu > 0} U_\mu V_\mu. \quad (8-108)$$

Note that e'_ν is the renormalized single-particle energy in the orbital ν , which includes the contribution $-GV_\nu^2$ of the pairing interaction to the one-body field. By squaring Eq. 8-107 and making use of the relation $U_\nu^4 + V_\nu^4 = 1 - 2U_\nu^2V_\nu^2$, we obtain

$$U_\nu^2 V_\nu^2 = \frac{\Delta^2}{4[(e'_\nu - \lambda)^2 + \Delta^2]} = \frac{1}{4} \left[1 - \frac{(e'_\nu - \lambda)^2}{(e'_\nu - \lambda)^2 + \Delta^2} \right]. \quad (8-109)$$

A little algebra will now yield the important relations

$$U_\nu^2 = \frac{1}{2} \left[1 + \frac{e'_\nu - \lambda}{\sqrt{(e'_\nu - \lambda)^2 + \Delta^2}} \right] \quad \text{and} \quad (8-110)$$

$$V_\nu^2 = \frac{1}{2} \left[1 - \frac{e'_\nu - \lambda}{\sqrt{(e'_\nu - \lambda)^2 + \Delta^2}} \right].$$

Two more equations may be written down in a neat form to solve for the parameters Δ and λ , starting from the Hamiltonian 8-97. The first can be obtained by substituting for $U_\nu V_\nu$ from Eq. 8-109 into Eq. 8-108, giving

$$\frac{1}{G} = \frac{1}{2} \sum_{\nu > 0} \frac{1}{\sqrt{(e'_\nu - \lambda)^2 + \Delta^2}}. \quad (8-111)$$

The other equation is simply a statement of the condition that the mean number of particles is N :

$$N = 2 \sum_{\nu > 0} V_\nu^2 = 2 \sum_{\nu > 0} \left[1 - \frac{e'_\nu - \lambda}{\sqrt{(e'_\nu - \lambda)^2 + \Delta^2}} \right]. \quad (8-112)$$

Note the similarity of Eq. 8-111 and the Cooper formula 8-88; as before, we can expect an energy gap in the excitation spectrum of the nucleus. For a given choice of G and the single-particle spectrum, the coupled equations 8-111 and 8-112 have to be solved for λ and Δ .

Note, from Eq. 8-106, that the ground-state energy is given by

$$\langle \text{BCS} | H | \text{BCS} \rangle = \sum_{\nu > 0} 2e'_\nu V_\nu^2 - \frac{\Delta^2}{G} - G \sum_{\nu > 0} V_\nu^4, \quad (8-113)$$

which reduces, for $G = 0$, to a sum over occupied single-particle energies, which is different from the self-consistent Hartree-Fock result (Eq. 10-21).

It is clear from Eq. 8-100 that the wave function $|\text{BCS}\rangle$ represents an admixture of states with an even number of particles of one kind; the constraint is therefore made that the mean number $N = 2 \sum_{\nu > 0} V_\nu^2$ is even. The $|\text{BCS}\rangle$ state may be regarded as an average of the wave functions of a few neighboring nuclides with particle numbers $N, N - 2, N + 2, \dots$. However, for large N , the spread $\langle \text{BCS} | (\hat{N} - N)^2 | \text{BCS} \rangle$ is small, and the contribution of the desired nuclide N is predominant. With this limitation, the state $|\text{BCS}\rangle$ represents the ground state of an even-even nucleus, and it is a quasi-particle vacuum.

To see the structure of excited states, it is useful to express the particle-number operator \hat{N} in terms of quasiparticle operators by using Eq. 8-103. A little algebra yields

$$\hat{N} = \sum_{\nu>0} [2V_\nu^2 + \hat{\mathcal{N}}_\nu(U_\nu^2 - V_\nu^2) + 2U_\nu V_\nu(\alpha_\nu^+ \alpha_\nu^- + \alpha_\nu^- \alpha_\nu^)], \quad (8-114)$$

where $\hat{\mathcal{N}}_\nu = (\alpha_\nu^+ \alpha_\nu^- + \alpha_\nu^- \alpha_\nu^+)$. Consider now the one quasiparticle state $\alpha_\mu^+ |\text{BCS}\rangle$. Since $\langle \text{BCS} | \hat{N} | \text{BCS} \rangle = N$, it follows from Eq. 8-114 that

$$\langle \text{BCS} | \alpha_\mu^+ \hat{N} \alpha_\mu^+ | \text{BCS} \rangle = N + (U_\mu^2 - V_\mu^2) = N + 1 - 2V_\mu^2.$$

If the state μ is far above the Fermi sea, V_μ^2 is negligible and the expectation value is just $N + 1$. In this situation, the state $\alpha_\mu^+ |\text{BCS}\rangle$ represents an odd nucleus. A state with two quasiparticle excitations, $\alpha_\mu^+ \alpha_\mu^- |\text{BCS}\rangle$, yields the expectation value of \hat{N} as

$$N + 2(U_\mu^2 - V_\mu^2) = N + 2 \left[\frac{e_\mu' - \lambda}{\sqrt{(e_\mu' - \lambda)^2 + \Delta^2}} \right].$$

Only if e_μ is close to λ is this N ; at the other extreme, with $(e_\mu - \lambda) \gg \Delta$, it is $N + 2$. Consequently, the low-lying intrinsic states of even-even nuclei are double quasiparticle excitations. Triple quasiparticle excitations are rather high excited states of odd- A nuclei.

The energy of a quasiparticle can be calculated by evaluating the quantity $\langle \text{BCS} | (\alpha_\nu H \alpha_\nu^+) - H | \text{BCS} \rangle$, which turns out to be

$$E_\nu = \sqrt{(e_\nu' - \lambda)^2 + \Delta^2}. \quad (8-115)$$

As we have seen, for an even-even nucleus, the ground state is a quasiparticle vacuum, while the first excited state must have at least two quasiparticles present, say in orbitals ν and ν' . Thus the excitation energy of the first excited state in an even-even nucleus is $E_\nu + E_{\nu'} \geq 2\Delta$. This is so because in the BCS approximation the quasiparticles are noninteracting. There is thus an energy gap of at least 2Δ between the ground state and the first excited state. We should point out that we are here considering the first excited state of an intrinsic (as opposed to collective) nature; a coherent combination of these two-quasiparticle intrinsic states may, of course, give rise to a collective excitation (like the first 2^+ state in a near-spherical nucleus) at an energy lower than 2Δ . In a nucleus containing an odd number of particles, however, the ground state already contains a quasiparticle in an orbital ν (say), and an excited state may be obtained by changing this orbital to ν' , so that the excitation energy is simply $E_\nu - E_{\nu'}$, with no gap in the energy spectrum.

In the absence of pairing, it is clear from Eq. 8-108 that Δ vanishes, with U_ν and V_ν becoming 0 and 1, respectively, if $e_\nu < \lambda$, and 1 and 0 if $e_\nu > \lambda$. In other words, in the absence of pairing, λ is the sharp Fermi surface of the independent-particle model. The presence of the pairing force, however,

"smears" the Fermi level; particle states ν such that $|e_\nu - \lambda| \gg \Delta$ are still almost completely full or completely empty, but states with $|e_\nu - \lambda| \sim \Delta$ are only partially occupied. In this sense, λ is an average Fermi level. More precisely, since it is the Lagrange multiplier of the number operator, it is the chemical potential of the system.

From Eq. 8-111 it is clear that, if the pairing strength G is so small that

$$\frac{G}{2} \sum_{\nu>0} \frac{1}{|e_\nu' - \lambda|} < 1, \quad (8-116)$$

no real solution for Δ can be found from the gap equation. One would suspect from the Cooper pair problem, however, that a gap should exist no matter how weak G is (as long as the pairing interaction is attractive), provided there are pairs in an unfilled shell. The accuracy of the BCS solution may be tested in an exactly solvable two-level model [47], in which the two levels, each of degeneracy η , are separated by an energy $\hbar\omega$. In the symmetric model, the number of particles is η , so that in the absence of interaction the lower level is completely filled. The chemical potential λ is halfway between the two levels, so that $|e_\nu' - \lambda| = \frac{1}{2}\hbar\omega$ for all ν . It is clear from Eq. 8-116, then, that no gap would be found in the BCS solution for $G \leq G_c$, where

$$\frac{G_c}{2} \cdot 2\eta \frac{2}{\hbar\omega} = 1, \quad \text{or} \quad G_c = \frac{\hbar\omega}{2\eta}. \quad (8-117)$$

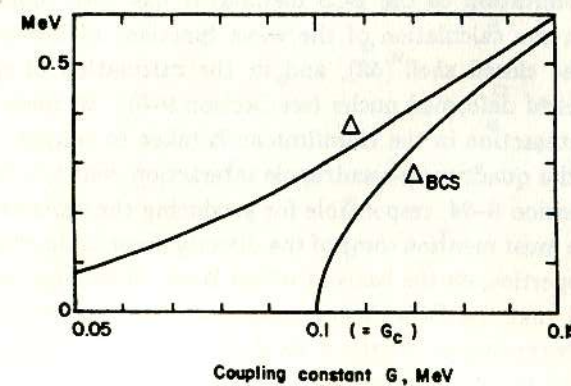


Fig. 8-16 Behavior of the BCS and the "exact" solutions for the gap parameter as a function of the coupling constant G in the symmetric two-level model. The degeneracy factor $\eta = 5$, and the level spacing $\hbar\omega = 1$ MeV here. (After Nogami [49].)

The calculated gap in the BCS approximation, Δ_{BCS} , for $\eta = 5$ and $\hbar\omega = 1$ MeV is shown in Fig. 8-16; it will be seen that this vanishes at $G_c = 0.1$ MeV, in agreement with Eq. 8-117. The inaccuracy in the BCS solution is due to the particle number fluctuation in the wave vector $|\text{BCS}\rangle$. Ideally, one should project out from this state the component with N particles and then solve the variational problem with respect to V_v^2 , a very complicated procedure [48]. Nogami and his coworkers [49] have devised a simpler technique of suppressing the number fluctuations in $|\text{BCS}\rangle$, and the Δ calculated by their method (which is very close to the exact value) is also shown in Fig. 8-16. It will be seen that Δ approaches zero smoothly as $G \rightarrow 0$, in contrast to Δ_{BCS} .

We should emphasize that our discussion in this section has been based on the physical picture of pairs of nucleons, coupled to $J = 0$, being scattered by the pairing interaction, resulting in a depression of the $J = 0$ ground state from all the other excited states. This is true for pairs interacting in the i -spin $T = 1$ state; for example, the two valence neutrons in the $d_{5/2}$ -shell in ^{18}O form a $0^+, T = 1$ ground state (see Chapter 10). However, for a $n-p$ pair, there is a strong attractive interaction in the $T = 0$ state too. The situation is complicated by the fact that two nucleons in a j -shell with $T = 0$ may form only angular-momentum states $1^+, 3^+, 5^+, \dots$ (Problem 10-1), and several of these states may occur in energy near the $J = 0, T = 1$ paired state. The formalism developed in this section is thus applicable directly to pairing between $n-n$ and $p-p$ pairs, but not $n-p$ pairs. This is a serious limitation of the method. Various attempts have been made to incorporate $n-p$ pairing in a more general formalism, and Lane [50] and Rowe [51] review these methods. Despite this limitation of the BCS method, it has been highly successful, particularly in the calculation of the wave functions of low-lying states of nuclei with one closed shell [52], and in the calculation of the potential-energy surfaces of deformed nuclei (see Section 9-6). In these calculations, the residual interaction in the Hamiltonian is taken to consist of the pairing interaction and a quadrupole-quadrupole interaction, which is the $l = 2$ part of V_{12} in expansion 8-94, responsible for producing the deformed field.

Finally, we must mention some of the directly observable effects of pairing on nuclear properties, on the basis of which Bohr, Mottelson, and Pines [53] first suggested that the BCS theory of metallic superconductivity could be applied to nuclear physics. Figure 8-17 shows a plot of the energy of the first excited *intrinsic* state of stable nuclei against the mass number A . In this plot, we have not included the low-lying collective excited states of rotational or vibrational nature, and that is why the term *intrinsic* is used. It will be seen that there is an energy gap of at least 900 keV in the intrinsic excitation

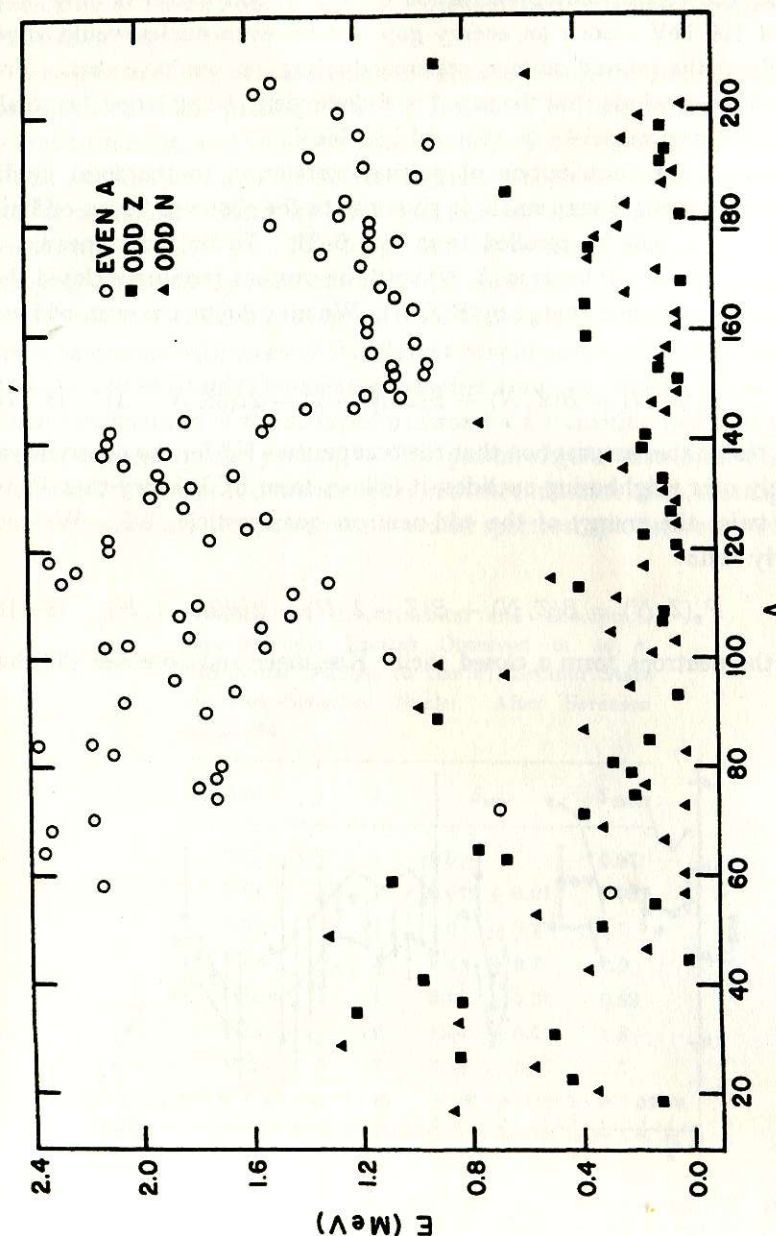


Fig. 8-17 The energy of the first excited *intrinsic* state of stable nuclei. (After Bes and Sorensen [55].)

of even-even nuclei, and the gap is in fact much larger for lighter nuclei. In contrast, the corresponding excitation energy in odd nuclei is only of the order of 100 keV. Such an energy gap in even-even nuclei would appear naturally if the ground state is superconducting, as we have seen. From Fig. 8-17 we conclude that the gap Δ is A -dependent, being larger for smaller A and for heavy nuclei ($A > 140$), $2\Delta \gtrsim 1$ MeV.

Although the contribution of pairing correlation to the total binding energy of a nucleus is very small, it gives rise to the observed "even-odd mass difference," as will be recalled from Eq. 6-21. To be more specific, we consider an even-even nucleus (Z, N) with the protons forming a closed shell, and denote its binding energy by $B(Z, N)$. We may define the even-odd mass difference by

$$P_n(Z, N) = B(Z, N) + B(Z, N - 2) - 2B(Z, N - 1). \quad (8-118a)$$

On the reasonable assumption that the occupancies V_v^2 for the neutrons vary smoothly over neighboring nuclides, it follows from BCS theory that P_n just equals twice the energy of the odd-neutron quasiparticle, $2E_v$. We could similarly define

$$P_p(Z, N) = B(Z, N) + B(Z - 2, N) - 2B(Z - 1, N), \quad (8-118b)$$

where the neutrons form a closed shell. Kisslinger and Sorensen [52] have

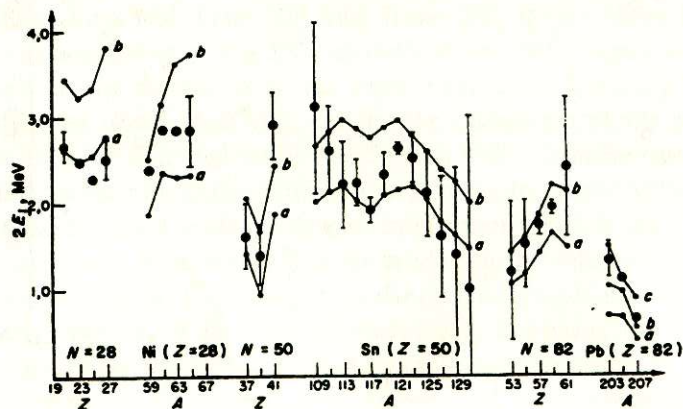


Fig. 8-18 The heavy dots with error bars show the experimental even-odd mass differences P_n or P_p , defined by Eq. 8-118. The little dots are theoretical points, corresponding to twice the energy of the lowest-lying quasiparticle for the odd- A isotopes. Curves *a* and *b* correspond to $G = 19/A$ and $23/A$, respectively, while curve *c*, for lead only, corresponds to $G = 30/A$. (After Kisslinger and Sorensen [52].)

compared the experimental quantities P_n and P_p with the corresponding predictions of the BCS calculation for various choices of G , and this comparison is shown in Fig. 8-18.

The partial filling of states near the Fermi level is one of the most important consequences of the pairing force. It is similar in many ways to interconfiguration mixing, and will have the same type of effects on the energy levels in odd nuclides and also on electromagnetic moments, transition rates, and nuclear reactions. Here we shall mention an experiment which directly measures U_v^2 and V_v^2 . The (d, p) and (d, t) reactions are, respectively, stripping and pick-up reactions in which a deuteron loses and picks up a neutron when it strikes a heavier nucleus. Consider, for example, the deuteron stripping process with an even-even target of spin parity 0^+ . The conservation of parity and of angular momentum requires a unique value, l , for the orbital angular momentum of the stripped neutron for a transition to a final state of angular momentum and parity j, π . The proton angular distribution fixes the l -value and thus helps to determine the j, π of the final state. Also, the magnitude of the cross section determines the so-called spectroscopic factor, which is the

TABLE 8-9 Experimental and Theoretical Spectroscopic Factors Observed in (d, p) Reactions Leading to the 0^+ Ground State of Near-Spherical Nuclei. After Sorensen et al. [54].

Target	j	l	S_{exp}	S_{theor}
^{53}Cr	$\frac{3}{2}$	1	0.91	0.97
^{57}Fe	$\frac{1}{2}$	1	0.072 ± 0.01	0.067
^{61}Ni	$\frac{3}{2}$	1	2.0 ± 0.3	1.7
^{67}Zn	$\frac{5}{2}$	3	2.2 ± 0.3	2.9
^{77}Se	$\frac{1}{2}$	1	0.68 ± 0.01	0.83
^{91}Zr	$\frac{5}{2}$	2	1.44 ± 0.21	1.6
^{95}Mo	$\frac{5}{2}$	2	2.48 ± 0.37	2.7
$^{99,101}\text{Ru}$	$\frac{5}{2}$	2	2.74 ± 0.4	3.3
^{105}Pd	$\frac{5}{2}$	2	1.74 ± 0.25	2.8
^{115}Sn	$\frac{1}{2}$	0	1.08 ± 0.16	1.03
^{117}Sn	$\frac{1}{2}$	0	1.4 ± 0.2	1.2
^{119}Sn	$\frac{1}{2}$	0	1.3 ± 0.2	1.4
^{125}Te	$\frac{1}{2}$	0	1.2 ± 0.3	0.99

fraction of the "even 0^+ state plus neutron" in the final-state wave function. In this example, the cross section should be proportional to the probability of an even nucleus picking up a neutron in state j, m , which is determined by the probability that this state is vacant, that is, by U_j^2 . As another example, if the (d, p) reaction from the j -state of an odd target (Z even, N odd) is studied, for example, $^{53}\text{Cr}(d, p)^{54}\text{Cr}$, the cross section is proportional to V_j^2 .

In Table 8-9, we compare the theoretical and experimental occupation factors $S = (2j + 1)V_j^2$ observed in deuteron stripping leading to the 0^+ ground state of near-spherical nuclei [54]. The theoretical numbers are determined from a BCS calculation, using the pairing plus quadrupole model of Kisslinger and Sorensen [52], and a small correction in S is included because of the small admixture of collective components in the odd- A ground state. More examples of nuclear reactions (including two-nucleon transfer) in which pairing is important are given by Bes and Sorensen [55].

Finally, we shall see in Section 10-8 that in microscopic calculations of the collective inertial parameters of a deformed nucleus the pairing interaction plays a very important role.

REFERENCES

1. H. A. Bethe, *Ann. Rev. Nucl. Sci.* **21**, 93 (1971).
2. D. W. L. Sprung, *Advan. Nucl. Phys.* **5**, 225 (1972).
- References 1 and 2 are comprehensive reviews of the theory both of nuclear matter and of finite nuclei.
3. B. H. Brandow, unpublished thesis, Cornell University, 1964.
4. L. C. Gomes, J. D. Walecka, and V. F. Weisskopf, *Ann. Phys. (N.Y.)* **3**, 241 (1958); An *anschaulich* presentation of the basic principles of nuclear-matter calculations.
5. H. A. Bethe and J. Goldstone, *Proc. Roy. Soc. (London)* **A238**, 551 (1957); J. Goldstone, *Proc. Roy. Soc. (London)* **A239**, 267 (1957).
6. B. D. Day, *Rev. Mod. Phys.* **39**, 719 (1967).
7. H. A. Bethe, *Phys. Rev.* **B138**, 804 (1965); L. D. Faddeev, *Zh. Eksp. Teor. Fiz.* **39**, 1459 (1960), and *Dokl. Acad. Nauk S.S.R.* **138**, 565 (1961); English translation, *Sov. Phys. JETP* **12**, 1014 (1961), and *Dokl. 6*, 384 (1962); R. Rajaraman and H. A. Bethe, *Rev. Mod. Phys.* **39**, 745 (1967).
8. H. A. Bethe, B. H. Brandow, and A. G. Petschek, *Phys. Rev.* **129**, 225 (1963).
9. T. K. Dahlblom, *Acta Acad. Aboensis* **B29**, 6 (1969); T. K. Dahlblom, K. G. Fogel, B. Qvist, and A. Törn, *Nucl. Phys.* **56**, 177 (1964); B. D. Day, *Phys. Rev.* **187**, 1269 (1969).
10. B. D. Day, *Phys. Rev.* **151**, 826 (1966).
11. K. A. Brueckner and C. A. Levinson, *Phys. Rev.* **97**, 1344 (1955); K. A. Brueckner, *Phys. Rev.* **97**, 1353 (1955), and **100**, 36 (1955); K. A. Brueckner and J. L. Gammel, *Phys. Rev.* **109**, 1023 (1958).

References

12. B. H. Brandow, *Phys. Rev. Lett.* **22**, 173 (1969); *Ann. Phys. (N.Y.)* **57**, 214 (1970).
13. R. L. Becker, *Phys. Rev. Lett.* **24**, 400 (1970).
14. M. I. Haftel and F. Tabakin, *Nucl. Phys.* **A158**, 1 (1970).
15. M. A. Preston and R. K. Bhaduri, *Phys. Lett.* **6**, 193 (1963); *Can. J. Phys.* **42**, 696 (1964).
16. P. J. Siemens, *Nucl. Phys.* **A141**, 225 (1970).
17. P. Grangé and M. A. Preston, *Nucl. Phys.* **A204**, 1 (1973).
18. P. K. Banerjee and D. W. L. Sprung, *Can. J. Phys.* **49**, 1899 (1971).
19. P. Grangé and M. A. Preston, *Phys. Lett.* **42B**, 35 (1972).
20. F. Calogero and Yu. A. Simonov, *Nuovo Cimento* **B64**, 337 (1969); *Phys. Rev. Lett.* **25**, 881 (1970); *Lett. Nuovo Cimento* **4**, 219 (1970).
21. C. Michael and C. Wilkin, *Nucl. Phys.* **B11**, 99 (1969).
22. I. R. Afnan, D. M. Clement, and F. J. D. Serduke, *Nucl. Phys.* **A170**, 625 (1971).
23. A. M. Green, T. K. Dahlblom, and T. Kouki, *Nucl. Phys.* **A209**, 52 (1973).
24. B. H. J. McKellar and R. Rajaraman, *Phys. Rev. C3*, 1877 (1971).
25. B. A. Loiseau, Y. Nogami, and C. K. Ross, *Nucl. Phys.* **A165**, 601 (1971).
26. G. E. Brown, A. D. Jackson, and T. T. S. Kuo, *Nucl. Phys.* **A133**, 481 (1969).
27. J. W. Negele and D. Vautherin, *Nucl. Phys.* **A207**, 321 (1973).
28. J. Nemeth and D. W. L. Sprung, *Phys. Rev.* **176**, 1496 (1968).
29. J. R. Buchler and L. Ingber, *Nucl. Phys.* **A170**, 1 (1971).
30. S. L. Schlenker and E. L. Lomon, *Phys. Rev. C3*, 1487 (1971).
31. V. R. Pandharipande, *Nucl. Phys.* **A174**, 641 (1971).
32. M. Miller, C. W. Woo, J. W. Clark, and W. J. TerLouw, *Nucl. Phys.* **A184**, 1 (1972).
33. P. Grangé and M. A. Preston, *Nucl. Phys.* **A219**, 266 (1974).
34. K. T. R. Davies and R. J. McCarthy, *Phys. Rev. C4*, 81 (1971).
35. K. T. R. Davies, R. J. McCarthy, and P. U. Sauer, *Phys. Rev. C6*, 1461 (1972).
36. K. A. Brueckner, J. L. Gammel, and H. Weitzner, *Phys. Rev.* **110**, 431 (1958).
37. I. J. Donnelly, *Nucl. Phys.* **A111**, 201 (1968); R. K. Bhaduri and C. S. Warke, *Phys. Rev. Lett.* **24**, 1379 (1968); J. W. Negele, *Phys. Rev. C1*, 1260 (1970); P. Siemens, *Nucl. Phys.* **A141**, 225 (1970).
38. D. W. L. Sprung and P. K. Banerjee, *Nucl. Phys.* **A168**, 273 (1971); P. K. Banerjee and D. W. L. Sprung, *Can. J. Phys.* **49**, 1899 (1971); D. W. L. Sprung, *Nucl. Phys.* **A182**, 97 (1972).
39. X. Campi and D. W. L. Sprung, *Nucl. Phys.* **A194**, 401 (1972); J. W. Negele, ref. 37.
40. B. H. Brandow, *Rev. Mod. Phys.* **39**, 771 (1967).
41. L. N. Cooper, *Phys. Rev.* **104**, 1189 (1956).
42. E. Jakeman and S. A. Moszkowski, *Phys. Rev.* **141**, 933 (1966); S. Nagata and H. Bando, *Phys. Lett.* **11**, 153 (1964).
43. J. R. Schrieffer, 1972 Nobel lecture, reprinted in *Phys. Today*, **26**, 23 (1973).
44. J. Bardeen, L. N. Cooper, and J. R. Schrieffer, *Phys. Rev.* **108**, 1175 (1957).
45. N. N. Bogolyubov, *Nuovo Cimento* **7** (ser. 10), 794 (1958).
46. J. G. Valatin, *Nuovo Cimento* **7** (ser. 10), 843 (1958).
47. M. Rho and J. O. Rasmussen, *Phys. Rev.* **135**, B1295 (1964).
48. A. K. Kerman, R. D. Lawson, and M. H. Macfarlane, *Phys. Rev.* **124**, 162 (1961).
49. Y. Nogami, *Phys. Lett.* **15**, 335 (1965); H. C. Pradhan, Y. Nogami, and J. Law, *Nucl. Phys.* **A201**, 357 (1973).

50. A. M. Lane, *Nuclear Theory*, Benjamin, New York, 1964, p. 67.
 51. D. J. Rowe, *Nuclear Collective Motion*, Methuen, London, 1970, p. 202.
 52. L. S. Kisslinger and R. A. Sorensen, *K. Danske Vidensk. Selsk. Mat.-Fys. Medd.* 32, No. 9 (1960); *Rev. Mod. Phys.* 35, 853 (1963).
 53. A. Bohr, B. R. Mottelson, and D. Pines, *Phys. Rev.* 110, 936 (1958).
 54. R. A. Sorensen, E. D. Lin, and B. L. Cohen, *Phys. Rev.* 142, 729 (1966).
 55. D. R. Bes and R. A. Sorensen, *Advan. Nucl. Phys.* 2, 129 (1969).

PROBLEMS

8-1. In the text, in considering exclusion-principle correlations in ^{16}O , we defined a function F_2 as the ratio of the actual joint probability $P_F(1, 2)$ to the classical joint probability $P_{cl} = \rho(1)\rho(2)$. However, it would be useful to define the ratio of $P_F(1, 2)$ to the classical probability of finding both fermions at the same radius as their mass center, that is, $[\rho(\frac{1}{2}\mathbf{R})]^2$. Show that this quantity is

$$F_3(\mathbf{r}, \mathbf{R}) = \left(1 - \frac{\alpha^2 r^2}{2 + \alpha^2 R^2}\right)^2 \exp(-\frac{1}{2}\alpha^2 r^2).$$

8-2. There is a formula connecting the spherical Bessel function j_l with the harmonic-oscillator radial function R_{nl} . It is given in Problem 8-11b.

Consider like particles in ^{16}O , separated by a distance r with mass center at the position of maximum density in the nucleus and with (i) \mathbf{r} perpendicular to \mathbf{R} and (ii) \mathbf{r} at 45° to \mathbf{R} . Obtain the exclusion-principle correlations and consider how best to represent them by a careful choice of k_F in a function $F_1(k_F r)$, coming from nuclear matter.

8-3. Considering the derivation of Eq. 8-37, show that with

$$\Psi = \binom{A}{2}^{-1} \sum_{kl} \Psi_{kl}$$

it follows that

$$\langle \Psi | \Psi \rangle = \binom{A}{2}^{-1} \sum_{kl} \langle \psi_{kl} | \psi_{kl} \rangle.$$

Show further that in nuclear matter $\langle \psi_{kl} | \psi_{kl} \rangle$ is independent of k and l , and hence

$$\langle \Psi | \Psi \rangle = \langle \psi_{kl} | \psi_{kl} \rangle.$$

Note also that $\langle \Psi | \Phi_0 \rangle = 1$.

Establish that

$$\langle \Phi_0 | \sum v(i, j) | \Psi \rangle = \langle \Phi_0 | v(1, 2) | \sum \Psi_{kl} \rangle.$$

8-4. It is asserted in the caption to Fig. 8-8 that, by considering Eq. 8-41, one can show that the most frequently occupied intermediate state in nuclear matter lies near the maximum of the Fourier transform of $v(r)\zeta(r)$. Show that this is true.

8-5. Consider two G -matrices, G_A and G_B , one associated with potential v_A , Pauli operator Q_A , and energy denominator $e_A = H_{0A} - \omega_A$, and the other with v_B , Q_B , e_B . Define $\Omega = 1 - (Q/e)G$.

(a) Note that $\psi = \Omega\phi$.

$$(b) \quad G_A(\omega_A) = v_A - \frac{Q_A}{H_{0A} - \omega_A} G_A.$$

Show that G is Hermitian, given that v and H_0 are.

(c) Show that

$$G_A - G_B = \Omega_B^\dagger (v_A - v_B) \Omega_A - G_B \left(\frac{Q_A}{e_A} - \frac{Q_B}{e_B} \right) G_A.$$

(This is shown in Appendix A of ref. 8.)

(d) If $v_A = v_B$ and $Q_A = Q_B = Q = Q^2$, note that

$$G_A - G_B = G_B \frac{Q}{e_B} (e_A - e_B) \frac{Q}{e_A} G_A = (1 - \Omega_B^\dagger)(e_A - e_B)(1 - \Omega_A)$$

and show that

$$\left\langle \phi_{kl} \left| \frac{\partial G(\omega)}{\partial \omega} \right| \phi_{kl} \right\rangle = - \langle \zeta_{kl} | \zeta_{kl} \rangle.$$

(e) Indicate how this leads to the formula

$$P_k = \left(1 - \sum_l \left\langle \phi_{kl} \left| \frac{\partial G}{\partial \omega} \right| \phi_{kl} \right\rangle_A P_l \right)^{-1}$$

and discuss the usefulness of this formula in a Brueckner calculation. [See refs. 34 and 35 and R. J. McCarthy and K. T. R. Davies, *Phys. Rev.* C1, 1640 (1970).]

8-6. Deduce Eq. 8-59a; that is, starting with the antisymmetrized state ϕ_A in which two nucleons have momenta \mathbf{p}_a and \mathbf{p}_b and specified third components M_S and M_T of spin and i -spin, write it as in the text. You will want to use the angular-momentum expansion of the plane wave and also to introduce suitable complete sets of angular-momentum states.

8-7. In Eq. 8-76 we defined the incompressibility K for nuclear matter. In thermodynamics the isothermal compressibility is defined as

$$K_T^{\text{th}} = - \frac{1}{V} \left(\frac{\partial V}{\partial P} \right)_T,$$

where P , V , and T are the pressure, volume, and temperature, respectively, of the system. Also, the free energy is defined as $F = E - TS$, where E is the energy of the system and S is the entropy. The pressure is the rate of change of free energy with volume at constant temperature:

$$P = - \left(\frac{\partial F}{\partial V} \right)_T.$$

(a) Prove the equivalence of the two forms of K in Eq. 8-76 and show that still another form is

$$K = \left[r_0^2 \frac{\partial^2}{\partial r_0^2} \left(\frac{E}{A} \right) \right]_{\text{equil}},$$

where r_0 is a length (e.g., the radius of a sphere) specifying the volume per particle.

(b) For a zero-temperature system like the nucleus, prove that

$$P = \rho^2 \frac{\partial}{\partial \rho} \left(\frac{E}{A} \right)_{T=0},$$

which shows that the net pressure vanishes at equilibrium density. Hence show from the definition of isothermal compressibility that at equilibrium of a zero-temperature system

$$K_{T=0}^{\text{th}} = \left[\rho^3 \frac{\partial^2}{\partial \rho^2} \left(\frac{E}{A} \right) \right]_{\rho=\rho_{\text{sat}}}^{-1}.$$

Note that the nuclear physics definition of incompressibility is not very different from the reciprocal of the thermodynamic definition of compressibility; in fact,

$$\frac{1}{9} \rho K = \frac{1}{K_{T=0}^{\text{th}}}.$$

In thermodynamics, the name compressibility for K_T^{th} is a reasonable one; if K_T^{th} is numerically large, it signifies that the system is easily compressible. On the other hand, in nuclear physics, it is reasonable to call K the incompressibility. Nevertheless one does find K referred to in the literature as the compression modulus.

8-8. Consider a spherical nucleus of uniform density, and suppose that the density oscillates, each nucleon moving radially in and out. When the density is $\rho = \rho_0(1 + x)$, a particle that is a distance r from the center when the density is ρ_0 will have radial velocity $-\frac{1}{3}r\dot{x}$. Deduce that the kinetic energy associated with these oscillations is $\frac{1}{30}Mr_0^2 A^{5/3} \dot{x}^2$ and that the potential energy is $\frac{1}{16}AKx^2$, where M is the mass of a nucleon, r_0 is the constant in the $A^{1/3}$ -law for nuclear radius, and K is the incompressibility. Find the frequency of oscillation and show that, unless K is at least 120 MeV, there will be such oscillations at energies as low as 15 MeV in medium-mass nuclei.

8-9. Consider Eq. 8-29 for the motion of two nucleons in states k_1 , k_2 in nuclear matter. In this case, as discussed in the text, we may replace e_{k_1, k_2} by

$$e_{k_1} + e_{k_2} = \frac{\hbar^2}{2M} (k_1^2 + k_2^2) + U(k_1) + U(k_2).$$

In short-hand notation, we can write Eq. 8-29 as

$$G = v + v \frac{Q}{e} G, \quad (1)$$

where it is understood that the operator Q/e is diagonal, and

$$\begin{aligned} & \left\langle k_1', k_2' \middle| \frac{Q}{e} \middle| k_1', k_2' \right\rangle \\ &= \frac{Q(k_1', k_2')}{(\hbar^2/2M)(k_1^2 + k_2^2 - k_1'^2 - k_2'^2) + U(k_1) + U(k_2) - U(k_1') - U(k_2')}. \end{aligned}$$

Let us study the effect of splitting the two-nucleon potential v into two parts,

$$v = v_s + v_t, \quad (2)$$

where the short-range part v_s contains the strong repulsive core plus most of the attraction, while v_t consists of the weak long-range tail.

(a) Define the following G -matrices for the short-range potential v_s :

$$G_s = v_s + v_s \frac{1}{e} G_s, \quad (3)$$

and

$$G_s^F = v_s + v_s \frac{1}{e_0} G_s^F. \quad (4)$$

Note that in both these definitions the Pauli operator Q is absent. In Eq. 3 the energy denominator is the same as in Eq. 1, while in Eq. 4 e_0 is the free-energy denominator, without the one-body potentials U . Assuming the Hermiticity of G_s and G_s^F , prove that

$$G_s = G_s^F + G_s^F \left(\frac{1}{e} - \frac{1}{e_0} \right) G_s. \quad (5)$$

(b) Noting the relation

$$v_s = \left(1 + G_s \frac{1}{e} \right)^{-1} G_s,$$

prove that, to second order in v_t and G_s ,

$$G = v_i + G_s + G_s \left(\frac{Q-1}{e} \right) G_s + v_i \frac{Q}{e} v_i + v_i \frac{Q}{e} G_s + G_s \frac{Q}{e} v_i, \quad (6)$$

and, to the same order,

$$\begin{aligned} G &= v_i + G_s^F + G_s^F \left(\frac{1}{e} - \frac{1}{e_0} \right) G_s^F + G_s^F \left(\frac{Q-1}{e} \right) G_s^F \\ &\quad + v_i \frac{Q}{e} v_i + v_i \frac{Q}{e} G_s^F + G_s^F \frac{Q}{e} v_i. \end{aligned} \quad (7)$$

This equation was first obtained by Moszkowski and Scott [*Ann. Phys.* **11**, 65 (1960)]. Note that, since the short-range part v_s is very strong, it scatters nucleons high above the Fermi sea in the intermediate states, and the Pauli principle has, therefore, only a small effect on the two-particle wave function at short distances. Thus G_s^F , the free G -matrix for the short-range part, should be adequate for v_s . The long-range part v_i is rather weak, and the Pauli principle drastically suppresses its effects in higher orders; in Eq. 7, the second-order term $v_i(Q/e)v_i$ has been taken into account. The term

$$G_s^F \left(\frac{1}{e} - \frac{1}{e_0} \right) G_s^F$$

is called the dispersion term; it takes into account the fact that the nucleons are moving in the presence of an average field U . The other terms in Eq. 7 are the Pauli correction term and the two interference terms. With the choice of v_s to be described below, the convergence of expansion 7 is very good for central potentials.

(c) In binding-energy calculations, one is interested in the diagonal matrix elements $\langle k | G | k \rangle$, summed over the relative momenta k of the occupied states (Eq. 8-37). Moszkowski and Scott chose the separation distance so that, for a given k ,

$$\langle k | G_s^F | k \rangle = 0. \quad (8)$$

This makes v_s dependent on k , and hence it becomes non-Hermitian, introducing some correction terms into expansion 7 in third order. Note that

$$\langle k | G_s^F | k \rangle = \int_0^{r=d} \Phi_k^* v_s \Psi_k^F d^3 r, \quad (9)$$

where Φ_k is the relative unperturbed two-nucleon wave function, and Ψ_k^F is given by

$$-\frac{\hbar^2}{M} \nabla^2 \Psi_k^F + v_s \Psi_k^F = \frac{\hbar^2}{M} k^2 \Psi_k^F.$$

Prove that Eq. 8 will be satisfied if

$$\frac{\nabla \Psi^F}{\Psi^F} \Big|_{r=d} = \frac{\nabla \Phi^*}{\Phi^*} \Big|_{r=d}. \quad (10)$$

With this choice of d , the net effect of the second-order terms in expansion 7 is found to be rather small, and in the first approximation G is just the long-range potential v_i . For example, for a central potential with a hard core and a spin-averaged strength acting in the S -state, v_i contributed -37.29 MeV to the potential energy per particle in nuclear matter at $k_F = 1.4$ fm $^{-1}$, while all the second-order terms contributed only 1.65 MeV. In the more realistic situation in which tensor force is present, there are some technical complications in the method because different partial waves are coupled and Eq. 8 cannot be simultaneously satisfied for two partial waves with the same d . Also, since the first-order contribution of the tensor component of v_i to nuclear-matter binding vanishes, and its second-order contributions are large, one is less sure of the convergence of Eq. 7.

8-10. Consider the equation

$$|\Psi_{k,\omega}\rangle = |\mathbf{k}\rangle + \frac{P}{\omega - t_{\text{rel}}} v |\Psi_{k,\omega}\rangle, \quad (1)$$

where v is the two-body potential, P denotes the principal value, and t_{rel} is the relative kinetic-energy operator,

$$t_{\text{rel}} |\mathbf{k}\rangle = \frac{\hbar^2}{M} k^2 |\mathbf{k}\rangle.$$

This equation, for the choice of $\omega = (\hbar^2/M)k^2$, is identical to the Lippmann-Schwinger equation 5-49, and describes the scattering of two nucleons. It is also of the same structure as Eq. 8-29, except that the propagator here is for free scattering, without the Pauli operator Q .

(a) Consider the case when $\omega < 0$. In such a situation, there can be no singularity in the propagator, and the principal value sign P is superfluous. Show in this case that the coordinate space representation of Eq. 1 is

$$\langle \mathbf{r} | \Psi_{k,\omega} \rangle = \exp(i\mathbf{k} \cdot \mathbf{r}) - \frac{M}{4\pi\hbar^2} \int \frac{\exp(-\gamma|\mathbf{r} - \mathbf{r}'|)}{|\mathbf{r} - \mathbf{r}'|} v(\mathbf{r}') \langle \mathbf{r}' | \Psi_{k,\omega} \rangle d^3 r', \quad (2)$$

where $|\omega| = \hbar^2 \gamma^2 / M$. We have taken unit normalization volume for plane waves, that is, $\langle \mathbf{r} | \mathbf{k} \rangle = \exp(i\mathbf{k} \cdot \mathbf{r})$, and used the relation

$$\sum_{\mathbf{k}'} = \frac{1}{(2\pi)^3} \int d^3 k'.$$

(b) Making the expansion

$$\langle \mathbf{r} | \Psi_{k,\omega} \rangle = \sum_{l=0}^{\infty} [4\pi(2l+1)]^{1/2} i^l u_l(k, \gamma; \mathbf{r}) Y_l^0(\hat{\mathbf{k}}, \hat{\mathbf{r}}), \quad (3)$$

show that the asymptotic form for the radial function u_i is given by

$$u_i(k, \gamma; r) \sim j_i(kr) + b_i(k, \gamma) \frac{\exp(-\gamma r)}{r}, \quad (4)$$

where b_i is real. Equation 4 shows that for negative ω the two-body relative wave function "heals" to its unperturbed value $j_i(kr)$, the healing distance being governed by the parameter γ . For nuclear matter, the healing is due to the Pauli operator Q in Eq. 8-29; however, its effect may be simulated by making the parameter ω negative in the free-scattering equation. This is the essence of the so-called reference spectrum method due to Bethe, Brandow, and Petschek [8].

8-11. (a) Harmonic-oscillator wave functions in relative coordinates and the Brody-Moshinsky transformation brackets. Consider a particle of mass M moving in a harmonic-oscillator potential $\frac{1}{2}M\omega^2 r_1^2$, r_1 being the position coordinate of the particle with respect to the center of the oscillator well. The eigenfunction of the particle, in an orbital (n_1, l_1, m_1) , is denoted by

$$\langle \mathbf{r}_1 | n_1 l_1 m_1 \rangle = \phi_{n_1 l_1 m_1}(\mathbf{r}_1)$$

and is defined by Eqs. 1 and 3 of Problem 4-10, the corresponding eigen-energy being $(2n_1 + l_1 + \frac{3}{2})\hbar\omega$. For two particles of identical mass M , moving in a common harmonic-oscillator well without interaction, the Hamiltonian is

$$H = \frac{\dot{p}_1^2}{2M} + \frac{1}{2}M\omega^2 r_1^2 + \frac{\dot{p}_2^2}{2M} + \frac{1}{2}M\omega^2 r_2^2. \quad (1)$$

Transform this Hamiltonian to a relative frame by making the transformation

$$\mathbf{r} = \frac{\mathbf{r}_1 - \mathbf{r}_2}{\sqrt{2}}, \quad \mathbf{R} = \frac{\mathbf{r}_1 + \mathbf{r}_2}{\sqrt{2}}, \quad (2)$$

and likewise for the momenta. Show that Eq. 1 is exactly separable into relative and center-of-mass variables, and remains identical in form. If we denote the quantum numbers for relative and CM motion by n, l and N, L , it follows from conservation of angular momentum that

$$l_1 + l_2 = \lambda = l + L, \quad (3a)$$

and from conservation of energy that

$$2n_1 + l_1 + 2n_2 + l_2 = 2n + l + 2N + L. \quad (3b)$$

Denoting the eigenvector of the two particles coupled to angular momentum λ and z -component μ by $|n_1 l_1, n_2 l_2; \lambda \mu\rangle$, we may make the transformation

$$|n_1 l_1, n_2 l_2; \lambda \mu\rangle = \sum_{NL} |nl, NL; \lambda \mu\rangle \langle nl, NL; \lambda \mu| n_1 l_1, n_2 l_2; \lambda \mu\rangle. \quad (4)$$

It can be shown that the brackets in the extreme right of Eq. 4 are independent of the magnetic quantum number μ , and they vanish if conditions 3 are

not obeyed. These transformation brackets, commonly known as the Brody-Moshinsky coefficients, are tabulated by T. A. Brody and M. Moshinsky "Table of transformation brackets for nuclear shell model calculations." (Gordon and Breach, New York, 1967) and are extensively used in finite-nucleus calculations.

(b) The Kallio approximation for the relative radial wave function. As seen in (a), making the transformation to relative and CM coordinates leaves the Hamiltonian of Eq. 1 identical in form, and consequently we may write for the relative radial wave function in the relative coordinate an expression identical in form to Eq. 3 of Problem 4-10:

$$R_{nl}(r) = \sqrt{\frac{2n! \alpha^3}{\Gamma(n+l+\frac{3}{2})}} (\alpha r)^l \exp(-\frac{1}{2}\alpha^2 r^2) L_n^{l+1/2}(\alpha^2 r^2), \quad (5)$$

where $\alpha = (M\omega/\hbar)^{1/2}$; n, l are now the quantum numbers for relative motion, and the Laguerre polynomial $L_n^{l+1/2}$ was defined in Problem 4-10.

Consider the special case of $l = 0$. Using the asymptotic expansion, valid for large n ,

$$L_n^{l=0}(\alpha^2 r^2) \sim \exp(\alpha^2 r^2/2) \frac{1}{\sqrt{\pi}} \frac{\sin(\sqrt{n} 2\alpha r)}{\alpha r},$$

and the limit

$$\lim_{n \rightarrow \infty} \frac{n!}{\Gamma(n+\frac{3}{2})} = \frac{1}{\sqrt{n}},$$

show that, for $n \rightarrow \infty$,

$$R_{n0}(r) = \sqrt{\frac{2\Gamma(n+\frac{3}{2})\alpha^3}{\pi n!}} 2j_0(2\sqrt{n} \alpha r). \quad (6)$$

Note that here

$$\mathbf{r} = \frac{1}{\sqrt{2}} (\mathbf{r}_1 - \mathbf{r}_2) \equiv \mathbf{r}_{12} \equiv \frac{\mathbf{r}_{12}}{\sqrt{2}}.$$

Expression 6 can be generalized for any l , as was shown by A. Kallio [*Phys. Lett.* 18, 53 (1965)]. He gave the approximate relation

$$R_{nl}(r_{12}) \approx \sqrt{\frac{2\Gamma(n+l+\frac{3}{2})\alpha^3}{\pi n! r^l}} \cdot 2^{l+1} j_l(\sqrt{2n+l+\frac{3}{2}} \alpha r_{12}), \quad (7)$$

with[†] $r = 4n + 2l + 3$. Note that this equation is consistent with Eq. 6. Equation 7 is surprisingly accurate for low values of n , including $n = 0$, provided $r_{12} \lesssim 2$ fm. The accuracy increases for large n .

[†] There is a misprint in Kallio's paper in the definition of r .

(c) Recall that the l th partial wave of the plane wave is proportional to $j_l(k_{12}r_{12})$, where we are using the definitions $\mathbf{r}_{12} = \mathbf{r}_1 - \mathbf{r}_2$, $\mathbf{k}_{12} = \frac{1}{2}(\mathbf{k}_1 - \mathbf{k}_2)$. The relative kinetic energy of two free particles is of course $\hbar^2 k_{12}^2/M$, whereas for two particles moving in a harmonic well the relative energy is $e_{nl} = (2n + l + \frac{3}{2})\hbar\omega$. However, only half of this, that is,

$$\frac{1}{2}e_{nl} = \left(n + \frac{l}{2} + \frac{3}{4}\right)\hbar\omega$$

is the relative kinetic energy. We may think, then, that $R_{nl}(r_{12})$ may be proportional to $j_l(k_{\text{eff}}r_{12})$, where

$$\frac{\hbar^2 k_{\text{eff}}^2}{M} = \frac{1}{2}e_{nl}.$$

We see from Eq. 7, however, that

$$k_{\text{eff}} = \sqrt{2n + l + \frac{3}{2}\alpha},$$

so that

$$\frac{\hbar^2 k_{\text{eff}}^2}{M} = e_{nl}. \quad (8)$$

Can you explain this result qualitatively, remembering that Eq. 7 is valid only for small values of r_{12} ?

8-12. Consider the model of a single shell in which there are η equally spaced single-particle levels in an energy interval $\hbar\omega$. Since each level is doubly degenerate, the shell can accommodate a maximum of up to 2η fermions of one kind. Assume that a pairing interaction of constant strength G acts in this shell, and that the total number of particles in the shell is η .

(a) Using Eq. 8-112, show that the chemical potential λ is in the middle of the shell, symmetrically placed with respect to the single-particle levels.

(b) Noting that the average level density in the shell is $\eta/\hbar\omega$, and replacing the sum over the levels by an integral in the gap equation 8-111, show that

$$\Delta = \frac{\hbar\omega}{2 \sinh(\hbar\omega/G\eta)}. \quad (1)$$

In the limit $G\eta \gg \hbar\omega$, this gives

$$\Delta \approx \frac{1}{2}G\eta, \quad (2)$$

while for $G\eta \ll \hbar\omega$ we obtain

$$\Delta \approx \hbar\omega \exp\left(-\frac{\hbar\omega}{G\eta}\right). \quad (3)$$

This model may roughly represent the situation in the half-filled shell of a well-

deformed nucleus, where, in the first approximations, the single-particle levels (each doubly degenerate) may be taken to be uniformly spaced. Taking the "experimental" values of Δ and $\hbar\omega$ in the deformed rare-earth region, which of the above limiting equations (2 or 3) would you use to estimate $G\eta$? What is your numerical estimate for $G\eta$?

8-13. The pairing strength G , defined by Eq. 8-93, is not a constant for the realistic case of a finite-range interaction V_{12} . A rough estimate of the numerical value of G and its A -dependence may be obtained using the plane-wave approximation and assuming that V_{12} is the S -wave, $T = 1$ nucleon-nucleon potential. Using these assumptions and the definitions $\mathbf{r} = \mathbf{r}_1 - \mathbf{r}_2$, $\mathbf{k} = \frac{1}{2}(\mathbf{k}_1 - \mathbf{k}_2)$, show from Eq. 8-93 that the diagonal matrix element is given by

$$G(k, k) = -\frac{1}{\Omega} \int V_{12}(r) j_0^2(kr) d^3r.$$

Using Eq. 5-39, show that this may be written as

$$G(k, k) \approx -\frac{4\pi\rho}{A} \frac{\hbar^2}{Mk} \delta_0^{\text{Born}}(k), \quad (1)$$

where $\delta_0^{\text{Born}}(k)$ is the S -wave, $T = 1$ Born phase shift of the two-nucleon potential, and ρ is the nuclear density.

For numerical estimate, we may take for k the value corresponding to the head-on collision of two nucleons at the Fermi surface, that is, $k = k_F$. Also, for such large values of k , we may assume $\delta_0^{\text{Born}}(k) \approx \delta_0(k)$. For large nuclei, taking the nuclear-matter value of $k_F = 1.36 \text{ fm}^{-1}$, and using Fig. 5-12a to estimate δ_0 , show that Eq. 1 gives $G \approx 14/A \text{ MeV}$, whereas using an average value of $k_F = 1.25 \text{ fm}^{-1}$ for a nucleus gives $G \approx 21/A \text{ MeV}$. The latter number is close to the value of G actually chosen in calculations.

Collective Nuclear Motion

9-1 INTRODUCTION

We have pointed out that the shell and independent-particle models explain many nuclear properties, but fail to account for the large nuclear quadrupole moments and spheroidal shapes which many nuclei have. It is clear that such effects cannot be obtained from any model that considers the pairwise filling of the individual orbits of a spherical potential to be a good approximation to nuclear structure. Such large effects can arise only from coordinated motion of many nucleons. Let us visualize the nucleons as moving in essentially single-particle paths, such as the properties of nuclear matter would lead us to expect in a finite nucleus; at each instant the nucleons form a pattern in space. Let us suppose that at some moment this pattern is, say, ellipsoidal. The motion is collective, or cooperative, if this pattern changes very slowly, or, in the extreme case, is permanent. The particles move through many circuits of their orbits, but in a sufficiently correlated manner, so that at all times the overall space pattern is essentially the same or slowly changing. This type of correlation is very different from the short-range correlations in nuclear matter; it is a long-range correlation and may be thought of as a surface effect. Also, the specific values of the parameters involved depend on the exact number of nucleons in the nucleus.

We may characterize such motion by saying that the particle motion and surface motion are coupled. Because the surface is distorted at some moment, the potential "felt" by a particle is not spherically symmetric. If this distortion lasts for a sufficient time—a few nucleon periods—the

particles will move in orbits appropriate to an aspherical shell-model potential. This particle motion in turn preserves the nuclear shape. In nearly spherical nuclei, there is only very weak coupling of this type, the particles have no directional correlation, and the resultant average shape is spherical.

To express the particle-surface coupling mathematically, it is necessary to introduce some *collective variables* to describe the cooperative modes of motion. It is also convenient to take parts of the energy, angular momentum, and other dynamical variables and to ascribe these parts to collective motion. For example, the correlated particle motion may be such that the pattern of particles changes slowly, maintaining a fixed shape, but with the orientation in space altering. Looked at from outside, the nucleus of constant shape is rotating. It is natural to attribute kinetic energy and angular momentum to this rotating mass and to consider the rest of the nuclear kinetic energy and angular momentum to be internal. Also, we may remove from the potential energy of the system a term to express the work done in deforming it from spherical shape; such a term will depend only on collective variables if they are suitably chosen, and we may call it the deformation energy. It will include the change in Coulomb energy of a continuous distribution of charge, as well as the change in surface energy. If this potential energy is a minimum for the smallest surface of a given volume, the first terms in a Taylor-series expansion will be quadratic in the parameters describing the departure from sphericity. Because of the great resistance of nuclear matter to compression, it is usual to consider deformations of fixed volume only and to treat the collective potential energy as quadratic in the simplest approximation.

Collective variables are useful only if the energy can be separated in this way into terms that depend on the collective variables and terms that do not. The other variables may be called intrinsic. If there is only a weak collective-intrinsic coupling, the system may be studied by perturbation theory:

$$H = H_c \text{ (collective variables)} + H_i \text{ (intrinsic variables)} + H_{\text{coup}}$$

An important question concerns the identity of the intrinsic variables; this is, in general, a difficult problem. A simple example of a collective variable is the mass center; for a two-body system, the corresponding intrinsic variable is the particle separation $\mathbf{r}_1 - \mathbf{r}_2$, and there is no coupling. But, as we mentioned in connection with the shell model, there are no such simple intrinsic variables for the N -body system. If we continue to use as intrinsic variables the coordinates of the particles with respect to a fixed origin, we have too many variables, since we also have the collective coordinates. On

the other hand, if we use the correct number of variables, the intrinsic variables are complicated. We shall say more about the separation of collective and intrinsic motions and their interactions after we have formalized the concepts.

A nonspherical equilibrium shape might be thought of as arising as a result of the opposing tendencies of the "outer" nucleons to polarize the nuclear core and of the core to resist this polarization and maintain a spherical shape; this possibility was first suggested by Rainwater [1] in 1950. The model was worked out in detail by Aage Bohr and extended and generalized principally by Bohr and Ben R. Mottelson and various coauthors in a comprehensive series of papers during the decade 1950–1960. The most instructive of these papers are probably refs. 2, 3, 4, and 5.

Two different nuclear models are considered in these works. The earlier (and for many purposes the simpler) separates the nucleus into a core and extracore nucleons. The core is treated macroscopically as a deformable drop of nuclear "liquid," in interaction with the few extra nucleons in an unfilled shell. The second model is really an extended shell model; the shell-model potential is assumed to be nonspherical, the energies of the single particles in the nonspherical potential are calculated, and the distortion that gives the minimum energy is taken as the distortion actually found. One is faced here with the problem inherent in any nuclear shell model: the need to understand the model in terms of more fundamental interactions. The long-range correlations are replaced by the assumption of a permanently distorted potential.

In the early development of a collective model, all nuclei were broadly classified into two categories: spherical and permanently deformed. In spherical nuclei the nuclear excitations were assumed to be small-amplitude vibrations of the harmonic type about the equilibrium spherical shape, while in deformed nuclei the low-energy modes were rotations and small-amplitude vibrations about the deformed shape. The experimental data accumulated in the last decade or so have revealed that, while there do exist many well-deformed nuclei with rotational spectra, the simple vibrational picture for spherical nuclei is not a realistic one. Recent experimental techniques make it possible to measure the quadrupole moments of excited states, and it is found [6] that even the first excited 2^+ states of most of the so-called spherical nuclei (e.g., the Sn and Te isotopes) are appreciably deformed. Furthermore, when we examine the level structures of many of these so-called vibrational nuclei up to an excitation of about 5 MeV, well-defined rotation-like bands appear, just as in permanently deformed nuclei. We shall give examples of these quasi-rotational bands in a later section.

These experimental findings make us believe that the concept of a spherical nucleus making small harmonic vibrations about its spherical shape is too naive and does not conform with reality. The concept of a nucleus having a spherical shape in its *ground state*, however, is a valid one. If the potential energy for deformation from this shape goes up steeply, the nucleus is stiff, while if the potential-energy curve against deformation is very flat, the nucleus is soft and may contain many modes of deformation. Nuclei of the latter type are called transitional and occur in regions where either permanent deformation or stiff sphericity is about to set in (e.g., some of the Nd isotopes, where deformation is setting in, and others in the Pt-Os region, where stiff sphericity is about to set in). An important advance in recent times has been a gain in understanding these transitional nuclei. Before going into these more complicated cases, we give, in the next few sections, accounts of the simplest vibrational and rotational models for stiff nuclei.

9-2 THE VIBRATIONAL MODES OF A SPHERICAL NUCLEUS

A spherical nucleus, in the simplest model, may be assumed to be a charged liquid drop, its excitation modes arising from small oscillations about the equilibrium spherical shape. Although, as mentioned in Section 9-1, this is not too realistic, this model introduces the concept of phonon excitations in an elegant manner and is useful for more sophisticated theories. We therefore first consider the modes of small oscillations of a charged liquid drop. The case of an incompressible liquid was first worked out by Lord Rayleigh [7]. The assumption of incompressibility is reasonable for the low-lying states of a nucleus; it means that, for a given mass of nuclear matter, shape changes can take place only with the restriction of volume conservation. For a nucleus, Lord Rayleigh's classical equations of motion must be quantized, and we should allow for a type of motion more general than the irrotational[†] fluid flow considered by him.

Consider a spherical drop of radius R_0 . When distorted, its surface is conveniently parametrized by the expression

$$R(\theta, \phi) = R_0 \left[1 + \sum_{\lambda=0}^{\infty} \sum_{\mu=-\lambda}^{\lambda} \alpha_{\lambda\mu} Y_{\lambda\mu}(\theta, \phi) \right], \quad (9-1)$$

[†] *Irrational* is used here in the technical hydrodynamic sense; it does *not* imply that elementary volumes of the fluid may not move in circular paths, but it does imply that each elementary volume is not rotating about an axis moving with its own center. In other words, in successive positions of the volume element, the orientations of its sides in space are unaltered. The general motion of a rigid body is *not* irrotational, but fluids may move in this way.

where θ and ϕ are polar angles with respect to an arbitrary space-fixed axis, and R_α is chosen to preserve volume conservation. For reality, $\alpha_{\lambda\mu} = (-)^\mu \alpha_{\lambda-\mu}^*$. Volume conservation implies that

$$\begin{aligned}\frac{4\pi}{3} R_0^3 &= \int_0^{2\pi} d\phi \int_0^\pi \sin \theta d\theta \int_0^{R(\theta, \phi)} r^2 dr \\ &= \frac{4\pi}{3} R_\alpha^3 \left[1 + \frac{3\alpha_{00}}{\sqrt{4\pi}} + \frac{3}{4\pi} \sum_{\lambda, \mu} |\alpha_{\lambda\mu}|^2 + O(\alpha^3) + \dots \right],\end{aligned}\quad (9-2)$$

where the higher-order terms are neglected, assuming the deformation to be small. Deformation of the type α_{00} in the first order causes a volume change costing too much deformation energy and is therefore discarded in the treatment of low-lying modes. Furthermore, the potential energy of the drop should not depend on the location of the center of mass, which, to first order, is given by $\alpha_{1\mu}$ ($\mu = -1, 0, 1$). By constraining the center of mass at the origin, we obtain $\alpha_{1\mu} = 0$. Hence we can write

$$R(\theta, \phi) = \frac{R_0}{\xi} \left[1 + \sum_{\lambda=2}^{\infty} \sum_{\mu=-\lambda}^{\lambda} \alpha_{\lambda\mu} Y_{\lambda\mu}(\theta, \phi) \right], \quad (9-3)$$

where ξ is a scale factor required by the condition of constant volume and is given by

$$\xi \approx 1 + \frac{1}{4\pi} \sum_{\lambda=2}^{\infty} \sum_{\mu} |\alpha_{\lambda\mu}|^2. \quad (9-4)$$

If we ignore the volume changes to second order in the α 's, then ξ is unity, and we obtain

$$R(\theta, \phi) = R_0 \left[1 + \sum_{\lambda=2}^{\infty} \sum_{\mu=-\lambda}^{\lambda} \alpha_{\lambda\mu} Y_{\lambda\mu}(\theta, \phi) \right]. \quad (9-5)$$

an expression which we use in the following treatment for simplicity. Of course, the nucleus does not have a sharp surface like that of a liquid drop, but appropriate modifications can be made in the calculation of deformation energy for the case of a diffuse surface. Any collective motions are expressed by letting $\alpha_{\lambda\mu}$ vary with time. In the quadratic approximation, the kinetic energy is of the form

$$T = \frac{1}{2} \sum_{\lambda, \mu} B_\lambda |\dot{\alpha}_{\lambda\mu}|^2. \quad (9-6)$$

In the particular case of the irrotational flow of a constant-density fluid, Rayleigh's calculations show that

$$B_\lambda = \frac{\rho R_0^5}{\lambda}, \quad (9-7)$$

where ρ is the density. This expression for the inertial parameter B_λ turns out to be quite unrealistic in the nuclear case, and a microscopic model is necessary for a more realistic estimate. Because of distortion from sphericity, the potential energy changes: the surface energy increases as a result of an increase in the surface area of the drop, and the Coulomb energy decreases with increasing distortion. This change in the potential energy from its spherical value is denoted by V and is given in the quadratic approximation by

$$V = \frac{1}{2} \sum_{\lambda, \mu} C_\lambda |\alpha_{\lambda\mu}|^2. \quad (9-8)$$

For the classical liquid,

$$C_\lambda = C_\lambda^{(1)} - C_\lambda^{(2)}, \quad (9-9)$$

with

$$C_\lambda^{(1)} = SR_0^2(\lambda - 1)(\lambda + 2), \quad (9-10)$$

and

$$C_\lambda^{(2)} = \frac{3}{2\pi} \frac{Z^2 e^2}{R_0} \frac{\lambda - 1}{2\lambda + 1}, \quad (9-11)$$

where S in Eq. 9-9 is the surface tension. For a charged drop to perform oscillations about the spherical shape, the C_λ 's should be positive. This classical estimate of C_λ is useful for nuclei, as we shall see in Chapter 12 on fission, provided we use appropriate values of R_0 and S based on the semiempirical mass formula.

With expressions 9-6 and 9-8 for T and V , the Lagrangian $L = T - V$ is seen to be a sum of separate terms for each of the generalized coordinates $\alpha_{\lambda\mu}$, and each of these terms is the Lagrangian of a simple harmonic oscillator. The frequency associated with the variable $\alpha_{\lambda\mu}$ is

$$\omega_\lambda = \left(\frac{C_\lambda}{B_\lambda} \right)^{1/2}. \quad (9-12)$$

As mentioned earlier, we have excluded from our considerations the $\lambda = 0$ mode, whose excitation should be at a much higher energy than the incompressible shape vibrations, as well as the $\lambda = 1$ modes, which merely describe the vibrations of the center of mass of the drop.

In order to quantize the collective modes of the drop and to introduce the concept of phonon excitations [2], we first define the momentum conjugate to the variable $\alpha_{\lambda\mu}$ as

$$\pi_{\lambda\mu} = \frac{\partial T}{\partial \dot{\alpha}_{\lambda\mu}} = B_\lambda \dot{\alpha}_{\lambda\mu}^*$$

The Hamiltonian for the drop then becomes

$$H = T + V = \sum_{\lambda,\mu} \left(\frac{1}{2B_\lambda} |\pi_{\lambda\mu}|^2 + \frac{1}{2} C_\lambda |\alpha_{\lambda\mu}|^2 \right). \quad (9-13)$$

As the different λ -modes of oscillation are completely uncoupled in this approximation, we consider, for quantization, only the case of $\lambda = 2$, and drop the $\lambda = 2$ suffix from B_2 and $\alpha_{2\mu}$ for simplicity. In the quantization procedure, the dependence of the inertial parameter B on the coordinates α_μ is ignored, and the variables α_μ and π_μ are observables with the commutator $[\alpha_\mu, \pi_\mu] = i\hbar$. In the usual way, we define

$$\begin{aligned} \alpha_\mu &= \sqrt{\frac{\hbar}{2B\omega}} (b_\mu + (-)^\mu b_{-\mu}^+), \\ \pi_\mu &= i \sqrt{\frac{\hbar B \omega}{2}} (b_\mu^+ - (-)^\mu b_{-\mu}), \end{aligned} \quad (9-14)$$

where $\omega = \omega_2$ is given by Eq. 9-12, and the operator b_μ and its Hermitian conjugate b_μ^+ will turn out to be the annihilation and creation operators for phonons. When the number operator \hat{n}_μ is introduced by the definition

$$\hat{n}_\mu = b_\mu^+ b_\mu, \quad (9-15)$$

the Hamiltonian of Eq. 9-13 is diagonal in the n_μ -representation,[†] so that any eigenstate of the Hamiltonian can be specified by the number of phonons present in the state. The energy eigenvalues are given by

$$E_N = \hbar\omega \sum_\mu (\frac{1}{2} + n_\mu) = \hbar\omega(\frac{1}{2} + N), \quad (9-16)$$

where $N = \sum n_\mu = 0, 1, 2, \text{etc.}$, and $\lambda = 2$. Thus the ground state is a state with no phonons present, while the first excited state has only one phonon excitation and is fivefold degenerate, since the azimuthal quantum number μ can take any of the integral values $-2, -1, \text{to } +2$. A similar analysis can be carried through for any λ , except that the phonon excitation energies

[†] Indeed, $H = \sum_{\lambda,\mu} \hbar\omega_\lambda (b_{\lambda\mu}^+ b_{\lambda\mu} + \frac{1}{2})$.

are higher. In general, a state with $n_\lambda = 1$ is $(2\lambda + 1)$ -fold degenerate and, therefore, presumably has angular momentum λ . It can be shown for irrotational motion that a phonon of type $\lambda\mu$ carries angular-momentum quantum number λ , with z -component μ and parity $(-)^{\lambda}$.

The energy $\hbar\omega_\lambda$ is a fairly rapidly increasing function of λ . If we use the classical hydrodynamic expressions 9-7 and 9-9, we readily see that $\omega_3 \approx 2\omega_2$ and $\omega_4 = 3\omega_2$. Consequently, we need consider only low values of λ in order to examine low-lying nuclear states. If there are nuclei that can oscillate collectively about a spherical shape, the first excited vibrational state would have one $\lambda = 2$ phonon present and would therefore be a 2^+ state. One $\lambda = 3$ phonon has about the same energy as two $\lambda = 2$ phonons, so the second vibrational state would be either a 3^- state or one of the states formed from coupling the two angular momenta of two units, namely, $0^+, 2^+$ or 4^+ . The degeneracy of the last three states will normally be removed by perturbations which have not been considered, but at least the center of gravity of the three levels should be at an energy about twice the first

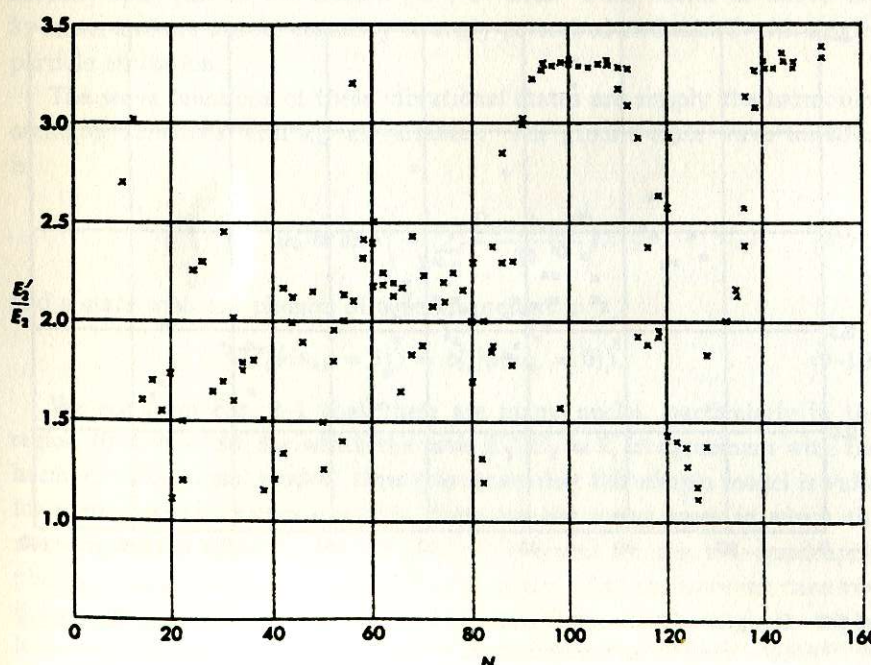


Fig. 9-1 Energy ratios of the first two excited states of even-even nuclides as a function of N .

2^+ level. For a rough indication of the excitation energy to be expected we could use the irrotational fluid approximations 9-7, 9-10, and 9-11; for A near 100, $\hbar\omega_2$ is slightly over 2 MeV, falling to about 1 MeV for A near 200. These energies are thus somewhat smaller than particle excitations for even-even nuclei, especially near closed shells, and we might very well expect to find that the lowest levels of even-even spherical nuclei are collective vibrations.

One test of this hypothesis would be to examine the ratio E_2'/E_2 of the energies of the first and second 2^+ states; it should be about 2. Figure 9-1 shows the ratio for the first and second excited states[†] of even-even nuclides; we see that there are regions where the ratio is slightly over 2, with abrupt transitions where it is 3.3 and the second state is 4^+ , not 2^+ . For nuclides with E_2'/E_2 near 2, the energies E_2 are smaller than the hydrodynamic estimate by a factor of about 2, but this is not inconsistent with the assumption that they are vibrational levels. It does mean that the hydrodynamic model for C_A and B_A is not very good. Figure 9-2 shows a plot of the energies

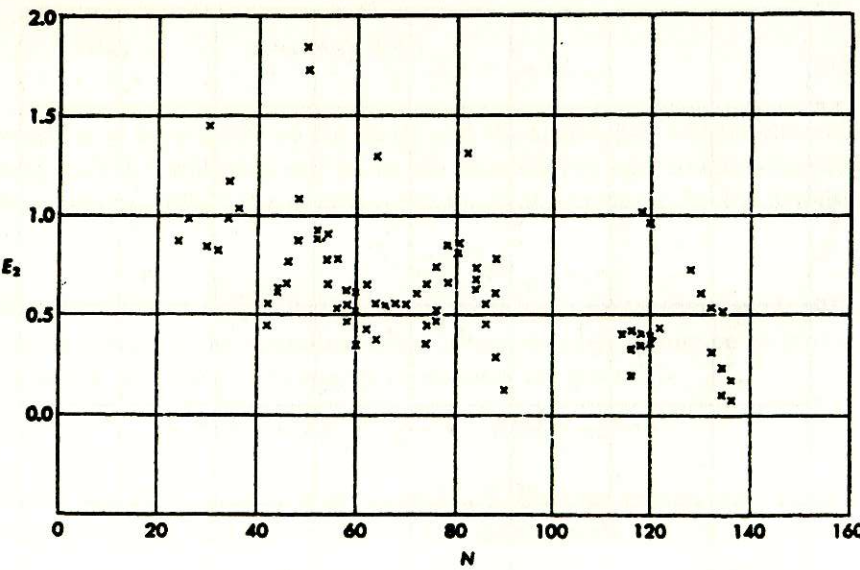


Fig. 9-2 Energies of first excited states in even-even nuclides, for which the energy is presumably vibrational, as a function of N (E_2 in MeV).

[†] There are only seven known exceptions in which the first excited state of an even-even nucleus is not a 2^+ . These are ${}^4\text{He}$ (0^+), ${}^{14}\text{C}$ (1^-), ${}^{16}\text{O}$ (0^+), ${}^{40}\text{Ca}$ (0^+), ${}^{72}\text{Ge}$ (0^+), ${}^{90}\text{Zr}$ (0^+), and ${}^{208}\text{Pb}$ (3^-).

E_2 against N , and it is seen that there is a general decrease of E_2 , as forecast by the theory.

Many items of information, both from nuclear reactions and from γ -ray spectra, indicate the presence of 3^- levels at an energy of about 2-3 MeV, decreasing with A . This result gives further support to the collective picture. If the energy of the collective mode is close to that of some single-particle excitations, these may be mixed by interaction between the particle degrees of freedom and the collective degrees of freedom. The wave functions of the actual nuclear states are then only partially collective, and the collective state is distributed over several actual states. Specifically collective properties are not so pronounced. For 3^- states this mixing is important in some cases, and we should expect even higher vibrational states to be so distributed among the nuclear states that the collective description loses its validity almost entirely.

Negative-parity states can also be obtained in spherical even-even nuclei by the combination of one quadrupole and one octupole phonon. There are five states, $1^-, 2^-, \dots, 5^-$, which, though degenerate in first approximation, actually split just as the triad $0^+, 2^+, 4^+$ does. Such states lie above the 3^- state, and are almost certainly strongly perturbed and mixed with single-particle excitation.

The wave functions of these vibrational states are simply the harmonic-oscillator functions with $\alpha_{\lambda\mu}$ as variables. The ground-state wave function is

$$\psi_0 \propto \exp\left(-\sum_{\lambda,\mu} \frac{B_\lambda \omega_\lambda |\alpha_{\lambda\mu}|^2}{2\hbar}\right), \quad (9-17)$$

and a state with one phonon of type $\lambda\mu$ present is

$$|\psi(n_{\lambda\mu} = 1)\rangle = b_{\lambda\mu}^+ |\psi(n_{\lambda\mu} = 0)\rangle. \quad (9-18)$$

We see from Fig. 9-1 that there are many nuclei, particularly in the region $40 < N < 80$, for which the ratio $E_2'/E_2 \approx 2$, in agreement with the harmonic vibrational model. Does this mean that this simple model is valid for these nuclei? Experimentally, there are not many cases in which the near-degenerate triplet of 0^+ , 2^+ , and 4^+ is found for the two-quadrupole phonon states, casting some doubt on the model. Let us, however, take two particularly favorable examples in which all three members of the triplet have been detected, and examine the experimental data more closely. In Fig. 9-3, we show the low-lying spectra of ${}^{114}_{48}\text{Cd}$ and ${}^{122}_{52}\text{Te}$ for this purpose. In ${}^{114}_{48}\text{Cd}$, we find the first excited 2^+ state at 0.558 MeV, followed by five,

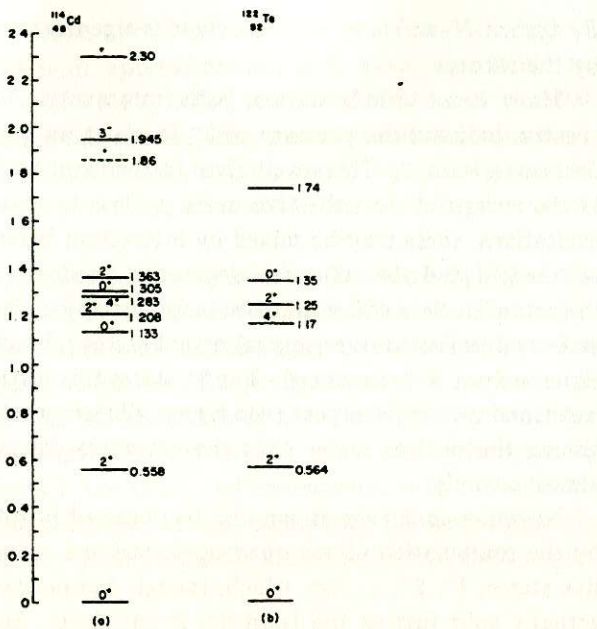


Fig. 9-3 Low-lying excited states of (a) $^{114}_{48}\text{Cd}$ and (b) $^{122}_{52}\text{Te}$.

not three, excited states at about twice this energy. There is also a 3⁻ state at 1.945 MeV. In order to salvage the vibrational model, we could assume that the lowest three of the five excited states starting at 1.133 MeV are two-phonon states, while the other two, the 0⁺ at 1.305 MeV and the 2⁺ at 1.363 MeV, are three-quadrupole phonon states somehow brought down in energy. Actually, it can be shown that three bosons of spin 2⁺ each can combine symmetrically to form $J = 0^+, 2^+, 3^+, 4^+,$ and 6^+ ; this would mean that the 3⁺, 4⁺, and 6⁺ states have been pushed up in energy, with the centroid of the quintuplet lying around the three-phonon energy of about 1.8 MeV. The spectrum of the other nucleus, ^{122}Te , is much simpler, and we find the expected triplet at the two-phonon energy. These energy considerations alone, then, may convey the impression that the vibrational model is reasonable for these nuclei. We shall now see, however, that a consideration of the electromagnetic properties of these states will lead us to believe that something is seriously wrong with the model even in the case of ^{122}Te , and will point to the pitfalls of judging the validity of a model from energy considerations alone.

To consider the electromagnetic properties of these states, we modify the definition of the electric 2^λ-pole moment operator, given by Eq. 3-6, to

$$Q_{\lambda\mu} = \int r^\lambda Y_\lambda^\mu(\Omega) \rho(r) d^3r, \quad (9-19)$$

for a continuous charge distribution with charge density ρ . In our model of the oscillating drop, the charge density is constant up to a radius $R(\theta, \phi)$, given by Eq. 9-5, with a value $3Ze/4\pi R_0^3$, and is zero outside. Thus we obtain, for a charged drop,

$$Q_{\lambda\mu} = \frac{3Ze}{4\pi R_0^3} \int Y_\lambda^\mu(\theta, \phi) \sin \theta d\theta d\phi \int_0^{R(\theta, \phi)} r^{\lambda+2} dr.$$

A straightforward evaluation of this integral yields

$$Q_{\lambda\mu} = \frac{3Ze}{4\pi} R_0^\lambda \alpha_{\lambda\mu}^* + O(\alpha^2). \quad (9-20)$$

If we now use the second-quantized expression 9-14 for $\alpha_{\lambda\mu}$, we note that the multipole operator $Q_{\lambda\mu}$ contains only a single creation and a single annihilation operator for a phonon of the type $\lambda-\mu$; therefore $Q_{\lambda\mu}$ can connect states differing by only one phonon of multipole λ . Applying this result to the low-lying quadrupole states, we find that

- (i) there should be strong $E2$ -transitions from the first excited 2⁺ state to the ground state and from the members of the two-phonon triplet to the first excited 2⁺ state;
- (ii) there should be no crossover $E2$ -transition from the second 2⁺ state to the ground state; and
- (iii) since the diagonal matrix element $\langle 1 \text{ phonon} | Q_{2\mu} | 1 \text{ phonon} \rangle = 0$ in this model, the quadrupole moment of the first excited 2⁺ state should be zero.

Experimentally, information about electromagnetic transitions can be obtained by Coulomb excitation of a nucleus from its ground state by scattering with ions, or by measuring the electromagnetic decay widths of excited states. To be more quantitative, let us define the transition probability for emission of a photon of energy $\hbar\omega = \hbar kc$, angular momentum λ , μ , and electric or magnetic type, with the nucleus going from an initial state $|J_i M_i\rangle$ to a final state $|J_f M_f\rangle$, as in Appendix E, viz.

$$T_{if}(\sigma\lambda\mu) = \frac{8\pi(\lambda+1)}{\lambda[(2\lambda+1)!]^2} \frac{\hbar^{2\lambda+1}}{\hbar} |\langle J_f M_f | O_{\lambda\mu} | J_i M_i \rangle|^2, \quad (9-21)$$

where $O_{\lambda\mu}$ stands for the electric or magnetic multipole operator, and the states $|JM\rangle$ are normalized to unity. Since we are not usually interested in the orientation of either the initial or the final nucleus, we sum over M , and average over M_i , defining the so-called reduced matrix element, which contains information about the nuclear wave function,

$$B(\sigma\lambda, J_i \rightarrow J_f) = (2J_i + 1)^{-1} \sum_{M_i, M_f} |\langle J_i M_i | O_{\lambda\mu} | J_f M_f \rangle|^2, \quad (9-22)$$

and obtain the relation

$$T(\sigma\lambda\mu, J_i \rightarrow J_f) = \frac{8\pi(\lambda + 1)}{\lambda[(2\lambda + 1)!]^2} \frac{k^{2\lambda+1}}{\hbar} B(\sigma\lambda, J_i \rightarrow J_f). \quad (9-23)$$

For electric transitions, the multipole operator $Q_{\lambda\mu}$ for a continuous charge distribution is given by Eq. 9-20, and the reduced matrix element from a one-phonon state ($n_\lambda = 1$) to a no-phonon state ($n_\lambda = 0$) is found easily:

$$B(E\lambda, n_\lambda = 1 \rightarrow n_\lambda = 0) = \left(\frac{3}{4\pi} ZeR_0^{-1} \right)^2 \frac{\hbar}{2\sqrt{B_\lambda C_\lambda}}, \quad (9-24)$$

where we have made use of expansion 9-14. Characteristics (i) and (ii) listed above are thus subject to the selection rule

$$\Delta n_\lambda = \pm 1. \quad (9-25)$$

Furthermore, using the properties of b_μ , we can obtain the following sum rule:

$$\sum_f B(E\lambda, n_\lambda J_i \rightarrow (n_\lambda - 1), J_f) = n_\lambda B(E\lambda, n_\lambda = 1 \rightarrow n_\lambda = 0), \quad (9-26)$$

where the summation f is over all states with a given J_f and $n_\lambda - 1$ phonons. If we take the particular case of $n_\lambda = 2$, there is only one state with $n_\lambda = 1$, and we obtain

$$B(E2, 2' \rightarrow 2) = 2B(E2, 2 \rightarrow 0), \quad (9-27a)$$

$$B(E2, 4 \rightarrow 2) = 2B(E2, 2 \rightarrow 0), \quad (9-27b)$$

where $2'$ denotes the second excited 2^+ state, and 4 the first excited 4^+ state.

Experimental analyses confirm point (i) above—that the $E2$ -transition from the ground state to the one-phonon 2^+ state is several times stronger than the single-particle estimate. In ^{114}Cd and ^{122}Te , for example, this transition is about 35 times stronger than the noncollective value. It is also found that, although the crossover transition is not zero, it is very small

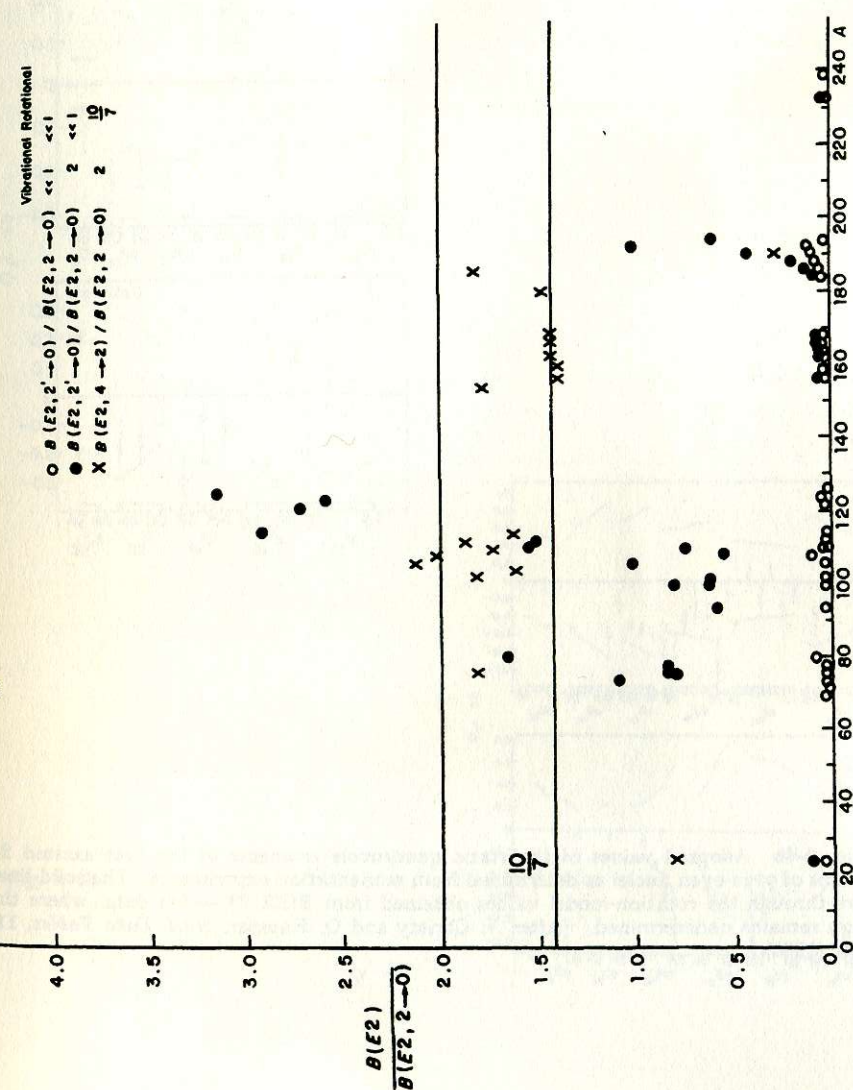


Fig. 9-4a The reduced $E2$ -transition probabilities for the decay of the second excited 2^+ state ($2'$) and the first excited 4^+ state, relative to the probability for the first 2^+ state. (After Nathan and Nilsson [8].)

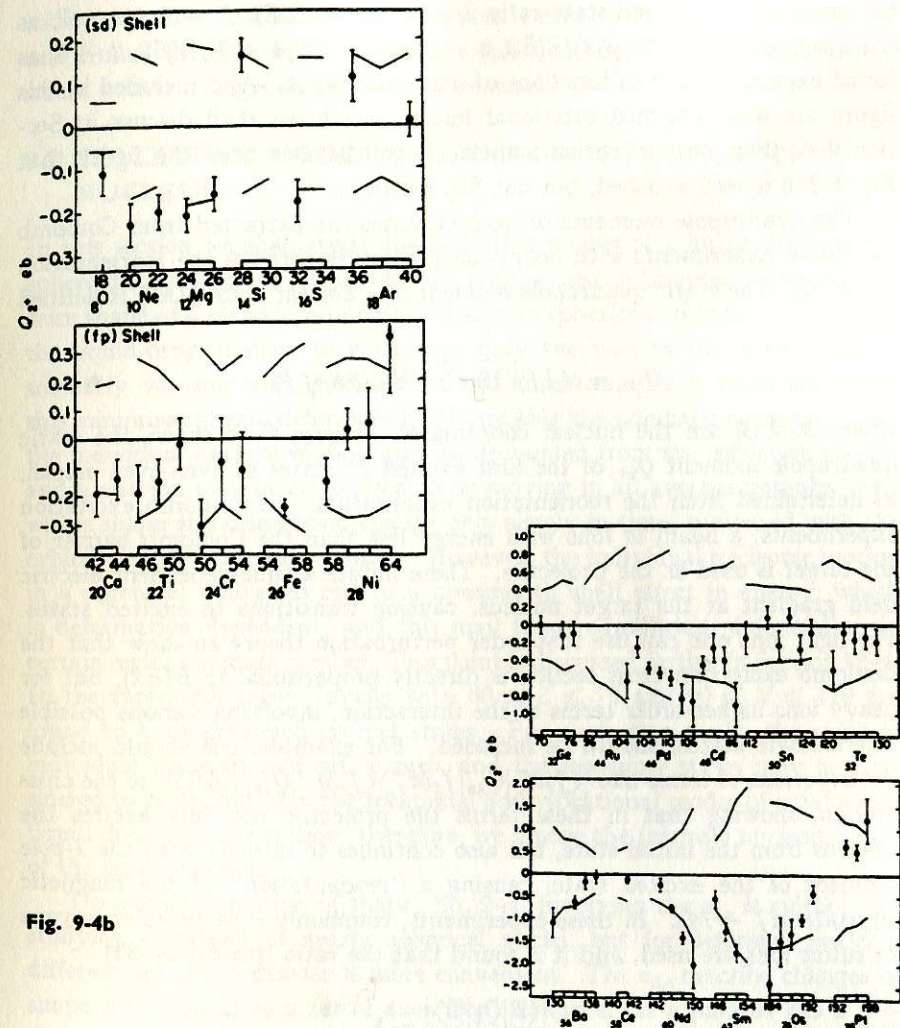


Fig. 9-4b

Fig. 9-4b Adopted values of the static quadrupole moments of the first excited 2^+ states of even-even nuclei as determined from reorientation experiments. The solid lines are through the rotation-model values obtained from $B(E2, 0^+ \rightarrow 2^+)$ data, where the sign remains undetermined. [After A. Christy and O. Hausser, *Nucl. Data Tables*, 11, 281 (1973).]

when compared with the probability of direct transition between adjacent 2^+ and 0^+ , confirming conclusion (ii). It is generally found, however, that Eq. 9-27a is not quantitatively satisfied in most cases, typical deviations being about 30–50%. Following Nathan and Nilsson [8], we show in Fig. 9-4a

the crossover to ground-state ratio $B(E2, 2' \rightarrow 0)/B(E2, 2 \rightarrow 0)$, as well as the quantities $B(E2, 2' \rightarrow 2)/B(E2, 2 \rightarrow 0)$ and $B(E2, 4 \rightarrow 2)/B(E2, 2 \rightarrow 0)$ as found experimentally as functions of mass number A . Also included in this figure are well-deformed rotational nuclei, which we shall discuss in Section 9-5. For most vibrational nuclei, it will be seen from the figure that Eq. 9-27b is well satisfied, but not Eq. 9-27a.

The quadrupole moments of excited states are extracted from Coulomb excitation experiments with heavy-ion projectiles through the reorientation effect [6]. The static quadrupole moment of a nuclear state $|JM\rangle$ is defined by

$$Q_{jn} = e\langle JJ|V\sqrt{16\pi/5}r^2Y_{20}(\theta\phi)|JJ\rangle,$$

where (r, θ, ϕ) are the nuclear coordinates. Figure 9-4b shows the static quadrupole moment Q_{2+} of the first excited 2^+ states of even-even nuclei, as determined from the reorientation experiments. In Coulomb excitation experiments, a beam of ions with energy less than the Coulomb barrier of the target is used as the projectile. These induce a time-dependent electric field gradient at the target nucleus, causing transitions to excited states. For light ions one can use first-order perturbation theory to show that the Coulomb excitation cross section is directly proportional to $B(E\lambda)$, but for heavy ions higher-order terms of the interaction, involving various possible intermediate states, should be included. For example, one should include contributions of terms like $|\langle J_i M_i | Q_{\lambda\mu} | J_f M_f' \rangle \langle J_f M_f' | Q_{\lambda\mu} | J_i M_i \rangle|^2$ to the cross section, showing that in these terms the projectile not only excites the nucleus from the initial state, but also continues to interact with the λ -pole moment of the excited state, causing a "reorientation" of the magnetic substate $M_f' \rightarrow M_f$. In these experiments, commonly α -particles or oxygen or sulfur ions are used, and it is found that the ratio (see Eq. A-83)

$$\frac{|\langle 2 || Q_2 || 2 \rangle|}{|\langle 2 || Q_2 || 0 \rangle|} \approx 1$$

for many of the vibrational nuclei. This implies a substantial quadrupole moment for the first 2^+ excited states of these nuclei, contradicting conclusion (iii) of the harmonic model, and pointing to the fact that modifications should be made for possibly large anharmonic effects in the model. It is expected that the quadrupole moment of an excited state will depend sensitively on the density distribution of the nucleus in the excited state. Anharmonic effects will introduce into the first 2^+ state some admixture of two-phonon contribution, thus changing its wave function and the quadrupole

moment [9, 10]. In a later section, we shall outline a theory, due to Baranger and Kumar [11, 12], which can handle spherical, deformed, and transitional nuclei within a single semiclassical framework.

9-3 COLLECTIVE MODES OF A DEFORMED EVEN-EVEN NUCLEUS

In this section we shall study the collective modes of a liquid drop with a spheroidal equilibrium shape. As was emphasized in Chapter 6, the equilibrium shape of a classical liquid drop is always spherical. However, in making the liquid-drop analogy to a nucleus, only the part of the energy that is smoothly varying with deformation and mass number is considered, and this minimizes at zero deformation. By making the adiabatic approximation, the individual nucleon motion may be decoupled from the collective modes, and a nucleon may be considered to be moving in an average potential well whose shape and orientation change only slowly in time, compared with the orbital periods of intrinsic motion. However, the individual nucleonic motion in a potential well gives rise to a nonsmooth shell effect in energy, which is deformation dependent, and this may favor equilibrium deformation in certain regions of mass number. This point is discussed further in Section 12-4. In the rare-earth region, nuclei with $60 \leq Z \leq 72$ and $90 \leq N \leq 110$ are found to have deformed ground states. For even-even nuclei the spins of individual nucleons pair off to zero, and the low-lying states may be considered to be arising from the rotational and vibrational modes of a deformed liquid drop. In this section, therefore, we ignore the intrinsic nucleonic part of the wave function.

The general equation of shape, Eq. 9-5, involving the $\alpha_{\lambda\mu}$ is suitable for studying vibrations of nearly spherical nuclei, but for deformed nuclei a different set of coordinates is more convenient. The $\alpha_{\lambda\mu}$ describe changes of shape with respect to a set of axes fixed in space. If a nucleus has a permanent nonspherical shape which is rotating, the $\alpha_{\lambda\mu}$ will change in time, although we would not say that the nuclear shape is altering. Consequently, we prefer to specify the orientation of the nucleus by giving the Euler angles $(\theta_1, \theta_2, \theta_3)$ of the principal axes of the nucleus with respect to the space-fixed axes,[†] and by introducing other parameters that specify the shape of the nucleus with respect to its own principal (body-fixed) axes.

We shall confine our attention to quadrupole shapes $\lambda = 2$. In the body-fixed system, we define the nuclear surface by

[†] For definitions of Euler angles and D -functions, see Section A-2.

$$R = R_0 [1 + \sum_{\mu} \alpha_{2\mu} Y_2^{\mu}(\theta', \phi')] . \quad (9-28)$$

Comparing this with Eq. 9-5, we have

$$\sum_{\mu} \alpha_{2\mu} Y_2^{\mu}(\theta, \phi) = \sum_{\mu} \alpha_{2\mu} Y_2^{\mu}(\theta', \phi'). \quad (9-29)$$

In the rotation $(\theta_1, \theta_2, \theta_3)$ from the space-fixed to the body-fixed axes, the spherical harmonics transform according to Eq. A-73:

$$Y_{\lambda}^{\mu}(\theta, \phi) = \sum_{\rho} Y_{\lambda}^{\rho}(\theta', \phi') \mathcal{D}_{\mu\rho}^{\lambda}(\theta_1, \theta_2, \theta_3), \quad (9-30)$$

where the rotation matrix $\mathcal{D}_{\mu\rho}^{\lambda}(\theta_i)$ is defined in Eq. A-53. Substituting the above expression for $Y_{\lambda}^{\mu}(\theta, \phi)$ into Eq. 9-29, we obtain

$$\alpha_{2\rho} = \sum_{\mu} \alpha_{2\mu} \mathcal{D}_{\mu\rho}^2(\theta_i) \quad (9-31a)$$

and

$$\alpha_{2\rho} = \sum_{\rho} \alpha_{2\rho} (\mathcal{D}_{\mu\rho}^2)^*. \quad (9-31b)$$

The body-fixed frame is chosen to be the principal axes, such that $\alpha_{21} = \alpha_{2,-1} = 0$ and $\alpha_{22} = \alpha_{2,-2}$ (see Problem 9-3). Thus α_{20} and α_{22} , together with the three Euler angles $(\theta_1, \theta_2, \theta_3)$, completely describe the system, replacing the five $\alpha_{2\mu}$. It is more convenient to use the variables β and γ instead of α_{20} and α_{22} :

$$\alpha_{20} = \beta \cos \gamma, \quad \alpha_{22} = \frac{1}{\sqrt{2}} \beta \sin \gamma. \quad (9-32)$$

Using these expressions in Eq. 9-28 and looking up the relevant Y_2^{μ} 's in Eq. A-14, we find

$$R - R_0 = \sqrt{\frac{5}{16\pi}} R_0 \beta [\cos \gamma (3 \cos^2 \theta' - 1) + \sqrt{3} \sin \gamma \sin^2 \theta' \cos 2\phi']. \quad (9-33)$$

The quantity β is a measure of the total deformation of the nucleus from sphericity, since

$$\beta^2 = \sum_{\mu} \alpha_{2\mu}^2 = \sum_{\mu} |\alpha_{2\mu}|^2. \quad (9-34)$$

The significance of γ is seen by writing the increments in lengths along the body-fixed axes x' , y' , and z' :

$$\delta R_{z'} = R(0, \phi') - R_0 = \sqrt{\frac{5}{4\pi}} R_0 \beta \cos \gamma,$$

$$\delta R_{x'} = R\left(\frac{\pi}{2}, 0\right) - R_0 = \sqrt{\frac{5}{4\pi}} R_0 \beta \cos\left(\gamma - \frac{2\pi}{3}\right),$$

$$\delta R_{y'} = R\left(\frac{\pi}{2}, \frac{\pi}{2}\right) - R_0 = \sqrt{\frac{5}{4\pi}} \beta R_0 \cos\left(\gamma - \frac{4\pi}{3}\right).$$

If we denote, for convenience in notation, the body-fixed axes x' , y' , z' by 1, 2, 3, the above expressions may be summarized as follows:

$$\delta R_{\kappa} = \sqrt{\frac{5}{4\pi}} \beta R_0 \cos\left(\gamma - \frac{\kappa 2\pi}{3}\right), \quad \kappa = 1, 2, 3. \quad (9-35)$$

The value $\gamma = 0$ yields a prolate (cigar-shaped) ellipsoid with the 3-axis as its symmetry axis, while $\gamma = 2\pi/3$ and $\gamma = 4\pi/3$ are prolate ellipsoids with the 1- and 2-axes as symmetry axes. Similarly $\gamma = \pi$, $\gamma = \pi/3$, and $\gamma = 5\pi/3$ are oblate ellipsoids about the 3, 2, and 1 symmetry axes, respectively.

Note that, if we make a cyclic permutation of the axes 1, 2, 3, the nuclear surface remains unaltered. It is easy to see from Eq. 9-35 that this cyclic permutation could be effected by changing γ to $(\gamma - 2\pi/3)$. Thus γ , $(\gamma - 2\pi/3)$, and $(\gamma - 4\pi/3)$ all describe the same nuclear surface. Furthermore, from Eq. 9-35 we see that γ and $-\gamma$ define the same nuclear surface. Therefore

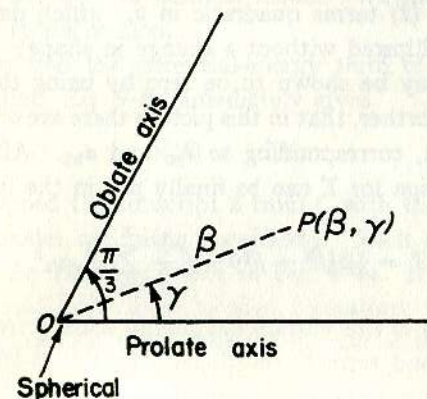


Fig. 9-5 The point P in the β - γ polar coordinates represents a definite asymmetric quadrupole shape. The length OP represents the magnitude of deformation β , and the angle that it makes with the horizontal axis measures the asymmetry parameter γ .

the γ -dependence of any physical quantity which is only a function of nuclear shape should be through the variable $\cos 3\gamma$. It is clear that the nuclear shape can be specified in a two-dimensional β - γ plane in polar coordinates, with the length of the vector representing β and its angular coordinate denoting γ , as shown in Fig. 9-5. Moreover, since only those functions of γ can come for which $f(\gamma) = f(\gamma - 2\pi/3)$, that is, $f(\gamma + \pi/3) = f(\gamma - \pi/3)$, and, in addition, $f(\gamma) = f(-\gamma)$, it follows that $f(\gamma)$ is symmetrical about the line $\gamma = \pi/3$. It is thus sufficient to take a 60° wedge in the β - γ plane, as in Fig. 9-5, to specify all possible quadrupole shapes. Any point on the $\gamma = 0$ line represents a prolate shape with the axis of symmetry along the 3-axis, while a point on the $\gamma = \pi/3$ line is an oblate shape with the 2-axis as the axis of symmetry. Any point within the wedge not lying on either of these lines is a deformed shape with no axis of symmetry.

We must now investigate the transformation of the kinetic energy

$$T = \frac{1}{2} \sum_{\mu} B |\dot{a}_{2\mu}|^2$$

to the body-fixed system. From Eq. 9-32, we find

$$\dot{a}_{2\mu} = \sum_{\nu} \dot{a}_{2\nu} \mathcal{D}_{\mu\nu}^{2*}(\theta_i) + a_{2\nu} \sum_{\nu} \dot{\theta}_i \frac{\partial}{\partial \theta_i} \mathcal{D}_{\mu\nu}^{2*}(\theta_i).$$

Substituting this in the expression for T , we find that there are three types of terms in the kinetic energy: (1) terms quadratic in $\dot{a}_{2\nu}$, which represent vibrations of the ellipsoid with change in shape, but the orientation θ_i unaltered in time; (2) terms quadratic in $\dot{\theta}_i$, which denote change in the orientation of the ellipsoid without a change in shape; and (3) cross terms like $\dot{a}_{2\nu} \dot{\theta}_i$, which may be shown to be zero by using the properties of the \mathcal{D} -matrices. Note, further, that in this picture there are only two independent modes of vibrations, corresponding to \dot{a}_{20} and \dot{a}_{22} . After some nontrivial algebra, the expression for T can be finally put in the form [2]

$$T = \frac{1}{2} B (\dot{\beta}^2 + \beta^2 \dot{\gamma}^2) + \frac{1}{2} \sum_{\kappa=1}^3 \mathcal{J}_{\kappa} \omega_{\kappa}^2, \quad (9-36)$$

where the first term is the vibrational energy arising from terms quadratic in $\dot{a}_{2\nu}$, and the second term is rotational. In Eq. 9-36, ω is the angular velocity of the principal axes with respect to the space-fixed axes,[†] and the effective moment of inertia \mathcal{J}_{κ} is given by

[†] Expressions for ω are given, for example, in Eq. 4-103 of H. Goldstein, *Classical Mechanics*, Addison-Wesley, Reading, Mass., 1950.

$$\mathcal{J}_{\kappa} = 4B\beta^2 \sin^2 \left(\gamma - \frac{\kappa 2\pi}{3} \right). \quad (9-37)$$

Note that, if there is an axis of symmetry, the moment of inertia for collective rotations about this axis vanishes, that is, if $\gamma = 0$ or π , $\mathcal{J}_3 = 0$. In this case, the moments about the other axes are equal:

$$\mathcal{J}_1 = \mathcal{J}_2 = \mathcal{J} = 3B\beta^2. \quad (9-38)$$

We note that to obtain the moment of inertia we must first obtain the inertial parameter B from a more basic model. If we use the value of B given by Eq. 9-7 for the irrotational fluid, \mathcal{J} can easily be expressed in terms of the moment of inertia of a rigid sphere of the same radius and density:

$$\mathcal{J} = \left(\frac{45}{16\pi} \right) \mathcal{J}_{\text{rig}} \beta^2, \quad (9-39)$$

with

$$\mathcal{J}_{\text{rig}} = \frac{2}{5} A M R_0^2, \quad (9-40)$$

where M , as usual, is the nucleon mass. We see that, since β is small, very little of the nuclear matter is actually taking part in the effective rotation. Although β and γ are fixed so that a given shape is rotating, it is more realistic to think of the rotation as the motion of a wave around the nuclear surface, carrying relatively little matter with it. These conclusions, including in particular the belief that the moment of inertia is zero about the symmetry axis, are based on the hydrodynamical model. We shall have more to say on this point later in the section.

We should now find the potential-energy term of the deformed drop. For the spherical drop, Eq. 9-8 immediately gives

$$V(\beta) = \frac{1}{2} C \beta^2, \quad (9-41)$$

where we have dropped the subscript 2 from C with the understanding that only quadrupole modes are being considered. Such a potential could be represented in the β - γ plane as shown in Fig. 9-6a. If we were to quantize the motion of a liquid drop in the present formalism, we would replace the velocities in the kinetic-energy expression by the conjugate momenta, and these in turn by differential operators in the Schrödinger representation. For the spherical case, the Hamiltonian takes the form

$$H = T_{\beta} + T_{\gamma} + \sum_{\kappa=1}^3 \frac{L_{\kappa}^2}{2\mathcal{J}_{\kappa}} + \frac{1}{2} C \beta^2, \quad (9-42)$$

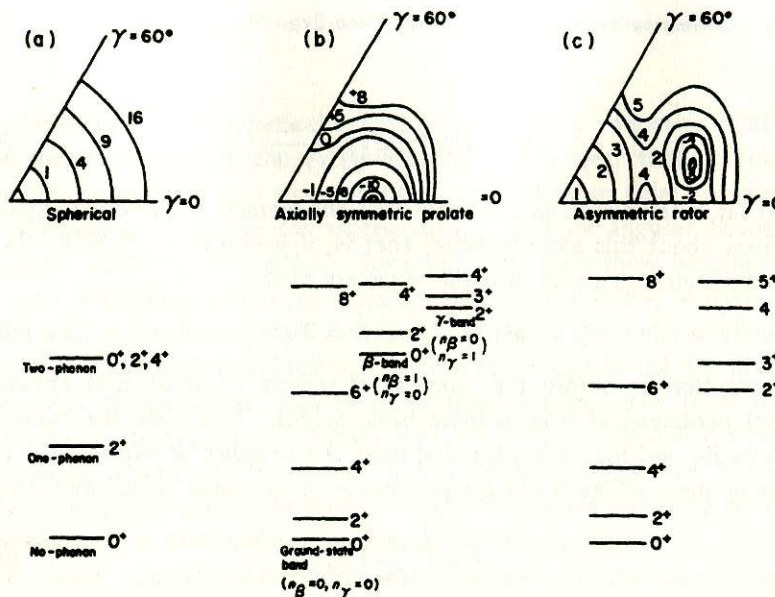


Fig. 9-6 Schematic plots of $V(\beta, \gamma)$ in arbitrary units for (a) spherical, (b) axially symmetric prolate, and (c) asymmetric shapes, with the corresponding low-lying energy levels.

where T_β and T_γ together constitute the vibrational kinetic energy, the third term is rotational, and L_κ is the component of angular momentum along the κ -axis. The quantities L_κ are referred to the moving axes and do not have the same commutation properties as angular-momentum components along fixed axes. The difference is only in the sign of the commutators:[†] $[L_1, L_2] = -iL_3$, but $[L_x, L_y] = iL_z$; consequently only slight changes are involved in handling them. In particular, although L^2 and L_z are constants of motion, in general no component of L_κ is. If we solve the Schrödinger equation with the Hamiltonian 9-42 and values of B and C given as before by Eqs. 9-7 and 9-11, we obtain the vibrational spectrum shown in Fig. 9-6a, which is identical to that of Eq. 9-16. This is not surprising, since we are solving essentially the same problem in the body-fixed frame, and actually making the analysis much more difficult by doing so.

This approach of describing the motion in terms of β - and γ -vibrations coupled with rotation is not of value if the equilibrium shape of the nucleus is strictly spherical; but, as we saw in the earlier section, this is too unrealistic a model. The vast majority of nuclei either seem to have a well-deformed equilibrium shape ("stiff" nuclei) or are transitional, being very soft to

nuclear deformation. For these "soft" nuclei, it is not meaningful to say that the equilibrium shape is characterized by a single point in the β - γ plane, since $V(\beta, \gamma)$ has no well-localized minimum in this plane. For such nuclei in particular, the method of solving the Schrödinger equation with the Bohr Hamiltonian

$$H = T_\beta + T_\gamma + \sum_{\kappa=1}^3 \frac{L_\kappa^2}{2J_\kappa} + V(\beta, \gamma) \quad (9-43)$$

is of great value. We shall return to transitional nuclei after discussing the simpler case of a stiff deformed nucleus.

If the inertial parameters and the potential-energy function $V(\beta, \gamma)$ are known (let us say from some basic microscopic calculation), the energy spectrum and the wave function can, in principle, be obtained by solving the Schrödinger equation with the Bohr Hamiltonian (Eq. 9-43). Much physical insight, however, can often be gained by examining the potential function $V(\beta, \gamma)$, which mainly governs the type of spectrum to be expected. In Fig. 9-6b, for example, a potential function which has a well-defined minimum for $\gamma = 0$ and $\beta = \beta_0$ is plotted. Although kinetic-energy effects are important, we can qualitatively argue that the nucleus in its ground state will tend to have the shape with $\gamma = 0$, $\beta = \beta_0$ in this case, so that the nuclear density has maximum overlap with $V(\beta, \gamma)$. As we have already seen, such a shape corresponds to an axially symmetric prolate ellipsoid with the 3-axis as its axis of symmetry. We can thus expect a rotational ground-state band of an axially symmetric rotor, where no vibrational quanta have been excited. We noted before that in the body-fixed axes two modes of vibrations are possible, a_{20} and a_{22} . In a spheroidal shape, the multipole order λ of phonons is not actually a good quantum number, but its projection along the symmetry axis, ν ($= 0$ or 2 here), is. The vibrations are expected to be about the equilibrium values $\beta = \beta_0$ and $\gamma = 0$. For small vibrations, at any instant of time t ,

$$\beta(t) = \beta_0 + \delta\beta(t) \quad \text{and} \quad \gamma(t) = \delta\gamma(t). \quad (9-44)$$

Using Eq. 9-32, we then obtain, to first order,

$$a_{20} = \delta\beta, \quad a_{22} = \frac{1}{\sqrt{2}} \beta_0 \delta\gamma. \quad (9-45)$$

There are thus two types of vibrational quanta: the β -type, with the phonon angular-momentum projection zero along the symmetry axis, and the γ -type, with projection 2 along the original symmetry axis. We may

[†] See, for example, Section 101 of L. D. Landau and E. M. Lifshitz, *Quantum Mechanics (Non-Relativistic Theory)*, Addison-Wesley, Reading, Mass., 1959.

picture β -vibrations as oscillations of the nuclear shape with its axis of symmetry preserved, while in γ -vibrations the nucleus loses its axial symmetry. If we denote the number of β -type phonons by n_β and the number of γ -type phonons by n_γ , in the ground-state rotational band $n_\beta = n_\gamma = 0$. We should then expect two more low-lying rotational bands, built on vibrational states $n_\beta = 0, n_\gamma = 1$ and $n_\beta = 1, n_\gamma = 0$. This kind of spectrum for a prolate axially symmetric nucleus is shown in Fig. 9-6b. Note that for the spheroid both the inertial parameter B and the force constant C can be quite different for β - and γ -vibrations, so that $\hbar\omega_\beta \neq \hbar\omega_\gamma$.

Another example of $V(\beta, \gamma)$ for a stiff nucleus is shown in Fig. 9-6c; in this case there is a well-defined minimum at a nonzero value of $\gamma = \gamma_0$ and $\beta = \beta_0$. From the preceding considerations, we can expect the low-lying spectrum to be that of an asymmetric rotor, and this is shown in Fig. 9-6c. In the following section, we shall consider both cases, Fig. 9-6b and Fig. 9-6c, in more detail.

9-4 SYMMETRIES OF THE COLLECTIVE WAVE FUNCTION FOR WELL-DEFORMED, EVEN-EVEN NUCLEI

In this section, we shall discuss in some detail the wave function of the so-called stiff, deformed nuclei, for which the potential function $V(\beta, \gamma)$ has a well-localized minimum. As before, we consider the low-lying states of even-even nuclei and disregard the intrinsic nucleonic part of the wave function. The potential function $V(\beta, \gamma)$ is such that there is a minimum for $\beta = \beta_0, \gamma = \gamma_0$; γ_0 may or may not be zero. In addition to rotation, the nucleus will vibrate around the equilibrium shape; for small oscillations the potential can be expanded about (β_0, γ_0) and written in the form

$$V(\beta, \gamma) \approx V_0 + \frac{1}{2}C_\beta(\beta - \beta_0)^2 + \frac{1}{2}C_\gamma(\gamma - \gamma_0)^2. \quad (9-46)$$

We also note that rotations and vibrations are actually coupled because the moments of inertia \mathcal{J}_κ are functions of β, γ . To extract the rotation-vibration coupling term in an approximate manner, we can expand $1/\mathcal{J}_\kappa(\beta, \gamma)$ in Eq. 9-43 about the equilibrium (β_0, γ_0) :

$$\begin{aligned} \frac{1}{\mathcal{J}_\kappa(\beta, \gamma)} &= \frac{1}{\mathcal{J}_\kappa(\beta_0, \gamma_0)} + \left[\frac{\partial}{\partial \beta} \frac{1}{\mathcal{J}_\kappa(\beta, \gamma_0)} \right]_{\beta_0} (\beta - \beta_0) \\ &\quad + \left[\frac{\partial}{\partial \gamma} \frac{1}{\mathcal{J}_\kappa(\beta_0, \gamma)} \right]_{\gamma_0} (\gamma - \gamma_0) + \dots \end{aligned} \quad (9-47)$$

Using expressions 9-46 and 9-47, we can now write, for a well-deformed

nucleus, the Hamiltonian 9-43 as,

$$\begin{aligned} H &= T_\beta + \frac{1}{2}C_\beta(\beta - \beta_0)^2 + T_\gamma + \frac{1}{2}C_\gamma(\gamma - \gamma_0)^2 \\ &\quad + \sum_{\kappa=1}^3 \frac{L_\kappa^2}{2\mathcal{J}_\kappa(\beta_0, \gamma_0)} + (U_1 + U_2), \end{aligned} \quad (9-48)$$

where U_1, U_2 are the rotation-vibration interaction terms. If we take the hydrodynamic form 9-37 for the moment of inertia and $\gamma_0 = 0$, then, to first order in $\beta - \beta_0$ and γ , we obtain

$$\begin{aligned} U_1 &= -\frac{\hbar^2}{\mathcal{J}_0} (L^2 - L_z^2) \frac{\beta - \beta_0}{\beta_0}, \\ U_2 &= -\frac{\hbar^2}{2\mathcal{J}_0} (L_+^2 + L_-^2) \frac{\gamma}{\sqrt{3}}, \end{aligned} \quad (9-49)$$

where the operators L_+ and L_- are the raising and lowering operators defined in Eq. A-1. Whereas U_1 is diagonal in K , U_2 can mix different bands with $\Delta K = \pm 2$. The effect of $U_1 + U_2$ may be treated in perturbation theory in an approximate manner; in a more careful treatment [13], expansion 9-47 is carried up to second order, and the total Hamiltonian is diagonalized in the basis generated by neglecting the coupling.

We shall soon examine the effects of such terms on the rotational spectrum. If this coupling is neglected, the Bohr Hamiltonian (Eq. 9-48) is separable in vibrational and rotational parts. In the general case of three unequal \mathcal{J}_κ , the projection of the angular momentum about the 3-axis, K , is not a good quantum number. The wave function, however, can still be expressed as a linear combination of the $(2J + 1) \mathcal{D}^J$'s. We can write

$$\Psi = f_{J,\tau,\nu}(\beta) \sum_{K=-J}^J g_K^{J,\tau}(\gamma) \mathcal{D}_{MK}^J(\theta_1, \theta_2, \theta_3). \quad (9-50)$$

The rotational wave functions \mathcal{D}_{MK}^J are simultaneous eigenfunctions of J^2 , J_z , and J_3 as given in Eq. A-71. Besides J and M , three other quantum numbers are required to specify the state completely. For the axially symmetric case, for example, these could be K and the phonon numbers n_β and n_γ , as mentioned in the preceding section. In the general case of Eq. 9-50, τ stands for two of the quantum numbers, associated with γ -vibrations and rotations, and ν stands for the third, associated with β -vibrations.

Certain symmetries restrict the generalities of the function $g(\gamma)$ and the allowed values of J and K in this model. Using Eq. 9-32, we see that the space-fixed $\alpha_{2\mu}$'s are expressible in terms of the body-fixed parameters as

$$\alpha_{2\mu} = \beta \cos \gamma \mathcal{D}_{\mu 0}^{2*}(\theta_i) + \frac{1}{\sqrt{2}} \beta \sin \gamma [\mathcal{D}_{\mu 2}^{2*}(\theta_i) + \mathcal{D}_{\mu -2}^{2*}(\theta_i)], \quad (9-51)$$

where we have chosen the body-fixed frame to be right-handed. The wave function should be single valued in the quantities α_μ (we drop the suffix 2), which specify the shape of the nucleus uniquely, but various choices of the body-fixed variables[†] (β , γ , and the Euler angles θ_1 , θ_2 , θ_3) are possible which all give the same α_μ 's. The wave function 9-50 must be invariant under any change of the body axes which does not alter the α_μ 's. It is important to note that the body-fixed frame (1, 2, 3) is specified by a set of Euler angles (θ_1 , θ_2 , θ_3), and we have chosen a right-handed system. By making changes in these values of Euler angles (i.e., by performing a set of rotations), we can never go from the right-handed frame (1, 2, 3) to the left-handed frame (-1, -2, -3) in this three-dimensional system. It is possible, as we shall see, to go from (1, 2, 3) to (-3, -2, -1) by a series of rotations, but this is still a right-handed system and does *not* mean an inversion. Since we describe the \mathcal{D} -functions in terms of the Euler angles, and these variables cannot take a right-handed system to a left-handed one, we cannot attach a parity quantum number to the rotational function $\mathcal{D}_{MK}^J(\theta_i)$ in the general case (when M and K are non-zero). However, in the special case when $K = 0$, it may be seen from Eq. A-66 that $\mathcal{D}_{M0}^J(\theta_1, \theta_2, \theta_3) = [4\pi/(2J+1)]^{1/2} \cdot Y_J^M(\theta_2, \theta_1)$, and θ_3 is redundant. The variables θ_2 , θ_1 can now be considered to specify the orientation of a single vector \mathbf{r} . By changing θ_2 to $\pi - \theta_2$, θ_1 to $\pi + \theta_1$, we can transform \mathbf{r} to $-\mathbf{r}$, that is, a parity operation. Thus the spherical harmonics have parity, $(-)^J$, in this sense. In the general case, the total wave function of the rotating nucleus will still have a parity, but it will be the parity of the intrinsic nucleonic wave function $\chi(\mathbf{r}_i)$, which we have ignored in this discussion.

We now consider the group of transformations on the body axes (1, 2, 3) which retain the right-handedness, but change the variables γ , θ_i in such a manner as to keep the α_μ 's invariant. Any such transformation can be described by a group of rotations, and these should leave the wave function 9-50 invariant. These transformations describe all possible ways in which the *right-handed* body axes can be relabeled: (1) without changing any of the signs of the axes 1, 2, or 3; (2) changing only one of the signs; (3) changing any two of the signs; and finally (4) changing all three signs, but in all cases retaining the right-handedness. We consider each of these cases, 1-4, in turn.

[†] The variable β , by Eq. 9-34, is a scalar and remains invariant under rotation.

1. These are simply the cyclic permutations of the axes (1, 2, 3), and we define the operator R_3 so that $R_3(1, 2, 3) = (3, 1, 2)$. Obviously, there are three such possibilities, and $R_3^3 = 1$.

2. The sign of one axis can be reversed, while maintaining the right-handedness, by making a rotation of $\pi/2$ about any one of the axes. For example, if we rotate (1, 2, 3) about the 3-axis by $\pi/2$, we obtain (1', 2', 3'), where $1' = 2$, $2' = -1$, and $3' = 3$. This operator is denoted by $R_2^{(3)}$, where the parenthetical superscript denotes the axis about which the rotation has been performed:

$$R_2^{(3)}(1, 2, 3) = (2, -1, 3). \quad (9-52)$$

These indices can be cyclically permuted in three possible ways. Furthermore, we could have applied any *one* of the operators $R_2^{(1)}$, $R_2^{(2)}$, or $R_2^{(3)}$ to (1, 2, 3); thus there are nine possible combinations (1', 2', 3') where only one sign is negative and the system is right-handed.

3. Similarly, two of the signs in the axes could be reversed in (1, 2, 3) by making a rotation of π about any one of the axes. Defining this rotation by $R_1^{(*)}$, we see, for example, that

$$R_1^{(1)}(1, 2, 3) = (1, -2, -3). \quad (9-53)$$

As in case (2), there are again nine such transformations in the right-handed system with two of the signs negative.

4. Finally, we note that, by taking suitable combinations of R_1 and R_2 , we can reverse all the signs in (1, 2, 3). For example,

$$R_2^{(3)}R_1^{(1)}(1, 2, 3) = R_2^{(3)}(1, -2, -3) = (-2, -1, -3), \quad (9-54)$$

where we have used Eqs. 9-52 and 9-53. Note that we cannot obtain the left-handed system (-1, -2, -3) from (1, 2, 3) by any set of rotations. There are, clearly, three different possibilities, corresponding to the three cyclic permutations of (-2, -1, -3).

In all, therefore, there are 24 different sets of axes (1', 2', 3') in the right-handed frame which can alter the body-fixed variables in such a way as to keep the α_μ 's invariant. Since these are all obtainable through various combinations of the operators R_1 , R_2 , and R_3 , we should demand that the wave function 9-50 be invariant under these operations. An alternative, but less transparent, way of noting that there are 24 such combinations is to realize that $(R_3)^3 = 1$, $[R_2^{(3)}]^4 = 1$, and $[R_1^{(1)}]^2 = 1$, that all possibilities are covered by the operators $[R_1^{(1)}]^a \cdot [R_2^{(3)}]^b \cdot (R_3)^c$, and that there are

$3 \times 4 \times 2 = 24$ such distinct operators. We can now examine how the \mathcal{D} -functions and γ transform under the transformations R_1 , R_2 , and R_3 . The rotation operator $R_1^{(1)}$ is a rotation of π around the 1-axis, changing 2 to -2 and 3 to -3 . From Eq. 9-35, this does not change γ , but geometrical considerations show that $\theta_1 \rightarrow (\pi + \theta_1)$, $\theta_2 \rightarrow (\pi - \theta_2)$, and $\theta_3 \rightarrow (2\pi - \theta_3)$. Thus

$$\begin{aligned} R_1^{(1)} \mathcal{D}_{MK}^J(\theta_1, \theta_2, \theta_3) &= \mathcal{D}_{MK}^J(\pi + \theta_1, \pi - \theta_2, 2\pi - \theta_3) \\ &= \exp[iM(\pi + \theta_1)] \mathcal{D}_{MK}^J(\pi - \theta_2) \exp(-iK\theta_3), \text{ using Eq. A-53,} \\ &= \exp(iM\theta_1) (-)^J \mathcal{D}_{M,-K}^J(\theta_2) \exp(-iK\theta_3), \text{ using Eq. A-59,} \\ &= (-)^J \mathcal{D}_{M,-K}^J(\theta_1, \theta_2, \theta_3). \end{aligned} \quad (9-55)$$

The rotation operator $R_2^{(3)}$ is a rotation by $\pi/2$ about the 3-axis; it changes γ to $-\gamma$ and the Euler angles transform as $\theta_1 \rightarrow \theta_1$, $\theta_2 \rightarrow \theta_2$, $\theta_3 \rightarrow \theta_3 + \pi/2$. Thus

$$\begin{aligned} R_2^{(3)} \mathcal{D}_{MK}^J(\theta_1, \theta_2, \theta_3) &= \mathcal{D}_{MK}^J\left(\theta_1, \theta_2, \theta_3 + \frac{\pi}{2}\right) \\ &= \exp(iK\pi/2) \mathcal{D}_{MK}^J(\theta_1, \theta_2, \theta_3). \end{aligned} \quad (9-56)$$

Finally, R_3 , a cyclic permutation of the axes, is equivalent to the rotation $\theta_1 = 0$, $\theta_2 = \pi/2$, $\theta_3 = \pi/2$, and changes γ to $(\gamma - 2\pi/3)$. We can therefore write

$$R_3 \mathcal{D}_{MK}^J(\theta_1, \theta_2, \theta_3) = \sum_{K'} \mathcal{D}_{K'K}^{J*}(0, \pi/2, \pi/2) \mathcal{D}_{MK'}^J(\theta_i). \quad (9-57)$$

By using Eqs. 9-55 to 9-57, it can be verified that under the transformations R_1 , R_2 , and R_3 the expression for α_{2u} as given in Eq. 9-51 remains invariant. We now apply these transformations to the wave function 9-50 to find its symmetry properties. It should be realized that the intrinsic part of the wave function, χ , is not included in Eq. 9-50, and this part will also transform under the symmetry operations. For even-even nuclei, the low-lying states are given, however, by the rotational and vibrational modes with the intrinsic spin zero, and we can ignore the intrinsic part. For odd nuclei, this is not the case, and it is necessary to consider the transformation of χ explicitly under the symmetry operations.

Consider first the effect of $R_2^{(3)}$ on the wave function 9-50. If we demand that $R_2^{(3)}\Psi = \Psi$, then, using Eq. 9-56 and recalling that $\gamma \rightarrow -\gamma$ under the operation of $R_2^{(3)}$, we obtain

$$g_K^J(-\gamma) \exp(iK\pi/2) = g_K^J(\gamma). \quad (9-58)$$

Applying then the condition $[R_2^{(3)}]^2\Psi = \Psi$, we see that $g_K^J(\gamma) = g_K^J(-\gamma)$; hence K must be an even integer for g_K^J to be nonzero.

Next, we consider the operator $R_1^{(1)}$ on Ψ , noting that γ remains unchanged. Since $[R_1^{(1)}]^2 = 1$, it follows that, if we take a wave function $[1 + R_1^{(1)}]\Psi$, it will be invariant under the operation $R_1^{(1)}$. Recalling Eq. 9-55, we can therefore write an invariant wave function:

$$\Phi = f_{J,\tau,v}(\beta) \sum_{\substack{K=0 \\ (\text{even})}}^J g_K^{J,\tau}(\gamma) |JMK\rangle, \quad (9-59)$$

where $|JMK\rangle$ is a normalized rotational wave function given by

$$|JMK\rangle = \left[\frac{2J+1}{16\pi^2(1+\delta_{K0})} \right]^{1/2} (\mathcal{D}_{MK}^J + (-)^J \mathcal{D}_{M,-K}^J). \quad (9-60)$$

If there is axial symmetry, K is a good quantum number, and the collective wave function can simply be written as

$$\Phi = f_{J,K,n,\beta}(\beta) g_K^J(\gamma) |JMK\rangle. \quad (9-61)$$

Note that, for $K = 0$, Eq. 9-60 implies that only even values of J are allowed. In this analysis, however, only the quadrupole oscillations were considered. More generally, it is possible to have rotational bands built on octupole vibrations, in which case, for $K = 0$, only an odd sequence of J values appears. Consider, for simplicity, an extra vibrational degree of freedom $a_{30}(t) Y_3^0(\theta', \phi')$ of the nuclear shape. The length of a vector in the body-fixed frame, given by Eq. 9-28, now generalizes to

$$R(\theta', \phi') = R_0 [1 + \sum_{\mu} a_{2\mu} Y_2^{\mu}(\theta', \phi') + a_{30} Y_3^0(\theta', \phi')].$$

If we apply the rotation operator $R_1^{(1)}$ to the body-fixed frame, the same vector length is given in a new frame with $\theta' \rightarrow (\pi - \theta')$, $\phi' \rightarrow (2\pi - \phi')$. Under this operation, then, the Y_2^{μ} 's do not change sign, but $Y_3^0(\pi - \theta', 2\pi - \phi') = -Y_3^0(\theta', \phi')$. In order that the length remain invariant under this transformation, the $a_{2\mu}$'s remain the same (i.e., β and γ do not change under $R_1^{(1)}$), but a_{30} must change sign. But a one-phonon harmonic-wave function always changes sign if the dynamic variable changes sign; hence the vibrational octupole one-phonon state $\phi_{\text{vib}}^{J=3}$ changes sign under the operation $R_1^{(1)}$. Thus an unsymmetrized wave function $\phi_{\text{vib}}^{J=3}(a_{30}) \cdot \mathcal{D}_{MK}^J(\theta_i)$ transforms as

$$R_1^{(1)}[\phi_{\text{vib}}^{\lambda=3}(a_{30}) \mathcal{D}_{MK}^J(\theta_i)] = -\phi_{\text{vib}}^{\lambda=3}(a_{30})(-)^J \mathcal{D}_{M,-K}^J(\theta_i). \quad (9-62)$$

In order to make the total wave function Φ invariant under $R_1^{(1)}$, we again take the combination

$$(1 + R_1^{(1)})\phi_{\text{vib}}^{\lambda=3}(a_{30}) \mathcal{D}_{MK}^J(\theta_i) = (\mathcal{D}_{MK}^J - (-)^J \mathcal{D}_{M,-K}^J)\phi_{\text{vib}}^{\lambda=3}(a_{30}),$$

which shows that for $K = 0$ only odd- J sequences are allowed.

We have thus generated the normal collective $K = 0$ bands in even-even nuclei:

$$K\pi = 0^+, \quad J = 0^+, 2^+, 4^+, \dots, \quad (9-63a)$$

$$K\pi = 0^-, \quad J = 1^-, 3^-, 5^-, \dots \quad (9-63b)$$

Sequence 9-63a is seen in the ground-state and β -vibrational rotational bands, while 9-63b is observed as the rotational band built on the $K = 0$ octupole vibration. It is worth mentioning that Das Gupta and Volkov [14] have pointed out the possibility of observing anomalous excited-state bands:

$$K\pi = 0^+, \quad J = 1^+, 3^+, 5^+, \quad (9-64a)$$

$$K\pi = 0^-, \quad J = 0^-, 2^-, 4^-, \dots, \quad (9-64b)$$

which may arise if the vibrational $\lambda = 2$ state changes sign under $R_1^{(1)}$ whereas the vibrational $\lambda = 3$ state does not. This is not the case for the normal surface vibrations that we have considered, but may be realized, for example, if surface vibrations of the Y_{20} -type are coupled to the intrinsic spins of the nucleons. The 0^- and 2^- states at 1819 and 1856.9 keV in ^{176}Hf have been identified [15] as members of the anomalous sequence 9-64b.

9-5 COLLECTIVE SPECTRA OF EVEN-EVEN NUCLEI

We first consider the simple case of a nucleus with a well-localized deformation in the β - γ plane and further simplify the situation by assuming that it possesses an axis of symmetry, which we choose to be the 3-axis. The wave function of such a system is then given by Eq. 9-61, which separates into a vibrational part $f(\beta)g(\gamma)$ and a rotational part, provided the rotation-vibration coupling terms are neglected. The rotational energy is simply given by

$$\begin{aligned} \langle JMK | \sum_k \frac{L_k^2}{2\mathcal{J}_k} | JMK \rangle &= \hbar^2 \left\langle \frac{L^2 - L_3^2}{2\mathcal{J}} + \frac{L_3^2}{2\mathcal{J}_3} \right\rangle \\ &= \hbar^2 \frac{J(J+1) - K^2}{2\mathcal{J}} + \frac{\hbar^2 K^2}{2\mathcal{J}_3}, \end{aligned} \quad (9-65)$$

where we have put $\mathcal{J}_1 = \mathcal{J}_2 = \mathcal{J}$. We consider first the ground-state rotational band of such a system, where $n_\beta = n_\gamma = 0$. The angular momentum \mathbf{J} in this band is arising solely from rotational motion ($\mathbf{J} = \mathbf{L}$), and K is its projection along the symmetry axis. Any rotation of the frame about the symmetry axis, 3, should leave the rotational wave function invariant or, at most, introduce a phase factor. If we apply such a rotation about the 3-axis by an arbitrary angle θ , then, by Eq. A-46, the wave function $|JMK\rangle$ transforms to

$$\begin{aligned} \exp(-i\theta J_3) |JMK\rangle &= \left[\frac{2J+1}{16\pi^2(1+\delta_{K0})} \right]^{1/2} \\ &\cdot [\exp(-i\theta K) \mathcal{D}_{MK}^J + (-)^J \exp(i\theta K) \mathcal{D}_{M,-K}^J] \end{aligned}$$

and hence axial symmetry demands that $K = 0$. This means that the rotational angular momentum \mathbf{L} is perpendicular to the 3-axis, with the result that the nucleus is actually rotating about *an axis perpendicular to the axis of symmetry*. We see from Eq. 9-60 that for $K = 0$ only even values of J are allowed; hence the ground-state rotational band is given by

$$E_J = \frac{\hbar^2}{2\mathcal{J}} J(J+1), \quad (9-66)$$

with

$$K = 0; \quad J = 0, 2, 4, \dots \quad (9-67)$$

We should remember that Eq. 9-67 is valid only for the quadrupole distortions that we have considered. If it is assumed that the intrinsic part of the wave function has positive parity, the parities of the rotational levels Eq. 9-67 are also positive. Note that for excited-state bands n_β or $n_\gamma \neq 0$, and it is possible to have nonzero values of K . For nonzero K , J takes all values $K, K+1, K+2$, etc.

In this section we have been considering only the collective modes of motion, with no reference to their coupling to intrinsic coordinates. In even-even nuclei where the intrinsic angular momentum is zero, we may expect a ground-state rotational band as given by Eq. 9-66. For the low-lying states of this rotational band, we may ignore the coupling due to vibrational and intrinsic modes of excitations of higher energy, and assume the moment of inertia to be a constant in the simplest approximation. Using Eq. 9-66, we then find that $E_4/E_2 = 10/3$, $E_6/E_2 = 7$, and $E_8/E_2 = 12$. The ground-state rotational band of ^{160}Dy , as found experimentally by Johnson, Ryde,

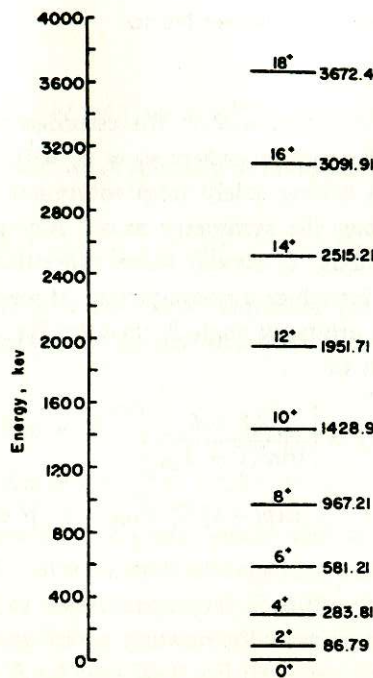


Fig. 9-7 The ground-state rotational band of ^{160}Dy . (After Johnson et al. [16].)

and Hjorth [16], is shown in Fig. 9-7. In this experiment, a beam of α -particles of energy near 43 MeV impinges on a target of ^{160}Gd . These α -particles impart a large amount of angular momentum to the compound nucleus, and a final state of ^{160}Dy in an angular-momentum state of $J \approx 20$ is formed with the ejection of four neutrons. The nucleus de-excites predominantly by cascading down the rotational band through $E2$ -transitions, and the associated γ -ray cascades are detected with Ge(Li) detectors. From the experimental spectrum of ^{160}Dy , we note that the ratios of E_4 , E_6 , and E_8 to E_2 are 3.27, 6.70, and 11.14, respectively, these being somewhat smaller than the values 3.33, 7, and 12 given by $J(J + 1)$. This decrease of a few per cent may be understood in terms of a weak coupling between these low-lying rotational modes and the vibrational modes. In general, such couplings depend on J^2 (see Eq. 9-49) and contribute to a change of energy in the second order of perturbation theory. Consequently, they introduce a correction term $-B[J(J + 1)]^2$. The first three or four excited states may be well fitted by the formula

$$E_J = \frac{\hbar^2}{2J} J(J + 1) - BJ^2(J + 1)^2, \quad (9-68)$$

9-5 | Collective Spectra of Even-Even Nuclei

with $\hbar^2/2J = 14.53$ keV and $B = 18$ eV. This situation is fairly typical for even-even nuclei in the region $A = 150\text{--}190$ and for $A > 220$. Such a perturbative approach for the rotation-vibration coupling is not adequate for the higher members ($J > 10$) of the rotational band or even for the low-lying states of transition nuclei like the Os isotopes, where the γ -vibrational levels are appreciably lowered in energy and the rotation-vibration interaction is substantial. Faessler, Greiner, and Sheline [13] have isolated the rotation-vibration interaction terms U_1 and U_2 by carrying expansion 9-47 up to the second order, assuming the hydrodynamical expression 9-37 for the moment of inertia. They diagonalize the Hamiltonian 9-48 with the basis states 9-50 to obtain the collective states.

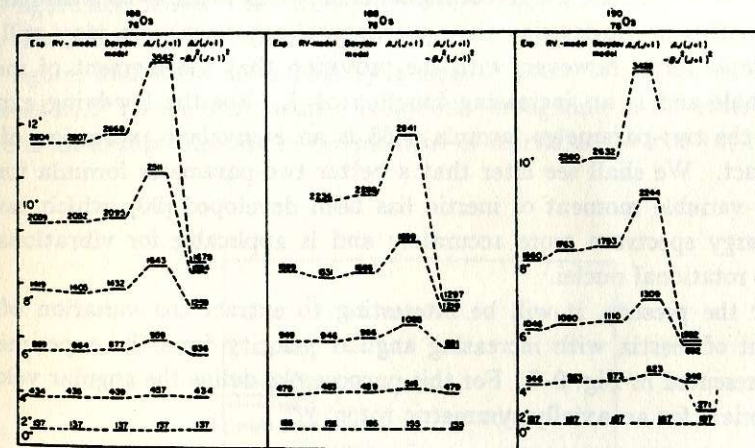


Fig. 9-8 Comparison of the various models for the energy spectra of Os isotopes (energies in keV). (After Faessler et al. [13].)

Figure 9-8 shows the results of their calculation for the Os isotopes, where their values (column 2) are compared with the experimental spectrum (column 1), as well as the predictions of Eqs. 9-66 (column 4) and 9-68 (column 5). In the Davydov model [17, 18, 19], whose predictions are shown in column 3, the levels are generated by the rotations of an asymmetric rotor. We shall discuss this model briefly later in this section; in general, its predictions are very similar to those of the axially symmetric model with rotation-vibration coupling included in the manner prescribed by Faessler et al. [13]. Although the success of this rotation-vibration model is impressive, as seen in Fig. 9-8, we should remember that the form of the rotation-

vibration interaction term was extracted from the hydrodynamical formula 9-37 for \mathcal{J}_κ , which cannot be realistic.

The moment of inertia \mathcal{J} obtained by empirical fitting of the first few low-lying levels is about half the rigid value $\mathcal{J}_{\text{rig}} = \frac{2}{5}AMR_0^2$ in the case of ^{160}Dy . As we shall see, the distortion β may be determined in the rotational model from the experimental determination of the reduced $E2$ -transition probability from the 0^+ to 2^+ state; using the hydrodynamical formula 9-39 with this value of β yields a moment of inertia that is about five times less than the observed \mathcal{J} . This poor agreement is typical of the irrotational fluid model and demonstrates the necessity of a microscopic model for the evaluation of the moment of inertia, as discussed in Section 10-8.

It is clear that the simple rotational-energy expression 9-66 with fixed \mathcal{J} is not sufficient to describe the experimental spectrum; we may still use this simple form, however, with the provision that the moment of inertia is variable and is an increasing function of J . For the low-lying excited levels, the two-parameter formula 9-68 is an equivalent expression of the same fact. We shall see later that a better two-parameter formula for E_J with a variable moment of inertia has been developed [20], which can fit the energy spectrum more accurately and is applicable for vibrational as well as rotational nuclei.

For the present, it will be interesting to extract the variation of the moment of inertia with increasing angular velocity from the experimental data presented in Fig. 9-7. For this purpose, we define the angular velocity appropriate for an axially symmetric rotor:

$$\hbar\omega_{\text{rot}} = \frac{dE}{d\sqrt{J(J+1)}}, \quad (9-69)$$

where we are identifying the angular momentum with $\hbar\sqrt{J(J+1)}$. Equation 9-69 can be rewritten as

$$\hbar^2\omega_{\text{rot}}^2 = 4J(J+1) \left[\frac{dE}{dJ(J+1)} \right]^2. \quad (9-70)$$

The moment of inertia is defined by the relation

$$\mathcal{J}\omega_{\text{rot}} = \hbar\sqrt{J(J+1)}. \quad (9-71)$$

Using Eqs. 9-70 and 9-71, we obtain

$$\frac{2\mathcal{J}}{\hbar^2} = \left[\frac{dE}{dJ(J+1)} \right]^{-1}. \quad (9-72)$$

Note that, by extracting the energy derivative $dE/dJ(J+1)$ from the experimental spectrum, we can calculate ω_{rot} and \mathcal{J} from Eqs. 9-70 and 9-72, and study the variation of \mathcal{J} with ω_{rot} . To evaluate the energy derivative from the experimental data, we may write

$$\frac{dE}{dJ(J+1)} = \frac{\Delta E}{\Delta J(J+1)} = \frac{E(J) - E(J-2)}{4J - 2}. \quad (9-73)$$

Also, the factor $J(J+1)$ in Eq. 9-70 is replaced by its mean value between J and $J-2$, which is $(J^2 - J + 1)$. It is now possible, using the experimental spectrum of Fig. 9-7, to calculate the variation of $2\mathcal{J}/\hbar^2$ with $(\hbar\omega_{\text{rot}})^2$, and the resulting plot is shown in Fig. 9-9. This figure also shows[†] the curves for ^{168}Yb , ^{158}Dy , and ^{162}Er [16]. Actually, only discrete points corresponding to discrete even J -values are obtained in this figure, and these are joined by a smooth line. It will be seen that, whereas in ^{168}Yb the increase in \mathcal{J} is smooth throughout, in the other nuclei there is an abrupt increase in the moment of inertia at $J \sim 14-16$, beyond

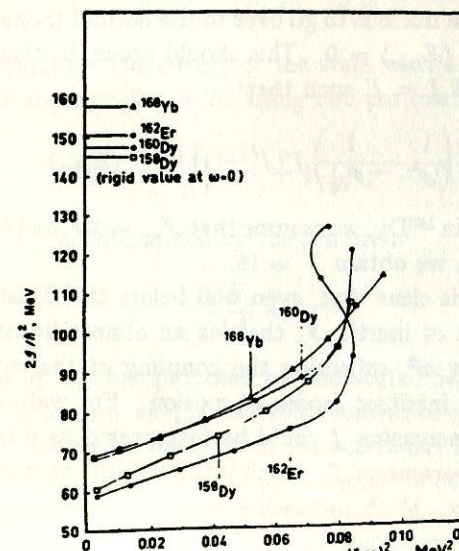


Fig. 9-9 The observed moments of inertia as functions of the square of the angular velocity. (After Johnson et al. [16].)

[†] Many other nuclides show the back-bending behavior. A detailed listing of experimental data is given by O. Saethre et al., *Nucl. Phys.* A207, 486 (1973).

which it tends to approach the rigid value. At least a partial explanation of this behaviour may be given in terms of the "Coriolis antipairing effect," predicted earlier by Mottelson and Valatin [21]. The following discussion is restricted to energy considerations.

Because of pairing interaction, as we have seen, the ground state of an even-even nucleus is lowered by the pairing energy $\langle E_{\text{pair}} \rangle$, which is typically only about -2 MeV in the rare-earth region. The pairing interaction, as we shall see, has a rather drastic effect on the moment of inertia, \mathcal{J} . Without the coherence of the pairing correlations, the moment of inertia of a system of fermions moving in an average potential is just the rigid value \mathcal{J}_{rig} [22]; with the pairing interaction it is about halved in ^{160}Dy . Let us write the energy of the rotating system as

$$E = \frac{\hbar^2}{2\mathcal{J}} J(J+1) + \langle E_{\text{pair}} \rangle, \quad (9-74)$$

where $\langle E_{\text{pair}} \rangle \approx -2$ MeV. For lower values of J , the nucleus prefers the superfluid state, because although the rotational energy has increased because of a drastic reduction in \mathcal{J} , this is more than compensated for by the gain in pairing energy. However, if J is large enough, it would be energetically more favorable for the nucleus to go over to the normal (nonsuperfluid) state, where $\mathcal{J} = \mathcal{J}_{\text{rig}}$ and $\langle E_{\text{pair}} \rangle = 0$. This should occur, in this simple picture, for a critical value of $J = J'$ such that^t

$$\frac{\hbar^2}{2} \left(\frac{1}{\mathcal{J}} - \frac{1}{\mathcal{J}_{\text{rig}}} \right) J'(J'+1) = -\langle E_{\text{pair}} \rangle. \quad (9-75)$$

For a rough estimate in ^{160}Dy , we assume that $\mathcal{J}_{\text{rig}} \approx 2\mathcal{J}$ and $\hbar^2/2\mathcal{J} \approx 15$ keV; then, using Eq. 9-75, we obtain $J' \approx 16$.

From Fig. 9-9 it is clear that, even well before this drastic change takes place in the moment of inertia \mathcal{J} , there is an almost linear increase in its value with increasing ω^2 , reflecting the coupling of the rotational motion with vibrational and intrinsic modes of motion. For well-deformed nuclei, this rise in \mathcal{J} with increasing J could be interpreted as due to an increase in the deformation parameter β , which adjusts itself to minimize the total energy of the nucleus. With increasing angular frequency, the energy of a state of given J is determined not only by the rotational kinetic energy, but also by a potential-energy term that represents the energy of other modes of motion. Furthermore, the two may be strongly coupled, the intrinsic wave functions being dependent on the angular velocity. We may

^t See Section 10-8.

thus generalize Eq. 9-66 to

$$E_J = \frac{\hbar^2 J(J+1)}{2\mathcal{J}(\omega)} + V(\omega), \quad (9-76)$$

where ω is the rotational frequency (the subscript "rot" has been dropped to make the notation less cumbersome), and $V(\omega)$ is the potential energy. The moment of inertia \mathcal{J} at any ω would adjust itself to minimize E_J , so that

$$\frac{dE_J}{d\mathcal{J}} = -\frac{\hbar^2 J(J+1)}{2\mathcal{J}^2(\omega)} + \frac{dV(\omega)}{d\mathcal{J}} = 0.$$

The above relation can be written, using Eq. 9-71, as

$$\frac{dV(\omega)}{d\mathcal{J}} = \frac{1}{2}\omega^2. \quad (9-77)$$

Since the experimental data displayed in Fig. 9-9 suggest that ω^2 is linearly related, up to a certain value of J , to $\mathcal{J} - \mathcal{J}_0$, \mathcal{J}_0 being the moment of inertia for $J = 0$, we can integrate Eq. 9-77 to obtain

$$V(\omega) = \frac{1}{2}C(\mathcal{J} - \mathcal{J}_0)^2,$$

where C is a constant. The energy of the state with angular momentum J can thus be written, from Eq. 9-76, using two parameters \mathcal{J}_0 and C :

$$E_J = \frac{\hbar^2 J(J+1)}{2\mathcal{J}} + \frac{1}{2}C(\mathcal{J} - \mathcal{J}_0)^2, \quad (9-78)$$

where \mathcal{J} for each J is determined by the condition

$$\frac{dE_J}{d\mathcal{J}} = 0. \quad (9-79)$$

Expression 9-78 for E_J was proposed by Mariscotti, Scharff-Goldhaber, and Buck [20] and is known as the variable-moment-of-inertia (VMI) model. It has been very successful not only in the rotational but also in the vibrational and transitional regions. As an example of this, in Fig. 9-10 the experimental ground-state bands of a few even-even nuclei, together with the calculated values in the VMI model, are shown.

To appreciate that the above form of variable moment of inertia may arise from stretching of the effective radius during rotation, it is instructive to consider a very simple classical problem [23]: a diatomic rotor with an interaction potential, shown in Fig. 9-11. When the system is not rotating,

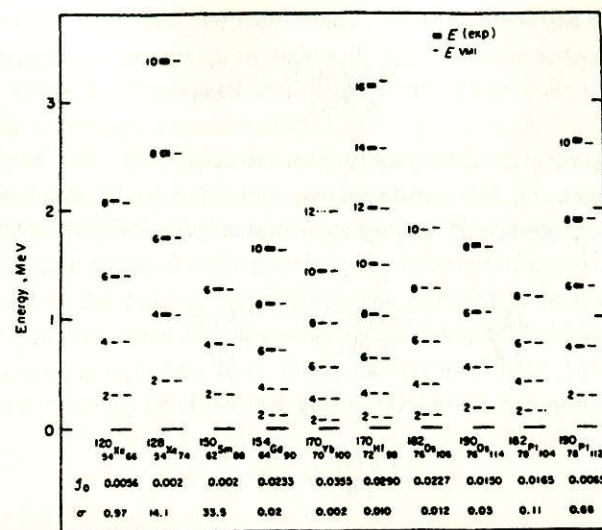


Fig. 9-10 Experimental and calculated ground-state bands of some even-even nuclei. For each nucleus, the experimental energies are shown on the left, and the calculated values, in the VMI model (Eq. 9-78), are on the right. The values of the parameters \mathcal{J}_0 and $\sigma = [\mathcal{J}^{-1}(d\mathcal{J}/dJ)]_{J=0} = \frac{1}{2}C\mathcal{J}_0^3$ are listed at the bottom of the figure. (After Mariscotti et al. [20].)

the masses rest at the equilibrium separation r_0 . With rotation, there is some stretching in this separation, and the total energy is given by

$$E = \frac{1}{2}m\dot{\mathbf{r}}_1^2 + \frac{1}{2}m\dot{\mathbf{r}}_2^2 + V(r), \quad (9-80)$$

where \mathbf{r}_1 and \mathbf{r}_2 are the coordinates of the two atoms with respect to some

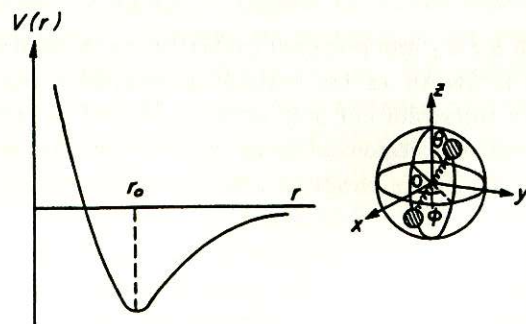


Fig. 9-11 A diatomic rotor with an interaction potential $V(r)$.

arbitrary origin, and $\mathbf{r} = \mathbf{r}_1 - \mathbf{r}_2$. We choose the center of mass $\mathbf{R} = \frac{1}{2}(\mathbf{r}_1 + \mathbf{r}_2)$ to be at rest and transform Eq. 9-80 to polar coordinates. The motion takes place in a plane, and, defining the angular momentum \mathbf{L} by

$$\mathbf{L} = \mu \mathbf{r}^2 \boldsymbol{\omega} = \mathcal{J} \boldsymbol{\omega}, \quad \mu = \frac{m}{2} \quad (9-81)$$

we obtain from Eq. 9-80

$$E = \frac{1}{2}\mu \mathbf{r}^2 + \frac{\mathcal{L}^2}{2\mu r^2} + V(r). \quad (9-82)$$

Now $\mathcal{J} = \mu \mathbf{r}^2$ and $\mathcal{J}_0 = \mu r_0^2$; and, assuming that \mathbf{r} does not deviate excessively from r_0 , we get

$$\mathcal{J} \approx \mathcal{J}_0 + 2\mu r_0(r - r_0)$$

or

$$r - r_0 = (\mathcal{J} - \mathcal{J}_0)C_1, \quad (9-83)$$

where $C_1 = 2\mu r_0$. Similarly, the potential may be expanded about the equilibrium position r_0 to give

$$\begin{aligned} V(r) &= V(r_0) + \frac{1}{2}C_2(r - r_0)^2 \\ &= V(r_0) + \frac{1}{2}C(\mathcal{J} - \mathcal{J}_0)^2, \end{aligned}$$

where $C = C_2/C_1^2$. Substituting this into Eq. 9-82, we obtain

$$E = [\frac{1}{2}\mu \mathbf{r}^2 + V(r_0)] + \frac{L^2}{2\mathcal{J}} + \frac{1}{2}C(\mathcal{J} - \mathcal{J}_0)^2. \quad (9-84)$$

In a given rotational band, the quantity in the brackets remains unchanged. Furthermore, the minimization condition $dE/d\mathcal{J} = 0$ immediately yields

$$\mathcal{J} - \mathcal{J}_0 = \frac{1}{2C} \omega^2,$$

showing that the increase in the moment of inertia is linearly proportional to ω^2 .

The preceding exercise is by no means a derivation of the VMI formula; rather, it is meant as an illustration of the stretching effect on the moment of inertia. An analogous quantum-mechanical treatment has been made by Volkov [24], and a many-body problem has been treated in a similar spirit

by Das, Dreizler, and Klein [25]. It is not well understood why the VMI equation 9-78 works so well for near-spherical and transitional nuclei.[†]

Coming back to axially symmetric deformed nuclei, we show the energy spectra of $^{164}_{68}\text{Er}$ and $^{232}_{92}\text{U}$ in Figs. 9-12 and 9-13, respectively, as typical examples. As mentioned before, in addition to the ground-state band,

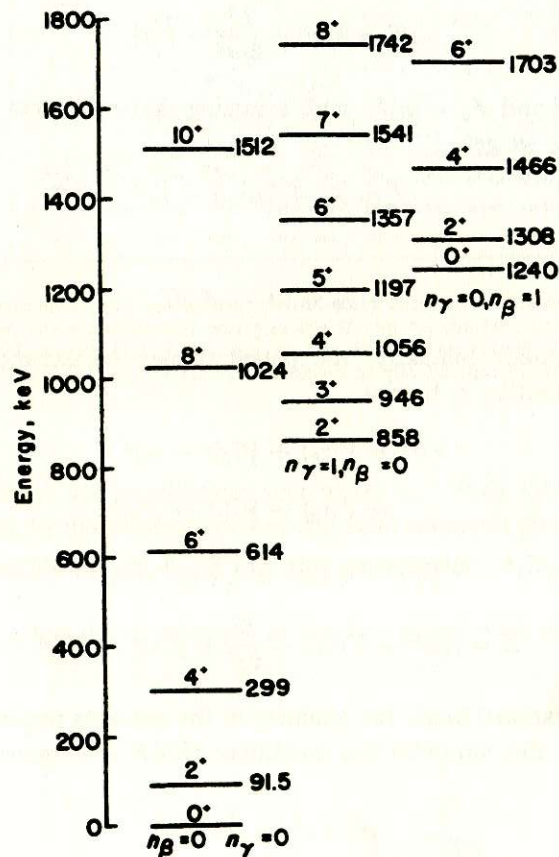


Fig. 9-12 The ground-state, γ -, and β -vibrational bands of $^{164}_{68}\text{Er}$.

[†] A more complicated and interesting behavior, termed "forking," is found in $^{100}_{46}\text{Pd}$ and $^{102}_{46}\text{Pd}$, where the ground-state band forks into two branches at $J = 6^+$ and 8^+ , with one branch exhibiting back-bending at this low value of J . See S. Scharff-Goldhaber, M. McKeown, A. H. Lumpkin, and W. F. Piel, Jr., *Phys. Lett.* **44B**, 416 (1973).

rotational bands are also built on collective vibrational excitations. The β -vibrational band head in ^{168}Er is at 1.24 MeV; while the γ -vibrational band head is somewhat lower in energy, at 858 keV. The β -band, on the other hand, is lower than the γ -band in ^{232}U , as shown in Fig. 9-13. Although small departures from axial symmetry take place in γ -vibrations, K can

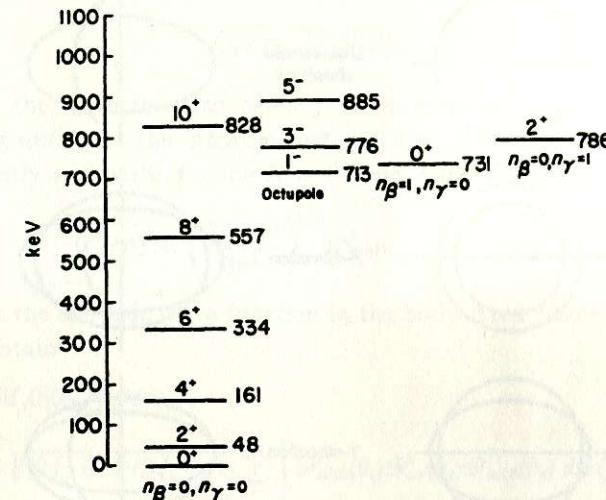


Fig. 9-13 The ground-state and the octupole bands in $^{232}_{92}\text{U}$. Also shown are the β - and γ -vibrational band heads. [After W. Elze and J. R. Huizinga, *Nucl. Phys.* **A187**, 545 (1972).]

still be considered to be approximately a good quantum number. In many deformed nuclei, there is a negative-parity rotational band, with its lowest level 1^- , as, for example, the 713-keV level of ^{232}U in Fig. 9-13. This band is interpreted as based on octupole vibrations of the prolate equilibrium shape. Such vibrations can carry 0–3 units of angular momentum parallel to the 3-axis. This vibrational angular momentum with 3-component ν is coupled to the angular momentum of a rotator with 3-component zero to give a resultant $K = \nu$. In general, the states have $J = K, K + 1$, etc., but we have seen that for the negative-parity $K = 0$ band the states are restricted to be $1^-, 3^-$, etc. These and other octupole states, as well as the rotational bands built on the quadrupole vibrations, have been recognized in a large number of deformed nuclei [26]. Because of the form of the Legendre polynomial $P_3(\cos \theta)$, octupole vibrations of the $K = 0^-$ type may be

described as pear-shaped, with the bulge alternating between one end of the nucleus and the other. The various simple forms of shape oscillations are schematically illustrated in Fig. 9-14.

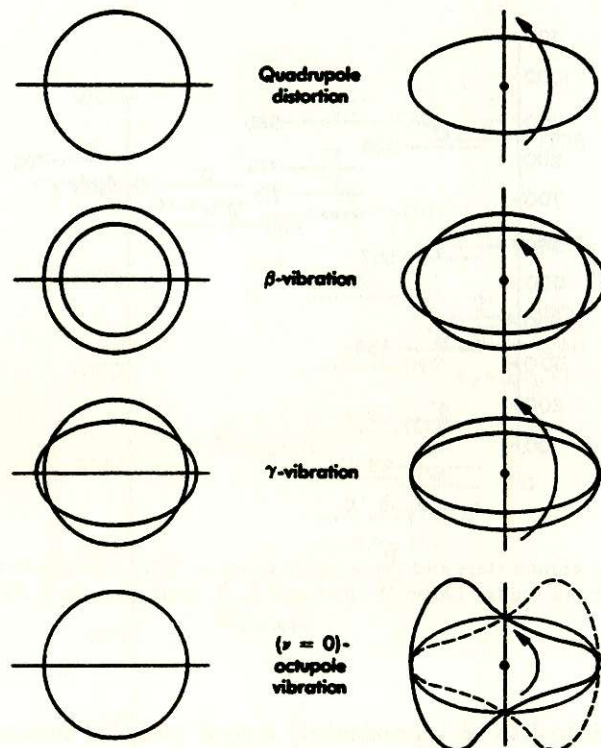


Fig. 9-14 The simple modes of vibrations of a distorted nucleus. The diagrams on the left represent cross sections perpendicular to the 3-axis; the lines are the 1-axis. In the diagrams on the right, the lines are the 3-axis and the cross sections are in the 2-3 plane; the arrows indicate the direction of rotation in a possible rotational state.

It will now be instructive to examine some of the electromagnetic transition properties in this model, one of the interesting quantities being the reduced transition probability $B(E2)$, defined in Eq. 9-22. We shall calculate this quantity for the ground-state rotational band with $K = 0$; more general results (e.g., interband transitions) can similarly be worked out. Adapting

Eq. 9-22 for the rotational case, quite generally, we obtain

$$B(E2, J_i, K \rightarrow J_f, K') = (2J_i + 1)^{-1} \sum_{M_i, M_f} |\langle J_i M_i, K' | Q_{2\mu} | J_f M_f, K \rangle|^2, \quad (9-85)$$

where the operator $Q_{2\mu}$ in the space-fixed coordinates is defined by Eq. 3-6. This operator can be expressed in terms of $Q'_{2\mu}$ in the intrinsic (body-fixed) frame as

$$Q_{2\mu} = \sum_{\nu} \mathcal{D}_{\mu\nu}^2 Q'_{2\nu}. \quad (9-86)$$

In writing the wave function $|JMK\rangle$ of the nuclear state, we have been suppressing until now the intrinsic part χ of the wave function; we now put it in explicitly and write, for the $K = 0$ band, from Eq. 9-60,

$$|JM0\rangle = \left(\frac{2J+1}{8\pi^2} \right)^{1/2} \mathcal{D}_{M0}^J(\theta_i) \chi_0(\mathbf{r}_1 \cdots \mathbf{r}_A), \quad (9-87)$$

where χ_0 is the intrinsic wave function in the body-fixed frame with $K = 0$. We then obtain

$$\begin{aligned} & \langle J_i M_i, 0 | Q_{2\mu} | J_f M_f, 0 \rangle \\ &= \frac{1}{8\pi^2} \sqrt{(2J_i + 1)(2J_f + 1)} \sum_{\nu} \int \mathcal{D}_{M_f 0}^{J_f}(\theta_i) \mathcal{D}_{\mu\nu}^2(\theta_i) \mathcal{D}_{M_i 0}^{J_i}(\theta_i) d\Omega \langle \chi_0 | Q'_{2\nu} | \chi_0 \rangle. \end{aligned} \quad (9-88a)$$

In this expression, the integral over the \mathcal{D} 's is nonzero only if $\nu = 0$; hence only this term contributes in the sum over ν . The integrations over the three \mathcal{D} 's can be done using Eq. A-78, and we get

$$\begin{aligned} & \langle J_i M_i, 0 | Q_{2\mu} | J_f M_f, 0 \rangle \\ &= \langle \chi_0 | Q'_{20} | \chi_0 \rangle \sqrt{\frac{2J_i + 1}{2J_f + 1}} (J_i 2M_i \mu | J_f M_f \rangle) (J_f 200 | J_f, 0 \rangle). \end{aligned} \quad (9-88b)$$

We therefore obtain

$$\begin{aligned} & \frac{1}{2J_i + 1} \sum_{M_i, M_f} |\langle J_i M_i, 0 | Q_{2\mu} | J_f M_f, 0 \rangle|^2 \\ &= |\langle \chi_0 | Q'_{20} | \chi_0 \rangle|^2 (J_i 200 | J_f, 0 \rangle)^2 \left[\frac{1}{2J_f + 1} \sum_{M_f} \sum_{M_i} |(J_i 2M_i \mu | J_f M_f \rangle)|^2 \right]. \end{aligned}$$

For a given M_f , $\sum_{M_i} (J_i 2M_i \mu | J_f M_f \rangle)^2 = 1$; hence the quantity in brackets is unity. We can therefore write

$$B(E2, J_i, 0 \rightarrow J_f, 0) = (J_i 200 | J_f, 0 \rangle)^2 |\langle \chi_0 | Q'_{20} | \chi_0 \rangle|^2. \quad (9-89)$$

The intrinsic quadrupole moment Q' in a given band K is defined by

$$Q'_K = \left(\frac{16\pi}{5}\right)^{1/2} \langle \chi_K | Q'_{20} | \chi_K \rangle, \quad (9-90)$$

which is related to the quadrupole moment Q in the space-fixed axes by Eq. 3-15. We can then write

$$B(E2, J_1 0 \rightarrow J_2 0) = \left(\frac{5}{16\pi}\right) Q_0'^2 \cdot (J_2 200 | J_1 0)^2. \quad (9-91)$$

For the reduced transition probability from the ground state 0^+ to the first excited 2^+ state in the $K = 0$ band, we simply obtain, from Eq. 9-91,

$$B(E2, 0^+ \rightarrow 2^+) = \left(\frac{5}{16\pi}\right) Q_0'^2 = 5B(E2, 2^+ \rightarrow 0^+). \quad (9-92)$$

Since the quadrupole moment in deformed nuclei is large, the $E2$ -transition rates will be enhanced greatly from the single-particle estimate. A rough single-particle estimate of the quadrupole moment was given in Eq. 3-17a; it varies as $A^{2/3}$. It is customary to take the single-particle (SP) unit for $B(E2)$ as ([27] and Appendix E)

$$B(E2, 0^+ \rightarrow 2^+)_{\text{SP}} = 2.95 \times 10^{-5} A^{4/3} e^2 b^2, \quad (9-93)$$

where the letter b stands for 1 barn = 10^{-24} cm 2 . A typical experimental $B(E2, 0^+ \rightarrow 2^+)$ for well-deformed rare-earth nuclei is about $5 e^2 b^2$, while in the actinides it is about twice this value. We thus see that there is an enhancement in the experimental value of $B(E2)$ by a factor of 100–200 from the single-particle estimates.

We can easily connect $B(E2, 0^+ \rightarrow 2^+)$ to the deformation parameter β , defined by Eq. 9-34. For a prolate nucleus, Eq. 9-33 reduces to

$$R(\theta') = R_0 \left[1 + \sqrt{\frac{5}{16\pi}} \beta (3\mu^2 - 1) \right], \quad \mu = \cos \theta'. \quad (9-33)$$

The intrinsic quadrupole moment of a prolate shape with a sharp surface defined by $R(\theta')$ and a density $\rho = 3Ze/4\pi R_0^3$ is then

$$Q'_0 = \int \rho r^2 Y_{20}(\theta', \phi') dr = \frac{3Ze}{4\pi R_0^3} \cdot 2\pi \sqrt{\frac{5}{16\pi}} \int_{-1}^{+1} (3\mu^2 - 1) d\mu \int_0^{R(\theta')} r^4 dr,$$

where we have used the relation

$$Y_{20} = \sqrt{\frac{5}{16\pi}} (3\mu^2 - 1).$$

A straightforward calculation then yields,[†] to second order in β ,

$$Q'_0 = \frac{3}{\sqrt{5\pi}} ZeR_0^2 \beta (1 + 0.36\beta + \dots). \quad (9.94)$$

Substituting this value of Q'_0 in Eq. 9-92, we find, to the leading order in β ,

$$B(E2, 0^+ \rightarrow 2^+) = \left(\frac{3ZeR_0^2}{4\pi}\right)^2 \beta^2, \quad (9-95)$$

so that the deformation β can be deduced from the experimental $B(E2)$ -values. These values are shown for the even-even rare-earth and actinide nuclei in Fig. 9-15.

Another interesting result that can immediately be deduced from Eq. 9-91 is that the ratio

$$\frac{B(E2, 4^+ \rightarrow 2^+)}{B(E2, 2^+ \rightarrow 0^+)} = \frac{(4200|20)^2}{(2200|00)^2} = \frac{10}{7}; \quad (9-96)$$

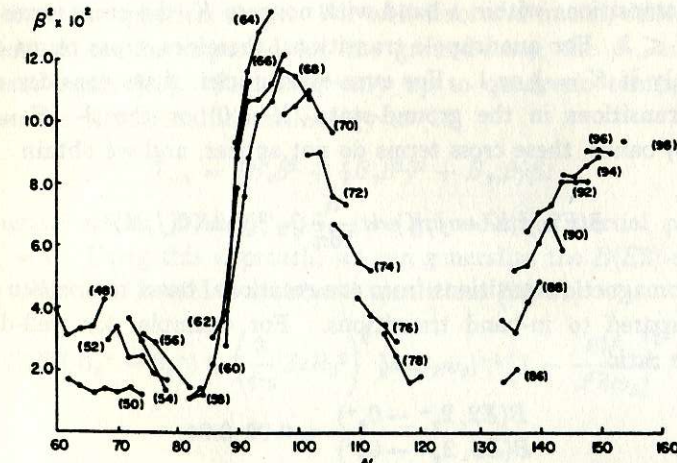


Fig. 9-15 Plot of β^2 as a function of the neutron number N as deduced from reduced $E2$ -transition probabilities to the first excited 2^+ state. The points of same Z are joined together, with Z shown within brackets on the figure.

[†] Note that the shape defined by Eq. 9-33 is not an ellipsoid. For an ellipsoid, one can define a parameter $\beta = (4/3)\sqrt{\pi/5}(\Delta R/R_0)$, ΔR being the difference between the major and minor semiaxes. For such a shape,

$$Q'_0 = \frac{3}{\sqrt{5\pi}} ZeR_0^2 \beta (1 + 0.16\beta + \dots).$$

this ratio was 2 for vibrational nuclei (cf. Eq. 9-27b). Experimentally this is found to be well satisfied for well-deformed nuclei, as shown in Fig. 9-4.

We derived Eq. 9-89 for $B(E2)$ -transitions within a $K = 0$ band; the result can be easily generalized for a nonzero K . In this case, the nuclear wave function $|JMK\rangle$ must be properly symmetrized (see Eq. 9-60), including the intrinsic state χ . There would, in principle, be cross terms in the matrix element 9-89 involving K and $-K$. Consider, for greater generality, transitions between different K -bands for a multipole operator $Q_{\lambda\mu}$; then the matrix element $\langle J_i M_i K_i | Q_{\lambda\mu} | J_i M_i K_i \rangle$ has to be evaluated. Consequently an integral of the type

$$\int D_{M_i K_i}^{J_i}(\theta_i) D_{\mu\nu}^{\lambda}(\theta_i) D_{M_i K_i}^{J_i}(\theta_i) d\Omega \quad (9-97)$$

is involved; this is nonzero only if

$$\Delta K = |K_i - K| \leq \lambda, \quad (9-98)$$

since $|\nu| \leq \lambda$. This is called the K -selection rule in electromagnetic transitions and is broken to the extent that K is not a good quantum number. Furthermore, for transitions within a band with nonzero K , the cross terms involve $\Delta K = 2K \leq \lambda$. For quadrupole transitions, therefore, cross terms can contribute only if $K = \frac{1}{2}$ or 1. For even-even nuclei, if we consider only the in-band transitions in the ground-state ($K = 0$) or the β - ($K = 0$) and γ - ($K = 2$) bands, these cross terms do not appear, and we obtain

$$B(E2, J_i K \rightarrow J_i K) = \frac{5}{16\pi} Q_K'^2 (J_i 2K0 | J_i K)^2. \quad (9-99)$$

Electromagnetic transitions from one rotational band to another are very weak compared to in-band transitions. For example, for well-deformed nuclei, the ratio

$$\frac{B(E2, 2_g^+ \rightarrow 0_g^+)}{B(E2, 2_g^+ \rightarrow 0_g^+)} \approx 0.02-0.04, \quad (9-100)$$

increasing to about 0.07 for the transitional Os isotopes. The other interesting ratio which is also experimentally extracted is

$$\frac{B(E2, 2_g^+ \rightarrow 2_g^+)}{B(E2, 2_g^+ \rightarrow 0_g^+)} \approx 0.10 \quad (9-101)$$

for well-deformed nuclei, but it increases rapidly for transition nuclei, reaching a value of about 0.7 for ^{192}Os and becoming larger than unity in

some of the Pt isotopes. Excluding for the moment these transitional nuclei, we have the concept of a "band" as one in which there are strong electromagnetic transitions within the states of the band, subject, of course, to the selection rules imposed by angular momentum, parity, and K -quantum number, with weak interband transitions. It should be emphasized that in a theoretical calculation of ratios 9-100 and 9-101, account must be taken of the rotation-vibration interaction. In its simplest form, we have seen, for example, that U_2 (defined in Eq. 9-49) can connect a state (J, K, n, \pm) with $(J, K \pm 2, n, \pm 1)$. Preston and Kiang [28] have given explicit expressions for interband $B(E2)$'s, using a perturbative approach in mixing the states, while a more complete treatment has been made by Faessler et al. [13]. The latter authors compare their theoretical values with experimental data, and the agreement is reasonable even in the transition region. As has been already pointed out, this success should be viewed with caution [29], however, since the rotation-vibration interaction term has been extracted from the hydrodynamical formula for the moment of inertia (see Eq. 9-37).

The hydrodynamical form of the moment of inertia (9-37) and the vibrational kinetic energy (Eq. 9-36) were derived for nuclei deviating slightly from the spherical shape. For well-deformed nuclei, different mass parameters B can be expected for the ground-state, the β -, and the γ -vibrational bands [30]. Retaining only up to quadratic terms, we may generalize the vibrational kinetic energy to [11]

$$T_{\text{vib}} = \frac{1}{2} B_\beta \dot{\beta}^2 + \frac{1}{2} B_\gamma \beta^2 \dot{\gamma}^2 + B_{\beta\gamma} \beta \dot{\gamma} \dot{\beta}. \quad (9-102)$$

For spherical nuclei, $B_\beta = B_\gamma = B_0$ (the ground-state inertial parameter) and $B_{\beta\gamma} = 0$. Using this approach, we can generalize the $B(E2)$ -expression 9-24 of vibrational nuclei to interband transitions [29, 31]

$$B(E2, 0_g^+ \rightarrow 2_g^+) = \left(\frac{3}{4\pi} ZeR_0^2 \right)^2 \frac{1}{2} \hbar (B_\beta \omega_\beta)^{-1} \left(1 - \frac{6\hbar^2}{J\hbar\omega_\beta} \right)^2 \quad (9-103a)$$

and

$$B(E2, 0_g^+ \rightarrow 2_g^+) = \left(\frac{3}{4\pi} ZeR_0^2 \right)^2 \beta_0^{-2} \hbar (B_\gamma \omega_\gamma)^{-1} \left(1 - \frac{2\hbar^2}{J\hbar\omega_\gamma} \right)^2, \quad (9-103b)$$

where the effects of rotation-vibration interactions have been included to first order. Using Eq. 9-103, one can extract the values of B_β and B_γ from the measured interband $B(E2)$ -values and the energies of the β - and γ -vibrational states. It is found that the values of B_β and B_γ , thus obtained exceed the ground-state mass parameter $B_0 (= J/3\beta_0^2)$ by a factor of 3-4.

Until now, the low-lying collective levels of an even-even nucleus with permanent quadrupole deformation have been described as rotations of an axially symmetric deformed shape, coupled with β - and γ -vibrational modes which are treated as dynamical variables. We should mention that there is an alternative description of these low-lying levels, due to Davydov and Filippov [17] and Davydov and Chaban [19], in which the nuclear shape is considered to be asymmetric, with all three components of the moment of inertia \mathcal{J}_κ unequal. In the simplest form of this model [17], β and γ are considered to be fixed parameters for a given nucleus (and not as dynamic variables) with $\gamma \neq 0$. In terms of the Bohr Hamiltonian 9-43, the potential function $V(\beta, \gamma)$ is assumed to have a very deep minimum for a well-defined value of β and $\gamma \neq 0$, so that the stiffness parameters C_β and C_γ of Eq. 9-46 are very large. This implies that the β - and γ -vibrational levels, although present in principle, come at very high excitations, and the low-lying collective levels are simply given by the eigenvalues of the asymmetric rotor

$$H_{AR} = \sum_{\kappa=1}^3 \frac{L_\kappa^2}{2\mathcal{J}_\kappa}, \quad (9-104)$$

where \mathcal{J}_κ , as before, is given by Eq. 9-37 in the hydrodynamical model, with β and γ as fixed parameters. To obtain the eigenvalues of H_{AR} , we can diagonalize it in the basis states (Eq. 9-60), that are eigenfunctions of an axially symmetric rotor,

$$|JMK\rangle = \left[\frac{2J+1}{16\pi^2(1+\delta_{K0})} \right]^{1/2} [\mathcal{D}_{MK}^J(\theta_i) + (-)^J \mathcal{D}_{M,-K}^J(\theta_i)], \quad (9-60)$$

with $K = 0, 2, 4$, etc., and

$$J = \begin{cases} K, K+1, K+2, \dots & \text{if } K \neq 0, \\ 0, 2, 4, \dots & \text{if } K = 0. \end{cases} \quad (9-105)$$

The eigenfunctions of H_{AR} may then be expressed as

$$|\Psi_{JM}\rangle = \sum_{K \leq J} g_{K,i}^J |\gamma\rangle |JMK\rangle, \quad (9-106)$$

where the coefficients $g_{K,i}^J$ are to be determined through diagonalization, and the index i indicates that several states of the same J may occur. An examination of Eqs. 9-105 and 9-106 immediately shows that in expansion 9-106 we get

- (i) only one term with $J = 0$ ($K = 0$),
- (ii) no possible state for $J = 1$,

- (iii) two terms with $J = 2$ ($K = 0, 2$),
- (iv) one term with $J = 3$ ($K = 2$),
- (v) three terms with $J = 4$ ($K = 0, 2, 4$),

and so on. Diagonalization of H_{AR} in the basis 9-60 would thus yield one 0^+ state, two 2^+ states, one 3^+ state, three 4^+ states, and so on. To determine these levels we simply form for each value of K the equation

$$\langle JMK | \sum_{\kappa=1}^3 \frac{L_\kappa^2}{2\mathcal{J}_\kappa} - E | \Psi_{JM} \rangle = 0.$$

Using the matrix elements[†] of L_κ^2 , we obtain for these equations

$$\begin{aligned} & g_{K+2}^J (\mathcal{J}_2 - \mathcal{J}_1) \mathcal{J}_3 [(J-K)(J-K-1)(J+K+1)(J+K+2)]^{1/2} \\ & + g_K^J \left[2(\mathcal{J}_1 + \mathcal{J}_2) \mathcal{J}_3 (J^2 + J - K^2) + 4\mathcal{J}_1 \mathcal{J}_2 K^2 - 8 \left(\frac{E}{\hbar^2} \right) \mathcal{J}_1 \mathcal{J}_2 \mathcal{J}_3 \right] \\ & + g_{K-2}^J (\mathcal{J}_2 - \mathcal{J}_1) \mathcal{J}_3 [(J+K)(J+K-1)(J-K+1)(J-K+2)]^{1/2} = 0. \end{aligned} \quad (9-107)$$

The determinant of the coefficients of the g 's must be zero for a solution. This yields an equation for E of the degree of the number of equations. For example, for $J = 2$, the equations are

$$\begin{aligned} & \sqrt{6} g_2 (\mathcal{J}_2 - \mathcal{J}_1) \mathcal{J}_3 + g_0 \left[6(\mathcal{J}_1 + \mathcal{J}_2) \mathcal{J}_3 - 4 \left(\frac{E}{\hbar^2} \right) \mathcal{J}_1 \mathcal{J}_2 \mathcal{J}_3 \right] = 0, \\ & g_2 \left[2(\mathcal{J}_1 + \mathcal{J}_2) \mathcal{J}_3 + 8\mathcal{J}_1 \mathcal{J}_2 - 4 \left(\frac{E}{\hbar^2} \right) \mathcal{J}_1 \mathcal{J}_2 \mathcal{J}_3 \right] + \sqrt{6} g_0 (\mathcal{J}_2 - \mathcal{J}_1) \mathcal{J}_3 = 0, \end{aligned}$$

and we obtain two states whose energies are the roots of

$$\begin{aligned} & \left(\frac{E}{\hbar^2} \right)^2 - 2 \left(\frac{E}{\hbar^2} \right) (\mathcal{J}_1^{-1} + \mathcal{J}_2^{-1} + \mathcal{J}_3^{-1}) \\ & + \frac{3}{8} [\mathcal{J}_1^{-2} + \mathcal{J}_2^{-2} + 6\mathcal{J}_1^{-1} \mathcal{J}_2^{-1} + 8(\mathcal{J}_1^{-1} + \mathcal{J}_2^{-1}) \mathcal{J}_3^{-1}] = 0. \end{aligned} \quad (9-108)$$

[†] The relevant matrix elements are

$$\langle JK | L_\kappa^2 | JK \rangle = \hbar^2 K^2, \quad \langle JK | L_1^2 | JK \rangle = \langle JK | L_2^2 | JK \rangle = \frac{\hbar^2}{2} [J(J+1) - K^2],$$

and

$$\begin{aligned} \langle JK | L_1^2 | J, K+2 \rangle &= - \langle J, K | L_2^2 | J, K+2 \rangle \\ &= \frac{\hbar^2}{4} [(J-K)(J-K-1)(J+K+1)(J+K+2)]^{1/2}. \end{aligned}$$

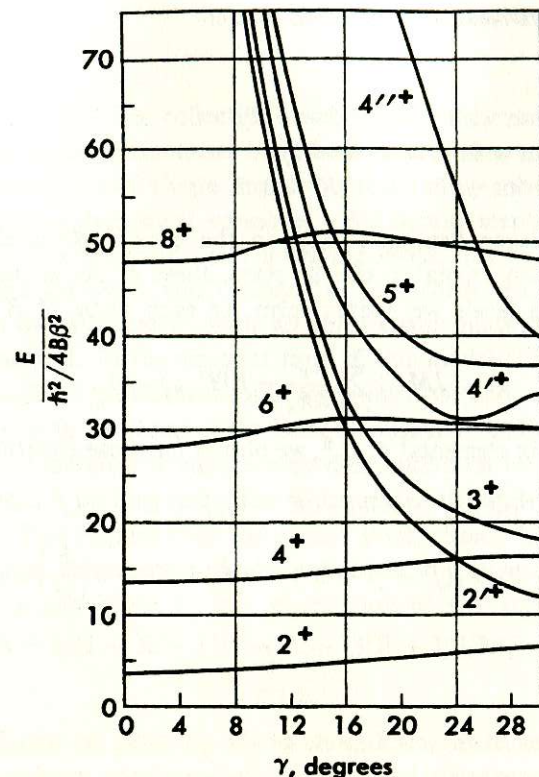


Fig. 9-16 Rotational levels of asymmetric distorted nuclei. [From G. R. De Mille et al., *Can. J. Phys.* 37, 1036 (1959).]

If we consider the axially symmetric case $\mathcal{J}_1 = \mathcal{J}_2, \mathcal{J}_3 \rightarrow 0$, we note that the two roots are $3\hbar^2/\mathcal{J}_1$ and $2\hbar^2/\mathcal{J}_3$; the first of these is the solution $(\hbar^2/2\mathcal{J})J(J+1)$ for axial symmetry, and the second is very large. As the asymmetry increases, the values become more nearly comparable. The energies of the lowest levels are shown in Fig. 9-16 as functions of the asymmetry, expressed in terms of the variable γ through the hydrodynamic equations 9-37 for \mathcal{J}_κ . The levels present at $\gamma = 0$ are only slightly affected by an increase in γ , but the levels that are infinite at this separation are brought down to comparable energies.

A slight departure of the energies of the normal 2^+ , 4^+ , etc., states from the $J(J+1)$ -ratios is predicted by the asymmetric model, but it would be difficult to disentangle this effect from the rotation-vibration coupling. There is a more significant test. Equations 9-108 and 9-107 show that the energies E_2 and E_2' of the two 2^+ states and the energy of the 3^+ state are related by

$$E_2 + E_2' = 2\hbar^2(\mathcal{J}_1^{-1} + \mathcal{J}_2^{-1} + \mathcal{J}_3^{-1}) = E_3. \quad (9-109)$$

This prediction is confirmed with an error of approximately 2% in about a dozen cases, and, in addition, the higher rotational levels also fit the model fairly well. Values of γ that fit experimental energies may therefore be deduced.

A rough plot of γ as a function of A is shown in Fig. 9-17. Although K is not a good quantum number, there is only small admixture for small γ -values, and even for larger ones the lowest energy levels for each J are predominantly $K = 0$. The values of some of the coefficients $g_{K\ell}^J$ are shown in Table 9-1, demonstrating the extent of mixing of different K -values in the states of nuclei without axial symmetry.

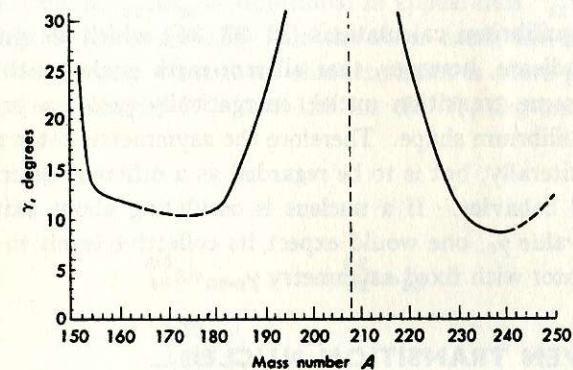


Fig. 9-17 Values of the asymmetry parameter γ , as a function of A . The smooth curve is based on values calculated from the values of E_2 and E_2' in ref. 18.

This simple model predicts only one 0^+ state, which is, in fact, the ground state. We saw, however, in Figs. 9-12 and 9-13, that there is another low-lying 0^+ state in many deformed nuclei which is interpreted as the β -vibrational band head in the axially symmetric model. Davydov and Chaban [19] have modified the asymmetric rotor model to incorporate β -vibrations; in this modified version β is considered to be a dynamic variable but γ is a fixed nonzero parameter. The results of this model, both in energy levels and in electromagnetic transition probabilities, are very similar to those of the axially symmetric model with rotation-vibration coupling included [13].

TABLE 9-1 Coefficients g_{Ki}^J . After Davydov et al. [17, 18].

γ	0	10°	20°	25°	30°
g_{01}^2	1	1.000	0.996	0.974	0.866
g_{21}^2	0	7.8×10^{-3}	0.0872	0.227	0.500
g_{02}^2	0	-7.5×10^{-3}	-0.0867	-0.226	-0.500
g_{22}^2	1	1.000	0.996	0.975	0.866
g_{01}^4	1	0.999	0.955	0.852	0.739
g_{21}^4	0	0.030	0.296	0.522	0.661
g_{41}^4	0	10^{-4}	0.010	0.043	0.125
g_{02}^4	0	-0.030	-0.296	-0.523	-0.559
g_{22}^4	1	0.999	0.954	0.842	0.500
g_{42}^4	0	0.004	0.043	0.128	0.661

Microscopic equilibrium calculations [32, 33, 34], which we shall discuss in Section 9-9 indicate, however, that all rare-earth nuclei, with the possible exception of some transition nuclei, energetically prefer a prolate axially symmetric equilibrium shape. Therefore the asymmetric-rotor model should not be taken literally, but is to be regarded as a different description of the same physical behavior. If a nucleus is oscillating about axial symmetry with an rms value γ_0 , one would expect its collective levels to be very like those of a rotator with fixed asymmetry γ_0 .

9-6 EVEN-EVEN TRANSITION NUCLEI

In the preceding sections, we considered the collective spectra of nuclei by making the simple assumption that the deformation potential $V(\beta, \gamma)$ in the Bohr Hamiltonian 9-43 has a well-defined minimum in $\beta\text{-}\gamma$ space, so that an expansion like Eq. 9-46 is meaningful about the equilibrium deformation (β_0, γ_0) . For the particular case of $V(\beta, \gamma)$ being γ -independent and $\beta_0 = 0$, we obtained the vibrational spectrum of spherical nuclei. In these simple models, the nonlinearity in the Bohr Hamiltonian 9-43 that is introduced due to the $\beta\text{-}\gamma$ dependence of the inertial parameter B and the moments of inertia \mathcal{J}_κ either was ignored by replacing β, γ in the inertial parameters by their equilibrium values, or at best was treated in a perturbative manner, using the hydrodynamical expression 9-37 for \mathcal{J}_κ . We found that this simple approach worked very well for permanently deformed rare-earth and actinide nuclei and fared rather poorly for spherical nuclei. We also mentioned that

there are nuclei in the transition region (e.g., the lighter isotopes of Sm, Gd, and Nd with $N < 90$ and the isotopes of Os and Pt) for which neither the vibrational nor the rotational model seems to apply in its simple form. We shall find in this section that the simple assumption of a well-localized minimum in $V(\beta, \gamma)$ is no longer applicable for these transitional nuclei, the minimum being very flat and spread out in the $\beta\text{-}\gamma$ space. For this reason, the inertial parameters can no longer be even approximately replaced by their values at a single point (β_0, γ_0) in the $\beta\text{-}\gamma$ space, but the nonlinearity of the Schrödinger equation with the Bohr Hamiltonian must be taken into account. Before outlining a theory due to Baranger and Kumar which tackles these points, let us examine some experimental data in the transition region.

It is found experimentally that permanent deformation sets in rather abruptly in the rare earths at neutron number $N = 90$. Thus, although the low-lying spectrum of $^{150}_{62}\text{Sm}_{88}$ is vibrational in appearance, $^{152}_{62}\text{Sm}_{90}$ is clearly rotational (Figs. 9-18a and 9-18b). On the other hand, the transition from rotational to apparently vibrational characteristics is more gradual in the region of neutron number $N = 110\text{--}120$ for the W, Os, and Pt isotopes.

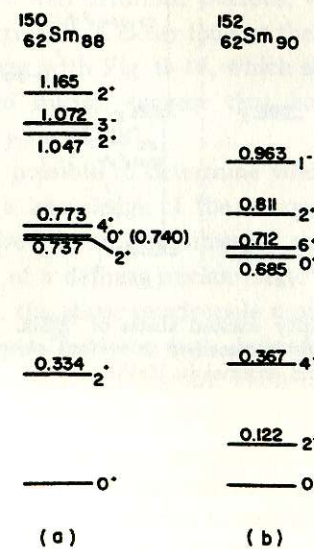


Fig. 9-18 Low-lying energy levels of (a) $^{150}_{62}\text{Sm}_{88}$ and (b) $^{152}_{62}\text{Sm}_{90}$ (energies in MeV).

These have been studied in great detail, both experimentally and theoretically.

Figure 9-19 shows a few positive-parity low-lying excited states of ^{148}Sm [35]. Vibrational characteristics are apparent in the spectrum, with $E(4+)/E(2+) \approx 2$ and the ratio $B(E2, 4^+ \rightarrow 2^+)/B(E2, 2^+ \rightarrow 0^+)$ being closer to 2 than to 10/7. However, a closer examination of the higher excited states suggests that these can be grouped into rotation-like bands with spin sequences $(0^+, 2^+, 4^+, 6^+, \dots)$, $(0^+, 2^+, 4^+, \dots)$, and $(2^+, 3^+, 4^+, \dots)$, which tend to go over, with increasing neutron number, to the rotational bands. These quasi-bands are present not only in transition nuclei but also throughout the vibrational region and have been systematically classified by Sakai [35].

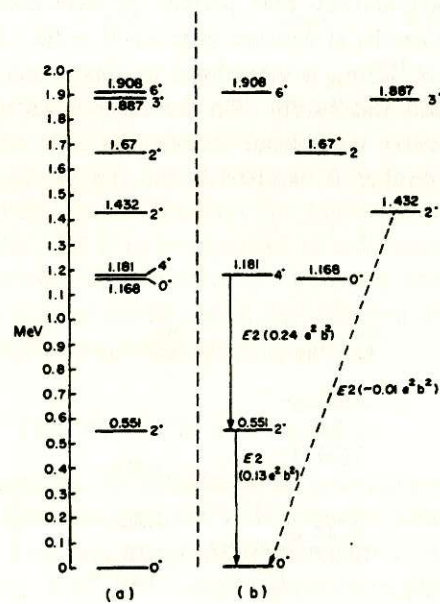


Fig. 9-19 A few positive-parity excited states of ^{148}Sm . In (a), the experimental sequence is shown; in (b), this is classified in various quasi-bands. A few measured $B(E2)$ -values are also shown (all energies in MeV).

The systematics of these quasi-rotational bands in spherical and transitional nuclei demonstrate that vibrational and rotational characteristics can coexist naturally, and indicates the need for a comprehensive theory that can treat vibrational, rotational, and transitional characteristics on an equal footing.

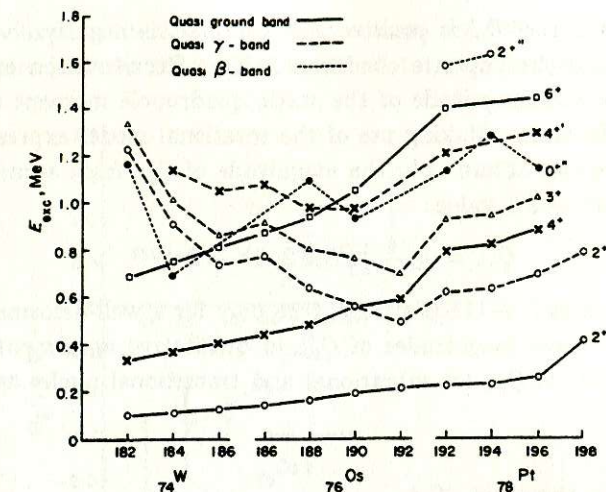


Fig. 9-20 The quasi-ground, quasi- β - and quasi- γ -bands for W, Os, and Pt isotopes. (After D. Cline, in *Colloquium on Intermediate Nuclei*, Institut de Physique Nucléaire d'Orsay, 1971.)

These quasi bands can be examined in detail in the W-Os-Pt region, as shown in Fig. 9-20. From this figure, it will be seen that $^{182}\text{W}_{108}$ has the rotational spectrum of a well-deformed nucleus, while the heavier isotopes of Pt appear to be vibrational. A closer look at the spectra of ^{190}Os and ^{192}Os and a comparison of these with Fig. 9-16, which shows the rotational levels of asymmetric distorted nuclei, suggest that both these nuclei may be asymmetric rotors with $\gamma \sim 24-28^\circ$.

In general, it is not possible to determine whether the nuclear shape is prolate or oblate from a knowledge of the energy spectrum or the $B(E2)$ -values. What is required is an experimental measurement of the static quadrupole moment Q_J of a definite nuclear state of angular momentum J . In the rotational model, the static quadrupole moment can be easily related to the intrinsic quadrupole moment Q_K' , defined in Eq. 9-90. The static quadrupole moment of a state with angular momentum J in the $K = 0$ band is given by

$$\begin{aligned} Q_J &= \langle J, M = J, K = 0 | Q_{20} | J, M = J, K = 0 \rangle \\ &= (J2J0|JJ)(J200|J0)Q_0', \quad \text{using Eq. 9-88b,} \\ &= -\frac{J}{2J + 3} Q_0'. \end{aligned} \quad (9-110)$$

For a prolate shape, Q_0' is positive and hence Q_2 is negative, whereas for an oblate shape the opposite condition holds. Reorientation experiments yield the sign and magnitude of the static quadrupole moment Q_{2+} of the first excited 2^+ state. Making use of the rotational model expressions 9-92 and 9-110, we can obtain only the magnitude of Q_{2+} from a measurement of the $B(E2, 0^+ \rightarrow 2^+)$ value:

$$Q_{2+} = \pm \frac{8}{7} \left[\frac{1}{5} \pi B(E2, 0^+ \rightarrow 2^+) \right]^{1/2}. \quad (9-111)$$

Although expression 9-111 is strictly true only for a well-deformed nucleus, it is found to yield magnitudes of Q_{2+} in qualitative agreement with the measured values of Q_{2+} for vibrational and transitional nuclei as well. As

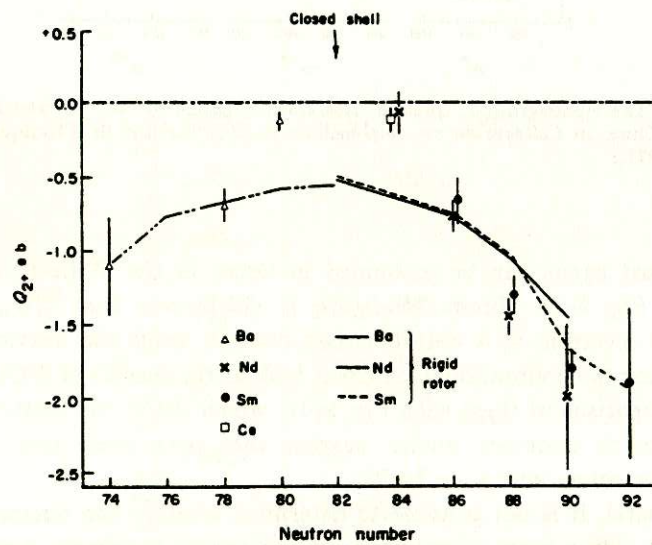


Fig. 9-21 The measured static quadrupole moments of the first 2^+ state of even-even isotopes in the $N = 82$ region as a function of N . The lines in this figure show the static quadrupole moments derived from the $B(E2, 0^+ \rightarrow 2^+)$ values, assuming a prolate rotor model. (From Gertzman et al. [36].)

an illustration of this, we show in Fig. 9-21 the measured Q_{2+} values and the corresponding predictions of Eq. 9-111, using the prolate rotor model for some near-spherical and transitional nuclei in the $N = 82$ region [36].

The static quadrupole moments Q_{2+} have been measured for some of the Os and Pt isotopes by Pryor and Saladin [37]. Their experimental results, displayed in Fig. 9-22, clearly indicate that, whereas the Os isotopes are

prolate in shape in the 2^+ state, the Pt isotopes are oblate. The dotted lines in the figure join the theoretical values of the calculations of Kumar and

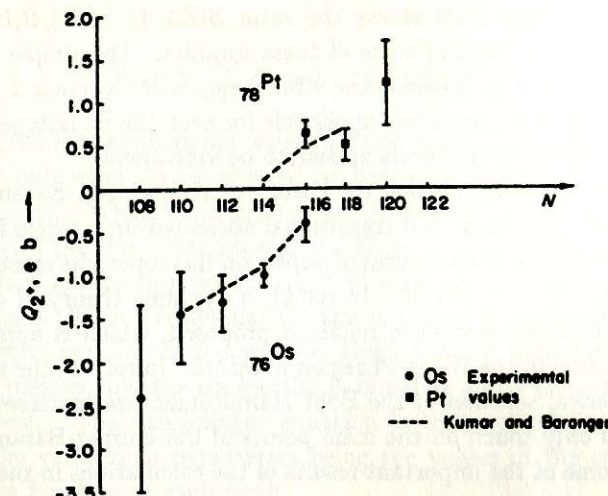


Fig. 9-22 The measured static quadrupole moments of the first 2^+ state, Q_{2+} , for Pt and Os isotopes. For comparison, we also show the theoretical values of Kumar and Baranger [12], through which dotted lines are drawn.

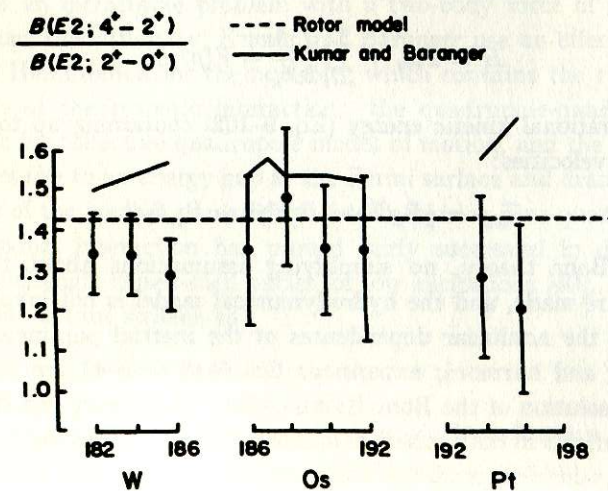


Fig. 9-23 The measured ratio $B(E2, 4^+ \rightarrow 2^+)/B(E2, 2^+ \rightarrow 0^+)$ for W, Os, and Pt isotopes. Also shown, by the dotted line, is the rotational model estimate ($= \frac{10}{7}$), and, by the solid line, the results of the calculation of Kumar and Baranger [12].

Baranger [12], which predicted successfully this prolate-to-oblate transition in these nuclei.

Detailed $B(E2)$ -measurements have been made for the W, Os, and Pt isotopes [38]. Figure 9-23 shows the ratio $B(E2, 4^+ \rightarrow 2^+)/B(E2, 2^+ \rightarrow 0)$ for the ground-state band of some of these isotopes. The simple rotational-model prediction is 10/7, whereas the vibrational-model value is 2. It is clear that the vibrational model is not applicable for even the Pt isotopes, in which the spacings of the energy levels appear to be vibrational.

We shall now briefly outline the theory of Kumar and Baranger, which treats spherical, deformed, and transitional nuclei within a single framework. These authors have written a series of papers on this topic, the most important ones being refs. 11, 12, and 39. In ref 11, a dynamic theory of quadrupole collective motion for even-even nuclei is proposed, which is applied to the transitional nuclei in the W-Os-Pt region in ref. 12. In ref. 39, the symmetries and the numerical solution of the Bohr Hamiltonian are discussed in detail. Here we shall only touch on the main points of the Kumar-Baranger theory and discuss some of the important results of the calculations in the transition region.

Baranger and Kumar, following Bohr, assume the collective quadrupole motion of a nucleus to be adiabatic and uncoupled to higher-lying octupole modes and single-particle excitations. As such, their theory is applicable only to doubly even nuclei. They consider the generalized Bohr Hamiltonian

$$H = T_{\text{vib}} + \sum_{\kappa=1}^3 \frac{L_\kappa^2}{2J_\kappa} + V(\beta, \gamma), \quad (9-112)$$

with the vibrational kinetic energy (Eq. 9-102) containing up to quadratic terms in the velocities:

$$T_{\text{vib}} = \frac{1}{2}B_\beta \dot{\beta}^2 + \frac{1}{2}B_\gamma \dot{\beta}^2 \dot{\gamma}^2 + B_\beta \beta \dot{\beta} \dot{\gamma}. \quad (9-102)$$

Unlike the Bohr theory, no simplifying assumptions about the inertial parameters are made, and the hydrodynamical model is not invoked. Most importantly, the nonlinear dependences of the inertial parameters on β, γ are retained, and harmonic expansions like 9-46 or 9-47 are *not* made to simplify the solution of the Bohr Hamiltonian. The theory can thus handle anharmonic effects in both spherical and deformed nuclei, as well as couplings between the ground-state and β - and γ -modes of vibrations. The six inertial parameters $B_\beta, B_\gamma, B_\beta$, and J_κ ($\kappa = 1-3$) and the potential energy V are calculated self-consistently as functions of β, γ , starting from a Hamiltonian that contains a spherical one-body potential, a quadrupole-quadrupole two-

body residual interaction, and the two-body pairing potential, in a manner to be described briefly. The full collective wave function with angular momentum J , z -component M , and other quantum numbers α is expanded as

$$\Phi_{\alpha JM} = \sum_{K \geq 0} A_{\alpha JK}(\beta, \gamma) \phi_{MK}^J(\theta_1, \theta_2, \theta_3), \quad (9-113)$$

where $\phi_{MK}^J(\theta_i)$ is the rotational wave function given by Eq. 9-60. As before, for $K = 0$, only even J 's are allowed, and for a nonzero K , J takes all values $K, K + 1$, etc. When expression 9-113 is substituted in the Schrödinger equation with the Bohr Hamiltonian 9-112, a set of coupled partial differential equations for the functions $A_{\alpha JK}(\beta, \gamma)$ is obtained. These equations are solved numerically in a triangular β - γ space, since $0 \leq \gamma \leq \pi/3$. The equilateral triangular area in the β - γ space is divided into a large number of small triangular meshes, and the six inertial parameters and $V(\beta, \gamma)$ are calculated in each mesh. The Schrödinger equation is then solved by a variational method, the variational parameters being the values of the component A_K of the wave function at each mesh.

The most important part of the Kumar-Baranger theory is the calculation of the inertial parameters and $V(\beta, \gamma)$; this should, ideally, be done starting from realistic nucleon-nucleon forces. It is crucial to identify the collective variables β and γ in terms of the particle coordinates in such a calculation, and this is an intractable problem with a two-body force of general form. To surmount this difficulty, Kumar and Baranger use an effective phenomenological Hamiltonian for the nucleons, which contains the two important ingredients of the realistic interaction: the quadrupole-quadrupole force, responsible for collective quadrupole modes of motion, and the pairing force, which gives rise to an energy gap at the Fermi surface and drastically affects the values of the inertial parameters. Such a pairing-plus-quadrupole model of the residual interaction has proved fairly successful in describing the properties of single closed-shell nuclei for low excitations [40]. The effective Hamiltonian is thus written as

$$\mathcal{H} = H_s + V_Q + V_P, \quad (9-114)$$

where H_s is a one-body spherically symmetric Hamiltonian generated by the core (e.g., a harmonic-oscillator potential with spin-orbit force), V_Q is the quadrupole interaction

$$V_Q = -\chi \sum_{i < j} r_i^2 r_j^2 \sum_{\mu} (-)^{\mu} Y_2^{\mu}(\hat{r}_i) Y_2^{-\mu}(\hat{r}_j) \quad (9-115)$$

acting between the nucleons in the partly filled major oscillator shell, and V_P is the pairing potential with matrix elements

$$\langle i\bar{i}|V_P|\bar{j}j\rangle = -G, \quad (9-116)$$

where i, j are two single-particle states, and \bar{i}, \bar{j} their time-reversed states. It is important to realize that this form of the pairing force with constant matrix element should be used only in a limited subspace in the neighborhood of the Fermi surface, and that the strength of the parameter G is dependent on the number of states i, j, \dots included around the Fermi surface. The pairing potential is assumed to act only between identical fermions, the neutron-proton pairing being neglected. Similarly, in doing calculations with V_Q , the oscillator space is restricted to the partly filled major shell and the adjacent major shell of opposite parity.

With a realistic effective force (such as the nuclear G -matrix), certain matrix elements are important for producing quadrupole deformation. It is found that with appropriate choices of G and χ these matrix elements can be reproduced approximately in the limited oscillator space defined above, but not outside it. It is therefore important to restrict the oscillator space while working with the phenomenological Hamiltonian 9-114.

It has been assumed that the nucleons in the filled shells give rise to a harmonic-oscillator type of spherical one-body potential in H_S (Eq. 9-114), whose central part is simply $\frac{1}{2}M\omega_0^2 r_i^2$ for the i th nucleon. If the contribution of the pairing force to the average potential is neglected, the noncentral quadrupole interaction V_Q should give rise to an average one-body potential which is noncentral. For simplicity, we may assume that the equipotential surface in a deformed nucleus has the same shape as the nuclear density. Consider, then, a point r_i on a distorted equipotential surface, given by

$$r_i = r_0[1 + \sum_{\mu} a_{2\mu} Y_2^{\mu}(\theta', \phi')] \quad (9-117)$$

in analogy with Eq. 9-28. For a different equipotential surface, r_0 would change. The value of the potential for the particular equipotential specified by r_0 is $V(r_0)$. We see that, if we take the harmonic form of the potential, denoted by V_h ,

$$\begin{aligned} V_h(r_0) &= \frac{1}{2}M\omega_0^2 r_0^2 \\ &= \frac{1}{2}M\omega_0^2 r_i^2 [1 + \sum_{\mu} a_{2\mu} Y_2^{\mu}(\theta', \phi')]^{-2} \end{aligned}$$

or

$$\begin{aligned} V_h(\beta, \gamma, r_i) &\approx \frac{1}{2}M\omega_0^2 r_i^2 \left\{ 1 - 2\beta \left[\cos \gamma Y_2^0(\theta', \phi') + \frac{1}{\sqrt{2}} \sin \gamma (Y_2^2 + Y_2^{-2}) \right] \right\} \\ &= V_{\text{spherical}}(r_i) + V_D(\beta, \gamma, r_i). \end{aligned} \quad (9-118)$$

Note that the deformation parameters (β, γ) now refer to the equipotential surfaces. Recall that the noncentral one-body potential V_D is arising because of the interaction of the i th particle with all the other extracore particles j through the two-body quadrupole interaction V_Q . If the exchange contribution is neglected (as is a reasonable approximation for a long-range potential), V_D should be given by

$$V_D(r_i) \approx - \sum_{\mu} r_i^2 Y_2^{\mu}(\hat{r}_i) D_{\mu},$$

with

$$\begin{aligned} D_{\mu} &= \chi \int \rho(r_j) r_j^2 (-)^{\mu} Y_2^{\mu}(\hat{r}_j) d^3 r_j, \\ &= \chi \langle Q_{\mu}' \rangle. \end{aligned} \quad (9-119)$$

Here ρ is the density of the intrinsic shape. For a nucleus with shape oscillations, ρ is a function of time, and the self-consistency condition is a dynamic one, to be satisfied at all times. The β - γ dependence in V_D arises through the density $\rho(\beta, \gamma)$, and we can put

$$D_0 = D \cos \gamma, \quad D_2 = \frac{1}{\sqrt{2}} D \sin \gamma,$$

obtaining the identical expression (9-118) for V_D , if we identify $D = M\omega_0^2 \beta$.

We now take the deformed one-body potential $H_S + V_D(\beta, \gamma)$, and, for each point of the β - γ mesh mentioned earlier, calculate the single-particle energy levels and the wave functions. Next, for each mesh point, the pairing potential V_P is used to do a BCS calculation on these single-particle levels, obtaining the neutron and proton pairing gaps and the occupation probabilities. Finally, the expectation value of the original Hamiltonian (Eq. 9-114) is taken with the BCS wave function to determine the collective potential energy $V(\beta, \gamma)$, to be used in the Bohr Hamiltonian. The inertial parameters B are calculated microscopically within this framework, using the time-dependent Hartree-Fock theory, with the dynamic self-consistency (Eq. 9-119) maintained. We shall not give any details of this calculation here, but a simpler formulation will be outlined in Section 10-8.

We now proceed to discuss some of the main results of the above calculation for the W-Os-Pt transition nuclei. Figure 9-24a shows $V(\beta, \gamma)$ for ^{184}W ,

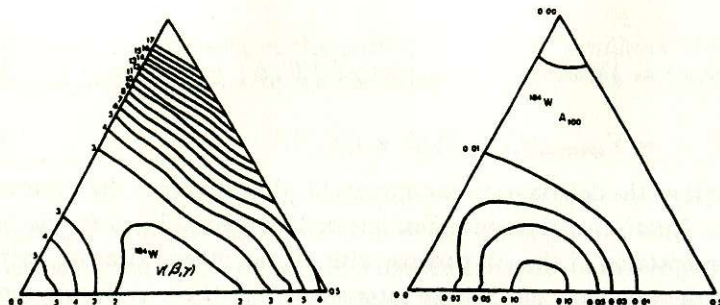


Fig. 9-24 The calculated contour maps of (a) $V(\beta, \gamma)$ and (b) the ground-state wave function A_{100} for the nucleus ^{184}W . The potential minimum occurs for a prolate shape ($\gamma = 0$). In this, as well as Figs. 9-25 and 9-26, the units for $V(\beta, \gamma)$ are arbitrary.

as calculated by Kumar and Baranger [12] by the above method, as a set of equipotential lines. The lowest potential minimum occurs for a prolate ($\gamma = 0$) deformed shape in this nucleus. It is also interesting to examine the coefficients $A_{\alpha J K}(\beta, \gamma)$ of the wave function defined in Eq. 9-113. The nuclear state of a given J may occur several times; $\alpha = 1$ denotes the particular J -state coming with the lowest energy, $\alpha = 2$ the state with the same J of next higher energy, and so on. Furthermore, since K need not be a good quantum number, a state of given α and J may have several K -values mixed. The K -probability of a particular state with given α and J may be defined as

$$N_K^{\alpha J} = \int |A_{\alpha J K}|^2 d\tau, \quad \sum_K N_K^{\alpha J} = 1, \quad (9-120)$$

where the integration is over the β - γ space. Thus, for a prolate well-deformed nucleus, we would expect for the first 2^+ state ($\alpha = 1, J = 2$) $N_0^{12} = 1$, and all other N_K 's to be zero.

Figure 9-24b depicts the contour plots of the ground-state A_{100} for ^{184}W in the β - γ plane, showing that the wave function is concentrated mostly in the prolate side around the potential minimum. For this nucleus, the first 2^+ state has $N_0^{12} = 0.995$ and $N_2^{12} = 0.005$, showing that this is a nearly pure $K = 0$ state, in agreement with the prolate rotor model (see Table 9-2). The calculated $V(\beta, \gamma)$ and A_{100} for ^{190}Os and ^{196}Pt are also shown in Figs. 9-25 and 9-26, respectively. In ^{190}Os , the lowest minimum in $V(\beta, \gamma)$ occurs for an asymmetric shape ($\beta > 0, \gamma = 30^\circ$), but the potential is very shallow as a function of γ . This results in the wave function A_{100}

TABLE 9-2 The K -Probability of the Nuclear Wave Functions. The probability measures the contribution of a K -component to the normalization integral. The $K = 0$ contribution can be deduced by subtracting from unity the $K = 2$ contribution (if $J = 2$) or the sum of the $K = 2, 4$ contributions (if $J = 4$). After Kumar and Baranger [12].

State ^a	K	^{182}W	^{184}W	^{186}W	^{186}Os	^{188}Os	^{190}Os	^{192}Os	^{192}Pt	^{194}Pt	^{196}Pt
2^+	2	0.002	0.005	0.013	0.013	0.033	0.066	0.174	0.275	0.414	0.512
$2'^+$	2	0.449	0.642	0.791	0.919	0.923	0.899	0.775	0.683	0.533	0.415
$2''^+$	2	0.528	0.328	0.170	0.093	0.110	0.190	0.236	0.159	0.188	0.373
4^+	2	0.005	0.011	0.027	0.027	0.071	0.132	0.218	0.302	0.365	0.380
4^+	4	0.000	0.001	0.002	0.002	0.006	0.015	0.049	0.099	0.185	0.279

State ^b	Prolate rotor	Oblate rotor	Harmonic vibrator
2^+	2. 0.0	0.75	0.275
$2'^+$	2. 1.0 (γ -band)	0.25 (γ -band)	0.661
$2''^+$	2. 0.0 (β -band)	0.75 (β -band)	0.275
4^+	2. 0.0	0.313	0.275
4^+	4. 0.0	0.547	0.107

^a W-Os-Pt region.

^b Some model cases.

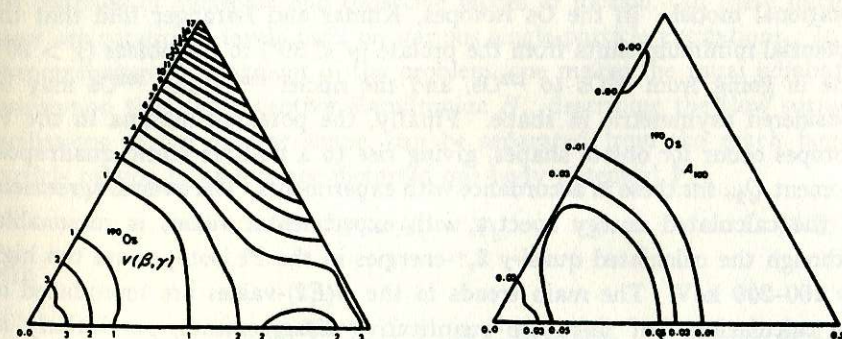


Fig. 9-25 (a) The calculated contour map $V(\beta, \gamma)$ for ^{190}Os . The potential is nearly γ -independent, although a very shallow minimum occurs for an asymmetric shape ($\beta > 0, \gamma = 30^\circ$). (b) The corresponding ground-state wave function A_{100} .

being spread over a large β - γ region instead of being concentrated around the minimum. Finally, in ^{196}Pt , although the minimum of $V(\beta, \gamma)$ occurs for an oblate shape, the wave function is spread out to an even greater degree over various β - γ values.

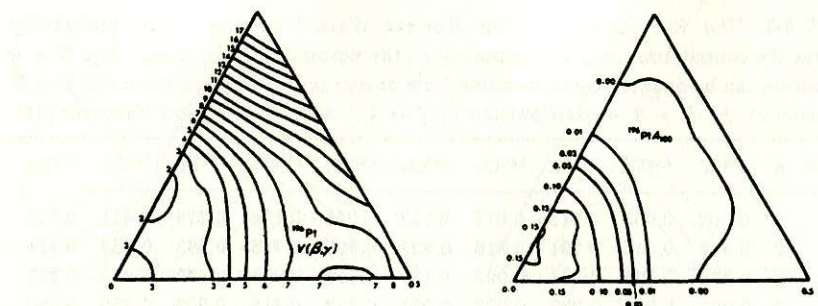


Fig. 9-26 (a) The calculated $V(\beta, \gamma)$ for ^{196}Pt . The minimum is on the oblate side. (b) The ground-state wave function A_{100} is spread over a large region of the β - γ plane.

Thus the various simple models for stiff nuclei—prolate or oblate rotor or harmonic vibrator—are no longer very meaningful for such cases. This is more evident in Table 9-2, where the calculated K -probabilities N_K (Eq. 9-120) are tabulated for these nuclei and compared with the model cases. Although the W isotopes are of prolate shape, there is strong coupling between the β - and γ -bands, resulting in large deviations from the simple rotational model. In the Os isotopes, Kumar and Baranger find that the potential minimum shifts from the prolate ($\gamma < 30^\circ$) to the oblate ($\gamma > 30^\circ$) side in going from ^{188}Os to ^{192}Os , and the nuclei ^{190}Os and ^{192}Os may be considered asymmetric in shape. Finally, the potential minima in the Pt isotopes occur for oblate shapes, giving rise to a positive static quadrupole moment Q_{2+} for these in accordance with experiments. The overall agreement of the calculated energy spectra with experimental values is reasonable, although the calculated quasi- γ $2, +$ -energies in the Pt isotopes are too high by 100–200 keV. The main trends in the $B(E2)$ -values are reproduced in the calculation, but there are quantitative disagreements, particularly in interband transitions. Perhaps the major triumph of the calculation lies in its correct prediction of the prolate-to-oblate transition in these nuclei, and in the applicability of the scheme to soft as well as stiff nuclei, irrespective of shape.

Finally, we should mention that the Davydov-Chaban model outlined in Section 9-5, which implicitly assumes a very steep γ -dependence of $V(\beta, \gamma)$ and a potential minimum for a fixed nonzero γ , also works reasonably well in this transition region, although its basic assumption seems to be in apparent contradiction with the microscopic calculation of $V(\beta, \gamma)$. The point to remember is that in the Os and Pt isotopes, as we have seen, the microscop-

ically calculated $V(\beta, \gamma)$ is nearly γ -independent, and this results in the nucleus sweeping a large range of γ -values, giving an appreciable rms value of the asymmetry parameter γ . The alternative phenomenological description of the Davydov model with a fixed $\gamma = \gamma_{\text{rms}}$ thus works reasonably well. Even before the detailed calculations of Kumar and Baranger were performed, these points were realized by Gunye, Das Gupta, and Preston [41] in a simple microscopic calculation of $V(\beta, \gamma)$ for these transition nuclei. They did not, however, carry out any quantitative calculation of the wave functions by solving the Bohr Hamiltonian.

9-7 STRONG COUPLING OF PARTICLE AND COLLECTIVE MOTIONS

The preceding discussions of collective modes of even-even nuclei were carried out without considering the coupling of these modes to single-particle excitations, which occur at higher energies in these nuclei because of the energy gap at the Fermi surface. For even-odd or odd-odd nuclei, however, the single-particle excitations are lowered in energy, and for a proper description of the low-lying levels of these nuclei it is necessary to take into account the coupling of nucleonic and collective modes of motion. In these nuclei, there are rotational levels built on various single-particle excitations. In a phenomenological treatment of the problem, one makes the usual adiabatic assumption that the collective Hamiltonian H_c , describing the slow surface oscillations of the nuclear shape, can be separated from the much faster particle motion in an average distorted one-body potential V_h :

$$H = H_c + H_p, \quad (9-121)$$

with

$$H_p = \sum_{i=1}^k [T_i + V_h(\beta, \gamma; \mathbf{r}_i, \mathbf{l}_i, \mathbf{s}_i)], \quad (9-122)$$

where H_p is the particle Hamiltonian. The shape of the distorted potential, V_h , is related to the nuclear shape and is described by the parameters β, γ in the body-fixed frame. The number of particles, k , summed over in the particle Hamiltonian, depends on the sophistication of our model. In the extreme single-particle model, we may consider only one particle in an odd nucleus and lump all others together in the core; or, with a little more sophistication, we may let i extend over all the particles in the last unfilled shell. Since the change in the shape of the nucleus in this model must be small during the time that a particle takes to complete several cycles of its

orbit, β and γ occurring in V_h are just average values and not dynamical variables. As before, we consider only the quadrupole deformations, and solve the single-particle Schrödinger equation

$$H_p \psi_\alpha = [T + V_h(\beta, \gamma; \mathbf{r}, \mathbf{l}, \mathbf{s})] \psi_\alpha = E_\alpha(\beta, \gamma) \psi_\alpha. \quad (9-123)$$

This calculation yields a set of single-particle states which constitutes a generalization of the shell model. In this simple model, for given β and γ , the k nucleons fill up the lowest orbitals beyond the filled core, and their total energy is simply the deformation potential $V(\beta, \gamma)$ of the Bohr Hamiltonian. In this static approach, the equilibrium shape of the nucleus is determined by the values of β, γ that minimize the total particle energy.

Recalling that the one-body potential V_h is generated by the two-body nucleon-nucleon interaction, we have thus traced the potential $V(\beta, \gamma)$ to the interparticle energy. However, the rotational energy, associated solely with the orientation of the distorted system, remains as the collective Hamiltonian H_c , for Eq. 9-123 yields particle wave functions ψ_α referred to a body-fixed coordinate system. This is a reasonable picture, since the nuclear orientation changes much more rapidly than does its shape; whereas β and γ may be considered constant at their average values, the same obviously does not apply to the Euler angles. Then the complete wave equation for the nucleus is taken as

$$(T_{\text{rot}} + \sum_p H_p) \Phi = E \Phi, \quad (9-124)$$

where

$$T_{\text{rot}} = \sum_{\kappa=1}^3 \frac{L_\kappa^2}{2J_\kappa} = \sum_\kappa \frac{(J_\kappa - j_\kappa)^2}{2J_\kappa}, \quad (9-125)$$

and \mathbf{J} , \mathbf{L} , and \mathbf{j} are the total, core, and particle angular momenta, respectively. The last, \mathbf{j} , is not necessarily for only one particle, but is the angular momenta of all the particles not included in the core.

Before examining the intrinsic particle wave functions, we shall look at the structure of the total wave function Φ , considering first the axially symmetric case, for which

$$T_{\text{rot}} = \frac{\hbar^2}{2J} [(\mathbf{J} - \mathbf{j})^2 - (J_3 - j_3)^2] + \frac{\hbar^2}{2J_3} (J_3 - j_3)^2. \quad (9-126)$$

For convenience, we have removed the factor \hbar from each angular-momentum operator. Because V_h is assumed to be axially symmetric, the azimuthal angles of the particles do not appear in the Hamiltonian, and therefore

j_3 is a constant of motion. We shall denote it by Ω . Moreover, J^2 is, of course, a constant of motion, and so is J_3 . We obtain

$$\begin{aligned} T_{\text{rot}} &= \frac{\hbar^2}{2J} [J(J+1) + \mathbf{j}^2 - 2\mathbf{J} \cdot \mathbf{j} - (K - \Omega)^2] + \frac{\hbar^2}{2J_3} (K - \Omega)^2 \\ &= \frac{\hbar^2}{2J} [J(J+1) - K^2 - \Omega^2] + \frac{\hbar^2}{2J_3} (K - \Omega)^2 \\ &\quad - \frac{\hbar^2}{2J} (J_+ j_- + J_- j_+) + \frac{\hbar^2}{2J} \mathbf{j}^2. \end{aligned} \quad (9-127)$$

The first two terms of Eq. 9-127 are now constants, whereas the last terms still involve operators. The quantities J_\pm and j_\pm are the operators $J_1 \pm iJ_2$ and $j_1 \pm ij_2$. The term containing these operators couples rotational and particle angular momenta and will be abbreviated as RPC. Since in classical mechanics the "potential" energy of the Coriolis force on a particle may be written as $\omega \cdot \mathbf{L}$, we see that the RPC-term is indeed of the same origin as a Coriolis force. The last term, $\hbar^2 \mathbf{j}^2/2$, contains only particle coordinates and can be absorbed in the particle Hamiltonian. We have

$$\left\{ \frac{\hbar^2}{2J} [J(J+1) - K^2 - \Omega^2] + \frac{\hbar^2}{2J_3} (K - \Omega)^2 + H_0 + \text{RPC} \right\} \Phi = E \Phi, \quad (9-128a)$$

$$H_0 = \sum_p H_p + \frac{\hbar^2}{2J} (\sum_p \mathbf{j}_p)^2. \quad (9-128b)$$

We shall presently prove that in the axially symmetric case $K = \Omega$. In this important special case, the Coriolis term may be treated as a perturbation. The operators J_\pm have matrix elements only for states that differ by one unit in K ; hence our assumption that K is a good quantum number is not valid in the presence of RPC. If we take a wave function with definite K as a zero-order approximation to Φ , RPC mixes in states of other K . But in a perturbation calculation, the admixture coefficient contains in the numerator the matrix elements of RPC and in the denominator the energy difference between the two states. Since for axial symmetry $K = \Omega$, states of different K are actually different particle states. The matrix element of RPC, on the other hand, is of the same order as rotational level spacing, proportional to $\hbar^2/2J$. Consequently (ignoring the special case of $K = \frac{1}{2}$), for nuclei with well-developed axial symmetry, such that the rotational spacing is small compared with particle-excitation energies, the Coriolis term

may be ignored, except when states of the same J and parity but different K come very close in energy. In the latter situation, although the matrix element of RPC between states of K and $K \pm 1$ is small, the small energy denominators in the perturbation terms make the higher-order terms important, and appreciable mixing is possible even between states differing in K by more than 1. For example, it is experimentally inferred that in $^{163}_{67}\text{Ho}_{96}$ the state of $J = \frac{7}{2}^+$, $K = \frac{1}{2}$ at 431.2 keV is mixed through RPC with the particle state $J = \frac{7}{2}^+$, $K = \frac{7}{2}$ at 439.9 keV [42], leading to appreciable $E1$ -transition from the 431.2-keV level to the $J = \frac{7}{2}^-, K = \frac{7}{2}$ ground state, which should otherwise be K -forbidden [$\Delta K > \lambda (= 1)$].

The effect of RPC for the special case of $K = \frac{1}{2}$ is especially large, since in the symmetrized zero-order wave function there are components of $K (= \frac{1}{2})$ and $-K (= -\frac{1}{2})$, which can become coupled by the RPC interaction.

Let the normalized intrinsic wave function χ_Ω be defined by

$$H_0\chi_\Omega = e_\Omega\chi_\Omega, \quad (9-129)$$

where we have shown explicitly only the quantum number Ω , although others are required to specify a state completely. Then a solution of Eq. 9-128a ignoring RPC is $\chi_\Omega \mathcal{D}_{MK}^J(\theta_i)$ in the body-fixed frame. This solution, however, is not invariant under the symmetry operation $R_1^{(x)}$, which is a rotation through π about the nuclear axis and leaves the space-fixed α_μ 's the same. We recall, from Eq. 9-55, that the rotation operator $R_1^{(1)}$ transforms \mathcal{D}_{MK}^J into $(-)^J \mathcal{D}_{M,-K}^J$, and we see that the properly symmetrized and normalized solution is

$$\Phi(JMK\Omega) = \left(\frac{2J+1}{16\pi^2}\right)^{1/2} [\mathcal{D}_{MK}^J(\theta_i)\chi_\Omega + (-)^J \mathcal{D}_{M,-K}^J(\theta_i)R_1^{(1)}\chi_\Omega]. \quad (9-130)$$

Because the potential V_h is not spherically symmetric, the average force on the particle is not central and \mathbf{j}^2 is not a constant of motion. Since in practice it is simpler to deal with states of constant angular momentum, we introduce the expansion

$$\chi_\Omega = \sum_j c_{j\Omega} \chi_{j\Omega}. \quad (9-131)$$

It is not difficult to determine the value of $R_1^{(1)}\chi_{j\Omega}$. The first step is to employ the very general property of the \mathcal{D} -matrix which allows the conversion of any angular function or any spherical tensor from the nuclear to the space-fixed axes. In this case, using Eq. A-72, we obtain

$$\chi_{j\Omega} = \sum_\mu \mathcal{D}_{\mu\Omega}^{j*} \chi'_{j\mu}, \quad (9-132)$$

where $\chi'_{j\mu}$ is the wave function in the space-fixed axes, and μ is the component of j on the z -axis. The operator $R_1^{(1)}$, of course, has no effect on χ' , and

$$R_1^{(1)}\chi_{j\Omega} = \sum_\mu \chi'_{j\mu} R_1^{(1)} \mathcal{D}_{\mu\Omega}^{j*}(\theta_i).$$

From Eqs. A-63 and A-64, we have

$$\mathcal{D}_{\mu\Omega}^{j*}(\theta_i) = (-)^{\mu-\Omega} \mathcal{D}_{-\mu,-\Omega}^j(\theta_i) \quad (9-133)$$

and

$$R_1^{(1)} \mathcal{D}_{\mu\Omega}^{j*}(\theta_i) = (-)^{\mu-\Omega} (-)^j \mathcal{D}_{-\mu,\Omega}^j(\theta_i).$$

Using these relations, it is straightforward to show that

$$R_1^{(1)}\chi_\Omega = \sum_j (-)^{j-2\Omega} c_{j\Omega} \chi_{j,-\Omega}, \quad (9-134)$$

with the result that the symmetrized wave function becomes

$$\Phi(JMK\Omega) = \left(\frac{2J+1}{16\pi^2}\right)^{1/2} [\mathcal{D}_{MK}^J \chi_\Omega + (-)^{J-2\Omega} \mathcal{D}_{M,-K}^J \sum_j (-)^j c_{j\Omega} \chi_{j,-\Omega}]. \quad (9-135)$$

This equation applies to the most general case, even with three unequal moments of inertia, for which the wave function is a linear superposition $\sum_{K,\Omega} A_{K\Omega} \Phi(JMK\Omega)$.

It is now easy to prove, using Eq. 9-135, that, for the axially symmetric case, $K = \Omega$. Rotation by an arbitrary angle θ about symmetry axis 3 should leave the wave function $\Phi(JMK\Omega)$ invariant or, at most, introduce a phase factor. Using Eqs. 9-131 to 9-133, we see that

$$\exp(-i\theta J_3) \mathcal{D}_{MK}^J \chi_\Omega = \exp[-i\theta(K - \Omega)] \mathcal{D}_{MK}^J \chi_\Omega, \quad (9-136)$$

so that the rotation operator $\exp(-i\theta J_3)$ acting on the two terms on the right-hand side of Eq. 9-135 would yield different phase factors unless $K = \Omega$. This implies that in the axially symmetric case the rotational angular momentum of the core, \mathbf{L} , is perpendicular to the symmetry axis, with the nucleus rotating about an axis perpendicular to the symmetry axis.

There are a few important cases in which Eq. 9-135 simplifies. For axial symmetry, $K = \Omega$, and the coefficient of the second term is $(-)^{J-1}$, since $2K$ is an odd number. Another important case is that of only one extracore particle—the extreme single-particle model. For this there is an

alternative representation for χ_{Ω} in terms of single-particle functions for which the constants of motion are the orbital angular momentum l , its component A on the 3-axis, and Σ , the component of spin on the 3-axis. Of course, $\Sigma = \Omega - A$. We have

$$\chi_{\Omega} = \sum_{l,A} a_{lA\Omega} \chi_{lA\Omega}. \quad (9-137)$$

Since parity is a good quantum number, the values of l are either all even or all odd. The coefficients $c_{j\Omega}$ are connected with the coefficients $a_{lA\Omega}$ simply by angular-momentum addition relations, and

$$c_{j\Omega} = \sum_{l,A} (\frac{1}{2} A \Sigma | j\Omega) a_{lA\Omega}. \quad (9-138)$$

By considering inversion of the 3-axis, we can show that $a_{lA\Omega}$ must equal $a_{l,-A,-\Omega}$. Using these results and the fact that

$$(l_1 l_2 m_1 m_2 | jm) = (-)^{l_1 + l_2 - j} (l_1 l_2 - m_1 - m_2 | j - m),$$

we find

$$c_{j\Omega} = (-)^{j-(1/2)} \Pi_x c_{j,-\Omega},$$

where $\Pi_x = (-)^l$ is the parity of χ . In this case, the last sum in Eq. 9-135 is $(-)^{2j-(1/2)} \Pi_x \chi_{-\Omega} = (-)^{1/2} \Pi_x \chi_{-\Omega}$; and if, furthermore, we have axial symmetry, then

$$\Phi(JMK) = \left(\frac{2J+1}{16\pi^2} \right)^{1/2} [\mathcal{D}_{MK}^J \chi_K + (-)^{J-(1/2)} \Pi_x \chi_{-K} \mathcal{D}_{M-K}^J]. \quad (9-139)$$

Let us now return to a consideration of the Coriolis term, which connects only collective states for which the K -values differ by 1. Since the nuclear state $\Phi(JMK)$ contains collective wave functions with both $\pm K$, the Coriolis term contributes directly to the energies of states with $K = \frac{1}{2}$, but in no other case. We see readily from Eq. 9-135 with $K = \Omega = \frac{1}{2}$ that

$$\langle \text{RPC} \rangle = \frac{\hbar^2}{2\mathcal{J}} a(-)^{J+(1/2)} (J + \frac{1}{2}), \quad (9-140)$$

where a , called the *decoupling parameter*, is given by

$$a = - \sum_j (-)^{j+(1/2)} (j + \frac{1}{2}) |c_{j(1/2)}|^2. \quad (9-141)$$

The energy of a nuclear state is given by Eqs. 9-128, 9-129, and 9-140 for the axially symmetric nucleus, as

$$E_{J,K} = e_K + \left(\frac{\hbar^2}{2\mathcal{J}} \right) [J(J+1) - 2K^2 + \delta_{K,(1/2)} a(-)^{J+(1/2)} (J + \frac{1}{2})]. \quad (9-142)$$

We see that a rotational band is built on each particle state. The collective angular momentum has no component on the 3-axis, and K is due entirely to the particle angular momentum and is constant throughout the band. All higher values of $J \geq K$ are permitted, and, when $K \neq \frac{1}{2}$, the lowest state has $K = J$, and successive states have $J = K+1, K+2, \dots$. The excitation above the ground state of a given band is

$$\Delta E_J = \left(\frac{\hbar^2}{2\mathcal{J}} \right) [J(J+1) - K(K+1)]. \quad (9-143)$$

When $K = \frac{1}{2}$, the level order is determined by the value of a in the manner shown in Fig. 9-27. For example, for a between -2 and -3 , the level order is $\frac{3}{2}, \frac{1}{2}, \frac{7}{2}, \frac{5}{2}, \frac{11}{2}, \frac{9}{2}$, etc.

Just as with even nuclei, the vibration-rotation interaction complicates these results. When this small correction is incorporated, the energies become

$$\begin{aligned} E_{J,K} = & e_K - 2 \left(\frac{\hbar^2}{2\mathcal{J}} \right) K^2 \\ & + \left(\frac{\hbar^2}{2\mathcal{J}} \right) [J(J+1) + \delta_{K,(1/2)} a(-)^{J+(1/2)} (J + \frac{1}{2})] \\ & - B[J(J+1) + \delta_{K,(1/2)} a(-)^{J+(1/2)} (J + \frac{1}{2})]^2. \end{aligned} \quad (9-144)$$

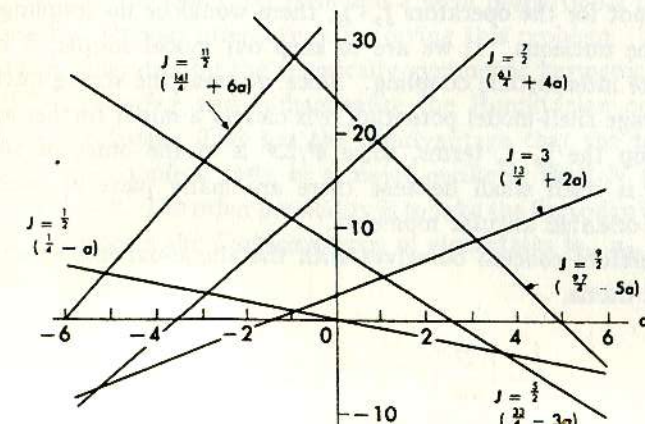


Fig. 9-27 The dependence of the rotational-energy levels on the decoupling parameter a in a $K = \frac{1}{2}$ band. The ordinate is $E_J - e$ in the notation of Eq. 9-142.

As we have already remarked, departures from Eq. 9-142 may also be produced by RPC in exceptional cases. This situation arises in ^{183}W , where a $K = \frac{1}{2}$ ground state and a $K = \frac{3}{2}$ excited state are fairly close in energy, with rotational bands built on both of these states. In these rotational bands, certain levels have very similar energies, and the band structure does not follow the level spacings of Eq. 9-142. Kerman [43] has shown that the perturbation due to the Coriolis term can explain the discrepancies. More interesting is the mixing of states with $\Delta K > 1$ because of RPC when the energies are very close, as was mentioned earlier in the case of ^{163}Ho . In such cases it is necessary to diagonalize RPC in the basis of the uncoupled states (Eq. 9-135) to determine the extent of K -mixing.

9-8 PARTICLE STATES IN DISTORTED NUCLEI

For further progress in studying odd nuclei, we must obtain an understanding of the states of motion of the particles outside the core. The fundamental paper on this subject was written by Nilsson [4] in 1955; he dealt only with an axially symmetric nucleus, and his work was extended to the nonaxial shape by Newton [44].

The intrinsic wave function is given by Eq. 9-129:

$$\left[\sum_p H_p + \left(\frac{\hbar^2}{2\mathcal{J}} \right) (\sum_p \mathbf{j}_p)^2 \right] \chi = e\chi.$$

If it were not for the operators $\mathbf{j}_p \cdot \mathbf{j}_q$, there would be no coupling whatever between the nucleons. If we are to keep our model simple, it is essential to eliminate interparticle coupling. Since we treat the strong nuclear forces by an average shell-model potential, it is clearly a minor further approximation to drop the $\mathbf{j}_p \cdot \mathbf{j}_q$ terms, since $\hbar^2/2\mathcal{J}$ is of the order of 15 keV and $\sum_{p,q} \mathbf{j}_p \cdot \mathbf{j}_q$ is itself small because there are many pairs of nucleons with oppositely oriented angular momenta.

We therefore concern ourselves with the single-particle equation in the body-fixed frame,

$$\left[-\left(\frac{\hbar^2}{2M} \right) \nabla^2 + V(\mathbf{r}_i, \mathbf{l}_i, \mathbf{s}_i) \right] \psi_\alpha = e_\alpha \psi_\alpha. \quad (9-145)$$

The one-body potential $V(\mathbf{r}_i, \mathbf{l}_i, \mathbf{s}_i)$ contains a spin-orbit term, a term proportional to \mathbf{l}_i^2 , and a distorted harmonic-oscillator potential of the form 9-118,

$$V_h(\beta, \gamma, \mathbf{r}_i) = \frac{1}{2} M \omega_0^2 r_i^2 \left\{ 1 - 2\beta \left[\cos \gamma Y_2^0(\theta', \phi') + \frac{1}{\sqrt{2}} \sin \gamma (Y_2^2 + Y_2^{-2}) \right] \right\}, \quad (9-146)$$

where in V_h we include the spherically symmetric part coming from the core. Just as in the spherical-shell model, the harmonic-oscillator form is used for convenience in calculation; a more realistic radial dependence like that of the Woods-Saxon form would involve more numerical work. For $\gamma = 0$, we obtain axial symmetry, with only a $P_2(\cos \theta')$ deformation remaining in Eq. 9-146. An alternative form for V_h is an anisotropic harmonic oscillator:

$$V_h = \frac{1}{2} M (\omega_1^2 x_1^2 + \omega_2^2 x_2^2 + \omega_3^2 x_3^2), \quad (9-147)$$

where (x_1, x_2, x_3) refer to the intrinsic body-fixed axes. For axial symmetry about x_3 , $\omega_1 = \omega_2$; and a little algebra shows that for this case the form 9-147 contains only P_2 -type deformation. It is assumed further that the volumes enclosed by the equipotential surfaces do not change with deformation, implying that

$$\omega_1 \omega_2 \omega_3 = \text{constant}. \quad (9-148)$$

The single-particle equation to be solved is therefore

$$\left(-\frac{\hbar^2}{2M} \nabla^2 + V_h + V_{l,s} \right) \psi_\alpha = e_\alpha \psi_\alpha, \quad (9-149)$$

where $V_{l,s}$ contains the spin-orbit term and a term proportional to \mathbf{l}^2 .

There are two obvious alternatives in solving this problem. The first is to take a basis generated by the spherically symmetric harmonic oscillator, $-\left(\hbar^2/2M\right)\nabla^2 + \frac{1}{2}M\omega_0^2 r_i^2$, and to diagonalize the Hamiltonian occurring in Eq. 9-149 in this basis. This has the disadvantage that the term $r_i^2 Y_2^0$ coming in V_h will couple a state in a major oscillator shell N ($= 2n + l$) with others of $N \pm 2$. The other possibility is to take the Cartesian form 9-147 for V_h and to generate the Cartesian basis of eigenstates $|n_1, n_2, n_3\rangle$ of the Hamiltonian

$$\sum_{\kappa=1}^3 \left(-\frac{\hbar^2}{2M} \frac{\partial^2}{\partial x_\kappa^2} + \frac{1}{2} M \omega_\kappa^2 x_\kappa^2 \right).$$

It is then necessary to diagonalize the total Hamiltonian of Eq. 9-149 in this basis. It is very difficult, however, to work with $\mathbf{l} \cdot \mathbf{s}$ and \mathbf{l}^2 -type potentials in a Cartesian basis.

The first alternative, therefore, is the more practical one, and Nilsson has shown that by using the following scale transformation one can eliminate the coupling between different major shells. This transformation is given by

$$\xi_\kappa = \left(\frac{M\omega_\kappa}{\hbar} \right)^{1/2} x_\kappa, \quad (9-150)$$

which corresponds to the adoption of different units of length along the three axes. When H_h is written for the anisotropic part of the Hamiltonian, it is transformed by Eq. 9-150 to

$$H_h = -\frac{\hbar^2}{2M} \nabla^2 + V_h = \sum_\kappa \frac{1}{2} \hbar \omega_\kappa \left(-\frac{\partial^2}{\partial \xi_\kappa^2} + \xi_\kappa^2 \right). \quad (9-151)$$

As before, this is simply the sum of the Hamiltonians of three linear oscillators; the corresponding quantum states have energies $\Sigma(n_\kappa + \frac{1}{2})\hbar\omega_\kappa$, where n_1, n_2, n_3 are the numbers of excitations in the respective linear oscillators. As we have mentioned, however, it is more convenient to use spherical coordinates; hence we define

$$\rho^2 = \sum_\kappa \xi_\kappa^2 \quad \text{and} \quad \nabla_\xi^2 = \sum_\kappa \frac{\partial^2}{\partial \xi_\kappa^2}.$$

Then it is easy to rewrite the Hamiltonian 9-151 as

$$H_h = H_0 + H_\epsilon \quad (9-152)$$

with

$$H_0 = \frac{1}{2} \hbar \omega_0 (-\nabla_\xi^2 + \rho^2),$$

$$H_\epsilon = \frac{1}{2} \hbar \omega_0 \sum_\kappa \epsilon_\kappa \left(-\frac{\partial^2}{\partial \xi_\kappa^2} + \xi_\kappa^2 \right), \quad (9-153)$$

and $\omega_\kappa = \omega_0(1 + \epsilon_\kappa)$. The ϵ_κ 's specify the deformation; for the axially symmetric case, we define[†]

$$\epsilon_1 = \epsilon_2 = \frac{1}{3}\epsilon, \quad \epsilon_3 = -\frac{2}{3}\epsilon, \quad (9-154)$$

yielding

$$\omega_1 = \omega_2 = \omega_\perp = \omega_0 \left(1 + \frac{\epsilon}{3} \right) \quad \text{and} \quad \omega_3 = \omega_0 \left(1 - \frac{2\epsilon}{3} \right).$$

[†] Our ϵ is the same as the one defined by Nilsson in the Appendix of ref. 4. In current literature, ϵ is taken to be the quadrupole deformation parameter, while deformations of higher multipoles are introduced as $\epsilon_l P_l(\cos \theta)$, $l > 2$.

The volume-conservation condition (Eq. 9-148) immediately shows that ω_0 is deformation dependent:

$$\omega_0(\epsilon) = \dot{\omega}_0(1 - \frac{1}{3}\epsilon^2 - \frac{2}{27}\epsilon^3)^{-1/3}, \quad (9-155)$$

with $\dot{\omega}_0 = \omega_0(0)$.

To construct a basis from the eigenfunctions of H_0 , we define a pseudo angular momentum

$$\lambda = -i\hbar\xi \times \nabla_\xi. \quad (9-156)$$

Of course, λ differs from the true angular momentum $-i\hbar r \times \nabla$ by terms of first order in ϵ . Nevertheless, the ξ -system is preferable, because, as is seen from the form of Eq. 9-153, the remaining term H_ϵ is diagonal in n_1, n_2 , and n_3 and hence in $N = n_1 + n_2 + n_3$. Thus the major-shell mixing has been eliminated from the ξ -system. We now define the basis $|N, l, \Lambda, \Sigma\rangle$ by

$$H_0|N, l, \Lambda, \Sigma\rangle = (N + \frac{3}{2})\hbar\omega_0|N, l, \Lambda, \Sigma\rangle,$$

$$\lambda^2|N, l, \Lambda, \Sigma\rangle = l(l+1)\hbar|N, l, \Lambda, \Sigma\rangle,$$

$$\lambda_3|N, l, \Lambda, \Sigma\rangle = \Lambda\hbar|N, l, \Lambda, \Sigma\rangle,$$

$$s_3|N, l, \Lambda, \Sigma\rangle = \Sigma\hbar|N, l, \Lambda, \Sigma\rangle. \quad (9-157)$$

It is more convenient now to take in the single-particle Hamiltonian[†] a spin-orbit potential of the form $C\lambda \cdot s$ and a quadratic potential $D\lambda^2$ in terms of the pseudo angular momentum rather than the true angular momentum. These terms are chosen phenomenologically to make the energy levels for spherical nuclei agree with the shell model. The λ^2 -dependent term decreases the energy of the higher angular-momentum states from their oscillator values, as observed empirically. Nilsson has shown [4, Appendix A] that there is very little difference in the energies found whether one uses the true or the pseudo angular momenta, and consequently we may now attempt to solve the single-particle wave equation

$$(H_0 + H_\epsilon + C\lambda \cdot s + D\lambda^2)\psi_\alpha = e_\alpha \psi_\alpha. \quad (9-158)$$

We can diagonalize the above Hamiltonian in the basis $|N, l, \Lambda, \Sigma\rangle$ defined in Eq. 9-157, so that ψ_α may be written as a linear combination of states $|N, l, \Lambda, \Sigma\rangle$. Note that C and D are constants in a given shell and that $H_\epsilon, C\lambda \cdot s$, or λ^2 cannot mix N ; hence it is enough to diagonalize within

[†] The coefficients C and D are both negative.

a single major shell. However, even in the absence of the $\lambda \cdot s$ potential, the pseudo angular momentum l is not a good quantum number because of H_ϵ , which can mix l with $l \pm 2$. This is readily seen by considering the matrix element $\langle N', l', \Lambda', \Sigma' | H_\epsilon | N, l, \Lambda, \Sigma \rangle$. By expanding the states $|N, l, \Lambda, \Sigma\rangle$ in the Cartesian basis $|n_1, n_2, n_3, \Sigma\rangle$ and noting the form of H_ϵ in Eq. 9-153, we find that $N' = N$ and, further, that the kinetic and potential parts in H_ϵ contribute equally. We then obtain

$$\begin{aligned} & \langle N', l', \Lambda', \Sigma' | H_\epsilon | N, l, \Lambda, \Sigma \rangle \\ &= \delta_{NN'} \delta_{\Sigma\Sigma'} \langle N', l', \Lambda', \Sigma' | \hbar \omega_0 \sum_\kappa \epsilon_\kappa \xi_\kappa^2 | N, l, \Lambda, \Sigma \rangle \\ &= \delta_{NN'} \delta_{\Sigma\Sigma'} \langle N', l', \Lambda', \Sigma' | \frac{1}{3} \hbar \omega_0 (\xi_1^2 + \xi_2^2 - 2\xi_3^2) | N, l, \Lambda, \Sigma \rangle. \end{aligned}$$

But $(\xi_1^2 + \xi_2^2 - 2\xi_3^2)$ is proportional to Y_2^0 , showing by the Wigner-Eckart theorem that l and l' may differ by ± 2 , whereas Λ cannot change because of H_ϵ .

We could also write V_h as given in Eq. 9-147 in terms of the deformation parameter ϵ in the axially symmetric case. A little algebra shows that

$$V_h = \frac{1}{2} M \omega_0^2 r^2 \left[\left(1 + \frac{2}{9} \epsilon^2 \right) - \frac{4}{3} \epsilon \left(1 - \frac{\epsilon}{6} \right) P_2(\cos \theta') \right], \quad (9-159a)$$

$$= \frac{1}{2} \hbar \omega_0 \rho^2 [1 - \frac{5}{3} \epsilon P_2(\cos \theta_i)], \quad (9-159b)$$

where $\cos^2 \theta' = x_3/r$, and $\cos^2 \theta_i = x_3/\rho$. If we neglect second-order terms in ϵ , the form 9-159a is equivalent to Eq. 9-146 for $\gamma = 0$, with the relation

$$\epsilon = \frac{3}{2} \sqrt{\frac{5}{4\pi}} \beta = 0.95\beta. \quad (9-160)$$

We have also seen in Eq. 9-155 that ω_0 is a function of the deformation parameter ϵ . It is sometimes more convenient to use the parameter

$$\eta = \frac{2\epsilon \hbar \omega_0(\epsilon)}{-C}, \quad (9-161)$$

where C is the coefficient of the $\lambda \cdot s$ term. The quantities C and D are chosen to yield the shell model for spherical nuclei; D is varied from shell to shell. In the literature the notations $\kappa = -C/2\hbar\omega_0$ and $\mu = 2D/C$ are used. Reasonable values are $\hbar\dot{\omega}_0 = 41A^{-1/3}$ MeV and $\kappa = 0.05$ for $N > 50$, increasing to $\kappa = 0.08$ for $N < 20$. Values of μ vary from 0 to 0.70, depending on the shell.

Nilsson's results are given in extensive tables and graphs in refs. 4 and 5. We reproduce these graphs as Figs. 9-28 to 9-32, for the regions of the periodic table in which there are large distortions. These graphs show the energy of each state as a function of the distortion ϵ . For Z and $N > 20$, only positive distortions are shown. The line representing each state is labeled

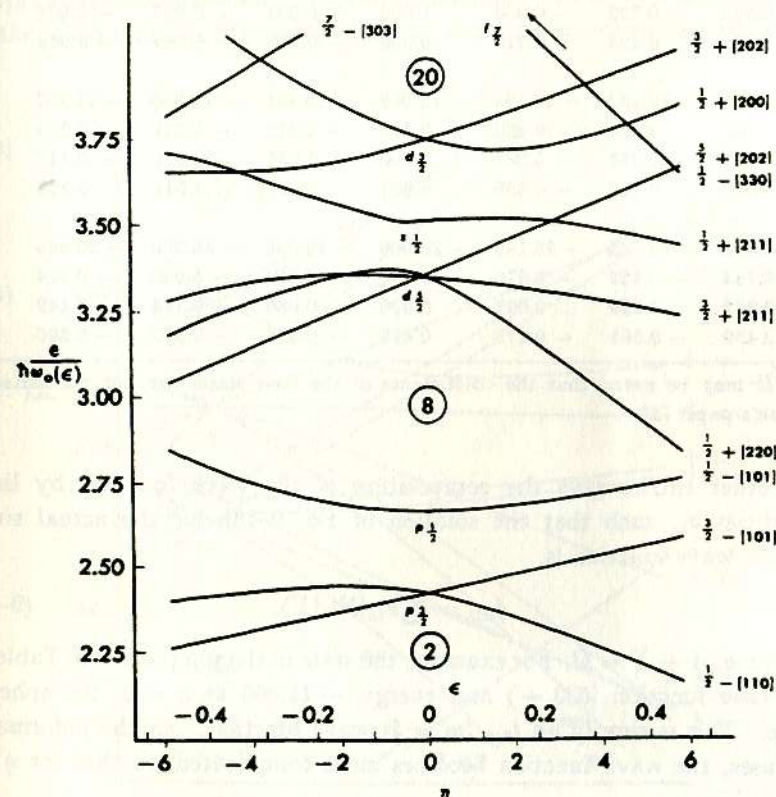


Fig. 9-28 Single-particle levels for $8 < Z < 20$, $8 < N < 20$. (After Mottelson and Nilsson [5].) The corresponding wave functions are given in ref. 4, Tables I and I(a).

by the value of Ω , the parity, and the triad $[N n_3 \Lambda]$. Although n_3 is not a constant of motion in the spherical representation, it becomes very nearly so for very large distortions. This would be expected physically as the energy difference $\hbar\omega_1 - \hbar\omega_3$ increases.

An example of Nilsson's wave-function tables is shown in Table 9-3. The energies in the first row of the table for each state are in units $\hbar\omega_0$.

TABLE 9-3 An Example of Nilsson's Wave Functions^a. $N = 5$, $\Omega = \frac{7}{2}$. Base vectors: $|553 +\rangle$, $|533 +\rangle$, $|554 -\rangle$.

$\eta = -6$	-4	-2	0	2	4	6	$+\infty$
-16.090	-15.493	-14.007	-11.400	-8.393	-5.255	-2.055	
-0.615	-0.485	-0.214	0.000	0.094	0.144	0.177	[503]
-0.583	-0.723	-0.954	1.000	-0.994	-0.987	-0.982	
0.531	0.493	0.210	0.000	-0.055	-0.067	-0.068	
<hr/>							
-20.498	-18.153	-16.194	-15.000	-13.961	-12.885	-11.757	
0.082	0.254	0.432	-0.426	-0.372	-0.321	-0.279	[514]
-0.717	-0.655	-0.285	0.000	-0.086	-0.111	-0.117	
-0.692	-0.712	-0.856	0.905	0.924	0.941	0.953	
<hr/>							
-27.812	-26.755	-26.199	-26.000	-26.046	-26.260	-26.588	
0.784	-0.837	-0.876	0.905	-0.924	-0.936	-0.944	[523]
-0.382	0.220	0.092	0.000	-0.066	-0.114	-0.149	
0.489	-0.501	-0.473	0.426	-0.378	-0.333	-0.295	

^a It may be noted that the coefficients of the base states are not normalized in Nilsson's paper [4].

The other entries give the composition of the wave function by listing quantities a_{IA} such that the solution of Eq. 9-158 for the actual single-particle wave function is

$$\psi_{\alpha\Omega} = \sum a_{IA} |NIA\Sigma\rangle. \quad (9-162)$$

Of course, $A + \Sigma = \Omega$. For example, the state in the top portion of Table 9-3 has wave function $|533 +\rangle$ and energy -11.400 at $\eta = 0$, the spherical shape. This is simply an $f_{7/2}$ ($m = \frac{7}{2}$) wave function. As the deformation increases, the wave function becomes more complicated, so that for $\eta = 2$ it is

$$0.094|553 +\rangle - 0.994|533 +\rangle - 0.055|554 -\rangle.$$

At this stage, the only valid quantum numbers are N and Ω . The wave functions could also be represented as a combination of states with fixed values of n_1 , n_2 , and n_3 ; instead we have used states of fixed l and A , and these states are themselves linear combinations of the (n_1, n_2, n_3) -states. As $\eta \rightarrow \infty$, the contribution of the state with $A = 4$, which is never very large, tends to zero, and we are left with the linear combination of $|553 +\rangle$ and $|533 +\rangle$ that describes the $n_3 = 0$ state. The entry [503] is therefore made for $[Nn_3A]$ in the final column of the table.

The second state in Table 9-3 is, for a spherical nucleus,

$$-0.426|553 +\rangle + 0.905|554 -\rangle.$$

The coefficients are simply specific values of Clebsch-Gordan coefficients, and this state is actually $h_{9/2}$ ($m = \frac{7}{2}$). The third state in the table is $h_{11/2}$ ($m = \frac{7}{2}$) at zero deformation. The two upper states can be seen in Fig. 9-31, and the third state in Fig. 9-29. Similar states for neutrons can be found

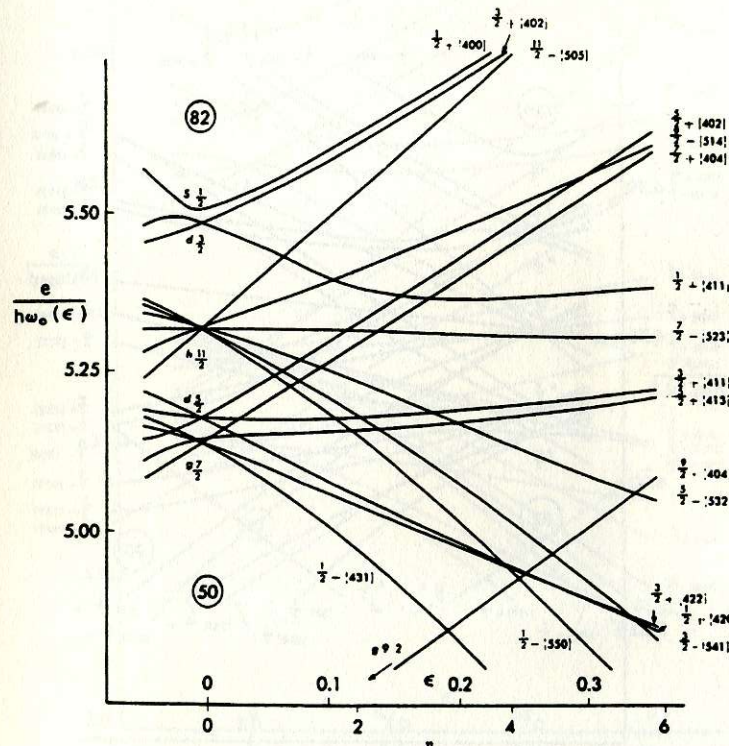


Fig. 9-29 Single-proton levels for $50 < Z < 82$. (After Mottelson and Nilsson [5].) The corresponding wave functions are given in ref. 4, Tables I and I(a).

in Fig. 9-30; the neutron states have rather different wave functions, because comparison with experiment suggests different values for the empirical constants in the theory.

The rule for determining the asymptotic quantum numbers n_3 and A is straightforward. For positive deformation, ω_3 is less than ω_1 and there-

fore, for a fixed N , the state of highest energy has the lowest value of n_3 : $n_3 = 0$. The next highest state is $n_3 = 1$, etc. In our example, the three states for $N = 5$, $\Omega = \frac{3}{2}$ are assigned successively the asymptotic numbers $n_3 = 0, 1, 2$. The oscillator motion is such that Λ is even or odd as $N - n_3$ is even or odd; this determines Λ . In our example, the highest state has $N - n_3 = 5$, and therefore $\Lambda = 3$; the next state has $n_3 = 1$ and $\Lambda = 4$; and the lowest state has again $\Lambda = 3$.

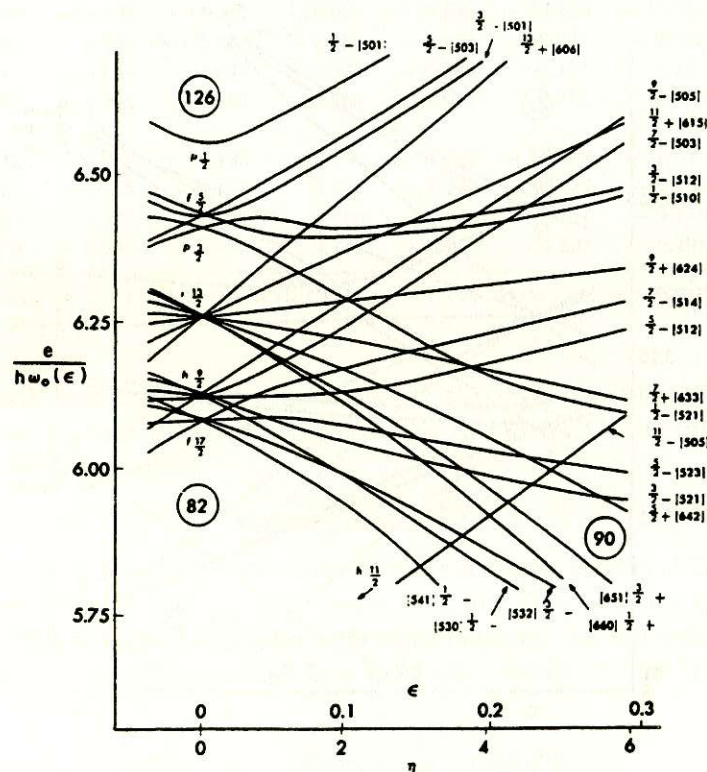


Fig. 9-30 Single-neutron levels for $82 < N < 126$. (After Mottelson and Nilsson [5].) The corresponding wave functions are given in ref. 4, Tables I and I(a).

In some processes selection rules (for β - and γ -radiation) are associated with changes in n_3 and Λ . Although these asymptotic quantum numbers are not strictly valid at the usual nuclear deformation, the rules are observed to hold. This implies that the actual wave function contains only a small

component corresponding to other than the asymptotic values of n_3 and Λ . To study this point, it is more convenient to express the wave functions as combinations of $|Nn_3\Lambda\Sigma\rangle$ than as Nilsson's base vectors $|N, l, \Lambda, \Sigma\rangle$. Such

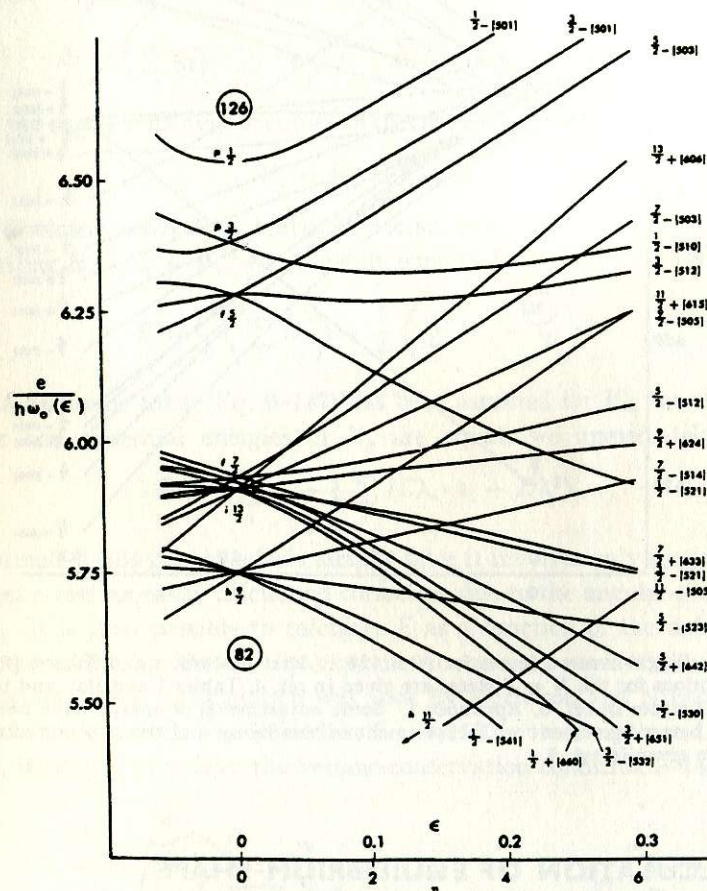


Fig. 9-31 Single-proton levels for $Z > 82$. (After Mottelson and Nilsson [5].) The wave functions of the $N = 4$ states are given in ref. 4, Tables I and I(a), and those for the $N = 5$ states in ref. 5, Appendix I.

a translation may be found in a paper by Rassey [45]. His Table II shows that the three states in our example are, respectively, 95% $|503\rangle$, 85% $|514\rangle$, and 86% $|523\rangle$ for $\eta = 4$; the corresponding figures for $\eta = 6$ are 97%, 89%, and 89%.

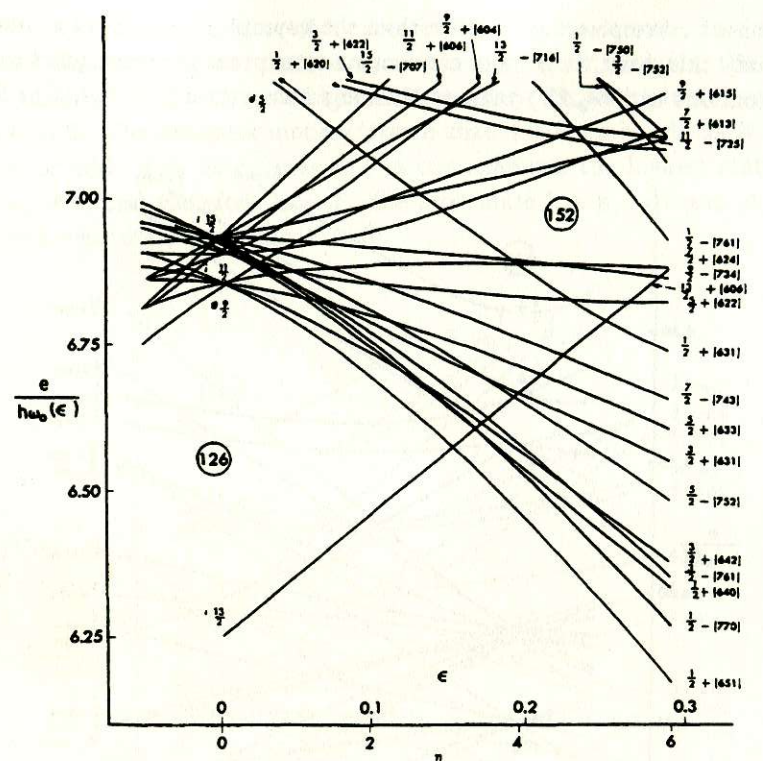


Fig. 9-32 Single-neutron levels for $N > 126$. (After Mottelson and Nilsson [5].) The wave functions for the $N = 6$ states are given in ref. 4, Tables I and I(a), and those for the $N = 7$ states in ref. 5, Appendix I. Some adjustments of energy have been made to obtain better agreement with experiment in this figure and the two preceding ones. Details are given in ref. 5.

9-9 CALCULATION OF EQUILIBRIUM SHAPE

In Section 9-6, we outlined how the nuclear potential energy $V(\beta, \gamma)$ is determined self-consistently from a phenomenological two-body Hamiltonian consisting of quadrupole-quadrupole and pairing interactions. It is possible to start with an even simpler approach and to assume that the nucleons are moving in a deformed one-body potential of the Nilsson or Newton type, with the single-particle energies e_i determined by Eq. 9-158 or a slightly generalized form to include axial asymmetry. Although it is implicitly assumed that this average potential is generated by two-body interactions, no attempt is made in this phenomenological approach to calculate it self-

consistently. All residual interactions are neglected in the simplest version, and the effect of Coulomb interaction is approximately taken into account by choosing different values of the oscillator parameter ω_0 for neutrons and protons. The total intrinsic energy of the nucleus is then

$$E = \left\langle \sum_i t_i + \sum_{i < j} V_{ij} \right\rangle = \left\langle \sum_i \frac{p_i^2}{2M} \right\rangle + \frac{1}{2} \left\langle \sum_i V_i \right\rangle,$$

where the sum i runs over occupied states only, and

$$V_i = V_h + V(\lambda, s)$$

is the distorted one-body potential of Section 9-8.

Writing $H_i = t_i + V_i$, we can easily express E as

$$E = \frac{3}{4} \left\langle \sum_i H_i \right\rangle - \frac{1}{4} \left\langle \sum_i (V_i - t_i) \right\rangle. \quad (9-163)$$

Since a harmonic form (Eq. 9-147) has been assumed for V_h , for which the kinetic and potential energies of V_h are equal, we immediately obtain

$$E = \frac{3}{2} \sum_i e_i - \frac{1}{4} \sum_i \langle C\lambda_i \cdot s_i + D\lambda^2 \rangle. \quad (9-164)$$

Formula 9-164 is particularly simple, since it involves only single-particle energies e_i and an easily calculated correction due to the angular-momentum terms. It is then possible to calculate E as a function of the deformation parameter ϵ (or, in the axially asymmetric case, ϵ_κ) and minimize it for equilibrium. Such a calculation was done by Mottelson and Nilsson [5] for the axially symmetric V_h defined in Eq. 9-159 for rare-earth and actinide nuclei, imposing, of course, the volume-conservation condition 9-148. Their

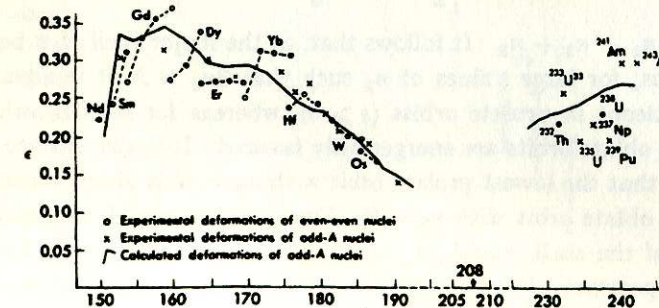


Fig. 9-33 Nuclear equilibrium deformation ϵ . The solid line is the calculated value. Circles denote experimental points for even-even nuclides; crosses, those for odd A . (After Mottelson and Nilsson [5].)

results, shown in Fig. 9-33, are in good agreement with experimentally extracted ϵ -values from $B(E2)$ -measurements. Bes and Szymanski [46] refined this method of calculation by the inclusion of two-body pairing correlations. In the presence of a pairing force, the occupation probability V_i^2 of a single-particle state i varies smoothly with energy, instead of being only 1 or 0. Thus pairing effects decrease the importance of any special ordering of single-particle levels, making the variation of E with ϵ gradual. Das Gupta and Preston [32] essentially used the same method for even-even rare-earth nuclei ^{156}Gd - ^{172}Yb , but with an anisotropic harmonic-oscillator potential with λ^2 and $\lambda \cdot s$ interactions, to demonstrate that an axially symmetric prolate shape is favored energetically in all cases. The preponderance of axially symmetric shapes over asymmetric ones is attributed by Kumar and Baranger [33] to the pairing force. Their calculations clearly show that the pairing force always energetically favors keeping the nucleus as symmetric as possible. A very strong pairing produces complete symmetry (i.e., the spherical shape), while a more reasonable weaker value yields axial symmetry. If the pairing interaction strength were reduced to half, for example, in their calculation, many nuclei (e.g., the W isotopes) would prefer an asymmetric rather than a symmetric shape.

The next question to be answered is, "Granted an axially symmetric shape, why do most nuclei prefer the prolate side ($\epsilon > 0$)?" We consider first whether the above statement is still true in an axially symmetric anisotropic harmonic-oscillator potential without any λ^2 or $\lambda \cdot s$ types of interactions. The energy of a nucleon in the quantum state (n_1, n_2, n_3) is given by

$$\begin{aligned} e_{n_1, n_2, n_3} &= (\frac{1}{2} + n_1)\hbar\omega_1 + (\frac{1}{2} + n_2)\hbar\omega_2 + (\frac{1}{2} + n_3)\hbar\omega_3 \\ &= \hbar\omega_0(\epsilon) \left[\frac{3}{2} + N + \frac{\epsilon}{3}(N - 3n_3) \right], \end{aligned} \quad (9-165)$$

with $N = n_1 + n_2 + n_3$. It follows that, as the major shell N is being filled by nucleons, for large values of n_3 such that $3n_3 > N$ it is advantageous to put nucleons in prolate orbits ($\epsilon > 0$), whereas for smaller values of n_3 ($3n_3 < N$) oblate orbits are energetically favored. It is also easy to see from Eq. 9-165 that the lowest prolate orbit with $n_3 = N$ is lower in energy than the lowest oblate orbit with $n_3 = 0$. Thus, in this model, the nuclei in the first half of the shell would be prolate and those in the latter half oblate.

In the presence of the $\lambda \cdot s$ and λ^2 potentials, however, this conclusion is no longer true. First, the $\lambda \cdot s$ force would split up a major shell into subshells. Second, it is no longer true that at the beginning of the shell the orbit on the prolate side is always the lowest. For example, in Fig. 9-31 for the

proton orbits for $Z > 82$, the $\frac{9}{2}-$ [505] level on the oblate side is lower in energy than the $\frac{1}{2}-$ [541] level on the prolate side for very small deformation. This results in a negative quadrupole moment for ^{209}Bi (Table 7-1), and a similar, more pronounced effect is found just beyond the shell closure of $Z = 50$. For larger values of ϵ , there is frequent crossing of levels between different subshells, and the λ^2 -dependent term can bring down in energy many levels with large angular-momentum components. Numerical calculations show that it is the λ^2 -dependent potential that favors the prolate shapes more than the oblate.

Until now, we have considered in this section only the Y_2^0 -type of deformation for axially symmetric well-deformed nuclei. It would be of

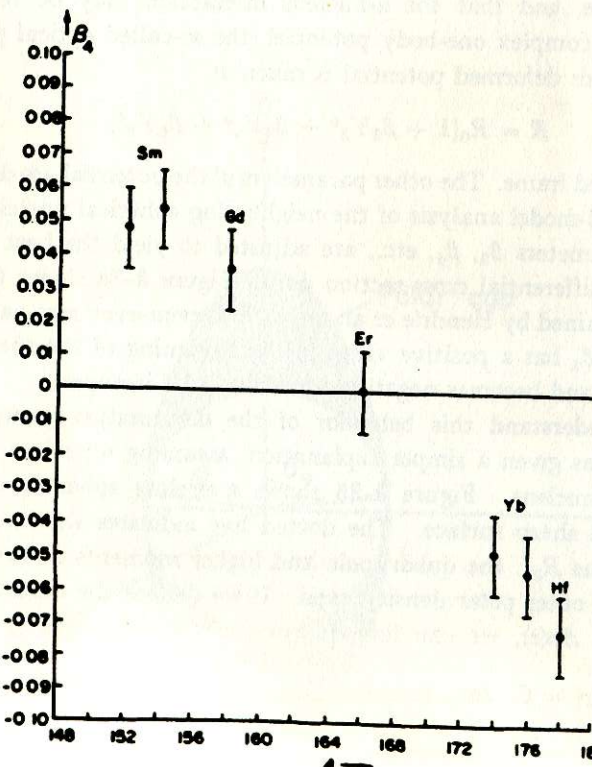


Fig. 9-34 Experimentally extracted β_4 -values of some doubly even rare-earth nuclei. (After Hendrie et al. [47].)

interest to investigate deformation modes involving higher multipoles. To find whether permanent deformations of Y_4^0 - and Y_6^0 -types are present in rare-earth nuclei, Hendrie et al. [47] have scattered α -particles off these targets, measuring the angular distribution of the scattered particles. These α -particles at an incident energy of 50 MeV carry enough angular momentum to transfer large units of angular momentum directly to members of the ground-state rotational band. The inelastically scattered α -particles interact mostly at the surface of the target nuclei because of strong absorption in the interior. For direct excitation of the target to a state J , the angular distribution of the inelastically scattered α 's is determined by the J th multipole component of the nuclear field. Hendrie et al. [47] measured the differential cross sections to the various rotational levels up to the 6^+ state, and analyses of the data yield the shape of the nuclear field up to the Y_6 -mode. In this analysis, they assume that the target nucleus is a perfect rotor at least up to the 8^+ state, and that the α -nucleus interaction may be represented by a deformed complex one-body potential (the so-called optical potential). The shape of this deformed potential is taken as

$$R = R_0(1 + \beta_2 Y_2^0 + \beta_4 Y_4^0 + \beta_6 Y_6^0) \quad (9-166)$$

in the body-fixed frame. The other parameters of the potential are determined from an optical-model analysis of the neighboring spherical nuclei. The deformation parameters β_2 , β_4 , etc., are adjusted to yield the best fit to the experimental differential cross-section data. Figure 9-34 shows the results for β_4 thus obtained by Hendrie et al. for various even-even rare-earth nuclei. We note that β_4 has a positive value in the beginning of the shell, goes to zero for ^{166}Er , and becomes negative for Yb and Hf isotopes.

Can we understand this behavior of the deformation parameter β_4 ? Bertsch [48] has given a simple explanation, assuming a prolate spheroidal shape of the nucleus. Figure 9-35 shows a prolate spheroid of uniform density with a sharp surface. The dotted line indicates the largest inside sphere of radius R_0 ; the quadrupole and higher moments of this spheroid arise from the outer polar density caps. If we denote the density of these polar caps by $\Delta\rho(\mathbf{r})$, we can introduce an azimuthal angle θ_0 such that

$$\begin{aligned} \Delta\rho(\mathbf{r}) &= C \quad \text{for } 0 < \theta < \theta_0 \quad \text{and} \quad \pi - \theta_0 < \theta < \pi, \\ &= 0 \quad \text{otherwise.} \end{aligned}$$

We can now expand $\Delta\rho(\mathbf{r})$, which is axially symmetric, in terms of $P_L(\mu)$, where $\mu = \cos\theta$. Let

$$\Delta\rho(\mathbf{r}) = \sum_L C_L P_L(\mu), \quad (9-167)$$

the coefficients C_L being directly related to the β_L 's defined in Eq. 9-166. Then

$$C_L = C \left[\int_{\mu_0}^1 P_L(\mu) d\mu + \int_{-1}^{-\mu_0} P_L(\mu) d\mu \right],$$

giving

$$\begin{aligned} C_L &= 0 && \text{for } L \text{ odd,} \\ &= 2C \int_{\mu_0}^1 P_L(\mu) d\mu && \text{for } L \text{ even.} \end{aligned} \quad (9-168)$$

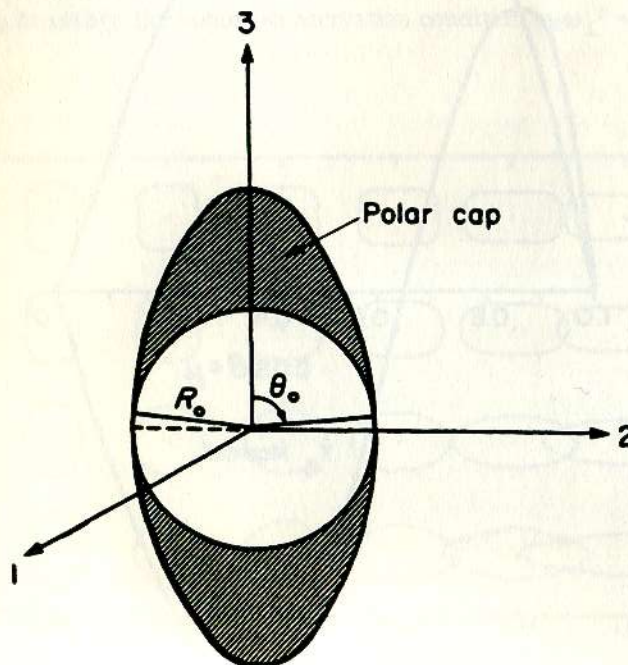


Fig. 9-35 A prolate spheroid of uniform density with a sharp surface. The dotted line shows the largest inside sphere of radius R_0 .

We can also calculate the L th moment of these caps, which is

$$\begin{aligned} Q_L &= 2\pi \sqrt{\frac{2L+1}{4\pi}} \int_{-1}^1 \Delta\rho(\mu) R_0^L P_L(\mu) R_0^2 d\mu \\ &= 2\pi \sqrt{\frac{2L+1}{4\pi}} R_0^{L+2} C_L. \end{aligned} \quad (9-169)$$

We thus see from Eqs. 9-168 and 9-169 that both C_L (i.e., β_L) and Q_L are

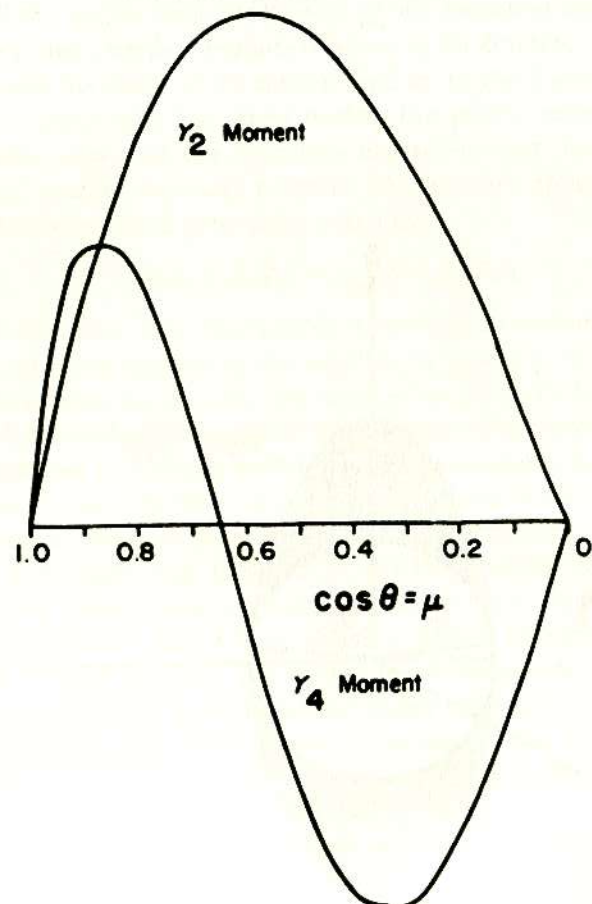


Fig. 9-36 Plots of $\int_{\mu_0}^1 P_L(\mu) d\mu$ as a function of μ_0 for $L = 2$ and $L = 4$. (After Bertsch [48].)

proportional to the integral $\int_{\mu_0}^1 P_L(\mu) d\mu$. At the beginning of the shell, added nucleons are placed in orbits as close to the 3-axis as possible for prolate orbitals. Eventually, the equatorial orbitals are filled to make a spherically symmetric distribution again with shell closure. The quantity μ_0 thus varies from 1 to 0 as more and more nucleons are added. In Fig. 9-36, the quantities $\int_{\mu_0}^1 P_L(\mu) d\mu$ are plotted as functions of μ_0 for $L = 2$ and 4. We see from this plot that, whereas β_2 and Q_2 are of the same sign and have a maximum in the middle of the shell, β_4 and Q_4 undergo a change in sign as shown, in agreement with the experimental findings of Hendrie et al. [47].

In a microscopic calculation, to obtain a hexadecapole (P_4) moment in the density distribution of a nucleus, we must generalize the form V_h of the deformed one-body potential, given by Eq. 9-159. Nilsson et al. [49] have used the form

$$V_h = \frac{1}{2}\hbar\omega_0(\epsilon, \epsilon_4)\rho^2[1 - \frac{2}{3}\epsilon P_2(\cos\theta_i) + 2\epsilon_4 P_4(\cos\theta_i)] \quad (9-170)$$

in the stretched coordinates. The oscillator constant ω_0 is now a function of ϵ and ϵ_4 to satisfy the volume-conservation condition $\omega_3\omega_1^{-2} = \omega_0^3$. Note

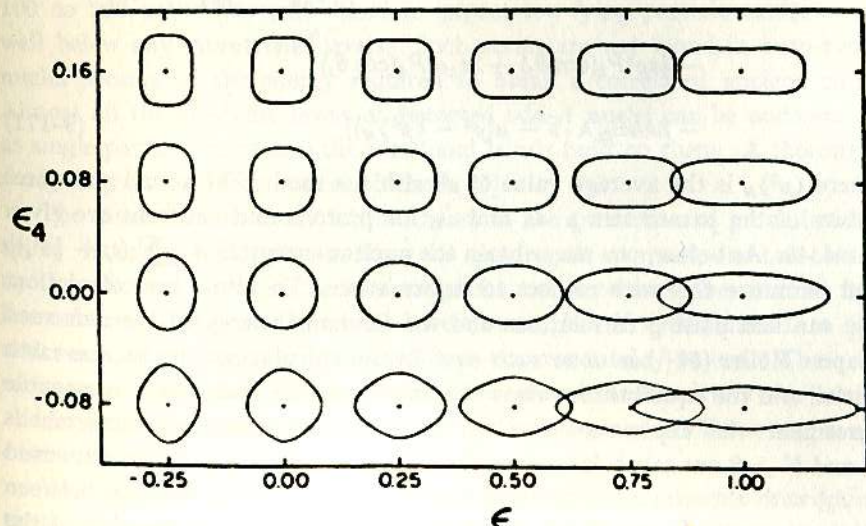


Fig. 9-37 The nuclear equipotential shapes for V_h given by Eq. 9-170 as a function of ϵ and ϵ_4 . (After Nilsson et al. [49].)

that in Eq. 9-170 we have only P_2 and P_4 degrees of freedom, but the potential could easily be generalized to include the mass asymmetry parameter P_3 and higher multipoles like P_6 . These additional modes of distortion are of importance in the calculation of fission barriers. With only the P_2 -type of deformation, we found in Section 9-8 that no major-shell mixing took place in stretched coordinates; this is no longer true for a potential of the form 9-170. Figure 9-37 shows the nuclear equipotential shapes as functions of ϵ and ϵ_4 . For the special case of $\epsilon = \epsilon_4 = 0$, the shape reduces to a sphere; for spheroids, $\epsilon_4 = 0$. We see that, even for large positive values of ϵ and ϵ_4 , the shape does not develop a prefission neck but instead remains cylinder-like. This parametrization of the shape is therefore not very suitable for calculation of fission barriers, as it is unable to describe the later stages of fission. For calculation of fission barriers, other parametrizations of the nuclear shape are also made [50].

In Section 9-8 we introduced a term proportional to λ^2 to correct the oscillator shape. Nilsson et al. [49] choose to use instead a term ρ^4 , whose matrix elements within one oscillator shell are the same as those of $-\frac{1}{2}\lambda^2$, apart from additive constants. Thus the generalized single-particle Hamiltonian of Nilsson in stretched coordinates is

$$H_{SP} = \frac{1}{2}\hbar\omega_0(\epsilon, \epsilon_4) \left[(-V_i^2 + \rho^2) + \frac{1}{2}\epsilon \left(2\frac{\partial^2}{\partial\xi_3^2} - \frac{\partial^2}{\partial\xi_2^2} - \frac{\partial^2}{\partial\xi_1^2} \right) \right. \\ \left. - \frac{3}{2}\epsilon\rho^2 P_2(\cos\theta_i) + 2\epsilon_4\rho^2 P_4(\cos\theta_i) \right] \\ - 2\kappa\hbar\dot{\omega}_0[\lambda \cdot s - \mu(\rho^4 - \langle\rho^4\rangle_N)], \quad (9-171)$$

where $\langle\rho^4\rangle_N$ is the average value of ρ^4 within a shell. The actual numerical values of the parameters μ , κ , and $\dot{\omega}_0$ for protons and neutrons are given in ref. 49. As before, one may obtain the nuclear energy $E = \langle \sum_i(t_i + \frac{1}{2}V_i) \rangle$ and minimize this with respect to deformation. To refine the calculation, one can add pairing correlations and the Coulomb energy of the deformed shape. Möller [51] has done such equilibrium calculations in the rare-earth nuclei, and the equilibrium values of ϵ and ϵ_4 that he finds are in reasonable agreement with experimental values if only couplings between major shells N and $N \pm 2$ are taken into account. The agreement for ϵ_4 (when converted to β_4) with experiment is partially destroyed, however, if coupling between all major shells is considered. This may be due to the inadequacy of the volume-conservation condition, which is not applied to the angular-momentum-dependent part of the one-body potential.

Finally, we mention that by calculating E in this one-body model as a function of deformation, although we obtain reasonable values of the equilibrium ground-state deformation, the value of E itself is found to be very unrealistic. Furthermore, this method of finding the deformation dependence of E is not accurate for large deformations and hence is not useful for the calculation of fission barriers, which involve delicate cancellation of the surface and Coulomb energies. The fission barriers of nuclei can be found accurately if the one-body Hamiltonian H_{SP} of Eq. 9-171 (or a more general form) is used only to calculate the shell correction in the total nuclear energy, which fluctuates with mass number and deformation, while the smooth part is taken directly from the semiempirical mass formula discussed in Chapter 6. This method is also capable of reproducing the equilibrium (ϵ, ϵ_4) values and the binding energy of the ground state accurately, and has been used by Möller [51] with the H_{SP} of Eq. 9-171 and by Götz et al. [34] with a one-body Woods-Saxon potential. We shall describe this method in some detail in Section 12-4.

9-10 LEVELS OF DISTORTED ODD- A NUCLEI

Examination of the levels in Figs. 9-28 through 9-32 shows that at reasonable distortions there is a fairly uniform level distribution with spacing from 100 to 200 keV. We can therefore expect low-lying particle excitations, well below any vibrational levels. Such states are not found in even-even nuclei because of the energy required to break a correlated nucleon pair. Almost all the low-lying levels of distorted odd- A nuclei can be understood as single-particle states and the rotational bands built on them. A thorough study is given by Mottelson and Nilsson [5].

The most obvious check of the theory is the prediction of ground-state spins. Knowing the distortion from the quadrupole moment, one can count up the occupied levels in the level diagrams and determine the orbit of the last nucleon. This gives Ω ; for the lowest state, $J = K = \Omega$ (unless $\Omega = \frac{1}{2}$), and one can compare the predicted and experimental J -values. There is often some doubt as to the predicted J because of the density of the levels and inversions of order which occur for small changes of ϵ . However, in all cases, the experimental value is one of those predicted.

We shall consider in detail three examples in different parts of the periodic table, rather than attempt to summarize all the data. The nuclides ^{25}Al and ^{25}Mg have been carefully studied by Litherland et al. [52]. Quadrupole moments in this region suggest $\epsilon \approx 0.3$. For this distortion, the $\frac{5}{2}^+$ [202]

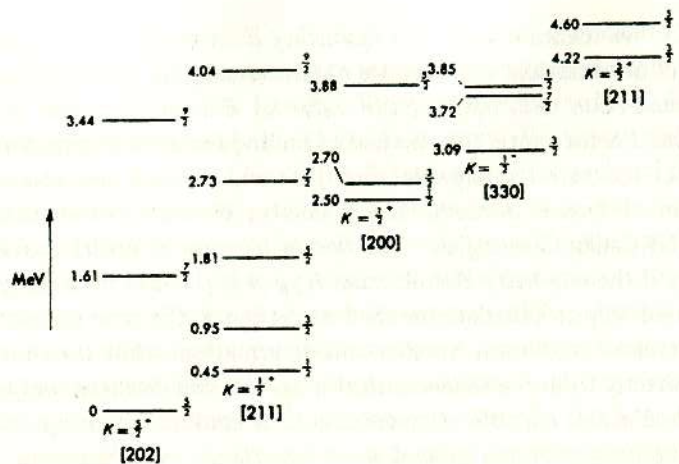


Fig. 9-38 The levels of ^{25}Al , displayed to show the various rotational bands.

level and the $\frac{1}{2}^+$ [211] level are very close (Fig. 9-28). Experimentally the ground state is $\frac{1}{2}^+$, and there is an excited state of $\frac{1}{2}^+$ at 450 keV. The other states are shown in Fig. 9-38; it is seen that they can be assigned to different states of the last particle, together with rotations of the intrinsic structure. The highest band shown corresponds to a hole in the $\frac{5}{2}^+$ [211] level and a pair in, presumably, the next state, $\frac{5}{2}^+$ [202]. We should not be content that these levels are correctly interpreted until the various consequences of the theory for electromagnetic properties, β -decay, and so forth, are examined.

One simple necessary condition is the level spacing in the various alleged rotational bands. The levels of the ground-state band satisfy quite well the $E \propto J(J + 1)$ rule, particularly if the small rotation-vibration correction is included. The $K = \frac{1}{2}$ bands, however, require more careful study, because of the Coriolis term. Equation 9-142 gives the relative energies in a given band as

$$E_J = \left(\frac{\hbar^2}{2J} \right) [J(J + 1) + \delta_{K,(1/2)} a (-)^{J+(1/2)} (J + \frac{1}{2})]. \quad (9-172)$$

In the special case of the single-particle χ 's calculated by Nilsson,

$$\chi_\alpha = \psi_{\Omega\alpha} = \sum_I a_{I\alpha} |NI\Lambda\Sigma\rangle, \quad (9-162)$$

equations 9-141 and 9-138 give for the decoupling parameter

$$a = (-)^l \sum_I [a_{I0}^2 + 2(l(l + 1))^{1/2} a_{I0} a_{I1}]. \quad (9-173)$$

The values of a depend on the distortion. To obtain exact fit for the levels of ^{25}Al , slightly different values of ϵ have to be used for the three $K = \frac{1}{2}$ bands, but this is neither unexpected nor physically unreasonable. Indeed, different equilibrium distortions arise from different configurations.

Further detailed consideration of other properties shows that the $A = 25$ nuclei are very well described by the rotations of intrinsic *distorted shell-model* states. There are indications that other nuclides from $A = 19$ -31 also display collective properties, although there are nuclides in this region to which the collective model does not seem to apply [45]. In addition to ^{25}Mg and ^{25}Al , the model is apparently successful in ^{19}F [53], ^{24}Mg [54], ^{28}Al [55], ^{29}Si [56], and ^{31}P [57].

In the rare-earth region, which includes A from about 150 to 190, we shall study the $A = 183$ isobars as typical examples. The level schemes of $^{183}_{74}\text{W}$ and $^{183}_{75}\text{Re}$ are shown in Fig. 9-39. The spins and parities of the low-lying levels of these two nuclides are well established; our simplified figure does not show all known states. If we count up from 90 neutrons in Fig. 9-30, we find that the 109th neutron is expected to be in the $\frac{1}{2}^-$ [510] state for $\epsilon \gtrsim 0.2$. This result is consistent with the ground-state assignments, and the levels labeled α can be considered to constitute a rotational band. Referring again to Fig. 9-30, we may expect a state caused by excitation to the $\frac{3}{2}^-$ [512] level at about 200 keV ($\hbar\omega_0 \approx 7$ MeV). It is natural, therefore, to associate the 209-keV level with this state. Two other states of its band appear; their energies above 209 keV are in the ratio 2.44, compared with the value 2.40 predicted by the $J(J + 1)$ law. Finally, it is reasonable to assign the 453-keV level to the $\frac{7}{2}^-$ [503] band. While we are still examining the odd-neutron diagram, let us consider ^{183}Os . We expect its ground state to be $\frac{9}{2}^+$ [624], and this appears to be confirmed. The $\frac{1}{2}^-$ level at 171 keV must then be the $\frac{1}{2}^-$ [510] state; the fact that it is only 171 keV above the ground state may suggest that ^{183}Os is less distorted than ^{183}W , with $\epsilon \sim 0.15$.

The theoretical expectations for the odd-proton nuclides Ta and Re are found from Fig. 9-29. Counting up from the 50-shell, we find that for $\epsilon \sim 0.3$ the 73rd proton would be either $\frac{9}{2}^-$ [514] or $\frac{5}{2}^+$ [402]. However, the ground states of all the Ta isotopes are $\frac{7}{2}^+$, as are those of the $_{71}\text{Lu}$ isotopes. It would appear that we have here an example of extra pairing energy in the state $\frac{9}{2}^-$ ($l = 5$), compared with the state $\frac{7}{2}^+$ [404] ($l = 4$). If $\epsilon \sim 0.3$, the two levels are very close, and the three protons 71-73 are presumably in the configuration $(\frac{7}{2}^+) (\frac{9}{2}^-)^2$. We would then expect the first particle excitation in Ta

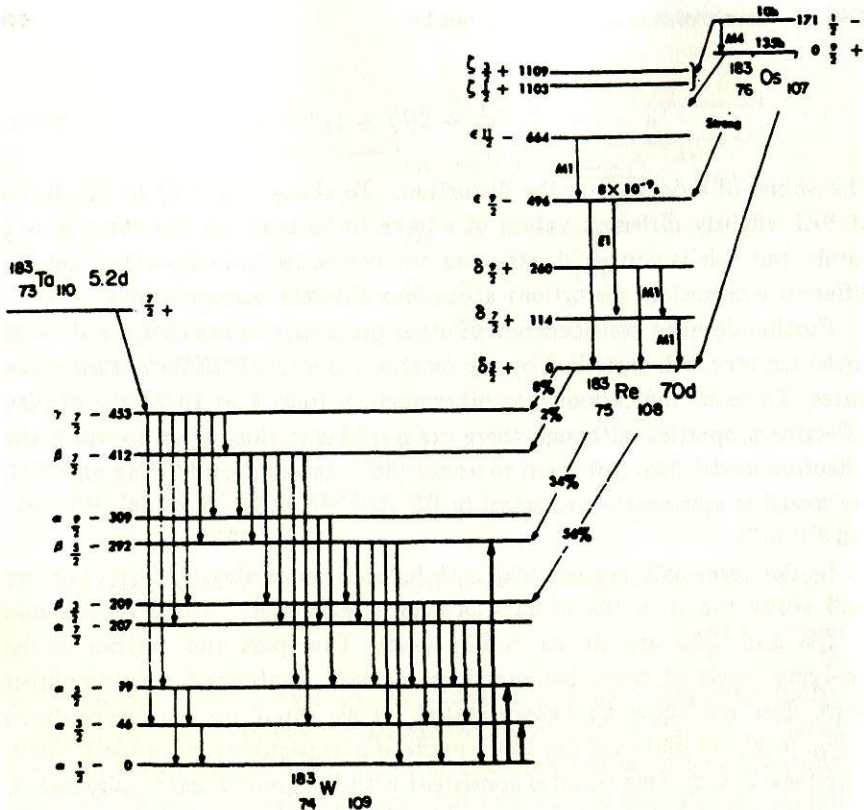


Fig. 9-39 The levels of the $A = 183$ nuclides (energies in keV). The Greek letters identify different rotational bands.

to be $(\frac{7}{2}^+)^2(\frac{9}{2}^-)$, with the configuration $(\frac{5}{2}^+ [402])(\frac{9}{2}^-)^2$ slightly higher. These expectations are borne out in ^{181}Ta . Also in ^{181}Ta , there is a $\frac{1}{2}^+$ state at 612 keV; this is presumably due to a hole in the $\frac{5}{2}^+ [411]$ state, so that the last five protons are $(\frac{1}{2}^+)(\frac{7}{2}^+)^2(\frac{9}{2}^-)^2$. Turning to ^{75}Re and consistently assuming high pairing energy for the $\frac{9}{2}^-$ state, we expect the last five protons to be $(\frac{3}{2}^+)^2(\frac{5}{2}^+)(\frac{9}{2}^-)^2$. The ground states of the Re isotopes are indeed $\frac{5}{2}^+$. In ^{183}Re we find also the expected particle excitations $(\frac{7}{2}^+)^2(\frac{5}{2}^+)^2(\frac{9}{2}^-)$ and $(\frac{1}{2}^+ [411])(\frac{7}{2}^+)^2(\frac{5}{2}^+)^2(\frac{9}{2}^-)^2$. Presumably there should be a $\frac{7}{2}^+ [404]$ excitation; if there is, it is not clear why it has not been observed in the Os decay. In Fig. 9-39, the level-spacing ratio $[E(\frac{9}{2}^-) - E(\frac{5}{2}^+)]/[E(\frac{7}{2}^-) - E(\frac{5}{2}^+)]$ in the band labeled δ is 2.28, compared with the theoretical value $\frac{16}{7} = 2.29$. We may also remark that the moments of inertia of excited bands differ from the value in the ground-state band.

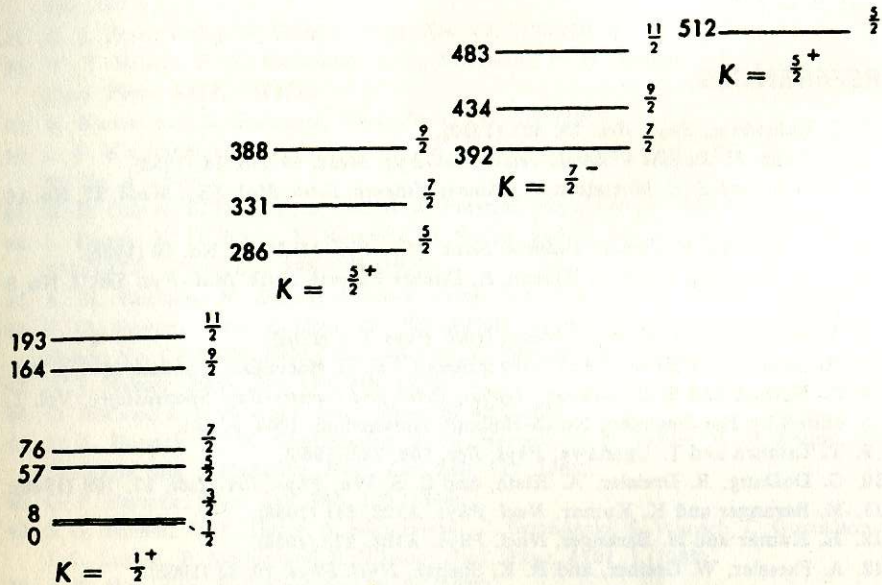


Fig. 9-40 The energy levels of ^{239}Pu , displayed to show the rotational bands (energies in keV).

The elements with $A > 224$ have rotational spectra. Figure 9-40 shows the levels of ^{239}Pu . It is left to the reader to make the detailed comparison with the level sequences deduced from Fig. 9-32. We mention only that the decoupling parameter $a = -0.58$ is consistent with the ground-state assignment $\frac{1}{2}^+ [631]$ and that reasonable assignments for the 286-, 392-, and 512-keV levels are $\frac{5}{2}^+ [622]$, $\frac{7}{2}^- [743]$, and $\frac{5}{2}^+ [633]$, respectively. The moments of inertia are, of course, greater than in the rare-earth region, with correspondingly smaller level spacing.

A noteworthy feature of the heavy-element region is the appearance of a "magic" number at 152 neutrons. Such a number cannot arise for spherical nuclei, but we see that at distortions $0.2 < \epsilon < 0.3$ there is a marked gap in the level spacing in Fig. 9-32. The $N = 152$ nuclides may then be magic, although they will not have the specially simple properties due to the spherical nuclei of the other magic nuclides. Experimental evidence for this energy gap is supplied by the unusually great α -decay energies of the $N = 154$ nuclides and the apparent instability against fission of the nuclides above

the energy gap. A gap of about 300 keV is indicated between $N = 151$ and $N = 153$.

REFERENCES

1. J. Rainwater, *Phys. Rev.* **79**, 432 (1950).
2. A. Bohr, *K. Danske Vidensk. Selsk. Mat.-Fys. Medd.* **26**, No. 14 (1952).
3. A. Bohr and B. R. Mottelson, *K. Danske Vidensk. Selsk. Mat.-Fys. Medd.* **27**, No. 16 (1953).
4. S. G. Nilsson, *K. Danske Vidensk. Selsk. Mat.-Fys. Medd.* **29**, No. 16 (1955).
5. B. R. Mottelson and S. G. Nilsson, *K. Danske Vidensk. Selsk. Mat.-Fys. Skr.* **1**, No. 8 (1959).
6. J. de Boer and J. Eichler, *Advan. Nucl. Phys.* **1**, 1 (1968).
7. Rayleigh, Third Baron, *The Theory of Sound*, Vol. II, Macmillan, London, 1877, p. 364.
8. O. Nathan and S. G. Nilsson, *Alpha-, Beta- and Gamma-Ray Spectroscopy*, Vol. I, edited by Kai Siegbahn, North-Holland, Amsterdam, 1965, p. 601.
9. T. Tamura and T. Ugadawa, *Phys. Rev.* **150**, 783 (1966).
10. G. DoDang, R. Dreizler, A. Klein, and C. S. Wu, *Phys. Rev. Lett.* **17**, 709 (1966).
11. M. Baranger and K. Kumar, *Nucl. Phys.* **A122**, 241 (1968).
12. K. Kumar and M. Baranger, *Nucl. Phys.* **A122**, 273 (1968).
13. A. Faessler, W. Greiner, and R. K. Sheline, *Nucl. Phys.* **70**, 33 (1965).
14. S. Das Gupta and A. B. Volkov, *Phys. Rev.* **C6**, 1893 (1972).
15. F. M. Bernthal, J. O. Rasmussen, and J. M. Hollander, *Phys. Rev.* **C3**, 1294 (1971).
16. A. Johnson, H. Ryde, and S. A. Hjorth, *Nucl. Phys.* **A179**, 753 (1972).
17. A. S. Davydov and G. F. Filippov, *Nucl. Phys.* **8**, 257 (1958).
18. A. S. Davydov and V. S. Rostovsky, *Nucl. Phys.* **12**, 58 (1959).
19. A. S. Davydov and A. A. Chaban, *Nucl. Phys.* **20**, 499 (1960).
20. M. A. J. Mariscotti, Gertrude Scharff-Goldhaber, and Brian Buck, *Phys. Rev.* **178**, 1864 (1969).
21. B. R. Mottelson and J. G. Valatin, *Phys. Rev. Lett.* **5**, 511 (1960).
22. B. R. Mottelson, *Cours de l'Ecole d'Eté de Physique Théorique des Houches*, 1958, Dunod, Paris, 1959; R. M. Rockmore, *Phys. Rev.* **116**, 469 (1959); G. E. Brown, *Unified Theory of Nuclear Models and Forces*, North-Holland, Amsterdam, 1967, p. 72.
23. C. K. Ross, private communication.
24. A. B. Volkov, *Phys. Lett.* **35B**, 299 (1971).
25. T. K. Das, R. M. Dreizler, and A. Klein, *Phys. Lett.* **34B**, 235 (1971).
26. See, for example, J. D. Immele and G. L. Struble, *Nucl. Phys.* **A187**, 459 (1972).
27. P. H. Stelson and L. Grodzins, *Nucl. Data* **A1**, 21 (1965).
28. M. A. Preston and D. Kiang, *Can. J. Phys.* **41**, 742 (1963).
29. E. R. Marshalek, *Phys. Rev.* **139B**, 770 (1965).
30. A. K. Kerman, *Ann. Phys.* **12**, 300 (1961).
31. B. L. Birbrair, L. K. Peker, and L. A. Sliv, *JETP* **9**, 566 (1959).
32. S. Das Gupta and M. A. Preston, *Nucl. Phys.* **49**, 401 (1963).
33. K. Kumar and M. Baranger, *Nucl. Phys.* **A110**, 529 (1968).
34. U. Götz, H. C. Pauli, K. Alder, and K. Junker, *Nucl. Phys.* **A192**, 1 (1972).
35. M. Sakai, *Nucl. Data* **A8**, 323 (1970).
36. H. S. Gertzman, D. Cline, H. E. Gove, and P. M. S. Lesser, *Nucl. Phys.* **A151**, 282 (1971).
37. R. J. Pryor and J. X. Saladin, *Phys. Rev.* **C1**, 1573 (1970).
38. W. T. Milner, F. K. McGowan, R. L. Robinson, P. H. Stelson, and R. O. Sayer, *Nucl. Phys.* **A177**, 1 (1971).
39. K. Kumar and M. Baranger, *Nucl. Phys.* **A92**, 608 (1967).
40. L. S. Kisslinger and R. A. Sorensen, *K. Danske Vidensk. Selsk. Mat.-Fys. Medd.* **32**, No. 9 (1960).
41. M. R. Gunye, S. Das Gupta, and M. A. Preston, *Phys. Lett.* **13**, 246 (1964).
42. L. Funke, K. H. Kaun, P. Kemnitz, H. Sodan, and G. Winter, *Nucl. Phys.* **A190**, 576 (1972); *Phys. Lett.* **39B**, 179 (1972).
43. A. K. Kerman, *K. Danske Vidensk. Selsk. Mat.-Fys. Medd.* **30**, No. 15 (1956).
44. T. D. Newton, *Can. J. Phys.* **38**, 700 (1960); *Atomic Energy of Canada Limited Report No. CRT-886*, 1960. See also *Can. J. Phys.* **37**, 944 (1959).
45. A. J. Rassey, *Phys. Rev.* **109**, 949 (1958).
46. D. Bes and Z. Szymanski, *Nucl. Phys.* **28**, 42 (1961).
47. D. L. Hendrie, N. K. Glendenning, B. G. Harvey, O. N. Jarvis, H. H. Duhm, J. Saudinos, and J. Mahoney, *Phys. Lett.* **26B**, 127 (1968).
48. G. F. Bertsch, *Phys. Lett.* **26B**, 130 (1968).
49. S. G. Nilsson, C. F. Tsang, A. Sobczewski, Z. Szymanski, S. Wycech, C. Gustafson, I.-L. Lamm, P. Möller, and B. Nilsson, *Nucl. Phys.* **A181**, 1 (1969).
50. J. R. Nix, *Ann. Rev. Nucl. Sci.* **22**, 65 (1972).
51. P. Möller, *Nucl. Phys.* **A142**, 1 (1970).
52. A. E. Litherland, H. McManus, E. B. Paul, D. A. Bromley, and H. E. Gove, *Can. J. Phys.* **36**, 378 (1958).
53. E. B. Paul, *Phil. Mag.* **2**, 311 (1957).
54. R. Batchelor, A. J. Ferguson, H. E. Gove, and A. E. Litherland, *Nucl. Phys.* **16**, 38 (1960).
55. R. K. Sheline, *Nucl. Phys.* **2**, 382 (1956).
56. D. A. Bromley, H. E. Gove, and A. E. Litherland, *Can. J. Phys.* **35**, 1057 (1957).
57. A. E. Litherland, E. B. Paul, G. A. Bartholomew, and H. E. Gove, *Can. J. Phys.* **37**, 53 (1959).

PROBLEMS

9-1. Prove Eq. 9-26.

9-2. The electric multipole operator has been defined as

$$Q_{\lambda\mu} = e \sum_{k=1}^Z r_k^\lambda Y_{\lambda\mu}(\theta_k, \phi_k) \equiv \sum_{k=1}^Z Q_{\lambda\mu}(r_k), \quad (1)$$

where (r_k, θ_k, ϕ_k) are the spherical polar coordinates of the k th proton, the sum in Eq. 1 extending over all the Z protons in the nucleus.

(a) Consider an even-even nucleus with ground-state angular momentum zero. Show, using Eq. 9-22, that

$$B(E\lambda, 0 \rightarrow f) = (2\lambda + 1)|\langle \lambda 0 | Q_{\lambda 0} | 0 \rangle|^2, \quad (2)$$

where $|0\rangle$ is the ground state and $|f\rangle$ the final state with angular momentum λ .

(b) Define the energy-weighted sum

$$S_\lambda = \sum_f (E_f - E_0) B(E\lambda, 0 \rightarrow f), \quad (3)$$

the sum going over all final states $|f\rangle$ with angular momentum λ , and E_f and E_0 being the energies of $|f\rangle$ and $|0\rangle$. Show that

$$S_\lambda = \frac{1}{2}(2\lambda + 1)\langle 0 | [Q_{\lambda 0}, [H, Q_{\lambda 0}]] | 0 \rangle, \quad (4)$$

where H is the Hamiltonian of the nucleus and a bracket denotes a commutator.

(c) Let

$$H = -\frac{\hbar^2}{2M} \sum_{i=1}^A \nabla_i^2 + V,$$

where V is assumed to contain no velocity-dependent or exchange interactions. It then follows that

$$[H, Q_{\lambda 0}] = -\frac{\hbar^2}{2M} \sum_{k=1}^Z [\nabla_k^2, Q_{\lambda 0}(\mathbf{r}_k)].$$

Prove that

$$S_\lambda = \frac{\hbar^2}{2M} (2\lambda + 1) \langle 0 | \sum_{k=1}^Z [\nabla_k Q_{\lambda 0}(\mathbf{r}_k)]^2 | 0 \rangle. \quad (5)$$

(d) Consider the particular case of $\lambda = 2$. Note, from Eq. 3-8, that

$$Q_{20}(\mathbf{r}_k) = \sqrt{\frac{5}{16\pi}} e(3z_k^2 - r_k^2),$$

and show that

$$[\nabla_k Q_{20}(\mathbf{r}_k)]^2 = 4r_k^2 + 12r_k^2 \cos^2 \theta.$$

Hence prove, assuming a spherically symmetric charge distribution $\rho(r_k)$, that

$$S_2 = \frac{Ze^2\hbar^2}{2M} \frac{25}{2\pi} \langle r^2 \rangle, \quad (6)$$

where

$$\langle r^2 \rangle = \frac{1}{Z} \int \rho(r_k) r_k^2 4\pi r_k^2 dr_k.$$

For the more general λ -pole transition, Eq. 5 may be evaluated to give

$$S_\lambda = \frac{Ze^2\hbar^2}{2M} \frac{\lambda(2\lambda + 1)^2}{4\pi} \langle r^{2\lambda-2} \rangle, \quad (7)$$

which is an energy-weighted sum rule and includes both the $T = 0$ and $T = 1$ contributions. For further discussion of Eq. 7 relating to relevant experimental data, see ref. 8, p. 641.

9-3. Show that the vanishing of the products of inertia of a nucleus with isodensity surfaces

$$R = R_0(1 + \sum a_{2\mu} Y_{2\mu})$$

implies that

$$a_{22} = a_{2,-2} \quad \text{and} \quad a_{21} = a_{2,-1} = 0.$$

9-4. In the simple vibrational model of a spherical nucleus, simplify Eq. 9-24 to show that the reduced $E2$ -transition probability from the ground state to the first excited 2^+ state is given by

$$B(E2, 0^+ \rightarrow 2^+) = \frac{45\hbar^2 e^2 r_0^4}{32\pi^2} \frac{Z^2 A^{4/3}}{E_2 B_2}, \quad (1)$$

where E_2 is the excitation energy of the first excited state, $R_0 = r_0 A^{1/3}$, and B_2 is the quadrupole inertial parameter.

Next, for the rotational model, use Eqs. 9-95 and 9-38 to show that the expression for the same quantity is given by

$$B(E2, 0^+ \rightarrow 2^+) = \frac{9\hbar^2 e^2 r_0^4}{16\pi^2} \frac{Z^2 A^{4/3}}{E_2 B_2}. \quad (2)$$

In both models we see that the inertial parameter B_2 is proportional to $[B(E2) \cdot E_2]^{-1}$.

Finally, for the ground-state band of a rotational nucleus, use Eqs. 9-38, 9-72, 9-73, 9-91, and 9-94 to show that

$$B(E2, J \rightarrow J-2) = \frac{3}{32\pi^2} \frac{\hbar^2 e^2 r_0^4 (4J-2)}{B_2(E_J - E_{J-2})} Z^2 A^{4/3} (J200|J-20)^2. \quad (3)$$

The $B(E2, J \rightarrow J-2)$ -value across the ground-state rotational band has been recently measured for ^{158}Er in the range $J = 2$ to $J = 16$ by Ward et al. [*Phys. Rev. Lett.* 30, 493 (1973)]. We list their data in the following table:

Transition	$E_J - E_{J-2}$, keV	$B(E2)$, $e^2 b^2$
$2 \rightarrow 0$	192.7	0.55 ± 0.03
$4 \rightarrow 2$	335.7	0.87 ± 0.04
$6 \rightarrow 4$	443.8	1.14 ± 0.19
$8 \rightarrow 6$	523.8	1.08 ± 0.34
$10 \rightarrow 8$	578.9	1.12 ± 0.50
$12 \rightarrow 10$	608.1	$\gtrsim 0.90$
$14 \rightarrow 12$	510.0	0.77 ± 0.18
$16 \rightarrow 14$	473.2	1.35 ± 0.48

Assuming the validity of Eq. 3 above, calculate the inertial parameter B_2 for each of these transitions and comment on the peculiarity of its behavior.

Comment also on the assumptions that have gone into the derivation of Eq. 3. In your opinion, should this equation be applied in analyzing the experimental data given for ^{158}Er ?

9-5. Prove Eq. 9-140, given

$$(JMK|J_{\pm}|JMK \pm 1) = \sqrt{(J \mp K)(J \pm K + 1)},$$

$$(j\Omega|j_{\mp}|j\Omega \pm 1) = \sqrt{(j \mp \Omega)(j \pm \Omega + 1)}.$$

The difference in sign in these two relations arises because J_{\pm} refer to the components of \mathbf{J} , the total angular momentum, along moving axes, whereas j is defined as an angular momentum in the moving coordinate system.

9-6. The levels of ^{25}Mg and ^{25}Al have been carefully studied by Litherland et al. [Can. J. Phys. 36, 378 (1958)]. Tables 9-4 and 9-5 list the rotational

TABLE 9-4

$K = \frac{5}{2}; \pi = +$			$K = \frac{1}{2}; \pi = +$		
J	E_{Mg} , MeV	E_{Al} , MeV	J	E_{Mg}	E_{Al}
$\frac{5}{2}$	0	0	$\frac{1}{2}$	0.58	0.45
$\frac{7}{2}$	1.61	1.61	$\frac{3}{2}$	0.98	0.95
$\frac{9}{2}$	3.44		$\frac{5}{2}$	1.96	1.81
			$\frac{7}{2}$	2.74	2.73

TABLE 9-5

$K = \frac{1}{2}; \pi = +$			$K = \frac{1}{2}; \pi = -$		
J	E_{Mg} , MeV	E_{Al} , MeV	J	E_{Mg}	E_{Al}
$\frac{1}{2}$	2.56	2.50	$\frac{3}{2}$	3.40	3.09
$\frac{3}{2}$	2.80	2.70	$\frac{5}{2}$	3.97	3.72
$\frac{5}{2}$	3.90	3.88	$\frac{7}{2}$	4.26	3.85

bands, each built on a different Nilsson orbit, that have been identified. The orbits for the ground state of each band are the ones that Nilsson labels 5, 9, 11, 14, respectively. With the notation

$$\chi_{\Omega} = \sum_l (A_{l+}|N, l, \Omega - \frac{1}{2}, +\frac{1}{2}\rangle + A_{l-}|N, l, \Omega + \frac{1}{2}, -\frac{1}{2}\rangle),$$

the wave functions for various distortions η are as follows:

Orbit 5: $N = 2, \Omega = \frac{5}{2}, A_{2+} = 1$ for all η ;

Orbit 9: $N = 2, \Omega = \frac{1}{2}$:

η	2	4	6
A_{2+}	1.000	1.00	1.000
A_{0+}	-15.696	15.901	6.635
A_{2-}	11.489	-25.472	-16.609

Orbit 11: $N = 2, \Omega = \frac{1}{2}$:

η	2	4	6
A_{2+}	1.000	1.000	1.000
A_{0+}	-0.717	-1.143	-1.287
A_{2-}	-1.066	-0.675	-0.454

Orbit 14: $N = 3, \Omega = \frac{1}{2}$:

η	2	4	6
A_{3+}	1.000	1.000	1.000
A_{1+}	0.359	0.637	0.809
A_{3-}	0.777	0.632	0.500
A_{1-}	0.164	0.198	0.183

Also listed is orbit 7: $N = 2, \Omega = \frac{3}{2}, \eta = 2, A_{2+} = 1.000, A_{2-} = 0.351$.

(a) The four given bands all fit the formula

$$E = A[J(J+1) + a(-)^{J+1/2}(J + \frac{1}{2})] \\ + B[J(J+1) + a(-)^{J+1/2}(J + \frac{1}{2})]^2,$$

where the respective bands have

A	272 keV	176 keV	160 keV	117 keV
$a = 0$		-0.03	-0.58	-3.16
$B = -1.69$		-0.70	-0.55	-0.21

Explain this formula and calculate the effective moments of inertia.

(b) (i) Find the coefficients $c_{\Omega\eta}$ necessary to express orbit 9 (for $\eta = 4$) in the form $\chi_{\Omega} = \sum_{\eta} c_{\Omega\eta} \chi_{\Omega\eta}$.

(ii) Calculate the decoupling parameter for $\eta = 4$, for orbit 9. Compare with experiment.

(iii) Determine the level order of the band built on level 14, for $\eta = 2$ and for $\eta = 4$.

9-7. According to Nilsson, the $\frac{1}{2}^-$ [510] level has the following wave functions:

$$\eta = 4, \psi = 1.000|550+\rangle - 2.730|530+\rangle + 2.440|510+\rangle \\ - 0.606|551-\rangle + 0.780|531-\rangle + 1.431|511-\rangle;$$

$$\eta = 6, \quad \psi = 1.000|550+> - 2.359|530+> + 1.981|510+> \\ - 0.469|551-> + 0.420|531-> + 0.993|511->.$$

Find the decoupling constant for $\eta = 4$ and $\eta = 6$ and compare the results with the experimental value for ^{183}W (Fig. 9-39).

9-8. The following level schemes are given. What would you expect the character of each state to be? At what energy would you look for a 10^+ state in ^{234}U ? an $\frac{11}{2}^+$ level in ^{237}Np ?

	MeV		MeV
	0+		0.810
4+	1.542	8+	0.499
2+	1.476	6+	0.296
?	1.473		
2+	0.658	4+	0.143
0+	0	2+	0.0435
		0+	0
^{110}Cd		^{234}U	
$\frac{9}{2}^-$	0.159		
$\frac{7}{2}^-$	0.103	$\frac{1}{2}^-$	0.747
$\frac{9}{2}^+$	0.076		
$\frac{5}{2}^-$	0.060	$\frac{9}{2}^+$	0
$\frac{7}{2}^+$	0.033		
$\frac{5}{2}^+$	0		
^{237}Np			

9-9. An odd-odd nucleus with $\Omega = 0$ and $K = 0$ has two possible intrinsic wave functions:

$$\chi(\pm) = \psi_\omega(n)\phi_{-\omega}(p) \pm \psi_{-\omega}(n)\phi_\omega(p),$$

where ψ_ω and ϕ_ω are Nilsson orbits with $j_3 = \omega$. Using Eqs. 9-131 and 9-132 and the relations following 9-138, show that, if the parities of ψ and ϕ are opposite, $\chi(-)$ is the ground state of a rotational band of odd J 's while $\chi(+)$ is the ground state of a band of even J 's; and that, if the parities are equal, the roles of $\chi(-)$ and $\chi(+)$ are reversed.

Similarly, show that there are only even spins in a $K = 0$ band in an even-even nucleus in which all particles are paired in Nilsson orbits.

Hartree-Fock and Particle-Hole Calculations

10-1 REFINEMENTS ON THE SPHERICAL-SHELL MODEL

We noted in Chapter 7 the successes of the extreme single-particle model in explaining the ground-state properties of spherical or near-spherical nuclei. In Chapter 9, this scheme was broadened to generate the intrinsic states of deformed nuclei, where the average potential well in which the particles move was taken to be deformed. Although it was understood that the average field was being generated by the two-body interaction between the nucleons, this field was chosen in an empirical manner to reproduce the experimental single-particle levels, rather than calculating it from first principles. At first sight it seems very puzzling that the realistic two-nucleon potential, which is so strong and may be singular at short ranges, is able to produce a smooth average one-body potential. This puzzle was essentially resolved in Chapter 8, where it was shown that the effective interaction (the so-called G -matrix) between the nucleons in a nucleus is well behaved and smooth. It becomes meaningful, then, to formulate a scheme for generating a self-consistent average field for nucleons interacting with a smooth two-body force. This is called the Hartree-Fock method and we shall outline it in Section 10-3, where the meanings of the vague terms "smooth" and "self-consistent" will be clarified.

Apart from the ground-state properties, we are also interested in the excited states of a nucleus and in the decay modes and transition probabilities between the various nuclear states. Ideally, starting with a smooth, density-dependent effective interaction which has been obtained from the realistic

two-nucleon potential, we should be able to reproduce the properties of the nucleus in the ground and excited states. In an earlier chapter we concentrated on how the effective interaction could be calculated starting from the fundamental two-nucleon force. In this chapter we shall concern ourselves primarily with the many-body problem of calculating the nuclear spectra, assuming the existence of a smooth effective interaction between the nucleons. In the next section, we shall first outline how the excited states of a nucleus can be calculated in a very simple-minded shell-model picture, and then compare the results with experimental observations. We shall find that some of the basic assumptions of this simple model have to be modified to explain the experimental results. In order to fix our ideas, we shall concentrate on the oxygen region, although the methods outlined are quite general.

10-2 THE SHELL-MODEL APPROACH TO CALCULATING NUCLEAR SPECTRA

To illustrate the method, we take the example of ^{18}O , which has two neutrons outside a closed shell of ^{16}O . The simplest empirical approach is to assume

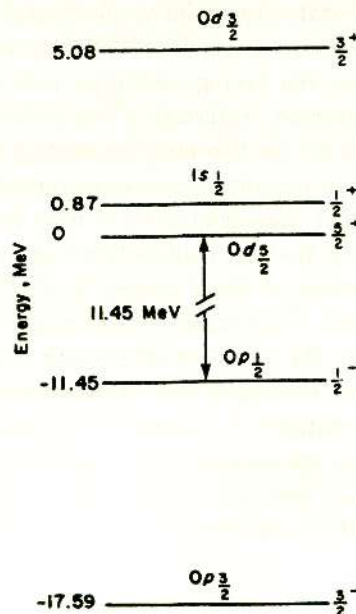


Fig. 10-1 Experimentally determined single-particle neutron levels in ^{18}O for the filled p -shell and the empty $s-d$ shell. The zero of energy has been arbitrarily taken at the $1d_{5/2}$ -level.

that the ^{16}O core is inert, in the sense that it provides an average field for the two neutrons, blocks states that would otherwise be available to the neutrons, but does not otherwise affect their motion. In the empirical approach, the single-particle levels generated by this potential are found from the experimental data. The energies of the levels in the $s-d$ shell are obtained in experiments in which a neutron is dropped into unfilled levels through the stripping reaction $^{16}\text{O}(d, p)^{17}\text{O}$. Correspondingly, the energies of the levels in the p -shell may be obtained by pulling out a neutron in a "pick-up" reaction like $^{16}\text{O}(d, t)^{15}\text{O}$. These experimental single-particle states are shown in Fig. 10-1, where it will be seen that there is a gap of 11.45 MeV between the $0p_{1/2}$ and the $0d_{5/2}$ levels. This is the basis of the assumption that the ^{16}O core is inert, because it should cost 11.45 MeV to excite a particle from the core.

To calculate the energy spectrum of ^{18}O , we now consider that the two valence neutrons in the $s-d$ shell interact through a two-body effective interaction, which may be completely phenomenological or may be derived from a realistic force. For simplicity, we ignore the continuum beyond the $s-d$ shell and consider virtual scattering of the two neutrons within the $s-d$ shell only. For example, a 0^+ shell state in ^{18}O could be composed of the following configurations:

$$|(0d_{5/2})^2 0\rangle, \quad |(1s_{1/2})^2 0\rangle, \quad \text{and} \quad |(0d_{3/2})^2 0\rangle.$$

The two-neutron interaction forms a 3×3 matrix within the space spanned by these three states; the eigenvalues of the matrix are the energies of distinct 0^+ states. The choice of appropriate single-particle wave functions is a matter of some subtlety. In calculations with phenomenological interactions they are taken to be harmonic-oscillator wave functions with the oscillator constant adjusted to fit the rms radius of the nucleus.

Similarly, the 2^+ state may be formed by five different unperturbed configurations, and it is necessary to diagonalize a 5×5 matrix. Figure 10-2 shows the experimental spectrum of ^{18}O , together with a typical calculated spectrum in this scheme, due to Kahana and Tomusiak [1]. The particular spectrum is obtained by assuming the two-neutron force to be an S -state free-reaction matrix, which fits only the low-energy phase-shift data. It is a characteristic feature of any short-range attractive interaction to push the 0^+ ground state far below the unperturbed configuration—a manifestation of the pairing effect.

Although we see that the correct level ordering has been reproduced and the energy spacings are qualitatively right, we cannot obtain, in this model,

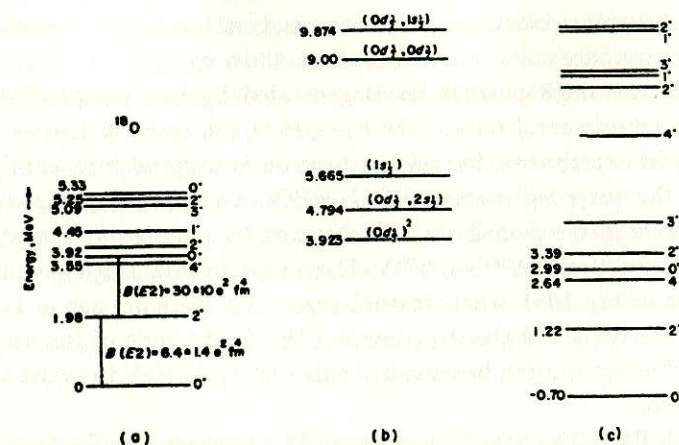


Fig. 10-2 (a) Experimental energy levels of ^{18}O . Also shown are the $B(E2)$ -values for the transitions from 2^+ to 0^+ and $0^- \rightarrow 0^+$ states. (b) The unperturbed energy levels due to two noninteracting neutrons in the $s-d$ shell. (c) The calculated spectrum in the inert-core model, using the Kahana-Tomusiak force.

the observed electric quadrupole transition rates between certain states. The electromagnetic transition rate between two states of a nucleus is directly proportional to the square of the matrix element of the electromagnetic operator between the initial and final states. A measure of the quadrupole transition is thus the reduced matrix element $B(E2)$. Two values are: $B(E2, 2^+ \rightarrow 0^+) = 6.4 \pm 1.4 e^2 \text{ fm}^4$ and $B(E2, 0^+ \rightarrow 2^+) = 30 \pm 10 e^2 \text{ fm}^4$. At first sight, since the two particles outside the closed shell are neutral, it would seem that in the simple shell model there can be no electric quadrupole transition in ^{18}O . But an extracore neutron is in a non-spherical orbit and it induces a small eccentricity of order A^{-1} in the motion of each core nucleon. Hence the Z protons produce a quadrupole moment of order Z/A times a single particle moment. One can simulate this effect by assigning an "effective charge" $\sim Ze/A$ to each extracore neutron. Distortion of an orbit is equivalent to admixture of excited states; hence Fig. 10-3 is a diagrammatic representation of this effect. With $e_{\text{eff}} = 0.5 e$ one can explain the value of $B(E2, 2^+ \rightarrow 0^+)$, but simple shell-model wave functions yield $B(E2, 0^+ \rightarrow 2^+) = 0.8 e^2 \text{ fm}^4$ [2], nearly 2 orders of magnitude too small. Large $B(E2)$ values indicate collective effects. This clearly shows that the simple two-neutron model of ^{18}O must be unrealistic and that the core must be taking an active

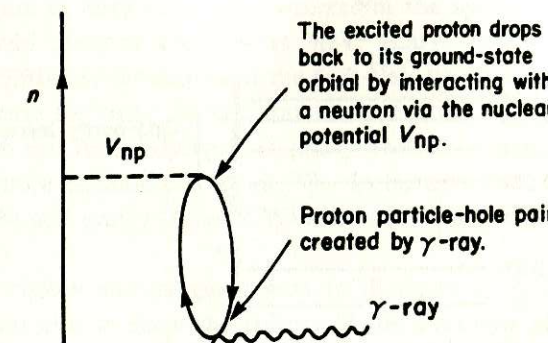


Fig. 10-3 The electric field couples to the extracore neutron through a proton particle-hole pair, giving rise to an effective charge of the neutron. If there is an extracore proton, its effective charge will similarly be increased. A calculation of the effective charge involves summing over all $p-h$ proton states.

rather than a passive role in the description of these states. Even in the description of the energy levels in ^{18}O from the simple model, there are some important discrepancies. The experimental spectrum (see Fig. 10-2) shows a 2^+ and a 0^+ state at 5.25 and 5.33 MeV, respectively. The stripping experiments show that both these states contain a large amount of two-neutron configurations. However, in the shell-model calculations, nearly all the two-particle strengths are absorbed in the five lowest states below 5 MeV. The rest go into states at about 8 MeV and higher.

Further clues that the ^{18}O core is not inert can be found by examining the experimental spectrum of ^{17}O in more detail, as shown in Fig. 10-4. It will be seen that there are three odd-parity levels around 4-MeV excitation, which cannot be generated at these energies by the one-body potential of our model. These must arise from the excitation of an odd number of particles from the p -shell of the core into the $s-d$ shell, leaving the appropriate number of holes in the core[†]. We should try to understand why these excitations from the core cost so little in energy.

Further evidence of core excitation can be obtained by examining the energy spectrum of ^{16}O , as shown in Fig. 10-5. In the simple shell-model picture, an odd-parity state can come only at an excitation energy of about

[†] These odd-parity states are primarily of two-particle, one-hole nature. See B. Margolis and N. de Takacsy, *Phys. Lett.* **15**, 329 (1965).

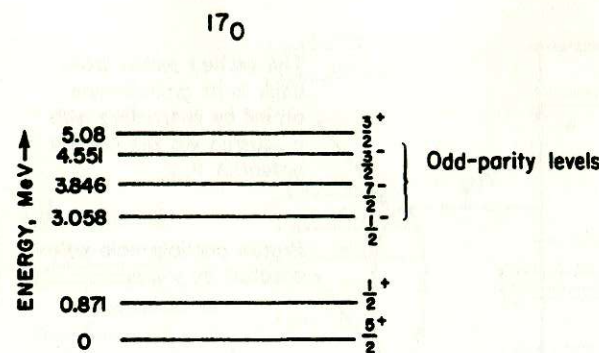


Fig. 10-4 Experimental spectrum of ¹⁷O for the first few levels.

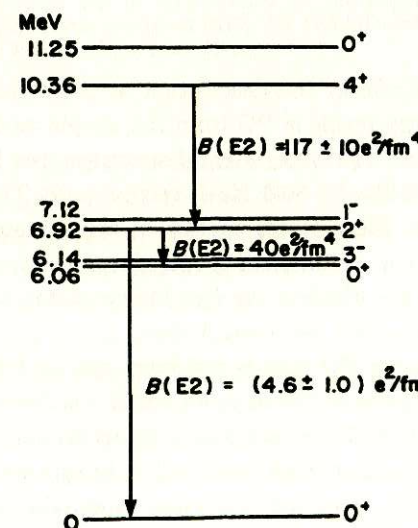


Fig. 10-5 Experimental spectrum of ¹⁶O. There are strong $E2$ -transitions from the 6.92-MeV 2⁺ to the 6.06-MeV 0⁺ state, and from the 10.36-MeV 4⁺ to the 6.92-MeV 2⁺ state.

12 MeV, whereas experimentally a 3⁻ level is seen at 6.14 MeV. One might suspect that this might be an octupole vibration state, which could show

that the core is far from inert. More surprising is the appearance of an 0⁺ excited state at only 6.06 MeV, whereas in the spherical single-particle model it should come at about ~ 24 MeV. Large $B(E2)$ -transition rates between the 6.92-MeV 2⁺ state and the 6.06-MeV 0⁺ state further suggest a collective nature for these excited states. In Section 10-5 we shall try to see how there can be low-lying even-parity excited states in ¹⁶O, and will then give a more realistic picture of ¹⁶O. In Section 10-6, we shall try to understand the odd-parity states of ¹⁶O within the framework of an extended shell model.

We have chosen the oxygen region to illustrate a simple shell model calculation and also to show the failings of the inert-core picture. Similar discrepancies are noted in the doubly closed-shell Ca and Ni regions as well. The shell model is more successful, however, when we consider the Pb region, where we have the doubly closed-shell nucleus ²⁰⁸Pb. Figure 10-6 shows plots of the experimentally determined low-lying levels of ²⁰⁹Pb from the reaction ²⁰⁸Pb(d, p)²⁰⁹Pb [3] and also the single-particles levels as generated by a suitably chosen Woods-Saxon potential with spin-orbit force [4]. It will

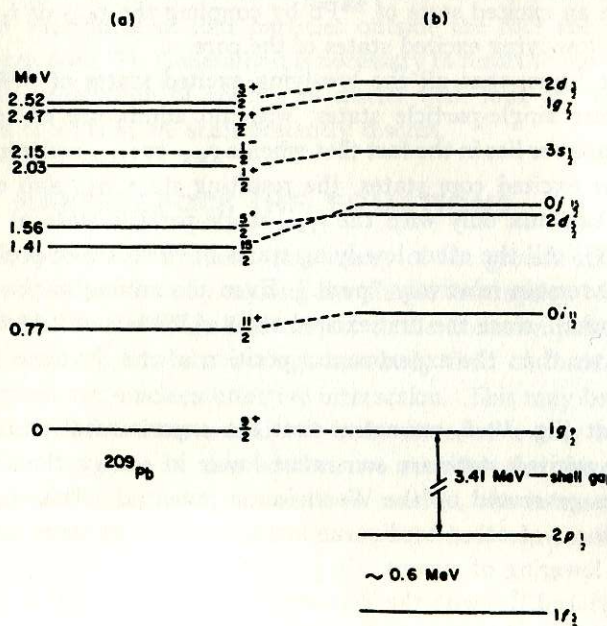


Fig. 10-6 (a) Experimental energy levels of the low-lying states in ²⁰⁹Pb. (b) Some levels generated by a neutron moving in an appropriate Woods-Saxon well with a spin-orbit potential [4].

be seen that seven out of eight excited states up to 2.52 MeV can be explained in the shell-model picture, which is a much better situation than that for ^{17}O , where there were three low-lying odd-parity states (Fig. 10-4) which could not be generated in the extreme single-particle model. Moreover, Mukherjee and Cohen [3] have shown that the experimental angular distribution of the proton in $^{208}\text{Pb}(d, p)^{209}\text{Pb}$ and the average cross sections over scattering angles 45–90° as functions of excitation energy could be reproduced fairly well by assigning to these excited states just the pure shell-model configurations, as shown in Fig. 10-6.

This is a classic example of the success of the simple model, where the core does seem to play a passive role. We naturally seek to know why this is so, since the shell gap between the $2p_{1/2}$ - and $1g_{9/2}$ -levels is only about 3.4 MeV. It should be realized, however, that the size of the energy gap should be considered in relation to the spacings of the occupied single-particle levels, which are only about 0.5 MeV for the top few levels in ^{208}Pb . In the spectrum of ^{208}Pb , all the low-lying excited states up to 4 MeV have odd parity. It is conceivable that in some of the excited states of ^{208}Pb , for example, the core of ^{208}Pb will be excited too. Within the framework of our model, we could describe such an excited state of ^{209}Pb by coupling the $g_{9/2}$ - or $i_{11/2}$ -neutron to one of the low-lying excited states of the core.

Why is it, then, that all the low-lying excited states of ^{209}Pb seem to be almost pure single-particle states, with no admixture of core-coupled states? The answer lies in the fact that when a $g_{9/2}$ - or $i_{11/2}$ -neutron is coupled to any of the excited core states, the resulting state has also odd parity. Therefore it can mix only with the $j_{15/2}$ single-particle state of odd parity (see Fig. 10-6). All the other low-lying states of ^{209}Pb are of positive parity and therefore remain relatively "pure." Even the mixing in the odd-parity $j_{15/2}$ -state is small, since the first excited state of ^{208}Pb is at 2.61 MeV, which is much greater than the experimental position of the $\frac{15}{2}^-$ state (1.41 MeV) in ^{209}Pb .

Looking at Fig. 10-6, we notice that the experimental positions of all but the first excited state are somewhat lower in energy than the single-particle states generated by the Wood-Saxon potential. This signifies that small admixtures of other configurations are present in these states which result in the lowering of energy. In particular, there is an inversion of the order of the $\frac{5}{2}^+$ and $\frac{15}{2}^-$, with the $\frac{15}{2}^-$ coming down, implying that the $\frac{5}{2}^+$ state has less admixture of higher configurations than the $\frac{15}{2}^-$. This is consistent with our earlier remarks. More specifically, we can describe the excited $\frac{15}{2}^-$ state in terms of the following configurations:

$$\begin{aligned} |\frac{15}{2}^-\rangle &= C_1 |\text{core ground state } 0^+ \otimes j_{15/2}; \frac{15}{2}^-\rangle \\ &\quad + C_2 |\text{core } 3^- \otimes g_{9/2}; \frac{15}{2}^-\rangle + C_3 |\text{core } 3^- \otimes i_{11/2}; \frac{15}{2}^-\rangle + \dots \end{aligned}$$

$$\text{with } \sum_i |C_i|^2 = 1.$$

The quantity $|C_1|^2$ gives the strength of the pure single-particle configuration and is called the "spectroscopic factor" in analyses of d - p reactions. It is possible to extract the spectroscopic factors of the single-particle configurations of the various excited states by analyzing the cross-section data for d - p reactions. These analyses confirm that the spectroscopic factors for all the even-parity excited states of ^{209}Pb are between 0.95 and 1.0, while for the $\frac{15}{2}^-$ state values range from 0.5 to 0.9 [5]. A great deal of experimental work has been done in the lead region [5], especially to examine how good the shell-model wave functions are, particularly when there are two or more valence particles or holes. It is found that in these nuclei the shell model is fairly successful.

Shell-model calculations escalate in complications with increasing number of particles outside the closed shell, because of the complexity of the angular-momentum algebra and the increasing dimension of the matrices. However, calculations with three or four particles outside the core are quite feasible and have been done [7]. Generally it is necessary to resort to more approximations in the calculation of spectra of nuclei with four or more extracore particles—a topic that we shall presently discuss.

10-3 THE HARTREE-FOCK (HF) EQUATIONS

In the shell model we have seen that many of the ground-state properties of nuclei can be described by making the simple assumption of independent particle motion in an average field subject to the exclusion principle. In this section we examine how the average one-body field of force is generated through a given two-nucleon effective interaction. This may be the reaction matrix calculated from the actual two-body force, or it may be a phenomenological interaction. In this section, we consider the theory when the effective interaction is local. In realistic models, the interaction may be nonlocal and density dependent, and these introduce some additional complications.

In the second quantized notation (see Appendix C), let us take the Hamiltonian to be

$$H = \sum_{\alpha, \beta} \langle \alpha | t | \beta \rangle a_\alpha^\dagger a_\beta + \frac{1}{2} \sum_{\alpha, \beta, \gamma, \delta} \langle \alpha \beta | V | \gamma \delta \rangle a_\alpha^\dagger a_\beta^\dagger a_\delta a_\gamma, \quad (10-1)$$

where V denotes the effective two-body interaction operator, and the single-particle states $|\alpha\rangle$, $|\beta\rangle$, etc., form an arbitrary complete set. The operator a_α^+ creates a particle in the state $|\alpha\rangle$, while a_β destroys a particle in the state $|\beta\rangle$. The sums in Eq. 10-1 are unrestricted, going over the complete set of states. Essentially, we seek to obtain the best possible ground-state wave function and energy of an A -body system in the independent-particle approximation. In this picture, each particle is moving in some average one-body potential U , which generates a set of single-particle states $|\alpha\rangle$, $|\beta\rangle$, ..., $|\ell\rangle$, $|m\rangle$, ... Of these single-particle states, A are singly occupied by the particles and we denote them by $|\ell\rangle$, $|m\rangle$, $|n\rangle$, ..., while the unoccupied states are $|\alpha\rangle$, $|\beta\rangle$, $|\gamma\rangle$, ... Our problem is to find U and the single-particle orbitals that are occupied in the ground state. Since the average field U is generated through the interaction V , we would expect its matrix element between two orbitals r and s to be

$$\langle r|U|s\rangle = \sum_{m=1}^A [\langle rm|V|sm\rangle - \langle rm|V|ms\rangle]. \quad (10-2)$$

The average field U thus depends on which orbitals m are occupied, and the orbitals in turn are generated by the single-particle Hamiltonian $H_{SP} = t + U$. In second-quantized form, we can write

$$H_{SP} = \sum_{k,i} \left[\langle k|t|i\rangle + \sum_{m=1}^A (\langle km|V|im\rangle - \langle km|V|mi\rangle) \right] a_k^+ a_i, \quad (10-3)$$

where the sums over k and i are unrestricted. The solution of the problem demands self-consistency: choosing a trial set of orbitals and selecting those which are occupied, we can calculate the one-body potential U by Eq. 10-2, and then solve the Schrödinger equation with U to obtain a new set of orbitals. The procedure is repeated until the process converges.

The procedure that we have described can be put on a firmer basis by using the variational principle. In the independent-particle picture, the many-body wave function $|\Phi\rangle$ is an antisymmetrized product of the single-particle orbitals. The optimum choice of these orbitals is such that the expectation value of the energy is stationary, that is,

$$\delta \frac{\langle \Phi_0 | H | \Phi_0 \rangle}{\langle \Phi_0 | \Phi_0 \rangle} = 0, \quad (10-4)$$

where by $|\delta\Phi_0\rangle$ we mean a first-order change (i.e., change in a single orbital) in $|\Phi_0\rangle$, such that $\langle \Phi_0 | \delta\Phi_0 \rangle = 0$. The determinantal ground state that satisfies Eq. 10-4 is

$$|\Phi_0\rangle = \prod_{m=1}^A a_m^+ |0\rangle, \quad (10-5)$$

where $|0\rangle$ denotes the true vacuum state with no particles. For $|\delta\Phi_0\rangle$, we choose

$$|\delta\Phi_0\rangle = \eta a_b^+ a_m |\Phi_0\rangle, \quad (10-6)$$

where η is a constant, $b > A$, and $m \leq A$. Then a straightforward but lengthy calculation to simplify Eq. 10-4 yields the condition (see Appendix C-3)

$$\langle m|t|b\rangle + \sum_{n=1}^A (\langle mn|V|bn\rangle - \langle nm|V|bn\rangle) = 0, \quad (10-7)$$

which must be obeyed for the optimum choice of orbitals, with $b > A$ and $m \leq A$. If we use the definition of H_{SP} as given in Eq. 10-3, it follows that

$$\langle m|H_{SP}|b\rangle = 0, \quad (10-8)$$

which implies that with this choice of H_{SP} there are no transitions between the occupied states $|m\rangle$ and the empty states $|b\rangle$. This, in fact, justifies our choice of U (Eq. 10-2), because it means that this U accounts for all the one-particle one-hole ($1p-1h$) transitions from the ground state that can be brought about by V . In other words, the matrix elements of the residual interaction ($V - U$) link the HF ground state only to states in which two particles are excited, that is, $2p-2h$ states. Since U is a one-body potential, this is the best that can be achieved. The inclusion of the multiple particle-hole state constitutes higher-order corrections to the HF ground state. The minimal condition (Eq. 10-8), obtained from the variational principle, implies that the occupied and empty states are completely decoupled so far as H_{SP} is concerned, and this means that H_{SP} may be diagonalized in these spaces separately. This is achieved if the HF orbitals are generated by H_{SP} :

$$(t + U)|m\rangle = e_m|m\rangle, \quad (10-9a)$$

that is,

$$\langle l|H_{SP}|m\rangle = e_l \delta_{lm}, \quad l, m \leq A. \quad (10-9b)$$

Since the occupied orbitals are distinct from the unoccupied ones, it also follows that Eq. 10-8 is satisfied.

It is worth while to write Eq. 10-9a in coordinate space to emphasize the nonlocal nature of U . Using Eq. 10-2, we find

$$-\frac{\hbar^2}{2M} \nabla_1^2 \phi_m(\mathbf{r}_1) + \left(\sum_{l=1}^A \int \phi_l^*(\mathbf{r}_2) V(|\mathbf{r}_1 - \mathbf{r}_2|) \phi_l(\mathbf{r}_2) d^3 r_2 \right) \phi_m(\mathbf{r}_1)$$

$$- \sum_{l=1}^A \int \phi_l^*(\mathbf{r}_2) V(|\mathbf{r}_1 - \mathbf{r}_2|) \phi_l(\mathbf{r}_1) \phi_m(\mathbf{r}_2) d^3 r_2 = e_m \phi_m(\mathbf{r}_1),$$

where $\langle \mathbf{r}|m\rangle = \phi_m(\mathbf{r})$ is a single-particle state.

Writing

$$U_H(\mathbf{r}_1) = \sum_{l=1}^A \int \phi_l^*(\mathbf{r}_2) V(|\mathbf{r}_1 - \mathbf{r}_2|) \phi_l(\mathbf{r}_2) d^3 r_2 \quad (10-10)$$

and

$$U_F(\mathbf{r}_1, \mathbf{r}_2) = \sum_{l=1}^A \phi_l^*(\mathbf{r}_2) V(|\mathbf{r}_1 - \mathbf{r}_2|) \phi_l(\mathbf{r}_1),$$

we obtain

$$-\frac{\hbar^2}{2M} \nabla_1^2 \phi_m(\mathbf{r}_1) + U_H(\mathbf{r}_1) \phi_m(\mathbf{r}_1) - \int U_F(\mathbf{r}_1, \mathbf{r}_2) \phi_m(\mathbf{r}_2) d^3 r_2 = e_m \phi_m(\mathbf{r}_1). \quad (10-11)$$

Here we have denoted the local part of U by U_H and the nonlocal part by U_F , the latter arising because of the antisymmetrization of the HF wave function.

We should mention here the modifications that take place in the HF equation 10-11 when the effective V is density dependent. For simplicity, we assume that V is still local and has the form

$$\langle \mathbf{r}_1, \mathbf{r}_2 | V | \mathbf{r}_1', \mathbf{r}_2' \rangle = V[\mathbf{r}_{12}, \rho(\mathbf{R}_{12})] \delta(\mathbf{r}_{12} - \mathbf{r}'_{12}) \delta(\mathbf{R}_{12} - \mathbf{R}'_{12}), \quad (10-12)$$

where $\mathbf{R}_{12} = (\mathbf{r}_1 + \mathbf{r}_2)/2$, $\mathbf{r}_{12} = \mathbf{r}_1 - \mathbf{r}_2$, and similarly for the primed variables. We are assuming that the interaction depends on the density ρ at the center of mass of the two particles. Since

$$\rho(\mathbf{R}) = \sum_{m=1}^A \phi_m^*(\mathbf{R}) \phi_m(\mathbf{R}),$$

an additional term arises when we minimize the ground-state energy with respect to the single-particle orbitals $\phi_m^*(\mathbf{r})$ at any point \mathbf{r} ; in fact,

$$\frac{\delta V}{\delta \phi_m^*(\mathbf{r})} = \frac{\delta V}{\delta \rho} \frac{\delta \rho(\mathbf{R})}{\delta \phi_m^*(\mathbf{r})} = \frac{\delta V}{\delta \rho} \phi_m(\mathbf{r}) \delta(\mathbf{R} - \mathbf{r}).$$

Consequently, for a density-dependent local V , the HF equation 10-11 is generalized to

$$-\frac{\hbar^2}{2M} \nabla_1^2 \phi_m(\mathbf{r}_1) + U_H \phi_m(\mathbf{r}_1) - \int U_F(\mathbf{r}_1, \mathbf{r}_2) \phi_m(\mathbf{r}_2) d^3 r_2$$

$$+ U_R(\mathbf{r}_1) \phi_m(\mathbf{r}_1) = e_m \phi_m(\mathbf{r}_1), \quad (10-13)$$

where $U_R(\mathbf{r}_1)$ is called the rearrangement potential. Its presence, of course, results in modifications of the values of the single-particle energies e_m and the total single-particle potential U . Explicit calculations show [8, 9] that U_R can be written as

$$U_R(\mathbf{r}_1) = \frac{1}{2} \sum_{l,m} \int \phi_l^*(\mathbf{r}_2) \phi_m^*(\mathbf{r}_3) \frac{\partial V(\mathbf{r}_{23}, \rho(\mathbf{R}_{23}))}{\partial \rho(\mathbf{R}_{23})} \delta(\mathbf{R}_{23} - \mathbf{r}_1)$$

$$\cdot [\phi_l(\mathbf{r}_2) \phi_m(\mathbf{r}_3) - \phi_l(\mathbf{r}_3) \phi_m(\mathbf{r}_2)] d^3 r_2 d^3 r_3. \quad (10-14)$$

In actual calculations, the HF orbitals are generally expressed in terms of some conveniently chosen basic set (denoted here by Greek symbols)

$$|\beta\rangle = \sum_{\beta} x_{\beta}^l |\beta\rangle, \quad (10-15)$$

with expansion coefficients x_{β}^l , where the basic set $|\beta\rangle$, for example, is generated by a spherically symmetric or axially symmetric harmonic-oscillator potential. In principle, the sum over β in Eq. 10-15 should be over all states; in practice, the space is truncated. In principle, of course, the choice of the space determines the effective interaction V (see Section 8-4). For example, for a calculation in the $0p$ -shell region like that of carbon, the basic states $|\beta\rangle$ may include all states up to the $1p$ - $0f$ levels of the harmonic oscillator. For convenience in notation, let us write

$$\langle ln | V | mn \rangle - \langle ln | V | nm \rangle = \langle ln | V | mn \rangle_A \quad (10-16)$$

and define the HF single-particle density operator

$$\rho = \sum_{m=1}^A |m\rangle \langle m|. \quad (10-17)$$

Then

$$\rho_{\gamma\delta} \equiv \langle \gamma | \rho | \delta \rangle = \sum_{m=1}^A (x_{\gamma}^m)^* (x_{\delta}^m). \quad (10-18)$$

Equation 10-9b may be rewritten as

$$\sum_i \langle l|t|m\rangle |l\rangle + \sum_l \sum_{m=1}^A \langle ln|V|mn\rangle_A |l\rangle = e_m |m\rangle. \quad (10-19)$$

Using Eqs. 10-15 and 10-18, we reduce this to

$$\sum_\beta \langle \alpha|t|\beta\rangle x_\beta m + \sum_{\beta,\gamma,\delta} \langle \alpha\gamma|V|\beta\delta\rangle_A \rho_{\gamma\delta} x_\beta m = e_m x_\alpha m. \quad (10-20)$$

Initially, a set of coefficients $x_\beta m$ for each orbital $|m\rangle$ is guessed, and $\rho_{\gamma\delta}$ is calculated by deciding which of these are filled. The left side of Eq. 10-20 can then be calculated in the given (truncated) space and diagonalized. This generates a new set of orbitals, and the procedure is repeated until successive diagonalizations produce the same set $x_\beta m$.

The ground-state energy of the system with the HF state $|\Phi\rangle$ is

$$\begin{aligned} E_{HF} &= \langle \Phi_0 | H | \Phi_0 \rangle \\ &= \sum_{l=1}^A \langle l|t|l\rangle + \frac{1}{2} \sum_{l,m=1}^A \langle lm|V|lm\rangle_A \end{aligned} \quad (10-21a)$$

or

$$E_{HF} = \sum_{l=1}^A e_l - \frac{1}{2} \sum_{l,m=1}^A \langle lm|V|lm\rangle_A \quad (10-21b)$$

$$= \sum_{l=1}^A \langle l|t + \frac{1}{2}U|l\rangle = \sum_{l=1}^A [e_l - \frac{1}{2}\langle l|U|l\rangle], \quad (10-21c)$$

where U is defined by Eq. 10-2.

It will be seen from Eq. 10-21 that the total ground-state energy is not simply the sum of the occupied eigenvalues e_l of H_{SP} . Nevertheless, we can interpret the e_l 's as the approximate excitation energies of the levels and call them the self-consistent single-particle energies. This can be seen by finding the expectation value of H with respect to a state $a_b + a_m |\Phi_0\rangle$, which is a configuration in which a particle in orbital $m \leq A$ has been excited to an orbital $b > A$. This is found to be $[E_{HF} + e_b - e_m - \langle bm|V|bm\rangle_A]$, implying that the excitation energy for this configuration is $e_b - e_m - \langle bm|V|bm\rangle_A$. For a system with large A , it is clear from Eq. 10-2 that the last term, $\langle bm|V|bm\rangle_A$, is of order $1/A$ compared to $e_b - e_m$ and hence may be ignored. If this is done, it follows that for the ground state the self-consistent energies of all the occupied orbitals should be less than those of the empty ones, so that only the lowest A HF orbitals are filled in the ground state.

Having established a variational principle for calculating the ground-state energy E_{HF} , we look for corrections to this expression in a perturbation scheme. Essentially, we started with a Hamiltonian for the A -nucleon system,

$$H = \sum_i t_i + \sum_{i < j} V_{ij}, \quad (10-22)$$

which we rewrote as

$$H = \sum_i (t_i + U_i) + (\sum_{i < j} V_{ij} - \sum_i U_i) \quad (10-23)$$

by introducing the one-body potential operator U defined in Eq. 10-2. The independent-particle A -body problem was then solved to obtain an expression for

$$E_{HF} = \sum_{l=1}^N \langle l|t + \frac{1}{2}U|l\rangle;$$

the factor $\frac{1}{2}$ appeared in U because it is being generated, by definition, by a two-body potential V_{ij} , subject to the condition that the pairs $i-j$ should not be double counted. For the HF approximation to be a good one, the contribution to the ground-state energy of the residual interaction $V - U$ appearing in Eq. 10-23 should be small compared to E_{HF} . In principle, the residual interaction, being a two-body operator, can cause transitions from the HF ground state $|\Phi_0\rangle$ to states $|\Phi_0'\rangle$, which differ only in one orbital, or to states $|\Phi_0''\rangle$, in which two orbitals are changed from $|\Phi_0\rangle$. Using perturbation theory, we find that the energy shift in the ground state due to the residual interaction is

$$\Delta E = \sum_{\Phi_0'} \frac{|\langle \Phi_0 | V - U | \Phi_0' \rangle|^2}{E_{HF} - E'} + \sum_{\Phi_0''} \frac{|\langle \Phi_0 | V | \Phi_0'' \rangle|^2}{E_{HF} - E''}. \quad (10-24)$$

The first term on the right side of Eq. 10-24, which is due to the one-particle one-hole transitions, drops out automatically because of the self-consistent definition of U , as given in Eq. 10-2. This is the bonus obtained by doing a self-consistent calculation. If we had chosen U arbitrarily, rather than through Eq. 10-2, the one-particle one-hole contribution could be substantial.

Let us now consider the last term in Eq. 10-24. Let

$$|\Phi_0''\rangle = a_b + a_d + a_m a_n |\Phi_0\rangle; \quad b \neq d > A, \quad m \neq n \leq A.$$

Then

$$\langle \Phi_0 | V | \Phi_0'' \rangle = \langle mn | V | bd \rangle_A \quad \text{and}$$

$$\sum_{\Phi_0''} \frac{|\langle \Phi_0 | V | \Phi_0'' \rangle|^2}{E_{HF} - E''} = \sum_{\substack{m,n \leq A \\ b,d > A}} \frac{|\langle mn | V | bd \rangle_A|^2}{e_m + e_n - e_b - e_d}, \quad (10-25)$$

where e_m , etc., are the self-consistent HF single-particle energies. In order for ΔE to be small, the effective interaction V should be weak, so that its matrix elements connecting two occupied orbitals to two unoccupied ones are small. In other words, the effective interaction should be smooth, in the sense that it may not have high Fourier components in momentum. Moreover, if there is a substantial gap in energy between the occupied single-particle levels and the unoccupied ones, the energy denominator $e_m + e_n - e_b - e_d$ will be large and ΔE small. Estimates of such second-order corrections to the HF energy have been made, for example, by Kerman and Pal [10] in ^{16}O and ^{40}Ca , using the Tabakin separable potential as the effective interaction V . They find that, whereas the first-order potential energies per particle in ^{16}O and ^{40}Ca are 21.8 and 25.6 MeV, respectively, the second-order corrections in the potential energy per particle in these nuclei are 4.3 and 7.2 MeV. These result in substantial corrections to the binding-energy values but indicate that higher-order corrections are probably small. Essentially, in this perturbation scheme, corrections to the HF ground state $|\Phi_0\rangle$ are introduced by adding $2p\text{-}2h$ correlations. Denoting the correlated ground state by $|\tilde{\Phi}_0\rangle$, we can write

$$|\tilde{\Phi}_0\rangle = |\Phi_0\rangle + \sum_{\Phi_0''} \frac{\langle \Phi_0'' | V | \Phi_0 \rangle}{E_{HF} - E''} |\Phi_0''\rangle. \quad (10-26)$$

We shall see in Section 10-6 that inclusion of $2p\text{-}2h$ correlations may have important effects on the equilibrium shape of the lowest intrinsic state of the nucleus. In the so-called random-phase approximation (RPA), a correlated ground state is introduced that has admixtures of $0p\text{-}0h$, $2p\text{-}2h$, $4p\text{-}4h$, and higher-order configurations. We shall not discuss this method in this book, and the reader is referred to Rowe [11] for further development.

10-4 BINDING ENERGIES OF CLOSED-SHELL NUCLEI IN THE HARTREE-FOCK APPROXIMATION

The HF method has been extensively applied in nuclear calculations. A basic project is the calculation of the binding energy, the density distribution, and the equilibrium density of nuclei—in particular, of closed-shell spherical

nuclei, for which the calculations are simpler. The binding energy and the saturation density of a system are very sensitive to the effective interaction and also to the nature of the approximations in the calculation. The first realistic attempt to do such a calculation on ^{16}O , ^{40}Ca , and ^{90}Zr was made by Brueckner, Lockett, and Rotenberg [12] and on ^{208}Pb by Masterson and Lockett [13]. They used the G -matrix from nuclear matter as the effective interaction, with the local-density approximation (see Chapter 8). Since the effective interaction itself is density dependent, there appears the extra rearrangement potential term with U_R in the HF equation 10-13. This extra term is of great importance in giving the right binding energy and saturation density. For an effective interaction that has no density dependence, we saw from Eq. 10-21 that the ground-state energy E_0 can be written as half the sum of the kinetic and the single-particle energies. If the radius of the nucleus is known, the kinetic energies are roughly known, and all the single-particle energies in a light nucleus like ^{16}O are also known. Adding these yields only about half the experimental binding of ^{16}O . In doing HF calculations for binding energy and saturation density, it is necessary, therefore, to take into account properly the density dependence of the effective interaction. The calculation of Brueckner et al. [12] included only the density dependence due to the repulsive core, omitting the strong density dependence brought about by the tensor force. This resulted in too little saturation, leading to unrealistically high central densities. In many subsequent calculations (see, e.g., Davies et al. [14]), the Brueckner G -matrix has been calculated in the harmonic-oscillator basis and the HF calculations have been performed with the matrix elements so obtained. In these calculations, the effect of the rearrangement potential and the contribution of higher order clusters have been omitted, resulting in too little binding.

The construction of a local, density-dependent interaction for finite nuclei, starting from the nuclear-matter G -matrix, was discussed in Chapter 8. Negele [15], Sprung and Banerjee [16], and Nemeth and Ripka [17] have constructed such interactions in the local-density approximation for HF calculations. As we have seen, realistic two-nucleon interactions that yield the correct equilibrium density of nuclear matter give a binding energy which is a few MeV less than the empirical value of 16 MeV. This additional binding may arise from higher-order clusters, from modifications in the tensor component of the force, and from a three-nucleon force [18]. The higher-order cluster contributions depend sensitively on the tensor component of the force. Negele, as well as Sprung and Banerjee, has accounted for these uncertainties of the nuclear-matter G -matrix by slightly

ormalizing it (mainly in the 3S_1 -state) to make it reproduce the correct binding and equilibrium density of nuclear matter. It has then been demonstrated [15, 19] that the effective density-dependent local interaction derived from such a G -matrix gives good results for finite spherical nuclei in the HF calculations.

In the following treatment, rather than describing in detail the more complicated calculations of Negele [15] or Campi and Sprung [19], we shall outline a HF calculation with a particularly simple, phenomenological interaction, due to Vautherin and Brink [20], which is density dependent. First, consider for simplicity the S -state diagonal matrix element of a local potential $V(r)$ in momentum space:

$$\langle k|V|k\rangle = \int V(r) j_0^2(kr) d^3r,$$

where k is the magnitude of the relative momentum of two nucleons inside the Fermi sea. If $V(r)$ is of very short range, we can expand $j_0^2(kr)$ in a power series, obtaining

$$\langle k|V|k\rangle = \int V(r) d^3r - \frac{1}{3}k^2 \int V(r)r^2 d^3r + \dots, \quad (10-27a)$$

where the higher-order terms can be neglected if the higher moments of $V(r)$ are very small. In coordinate space, the interaction may then be written as

$$V(p, r) = t_1 \delta(r) + t_2 [p^2 \delta(r) + \delta(r)p^2], \quad (10-27b)$$

where t_1, t_2 are constants and p is the momentum operator. Following this idea, Brink and Vautherin take the effective interaction to be

$$V = \sum_{i < j} V_{ij}^{(2)} + \sum_{i < j < k} V_{ijk}^{(3)}, \quad (10-28)$$

where the last term in this equation is a phenomenological three-body interaction, whose role we shall presently discuss. The matrix elements of the two-body interaction between plane-wave states are of the most general form, bilinear in relative momenta:

$$\langle \mathbf{k}|V^{(2)}|\mathbf{k}'\rangle = t_0(1 + x_0 P_\sigma) + \frac{1}{2}t_1(k^2 + k'^2) + t_2 \mathbf{k} \cdot \mathbf{k}' + iW_0(\boldsymbol{\sigma}_1 + \boldsymbol{\sigma}_2) \cdot \mathbf{k} \times \mathbf{k}'. \quad (10-29)$$

In Eq. 10-29, x_0 is the coefficient of the spin-exchange operator P_σ ; t_0, t_1, t_2 , and W_0 are constants; and the last term is a zero-range spin-orbit force.

A phenomenological effective interaction of this form was first proposed by Skyrme [21], and a very similar form has been used by Moszkowski [22] for the gross properties of nuclei. Note that the quadratic terms in k involving t_1 and t_2 not only make the interaction in coordinate space of finite range, but also give extra density dependence. This is so because the contribution to potential energy of a central, finite-range, static interaction goes dominantly like k_F^{-3} , whereas for a quadratically momentum-dependent interaction the contribution goes as k_F^{-5} . The three-body effective interaction is also taken to be of zero range:

$$V_{123}^{(3)} = t_3 \delta(\mathbf{r}_1 - \mathbf{r}_2) \delta(\mathbf{r}_1 - \mathbf{r}_3) \quad (10-30)$$

and represents empirically the effect of higher-order clusters. It may be regarded as a density-dependent, two-body interaction, since

$$\int V_{123}^{(3)} \rho(\mathbf{r}_3) d^3r_3 = \rho(\mathbf{r}_1) t_3 \delta(\mathbf{r}_1 - \mathbf{r}_2). \quad (10-31)$$

Delta-function interactions in HF calculations give rise to great simplicity because the direct and exchange terms have similar structures, and the self-consistent HF potential U turns out to be local.

The expectation value of the Hamiltonian with respect to a Slater determinant Φ can be expressed as

$$E = \langle \Phi | T + V | \Phi \rangle = \int \epsilon_\rho(\mathbf{r}) d^3r, \quad (10-32)$$

where $\epsilon_\rho(\mathbf{r})$, the spatial-energy density, is a function of the single-particle density ρ . The simplicity of interaction 10-29 makes it possible to express $\epsilon_\rho(\mathbf{r})$ in terms of $\rho(\mathbf{r})$, the kinetic-energy density $\tau(\mathbf{r})$, and the spin density $J(\mathbf{r})$:

$$\begin{aligned} \rho(\mathbf{r}) &= \sum_i |\phi_i(\mathbf{r})|^2, & \tau(\mathbf{r}) &= \sum_i |\nabla \phi_i(\mathbf{r})|^2, \\ J(\mathbf{r}) &= \frac{1}{r} \sum_i [\phi_i^*(\mathbf{l} \cdot \boldsymbol{\sigma}) \phi_i], \end{aligned} \quad (10-33)$$

where the sum i is over occupied orbitals only. For simplicity in algebra, we are assuming equal numbers of neutrons and protons and ignoring the Coulomb force. The results can be generalized by defining neutron and proton densities separately, as has been done by Brink and Vautherin [20]. Evaluating Eq. 10-32, we find

$$\epsilon_\rho(\mathbf{r}) = \frac{\hbar^2}{2M} \tau + \frac{3}{8} t_0 \rho^2 + \frac{1}{16} t_3 \rho^3 + \frac{1}{16} (3t_1 + 5t_2) \rho \tau +$$

$$+ \frac{1}{16}(9t_1 - 5t_2)(\nabla\rho)^2 + \frac{3}{4}W_0 \left(J \frac{d\rho}{dr} \right). \quad (10-34)$$

We should mention at this point that, although Eq. 10-34 has been obtained from the simplified interaction 10-29, Negele and Vautherin [23] have shown that form 10-34 for ϵ_ρ may also be obtained by starting from the nuclear-matter G -matrix derived from a realistic two-nucleon force, although in that case the coefficients t_i in Eq. 10-34 are somewhat density dependent.

The HF equation is obtained by varying Eq. 10-32 with respect to the single-particle states $\phi_i(r)$ and has the form

$$\left\{ -\nabla \left[\frac{\hbar^2}{2M^*(r)} \right] \cdot \nabla + U(r) \right\} \phi_i(r) = e\phi_i(r), \quad (10-35)$$

where, using Eq. 10-34, we find that

$$\frac{\hbar^2}{2M^*(r)} = \frac{\hbar^2}{2M} + \frac{1}{16}(3t_1 + 5t_2)\rho(r) \quad (10-36)$$

and

$$U(r) = \frac{3}{4}t_0\rho + \frac{3}{16}t_3\rho^2 + \frac{1}{16}(3t_1 + 5t_2)\tau \\ + \frac{1}{32}(5t_2 - 9t_1)\nabla^2\rho + \frac{3}{2r}W_0 \frac{d\rho}{dr} 1 \cdot s. \quad (10-37)$$

Note that now the HF equation is for a local $U(r)$, which itself depends on the orbitals $\phi_i(r)$ through the density. Assuming a form for $\rho(r)$, one can obtain U from Eq. 10-37 and then solve Eq. 10-35 to find the single-particle states ϕ_i . This procedure can be iterated to obtain self-consistency.

It will be seen from Eq. 10-36 that the parameter $3t_1 + 5t_2$ determines the density dependence of the effective mass M^* , which is important for the single-particle level spacings. On the other hand, the coefficient $5t_2 - 9t_1$ of $\nabla^2\rho$ is important in determining the surface thickness. The parameter t_3 , which is the coefficient of the three-body term in Eq. 10-30, is effective in giving saturation. The free parameters of the effective interaction V are fixed by fitting the binding energy and the equilibrium density of nuclear matter, and also the binding energies, radii, and separation energies of spherical nuclei. The parameters of one such set, S3, developed at Orsay [6] are as follows:

$$t_0 = -1128.75 \text{ MeV fm}^3, \quad t_1 = 395.0 \text{ MeV fm}^5, \\ t_2 = -95.0 \text{ MeV fm}^5, \quad t_3 = 14,000.0 \text{ MeV fm}^6, \\ x_0 = 0.45, \quad \text{and} \quad W_0 = 120 \text{ MeV fm}^5. \quad (10-38)$$

The numerical values of these parameters are by no means unique, and there are other sets of values that yield equally good results. The search for better parameters is a continuing process.

These parameters have also been evaluated by Negele and Vautherin [23], starting from a realistic nuclear-matter G -matrix. All the coefficients except t_2 are in qualitative agreement with the empirical set 10-38.

Vautherin and Brink [20] are able to reproduce, with good accuracy, the experimental binding energies and rms radii of ^{16}O , ^{40}Ca , ^{48}Ca , ^{90}Zr , and ^{208}Pb . We noted in Chapter 4 that the rms charge radius of ^{48}Ca , according to electron scattering and muonic X-ray data, is almost equal to (or is slightly smaller than) that of ^{40}Ca . This particular feature is not reproduced in HF calculations in general, and even with a density-dependent interaction some discrepancy remains. The single-particle levels calculated from the density-dependent interactions in the HF framework are much less bound and in much better agreement with experimental results than the corresponding density-independent calculations, because much of the binding comes from the rearrangement potential.

A detailed comparison of the calculated and experimental single-particle energies is given by Campi and Sprung [19]. In Fig. 10-7a we reproduce, from ref. 19, the perspective plots of the calculated density distributions of some spherical nuclei; the proton density is plotted on the left, and the neutron density on the right. The small oscillations in the density distribution, with a wavelength of the order of π/k_F , which arise because of shell effects,

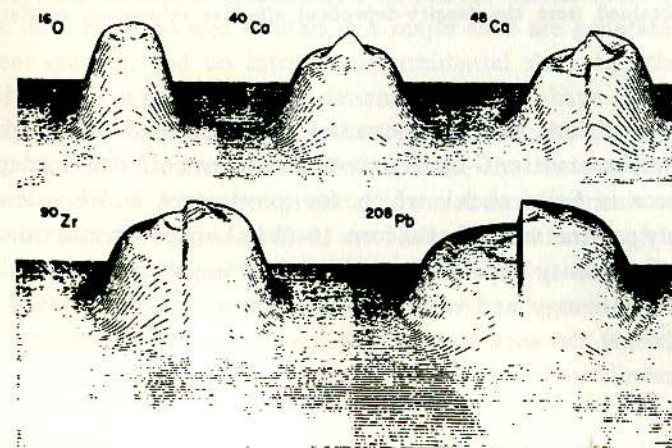


Fig. 10-7a Perspective plots of the calculated density distributions of some spherical nuclei. (After Campi and Sprung [19].)

are characteristic of HF calculations. In Fig. 10-7b we show, from ref. 15, the one-body self-consistent potential for ^{40}Ca obtained with the density-dependent effective interaction. This will be seen to be very state dependent, giving rise to charge form factors in reasonable agreement with electron-scattering data.

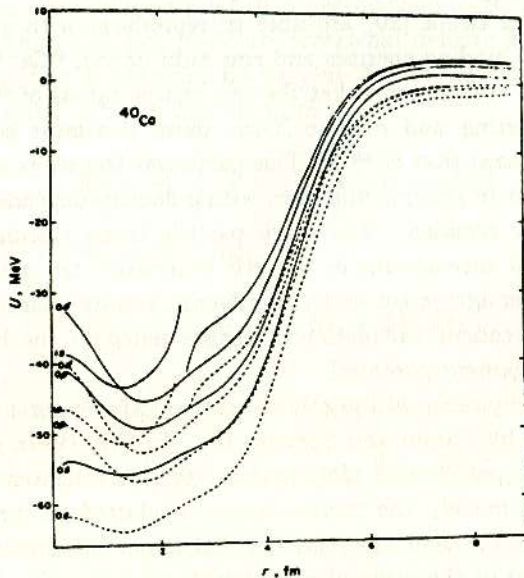


Fig. 10-7b Self-consistent single-particle proton (solid line) and neutron (dashed line) potentials obtained from the density-dependent effective interaction of Negele [15].

Summarizing these results, we can say that the local density approximation of the nuclear-matter G -matrix gives rise to a smooth density-dependent effective force in finite nuclei, which, for convenience in HF calculations, can be simply parameterized by the form 10-29 in k -space. Actual calculations show that the density dependence is of crucial importance in yielding the correct binding energy and saturation density in nuclei, and at the same time reproducing the experimental single-particle energies. Other phenomenological calculations [24] also bear out the last point.

Finally, it should be noted that the effective interaction (Eq. 10-29) has been used by Vautherin [25] to perform HF calculations in deformed nuclei, both in the $s-d$ shell and in the rare-earth region, with satisfactory results.

10-5 DEFORMED HARTREE-FOCK ORBITALS

In Section 10-4 we saw that a complete HF calculation can be done, starting with a given effective interaction V between all the particles in a nucleus, to obtain a self-consistent potential U . In this full HF approach, the single-particle states are obtained in minimizing the energy by adjusting the single-particle wave functions ϕ_i with respect to their dependence on all possible radial and angular variables. For spectroscopic calculations, however, it is often sufficient to perform a more restricted HF calculation in which the ϕ_i are taken from one major shell; their radial dependence is that of the states of a harmonic-oscillator potential which fits the size of the nucleus, and only the angular-momentum part of the orbitals is varied in order to minimize the energy. In such calculations, one is not attempting to study the saturation property of the nucleus, which is taken for granted, but is only treating the configuration interactions in a major shell, just as in a shell-model calculation.

We know that the assumption of a spherical nucleus is a reasonable approximation for the ground states of doubly closed-shell nuclei. But we have seen that, when a few particles are added to a closed core, deformation sets in and the average potential is no longer spherically symmetric. Even for the doubly closed-shell case, we cannot discount the possibility that the nuclei are deformed in some excited states. We have seen in the Nilsson model that the single-particle states can be generated in a deformed one-body potential which is chosen empirically. In the HF calculations that we will describe now, the deformed orbitals in a major shell are generated in a self-consistent manner, and an intrinsic determinantal state can then be constructed with these orbitals. After determining which shape of the nucleus is energetically most favorable, the results are compared with those of a Nilsson-type calculation. To find the nuclear spectra, the various states of total angular momentum J are then projected from such an intrinsic state.

As an example of the method, we shall describe a simple calculation by Kelson [26] for some nuclei in the $s-d$ shell which are known to have deformed shapes. At the end of this section, we shall refer to more involved and realistic calculations that have been done extensively by other groups.

In doing these calculations, it is convenient to take as a reference a closed-shell nucleus—in this particular case, ^{16}O . In the ground state of ^{16}O , it is assumed that the four $0s$ -shell orbits and twelve $0p$ -shell orbits are filled. Then ^{20}Ne , for example, can be considered to be a nucleus where four particles (two neutrons and two protons) are added in the $1s-0d$ shell orbits. In the

hypothetical situation of four noninteracting particles, these orbitals would be generated by the spherical field of the ^{16}O core; in the actual case there is some effective interaction between the four nucleons, which will modify the average field, and the orbitals should be determined self-consistently. This method is quite versatile; for example, the negative-parity states of ^{19}F can be formed by putting four nucleons in the $1s-0d$ shell orbitals, with a hole in the $0p$ -shell. To start with, we consider the simple case of ^{20}Ne .

In this model, there are only the four nucleons outside the closed core interacting with the Hamiltonian:

$$H = \sum_{\alpha, \beta} \langle \alpha | H_0 | \beta \rangle a_\alpha^\dagger a_\beta + \frac{1}{2} \sum_{\alpha, \beta, \gamma, \delta} \langle \alpha \beta | V | \gamma \delta \rangle a_\alpha^\dagger a_\beta^\dagger a_\delta a_\gamma. \quad (10-39)$$

Here H_0 is a one-body operator that represents the kinetic plus the potential energy of a particle moving in a field generated by the ^{16}O core. The single-particle j being a good quantum number in such a field, we have

$$\langle j'm' | H_0 | jm \rangle = e_j \delta_{jj'} \delta_{mm'}, \quad (10-40a)$$

where by e_j we denote the single-particle energy generated by H_0 . Since we are taking ^{16}O as the reference nucleus, the e_j 's may be considered to be the separation energies of the last neutron in ^{17}O from the various orbits, which are known to be

$$e_{d5/2} = -4.14 \text{ MeV}, \quad e_{s1/2} = -3.27 \text{ MeV}, \quad \text{and} \quad e_{d3/2} = 0.94 \text{ MeV}. \quad (10-40b)$$

In this calculation, only the e_j 's appear and the form of H_0 need not be specified. In our example, the effective interaction V is assumed to be simply a central force with Rosenfeld exchange mixture:

$$V = V_0 \frac{1}{3} (\boldsymbol{\tau}_1 \cdot \boldsymbol{\tau}_2) (0.3 + 0.7 \boldsymbol{\sigma}_1 \cdot \boldsymbol{\sigma}_2) f(r), \quad (10-41)$$

with $f(r) = e^{-r/a}/(r/a)$. The parameter a is taken as 1.37 fm, and the quantity V_0 remains adjustable. Of course, V should, in principle, be a given interaction, but in view of the numerous approximations, particularly the treatment of the ^{16}O core as inert, some flexibility in V is necessary in order to fit the experimental energy spacings. To obtain the HF orbitals and the single-particle energies, we have to apply the condition $\delta \langle \Phi_0 | H | \Phi_0 \rangle = 0$, where Φ_0 is a 4×4 determinant. As we have seen, this is equivalent to diagonalizing the single-particle operator H_{SP} in the occupied orbitals ϕ_m , ϕ_n :

$$\langle \phi_m | H_{SP} | \phi_n \rangle = \left\{ \langle \phi_m | H_0 | \phi_n \rangle + \sum_{\rho=1}^4 \langle \phi_m \phi_\rho | V | \phi_n \phi_\rho \rangle_A \right\} \delta_{mn}. \quad (10-42)$$

The HF orbitals ϕ_i are, in general, deformed, and consequently the single-particle j is no longer a good quantum number (see Sections 9-7 and 9-8). If axial symmetry is assumed, the projection Ω of j along the body-fixed symmetry axis is still a conserved quantity, and we may denote each HF orbital by $\phi_{\lambda, \Omega}$, where λ distinguishes various orbitals with the same Ω . We can then write

$$|\phi_{\lambda, \Omega} \rangle = \sum_j C_{j\Omega} |j\Omega\rangle, \quad (10-43)$$

where the coefficients $C_{j\Omega}^j$ are determined self-consistently.

In Eq. 10-43, the sum over j is restricted to the $1s-0d$ shell, and the radial dependence of the states $|j\Omega\rangle$ is taken to be that of harmonic-oscillator states, with the oscillator constant chosen to reproduce the rms radius of the nucleus. The states $|\phi_{1, \Omega}\rangle$ and $|\phi_{1, -\Omega}\rangle$ are degenerate in energy. Thus, in each self-consistent single-particle state with energy e_Ω , we can place two neutrons and two protons. Kelson [26], on doing the calculations for ^{20}Ne , found that the four extracore particles occupied the lowest deformed orbital ($\lambda = 1$), with $\Omega = \pm \frac{1}{2}$. For $V_0 = 50$ MeV, the structure of the HF orbital is

$$|\phi_{1, 1/2} \rangle = 0.71 |0d_{5/2}; \frac{1}{2}\rangle - 0.39 |0d_{3/2}; \frac{1}{2}\rangle + 0.58 |1s_{1/2}; \frac{1}{2}\rangle, \quad (10-44)$$

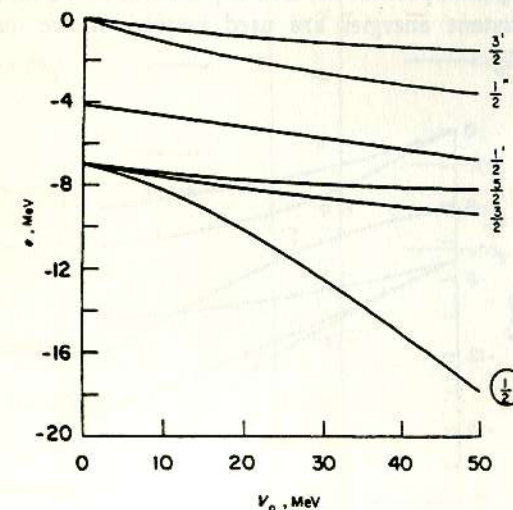


Fig. 10-8 The calculated single-particle self-consistent energies for ^{20}Ne , as a function of the strength V_0 of the attractive effective interaction. The single-particle energies e_j obtained from H_0 (Eq. 10-40) are taken to be somewhat different from those given in the text. Only the lowest $\Omega = \frac{1}{2}$ level is occupied by four nucleons. (After Kelson [26].)

which is quite similar to the Nilsson wave function. Figure 10-8 shows a plot of the self-consistent energies e_Ω for the HF orbitals as functions of the strength V_0 of the effective interaction. These energies are eigenvalues of a single-particle operator $H_{SP} = t + U$, where U is the self-consistent potential with the lowest $\Omega = \pm \frac{1}{2}$ levels occupied by four particles. It will be seen that, as V_0 increases, a marked gap appears between the occupied and the unoccupied levels. For a reasonable strength $V_0 = 50$ MeV, the gap is nearly 10 MeV. Qualitatively, this large gap indicates that it becomes increasingly difficult to promote particles from the occupied to the empty orbitals, making the deformed intrinsic state $|\Phi_{1,1/2}\rangle$ stable against vibrations as V_0 increases. We should remember, however, that if two particles are promoted to the $\Omega = \frac{3}{2}$ orbit the self-consistent potential U is no longer the same, with the result that the spectrum displayed in Fig. 10-8 will be modified. In general, the gap in this configuration between the $\Omega = \frac{1}{2}$ and the $\Omega = \frac{3}{2}$ levels will be less than that indicated by Fig. 10-8.

The energy levels shown in Fig. 10-8 have some similarity with the Nilsson levels of Fig. 9-28, which are plotted against the deformation parameter η . For $\eta = 2$, we get the same level ordering in the Nilsson levels as in Fig. 10-8, but the gap between the occupied and unoccupied levels in this case is less than 2 MeV. This has important effects in the calculation of the moment-of-inertia parameter, and improves the results of the cranking model if self-consistent energies are used instead of the energies of the Nilsson orbitals [27].

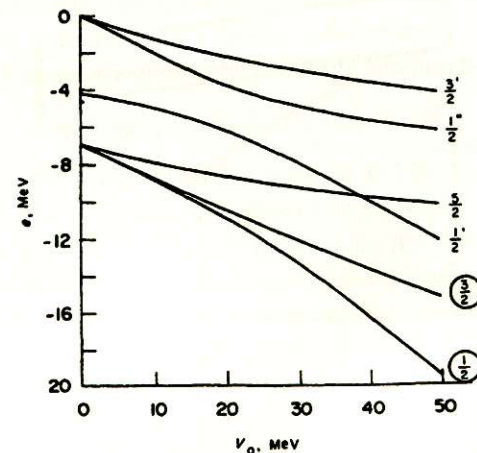


Fig. 10-9 The calculated self-consistent single-particle energies for ^{24}Mg as a function of the strength V_0 of the effective interaction, for the axially symmetric solution. Now the lowest $\Omega = \frac{1}{2}$ and $\frac{3}{2}$ levels are occupied. (After Kelson [26].)

Another important difference from the Nilsson model becomes apparent on examining the axially symmetric solution of ^{24}Mg . In Fig. 10-9 we have plotted the self-consistent single-particle energies of ^{24}Mg as a function of the strength V_0 of the effective interaction. In this case, the lowest two levels, with $\Omega = \pm \frac{1}{2}$ and $\Omega = \pm \frac{3}{2}$, are occupied by the eight extracore particles. For $V_0 = 50$ MeV, the $\Omega = \frac{1}{2}$ level is depressed only by about 2 MeV from its ^{20}Ne value, but the now-occupied $\Omega = \frac{3}{2}$ level has changed considerably, from about -8 MeV in ^{20}Ne to nearly -15 MeV in ^{24}Mg . This shows a very important characteristic of the self-consistent calculations, namely, the energy of a single-particle level is depressed markedly as it is occupied by more and more particles. This is due to the strong mutual attraction between particles in the same orbit. In the Nilsson model, this effect is nearly completely neglected, and the levels shift only slightly because of small changes in the equilibrium deformation of the nucleus.

Another important feature of the axially symmetric ^{24}Mg case is that the gap between the last occupied $\Omega = \frac{3}{2}$ level and the next unoccupied $\Omega = \frac{1}{2}$

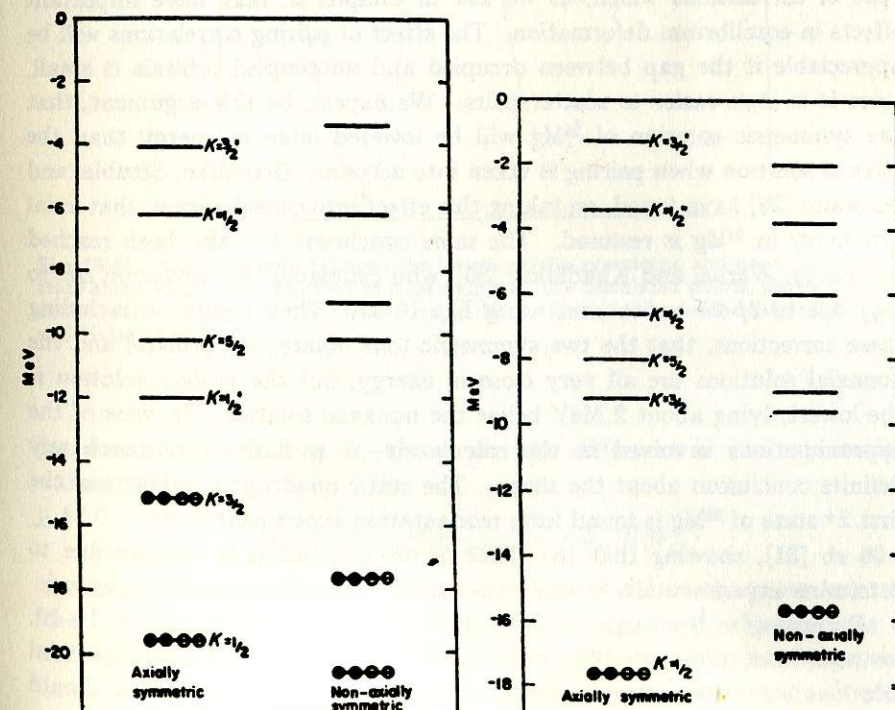


Fig. 10-10 A comparison of the calculated self-consistent single-particle energies for the axially symmetric and the nonaxial solutions: (a) ^{20}Ne , and (b) ^{24}Mg . (After Bar-Touv and Kelson [28].)

level is only about 3 MeV, in contrast to the gap of 10 MeV in ^{20}Ne . This suggests that the axially symmetric HF solution for ^{24}Mg is less stable than the one obtained for ^{20}Ne , since in mixing states of different Ω we create a state that does not have axial symmetry. Bar-Touv and Kelson [28], on doing a HF calculation without imposing the restriction of axial symmetry, found that a solution slightly lower in energy was obtained for an ellipsoidal shape with unequal axes.

In Fig. 10-10 we show the single-particle self-consistent spectra of ^{20}Ne and ^{24}Mg for both the axially symmetric and ellipsoidal shapes. Whereas for ^{20}Ne the axially symmetric shape is energetically favored, it is reversed for ^{24}Mg . There is also a larger gap between the occupied and empty single-particle levels in the triaxial solution than in the symmetric one. From this type of calculation, it would be concluded that the ground state of ^{24}Mg is asymmetric.

A note of caution must be added at this point about taking these results literally. We shall see shortly that HF calculations leave out the pairing type of correlations which, as we saw in Chapter 9, may have important effects in equilibrium deformation. The effect of pairing correlations will be appreciable if the gap between occupied and unoccupied orbitals is small, since it is then easier to scatter pairs. We expect, by this argument, that the symmetric solution of ^{24}Mg will be lowered more in energy than the triaxial solution when pairing is taken into account. Goodman, Struble, and Goswami [29] have found, on taking this effect into consideration, that axial symmetry in ^{24}Mg is restored. The same conclusion has also been reached by Gunye, Warke, and Khadkikar [30], who estimated the correction ΔE to E_{HF} due to $2p-2h$ excitations, using Eq. 10-25. They found, on including these corrections, that the two symmetric (one oblate, one prolate) and the nonaxial solutions are all very close in energy, but the prolate solution is the lowest, lying about 2 MeV below the nonaxial solution. In view of the approximations involved in the calculation, it is difficult to reach any definite conclusion about the shape. The static quadrupole moment of the first 2^+ state of ^{24}Mg is found from reorientation experiment to be -0.24 ± 0.06 eb [31], showing that the shape is prolate, but it is not possible to determine experimentally whether the shape is triaxial or axially symmetric.

Returning to the single-particle spectrum of ^{20}Ne or ^{24}Mg in Fig. 10-10, we note that, although the lowest axially symmetric and the ellipsoidal solutions are rather close in energy, this does not mean that there should be two *low-lying* 0^+ states; these two solutions are not orthogonal to each other, having been generated by two different single-particle Hamiltonians.

In fact, the close proximity of two such solutions may indicate that there is considerable overlap between these states. It is possible, however, to do "shape-mixing" calculations with nonorthogonal states, a point that we shall discuss in the next section.

Bar-Touv and Kelson [28] have done the HF calculations for all even-even nuclei in the $s-d$ shell by removing the restriction of axial symmetry. Usually, more than one stationary intrinsic state exists, and there is competition between the lowest axially symmetric and nonaxially symmetric

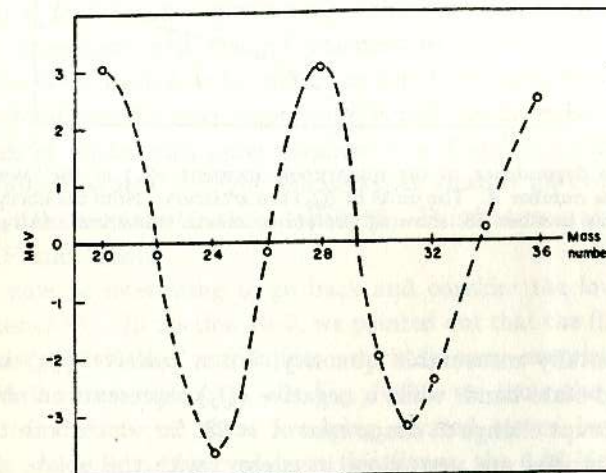


Fig. 10-11 The difference between the lowest axially symmetric and nonaxial intrinsic state energies, ΔE , as a function of mass number. The calculated points, shown by open circles, are joined by a dotted line to display the regularity of the curve. (After Bar-Touv and Kelson [28].)

intrinsic states. In Fig. 10-11 we plot the difference in the expectation values of H :

$$\Delta E = \langle \Phi_{\text{nonax}} | H | \Phi_{\text{nonax}} \rangle - \langle \Phi_{\text{ax}} | H | \Phi_{\text{ax}} \rangle$$

against the mass number A . Negative values of ΔE on the curve indicate that an axially asymmetric state is energetically favored. Two regions of axial asymmetry, around ^{24}Mg and ^{32}S , are clearly seen. An interesting result is shown in Fig. 10-12, where the expectation value of the mass quadrupole moment operator Q , with respect to the energetically lowest intrinsic state, is plotted against the mass number. This, of course, does not correspond to

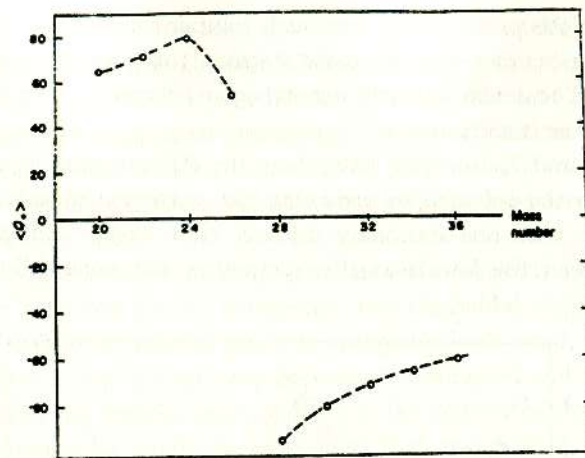


Fig. 10-12 The dependence of the quadrupole moment $\langle Q_0 \rangle$ of the lowest intrinsic state on the mass number A . The units of $\langle Q_0 \rangle$ are arbitrary. Note the abrupt change of sign around mass number 28, showing prolate to oblate transition. (After Bar-Touv and Kelson [28].)

any experimentally measurable quantity, but a positive $\langle Q_0 \rangle$ indicates a prolate ground-state band, while a negative $\langle Q_0 \rangle$ represents an oblate band. There is an abrupt change in shape near $A = 28$, for which both the prolate and oblate solutions are very close in energy, with the oblate shape only slightly lower.

It should be realized that in HF calculations of this type, in which only the particles in the $s-d$ shell are assumed to interact with an effective central interaction V (Eq. 10-41), it is not very reasonable to take the spin-orbit splitting between the $d_{5/2}$ - and $d_{3/2}$ -states from ^{19}O , as given in Eq. 10-40b. This spin-orbit splitting is likely to be modified by the noncentral interactions between the pairs of particles in the $s-d$ shell; therefore, if one takes a central interaction V as in Eq. 10-41, the $d_{5/2}-d_{3/2}$ input energies can be varied within reasonable limits to obtain the best result. In the case of ^{28}Si , the prolate-oblate energy difference is found to be very sensitive to the strength of the one-body spin-orbit force, the oblate solution being slightly lower in energy with reasonable values of the spin-orbit parameter. With more realistic effective interactions V containing noncentral components of force (like the Kuo-Brown G -matrix elements), it is reasonable to take the values of e_i given in Eq. 10-40b for the field of the core nucleons, and the oblate solution is then nearly 5 MeV lower in energy than the prolate one [30a]. Das Gupta

and Harvey [30b] have pointed out that the lowest oblate and prolate solutions in ^{28}Si are orthogonal to each other, and that the ground state and the lowest few states of ^{28}Si are generated from rotations or particle-hole excitations of the oblate intrinsic state, while the 0^+ state at 6.69 MeV is the band head of the prolate intrinsic state. The static quadrupole moment Q_{2+} of the first excited 2^+ state of ^{28}Si has been measured to be $0.17 \pm 0.05 \text{ eb}$ [31, 32], corresponding to an oblate shape,[†] in agreement with this calculation.

The position of the Fermi level in a nucleus can be obtained from experimental data by measuring the separation energy of a neutron from the top level. This is found to be substantially constant throughout the $s-d$ shell, a result in agreement with the HF calculations of Bar-Touv and Kelson. For an even-even nucleus with mass number A , the gap between the last occupied orbital and the next empty level is just the difference between the Fermi levels of nuclei with mass numbers $A + 1$ and A . Experimentally, this gap is about 10 MeV for ^{20}Ne , and decreases steadily for even-even nuclei as more particles are added in the $s-d$ shell [33]. This feature is also reproduced in these HF calculations.

It will now be interesting to go back and consider the low-lying even-parity states of ^{16}O . In Section 10-2, we pointed out that the first 0^+ excited state comes at 6.06-MeV excitation, which is very surprising from the spherical-shell-model viewpoint. In Fig. 10-13, we show the experimental evidence that certain of these low-lying excited states form rotational bands [34]. As will be observed from this figure, the 6.06-MeV 0^+ state is the band head of an even-parity rotational band, suggesting a deformed rotating nucleus in the excited states, although the ground state is spherical. If we turn back to the Nilsson diagram of Fig. 9-28, we find that, although there is a large gap of about 11.5 MeV between the occupied $0p_{1/2}$ - and the empty $0d_{5/2}$ -levels for the spherical shape, this gap decreases sharply as deformation sets in. To generate the even-parity excited states of ^{16}O , it is necessary to promote an even number of nucleons from the filled to the empty orbits. From the HF point of view, it is conceivable that, when this is done, the self-consistent field becomes highly deformed and much less energy is required to generate these excited states.

It is natural, therefore, to attempt a HF calculation in which the positive-parity intrinsic states are built from $2p-2h$ (two particle-two hole) and $4p-4h$ states. We have already noted a characteristic feature of HF calculations, in that a self-consistent orbital (in this case the lowest $\Omega = \frac{1}{2}^+$ orbit

[†]Note, from Eq. 9-110, that the intrinsic and static quadrupole moments have opposite signs for a given shape in the rotation-model approximation.

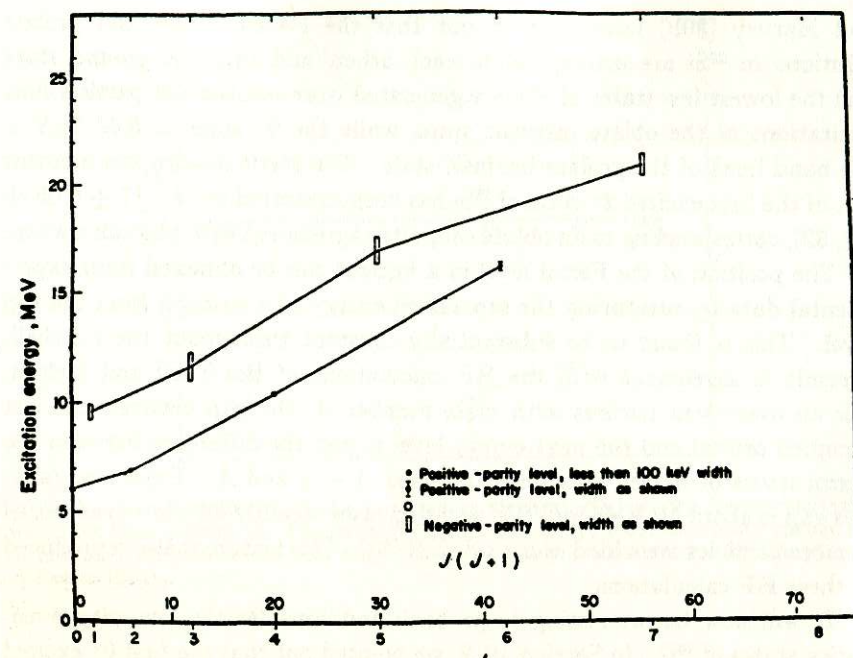


Fig. 10-13 States in ^{16}O excited strongly in the elastic scattering of α -particles by ^{12}C lie on a rotational band. (After Carter et al. [34].)

in the s - d shell) is sharply depressed as it is occupied by more and more particles. It may be possible, then, that the $4p\text{-}4h$ states are energetically more favored than the $2p\text{-}2h$ ones, since the gap between the occupied and empty orbitals is decreased drastically (see Fig. 9-28) for positive η . This has been demonstrated in a HF calculation by Bassichis and Ripka [35], assuming axially symmetric shape. In their calculation, they assumed an effective interaction V as given in Eq. 10-41, with a Gaussian form for $f(r)$. This calculation is very similar to the one on ^{20}Ne that we have described, except that instead of four particles in the s - d shell there are now two particles in the s - d shell and two holes in the p -shell with respect to the ground state ^{16}O configuration.

The lowest $4p\text{-}4h$ intrinsic state is the one in which the four particles are in the lowest $\Omega = \frac{1}{2}^+$ orbit and the four holes are in the highest $\Omega = \frac{1}{2}^-$ orbit, and this has isospin $T = 0$. In Fig. 10-14, we plot the energies of this intrinsic $4p\text{-}4h$ state and one of the $2p\text{-}2h$ intrinsic states obtained from the HF calculation, relative to the ground state, as functions of the strength V_0 .

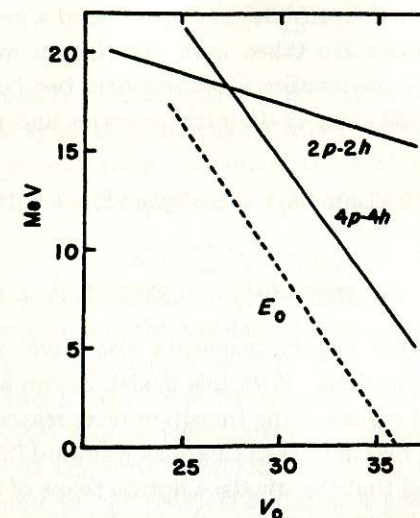


Fig. 10-14 The energies of the lowest $4p\text{-}4h$ and one of the $2p\text{-}2h$ intrinsic states of ^{16}O , relative to the ground state, plotted as a function of V_0 , the effective interaction. The position of the projected band head of the even-parity rotational band is shown by the dotted line. (After Bassichis and Ripka [35].)

of the effective interaction. The dotted line shows the position of the head of the rotational band based on the $4p\text{-}4h$ intrinsic state. It has been obtained by projecting out the 0^+ state from the intrinsic state, and experimentally its position is at 6.06 MeV. We shall indicate presently how this projection can be done in a simple-minded manner. It will be seen that, for $V_0 = 32$ MeV, the experimental position of the band head is reproduced. It is interesting to note that with a Gaussian interaction this value of V_0 is also close to what would be required to reproduce the ^{20}Ne spectrum. Thus the $4p\text{-}4h$ intrinsic state, which is well isolated from the $2p\text{-}2h$ ones, gives rise to a rotational band.

In the simplified analysis just described, the impression was given that the 6.06-MeV 0^+ state is the band head of a pure $4p\text{-}4h$ intrinsic HF state. If one goes one step further than the HF approximation, the residual interaction ($V - U$) will cause some mixing between the $0p\text{-}0h$, $2p\text{-}2h$, and $4p\text{-}4h$ configurations in all the low-lying even-parity states of ^{16}O . That there is some admixture of deformed orbitals even in the ground state is seen from the rather large $B(E2)$ -transition value of $4.6 \pm 1 e^2 \text{ fm}^4$ between the 6.92-MeV 2^+ state and the 0^+ ground state (see Fig. 10-5). To estimate the amount

of this mixing, Brown and Green [36] have performed a calculation in which the single-particle orbitals are taken from the Nilsson model, rather than self-consistently. They diagonalize a semirealistic two-body interaction in the space of $0p\text{-}0h$, $2p\text{-}2h$, and $4p\text{-}4h$ intrinsic states and find, for example, that

$$|0^+, 0 \text{ MeV}\rangle = 0.87|(0p\text{-}0h)\rangle + 0.47|(2p\text{-}2h)\rangle + 0.13|(4p\text{-}4h)\rangle$$

and

$$|0^+, 6.06 \text{ MeV}\rangle = -0.26|(0p\text{-}0h)\rangle + 0.23|(2p\text{-}2h)\rangle + 0.94|(4p\text{-}4h)\rangle.$$

Similarly, states of other angular momenta also have admixtures of the various intrinsic configurations. With this model, Brown and Green are able to fit the experimental values of the transition rates reasonably well.

We should mention that in later calculations Hayward [37] and Stephenson and Banerjee [38] found that the triaxial elliptical shape of the $4p\text{-}4h$ intrinsic state has considerably lower energy than the axially symmetric case discussed above. The reason for the triaxial shape may be understood in a simple manner by the following argument. If only four particles in the $s\text{-}d$ shell (as in ^{20}Ne) are considered, an axially symmetric prolate shape is obtained. Likewise, by considering four-hole states (as in ^{12}C), an axially symmetric oblate shape is obtained. In $4p\text{-}4h$ states of ^{16}O , these two intrinsic states are locked together at right angles to each other by the attractive particle-hole interaction, giving rise to maximum overlap between the prolate and oblate shapes, and yielding a triaxial intrinsic state which generates the rotational band. These assertions are confirmed by the detailed calculations of Engeland and Ellis, as well as de Takacsy and Das Gupta [38].

10-6 PROJECTION OF ANGULAR-MOMENTUM STATES FROM THE INTRINSIC STATE

The HF wave function $|\Phi\rangle$, being a product of single-particle orbitals, is not in general an eigenstate of the operator J^2 , where J is the total angular momentum of the state. For example, we have seen that, when there are some extra particles outside the closed core, the self-consistent potential U is deformed rather than spherically symmetric in space. This implies that the shape of the HF density distribution is also deformed, that is, it has a preferred direction in space with reference to a space-fixed system of axes. Thus rotational invariance has been lost in the HF approximation, and the deformed solution $|\Phi\rangle$ cannot be an eigenstate of J^2 . This is not at all satisfactory, since the total Hamiltonian

$$H = \sum_i t_i + \sum_{i < j} V_{ij}$$

is certainly rotationally invariant, and a physical state should have good J . In the case of axial symmetry, although J is not conserved in the HF approximation, its projection along the symmetry axis is still conserved; we denote this quantum number by

$$K = \sum_i \Omega_i = \langle J_z \rangle,$$

where Ω_i is the projection of the angular momentum of the i th particle along the symmetry axis. For example, in ^{20}Ne , four nucleons are placed in the $\Omega = \pm \frac{1}{2}$ orbits, and $K = 0$. The HF intrinsic state $|\Phi\rangle$ here represents a superposition of states with various values of J , but each of these has $K = 0$. Mathematically, it is tempting to project out of $|\Phi\rangle$ the states with good J and to identify these as the physical states of a given K -band. How can this procedure be justified on variational grounds (on which the HF approximation is based); moreover, under what circumstances can we expect to get a rotational band?

These questions have been examined by Hill and Wheeler [39] and by Peierls and Yoccoz [40]. The point to note is that for a deformed well U there is a directional degeneracy in the HF energy E_{HF} , since any orientation of the well in space generates a HF wave function with the same value of E_{HF} . In Chapter 9, we saw that the orientation of a body-fixed frame with respect to a space-fixed axis can be specified by three Euler angles θ_i , with $i = 1, 2$, and 3. Let $|\Phi_K\rangle$ be the HF solution for a given orientation of U ; then, for a different orientation, $R(\theta_i)|\Phi_K\rangle$ will be the HF solution with the same energy E_{HF} , where $R(\theta_i)$ is a rotation operator defined by Eq. A-47. We can take advantage of this directional degeneracy by constructing a trial wave function that is a linear combination of these degenerate wave functions with a given K , the coefficients being determined by the variational procedure of minimizing the energy. More specifically, we define a function $|\Psi_K^\alpha\rangle$, with an as yet unspecified quantum number α :

$$|\Psi_K^\alpha\rangle = \int f_K^\alpha(\theta_i) R(\theta_i) |\Phi_K\rangle \sin \theta_2 d\theta_2 d\theta_1 d\theta_3,$$

where the limits of θ_2 are from 0 to π , and θ_1, θ_3 extend from 0 to 2π . The trial wave function $|\Psi_K^\alpha\rangle$ is a superposition of all the degenerate HF solutions over all possible orientations, with the coefficients f_K^α to be determined. Since the state $|\Psi_K^\alpha\rangle$ has no preferred direction in space, it is rotationally

invariant. It is therefore possible for this to be an eigenstate of J^2 and J_z of the space-fixed axes, and we may write

$$|\Psi_{MK}^J\rangle = \int f_{MK}^J(\theta_i) R(\theta_i) |\Phi_K\rangle d\Omega, \quad (10-45)$$

where, in shorthand notation, we have put $d\Omega$ for $\sin \theta_2 d\theta_2 d\theta_1 d\theta_3$, with the limits of integration as specified above. The coefficients $f_{MK}^J(\theta_i)$ are to be determined by demanding that $\langle \Psi_{MK}^J | H | \Psi_{MK}^J \rangle / \langle \Psi_{MK}^J | \Psi_{MK}^J \rangle$ be stationary with respect to variations δf_{MK}^J , where H is the total Hamiltonian. It can be shown[†] that, to satisfy this requirement, f_{MK}^J is simply $\mathcal{D}_{MK}^J(\theta_i)$, as defined in Eq. A-53. We thus obtain

$$|\Psi_{MK}^J\rangle = \int \mathcal{D}_{MK}^J(\theta_i) R(\theta_i) |\Phi_K\rangle d\Omega. \quad (10-46)$$

To understand the physical significance of Eq. 10-46, consider the intrinsic wave function $|\Phi_K\rangle$ in the body-fixed axes, which may be expressed as a linear combination of good angular momentum states $|\Phi_{K'}^{J'}\rangle$:

$$|\Phi_K\rangle = \sum J' C_{J'} |\Phi_{K'}^{J'}\rangle. \quad (10-47)$$

If we want to express the same wave function in a rotated frame, we apply an appropriate rotation operator $R(\theta_i)$, obtaining, from Eq. A-50,

$$R(\theta_i) |\Phi_K\rangle = \sum J' \sum M' \mathcal{D}_{M'K}^{J'*}(\theta_i) |\Phi_{M'}^{J'}\rangle.$$

Substituting this in Eq. 10-46 yields

$$\begin{aligned} |\Psi_{MK}^J\rangle &= \sum_{J', M'} C_{J'} |\Phi_{M'}^{J'}\rangle \int \mathcal{D}_{MK}^{J*}(\theta_i) \mathcal{D}_{M'K}^{J'*}(\theta_i) d\Omega \\ &= \frac{8\pi^2}{2J+1} C_J |\Phi_M^{J'}\rangle, \end{aligned} \quad (10-48)$$

showing that the Peierls-Yoccoz wave function is essentially the projection of $|\Phi_K\rangle$ with angular momentum J . We have thus justified the projection procedure on a variational basis. Since the total Hamiltonian H commutes with J^2 , we can write the energy of the state with (J, K) as

$$E_{JK} = \frac{\langle \Psi_{MK}^J | H | \Psi_{MK}^J \rangle}{\langle \Psi_{MK}^J | \Psi_{MK}^J \rangle} = \frac{\langle \Phi_K | H | \Psi_{MK}^J \rangle}{\langle \Phi_K | \Psi_{MK}^J \rangle}. \quad (10-49)$$

[†] For the gory details in a simple two-dimensional model, see G. E. Brown, *Unified Theory of Models and Forces*, North-Holland, Amsterdam, 1967, p. 64.

Noting that the energy cannot depend on the choice of the space-fixed z -axis (i.e., the quantum number M), we can write

$$\begin{aligned} E_{JK} &= \frac{\langle \Phi_K | H | \Psi_{KK}^J \rangle}{\langle \Phi_K | \Psi_{KK}^J \rangle} \\ &= \frac{\int_0^\pi d\theta_2 \sin \theta_2 d_{KK}^J(\theta_2) \langle \Phi_K | H \exp(-i\theta_2 J_2) | \Phi_K \rangle}{\int_0^\pi d\theta_2 \sin \theta_2 d_{KK}^J(\theta_2) \langle \Phi_K | \exp(-i\theta_2 J_2) | \Phi_K \rangle}, \end{aligned} \quad (10-50)$$

where we have used Eqs. 10-46 and A-53.

The next question to answer is whether the E_J 's in a given K -band form a rotational spectrum. If the wave function $|\Phi_K\rangle$ belongs to a well of large anisotropy, its overlap with $\exp(-i\theta_2 J_2) |\Phi_K\rangle$, an intrinsic state of a different orientation, is small unless the directions are nearly the same, that is, $\theta_2 = 0$ or π . Thus the overlap function $\langle \Phi_K | \exp(-i\theta_2 J_2) | \Phi_K \rangle$ as a function of θ_2 is expected to peak sharply about $\theta_2 = 0$ and π for a well-deformed well. A similar property may be assumed to be valid for the energy-overlap integral $\langle \Phi_K | H \exp(-i\theta_2 J_2) | \Phi_K \rangle$, since H operates on at most two particles simultaneously, so that for the remaining particles we have just the overlap of the intrinsic parts at different orientations. Under these conditions, Yoccoz [41] and Verhaar [42] have shown[†] that Eq. 10-50 gives rise to a rotational band for a given K , including the special case for $K = \frac{1}{2}$.

Bassichis, Giraud, and Ripka [43] applied Eq. 10-50 for the calculation of E_J for the light $s-d$ shell nuclei, using the lowest $K = 0$ intrinsic state and evaluating the overlap integrals numerically. In Fig. 10-15 we show their calculated overlap function $\langle \Phi_{K=0} | \exp(-i\theta_2 J_2) | \Phi_{K=0} \rangle$ as a function of θ_2 for ${}^{20}\text{Ne}$ and note that it does peak at $\theta_2 = 0$ and $\theta_2 = \pi$. Figure 10-16 reproduces the spectrum of ${}^{20}\text{Ne}$ as obtained by Macfarlane and Shukla [44]; column (a) is the result of projection from the lowest $K = 0$ intrinsic state. In this calculation, the interaction V given by Eq. 10-41 was used with a Yukawa form for $f(r)$, with range parameter $a = 1.37$ fm, $V_0 = -50$ MeV, and the oscillator constant $b = \hbar/M\omega = 1.65$ fm for the basis states. The input single-particle energies were taken to be $e(d_{5/2}) = -7.0$ MeV, $e(s_{1/2}) = -4.2$ MeV, and $e(d_{3/2}) = 0$. In column (d) of Fig. 10-16, the experimental positive-parity states of predominant configuration $(0d, 1s)^4$ in this energy range are shown for comparison. It will be seen that the projection from

[†] Note that for θ_2 close to zero one can write

$$d_{KK}^J(\theta_2) = 1 - \frac{1}{2}[J(J+1) - K^2]\theta_2^2 + \dots,$$

which, when inserted into Eq. 10-50, gives rise to a rotational spectrum to leading order.

the lowest $K = 0$ intrinsic state yields only five of the eight experimental levels, whereas a complete shell-model calculation with the same interaction, whose spectrum is shown in Fig. 10-16c, does not suffer from this deficiency. This indicates that other low-lying intrinsic states play a part in the description of these levels. We then inquire as to how to include the effects of the other intrinsic states in a more complete calculation.

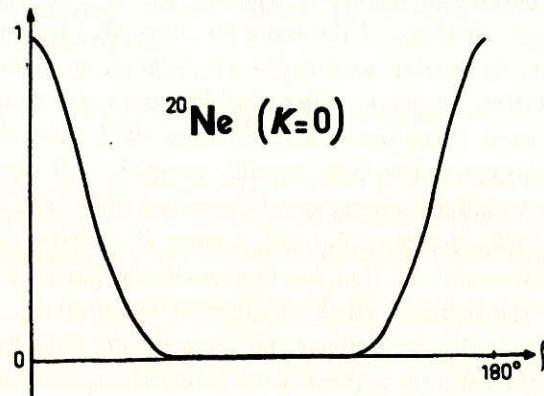


Fig. 10-15 The overlap function $\langle \Phi_K | \exp(-i\theta_2 J_2) | \Phi_K \rangle$ for ^{20}Ne , using the HF intrinsic state for $K = 0$, as a function of the Euler angle θ_2 . (After Ripka [33].)

We have already seen that for a given nucleus many solutions (i.e., intrinsic states) of the HF equation can be obtained by filling up different sets of orbitals, or by imposing different symmetries (i.e., axial or nonaxial shapes). For ^{20}Ne , five solutions of the HF equation are known [45]. Of these, four have axial symmetry—two are prolate and two oblate—and one is axially asymmetric. The lowest intrinsic state has a prolate shape and gives rise to the spectrum shown in Fig. 10-16a. In ^{28}Si the situation is even more complicated. Ripka [33] lists eight different solutions lying between $E_{\text{HF}} = -123$ and -124.44 MeV. In ^{24}Mg , we have seen that there are solutions corresponding to axially symmetric and triaxial ellipsoidal shapes, which are close in energy. In addition to these, other intrinsic states can be generated by filling up different orbitals, e.g. taking $1p-1h$ configurations based on the lowest intrinsic state. The point to note is that all these different intrinsic

states of a nucleus need not be orthogonal to each other, because they are not eigenstates of the same Hamiltonian.[†] This is so since the HF Hamiltonian

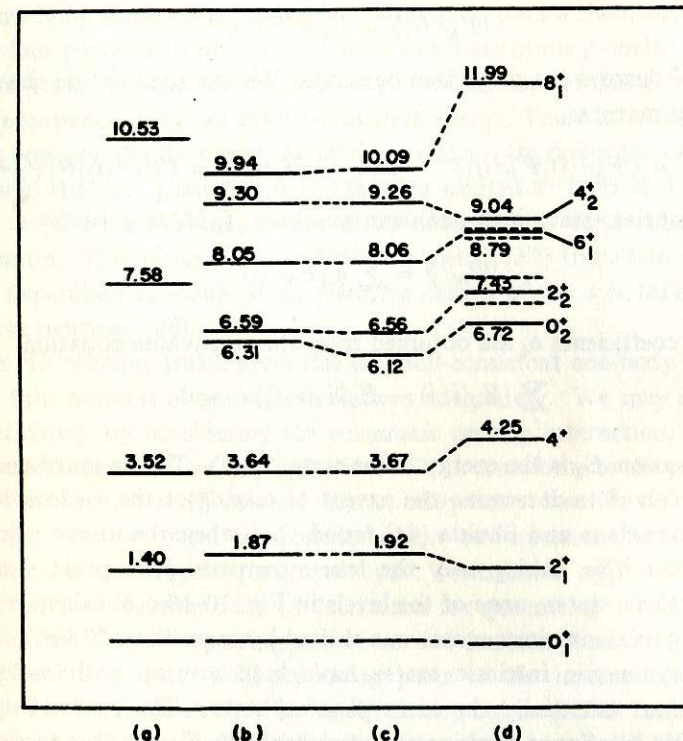


Fig. 10-16 Energy levels of ^{20}Ne : (a) the spectrum obtained from the lowest single intrinsic HF state; (b) the result of a shape-mixing calculation; (c) the spectrum of an exact shell-model calculation in the $(s, d)^4$ configuration; (d) the experimental spectrum. (After Macfarlane and Shukla [44].)

changes, through the one-body potential U , as the occupied orbitals are changed. Hence different intrinsic states, when they correspond to various local minima in a narrow energy region, cannot be interpreted as the different

[†] Under special conditions, of course, it is possible for two different intrinsic states to be strictly orthogonal. For example, in ^{19}F , the ground state is the band head of a positive-parity $K = \frac{1}{2}$ band, while the $\frac{1}{2}^-$ state at 0.110 MeV originates from the intrinsic state of negative parity with $K = \frac{1}{2}$.

excited states of the nucleus. In this case, there will be appreciable mixing of the intrinsic states via the effective interaction. We now illustrate this phenomenon by considering ^{20}Ne [44].

Let us denote the i th intrinsic state by $|\Phi(i)\rangle$. We can generate the states of good angular momentum J by the projection technique described earlier:

$$|\Psi_{M^J}(i)\rangle = P_{M^J}|\Phi(i)\rangle,$$

where P_{M^J} denotes the projection operator. We can then define the overlap and energy matrices,

$$N_J(i, j) = \langle \Psi_{M^J}(i) | \Psi_{M^J}(j) \rangle \quad \text{and} \quad H_J(i, j) = \langle \Psi_{M^J}(i) | H | \Psi_{M^J}(j) \rangle.$$

Then the nuclear state with quantum numbers (J, M) is given by

$$|\Psi_{M^J}\rangle = \sum_i a_i |\Psi_{M^J}(i)\rangle,$$

where the coefficients a_i are obtained from the eigenvalue equation

$$\sum_j [H_J(i, j) - E_J N_J(i, j)] a_j = 0.$$

In this equation, E_J is the energy of the state $|\Psi_{M^J}\rangle$. Thus a matrix equation has to be solved to determine the extent of mixing of the various intrinsic states. Macfarlane and Shukla [44] found that when the above calculation was done for ^{20}Ne , taking only the four symmetric (two prolate and two oblate) intrinsic states, none of the levels in Fig. 10-16a (obtained from just the lowest prolate intrinsic state) was shifted by more than 20 keV. In fact, all these symmetric intrinsic states have high overlap with each other; they represent essentially the same physical state. The nonaxial intrinsic state in ^{20}Ne is a linear combination of states with $K = 0, 2$, and 4 . When these states are mixed with the lowest prolate solution, significant improvement to the energy spectrum is obtained. Figure 10-16b shows the spectrum obtained by doing a mixing calculation with the lowest prolate, the nonaxial state ($K = 0$ and $K = 4$ components only), and five $1p-1h$ intrinsic states with $K = 0$ and 2 , based on the lowest prolate solution. Now the agreement with the shell-model calculation is excellent, and all the experimental levels believed to be coming from the $(0d, 1s)^4$ configuration have been reproduced.

We can now see that, in addition to the lowest intrinsic HF state, some others may also play an important part in the description of the nuclear states. This type of shape-mixing calculation may be of particular importance in ^{28}Si , where the projected spectrum from the lowest oblate intrinsic state is far too compressed in comparison with the experimental values.

We shall now make some comments about the even-parity states of ^{18}O , which we discussed in the simple shell-model picture in Section 10-2. It was noted that the experimental data indicated the ^{16}O core to be playing an active role in the description of even the low-lying states. We now realize that in the HF picture there should be two distinct intrinsic states describing these low-lying levels: one having two particles in the $s-d$ shell, and the other having four particles in the $s-d$ shell, with two holes in the p -shell. The latter intrinsic state, because of the increased deformation of the orbitals with higher occupancy, may not cost too much in energy. There is, of course, some mixing between the $2p$ and $4p-2h$ intrinsic states. On doing the calculation, it is found that the ground state 0^+ , the first excited 2^+ (1.98 MeV), and the second 0^+ (3.63 MeV) are mainly of $2p$ -nature, with some admixture of $4p-2h$ states. This admixture is sufficient to yield $B(E2)$ -transition rates close to the experimental values if an effective charge of $0.5 e$ is taken for the extracore neutrons [46].

The HF scheme, which gives rise to a self-consistent one-body potential, cannot take account of pairing correlations adequately. We may appreciate this deficiency by considering the schematic pairing interaction, with constant matrix element $G = \langle ii|V|jj\rangle$. Since G can contribute to the potential U only when $i = j$, the HF method cannot adequately describe pairing. This is not the case for other components of the two-nucleon interaction; for example, the quadrupole-quadrupole part contributes appreciably to U , giving rise to a deformation. A formalism for generating a self-consistent potential that treats the pairing part of the two-nucleon potential on an equal footing with the other field-producing parts of the interaction has been developed; this is called the Hartree-Fock-Bogolubov (HFB) formalism.[†]

Without going into any details of this method, we would like to draw attention to two effects of pairing correlations that are particularly relevant in affecting the HF results. First, depending on the gap between the occupied and empty single-particle states, some solutions of the HF equation may gain more energy from the pairing correlations than others, altering the symmetry of the ground-state band. This is possible because the various HF intrinsic states may differ very little in energy. As an example, we have noted that pairing correlations seem to restore axial symmetry in the ground-state band of ^{24}Mg . Second, when a HF calculation is done without taking pairing effects into account, it is often found that the projected spectra, although

[†] See, for example, the article "Theory of Finite Nuclei," by M. Baranger, in 1962 *Carg  e Lectures in Theoretical Physics*, Benjamin, New York, 1963.

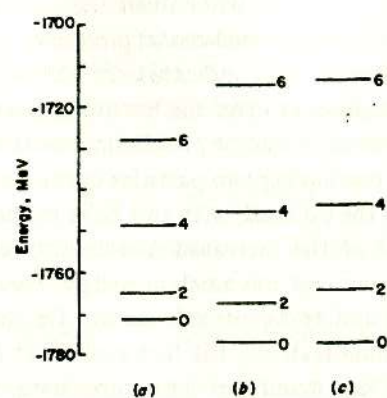


Fig. 10-17 The experimental energy spectrum of ^{22}Ne is shown in column (c). The energy spectra shown in columns (a) and (b) are computed in a space of the first four major oscillator shells by projecting good angular momentum states from the intrinsic HF and HFB states, respectively. The absolute energy scale (in MeV) is given at the left of the figure. (After Gunye and Khadkikar [48].)

reproducing the right level ordering, are too compressed in energy in comparison to the experimental levels. Some examples of this in the $s-d$ shell are ^{22}Ne , ^{24}Mg , and ^{28}Si , but this deficiency is even more prominent in heavier nuclei of the $p-f$ shell [47]. To the extent that we may use the concepts of the rotational model, the omission of the pairing correlations will result in the moment of inertia \mathcal{J} being too large in simple HF calculations. This is borne out by a calculation [48] of the energy spectra of ^{22}Ne . The HF and HFB calculations were done with all 22 nucleons, using a slightly modified version of the effective interaction of Elliot et al. [49]. The basis space consisted of the first four major shells of the oscillator potential. The energy spectrum of ^{22}Ne , when projected from the lowest intrinsic HF state, is shown in column (a) of Fig. 10-17 and is seen to be quite compressed when compared to the experimental values listed in column (c) of the same figure. There is a marked improvement in the spectrum shown in column (b), however, where the effect of pairing is taken into account in a HFB calculation and the states are then projected out.

10-7 PARTICLE-HOLE (TAMM-DANCOFF) CALCULATIONS

For simplicity, we continue with the example of ^{16}O , although the physical ideas that we develop here are quite general and may be used for other closed-

shell nuclei like ^{40}Ca or ^{208}Pb , and even, with some modifications, in other regions of the periodic table. In this section, we shall concentrate on the odd-parity excited states of ^{16}O . In particular, a sharp 3^- level (with $T = 0$) is seen at 6.13 MeV in reactions like the inelastic electron-scattering experiment $^{16}\text{O}(e, e')^{16}\text{O}^*$, brought about by the electromagnetic interaction between the incident electron and ^{16}O . Although a host of other excited states are identified in this reaction at excitation energies of up to 30 MeV or more, no other 3^- state is found. In some other reactions like $^{12}\text{C}(\alpha, \alpha)^{12}\text{C}$ other 3^- ($T = 0$) states at 11.63 and 13.14 MeV are detected; these are rather weak, in the sense that it is difficult to excite the nucleus to these states.

A similar situation prevails with respect to the 1^- excited states. These are most commonly studied by incident γ -rays on the nucleus in reactions like $^{16}\text{O}(\gamma, \gamma)^{16}\text{O}^*$, $^{16}\text{O}(\gamma, n)^{15}\text{O}$, and $^{16}\text{O}(\gamma, p)^{15}\text{N}$. When the incident γ -ray energy is small compared to the excited states of the nucleus, a photon can only shake the whole nuclear charge, producing Thomson (i.e., elastic) scattering. At higher excitations, but below the particle threshold, individual levels may be excited by the reaction $^{16}\text{O}(\gamma, \gamma)^{16}\text{O}^*$. A reaction like $^{16}\text{O}(\gamma, n)^{15}\text{O}$, involving particle emission, can occur only when the incident γ -ray energy is sufficient to provide the separation energy of the neutron and the difference between the ground-state energies of ^{16}O and ^{15}O ; these require a minimum γ -ray energy of 15.7 MeV.

For higher energies, many other reaction modes are possible, involving multiparticle emission. Because so many decay modes are possible at higher energies, the γ -ray absorption cross section is no longer sharp but shows broad structures. For example, measurement of the $^{16}\text{O}(\gamma, \gamma)^{16}\text{O}^*$ cross section shows very broad resonance peaks located at about 22 and 25 MeV with spin 1^- , $T = 1$, indicating electric dipole absorption. These are called giant dipole resonances. From the shell-model point of view, the simplest odd-parity excited states in ^{16}O should result from the excitation of an odd number of nucleons from the filled p -orbitals to the vacant $s-d$ shell. The simplest intrinsic states, in the HF picture, describing such excited states differ from the ground-state configuration in $1p-1h$ orbitals only. One should then expect such excited states to have energies ≈ 11 MeV, close to the shell gap between the $0p_{3/2}$ - and the $0d_{5/2}$ -orbitals (see Fig. 10-1). Experimentally, as we have mentioned, the 3^- ($T = 0$) state occurs only at about half this excitation, while the 1^- ($T = 1$) state is at about twice the shell gap. Moreover, from the single-particle point of view, there should be many such states, whereas experimentally the strength is concentrated only in a single 3^- and in a broad 1^- with some structure in it. In this section we shall try to under-

stand this behavior of these excited states within the framework of the single-particle model.

First we shall have to formulate more precisely, in terms of angular-momentum algebra, the meaning of expressions like "hole states" and "particle-hole configuration." We consider the special case of a filled j -shell in the spherical basis, and denote this closed-core state by $|c\rangle$:

$$|c\rangle = a_{j,j}^+ a_{j,j-1}^+ \cdots a_{j,m}^+ \cdots a_{j,-j}^+ |0\rangle, \quad (10-51)$$

where $|0\rangle$ is the vacuum with no particles present. If a particle in the orbit (jm) is missing from this core, we call this vacancy a hole, and denote the state as $|h\rangle_{jm}$:

$$|h\rangle_{jm} = a_{j,j}^+ a_{j,j-1}^+ \cdots a_{j,m+1}^+ a_{j,m-1}^+ \cdots a_{j,-j}^+ |0\rangle. \quad (10-52)$$

Since the a 's are Fermion operators, a pair like $(a_{jm} a_{jm}^+)$ commutes with every a or a^+ and hence can be inserted into Eq. 10-52 without altering its value:

$$\begin{aligned} |h\rangle_{jm} &= a_{j,j}^+ a_{j,j-1}^+ \cdots a_{j,m+1}^+ (a_{jm} a_{jm}^+) a_{j,m-1}^+ \cdots a_{j,-j}^+ |0\rangle \\ &= (-)^{j-m} a_{jm} |c\rangle. \end{aligned} \quad (10-53)$$

It can be readily shown that the hole state $|h\rangle_{jm}$ transforms under rotation as if it has an angular momentum j and azimuthal quantum number $-m$. We can therefore put

$$|h\rangle_{jm} \equiv (-)^{j-m} |j, -m\rangle.$$

We can now construct particle-hole configurations of a given angular momentum. Let there be a particle in an unfilled shell of angular momentum j_a , coupling to a hole of angular momentum j_n to give a state with resultant J, M :

$$|an^{-1}; JM\rangle = \sum_{m_a, m_n} (-)^{j_n - m_n} (j_a j_n m_a - m_n |JM\rangle) a_{j_a m_a}^+ a_{j_n m_n} |c\rangle. \quad (10-54)$$

Since there is a two-body effective interaction V between the nucleons,

$$V = \frac{1}{2} \sum_{\alpha, \beta, \gamma, \delta} \langle \alpha \beta | V | \gamma \delta \rangle a_\alpha^+ a_\beta^+ a_\gamma a_\delta, \quad (10-55)$$

it follows that there will be matrix elements of V between particle-hole states of type 10-54. We have seen that, if the ground state $|\Phi_0\rangle$ has been constructed from self-consistent orbitals, the residual interaction ($V - U$) cannot cause $1p-1h$ transitions, so that the ground state would have no admixture of $1p-1h$ states. However, here we are trying to describe odd-parity excited

states through the $1p-1h$ configuration, which may be formed, for example, because of the absorption of a photon of a certain multipolarity. The unperturbed $1p-1h$ states would then become mixed through the interaction V . We want to see whether it is possible for certain excited states to have a collective character, with excitation energies very different from their unperturbed values. For simplicity, we suppress the angular-momentum coupling in Eq. 10-54 and denote the $1p-1h$ state by $|an^{-1}\rangle$; then an excited state $|\Psi_1\rangle$ of the nucleus contains admixtures of such states

$$|\Psi_1\rangle = \sum_{n,a} C_{an} |an^{-1}\rangle, \quad (10-56)$$

where, if we ignore multiparticle excitations, the coefficients are such that

$$\sum_{n,a} |C_{an}|^2 = 1. \quad (10-57)$$

We can rewrite Eq. 10-23 for the Hamiltonian as

$$H = H_0 + V', \quad (10-58)$$

where $H_0 = \sum_i (t_i + U_i)$, and

$$V' = \sum_{i < j} V_{ij} - \sum_i U_i$$

is the residual interaction. Then, for an excited state $|\Psi_1\rangle$ with energy E_1 , we must have

$$(E_1 - H_0) |\Psi_1\rangle = V' |\Psi_1\rangle. \quad (10-59)$$

Noting that a state like $|an^{-1}\rangle$ is an eigenstate of H_0 with energy $e_a - e_n \equiv e_{an}$ relative to the ground state, where the e 's are the HF single-particle orbitals of the self-consistent ground state, we immediately obtain

$$(E_1 - e_{bm}) C_{bm} = \sum_{n,a} \langle bm^{-1} | V' | an^{-1} \rangle C_{an}. \quad (10-60)$$

In order to obtain the eigenvalues E_1 of the excited states, we therefore must evaluate $p-h$ matrix elements of the type $\langle bm^{-1} | V' | an^{-1} \rangle$. To avoid cumbersome notation, let us denote

$$a_{j_n m_n} \equiv a_n, \quad (10-61)$$

and similarly for the creation operators. Using Eqs. 10-54 and 10-55, we obtain

$$\langle bm^{-1} | V | an^{-1} \rangle = \frac{1}{2} \sum_{\alpha, \beta, \gamma, \delta} \langle c | a_m^+ a_\beta a_\alpha^+ a_\beta^+ a_\delta a_\alpha a_\delta^+ a_n | c \rangle \langle \alpha \beta | V | \gamma \delta \rangle. \quad (10-62)$$

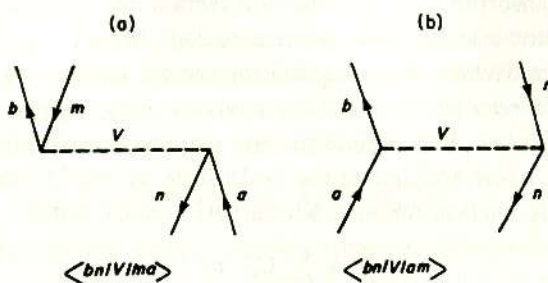


Fig. 10-18 The particle-hole matrix elements occurring in Eq. 10-63.

In Appendix C (Eq. C-38), we show how such matrix elements can be simplified in a systematic manner. It is shown there that the result is simply

$$\langle bm^{-1}|V|an^{-1} \rangle = \langle bn|V|ma \rangle - \langle bn|V|am \rangle, \quad (10-63)$$

which is displayed diagrammatically in Fig. 10-18. By convention, the first term on the right side of Eq. 10-63 is called the direct and the second the exchange term. Substitution of expression 10-63 for $\langle bm^{-1}|V|an^{-1} \rangle$ in Eq. 10-60 and subsequent diagonalization should yield the excited state energies E_1 and the corresponding wave functions.

The earliest calculations of this type, with phenomenological residual interaction, were due to Elliott and Flowers [50]. Their calculation agreed well with the experimental energies and lifetimes of the odd-parity levels of ^{16}O . They found, for example, that out of all the 1^- ($T = 1$) states one linear combination of the unperturbed p - h states separates markedly in energy and is pushed up. Furthermore, it has collective properties in the sense that this is the state most easily excitable by the electric dipole absorption of the γ -ray. Similarly, for the 3^- ($T = 0$) states, one particular state again has most of the collective strength, but it is pushed down in energy by the p - h residual interaction. These results are in agreement with the experimental observations.

To understand these results physically, we shall follow a model suggested by Brown and Bolsterli [51]. In this model, the exchange term in Eq. 10-63 is neglected, resulting in great simplicity. Some justification for this omission is based on the fact that the exchange term is almost identical to the direct one for a very short-range force, except that it has a different spin-isospin

weight factor. This results in the right side of Eq. 10-63 having approximately just the direct term with a certain weight. In this model, then,

$$\langle bm^{-1}|V|an^{-1} \rangle \approx \langle b(1)n(2)|V|m(1)a(2) \rangle. \quad (10-64)$$

A general expansion of the two-body operator V in terms of the spherical harmonics is

$$V(|\mathbf{r}_1 - \mathbf{r}_2|) = \sum_{J'} (2J' + 1) V_{J'}(\mathbf{r}_1, \mathbf{r}_2) P_{J'}(\cos \theta_{12}),$$

where J' can take only integral values, and $V_{J'}(\mathbf{r}_1, \mathbf{r}_2)$ is a function of the scalars r_1, r_2 . Using Eq. A-70, we obtain

$$V(|\mathbf{r}_1 - \mathbf{r}_2|) = 4\pi \sum_{J', M'} V_{J'}(\mathbf{r}_1, \mathbf{r}_2) Y_{J'}^{M'}(\hat{\mathbf{r}}_1) Y_{J'}^{M'*}(\hat{\mathbf{r}}_2). \quad (10-65)$$

Considerable simplification takes place if a separable assumption is made for $V_{J'}(\mathbf{r}_1, \mathbf{r}_2)$:

$$4\pi V_{J'}(\mathbf{r}_1, \mathbf{r}_2) = \chi f_{J'}(\mathbf{r}_1) f_{J'}(\mathbf{r}_2), \quad (10-66)$$

where $f_{J'}$ is some function still to be specified, and χ is a constant. Substituting Eqs. 10-65 and 10-66 into 10-64, we obtain the p - h matrix element as

$$\langle bm^{-1}|V|an^{-1} \rangle \approx \chi \sum_{J', M'} \langle b(1)|f_{J'}(\mathbf{r}_1) Y_{J'}^{M'}(\mathbf{r}_1)|m(1) \rangle \langle n(2)|f_{J'}(\mathbf{r}_2) Y_{J'}^{M'*}(\mathbf{r}_2)|a(2) \rangle. \quad (10-67)$$

If we now consider an excited state of angular momentum J, M , the unperturbed p - h states $|bm^{-1}\rangle$ and $|an^{-1}\rangle$ are each coupled to angular momentum J . We show in Appendix C (Eq. C-39) that, for any one-body operator defined by

$$O_{J'} = \sum_{\alpha, \beta} \langle \alpha|f(r) Y_{J'}^{M'}|\beta \rangle a_\alpha^+ a_\beta, \quad (10-68)$$

$$\langle b|f(r) Y_{J'}^{M'}|m \rangle = \langle bm^{-1}|O_{J'}|c \rangle. \quad (10-69)$$

If $|c\rangle$ has angular momentum zero, the above matrix element is nonzero only for $J', M' = J, M$, since $|bm^{-1}\rangle$ has angular momentum J, M . This results in only one term contributing in the sum in Eq. 10-67. We saw in Chapter 3 that the Hamiltonian for the electromagnetic field can be expanded in multipole operators. Defining the transition matrix element of the electric multipole operator of order J by

$$D_{bm}^J = \langle b|r^J Y_J^0|m \rangle, \quad (10-70)$$

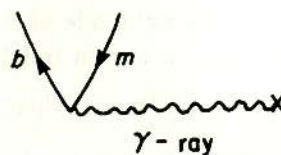


Fig. 10-19 The incident γ -ray creates a particle-hole pair as shown. For the J th electric multipole of the electromagnetic field, the matrix element is denoted by D_{bm}^J .

we see that it can be represented graphically by Fig. 10-19, which has the same structure as the direct p - h matrix element of Fig. 10-18, cut in half. If it were possible to write $f_J(r) = r^J$, Eqs. 10-67 and 10-70 would yield

$$\langle bm^{-1}|V|an^{-1}\rangle \approx \chi D_{bm}^J D_{an}^{J*}. \quad (10-71)$$

thus relating the direct p - h matrix element to the transition amplitudes of the multipole operator. Even though $V_J(r_1, r_2)$ cannot be expected to have the simple form $r_1^J r_2^J$, Eq. 10-71 should be an order-of-magnitude approximation. The special property of this matrix element, namely, that only the J th multipole of the interaction is involved in the mixing of p - h states coupled to J , is characteristic of the direct term only—other multipoles can certainly contribute in the exchange term. Substitution of Eq. 10-71 in Eq. 10-60 yields

$$(E_1 - e_{bm})C_{bm} = \chi D_{bm}^J \sum_{n,a} C_{an} D_{an}^{J*}.$$

Using the fact that

$$\chi \sum_{n,a} C_{an} D_{an}^{J*} = N_J, \text{ a constant}, \quad (10-72)$$

we obtain

$$C_{bm} = \frac{N_J D_{bm}^J}{E_1 - e_{bm}},$$

where these coefficients must obey the normalization condition 10-57.

Multiplying the left-hand side of the above equation by D_{bm}^{J*} and summing over b, m yields

$$\sum_{b,m} C_{bm} D_{bm}^{J*} = N_J \sum_{b,m} \frac{|D_{bm}^J|^2}{E_1 - e_{bm}}.$$

Using Eq. 10-72, we obtain

$$\frac{1}{\chi} = \sum_{b,m} \frac{|D_{bm}^J|^2}{E_1 - e_{bm}}. \quad (10-73)$$

For a given χ , which is determined from the nature of the p - h interaction, the excited states E_1 may be obtained from a graphical solution of Eq. 10-73, as shown in Fig. 10-20. All the solutions except one are trapped between the

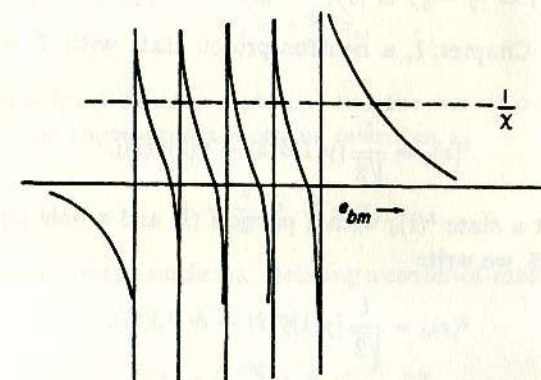


Fig. 10-20 Graphical solution of Eq. 10-73 for a positive χ , that is, a repulsive particle-hole interaction.

unperturbed energies. For a positive χ (i.e., a repulsive p - h interaction), one solution is pushed high up in energy and becomes collective, in the sense that it acquires a large share of the electromagnetic multipole strength. It is clear from Fig. 10-20 that for an attractive p - h interaction (negative χ) the collective solution will come down in energy. An extreme example is the degenerate limit, where all the e_{bm} 's equal e . Then, from Eq. 10-73, we obtain

$$\frac{1}{\chi} = \frac{D^2}{E_1 - e}, \quad \text{with} \quad D^2 = \sum_{b,m} |D_{bm}^J|^2. \quad (10-74)$$

In this case, all the solutions except one have the unperturbed energy e . The collective state has the eigenvalue $E_1 = e + \chi D^2$, and it contains all the multipole strength D^2 .

Experimentally, we have seen that the $T = 1$ collective states are pushed up in energy, indicating a repulsive p - h interaction, whereas the $T = 0$ collective state comes down, showing the effect of an attractive p - h interaction. We would like to understand this behavior of the p - h interaction, starting with a short-range attractive particle-particle force that is independent of spin and i -spin. The results can then be generalized for a more realistic nucleon-nucleon force. In the i -spin space, we denote a proton state by $|\gamma\rangle = |\frac{1}{2}\frac{1}{2}\rangle$ and a neutron state by $|\delta\rangle = |\frac{1}{2}-\frac{1}{2}\rangle$. Then, using the phase convention defined in Eq. 10-53, a proton hole $|\bar{\gamma}\rangle$ and a neutron hole $|\bar{\delta}\rangle$ are given by

$$|\bar{\gamma}\rangle = |\frac{1}{2}-\frac{1}{2}\rangle \equiv |\delta\rangle, \quad |\bar{\delta}\rangle = -|\frac{1}{2}\frac{1}{2}\rangle \equiv -|\gamma\rangle. \quad (10-75)$$

As we noted in Chapter 1, a neutron-proton state with $T = 1$, $T_3 = 0$ is given by

$${}^3(\tau)_0 = \frac{1}{\sqrt{2}} [\gamma(1)\delta(2) + \gamma(2)\delta(1)].$$

Let us construct a state ${}^3(\tau)_0$ with a particle (1) and a hole (2). Making use of relation 10-75, we write

$${}^3(\tau)_0 = \frac{1}{\sqrt{2}} [\gamma(1)\bar{\gamma}(2) - \delta(1)\bar{\delta}(2)]. \quad (10-76)$$

Similarly,

$${}^3(\tau)_1 = -\gamma(1)\bar{\delta}(2), \quad {}^3(\tau)_{-1} = \delta(1)\bar{\gamma}(2)$$

and

$${}^1(\tau)_0 = \frac{1}{\sqrt{2}} [\gamma(1)\bar{\gamma}(2) + \delta(1)\bar{\delta}(2)]. \quad (10-77)$$

In a given nucleus like ^{16}O , all the states should have $T_3 = 0$; hence the excited p - h configurations may be described by ${}^3(\tau)_0$ or ${}^1(\tau)_0$. Schematically, therefore, the p - h states can be denoted by

$$|ph\rangle = \frac{1}{\sqrt{2}} (\gamma\bar{\gamma} \pm \delta\bar{\delta}) \quad (10-78)$$

with the positive sign for $T = 0$ and negative sign for $T = 1$. With a spin-isospin-independent potential V , it can be easily seen that

$$\langle\gamma\bar{\gamma}|V|\gamma\bar{\gamma}\rangle = (\text{direct}) - (\text{exchange}) \quad \text{and} \quad \langle\gamma\bar{\gamma}|V|\delta\bar{\delta}\rangle = (\text{direct}), \quad (10-79)$$

where (direct) and (exchange) stand for the matrix elements shown in Figs. 10-18a, 10-18b, respectively. It then follows that

$$\begin{aligned} \langle ph|V|ph\rangle &= 2(\text{direct}) - (\text{exchange}) \quad \text{for } T = 0, \\ &= -(\text{exchange}) \quad \text{for } T = 1. \end{aligned} \quad (10-80)$$

For a short-range V , we have (direct) \approx (exchange); and if the particle-particle interaction is attractive, it follows that the p - h matrix elements of V are attractive in $T = 0$ and repulsive in $T = 1$ states. This general result still holds for any reasonable exchange mixture.

To understand these results in physical terms, let us examine the form of the dipole operator

$$Q_1 = e \sum_p \mathbf{r}_p,$$

where the subscript p denotes a proton, and the sum is over all protons in the nucleus. The above equation can be rewritten as

$$Q_1 = \frac{e}{2} \sum_i (1 + \tau_{3i}) \mathbf{r}_i,$$

where the sum i is over all nucleons. Defining a center-of-mass $\mathbf{R} = (1/A) \sum_i \mathbf{r}_i$, we obtain

$$Q_1 = \frac{e}{2} \sum_i \tau_{3i} \mathbf{r}_i + \frac{e}{2} A \mathbf{R}, \quad (10-81)$$

which implies that Q_1 consists of a $T = 1$ part and a $T = 0$ component which is spurious in the sense that it only affects the center-of-mass motion. For a nucleus with $T_3 = 0$ ($N = Z$), this component can be eliminated by redefining the dipole operator with respect to the center of mass:

$$Q'_1 = \frac{e}{2} \sum_i \tau_{3i} \mathbf{r}_i = e \sum_p (\mathbf{r}_p - \mathbf{R}). \quad (10-82)$$

If we now define the centers of mass of protons and neutrons separately,

$$\mathbf{R}_Z = \frac{1}{Z} \sum_p \mathbf{r}_p, \quad \mathbf{R}_N = \frac{1}{N} \sum_n \mathbf{r}_n,$$

a little algebra shows that

$$Q_1' = \frac{eNZ}{A} \mathbf{r}, \quad (10-83)$$

where $\mathbf{r} = (\mathbf{R}_Z - \mathbf{R}_N)$.

In Eq. 10-83, we have expressed the dipole operator in a collective coordinate, which is the relative distance between the proton and neutron mass centers. Thus absorption of dipole radiation ($T = 1$) can be interpreted as setting up relative motion between the protons and neutrons as a whole, which is opposed by the attractive $n-p$ interaction. This requires additional energy for the $T = 1$ collective states, which are therefore pushed up from their unperturbed values. On the other hand, in a $T = 0$ excitation the neutrons and protons move in phase, bringing the collective state down in energy.

These ideas are fully exploited in the hydrodynamical model [64, 65], where giant dipole resonance results from the vibrations of a proton fluid against a neutron fluid. The resonance frequency in this model is inversely proportional to the linear dimension of the nucleus along which the vibrations take place, that is, to $A^{-1/3}$. An excellent and detailed treatment of this model, which is applicable for medium-mass and heavy nuclei, is given by

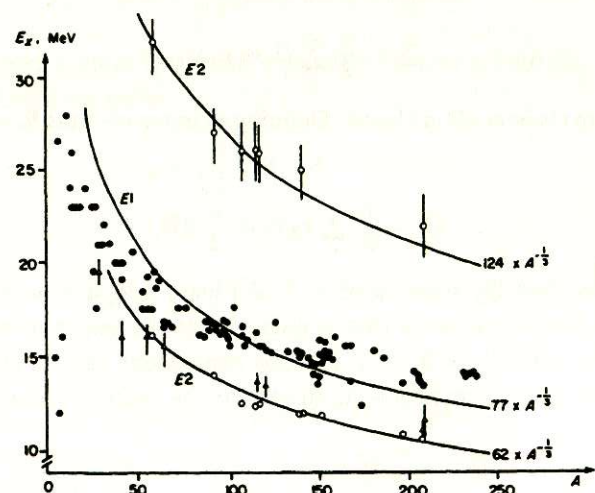


Fig. 10-21 Giant resonance energies as a function of A . The dark dots are for giant dipole $E1$ -resonances, and the curve $77A^{-1/3}$ is the prediction of the hydrodynamical model. The upper curve $E2$ is through the $T = 1$ giant $E2$ -resonances, while the lower curve $E2$ is through the $T = 0$ $E2$ -resonances. The open circles are from (e, e') experiments; the triangles, from (p, p') experiments [67]. (After Walcher [68].)

Eisenberg and Greiner [65]. In Fig. 10-21, the experimentally found giant-dipole-resonance energies are shown by dark dots as a function of A . It will be seen that the smooth curve $E1$ given by the hydrodynamical model fits the gross experimental trend for $A > 100$. In the hydrodynamical model, one expects two peaks in the giant dipole resonance for axially symmetric deformed nuclei, corresponding to the two different frequencies of oscillation along the major and minor axes of the nucleus. This is found to be so experimentally; for example, in Nd isotopes, ^{150}Nd , which is deformed, exhibits two peaks, whereas the lighter isotopes show only one peak [66].

Finally, we should mention that (e, e') and (p, p') experiments have also revealed giant $E2$ - (both $T = 0$ and $T = 1$) and giant $M1$ -resonances [67]. A review of these findings is given by Walcher [68]. In Fig. 10-21, the upper $E2$ curve goes through the $T = 1$ giant quadrupole resonances, while the lower $E2$ curve is through the $T = 0$ resonances. Note that again the $T = 0$ resonances are lowered in energy, whereas the $T = 1$ resonances are pushed up, the dependence on mass number in both cases being $A^{-1/3}$. These characteristics for the giant $E2$ -resonances were predicted by Bohr and Mottelson [69], whose theory fits the experimental data very well.

10-8 CALCULATION OF INERTIAL PARAMETERS

In the discussion of the rotational motion of well-deformed nuclei, we derived expression 9-37 for the moment of inertia \mathcal{I} in the hydrodynamical model. We see in Fig. 10-22 that this expression fares very poorly when compared with the experimental data. The situation does not improve if we take the other extreme model, that of a rigid deformed shape, and modify Eq. 9-40 accordingly. In Section 10-6, we saw how states of good angular momenta J could be projected from an intrinsic wave function in a body-fixed system. In this section, we shall first attempt to find how the moment-of-inertia parameter \mathcal{I} can be calculated for well-deformed nuclei, and then briefly discuss the microscopic basis of calculating the inertial parameter B_2 for quadrupole vibrations of spherical nuclei.

Consider a nucleus that is rotating with an angular velocity ω about a body-fixed 1-axis and has an axis of symmetry about the 3-axis. The same nucleus could be described in a space-fixed system, where, without any loss of generality, we may assume that the spaced-fixed x -axis coincides with the body-fixed 1-axis. If we denote the Hamiltonian in the space-fixed frame by H , the state $|\Psi\rangle$ will be a solution of the time-dependent wave equation,

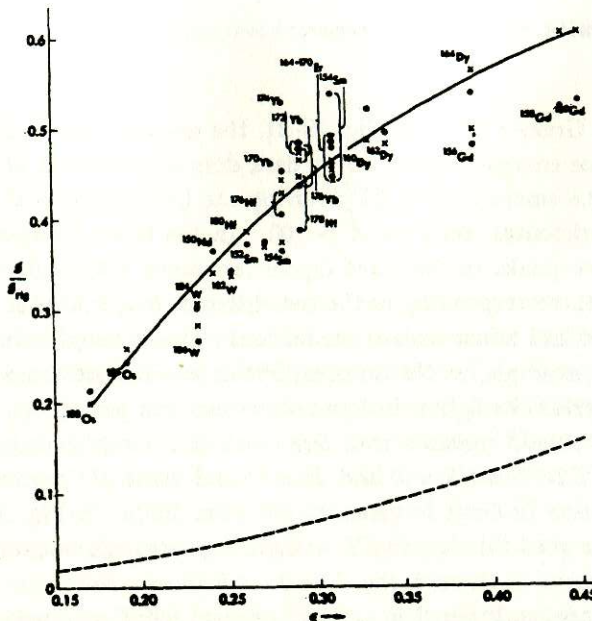


Fig. 10-22 The dependence of moments of inertia on deformation for even-even rare-earth nuclides. The circles indicate experimental values, the crosses are values calculated by superfluid theory [58], and the dashed line shows the prediction for irrotational fluid flow. The experimental values of \mathcal{J} are deduced from the level spacing in rotational bands; the values of the deformation parameter are deduced from the electric quadrupole moments. Units of \mathcal{J} : $\mathcal{J}_{\text{rig}} = \frac{2}{5}AMR_0^2(1 + 0.31\beta + \dots)$.

$$H|\Psi\rangle = i\hbar \frac{\partial|\Psi\rangle}{\partial t}. \quad (10-84)$$

The wave function in the rotating frame, $|\Phi_\omega\rangle$, is related to $|\Psi\rangle$ by the transformation

$$|\Psi\rangle = R_1(\omega t)|\Phi_\omega\rangle, \quad (10-85)$$

where R_1 is the rotation operator about the 1-axis,

$$R_1(\omega t) = \exp(-iJ_1\omega t). \quad (10-86)$$

Substituting Eq. 10-85 into 10-84, we obtain

$$H_\omega|\Phi_\omega\rangle = i\hbar \frac{\partial}{\partial t}|\Phi_\omega\rangle \quad (10-87)$$

with

$$H_\omega = R_1^{-1} \left(H R_1 - i\hbar \frac{\partial R_1}{\partial t} \right). \quad (10-88)$$

Recalling the simple form of R_1 from Eq. 10-86, we note that H_ω simplifies to

10-8 | Calculation of Inertial Parameters

$$H_\omega = \exp(+iJ_1\omega t) H \exp(-iJ_1\omega t) - \hbar\omega J_1. \quad (10-89)$$

If we demand stationary solutions of Eq. 10-87, we can put

$$H_\omega|\Phi_\omega\rangle = E_\omega|\Phi_\omega\rangle, \quad (10-90)$$

obtaining the relation between the energy eigenvalues in the two frames:

$$E = \langle \Psi | H | \Psi \rangle = E_\omega + \hbar\omega \langle \Phi_\omega | J_1 | \Phi_\omega \rangle. \quad (10-91)$$

Note that, if we had started with the total Hamiltonian

$$H = \sum_i t_i + \sum_{i < j} V_{ij},$$

which is rotationally invariant, Eq. 10-89 would simply reduce to

$$H_\omega = H - \hbar\omega J_1, \quad (10-92)$$

showing that in a rotating frame an extra term $-\hbar\omega J_1$ arises in the Hamiltonian. If, on the other hand, we take the simple-minded approach of the independent-particle model with neglect of all residual interaction, we can assume that the quantity $\exp(iH_1\omega t) H \exp(-iJ_1\omega t)$ occurring in Eq. 10-89 is simply the sum of the time-independent one-body operators in the body-fixed frame, and denote this by H_0 :

$$H_0 \equiv \exp(iJ_1\omega t) H \exp(-iJ_1\omega t) \approx \sum_i (t_i + U_i). \quad (10-93)$$

In the absence of any cranking (or rotation) the energy of the system is given by

$$H_0|\Phi_0\rangle = E_0|\Phi_0\rangle, \quad (10-94)$$

while in the presence of rotation the system energy is given by E of Eq. 10-91.

The quantity $E - E_0$ is the rotational energy and is given by

$$E - E_0 = \frac{1}{2}\mathcal{J}\omega^2. \quad (10-95)$$

If we assume ω to be small, E may be evaluated by taking $-\hbar\omega J_1$ as a perturbation. To do this, we note from Eqs. 10-89 and 10-93 that

$$H_\omega = H_0 - \hbar\omega J_1,$$

so that from perturbation theory

$$|\Phi_\omega\rangle = |\Phi_0\rangle - \hbar\omega \sum_{\Phi \neq \Phi_0} \frac{\langle \Phi_0 | J_1 | \Phi \rangle}{E_0 - E'} \quad (10-96)$$

where $|\Phi'\rangle$ is a state connected through the operator J_1 with $|\Phi_0\rangle$, so that $H_0|\Phi'\rangle = E'|\Phi'\rangle$. Note further that, in the independent-particle model with axial symmetry, $|\Phi_0\rangle$ is a determinantal state with a definite value of $J_3 = \Omega$; and since J_1 is a linear combination of the raising and lowering operators J_+ and J_- , which alter Ω by ± 1 , the diagonal matrix element

$$\langle\Phi_0|J_1|\Phi_0\rangle = 0. \quad (10-97)$$

When Eqs. 10-96 and 10-97 are used, it follows immediately that

$$\langle\Phi_\omega|J_1|\Phi_\omega\rangle = 2\hbar\omega \sum_{\phi' \neq \phi_0} \frac{|\langle\Phi'|J_1|\Phi_0\rangle|^2}{E' - E_0}. \quad (10-98)$$

Likewise, using perturbation theory up to second order and noting that the first-order term (10-97) is zero, we obtain

$$E_\omega = E_0 - (\hbar\omega)^2 \sum_{\phi' \neq \phi_0} \frac{|\langle\Phi'|J_1|\Phi_0\rangle|^2}{E' - E_0}. \quad (10-99)$$

We can now substitute the expressions for E_ω and $\langle\Phi_\omega|J_1|\Phi_\omega\rangle$ obtained in Eqs. 10-99 and 10-98 into expression 10-91 for E to get

$$E = E_0 + (\hbar\omega)^2 \sum_{\phi' \neq \phi_0} \frac{|\langle\Phi'|J_1|\Phi_0\rangle|^2}{E' - E_0}. \quad (10-100)$$

Comparing this expression with Eq. 10-95, we find

$$\mathcal{J} = 2\hbar^2 \sum_{\phi' \neq \phi_0} \frac{|\langle\Phi'|J_1|\Phi_0\rangle|^2}{E' - E_0}. \quad (10-101)$$

The same expression for \mathcal{J} could be obtained by recalling that

$$\langle\Phi_\omega|\hbar J_1|\Phi_\omega\rangle = \mathcal{J}\omega \quad (10-102)$$

and equating this to expression 10-98. Since the operator J_1 is a sum of one-body angular-momentum operators j_1 about the 1-axis, $|\Phi'\rangle$ can differ from $|\Phi_0\rangle$ only in one of the orbitals: namely, a hole is created in a single-particle orbital m and a particle in an originally unoccupied orbital b . Equation 10-101 thus simplifies to

$$\mathcal{J} = 2\hbar^2 \sum_m \sum_b \frac{|\langle b|j_1|m\rangle|^2}{e_b - e_m}. \quad (10-103)$$

This formula, originally derived by Inglis [52], is known as the cranking formula. In order to evaluate \mathcal{J} by Eq. 10-103, it is necessary to choose an appropriate H_0 whose single-particle energies e_i are known—this could be, for example, the Nilsson Hamiltonian. In a more rigorous approach to the

problem, however, one should calculate the self-consistent field in a rotating frame by performing a Hartree-Fock calculation on the Hamiltonian $(H - \hbar\omega J_1)$, with the constraint 10-102. This would take into account the changes brought about in the intrinsic state because of the cranking of the nucleus.[†] This self-consistent approach to cranking was formulated by Thouless [53], and a simplified formula developed by Thouless and Valatin [54]. A review of these methods is given by Rowe [55].

It has been shown [56] that, if the cranking formula 10-103 is applied to a rotating anisotropic harmonic-oscillator well, the rigid moment of inertia is obtained. As will be seen from Fig. 10-21, the experimental values are only 20–50% of the rigid values. Although the nucleons in the deformed well are moving independently of each other, they are frozen in their orbits because of the Pauli principle, and no scattering can take place in the absence of two-body interactions. In Eq. 10-103, we have assumed the occupancy of the orbitals to be either zero or one; furthermore, the equation also reveals that \mathcal{J} should be very sensitive to the energy gap between the occupied and unoccupied orbitals. These considerations suggest that the two-body pairing force, which smears the occupancy of the orbitals near the Fermi energy and also introduces a gap of at least 2Δ (in even-even nuclei) between the ground state and the excited states, may modify \mathcal{J} drastically from its rigid value. Consider an even-even nucleus, where we are taking into account the pairing force between identical nucleons. On solving the pairing problem in the BCS approximation (see Chapter 8), the ground state $|\Phi_0\rangle$ is described by a state with no quasiparticles, and the excited states $|\Phi'\rangle$ contain two quasiparticles. Thus we write

$$|\Phi'\rangle = \alpha_\mu^+ \alpha_\nu^+ |\Phi_0\rangle, \quad (10-104)$$

where μ (or ν) stands for the quantum numbers required to specify a single-particle state in an axially symmetric well, that is, in a Nilsson potential, $\mu \equiv (N, \Omega)$, N being the principal quantum number and Ω the 3-component of the angular momentum. The operator α_μ^+ creates a quasiparticle in the state μ . We may now apply the cranking formula 10-101 for the moment of inertia, obtaining

$$\mathcal{J} = \hbar^2 \sum_{\mu, \nu} \frac{|\langle\Phi_0|J_1\alpha_\mu^+\alpha_\nu^+|\Phi_0\rangle|^2}{E_\nu + E_\mu}, \quad (10-105)$$

[†] A self-consistent calculation of this type, with pairing taken into account, can reproduce the “back-bending” of the moment of inertia against ω^2 for high spins, described in Section 9-5. Details are given in ref. 63.

where $E_\mu = \sqrt{(e_\mu - \lambda)^2 + \Delta^2}$ is the quasiparticle energy. Note that the factor 2 is not present in front of the right-hand side of Eq. 10-105; it is canceled by the factor $\frac{1}{2}$, introduced to avoid double-counting μ and ν . On simplifying this expression, we obtain the formula [57]

$$\mathcal{I} = 2\hbar^2 \sum_{\substack{\mu > 0 \\ \nu \text{ all}}} \frac{|\langle \mu | j_1 | \nu \rangle|^2}{E_\nu + E_\mu} (V_\mu U_\nu - V_\nu U_\mu)^2. \quad (10-106)$$

In this equation, $\mu > 0$ means that no time-reversed states of μ are included; while for ν both $|N, \Omega_\nu\rangle$ and the time-reversed state $|N, -\Omega_\nu\rangle$ are taken in the sum. When this formula is used for the evaluation of \mathcal{I} for rare-earth nuclei with Nilsson wave functions, good agreement with experimental values is obtained [58, 59], as will be seen from Fig. 10-22.

Other collective parameters may also be calculated in the cranking approximation. Equation 10-101 for the moment of inertia is only a special case of a more general theorem when the adiabatic approximation for the collective mode is invoked. If any collective variable α which changes slowly compared to the intrinsic motion provides a term $\frac{1}{2}B\dot{\alpha}^2$ in the kinetic energy, the inertial parameter B is given by

$$B = 2\hbar^2 \sum_{\phi' \neq \phi} \frac{|\langle \Phi' | \partial/\partial\alpha | \Phi_0 \rangle|^2}{E' - E_0}. \quad (10-107)$$

The analogy to Eq. 10-101 is clear if we recall that an angular-momentum component is the canonically conjugate variable to a rotation angle, and that the quantum-mechanical operator conjugate to any variable α is $-i\hbar \partial/\partial\alpha$. In applying formula 10-107 to obtain the quadrupole inertial-vibrational parameter B_2 of spherical nuclei, we should remember that the first excited 2^+ state is often in the range 1–2 MeV, and that the adiabatic approximation is not as good in this case as for the low-lying rotational states.

From the microscopic point of view, the first excited 2^+ state of a spherical nucleus may be considered to be a coherent combination of one-particle, one-hole states, brought down in energy by the quadrupole-quadrupole part of the two-nucleon force. The mechanism by which a particular combination of $1p$ - $1h$ states may show collective effects was discussed in a schematic model in Section 10-7, with emphasis on the giant dipole state. In the presence of pairing force, a $1p$ - $1h$ state goes over to a two-quasi-particle state with a minimum energy of $\sim 2\Delta$. But a coherent combination of these two-quasi-particle states can be appreciably lowered in energy through the

attractive quadrupole-quadrupole interaction. In this pairing plus quadrupole-quadrupole model, not only the energy of the 2^+ state but also its wave function can be calculated. It is then possible to calculate quantities like $B(E2)$ or the inertial parameter B_2 in a microscopic manner in this model. The quadrupole-quadrupole potential V_Q was defined earlier in Eq. 9-115, and an equation of form 10-73 can be obtained to determine the energy of the excited 2^+ state, which we denote by E_2 . Modification due to pairing is straightforward, and the detailed formula is given by Bes and Sorensen [60]. One point in this modification is worth noting. We found in Eq. 10-106 for the moment of inertia an occupancy factor $(V_\mu U_\nu - V_\nu U_\mu)^2$, where the negative sign arose because the operator j_1 changes sign with time reversal. When Eq. 10-73 for the quadrupole force is modified because of pairing, however, the occupancy factor is $(V_\mu U_\nu + V_\nu U_\mu)^2$, due to the fact that $r^2 Y_2$ does not change sign with time reversal.

These particle-hole calculations can be refined by including the possibility that in the ground state, which was previously taken to be a HF determinant, there can be present $2p$ - $2h$ excitations caused by residual interactions. This is called the random-phase approximation (RPA), and in the schematic model of Section 10-7 the resulting equations are only slightly more complicated. In this RPA calculation for E_2 , it is found that, if $(E_2)^2 \ll (2\Delta)^2$ (i.e., the collective effect of lowering the energy of the 2^+ state is appreciable), the resulting equations for the inertial parameter B_2 becomes identical to the cranking-model expression 10-107. Kisslinger, Sorensen, and Uher [61, 62] have calculated the $B(E2)$ -transition rates from the ground state 0^+ to the first excited 2^+ state of even-even spherical nuclei with the RPA equations in the pairing plus quadrupole-quadrupole model, obtaining reasonable agreement with experiment. For well-deformed nuclei, the same physical ideas can be applied for the calculation of the excitation energy and transition rate, *not* for the first excited 2^+ state (which is obtainable from the rotation of the same intrinsic state), but for the γ -vibrational state.

REFERENCES

1. S. Kahana and E. L. Tomusiak, *Nucl. Phys.* **71**, 402 (1965).
2. T. Engeland, *Nucl. Phys.* **72**, 68 (1965).
3. P. Mukherjee and B. L. Cohen, *Phys. Rev.* **127**, 1284 (1962).
4. J. Blomquist and S. Wahlborn, *Ark. Fysik* **16**, 545 (1960).
5. N. Stein, *Proceedings of the International Conference on Properties of Nuclear States, Montreal, 1969*, University of Montreal Press, 1969; see Fig. 4 on p. 342.
6. H. Flocard, M. Beiner, P. Quentin and D. Vautherin, *Proc. Int. Conf. on Nucl. Phys.* Vol. 1, Munich, 1973; North-Holland, Amsterdam, 1974; p. 40.

7. For a detailed list of references to these and other shell-model calculations, see the review by J. M. Irvine, *Rep. Progr. Phys.* **21**, Part I, 1 (1968).
8. K. A. Brueckner and D. Goldman, *Phys. Rev.* **116**, 424 (1959).
9. Kailash Kumar, *Perturbation Theory and the Nuclear Many-Body Problem*, North-Holland, Amsterdam, 1962, p. 172.
10. A. K. Kerman and M. K. Pal, *Phys. Rev.* **162**, 970 (1967).
11. D. J. Rowe, *Nuclear Collective Motion*, Methuen, London, 1970, Chap. 14.
12. K. A. Brueckner, A. M. Lockett, and M. Rotenberg, *Phys. Rev.* **121**, 255 (1961).
13. K. A. Masterson and A. M. Lockett, *Phys. Rev.* **129**, 776 (1963).
14. K. T. R. Davies, M. Baranger, R. M. Tarbutton, and T. T. S. Kuo, *Phys. Rev.* **177**, 1519 (1969).
15. J. W. Negele, *Phys. Rev.* **C1**, 1260 (1970).
16. D. W. L. Sprung and P. K. Banerjee, *Nucl. Phys.* **A168**, 273 (1971).
17. J. Nemeth and G. Ripka, *Nucl. Phys.* **A194**, 329 (1972).
18. B. A. Loiseau, Y. Nogami, and C. K. Ross, *Nucl. Phys.* **A165**, 601 (1971).
19. X. Campi and D. W. L. Sprung, *Nucl. Phys.* **A194**, 401 (1972).
20. D. Vautherin and D. M. Brink, *Phys. Lett.* **32B**, 149 (1970); *Phys. Rev.* **C5**, 626 (1972).
21. T. H. R. Skyrme, *Phil. Mag.* **1**, 1043 (1956).
22. S. A. Moszkowski, *Phys. Rev.* **C2**, 402 (1970).
23. J. W. Negele and D. Vautherin, *Phys. Rev.* **C5**, 1472 (1972).
24. H. Meldner, *Phys. Rev.* **178**, 1815 (1969); A. B. Volkov, unpublished results.
25. D. Vautherin, *Phys. Rev.* **C7**, 296 (1973).
26. I. Kelson, *Phys. Rev.* **182**, 2189 (1963).
27. I. Kelson and C. A. Levinson, *Phys. Rev.* **184**, B269 (1964).
28. J. Bar-Touv and I. Kelson, *Phys. Rev.* **188**, B1035 (1965).
29. A. L. Goodman, G. L. Struble, and A. Goswami, *Phys. Lett.* **26B**, 260 (1968).
30. M. R. Gunye, C. S. Warke, and S. B. Khadkikar, *Phys. Rev.* **C3**, 1936 (1971).
- 30a. S. K. M. Wong, J. Le Tourneau, N. Quang-Hoc, and G. Saunier, *Nucl. Phys.* **A187**, 318 (1969).
- 30b. S. Das Gupta and M. Harvey, *Nucl. Phys.* **A94**, 602 (1967).
31. D. Schwalm, A. Bamberger, P. G. Bizzeti, B. Povh, G. A. P. Engelbertink, J. W. Oiness, and E. K. Warburton, *Nucl. Phys.* **A192**, 449 (1972).
32. O. Hausser, B. W. Hooton, D. Pelte, T. K. Alexander, and H. C. Evans, *Phys. Rev. Lett.* **22**, 359 (1969); *Can. J. Phys.* **48**, 35 (1970).
33. G. Ripka, *Advan. Nucl. Phys.* **1** (1968); see Table VI on p. 209.
34. E. B. Carter, G. Mitchell, and R. Davies, *Phys. Rev.* **183**, B1421 (1964).
35. W. H. Bassichis and G. Ripka, *Phys. Lett.* **15**, 320 (1966).
36. G. E. Brown and A. M. Green, *Phys. Lett.* **15**, 320 (1966). Also see the article by G. E. Brown in the *Proceedings of the International School of Physics, "Enrico Fermi"* Course, Vol. 36, p. 524.
37. J. Hayward, *Nucl. Phys.* **81**, 193 (1966).
38. G. J. Stephenson, Jr., and M. K. Banerjee, *Phys. Lett.* **24B**, 209 (1967); T. Engeland and P. J. Ellis, *Phys. Lett.* **25B**, 57 (1967); N. de Takacsy and S. Das Gupta, *Nucl. Phys.* **A152**, 657 (1970).

39. D. L. Hill and J. A. Wheeler, *Phys. Rev.* **89**, 1102 (1953).
40. R. E. Peierls and J. Yoccoz, *Proc. Phys. Soc. (London)* **70**, 381 (1957).
41. J. Yoccoz, *Proc. Phys. Soc. (London)* **70**, 388 (1957).
42. B. J. Verhaar, *Nucl. Phys.* **54**, 641 (1964).
43. W. H. Bassichis, B. Giraud, and R. Ripka, *Phys. Rev. Lett.* **15**, 980 (1965).
44. M. H. Macfarlane and A. P. Shukla, *Phys. Lett.* **35B**, 11 (1971).
45. J. C. Parikh, *Phys. Lett.* **25B**, 181 (1967).
46. H. G. Benson and J. M. Irvine, *Proc. Phys. Soc. (London)* **89**, 249 (1966); A. Bottino and B. Carazza, *Nuovo Cimento* **46B**, 137 (1967).
47. S. B. Khadkikar and M. R. Gunye, *Nucl. Phys.* **A110**, 472 (1968).
48. M. R. Gunye and S. B. Khadkikar, *Phys. Rev. Lett.* **24**, 910 (1970).
49. J. P. Elliott, A. D. Jackson, H. A. Mavromatis, E. A. Sanderson, and B. Singh, *Nucl. Phys.* **A121**, 241 (1968).
50. J. P. Elliott and B. H. Flowers, *Proc. Roy. Soc. (London)* **242A**, 57 (1957).
51. G. E. Brown and M. Bolsterli, *Phys. Rev. Lett.* **3**, 472 (1959).
52. D. Inglis, *Phys. Rev.* **96**, 1059 (1954). For higher-order corrections to the Inglis formula, see S. M. Harris, *Phys. Rev.* **138**, B509 (1965).
53. D. J. Thouless, *Nucl. Phys.* **21**, 225 (1960).
54. D. J. Thouless and J. G. Valatin, *Nucl. Phys.* **31**, 211 (1962).
55. D. J. Rowe, *Nuclear Collective Motion*, Methuen, London, 1970. Chapter 10.
56. B. R. Mottelson, *Rendiconti della Scuola Internationale di Fisica, Varenna 1960*, Zanichelli, Bologna, 1962, p. 44.
57. S. T. Belyaev, *K. Danske Vidensk. Selsk. Mat.-Fys. Medd.* **31**, No. 11 (1959).
58. J. J. Griffin and M. Rich, *Phys. Rev.* **118**, 850 (1960).
59. S. G. Nilsson and O. Prior, *K. Danske Vidensk. Selsk. Mat.-Fys. Medd.* **32**, No. 16 (1961).
60. D. R. Bes and R. A. Sorensen, *Advan. Nucl. Phys.* **2**, 129 (1969).
61. L. S. Kisslinger and R. A. Sorensen, *K. Danske Vidensk. Mat.-Fys. Medd.* **32**, No. 9 (1960).
62. R. A. Uher and R. A. Sorensen, *Nucl. Phys.* **86**, 1 (1966).
63. P. C. Bhargava, *Nucl. Phys.* **A207**, 258 (1973); B. Banerjee, H. J. Mang, and P. Ring, *Nucl. Phys.* **A215**, 366 (1973).
64. M. Goldhaber and E. Teller, *Phys. Rev.* **74**, 1946 (1948); H. Steinwedel and J. H. D. Jensen, *Z. Naturforsch.* **5a**, 413 (1950).
65. J. M. Eisenberg and W. Greiner, *Nuclear Models*, Vol. 1, North-Holland, Amsterdam, 1970, Chap. 10.
66. P. Carlos, H. Beil, R. Bergère, A. Leprêtre, and A. Veyssiére, *Nucl. Phys.* **A172**, 437 (1972).
67. R. Pitthan and Th. Walcher, *Phys. Lett.* **36B**, 563 (1971); *Z. Naturforsch.* **27a**, 1683 (1972); R. Pitthan, *Z. Physik* **260**, 283 (1973); S. Fukuda and Y. Torizuka, *Phys. Rev. Lett.* **29**, 1109 (1972); M. B. Lewis and F. E. Bertrand, *Nucl. Phys.* **A196**, 337 (1972).
68. Th. Walcher, Proc. Int. Conf. on Nucl. Phys., Vol. 2, Munich, 1973; North-Holland, Amsterdam, 1974, p. 509.
69. A. Bohr and B. R. Mottelson, *Nuclear Structure*, Vol. 2, Addison-Wesley, Reading, Mass. (in press).

PROBLEMS

10-1. Very detailed and thorough experimental studies of ^{18}F were recently performed by two groups at Strasbourg and Toronto [see *Nucl. Phys.* A199, 232–398 (1973)]. The level scheme of ^{18}F up to the excitation energy of 5 MeV, shown in Fig. 10-23, is taken from the paper of C. Rolfs, A. M. Charlesworth, and R. E. Azuma [*Nucl. Phys.* A199, 257 (1973)].

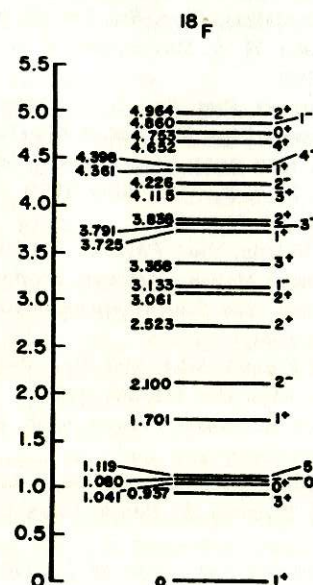


Fig. 10-23 Energy levels of ^{18}F .

(a) Comparing this spectrum of ^{18}F with that of ^{18}O , given in Fig. 10-2a, we find that far more levels (within about 5 MeV excitation) are present in ^{18}F . Explain why you expect this on theoretical grounds.

(b) If two nucleons are put in the $(1d_{5/2})^2$ configuration, then, for the $T = 0$ states, the resultant $J = 1^+, 3^+, 5^+$ only, while for $T = 1$ states $J = 0^+, 2^+, 4^+$ only are possible. Prove this.

(c) As discussed in the text, a simple model for ^{18}O consists of an inert ^{16}O -core and two neutrons in the $s-d$ shell with $T = 1$. In ^{18}F , however, there are one neutron and one proton outside the ^{16}O -core, and both $T = 0$ and $T = 1$ states are possible. By comparing the given spectrum of ^{18}F with that of ^{18}O (Fig. 10-2a), identify the first five $T = 1$ excited states in ^{18}F .

Problems

Also, look up the low-lying levels of ^{18}Ne given by Ajzenberg-Selove, *Nucl. Phys.* A190, 1 (1972), and comment.

10-2. Two identical spin- $\frac{1}{2}$ particles in the spin singlet state are each moving in an average harmonic potential and further interacting via a two-body harmonic potential. The Hamiltonian of the system is given by (for convenience we take the mass M of each particle to be unity and the oscillator constant $\omega = 1$)

$$H = \frac{1}{2}(\dot{r}_1^2 + r_1^2) + \frac{1}{2}(\dot{r}_2^2 + r_2^2) + \chi \left[\frac{1}{\sqrt{2}} (\mathbf{r}_1 - \mathbf{r}_2) \right]^2,$$

where χ is a measure of the interaction strength.

(a) Define, for this problem, the relative and center-of-mass coordinates

$$\mathbf{r} = \frac{\mathbf{r}_1 - \mathbf{r}_2}{\sqrt{2}}, \quad \mathbf{R} = \frac{\mathbf{r}_1 + \mathbf{r}_2}{\sqrt{2}}.$$

Show that the exact ground-state wave function for the system separates into relative and CM coordinates, and is given by (normalization = 1)

$$\Psi_{\text{ex}}(\mathbf{r}, \mathbf{R}) = \frac{1}{(\pi\hbar)^{3/4}} \exp(-R^2/2\hbar) \left(\frac{\sqrt{2\chi + 1}}{\pi\hbar} \right)^{3/4} \exp\left(-\left(\frac{\sqrt{2\chi + 1}}{2\hbar} r^2\right)\right), \quad (1)$$

and the ground-state energy is

$$E_{\text{ex}} = \frac{3}{2}\hbar + \frac{3}{2}\hbar\sqrt{2\chi + 1} \quad (2)$$

(b) Since the spin part of the wave function is asymmetric, the spatial wave function is symmetric, and the Hartree-Fock solution for the spatial part is the same as the Hartree solution in the s -state. Write down the Hartree equation and show that it can be solved analytically. Show that the normalized Hartree solution is

$$\Psi_{\text{H}}(\mathbf{r}_1, \mathbf{r}_2) = \left(\frac{\sqrt{\chi + 1}}{\hbar\pi} \right)^{3/2} \exp\left(-\frac{\sqrt{\chi + 1}}{2\hbar} r_1^2\right) \exp\left(-\frac{\sqrt{\chi + 1}}{2\hbar} r_2^2\right), \quad (3)$$

and the ground-state energy in this approximation is

$$E_{\text{H}} = 3\hbar\sqrt{\chi + 1}. \quad (4)$$

(c) Show that the overlap of the exact solution (1) and the Hartree solution (3) is simply given by

$$\langle \Psi_{\text{ex}} | \Psi_{\text{H}} \rangle = 8(\sqrt{2\chi + 1})^{3/4} \left[\frac{\sqrt{\chi + 1}}{(1 + \sqrt{\chi + 1})(\sqrt{2\chi + 1} + \sqrt{\chi + 1})} \right]^{3/2}. \quad (5)$$

Plot the overlap function (5) and the fractional error in the energy $(E_{\text{ex}} - E_{\text{H}})/E_{\text{ex}}$ as a function of the interaction strength χ , varying χ from 0 to 3 in steps of 0.5. What is your conclusion from these plots?

If you have difficulty in solving this problem, you may consult the article by M. Moshinsky, *Am. J. Phys.* **36**, 52 (1968), and the erratum, *Am. J. Phys.* **36**, 763 (1968).

10-3. L. Zamick [*Phys. Lett.* **45B**, 313 (1973)] has proposed a simple model to determine the dependence of the nuclear incompressibility K on the density dependence of the effective interaction and the binding energy of the nucleus. Assume that the effective interaction is such that it yields the observed binding energy E_B at the right saturation density, and that it is parameterized by the expression

$$V = -\alpha \delta(\mathbf{r}) + \gamma \rho^\sigma(R) \delta(\mathbf{r}), \quad (1)$$

where the parameters α , γ , and σ are chosen to fit the experimental data, and \mathbf{r} is the relative and R the center-of-mass coordinate of the two interacting nucleons. Assume further that the single-particle wave functions of the finite nucleus may be well approximated by harmonic-oscillator wave functions (see Problem 4-10), characterized by the oscillator length $b = (\hbar/M\omega)^{1/2}$.

(a) Show, on dimensional grounds, that the energy of the nucleus may be written in the form

$$E = -E_B = \frac{A'}{b^2} + \frac{B'}{b^3} + \frac{C'}{b^{3+3\sigma}}, \quad (2)$$

where A' , B' , and C' are independent of b . In this model, find an expression for the kinetic energy $\langle T \rangle$ of the nucleons and show that it may be identified with the first term in Eq. 2, that is,

$$\langle T \rangle = \frac{A'}{b^2}. \quad (3)$$

At saturation, we must have

$$\frac{\partial E}{\partial b} = 0. \quad (4)$$

Using relations 2, 3, and 4, verify that

$$B' = b^3 \left(E_B \frac{1+\sigma}{\sigma} + \langle T \rangle \frac{1+3\sigma}{3\sigma} \right)$$

and

$$C' = \frac{b^{3+3\sigma}}{\sigma} (E_B + \frac{1}{3}\langle T \rangle). \quad (5)$$

In this model, the nuclear incompressibility K may be defined as

$$K = \left(b^2 \frac{\partial^2 E}{\partial b^2} \right)_{\text{equil.}} \quad (6)$$

which is consistent with the definition given in Problem 8-7.

(b) Show that in this model the incompressibility K is

$$K = \frac{1}{A} [\langle T \rangle + 9E_B + \sigma(9E_B + 3\langle T \rangle)]. \quad (7)$$

For a medium-heavy or heavy nucleus it is not unreasonable to take $\langle T \rangle/A \approx 20$ MeV and $E_B/A \approx 8$ MeV; thus Eq. 7 yields

$$K = (92 + 132\sigma) \text{ MeV for a finite nucleus.}$$

For nuclear matter, $\langle T \rangle/A \approx 24$ MeV and $E_B/A \approx 16$ MeV, and the incompressibility expression 7 extrapolated to very large A is

$$K = (168 + 216\sigma) \text{ MeV.}$$

Unfortunately, since no experimental value of K is known, the parameter σ cannot be determined. Nuclear-matter calculations with reasonable forces yield a value for K in the range of 80–150 MeV, showing that a simple interaction of type 1 overestimates K .

10-4. The distribution of angular-momentum states in the deformed intrinsic state $|\Phi_K\rangle$, according to Eq. 10-47, is determined by the quantities $|C_J|^2$.

(a) Using the notation of the text, show that

$$|C_J|^2 = \frac{2J+1}{8\pi^2} \int [D_{KK}^J(\theta_i)]^* \langle \Phi_K | R(\theta_i) | \Phi_K \rangle d\Omega. \quad (1)$$

For the ground-state $K=0$ band of an even-even nucleus, show that Eq. 1 reduces to the form

$$|C_J|^2 = \frac{1}{2}(2J+1) \int_0^\pi \sin \theta_2 d\theta_2 P_J(\cos \theta_2) \langle \Phi_0 | \exp(-i\theta_2 J_2) | \Phi_0 \rangle. \quad (2)$$

(b) The overlap function $\langle \Phi_0 | \exp(-i\theta_2 J_2) | \Phi_0 \rangle$ is symmetric about $\theta_2 = \pi/2$ (see Fig. 10-15) and is well approximated, for a well-deformed nucleus, by the expression

$$\langle \Phi_0 | \exp(-i\theta_2 J_2) | \Phi_0 \rangle \approx \exp\left(-\frac{\theta_2^2 \langle J^2 \rangle}{4}\right), \quad 0 \leq \theta_2 \leq \frac{\pi}{2}, \quad (3)$$

where $\langle J^2 \rangle = \langle \Phi_0 | J^2 | \Phi_0 \rangle$ is typically 15–20 for *s-d* shell nuclei and of the order of 100 for rare-earth nuclei. Making approximation (3) in the exact expression (2) for $|C_J|^2$, one obtains

$$|C_J|^2 \approx (2J+1) \int_0^{\pi/2} \sin \theta_2 d\theta_2 P_J(\cos \theta_2) \exp\left(-\frac{\theta_2^2 \langle J^2 \rangle}{4}\right). \quad (4)$$

Since the dominant contribution to this integral comes from small values of θ_2 , one can make the following small-angle approximation, valid for all J :

$$P_J(\cos \theta_2) \approx J_0 \left[2\sqrt{J(J+1)} \sin \frac{\theta_2}{2} \right], \quad (5)$$

where J_0 is the cylindrical Bessel function of order zero.

(a) Show that, with this approximation,

$$|C_J|^2 \approx \frac{2(2J+1) \exp[-J(J+1)/\langle J^2 \rangle]}{\langle J^2 \rangle}. \quad (6)$$

In deducing Eq. 6, you will have to make use of the relation

$$\int_0^\infty \sqrt{x} \exp(-\alpha x^2) J_0(xy) \sqrt{xy} dx = \frac{\sqrt{y}}{2\alpha} \exp(-y^2/4\alpha).$$

(b) Using expression 6, find which angular-momentum states contribute importantly to $|\Phi_0\rangle$ for (i) $s-d$ shell nuclei, and (ii) rare-earth nuclei.

Part III

Alpha Disintegration and Fission of Nuclei

1. INTRODUCTION

The fact that most of the naturally occurring elements decay radioactive is due to one of man's discoveries in the very early days of science, that Rutherford had successfully demonstrated the existence of the nucleus. There are 200 isotopes in three naturally occurring elements, known as the uranium, thorium, and actinium series. The elements U^{238} , Th^{232} , and Ac^{228} are the only ones which are stable, based on the stable nuclides U^{238} , Th^{232} , and Ac^{228} . In addition, the radioactive decay of the intermediate chain nuclides, which are lighter and/or more unstable, such as U^{235} , Th^{230} , U^{234} , Th^{228} , U^{233} , Th^{226} , U^{232} , and Th^{222} , also produce a number of other nuclides which have been studied to appear as fission products. These different isotopes have different properties, and some have been separated.

In the early days of nuclear experimentation, it was thought that the atomic nucleus could be broken up like a brittle piece of chalk, and that the energy released would be proportional to the mass of the nucleus. This was called the fission hypothesis, and it was proposed by

Alpha Radioactivity

11-1 INTRODUCTION

The fact that certain of the naturally occurring radioactive elements emit α -particles was one of the first discoveries in the early days of modern physics; by 1908 Rutherford [1] had conclusively demonstrated that α -particles are ${}^4\text{He}$ nuclei. There are 30 α -emitters in three naturally occurring radioactive chains, known as the uranium, actinium, and thorium series. These start at ${}^{238}\text{U}$, ${}^{235}\text{U}$ (AcU), and ${}^{232}\text{Th}$ and, after a number of radioactive transformations, finish at the stable nuclides ${}^{206}\text{Pb}$, ${}^{207}\text{Pb}$, and ${}^{208}\text{Pb}$, respectively. In addition, the great majority of the artificially created isotopes of the elements above Pb are α -active; so are some lighter nuclides, notably certain isotopes of Sm, Cm, Hf, Nd, Eu, Gd, Tb, Dy, Au, and Hg [2, 3]. Altogether there are over 150 α -active nuclides, which have been studied to some extent. In this section we shall set forth the main features of the pattern that can be seen in the experimental data.

In the earliest days of nuclear experimentation, it was thought that, in general, each nuclide emitted α -particles of a distinct and characteristic energy. In 1930 Rosenblum [4], analyzing the charged α -particles in a strong magnetic field, discovered that many nuclides emit several groups of α -particles of distinct energy. For example, ${}_{88}^{224}\text{Ra}$ emits two main groups of α -particles: 95% of the emitted particles have energy 5.681 MeV; 5% have 5.445 MeV. Thus it is apparent that the decay need not leave the final nucleus in its ground state; in our example, when the 5.681-MeV α -particles are emitted, the daughter nucleus is ${}_{86}^{220}\text{Rn}$ in its ground state, but when a

5.445-MeV α -particle is emitted, the ^{220}Rn is in a state excited by 226 keV. The pattern for ^{224}Ra is typical of even-even nuclides; the feature to be noted at the moment is that the ground-state transition is considerably more frequent than the modes of decay which produce lower-energy particles. On the other hand, the odd- A and odd-odd nuclei have a different pattern, of which ^{223}Ra and ^{241}Am are typical representatives. Their spectra are shown in Table 11-1, which also includes the spectra of a number of other nuclides.

TABLE 11-1

Nuclide	E_α , MeV	Abundance, %	Half-life	Partial half-life, years	Hindrance factor
$^{241}_{95}\text{Am}$	5.535	0.34	470y	1.38×10^5	560
	5.503	0.21		2.24×10^5	560
	5.476	84.4		5.60×10^2	1
	5.433	13.6		3.46×10^3	4
	5.379	1.4		3.36×10^4	16
	5.314	0.015		3×10^6	
$^{223}_{88}\text{Ra}$	5.860	Weak	11.2d	$\gtrsim 2$	$\sim 10^5$
	5.735	9		0.340	65
	5.704	53		0.0580	8
	5.592	24		0.128	5
	5.525	9		0.340	6
	5.487	2		1.5	17
	5.419	3		1.0	5
$^{224}_{88}\text{Ra}$	5.681	95.1	3.64d	1.053×10^{-2}	
	5.445	4.9		0.218	
	5.15	0.009		1.0×10^2	
$^{211}_{84}\text{Po}$	7.434	99	0.52s	1.6×10^{-8}	530
	6.88	0.50		3.3×10^{-6}	1700
	6.56	0.53		3.1×10^{-6}	100

It will be seen that in these non-even-even cases the α -particles of highest energy are not usually the most abundant, but may be quite weak relative to a group of somewhat smaller energy. Also, a comparison of the absolute half-lives shows a characteristic difference. In fact, one of the most remarkable things about α -radioactivity is the great range of half-lives. If λ is the probability per second that a radioactive nucleus will decay, the half-life $\tau_{1/2} = (\ln 2)/\lambda$. We shall often call these λ 's *decay constants*. Each mode

has its own decay constant λ_i , and the total decay constant of the nuclide is $\lambda_{\text{tot}} = \sum \lambda_i$. The *partial half-life* of a mode is

$$\tau_{1/2,i} = \frac{\ln 2}{\lambda_i}$$

The great range of decay probabilities in α -activity is illustrated by the fact that the half-life of ^{213}Po , emitting 8.336-MeV α -particles, is 4.2×10^{-6} sec or 1.33×10^{-13} yr, whereas the half-life of ^{232}Th , which emits 3.98-MeV particles, is 1.39×10^{10} yr. A table of energies and half-lives illustrates clearly that the greater decay rates correspond to greater energies. As early as 1911, Geiger and Nuttall [5] showed that a good straight line was obtained by plotting the logarithm of the half-life against the logarithm of the range of the α -particles in air. This range is connected with the energy. Now that we have more data, of greater accuracy, we prefer to draw our curves only through the points belonging to the same element. Figure 11-1 shows the experimental points for even-even nuclides, and it is seen that joining the

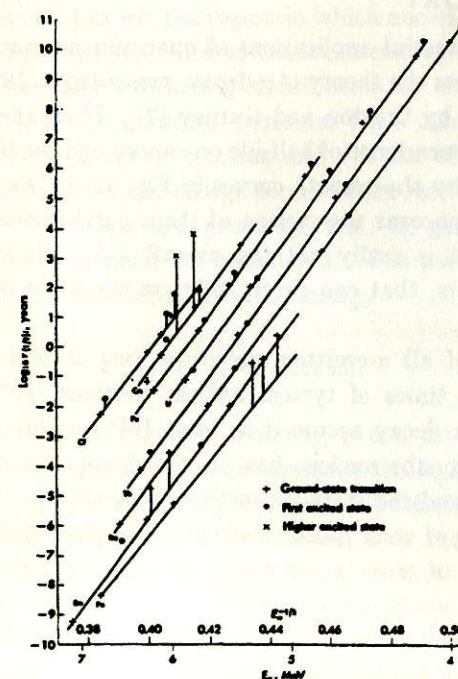


Fig. 11-1 Half-life versus energy relation for even-even α -emitters. The points appreciably off the empirical curves are either transitions to second excited states or pertain to isotopes of Em and Po whose decay involves a magic number.

points of the same Z produces a very regular family of lines. Moreover, with the exception of two isotopes of Rn and three of Po, the points for all the ground-state components of the α -spectra are seen to lie very close to the empirical lines.

If we were to plot the corresponding data for even- Z , odd- N nuclides on this diagram, we would see immediately that there are great discrepancies. In most cases, the half-life is 100–1000 times that for an even-even nuclide of the same Z and same energy; in no case is the half-life shorter than the corresponding even-even value. The ratio of the actual half-life to that predicted by the empirical even-even line is called the *hindrance factor*. There is no apparent correlation between hindrance factor and energy; it will be one of our tasks to try to "explain" the hindrance factor and to see what information concerning nuclear structure it can suggest to us. The pattern for odd-even and odd-odd nuclides is similar. The average hindrance factor for the odd-odd nuclides is perhaps greater than that for the odd-even cases.

11-2 BASIC THEORY

One of the first successful applications of quantum mechanics to a problem in nuclear physics was the theory of α -decay, presented in 1928 independently by Gamow [6] and by Condon and Gurney [7]. Their theory accounts for the very sensitive dependence of half-life on energy and predicts a relationship like that described by the smooth curves in Fig. 11-1. As we shall see, this theory essentially concerns the motion of the α -particle outside the nucleus, and consequently it is really not the overall $\lambda-E_\alpha$ relationship, but only the hindrance factors, that can throw light on the more interesting details of nuclear structure.

The half-lives of all α -emitters are very long indeed (10^{-6} to 10^{17} s) compared with the times of typical nuclear motions (10^{-21} s). Thus the average time before decay occurs is at least 10^{15} nuclear periods and may be as many as 10^{28} ; the nucleus has plenty of opportunity to establish a pattern of motion, and the state is practically stationary. We might expect the wave functions of such quasi-stationary decaying states to differ only slightly from those of true bound states, at least over time intervals that are not too great a fraction of the half-life. It is clear that over longer intervals the part of the wave function which describes the probability of finding the α -particle in the nucleus must decrease, with a corresponding increase in the probability of finding that the particle has reached "infinity," that is, has been emitted from the nucleus.

The concept of the slowly decaying, almost stationary, state arises in many problems and is handled in a variety of ways. In β - and γ -transitions one uses first-order time-dependent perturbation theory, but in cases like α -decay, which involve a leakage through a potential barrier of particles going from one region of space to another, one normally deals with the problem as a time-independent one, ignoring the very slow change in the flux onto the barrier. Alternatively, one explicitly takes account of the time rate of change by allowing the energy to have a small imaginary part, so that the factor $\exp(-iEt/\hbar)$ introduces a decaying exponential $\exp(-\lambda t)$ into the otherwise steady-state wave function. In some ways the introduction of a complex energy provides a neat formulation of the theory, and it has been applied extensively to α -decay (e.g., refs. 6, 11). Here, however, we shall derive the results by the perhaps more readily understood WKB formulation of barrier penetration.

Our picture is that from time to time, as the nucleons move in the nucleus, an α -particle is formed near the surface and moving outward. It is subject to strong attractive nuclear forces while it is close to the rest of the nucleus; but once the α -particle has left the region in which nuclear forces act between it and the product nucleus, the interaction is electromagnetic. If the nucleus were a static spherically symmetric distribution of charge, the potential energy would be just the Coulomb potential $V_C = 2Ze^2/r$, where Z is the charge number of the *daughter* nucleus and r is the distance between the center of the α -particle and the charge center of the nucleus. Actually, since nuclear-charge distributions are nonstatic and, in general, nonspherical, higher electric moments must be considered. The most important is the quadrupole, which contributes a potential energy

$$V_Q = \frac{2Qe^2}{r^3} P_2(\cos \omega), \quad (11-1)$$

where Q is the nuclear quadrupole moment, and ω is the angle between r and the nuclear axis. Since Q is of the order of the square of nuclear radii, and since Eq. 11-1 applies only for r greater than the nuclear radius, $V_Q < V_C$, and it is reasonable first to solve the problem with the Coulomb potential only, and to use these solutions as a basis for the solution of the more complete problem.

What can be said about the nuclear force felt by the α -particle near the nucleus or in its surface region? Just as nucleon scattering yields the potential between nucleons, and electron scattering reveals the nuclear-charge distribution, it seems reasonable to attempt to discover the actual force on an

α -particle in a nucleus by studying the scattering of α -particles from nuclei. In addition to elastic scattering, it is possible to have inelastic scattering or nuclear reactions in which the α -particle is not re-emitted. The cross sections for all these processes involve a single potential, called the *optical* potential for the α -particle. Optical potentials are discussed at length in Chapter 18 of M. A. Preston, *Physics of the Nucleus* (Addison-Wesley, 1962) and in other standard accounts of nuclear reactions. For the present discussion, we need to remark only that this potential is complex: the real part gives directly the force causing elastic scattering, whereas the imaginary part is present to take account of the "disappearance" of α -particles as they initiate nuclear reactions. The imaginary part therefore yields information on how far an α -particle can penetrate nuclear matter without breaking up, or at any rate ceasing to be a recognizable α -particle cluster. The real part represents the potential barrier that the α -particle must traverse.

Data for these potentials have been given by Igo [8]. However, the optical potential is accurately known only in the extreme outer region of the nucleus. Igo's analysis shows that in the uranium nucleus no appreciable number of elastically scattered α -particles gets closer to the center than 9.9 fm. Consequently the potential is known accurately only in this surface region, which is in the very diffuse nuclear tail; in uranium, the density has fallen to one-tenth its central value at about 8.5 fm.[†] This very fast absorption of incident α -particles might suggest a very short lifetime for α -particle clusters formed in the nucleus. However, we must remember that we expect an important amount of granular structure in the region outside the half-density radius, with the possibility of α -particle clustering being favored; hence it is difficult to relate directly the fate of externally incident α -particles to the α -particle flux incident on the barrier of a decaying nucleus.

On the other hand, although the optical potential does not give information about the motion of α -particles in the nuclear interior, it does yield the barrier which must be penetrated. The nuclear potential, to which must be added the Coulomb energy, is [8]

$$V(r) = -1100 \exp\left[-\left(\frac{r - 1.17A^{1/3}}{0.574}\right)\right] \text{ MeV}, \quad (11-2)$$

with r measured in femtometers. This expression is valid in the region in which $|V(r)| \lesssim 10$ MeV and yields a potential barrier with a very sharp inner surface. For example, the ground-state α -particles of the U isotopes,

[†] Since the α -particle has a rms radius of 1.6 fm, some of the matter of an α -particle at 9.9 fm reaches a short way inside the one-tenth-density shell.

with energies ranging from 4.2 to 6.7 MeV, all strike the inner side of the barrier at radii between 9.38 and 9.42 fm.

Consequently, the potential felt by the α -particle is of the nature shown by the solid line in Fig. 11-2. This figure also shows, as a dashed line, the "traditional" potential, a spherical well of sharp radius R and constant potential inside R . Of course, the assumption of constant potential inside the nucleus is an oversimplification, but it is of some value in understanding the process since it permits analytic solutions for the decay rate. On the other hand, it would seem more reasonable to assume some potential that fits smoothly onto Eq. 11-2. Such an expression, for example, would be a Woods-Saxon form

$$V_{\text{int}} = -V_0 \left[1 + \exp\left(\frac{r - R_0}{a}\right) \right]^{-1} \quad (11-3)$$

with appropriate constants. We shall discuss later the sensitivity of the results to the form of V_{int} .

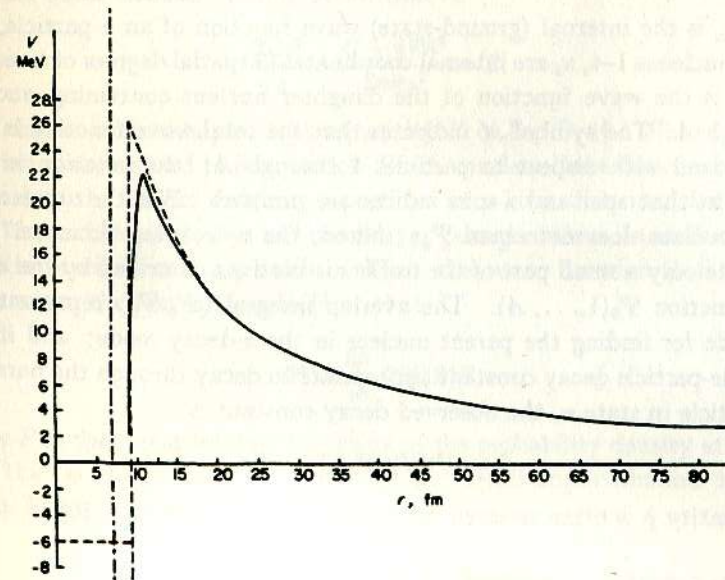


Fig. 11-2 Models of α -nucleus potential. The solid line is the optical potential of Eq. 11-2. The dashed line is the traditional model and the dot-dash line is the "surface well" model (see text).

So far the formulation ignores the imaginary part of the optical potential or, more physically, the fact that α -particles in a nucleus have a finite mean free path against losing their identity. One simple way of representing this phenomenon is to insist that α -particles can be found only within a short distance of the nuclear radius R , and to achieve this by postulating an infinite repulsion at a small distance from R . This has been called the surface-well model [9] and is represented in Fig. 11-2. It is not a very precise representation of the situation in which α -particles disappear, since the repulsive barrier is not absorptive but indeed reflects all particles striking it.

It is more satisfactory to consider the probability of finding an α -particle near the surface from the microscopic point of view of the dynamics of the nucleons. If an α -particle is to be considered as subject to a single-particle potential V similar to those in Fig. 11-2, its motion as it moves within the nucleus and through the barrier is described by a wave function $u(\mathbf{R})$, where \mathbf{R} is the position of the center of mass of the α -particle referred to the center of the nucleus and u is a suitable eigenfunction of V . From the nucleonic point of view the wave function to describe this state of an escaping α -particle is

$$\Psi_\alpha = \mathcal{A}\{u(\mathbf{R})\psi_\alpha(x_1, x_2, x_3)\Psi_r(r_5, \dots, r_A)\}, \quad (11-4)$$

where ψ_α is the internal (ground-state) wave function of an α -particle, containing nucleons 1–4, x_i are internal coordinates (9 spatial degrees of freedom), and Ψ_r is the wave function of the daughter nucleus containing nucleons 5 through A . The symbol \mathcal{A} indicates that the total wave function is antisymmetrized with respect to particles 1 through A ; the notation is compressed in that spin and i -spin indices are omitted. But the state of the parent nucleus does not equal Ψ_α ; indeed, the α -decaying “channel” may constitute only a small part of the nucleonic motions described by the actual wave function $\Psi_0(1, \dots, A)$. The overlap integral $\langle\Psi_0|\Psi_\alpha\rangle$ represents the amplitude for finding the parent nucleus in the α -decay mode; and if λ^0 is the single-particle decay constant appropriate to decay through the barrier V of a particle in state u , the observed decay constant is

$$\lambda = \lambda^0 |\langle\Psi_0|\Psi_\alpha\rangle|^2 = \lambda^0 p. \quad (11-5)$$

The quantity p is often referred to as the “formation factor” [10].

11-3 ONE-BODY THEORY

We first consider the simplest one-body form of the theory, in which the barrier is entirely Coulomb and the potential inside the barrier is constant,

that is, the “traditional” potential of Fig. 11-2. We make use of the WKB approximation described in Appendix D in order to write the barrier penetration. It is $e^{-2\omega}$, where

$$\omega = \int_R^{r_E} \left[\frac{2\eta k}{r} + \frac{(l + \frac{1}{2})^2}{r^2} - k^2 \right]^{1/2} dr. \quad (11-6)$$

Here we are considering an emission in which E is the total kinetic energy of the α -particle and residual nucleus,[†] $k^2 = 2mE/\hbar^2$, m is the reduced mass:

$$m = \frac{m_\alpha m_Z}{m_\alpha + m_Z},$$

$$\eta = \left(\frac{2Ze^2}{\hbar} \right) \left(\frac{m}{2E} \right)^{1/2}. \quad (11-7)$$

Z is the charge of the daughter nucleus, and in the centrifugal-energy term $l(l + 1)$ has been replaced by $(l + \frac{1}{2})^2$ since this gives greater numerical accuracy in the first-order WKB approximation. The range of integration in Eq. 11-6 is between the two points where the total energy equals the energy of the potential barrier; in this case R is the “nuclear radius” and r_E is the outer classical turning point, that is,

$$\frac{2Ze^2}{r_E} + \frac{(l + \frac{1}{2})^2 \hbar^2}{2mr_E^2} = E.$$

Note that ω in this chapter is the quantity K of Eq. D-10. When the wave function is normalized to one particle “in the nucleus,” the decay constant λ^0 is equal to the flux of outgoing α -particles at a large distance, since this is then the number of decays per second per parent nucleus, in each of which there is precisely one α -particle. When the wave function ψ is an outgoing wave, the flux is $(\hbar/m)k|\psi|^2$, so that

$$\lambda^0 = \frac{\hbar k}{m} P |\psi(R)|^2, \quad (11-8)$$

where P is the factor relating the value of the probability density at infinity with that at the radius R . In terms of the WKB approximation described in Eq. D-11, P is given as

$$P = \left| \frac{k(R)}{k(\infty)} \right| \exp(-2\omega), \quad (11-9)$$

[†] More precisely, the total energy should be reduced by approximately $65.3(Z + 2)^{7/5}$ eV to allow for electron screening [11].

where $k(r)$ is the local wave number, that is,

$$k^2(r) = \frac{2m|E - V|}{\hbar^2}. \quad (11-10)$$

Hence, for the "traditional" model,

$$\begin{aligned} P &= \left[\frac{2Ze^2}{RE} + \frac{(l + \frac{1}{2})^2 \hbar^2}{2mR^2 E} - 1 \right]^{1/2} e^{-2\omega} \\ &= \left[\frac{2\eta}{Rk} + \frac{(l + \frac{1}{2})^2}{k^2 R^2} - 1 \right]^{1/2} e^{-2\omega}. \end{aligned} \quad (11-11)$$

It is convenient to define a number α by the relationship

$$\tan^2 \alpha = \frac{2\eta}{Rk} + \frac{(l + \frac{1}{2})^2}{k^2 R^2} - 1. \quad (11-12)$$

Then it is readily seen that

$$\omega = \eta(2\alpha - \sin 2\alpha). \quad (11-13)$$

To obtain this last result, we have ignored the square of the ratio of the centrifugal term to the Coulomb term, which is small compared with unity. Assembling these results, we find

$$\lambda^0 = \frac{\hbar k}{m} \tan \alpha e^{-2\omega} |\psi_0(R)|^2, \quad (11-14)$$

where ψ_0 is the wave function for the α -particle inside the barrier.

The normalization of ψ_0 can be found to a good approximation from the condition that there be one α -particle in the nucleus, namely,

$$\int_0^R |\psi_0(r)|^2 dr = 1. \quad (11-15)$$

It follows that we can write

$$\lambda^0 = \frac{2v}{R} \tan \alpha e^{-2\omega} \frac{1}{F} \quad (11-16)$$

where

$$F = \frac{2}{R} \frac{\int_0^R |\psi_0|^2 dr}{|\psi_0(R)|^2}. \quad (11-17)$$

Note that F is a dimensionless quantity dependent only on the wave function *inside* the nucleus.[†]

The factors in Eq. 11-16 for λ^0 can be interpreted physically. The number of times per second that an α -particle in the nucleus will hit the boundary of the nucleus is of the order of the velocity of the particle in the nucleus divided by the nuclear radius. Now, the velocity in the nucleus is not the same as the velocity v which the particle has at infinity, but the two are of the same order of magnitude. The last factor in Eq. 11-16 depends on the inside wave function. Hence it is reasonable to regard $2v/RF$ as the frequency with which the particle hits the wall. The other two terms depend only on the outside behavior and can be interpreted as the probability that the particle striking the wall will penetrate the barrier. For the energies of actual α -particles, η is about 20–25. Thus the variation in λ^0 comes essentially from the exponential. Also, because of the large value of η , the absolute value of λ^0 is very sensitive to the value of R used in determining α . In actual practice E and λ are known experimentally, and the equations have been used to determine the nuclear radius and a parameter in F . This was one of the earliest methods of finding the radii of heavy nuclei.

For example, with the traditional model of Fig. 11-2 and for the special case $l = 0$, the explicit form of the interior solution is

$$u_i = c_i \sin Kr,$$

where $K^2 = (2m/\hbar^2)(E - V_0)$ and V_0 is the constant interior potential. In order to fix two parameters we need a relationship in addition to Eq. 11-16. This arises from the realization that K is not arbitrary, since the wave function and its derivative must be continuous everywhere, in particular at the nuclear radius; we express this as the equality of the logarithmic derivative du/dr . Inside the well this is simply $K \cot KR$. To obtain its value just inside the Coulomb barrier we have resorted to the WKB approximation, which indicates that the solution under the barrier is

[†] One can generally demonstrate for the regular solution of a one-body Schrödinger equation that F can be alternatively expressed as

$$F = \frac{\hbar^2}{mR} \frac{d}{dE} \left(\frac{1}{\psi_0} \frac{d\psi_0}{dr} \right)_{r=R}. \quad (11-17a)$$

In other words, it is essentially the derivative with respect to the energy of the state of the logarithmic derivative of the wave function. This form of F arises naturally in the alternative derivation, which assigns the energy an imaginary part, and the fact that expressions 11-17 and 11-17a are equal provides the connection between the two derivations. See, for example, M. A. Preston, *Physics of the Nucleus*, Addison-Wesley, 1962, p. 362.

$$u(r) = c[k(r)]^{-1/2}(e^{\omega} + \frac{1}{2}ie^{-\omega}),$$

of which only the first term is significant at $r = R$. It is straightforward to see that the logarithmic derivative is $-k \tan \alpha$. Thus the two equations governing the simplest case of one-body α -decay are

$$K \cot KR = -k \tan \alpha \quad (11-18a)$$

and

$$\lambda^0 = \frac{2v \tan \alpha}{R F} e^{-2\omega} \quad (11-18b)$$

with F given by Eq. 11-17 as

$$F = \operatorname{cosec}^2 KR - (\cot KR)/KR. \quad (11-18c)$$

In these equations certain terms in $1/\eta$ have been omitted, causing an error of about 2%. The procedure used in a number of papers [12, 13] has been to solve Eq. 11-18a for K with an assumed value of R , and then to calculate λ^0 using this value of K . If the experimental value of λ is not obtained, a different choice of R is made, and the procedure is repeated until agreement is reached. Since λ^0 is the decay constant after the α -particle has formed (i.e., the λ^0 of Eq. 11-5), the procedure is equivalent to assuming that the formation factor ρ has a value of 1. This is certainly an overestimate of ρ ; λ is an underestimate of λ^0 . If more correct (i.e., higher) values of λ^0 were used, higher values would be obtained for R , since increasing the radius makes the barrier thinner and increases the penetration probability. However, some correction to R for the finite size of the α -particle is presumably necessary. Thus we say that a precise correlation of R with nuclear radius is not possible.

Nevertheless, for the ground-state transitions in even-even nuclei, the values of R calculated from Eq. 11-18 with the assumption that $\rho = 1$ are in excellent agreement with $R = r_0 A^{1/3}$, where $r_0 = 1.57 \pm 0.015$ fm. Also, the values of V_0 are found to satisfy the equation $E + V_0 = 0.52 \pm 0.01$ MeV. Although the physical significance of V_0 is not very clear, this result for $E + V_0$ has a simple meaning: it implies that KR is always just a little less than π , so that the interior wave function is very small at the boundary, as indicated in Fig. 11-3. (Actually $KR = 2.986 \pm 0.005$.)

The above value for r_0 is higher than that found from experiments involving electron and neutron scattering, for which the interpretation is

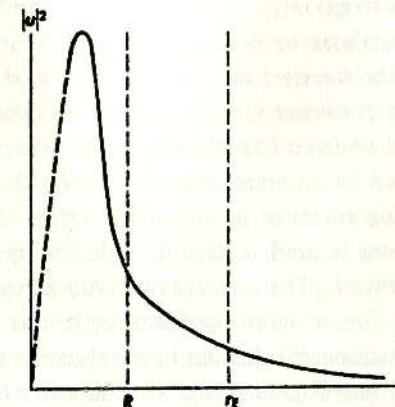


Fig. 11-3 The α -decay probability density.

much less ambiguous. These experimental results suggest $r_0 < 1.2$ fm. Let us assume as a simple model that R is made up of a true nuclear radius R_0 and an α -particle radius, $R = R_0 + R_\alpha$. If we demand that $R_0 = 1.2 A^{-1/3}$ fm, and that the λ^0 's from Eq. 11-18 agree with the experimental decay constants, we find that $R_\alpha = 2.2$ fm. In other words, with $r_0 = 1.2$ fm and $R_\alpha = 2.2$ fm, we find that the formation factor ρ is unity. The rms radius of ${}^4\text{He}$ measured by electron scattering is 1.6 fm, which gives an equivalent square-well value of 2.1 fm. To decrease ρ it would be necessary to increase R_α to unreasonable values. The great regularity of the empirical values for R and $E + V_0$ suggests that, whatever the value of ρ , it is fairly constant for most even-even nuclides. This is the significance of the close agreement of the experimental data with the lines in Fig. 11-1. Indeed, we see that Eqs. 11-5, 11-13, and 11-18b yield

$$\ln \lambda = \ln \rho + \ln \left(\frac{2v}{RF} \tan \alpha \right) - (2m)^{1/2} \frac{Ze^2}{\hbar} (2\alpha - \sin 2\alpha) E^{-1/2}. \quad (11-19)$$

For the observed disintegration energies, the values of α turn out to be in the region of $\pi/3$, and the function $(2\alpha - \sin 2\alpha)$ does not vary too greatly over the observed energy range. Since the second logarithmic term in Eq. 11-19 also turns out to be fairly insensitive to the energy, we see that $\log \lambda$ is approximately a linear function of $E^{-1/2}$ apart from fluctuations in ρ .

Apart from variations in ρ , experimental values of λ may be expected to depart from the smooth curves of Eq. 11-19 if the relative angular

momentum is different from zero. The effect of angular momentum on the outside solution is such as to decrease λ , since $l(l+1)/r^2$ may be considered an addition to the barrier, making it higher and thicker. At first, this was the only effect considered; however, to be consistent one should also include the effect of nonzero l on the interior solution, and such considerations can actually lead to an increased value of λ [12, 14]. In the traditional model the interior solution is $u_i = c_i K r j_i(Kr)$. If the logarithmic derivative of this function is used as the left side of Eq. 11-18a, it will be found that K increases with l . The increase indicates a greater kinetic energy inside the nucleus and hence more frequent collisions with the surface. Mathematically, this situation is reflected in a reduced value of F , which in turn tends to increase λ^0 (see Eq. 11-18b). On the other hand, the increased barrier reduces $e^{-\omega}$ and tends to reduce λ . For $l \lesssim 4$, the result is an increase in λ^0 ; for $l > 4$, the exponential decrease becomes the deciding factor.

As we have already remarked, the traditional model is seen in Fig. 11-2 to be a not unreasonable approximation to the optical potential with, say, a Woods-Saxon potential inside the nucleus. But our results, typified by the exponential dependence in Eq. 11-18, show a very marked sensitivity to R or, more precisely, to the behavior of the wave function near the nuclear surface. The result for λ^0 is clearly affected by both the shape of the potential barrier and the approximations arising in the calculation. Both factors have been considered [15, 16]. By replacing a constant potential by a more physically reasonable Woods-Saxon shape joining smoothly onto the Igo optical potential, the quantity RF can be changed by 50–75%. Replacing the WKB approximation by numerical integration through the barrier is a time-consuming procedure, since the accurate calculation of an exponentially decreasing function requires great numerical accuracy; nevertheless, it has been done and, for reasonable values of R , causes about 10% effects.

Another consideration is the effect of abandoning the assumption that the one-body potential is local. One would, in fact, expect an effective α -nucleus potential to be momentum dependent or nonlocal, at least at short distances. Such potentials have been considered [17, 18]. Unfortunately, α -particle scattering has not been done at sufficient energies to sample much of the nuclear interior, so that considerable ambiguity is available to the theorist. One should, of course, use potentials that give the correct scattering cross sections; on the basis of the results of refs. 17 and 18, it is probably reasonable to consider that the use of nonlocal potentials restricted in this way will produce changes in the one-body factor ranging over about the same values as are covered by a sequence of acceptable Woods-Saxon potentials.

To summarize the above, we may note that the major uncertainty of the one-body model is connected with the potential and wave function at distances inside about 9 fm. We recall that the well-known part of the optical potential of Eq. 11-2 is outside this distance, and that the inner turning point R is near 9.4 fm for the observed range of α -particle energies. Consequently, it is reasonable to calculate the penetrability P of the barrier and to interpret λ/P as the single-body α -particle probability at R , subsuming in λ/P all the internal effects. Of course, P must be calculated with the most realistic possible barrier, that is, the nuclear potential of Eq. 11-2, together with the Coulomb and angular-momentum barriers.

These calculations have been made by Rasmussen [19]. He lists penetration factors for most well-known transitions and expresses the flux in terms of the *reduced width* δ^2 (MeV), defined as

$$\delta^2 = \frac{\lambda}{P} h, \quad (11-20)$$

where h is Planck's (uncrossed) constant. The quantity δ^2/h is the hypothetical decay rate in the absence of a barrier. It is, of course, related to the formation factor ρ . From the point of view of nuclear dynamics, the interesting aspect of α -decay is the determination of δ^2 . Rasmussen's values of δ^2 have been calculated with a realistic barrier and therefore may be considered good empirical values. Since they are based on the WKB approximation, they are subject to a correction of the order of magnitude noted above. The values might also change slightly if the Igo potential were replaced by a nonlocal one; but, as we have suggested, values of P are likely to be quite close for formally different potentials that are equivalent in elastic α -nucleus scattering.

Of course, the single-particle models, including the optical model, do not provide an understanding of the values of δ^2 beyond the rough order of magnitude v/R ; one must find ρ from microscopic theory.

11-4 HIGHER ELECTRIC MOMENTS

The quadrupole potential (Eq. 11-1) involves the angle between the radius to the α -particle and the axis of the nucleus; it is a particular case of noncentral interactions for which the relative orbital angular momentum is not constant. A particle can leave the nucleus with angular-momentum quantum number l_1 , and later, through the intermediary of such noncentral potentials, it can acquire a different value of l , say l_2 , with the nucleus going to a state

such that the total angular momentum and parity of the system are conserved. Of course, there is also an exchange of energy. For example, an even-even nucleus might undergo its ground-state transition, emitting an α -particle with $l = 0$. Then, before the particle had moved too far away, the quadrupole interaction could raise the nucleus to an excited state with $J = 2$, simultaneously reduce the kinetic energy of the particle, and change l to 2. Since the barrier would then have been penetrated partially at one energy and partially at another, the λ 's of the two groups of particles would not have the values obtained by the theory discussed in Section 11-3. Moreover, we also see that the observed ratio of the intensity of the l_1 -group to that of the l_2 -group is not the same at infinity as at the nuclear radius, for the number of particles going from l_1 to l_2 is not the same as the number of particles involved in the reverse transition. In other words, the quantities $w_1 = \lambda_1/\lambda_1^0$ and $w_2 = \lambda_2/\lambda_2^0$, which, according to the previous theory, would be the formation factors p_1 and p_2 , now differ from them because of the effect of the noncentral forces. In addition to the change in the amplitude of different angular momenta as the α -particles move out from the nucleus, a nonspherical shape may cause a different angular distribution of α -particles over a sphere *near* the nucleus.

Let us consider a spheroidal even-even nucleus, emitting α -particles in transitions to both the ground state and the various rotational states of its daughter. The angular distribution of a wave is closely related to the relative amplitudes of the constituent angular-momentum states. A com-

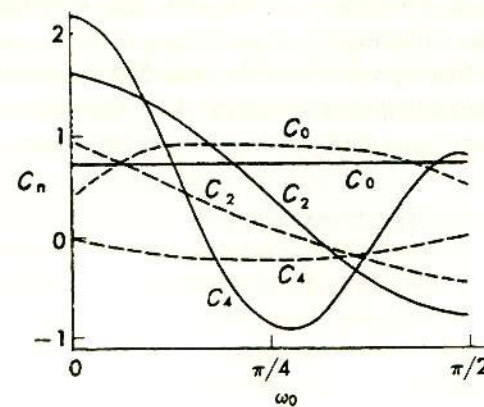


Fig. 11-4 Components of distribution functions peaked at angle ω_0 .

pletely isotropic distribution is entirely an $l = 0$ wave. As the distribution becomes more peaked, the higher components become more important, and the relative amounts of various l 's present depend on the angle about which the distribution is peaked. For example, the relative amounts of $l = 0, 2$, and 4 are shown for various angles and for two different distributions in Fig. 11-4, in which $|C_n|^2$ is the relative proportion of the state with $l = n$. If $|f(\omega)|^2$ is the angular distribution of α -particles, the solid lines represent the very peaked distribution

$$f(\omega) = \frac{1}{2} \delta(\omega - \omega_0) + \frac{1}{2} \delta(\omega - \pi - \omega_0),$$

and the dotted lines the broad distribution

$$f(\omega) = \cos^2(\omega - \omega_0), \quad \omega \leq \frac{\pi}{2}.$$

Now, for a nucleus of positive quadrupole moment, the greatest excursions of nuclear matter from the center are in the directions 0 and π , with the angles measured from the symmetry axis. Consequently, to reach the same distance from the center of the nucleus, particles traveling out in different directions have to cover varying distances within the Coulomb barrier; and, assuming that the encounters of nascent α -particles with the nuclear surface are uniformly distributed over the surface, we might therefore expect that near the nucleus the distribution of α -particles would be peaked around the angles 0 and π . On the other hand, the quadrupole potential V_Q is greatest in the directions 0 and π , so that, although particles moving in these directions have a head start through the barrier, they also encounter a higher barrier. Thus during the progress through the barrier the intensity in these directions will suffer a relative decrease, or, in other words, the effect of the quadrupole moment is to shift the peak in the angular distribution toward angles 90° from the maximum of V_Q . It is clear that the same considerations apply also to negative Q 's, where the initial maximum at $\pi/2$ would be swung toward 0 and π .

Figure 11-4 shows that, as the peak of the distribution moves toward $\pi/2$, the proportions of the $l = 4$ and $l = 2$ components decrease with respect to the $l = 0$ wave. Consequently, for positive Q , the waves with $l = 2$ and $l = 4$ will lose intensity to the $l = 0$ wave as the particles move out. Thus the ratio of the apparent formation factors w_2/w_0 will be less than p_2/p_0 . If we assume that all even-even nuclei have about the same ratio of actual formation factors (p_2/p_0), we expect w_2/w_0 to decrease as Q increases. Since the natural α -emitters are located in the part of the periodic table where

increasing Z corresponds to the filling of proton and neutron shells with increasing Q , w_2/w_0 should decrease if Z increases. If $l = 4$ states are involved, Fig. 11-4 would indicate that the ratio w_4/w_0 should exhibit this decrease even more markedly. Both effects are found.

These considerations have been formulated quantitatively [20]. The electrostatic interaction of the α -particle with the nucleus is expanded in spherical harmonics,

$$V(r) = \sum_{p=1}^A \frac{2ee_p}{|r - r_p|} = 2e \sum_p \sum_\lambda e_{\lambda p} r_p^{-\lambda} P_\lambda[\cos(r, r_p)] r^{-(\lambda+1)}, \quad (11-21)$$

where $e_{\lambda p}$ is the effective nucleon charge. The similarity between this expression and the multipole expansion of the electromagnetic field in appendix E suggests that the same nuclear matrix elements $B(E\lambda)$ will enter the calculation. We may write the wave function of the final state as a superposition of waves with the angular momentum of the initial nucleus shared in various ways between the α -particle and the residual nucleus:

$$\Psi = \sum_{l, J_f, \tau} r^{-1} u_\nu(r) \chi_\nu^M(\theta, \phi, \xi),$$

$$\chi_\nu^M(\theta, \phi, \xi) = \sum_m (lJ_f m M - m|J_i M) Y_i^m(\theta, \phi) \psi_{f, \tau}^{M-m}(\xi), \quad (11-22)$$

where ν stands for (l, J_f, τ) , τ represents all unspecified quantum numbers of the residual nucleus, ξ represents all coordinates of the residual nucleus, and r is the coordinate of the α -particle. (Since the α -particle is supposed to be in the same state initially and finally, its internal wave function is not included.) Equation 11-22 is substituted in the Schrödinger equation for the whole system,

$$\left[H_\xi - \frac{\hbar^2}{2m} \nabla^2 + V(r) - E \right] \Psi = 0,$$

the scalar product is taken with χ_ν^M , use is made of the fact that

$$H_\xi \psi_\nu(\xi) = E_\nu^{\text{nuc}} \psi_\nu(\xi),$$

and, after some simplification of the angular-momentum coefficients, we obtain [11]

$$\begin{aligned} & -\frac{\hbar^2}{2M} \frac{d^2 u_\nu}{dr^2} + \left[\frac{l(l+1)\hbar^2}{2mr^2} + E_\nu^{\text{nuc}} - E + \frac{2Ze^2}{r} \right] u_\nu \\ & = \sum_{\lambda=1}^{\infty} \frac{2e}{r^{\lambda+1}} \sum_\nu u_\nu(r) [B_{\nu \rightarrow \nu}(E\lambda)]^{1/2} c(l, l', J_f, J_f'; \lambda). \end{aligned} \quad (11-23)$$

Here

$$\begin{aligned} c(l, l', J_f, J_f'; \lambda) &= \pm (-)^{J_f'-1} \frac{[4\pi(2l+1)(2l'+1)(2J_f'+1)]^{1/2}}{2\lambda+1} \\ &\times (l'00|\lambda 0) W(l, l' J_f'; J_f \lambda), \end{aligned}$$

where W is a Racah function. The uncertainty in sign comes from taking the square root of $B(E\lambda)$ at a certain point in the calculation; it relates to the two possible phases of the corresponding γ -transition. Sometimes angular γ -distributions will fix the sign experimentally; in other cases, it is fixed by a sufficiently detailed theoretical model.

The left side of Eq. 11-23 is the equation for the radial function u_ν , in the absence of noncentral interaction, which we have already studied in detail. The solutions for the different angular-momentum states are coupled by the right side. The coupling gives mathematical expression to the physical idea that an α -particle could start at the nucleus with a single specific angular momentum and energy [$u_\nu(R)$ finite, $u_\nu(R) = 0$ for $\nu \neq \nu'$] and, after traveling to some distance r , would have exchanged energy and angular momentum with the nucleus with a certain probability related to the now nonzero amplitude $u_\nu(r)$. The experimentally measured intensities of the different groups E_ν in the decay of a nuclide are proportional to $|u_\nu(\infty)|^2$. Internal nuclear dynamics determine $u_\nu(R)$, and the set of coupled differential equations 11-23 provides the link between the relative intensities at the nucleus and at infinity.

It is clear that the extent to which the population of one group (ν) is increased at the expense of another (ν') as the particles travel out is dependent on the size of the reduced matrix element $B_{\nu \rightarrow \nu'}$. The magnitude of the effect also depends on the energy difference $|E_\nu - E_{\nu'}|$, and is greater for smaller energy differences.

It has been shown that electric dipole oscillations are unimportant. Two groups are emitted by ^{241}Am decaying to levels of ^{237}Np separated by only 60 keV and connected by an $E1$ -transition. With matrix elements of single-proton magnitude, the coupling effect is of the order of 10^{-2} of the intensity of the strong transition; but when the actual retarded value for $M(E1)$ is used, the result is reduced to 10^{-7} [11].

The noncentral effect is appreciable only in transitions to different states of the same rotational band in spheroidal nuclei. Here the quadrupole matrix element $B(E2)$ is large, and the energy differences are reasonably small. Since most natural α -emitters are spheroidal nuclei, the effects of quadrupole coupling have been extensively studied [11, 21, 22, 23, 24, 25].

The wave functions u_r in Eq. 11-23 are known at large distances, for as r tends to infinity, the coupling terms become negligible, and u_r is simply a Coulomb wave function for a particle of energy $E - E_v^{\text{nuc}}$ and charge $2e$, moving out from the charge Ze . When F_v and G_v are the regular and irregular Coulomb functions discussed in Appendix B, then

$$u_r \sim A_v e^{i\delta_v} (G_v + iF_v). \quad (11-24)$$

The magnitudes A_v are fixed by the experimentally measured intensities of the different groups, since the intensity $I_v = v_v A_v^2$, where v_v is the velocity of the particles in group v . However, the phases δ_v are not fixed by this consideration. To determine them experimentally, one would have to measure some quantity that depends on the interference between the various terms of Ψ . Such experiments (e.g., the measurement of the angular distribution of α -particles from oriented nuclei) are difficult to perform. Fortunately the phases must also satisfy a condition imposed by theory. Since the α -particles are emitted by quasi-stationary states, the α -particle flux at the nuclear surface must be due entirely to the imaginary part of the energy. In other words, in a calculation using only the real part of the energy, there must be no current of α -particles at the nuclear surface; this condition requires that the imaginary part of u_r vanish on the surface.

One can then envisage obtaining the physical solution of the set of equations 11-23 by starting at some large value of r with form 11-24, in which the A_v 's are known. By numerical computation, the equations are integrated inward for various values of δ_v , and those values of δ_v are selected which make the imaginary parts vanish on the nuclear surface. It turns out that this condition permits two solutions for each δ_v , one near zero and one near π . (Of course, one of the δ_v 's, say δ_0 , can always be equated to zero, because of the arbitrary phase of the total wave function.) Consider

TABLE 11-2 Relative Amplitudes of the Waves of α -Particles of Different Angular Momenta on the Surface of the ^{242}Cm Nucleus. After Chasman and Rasmussen [25].

Case:	A	B	C	D	E	F	G	H
$\frac{u_2}{u_0}$	1.208	1.175	-1.013	-1.080	1.204	1.171	-1.005	-1.071
$\frac{u_4}{u_0}$	0.423	0.221	-0.276	-0.626	0.348	0.145	-0.148	-0.496
$\frac{u_6}{u_0}$	0.336	0.261	-0.431	-0.562	-0.188	-0.264	0.461	0.334

an even-even decay. The quadrupole moment couples the transitions to the ground state and to the first excited state $J = 2$ of the rotational band, that is, u_0 and u_2 are coupled. Also u_2 is coupled to u_4 , the radial function for decay to the $J = 4$ rotational state. In turn u_4 is coupled to u_6 as well as to u_2 , and so on. However, the number of α -particles feeding the higher levels rapidly decreases, so that the effect of u_8 on the value of u_4 may be ignored. It is therefore a reasonable procedure to consider only the first four equations of the set 11-23 and include only u_0 , u_2 , u_4 , and u_6 . The ambiguity in δ_2 , δ_4 , and δ_6 means that there are eight possible sets of phases and eight different solutions. In general, if we keep n wave functions, there are 2^{n-1} solutions, and the selection of the correct one can be made satisfactorily only by an interference experiment.

The large number of numerical results may be typified by a single case, ^{242}Cm , for which we assume the quadrupole moment $Q_0 = 11 \text{ eb}$. We show in Table 11-2 the relative values of u_0 , u_2 , u_4 , and u_6 on a sphere of radius 9 fm, which lies in the nuclear surface. The squares of these numbers are

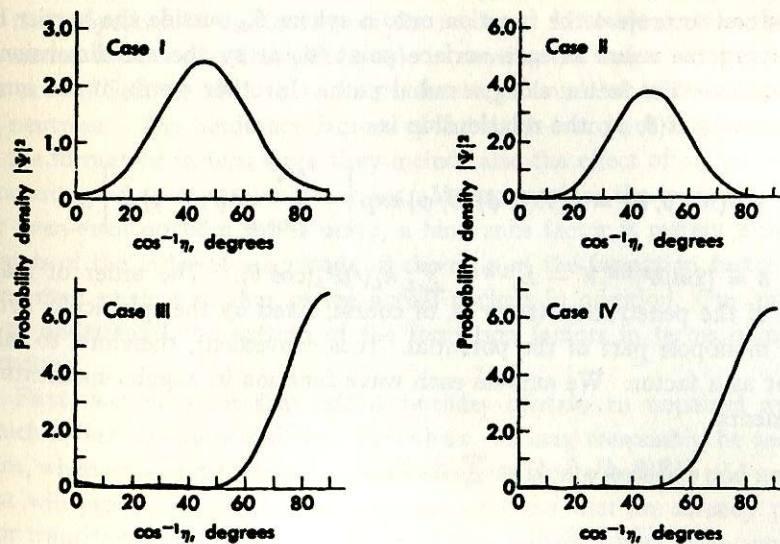


Fig. 11-5 Distribution of α -particles over the spheroidal surface of ^{242}Cm , based on the assumption that $Q_0 = 11.3 \text{ eb}$. The abscissa is $\cos^{-1} \eta$, where η is the difference of the distances between the point on the spheroid and the two foci divided by the interfocal distance: $\eta = (r_1 - r_2)/a$. The polar angle θ is approximately $\cos^{-1} \eta$. This graph is approximate, being based on calculations [23] which ignored the $l = 6$ wave.

therefore the relative probabilities of forming the four different groups of α -particles. It is seen that among the eight cases there are some quite different solutions, particularly in the amplitude of the particles with $l = 4$. These results demonstrate that the noncentral effect may be quite important, but that we cannot calculate surface amplitudes uniquely without knowing the phases at infinity as well as the intensities.

Another way of presenting the results is to show the distribution of α -particles over the nuclear surface. Figure 11-5 illustrates the angular variation of $|\Psi|^2$ on the spheroidal surface of ^{242}Cm for four of the eight typical cases. In the cases labeled III and IV, α -particle formation is confined to a band of approximately 30° on either side of the equator. On the basis of our ideas of nuclear structure this seems improbable, and hence we incline toward accepting one of the other solutions.

It would be tedious and expensive to perform numerical integration of the barrier penetration for each case of decay of a nonspherical nucleus. One looks, therefore, for an extension of the WKB method that will deal with penetration of a barrier containing the noncentral quadrupole force. Such a technique has been developed by Fröman [21]. Given an arbitrary wave function over an arbitrary surface near the nucleus, Fröman's method permits one to project the function onto a sphere R_0 outside the barrier by multiplying the value at each surface point (θ, ϕ) by the one-dimensional WKB exponential factor along a radial path. In other words, if the inner surface is $r = R(\theta, \phi)$, the relationship is

$$\psi(R_0, \theta, \phi) = \psi[R(\theta, \phi), \theta, \phi] \exp \left[- \int_{R(\theta, \phi)}^{R_0} k(r, \theta, \phi) dr \right],$$

where $k = (2m/\hbar^2)^{1/2}[V - E]^{1/2} = \sum_L k_L(r) P_L(\cos \theta)$. The order of magnitude of the penetration factor is, of course, fixed by the spherically symmetric monopole part of the potential. It is convenient, therefore, to take this out as a factor. We express each wave function in angular-momentum components

$$\psi[R(\theta, \phi), \theta, \phi] = \sum c_{lm} Y_{lm},$$

$$\psi(R_0, \theta, \phi) = \exp \left[- \int_R^{R_0} k_0(r) dr \right] \sum d_{lm} Y_{lm}.$$

where R is the radius of a spherical surface near the nuclear surface $R(\theta, \phi)$ —indeed, a convenient one is the sphere enclosing the same volume. We then define the matrix k by

$$d_{lm} = \sum_{LM} c_{LM} k_{IL}^{mm}.$$

If there were spherical symmetry, k would be the unit matrix, and in the general case it gives the angular-momentum distribution of the α -particles at a large distance R_0 in terms of their distribution on the nuclear surface. Of course, there is no change in the angular momentum once α -particles have traveled sufficiently far from the nucleus that the quadrupole field is negligible. Consequently, to evaluate the matrix k we need only calculate WKB integrals through the barrier. Fröman's initial calculations have been extended by Poggenburg, Mang, and Rasmussen [26].

11-5 FORMATION FACTORS

In addition to nonzero values of l and noncentral interactions, there is still a third factor which produces departures of the empirical lifetimes from the smooth values for even-even nuclides, namely, variation of the formation factor. It is the only one of the three that seems capable of producing factors of 10 or more in the half-life, and its value is potentially most informative about nuclear structure since it is the only one that depends sensitively on the properties of the interior of the nucleus. It seems certain that the formation factors play the leading role in causing the longer lifetimes which we saw in Section 11-1 to be characteristic of nuclides with odd protons or neutrons. The hindrance factors of Table 11-1 are not directly related to the formation factors, since they include also the effect of higher angular momenta and noncentral interactions. Moreover, since the formation factor for even-even nuclides is not unity, a hindrance factor is merely a number that is of the order of magnitude of the ratio of the formation factor of an even-even nucleus to that of the actual nucleus in question. Our problem is to understand the pattern of the formation factors in terms of nuclear structure.

First, we recognize that odd- A nuclides contain an unpaired nucleon which is less tightly bound than the others. It may reasonably be assumed that, when an α -particle forms, it is not likely to incorporate the odd nucleon, but will probably consist of protons and neutrons that are already paired. For transitions in which the odd nucleon does not change its quantum state, the formation factor would be expected to be about the same as for even-even nuclei, since the nucleons forming the α -particle would have very similar wave functions in the two cases. Consequently, if the ground state of the daughter nucleus differs from that of the parent, while an excited

state has a similar wave function, we expect the ground state to show a considerable departure factor, whereas the excited state may have essentially the lifetime appropriate for an even-even case. This would explain the typical pattern of odd- A nuclides, which we discussed in Section 11-1.

As an example of a considerable body of similar data, consider the decay of ^{243}Cm , shown in Fig. 11-6. The various quantum numbers of the single-particle levels in a spheroidal potential are shown. It is seen that only 13% of the transitions go to the ground-state band A of ^{239}Pu , whereas 86% go to the two levels of the band labeled B . It is not hard to find the

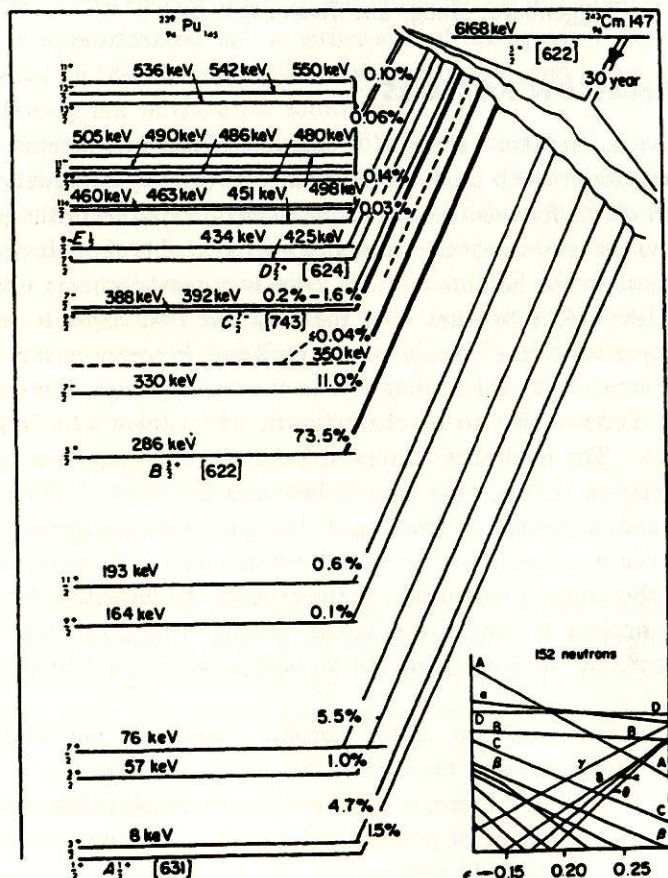


Fig. 11-6 Decay of ^{243}Cm . About 30 α -groups are known; the 24 of highest energy are shown. The notation for a band is $K\pi[N, n_z, A]$. Based on Nuclear Data Sheets B3, No. 2, 1969 and S. A. Baranov et al., *Yadern Fiz.* 4, 1108 (1966). The insert of a portion of a level diagram has the notation: $A \frac{1}{2}^+[631]$, $B \frac{5}{2}^+[622]$, $C \frac{7}{2}^-[743]$, $D \frac{7}{2}^+[624]$, $\alpha \frac{9}{2}^-[503]$, $\beta \frac{5}{2}^+[633]$, $\gamma \frac{1}{2}^-[501]$, $\delta \frac{5}{2}^-[503]$, $\epsilon \frac{3}{2}^-[501]$, $\theta \frac{13}{2}^+[606]$.

reason: the transitions to band A have $\Delta K = 2$ and $\Delta A = 1$, whereas there are no changes in quantum numbers in the transitions to band B . Another very typical example is provided by ^{241}Am , 84% of whose decays go to a $\frac{5}{2}^-$ level at 60 keV rather than a $\frac{5}{2}^+$ ground state; the quantum numbers of the decaying state of Am ($J = \frac{5}{2}$, $\pi = -1$, $N = 5$, $n_z = 2$, $A = 3$, $K = \frac{5}{2}$) are identical with those of the Np state preferentially fed, whereas the ground state of ^{237}Np is $\frac{5}{2}^+$ ($6, 4, 2, \frac{5}{2}$). Of course, the reason that it is an excited state of the daughter which resembles the ground state of the parent is simply that, with the addition of two more neutrons (or protons), the odd particle in the ground state has moved to the next Nilsson orbit. The atomic number of Np is 93; and, as Fig. 9-31 shows, for $\eta \sim 5$ the $\frac{5}{2}^+$ ($6, 4$) state and the $\frac{5}{2}^-$ ($5, 2$) state are, respectively, the ground and first excited states for the 93rd proton, and the latter is the ground state for the 95th proton.

Within a given rotational band, the states have the same internal structure, but in some transitions the α -particle may carry off zero angular momentum, whereas in others it must remove an appreciable amount. The decays requiring higher l -values for the α -particle are expected to be less probable, if only because of the increasingly greater radius at which the particle must be formed. This distinction is present in the cases cited in the last paragraph (note that all the levels which are appreciably fed have $\Delta J = 0$ or 1), and the additional hindrance with higher l 's is shown also in even-even decays. The decays to the first excited 2^+ states are not delayed; in fact, in many cases the reduced width δ^2 is actually greater for the $l = 2$ transition. However, all the $l = 4$ transitions to 4^+ rotational states are slow. A quantitative expression is readily given in terms of the *reduced hindrance factor*, which is the ratio δ_l^2 / δ_0^2 , where δ_l^2 is the reduced width $\hbar\lambda/P_l$, obtained with a barrier penetrability including the centrifugal barrier, and δ_0^2 is the reduced width of the ground state. The reduced hindrance factors for $l = 2$ range from 0.8 to 1.2, while those for $l = 4$ increase with nuclear distortion, ranging from 2 at $Z = 90$ to a maximum of 150 in ^{244}Cm , and then decrease [19]. However, these numbers do not measure the relative difficulty of forming an α -particle with $l = 4$, for they are based on the intensity of such particles at infinity, not at the nuclear surface, and we know that the quadrupole interaction can seriously affect the relative intensities.

We see that the α -decay of spheroidal nuclei is consistent with the collective model, both in its general features and in assignments of quantum numbers to specific states.

The spherical nuclei near ^{208}Pb also provide some interesting confirmations of the single-particle model. One of the simpler facts to understand is that the decay of all Bi isotopes ($Z = 83$) is strongly forbidden. The unpaired proton of Bi is in the $h_{9/2}$ state, while the 81st proton in the daughter is $s_{1/2}$; the α -particle must carry off at least four units of angular momentum and presumably must incorporate the $h_{9/2}$ proton. Both these factors make its formation difficult.

The shell model was tested by Mang [27] in a quantitative calculation of the formation factors of the Po and At isotopes. The most striking feature of the experimental data is the sharp drop by a factor of about 5 in the reduced width of α -emitters with 126 or fewer neutrons. Mang is able to explain this phenomenon in terms of a simple spherical shell-model nuclear structure.^t The essential idea of the calculation is that the probability of formation of an α -particle is proportional to the overlap of the wave function of the final state with that of the initial state.

Let the initial state be $\Psi_0(\mathbf{r}_1, \mathbf{r}_2, \dots, \mathbf{r}_A)$. Suppose that nucleons 1, 2, 3, and 4 form an α -particle of angular momentum l . If we write \mathbf{R} for the center of mass of the α -particle and $\mathbf{x}_1, \mathbf{x}_2$, and \mathbf{x}_3 for its internal coordinates (they are functions of $\mathbf{r}_1, \dots, \mathbf{r}_4$), the final-state wave function is of the form

$$\Psi_\alpha = \mathcal{A}\{R^{-1}u_i(R)\chi_{ij}^M(\mathbf{x}_1, \mathbf{x}_2, \mathbf{x}_3, \mathbf{r}_5, \dots, \mathbf{r}_A)\},$$

where

$$\chi = \sum_m (IJ, m M - m|J, M) Y_l^m(\Theta, \Phi) \Psi_j^{M-m}(\mathbf{r}_5, \dots, \mathbf{r}_A) \psi_\alpha(\mathbf{x}_1, \mathbf{x}_2, \mathbf{x}_3);$$

in this sum ψ_α is the internal wave function of an α -particle, and Ψ_j is the state of the daughter nucleus. With a nucleus in state Ψ_0 , the amplitude for finding this α -particle with its center at radius R is

$$A = \int d\mathbf{x}_1 d\mathbf{x}_2 d\mathbf{x}_3 d\mathbf{r}_5 \cdots d\mathbf{r}_A \sin \Theta d\Theta d\Phi \Psi_0^* \chi.$$

Factors must be introduced to take account of the other possible choices of four nucleons to constitute the particle, but A is the fundamental quantity in the formation factor. Mang obtained the general expression for the reduced width δ in terms of A , and then evaluated δ for the Po and At isotopes. It is necessary to assume wave functions for the various nuclei involved. For the α -particle Mang used a wave function that had been

^t An earlier explanation, which invoked a discontinuous change in nuclear radius at $N = 126$, is apparently incorrect.

successfully employed to predict the binding energy and the charge distribution, namely,

$$\psi_\alpha = {}^1\sigma_0(1, 2){}^1\sigma_0(3, 4) \exp[-\frac{1}{2}\beta(x_1^2 + x_2^2 + x_3^2)],$$

where (1, 2) are the protons, (3, 4) are the neutrons, and

$$x_1 = 2^{-1/2}(\mathbf{r}_1 - \mathbf{r}_2), \quad x_2 = 2^{-1/2}(\mathbf{r}_3 - \mathbf{r}_4),$$

$$x_3 = \frac{1}{2}(\mathbf{r}_1 + \mathbf{r}_2 - \mathbf{r}_3 - \mathbf{r}_4).$$

For heavy nuclei, simple shell-model wave functions were used, for example,

$$^{204}\text{Po}: \text{ protons } h_{9/2}^2, \text{ neutrons } p_{1/2}^{-2}f_{5/2}^{-4};$$

$$^{200}\text{Pb}: \text{ protons closed shell, neutrons } p_{1/2}^{-2}f_{5/2}^{-4}p_{3/2}^{-2}.$$

The radial wave functions of the single-particle states were taken as harmonic-oscillator functions, with the one adjustable parameter fixed to give a suitable rms radius for all nuclei. The values of the formation factor were calculated for $R = 9$ fm, a radius inside which most α -particle formation occurs; the penetration factors required to obtain empirical values of δ^2 have been calculated for a Coulomb barrier starting at the same radius.

A comparison of the calculated and empirical values of reduced widths is shown in Fig. 11-7. The absolute values of the calculated δ^2 can be altered by changing R and the parameters in the wave function, but the relative values are insensitive to such changes; the calculated data have been normalized by fitting the value for ^{210}Po to experiment.

It is seen that even the simple shell model provides very satisfactory agreement with the observed trend for these spherical nuclei. Mang's early calculations have been greatly extended in the direction of using Nilsson wave functions appropriate to the heavier nuclei and simultaneously introducing the configuration mixing caused by the pairing force [28]. One might expect that the superfluid smearing of the Fermi surface would be important. Consider the case of ^{243}Cm , discussed earlier (Fig. 11-6). Transitions to band A are strongly forbidden, while those to band B are unhindered; consequently, if the BCS quasiparticles should mix states in these bands to even a small extent, one might expect marked effects.

Mang and Rasmussen did find that the theoretical α -decay rates are quite sensitive to details of the pairing-force wave functions. In their later work [26] they therefore used a wave function which strictly conserves particle number; furthermore, they assumed an attractive δ -force interaction between like nucleons in Nilsson orbitals, rather than using the standard

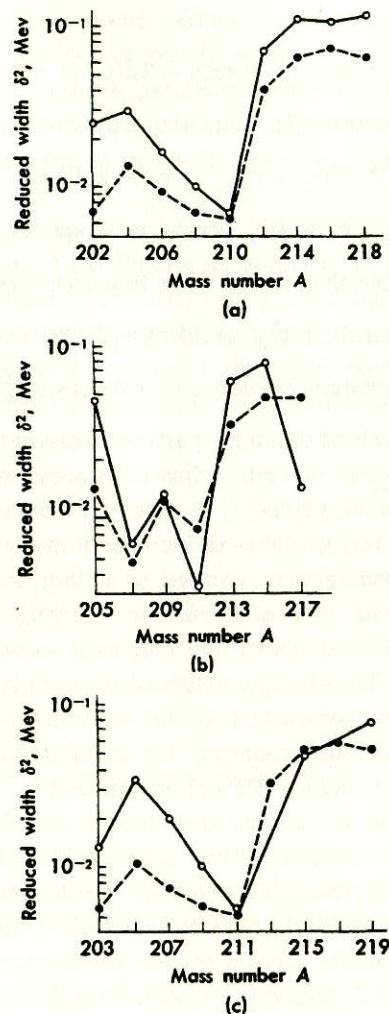


Fig. 11-7 Reduced widths of Po and At isotopes: (a) even-even Po, (b) even-odd Po, and (c) odd-even At. (After Mang [27].) The closed circles are Mang's calculated values, the open circles are empirical values. The calculated values are normalized at ^{210}Po .

assumption of a constant matrix element G between all pairing states. These calculations are rather lengthy, and it does not seem desirable to give all details here. These workers have calculated α -intensities for most of the

actinide region, using the wave functions mentioned to obtain formation factors $\langle \Psi_0 | \Psi_\alpha \rangle$ and employing the Igo potential and Fröman's method to calculate barrier penetrabilities.

The quality of the agreement of these calculations with experiment is well illustrated by the case of ^{243}Cm , shown in Fig. 11-6 and Table 11-3. The rotational bands labeled A , B , C , and D are consistent with the systematics of neighboring nuclei, correspond to neutron orbitals in this part of the Nilsson diagram, and have reasonable values of the moments of inertia and of the decoupling parameter for the A -band.

TABLE 11-3 Comparison of Calculated and Experimental Values of Relative Intensities in the α -Decay of ^{243}Cm . Calculated values from Ref. 26. Experimental values from *Nucl. Data Sheets* B3-2-8 (1969), based mostly on S. A. Baranov, V. M. Kulakov, V. M. Shatinsky, *Nucl. Phys.* **56**, 252 (1964).

Band	Daughter level	Calculated, %		Experimental, %
		Energy	%	
A	0	0.43		1.5
A	8	2.2		4.7
A	57	0.89		1.0
A	76	1.9		5.5
A	164	0.20		0.1
A	193	0.21		0.6
A	320 ^a	0.013		
B	286	76		73.5
B	330	11.5		11.0
B	388	1.8		1.6
B	463	0.022		0.01
B	436	0.004		0.002
C	392	0.068		0.2
C	434	0.028		0.14
C	486	0.008		0.02
C	542	0.00006		0.006
E	460	0.00028	0.06 or 0.03	
E	490	0.00056	0.009	
E	505	0.0005	0.007	

^a Calculated energy of $\frac{13}{2}^+$ state. Not seen in α -decay experiments.

It is seen that the agreement is impressive, particularly since the intensities vary over 4 orders of magnitude. This constitutes a sensitive test of the wave functions, since it is to their structure that one must attribute the very marked departure from a regular energy dependence of the intensities.

The band labeled *E* may be a $K = \frac{1}{2}$ band, containing the 451-, 460-, 490-, and 505-keV levels. However, none of the nearby Nilsson orbitals seems to have a decoupling parameter near the value necessary to fit the level scheme. The calculations for band *E* in Table 11-3 are based on the assumption that the three levels listed form the $\frac{1}{2}^-$ -[501] band; since the results are 1 or 2 orders of magnitude too small, this assumption is apparently wrong. Similarly the assignment of the 542-keV level to band *C* may be questioned because the calculated and experimental intensities differ by 2 orders of magnitude.

Although their relative intensities are in good agreement with experiment, the absolute values of decay rates calculated by Poggengburg, Mang, and Rasmussen [26] are too small by almost an order of magnitude. As we saw in Section 11-3, this is probably due to deficiencies in the α -nucleus potential and in the WKB approximation.

We may summarize this chapter by two remarks. First, we understand reasonably well the phenomena of α -decay, which occur "after the formation" of the α -particle, although great accuracy of calculation of barrier penetration may require tedious computation. Second, "formation of the α -particle" occurs continuously in the sense that the overlap $\langle \Psi_\alpha | \Psi_0 \rangle$ is nonzero, that is to say, the correlations of nucleons in the nuclear wave function Ψ_0 are such that "some of the time" four of the nucleons are an α -cluster. Moreover, the intrinsic correlations need not be known in great detail, for the wave functions of the Nilsson model with pairing-force configuration mixing are found to be quite adequate. This fact should not be very surprising; the only important aspects that such a wave function overlooks are the short-range two-body correlations which "wound" the single-particle wave functions, and these depend primarily on density, which in turn is essentially constant for nuclei throughout the α -active region. Hence, at the most, the neglect of short-range correlations in both the nuclear wave functions and the intrinsic α -particle wave functions will introduce a common normalization factor.

Alpha decay, at one time a source of puzzling phenomena, is now seen to provide a convincing confirmation of many aspects of the collective model.

REFERENCES

1. E. Rutherford and H. Geiger, *Proc. Roy. Soc. (London)* **A81**, 141, 162 (1908); also E. Rutherford and T. Royds, *Phil. Mag.* **17**, 281 (1909).
2. J. O. Rasmussen, S. G. Thompson, and A. Ghiorso, *Phys. Rev.* **89**, 33 (1953).
3. R. D. Macfarlane and T. P. Kohman, *Phys. Rev.* **121**, 1758 (1961).
4. S. Rosenblum, *J. Phys. Radium* **1**, 438 (1930), and many later papers.
5. H. Geiger and J. M. Nuttall, *Phil. Mag.* **22**, 613 (1911).
6. G. Gamow, *Z. Phys.* **51**, 204 (1928).
7. E. U. Condon and R. W. Gurney, *Nature* **122**, 439 (1928); *Phys. Rev.* **33**, 127 (1929). In addition to refs. 6 and 7, a number of accounts on α -decay theory was published in the years 1930–1937, of which the most commonly quoted are H. Bethe, *Rev. Mod. Phys.* **9**, 161 (1937), and F. Rasetti, *Elements of Nuclear Physics*, Prentice-Hall, Englewood Cliffs, N.J., 1936. Others are listed in ref. 12.
8. G. Igo, *Phys. Rev.* **115**, 1665 (1959).
9. G. H. Winslow, *Phys. Rev.* **96**, 1032 (1954).
10. I. Perlman, A. Ghiorso, and G. T. Seaborg introduced the concept of a formation factor in *Phys. Rev.* **77**, 26 (1950).
11. I. Perlman and J. O. Rasmussen, *Encyclopedia of Physics*, Vol. XLII, Springer-Verlag, Berlin, 1957, p. 109.
12. M. A. Preston, *Phys. Rev.* **71**, 865 (1947).
13. I. Kaplan, *Phys. Rev.* **81**, 962 (1951).
14. M. A. Preston, *Phys. Rev.* **83**, 475 (1951).
15. Gy. Bencze and A. Sandulescu, *Phys. Lett.* **22**, 473 (1966).
16. L. Scherk and E. Vogt, *Can. J. Phys.* **46**, 1119 (1968).
17. Gy. Bencze, *Phys. Lett.* **23**, 713 (1967).
18. M. L. Chaudhury, *J. Phys. A: Gen. Phys.* **4**, 328 (1971); *Nucl. Phys.* **76**, 181 (1966).
19. J. O. Rasmussen, *Phys. Rev.* **118**, 1593, and **115**, 1675 (1959).
20. M. A. Preston, *Phys. Rev.* **75**, 90 (1949), and **82**, 515 (1951).
21. P. O. Fröman, *K. Danske Vidensk. Selsk. Mat.-Fys. Skr.* **1**, No. 3 (1957).
22. R. R. Chasman and J. O. Rasmussen, *Phys. Rev.* **112**, 512 (1958).
23. E. M. Pennington and M. A. Preston, *Can. J. Phys.* **36**, 944 (1958).
24. J. O. Rasmussen and E. R. Hansen, *Phys. Rev.* **109**, 1656 (1958).
25. R. R. Chasman and J. O. Rasmussen, *Phys. Rev.* **115**, 1257 (1959).
26. J. K. Poggengburg, H. J. Mang, and J. O. Rasmussen, *Phys. Rev.* **181**, 1697 (1969).
27. H. J. Mang, *Phys. Rev.* **119**, 1069 (1960); *Z. Phys.* **148**, 572 (1957).
28. H. J. Mang and J. O. Rasmussen, *K. Danske Vidensk. Selsk. Mat.-Fys. Skr.* **2**, No. 3 (1962); H. J. Mang, *Ann. Rev. Nucl. Sci.* **14**, 1 (1964).

PROBLEMS

- 11-1. In 1964 (*Phys. Lett.* **13**, 73) Flerov et al. reported the synthesis of the nuclide ^{260}Ku in the reaction ^{242}Pu ($^{22}\text{Ne}, 4n$). The species was identified by spontaneous fission products and assigned a half-life of 0.3 s. The name kurchatovium was proposed. The nuclide ^{260}Ku should decay by α -emission to ^{260}No . From binding-energy systematics the *Q*-value for α -decay is estimated at 8.99 MeV.

Justify this estimate, calculate the half-life for α -decay, and comment on whether or not it should be observed.

11-2. The nuclide ^{253}Fm has a half-life of 3.0 days, decaying 88% by electron capture and 12% by α -decay. The energies and intensities of the α -groups are as follows:

E_α , MeV	I_α , %
7.092	1.3
7.032	6.7
6.952	42.7
6.910	9.8
6.876	0.9
6.855	8.4
6.682	23.2
6.659	2.4
6.639	2.6
6.550	1.5
6.496	0.3

Use these results to suggest Nilsson levels and rotational band structure for ^{249}Cf . You may find it useful to know that the ground state of ^{251}Cf has $J\pi = \frac{1}{2}^+$ and that the ground state of ^{252}Es is thought to have $J\pi = 7^+$.

Fission

12-1 THE PHENOMENON OF FISSION

Hahn and Strassmann [1] were the first to establish that uranium, when bombarded with neutrons, splits into lighter elements with about half the atomic number of uranium. The phenomenon of a nucleus undergoing a division into two more or less equal fragments, either spontaneously or induced by some projectile, is termed binary fission. Less frequently, division into three fragments has also been observed [2]; this is called ternary fission. It is easy to see, from the binding-energy versus mass-number curve shown in Fig. 6-1, why fission is an energetically favorable process for heavy nuclei. The binding energy per particle, B/A , is maximum for ^{56}Fe , being about 8.8 MeV, and falls off rather slowly with increasing A . The quantity B/A in the mass region $A = 240$ is about 7.6 MeV, while it is nearly 8.5 MeV for half this mass number. The mass of the atomic species (A, Z) is simply

$$M(A, Z) = ZM_H + (A - Z)M_n - B(A, Z). \quad (12-1)$$

It follows that, if a heavy nucleus of $A = 240$ splits into two nearly equal parts, the sum of the masses of the two fragments will be less than the mass of the fissioning nucleus by $240(8.5 - 7.6) = 216$ MeV, which should be released in the form of energy. At the instant that the division takes place (the scission point), the two fragments are in highly deformed excited states, and most of this energy is stored in the form of the deformation and excitation energy of the fragments and the mutual Coulomb energy between them, the latter being the dominant term. As a crude estimate,

if we assume that the charge centers of the two fragments ($Z_1 = 50, Z_2 = 44$) are separated by $D = 15$ fm at the time of scission, the Coulomb energy $(Z_1 Z_2 e^2)/D \approx 210$ MeV. In the postscission stages, the two fragments recede from each other because of Coulombic repulsion, picking up velocity and at the same time collapsing to their equilibrium shapes. By the time the separation D between the charge centers has become 150 fm, the mutual Coulomb energy has reduced to a tenth of its original value, the rest being converted to kinetic energy.[†] A very simple calculation shows that this implies a fragment velocity of the order of 10^9 cm/sec, and that each fragment has covered a distance of about 70 fm in roughly 10^{-20} s, by this time already attaining 90% of the maximum kinetic energy. Moreover, each of the intermediate-mass primary fragments is neutron rich, since the neutron excess increases with atomic number.

About two to four neutrons are emitted from the fragments after these have attained their full kinetic energy, within a time of 10^{-15} to 10^{-18} s [3] after scission. In the laboratory frame the angular distribution of these neutrons is strongly peaked in the directions of fragment motion; in the frame of the moving fragment the neutron distribution is very nearly isotropic. This supports the view that these neutrons are emitted from the fully accelerated fragments themselves and not at the time of scission. These prompt neutrons have a Maxwellian distribution in energy, and on the average each neutron carries away about 2 MeV of energy. In addition, of course, it costs energy for these neutrons to "evaporate" from the fragments—about 8 MeV for each neutron. When the fragment-excitation energy has been reduced below the neutron-emission threshold, the fragments de-excite by γ -emission ($< 10^{-11}$ s) to reach their ground state. These secondary fragments (also called primary products) are far removed from the β -stability line because their charges have not been readjusted. The primary products thus undergo the slow process of β -decay ($\sim 10^{-2}$ s or more), forming stable end products. Occasionally it may happen that certain β -decay paths lead to a level that is neutron unstable, causing the emission of delayed neutrons. The delayed neutron yield is only about 1% of the total neutron emission.

Now, using mass formula 6-21, we shall investigate at what point of the periodic table it becomes energetically more favorable for a nucleus to undergo binary fission. As we have seen, the mass formula with the parameters given in Eq. 6-24 reproduces the binding energies of nuclei very well, although small corrections like those for shell effects and deformation have

[†] Noncentral components of the electric field can also exchange energy with the internal degrees of freedom of the fragments.

been ignored in it. For simplicity, we consider only the most stable even-even isobar with mass $M(A, Z)$ undergoing symmetric fission into two identical fragments, each of mass $M(A/2, Z/2)$. This is an oversimplification of the actual situation, since very often the fragments have unequal masses. Using Eqs. 6-21 and 12-1, we find that

$$\begin{aligned} \Delta M &= M_0(A, Z) - 2M\left(\frac{A}{2}, \frac{Z}{2}\right) \\ &= a_s(1 - 2^{1/3})A^{2/3} + \kappa_c(1 - 2^{-2/3})\frac{Z^2}{A^{1/3}} \\ &\quad - a_{\text{surf sym}}(1 - 2^{1/3})I^2A^{-4/3} + a_{\text{pair}}(1 - \delta 2^{3/2})A^{-1/2}, \end{aligned} \quad (12-2)$$

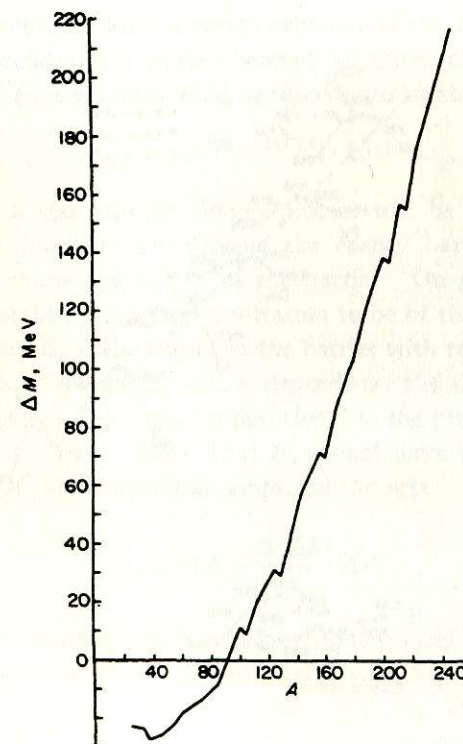


Fig. 12-1 The energy release ΔM in the symmetric fission of even-even nuclides, using Eq. 12-2. Only those even-even nuclides (A, Z) are considered which are the most stable isobars, and which yield fragments with $(A/2, Z/2)$ even-even, so that δ in Eq. 12-2 is $+1$. The kinks in the curve arise from discontinuous changes in $I = N - Z$ for the most stable isobars.

where $\delta = +1, -1$, or 0 , according as each fragment is even-even, odd-odd, or odd, while I as before is $N - Z$. In Fig. 12-1 we plot ΔM against A , and it will be seen that ΔM becomes positive at about $A \approx 90$, indicating that binary fission becomes energetically favorable.

Using similar arguments, we find that for heavier nuclei even more energy should be released for ternary fission into three equal fragments. The experimental observations that most nuclei are stable against spontaneous fission and that even the half-life of a heavy nucleus like ^{238}U is of the order of 10^{16} years, as well as the fact that ternary fission is rather infrequent, all point to the conclusion that there is an energy barrier which the fragments must either penetrate or surmount before fission can occur. We shall discuss the origin and implications of the fission barrier in the next section.

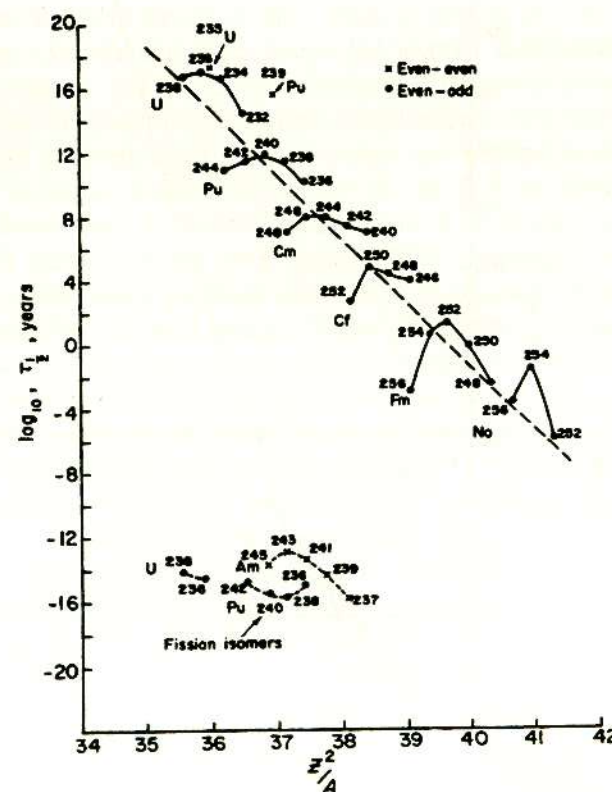


Fig. 12-2 The spontaneous fission half-lives of elements in the actinide region plotted against Z^2/A .

One can estimate the height of this barrier either from the spontaneous half-lives of heavy nuclei by making some assumptions about its shape, or more directly by inducing fission by the use of some external projectile (photon, neutron, deuteron, etc.) and obtaining the fission threshold energy. In Fig. 12-2 we plot on a logarithmic scale the spontaneous half-lives of some elements in the actinide region against Z^2/A . It will be seen that the general trend of the even-even nuclei can be roughly reproduced by a straight line, although the various even-even isotopes of a particular nuclide seem to fall on a smooth curve. Note that odd nuclides possess half-lives which are longer by a few orders of magnitude. Also shown are the lifetimes of the short-lived fission isomers, whose existence has led to new information about the barrier shapes, and which we shall discuss at some length in Section 12-5.

For the moment, we want a rough estimate of the barrier height, using the even-even nuclides as a guide. Seaborg [4] noted that the trend in the half-lives of even-even nuclides could be reproduced by the empirical formula[†]

$$\tau_{1/2} = (10^{178-3.75Z^2/A}) \cdot 10^{-21} \text{ s.} \quad (12-3)$$

The lifetime in a spontaneous fission process will be determined by the probability of a fragment penetrating the energy barrier, which in turn depends on the shape and height of the barrier. On general grounds, we expect the probability factor for penetration to be of the approximate form $\exp(-\kappa E_b)$, where E_b is the height of the barrier with respect to the ground state of the fissioning nucleus, and κ depends on the shape of the barrier. Since the half-life $\tau_{1/2}$ is inversely proportional to the probability of penetration, we expect, using Eq. 12-3, that E_b should have a linear dependence on Z^2/A . Seaborg [4] has given an empirical formula

$$E_b = 19.0 - \frac{0.36Z^2}{A} \text{ MeV} \quad (12-4)$$

based on such an analysis, which is approximately valid for even-even nuclei over a limited range of Z^2/A . We emphasize that Eq. 12-4 is just a rough estimate based on a one-humped barrier. We also find, from Eqs. 12-3 and 12-4, that each factor-of-10 increase in $\tau_{1/2}$ corresponds to an increase of about 0.13 MeV in the barrier height, showing the extreme sensitivity of half-life to barrier height.

[†] This form of the formula, in a simple barrier model, is derived in Section 12-3. See, in particular, Eqs. 12-26 to 12-29.

A more direct way of determining barrier height is to impart enough excitation energy to the nucleus by a projectile so that the barrier can be surmounted. A basic difficulty in this method is that there is no unique value of threshold energy, since, even if the excitation energy E_{ex} is less than E_b , fission can take place by barrier penetration. From our previous formula, below-the-barrier fission yield would be expected to rise exponentially with the increase in excitation energy, while for $E_{ex} > E_b$ the yield should level off until new reaction channels become available with increasing energy (see, e.g., Fig. 12-6).

One of the most direct methods of estimating the barrier height is by exciting the nucleus with γ -rays, although it is rather difficult to obtain a monochromatic source. As the γ -ray energy is increased from a low value, the fission yield increases exponentially and then levels off rather sharply but in a smooth fashion [5]. The bending of the fission-yield curve is also partly due to the opening up of (γ, n) channels, and it is not possible to determine E_b unambiguously. Typical uncertainties in E_b thus determined are in the range of 0.2–0.3 MeV.

The other commonly used method of determining E_b is to excite the target nucleus by a monoenergetic neutron beam. When a low-energy neutron is captured by the target nucleus, it forms a compound nucleus, with the energy of the incident neutron redistributed by many collisions over a time period very long ($\sim 10^{-14}$ s) compared to the time in the nuclear scale ($\sim 10^{-22}$ s). Above a certain threshold of neutron energy fission becomes dominant, while below this energy the compound nucleus de-excites by electromagnetic processes. A zero-energy incident neutron imparts an excitation energy B_n to the compound nucleus, where B_n is the binding energy of the neutron in the compound nucleus. Consequently, if the threshold kinetic energy of the neutron is E_n , the barrier height $E_b = E_n + B_n$. It is necessary, therefore, to know B_n from other sources in order to estimate E_b by this method. Furthermore, if the compound nucleus has an even number of neutrons, B_n may be larger than E_b , and even thermal neutrons can induce fission—in such cases this method is not applicable. On the other hand, the method works for a target nucleus like ^{234}U , where the compound nucleus ^{235}U has an odd number of neutrons, and $B_n = 5.3$ MeV. In this case, the threshold energy E_n is ~ 0.5 MeV, giving the barrier height in ^{235}U as 5.8 MeV. For most nuclei in the actinide region, E_b is between 5 and 6 MeV; for Cf and Fm isotopes the fission barrier is smaller, in the range 2.5–4 MeV.

For the case in which $E_b < B_n$, an ingenious method of measuring the threshold has been devised by Northrup, Stokes, and Boyer [6], using the

(d, pf) reaction. Fission thresholds are obtained by measuring the energy spectrum of protons in coincidence with fission events induced by deuterons of known kinetic energy E_d . If the outgoing proton energy is E_p , and the deuteron binding energy is ϵ_d , the captured neutron has an equivalent kinetic energy E_n , given by

$$E_d - E_p = \epsilon_d + E_n. \quad (12-5)$$

The excitation energy of the compound nucleus, as before, is

$$E_{ex} = E_n + B_n = (E_d - E_p - \epsilon_d) + B_n. \quad (12-6)$$

The point to note is that E_n now may be negative in cases where nearly all the kinetic energy is taken away by the proton, so that $E_d - E_p < \epsilon_d$. In this case the excitation energy $E_{ex} < B_n$, and by measuring the E_d and E_p at fission threshold it is possible to estimate the barrier height from Eq. 12-6. We shall discuss the results of such experiments later in this section while considering the variation of fission cross section with excitation energy.

We have already noted that in actinide nuclei with an odd number of neutrons (e.g., ^{233}U , ^{235}U , ^{239}Pu) a large fission rate can be induced by thermal

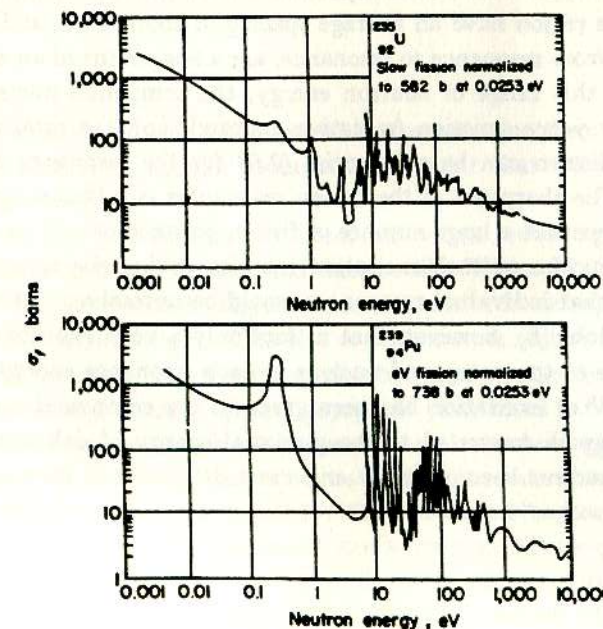


Fig. 12-3 Fission cross section σ_f as a function of neutron energy in the energy range 10^{-3} to 10^4 eV, incident on (a) ^{235}U and (b) ^{239}Pu . (After Hyde [7].)

neutrons, a fact which makes them technologically important. Some insight into the fission process is gained by examining the variation of the fission cross section with increasing neutron energy in this range. In Figs. 12-3a and 12-3b we plot the fission cross section σ_f of ^{235}U and ^{239}Pu against the incident neutron energy in the energy range 10^{-3} to 10^4 eV [7]. It will be seen that there is a drastic drop in σ_f , from about 1000 b at the lower energies to less than 10 b in the keV region.

From 0 to 0.2 eV, the cross section drops inversely with the velocity v of the incoming neutron. This reflects the fact that the slower neutrons spend a larger fraction of time in the vicinity of the target nucleus and therefore have a greater probability of being captured and imparting the excitation energy for fission.

Beyond 0.2 eV, there are many sharp resonances in the cross section. These occur when the incident kinetic energy plus the binding energy of the neutron equals the energy of one of the excited states of the compound nucleus, the density of such states being very large at an excitation energy of about 6 MeV. If the width of a resonance in the fission cross section is denoted by Γ_r , then Γ_r/\hbar is the probability per unit time that the compound nucleus will lose its excitation by fission. The many resonances that are found in this region have an average spacing of about 1 eV, and the widths, which vary from resonance to resonance, are a few tenths of an electron volt or less. In this range of neutron energy, the compound nucleus can also de-excite by γ -ray emission (radiative capture), and the ratio of radiative capture to fission can be substantial (0.69 for the resonance at 0.296 eV in ^{239}Pu). The sharpness of the fission resonances is rather surprising, since it would seem that a large number of fission channels would be open to the compound nucleus at such excitation energies, giving rise to a large fission width, and that individual resonances would be unresolved. It was pointed out by A. Bohr [8], however, that in fact only a very few fission channels are available to the compound nucleus at each resonance energy. Although about 6 MeV of excitation has been given to the compound nucleus, most of this energy is converted to the potential energy of deformation as the compound nucleus becomes more and more deformed on its way to fission. Bohr visualized a "transition state" of the nucleus: an unstable equilibrium near the top of the barrier, where the compound nucleus is "cold," most of its excitation energy having been spent in reaching this deformed state. A nucleus, on its way to fission, must pass through this transition state, which has only a few well-defined low-lying quantum states available to it, because of its low excitation (see Fig. 12-4). Further restrictions on the

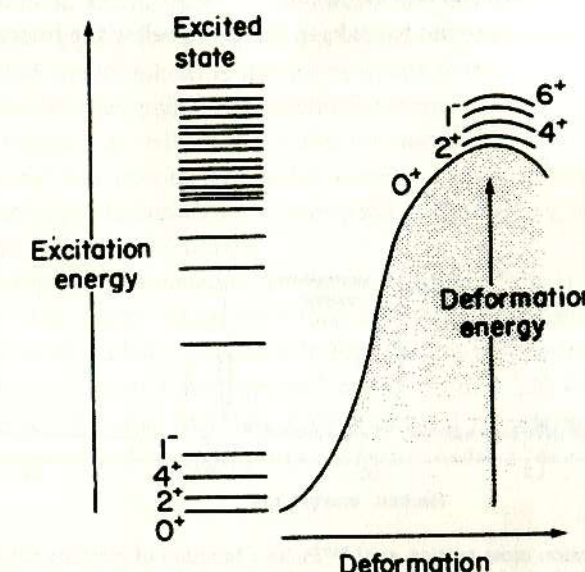


Fig. 12-4 Schematic view of the transition states of a nucleus in the liquid-drop picture.
(After Hyde [7].)

levels of the transition state through which fission can take place are imposed by the conservation of angular momentum, a point that we shall discuss at some length later.

An interesting phenomenon is observed when low-energy neutrons (0.2–8 keV) bombard an even-neutron nucleus like ^{240}Pu . In this case, the fission is in the subthreshold region, since the excitation energy imparted is less than the barrier height. The plot of fission cross section in Fig. 12-5 demonstrates that the fission widths are abnormally large (~ 50 eV) for some approximately equally spaced groups of resonances (at intervals of ~ 650 eV), and are extremely small between them, instead of being randomly distributed. This phenomenon, known as an intermediate structure effect, cannot be explained by the conventional one-humped barrier. We shall discuss the implications of this finding in Section 12-5 when we consider the barrier shape in detail.

In Fig. 12-6, we have plotted the fission cross section of ^{238}U in the MeV region, as an example of a nuclide that has a threshold energy in this range. In the subthreshold range of energies, the cross section rises expo-

nentially, until neutron emission becomes possible. The competition from neutron re-emission gives rise to kinks in the curve below the fission threshold.

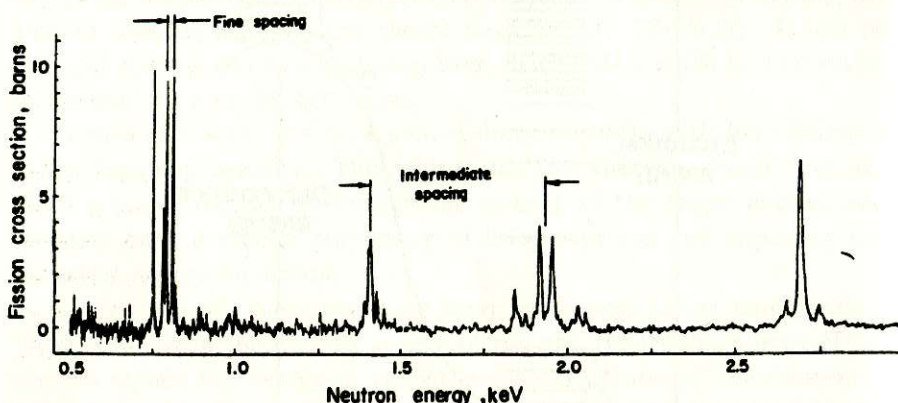


Fig. 12-5 The fission cross section σ_f of ^{240}Pu as a function of incident neutron energy, showing the grouping of resonances at regular intervals with large widths. [After E. Migneco and J. P. Theobald, *Nucl. Phys.* **A112**, 603 (1968).]

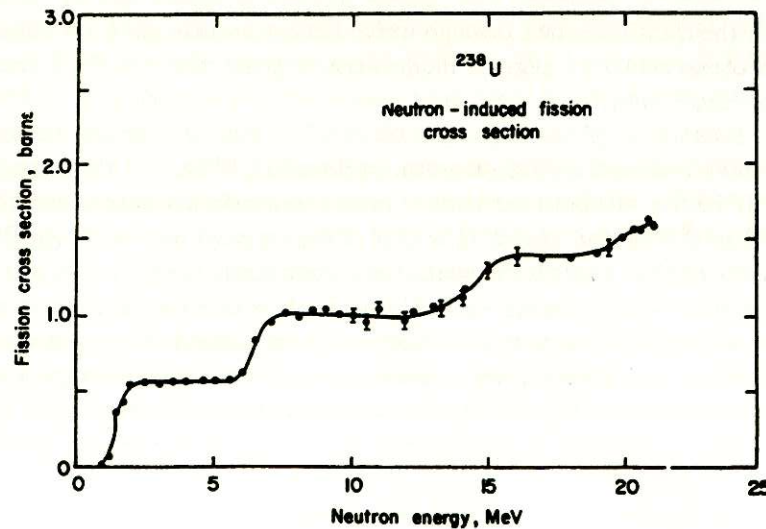


Fig. 12-6 Fission cross section σ_f for n -induced fission of ^{238}U as a function of energy. (After Hyde [7].)

The neutron-fission cross section in the MeV region is governed by the ratio of the widths Γ_f/Γ_n for fission as compared with neutron emission. The curve beyond the threshold is flat up to about 6 MeV, where there is again a sharp rise. At this point, the excitation energy is large enough to permit a neutron emission as well as fission over the barrier, so that a second reaction channel (n, nf) has opened up, giving increased cross section. The rises in the cross section at 14 and 20 MeV correspond to the opening up of "third-try" ($n, 2nf$) and "fourth-try" fission.

An interesting phenomenon is observed when ^{230}Th is bombarded by neutrons in the energy range 690–1230 keV [9]. The fission threshold in this case is about 1 MeV. As shown in Fig. 12-7, a well-developed maximum in σ_f is observed in the subthreshold region around 750 keV, and careful analysis shows [10] that this cannot be attributed to neutron-emission competition. One is forced to assume that the fission width Γ_f has a nonmonotonic

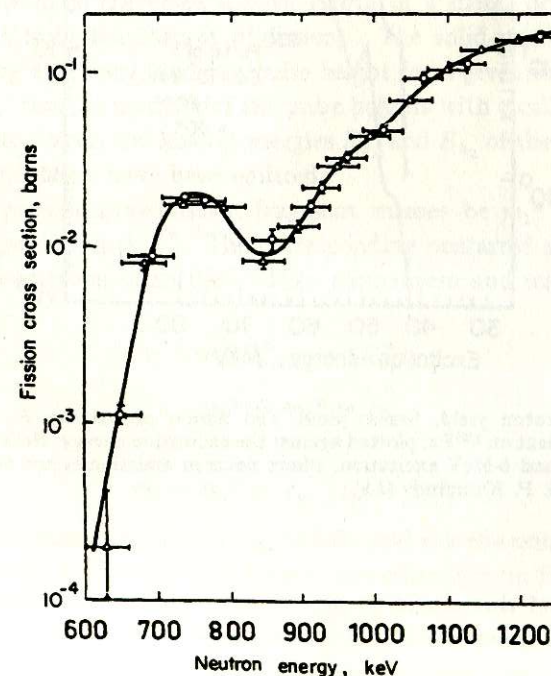


Fig. 12-7 Neutron-induced fission cross section of ^{230}Th , showing a marked resonance in the subthreshold neutron energy, around 750 keV. (After Vorotnikov et al. [9].)

dependence on the excitation energy, a behavior not allowed by a simple one-humped barrier. This anomaly, which is believed to be due to vibrational resonances in a double-humped barrier, will be discussed later. Further examples of such vibrational resonances have been found in the (d, pf) reactions in the compound nuclei ^{234}U , ^{236}U , ^{240}U , and ^{242}Pu [11]. In Fig. 12-8,

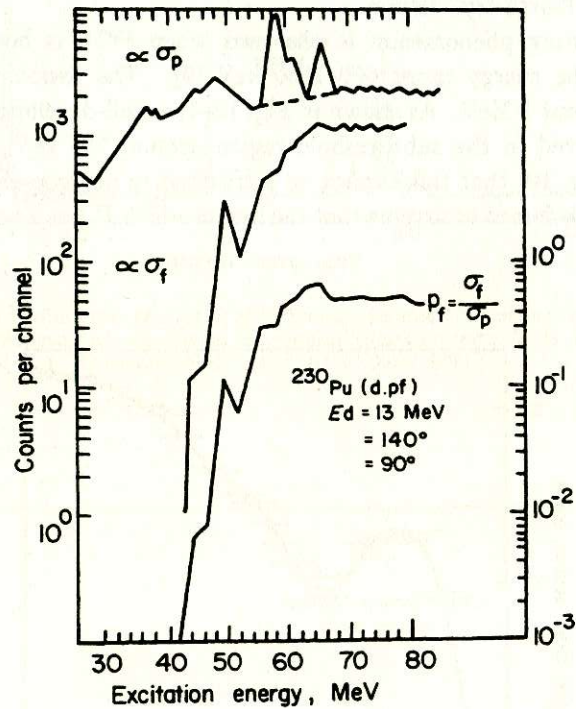


Fig. 12-8 The proton yield, fission yield, and fission probability P_f when 13-MeV deuterons are incident on ^{239}Pu , plotted against the excitation energy. Note the resonance-like structure around 5-MeV excitation, where neutron emission is not possible. (After J. Pedersen and B. P. Kuzminov [11].)

as an example of this phenomenon, we have plotted the curves of proton yield, coincident fission yield, and their ratio, which is the fission probability, against the excitation energy for 13-MeV deuterons on ^{239}Pu . The resonance at $E_{ex} \approx 5$ MeV appears below the neutron binding energy of 6.4 MeV and therefore cannot be explained by neutron competition. We shall see later

that these resonances have a natural explanation when the barrier shape has two minima, giving rise to vibrational states. The peculiar barrier shapes arise because of shell effects, which persist even for large deformations, and which we shall discuss after describing the simple liquid-drop picture of fission.

12-2 FISSION-FRAGMENT CHARACTERISTICS

In this section we discuss the mass and energy distributions of the fragments in binary fission and examine in more detail some properties of the emitted prompt neutrons. It is important, while discussing the experimental data, to distinguish between mass distributions before and after neutron emission—the difference between the two gives us information about the number of prompt neutrons emitted. Radiochemical and mass-spectroscopic analyses of the fission fragments are done with the final fission products or the cumulative yields. The post-neutron-fragment kinetic energies can also be obtained by detecting the fission fragments with solid-state detectors after the fragments have traversed a path length of a meter or two (i.e., after about 10^{-7} s from the instant of fission). The solid-state detectors have good counting efficiency, and the pulse height for a given ion mass is linear with energy; thus an analysis of the pulse heights with a calibrated detector enables one to obtain the kinetic energies E_{k_1} and E_{k_2} of the fragments *after* the prompt neutrons have been emitted.

Let the pre-neutron-emission fragment masses be m_1^* and m_2^* , with kinetic energies $E_{k_1}^*$ and $E_{k_2}^*$. The corresponding unstarred symbols refer to post-neutron-emission quantities. Then momentum and mass conservation imply

$$m_1^* E_{k_1}^* = m_2^* E_{k_2}^* \quad (12-7)$$

$$m_1^* + m_2^* = A, \quad (12-8)$$

and

$$m_i = m_i^* - \nu_i, \quad i = 1, 2, \quad (12-9)$$

where A is the mass of the fissioning nuclide, and ν_i is the number of neutrons emitted from the i th fragment. It follows immediately from Eqs. 12-7 to 12-9 that

$$m_1^* = \frac{AE_{k_1}^*}{E_{k_1}^* + E_{k_2}^*}, \quad (12-10)$$

and a similar relation exists for m_2^* .

To obtain the initial fragment masses m_1^* and m_2^* , it is therefore necessary to know the pre-neutron-emission kinetic energies. Experimentally, however, it is only possible to measure the post-neutron energies E_{k_1} and E_{k_2} . Schmitt, Neiler, and Walter [12] have developed a widely used approximate procedure to deduce m_1^* and m_2^* from the experimentally measured quantities. First, it is assumed that, although the kinetic energy of each fragment changes because of neutron emission, its velocity remains almost unaltered, that is, $v_i^* = v_i$. The plausibility of this assumption relies on the conservation of momentum, coupled with the fact that the neutrons evaporate isotropically from the fragment in its own reference frame and hence have an average velocity in the laboratory frame that is the same as the fragment velocity. It then follows that

$$E_{k_i}^* = E_{k_i} \left(\frac{m_i^*}{m_i} \right) \quad (12-11)$$

and

$$m_i^* = \frac{AE_{k_2}}{E_{k_2} + E_{k_1}(1 + \xi_1)}, \quad (12-12)$$

where

$$\xi_1 = \frac{1 + v_1/m_1}{1 + v_2/m_2} - 1 \approx \frac{v_1}{m_1} - \frac{v_2}{m_2}. \quad (12-13)$$

One could, therefore, obtain m_1^* and m_2^* from a measurement of E_{k_1} and E_{k_2} provided that the values of v_1 and v_2 were known as a function of fragment mass and energy. However, usually experiments have been able to determine only the average number $\bar{\nu}$ of neutrons emitted from a fragment of known mass, but distributed over the available energies. Consequently, some approximations must be made. The simplest comes from putting the small number $\xi_1 = 0$; the resulting m_i^* are referred to as "provisional" masses in some papers in the literature. Another approximation, which is sufficiently accurate for most purposes, is to replace v_i by \bar{v}_i . Fission-fragment double energy measurements have been made by several groups, using silicon-surface-barrier detectors and the fission yield $N(m^*)$ deduced from the above analysis. Work along these lines on several different nuclides has been done by Schmitt et al. [12], Bennet and Stein [13], Pleasonton [14], and John et al. [15]. Before discussing these results, we outline the other commonly used method of determining the pre-neutron-emission fragment distribution.

The most direct method of obtaining the primary fragment characteristics is to determine the velocities of the two fragments by time-of-flight measurements, the flight path of each fragment being about 2 meters. The fragments attain their full velocity when their separation is a few thousand fm, that is, within a time period of about 10^{-19} s, after which they should travel with uniform velocities through vacuum, provided their motion is not altered by subsequent neutron emission or through scattering from the walls of the flight tube. If, as before, it is assumed that $v_i = v_i^*$, then, since momentum conservation implies that

$$m_1^* v_1^* = m_2^* v_2^*, \quad (12-14)$$

the measured velocities v_1 and v_2 , together with relation 12-8, immediately

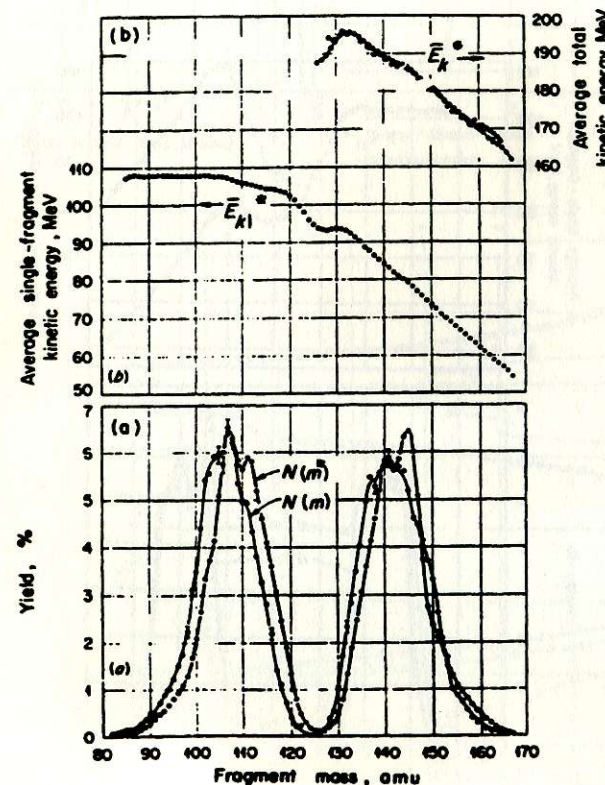


Fig. 12-9 Spontaneous fission of ^{252}Cf . (a) Pre-neutron-emission mass distribution $N(m^*)$ and post-neutron-emission mass distribution $N(m)$ as functions of fragment mass. (b) Average single-fragment and total pre-neutron-emission kinetic energy as functions of mass. (After Schmitt et al. [12].)

give the pre-neutron-emission fragment masses m_1^* and m_2^* . The double velocity measurements were pioneered by Stein [16] and Milton and Fraser [17, 18]. The latter workers studied the spontaneous fission of ^{252}Cf [17] and the thermal-neutron-induced fission of ^{233}U , ^{235}U , and ^{239}U [18]. Their results were somewhat inaccurate [12] because of the effects of fragment scattering from the walls of the flight tubes. The subsequent experiment of Whetstone [19] on the spontaneous fission of ^{252}Cf was free of such errors, and more accurate measurements on $^{235}\text{U} + n$ have been made by Signarbieux, Ribrag, and Nifenecker [20].

We now present a few experimental results. A very large body of experimental data is now available [21], but we shall confine our discussion largely to spontaneous fission and fission induced by low-energy neutrons. The most striking characteristic in these cases is the mass asymmetry of the

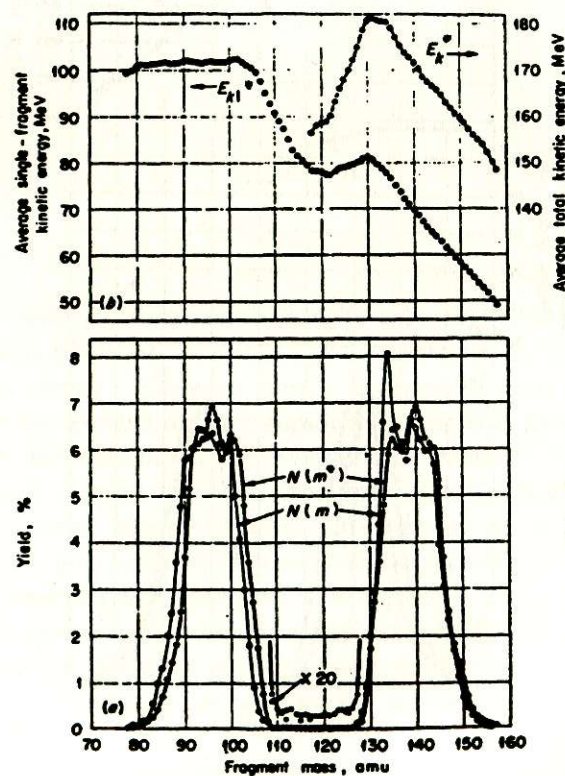


Fig. 12-10 Thermal-neutron-induced fission of ^{235}U . Captions for (a) and (b) are the same as in Fig. 12-9. (After Schmitt et al. [12].)

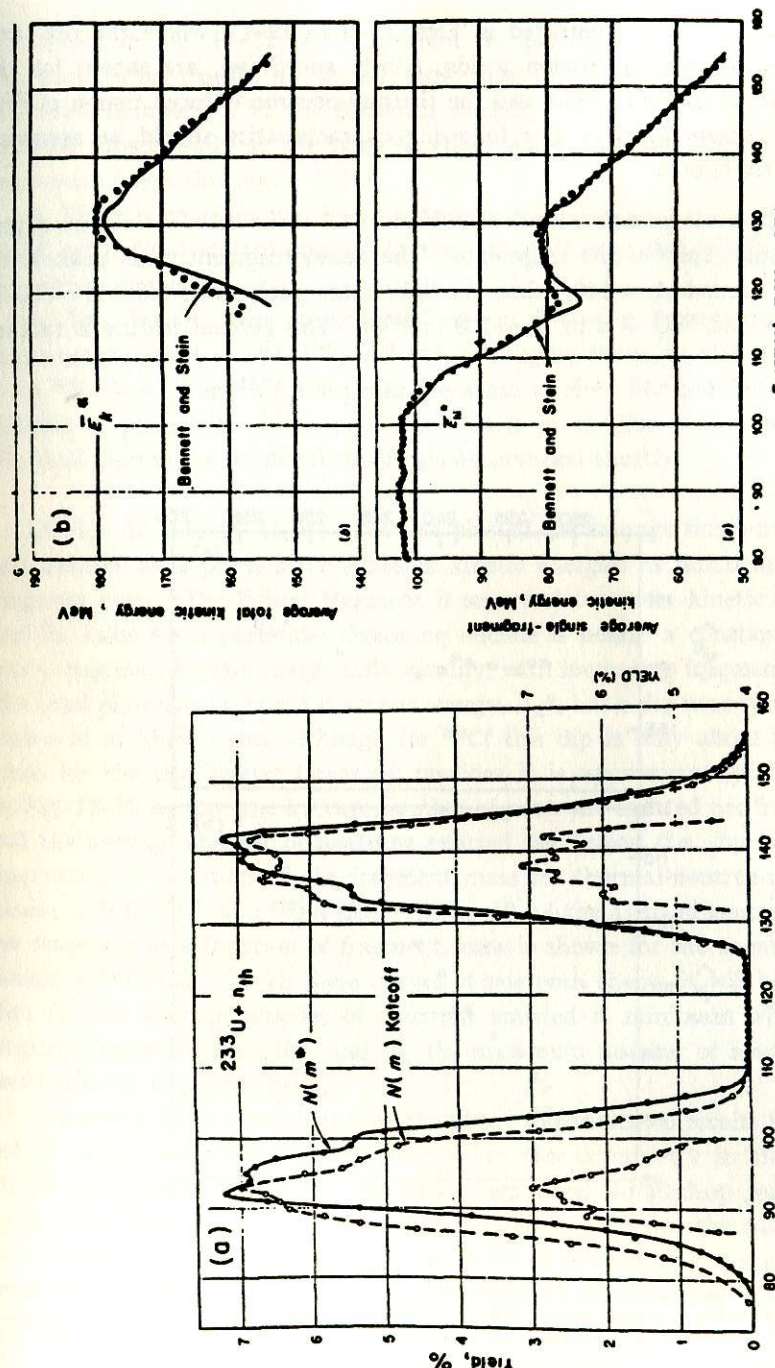


Fig. 12-11 Thermal-neutron-induced fission of ^{233}U . Captions for (a) and (b) are the same as in Fig. 12-9. (After F. Pleasonton [14].)

fragments. This is illustrated in Figs. 12-9 to 12-11, where the pre- and post-neutron-emission fission yields, $N(m^*)$ and $N(m)$, are shown for the spontaneous fission of ^{252}Cf and the thermal-neutron-induced fission of ^{235}U and ^{233}U , respectively. The following characteristics should be apparent from these figures:

1. The most probable mode of fission in all three cases is with an asymmetric mass split of the fragments. The heavy-fragment mass peak in all appears around $A \sim 140$, while the light mass peak shifts from $A \sim 95$ in $^{233}\text{U} + n$ and $^{235}\text{U} + n$ to $A \sim 108$ in ^{252}Cf . This general feature is further

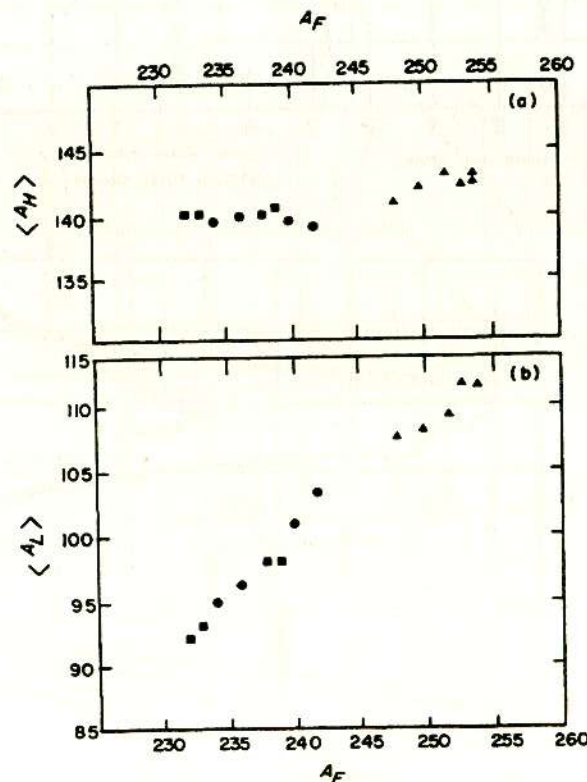


Fig. 12-12 Positions of the (a) heavy peak $\langle A_H \rangle$ and (b) light peak $\langle A_L \rangle$ in initial mass distribution as a function of the mass number A_F of the fissioning nucleus. (After Pappas et al. [21].) ▲: spontaneous fission; ●: thermal neutron fission; ■: fast neutron fission.

illustrated in Fig. 12-12, where we plot the positions of the heavy peak, \bar{A}_H , and the light peak, \bar{A}_L , in the initial mass distribution as a function of the mass number A_F of the fissioning nuclide. Whereas the heavy peak remains substantially at the same location, $\bar{A}_H \sim 140$, the position of the light peak keeps shifting.

2. There is considerable fine structure in the peaks of both $N(m^*)$ and $N(m)$, with $N(m)$ shifted slightly to the left of $N(m^*)$, showing the effect of neutron emission.

3. The fine-structure peaks of $N(m^*)$ in $^{233}\text{U} + n$ appear at heavy-fragment masses $A \sim 134, 139$, and 142 , at roughly the same mass numbers as in $^{235}\text{U} + n$. For ^{252}Cf , the peaks are again at $A \sim 140$ and 145 . These indicate a periodicity of about 5 mass units in the fine-structure peaks. We shall discuss the implications of this observation shortly.

In Figs. 12-9 to 12-11, we have also plotted the average single-fragment and average total pre-neutron-emission kinetic energies as functions of the fragment mass. The lighter fragment is seen to have more kinetic energy, and its value for a particular fissioning nuclide is nearly a constant. The heavy-fragment kinetic energy falls steadily, with increasing fragment mass. The total pre-neutron-emission kinetic energy, E_k^* , has a dip near symmetric fission in all three cases, although for ^{252}Cf this dip is only about 8 MeV, while for the two lighter fissioning nuclides it is approximately 22 MeV. In Fig. 12-13 we plot the average number of neutrons emitted per fragment and the average number of neutrons emitted per fission (i.e., by both the fragments) as functions of the fragment mass for thermal-neutron-induced fission of ^{233}U , ^{235}U , and ^{239}Pu [22]. In Fig. 12-14 the average neutron yield per fragment as a function of fragment mass is shown for the spontaneous fission of ^{252}Cf [23]. In all these curves of sawtooth shape, it will be noted that (a) the average number of neutrons emitted is minimum when the fragment mass is about 132, and (b) the maximum number of neutrons is emitted near symmetric fission.

It is worth while to discuss now the above experimental results in more detail. First, we make some comments on the asymmetry in the mass distribution of the fragments. From the empirical liquid-drop mass formula 6-21, there is no reason to expect this asymmetry, as the calculated energy release from this formula is found to be maximum for symmetric fission. We may then suspect that the mass asymmetry may be arising because of shell effects, implying thereby that shell effects persist even at the scission point, when the nucleus is in a highly deformed configuration.

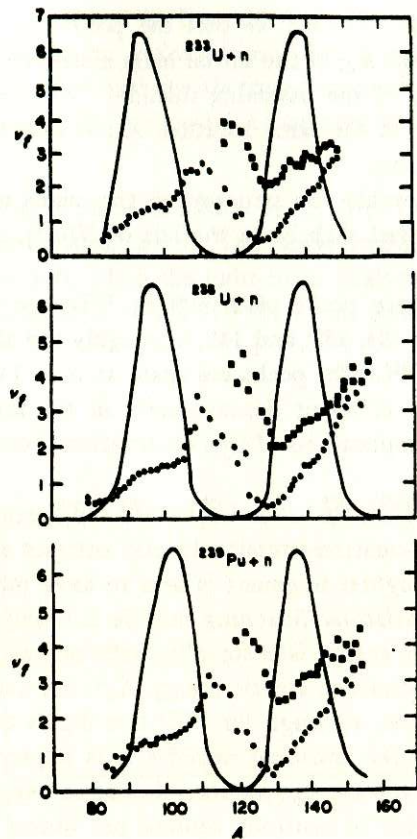


Fig. 12-13 Neutron yields of thermal-neutron-induced fission of ^{233}U , ^{235}U , and ^{239}Pu as a function of fragment mass. ●: The average number of neutrons emitted per fragment; ◆: the average number of neutrons emitted per fission as a function of the heavy-fragment mass. The mass distributions are shown for comparison. (After Apalín et al. [22].)

As will be seen from Figs. 12-9 to 12-11, appreciable asymmetric fission yield starts building up only when one of the fragments has at least 82 neutrons and 50 protons (two magic numbers), that is, beyond the heavy-fragment mass number 132.

As already discussed in Chapter 6, shell effects in the binding energy of a nucleus arise because of the bunching of single-particle quantum levels, due to the motion of a nucleon in an average potential well. This average potential well should change only slowly in a time compared to the time required for a nucleon to cross the nuclear diameter, which is of the order

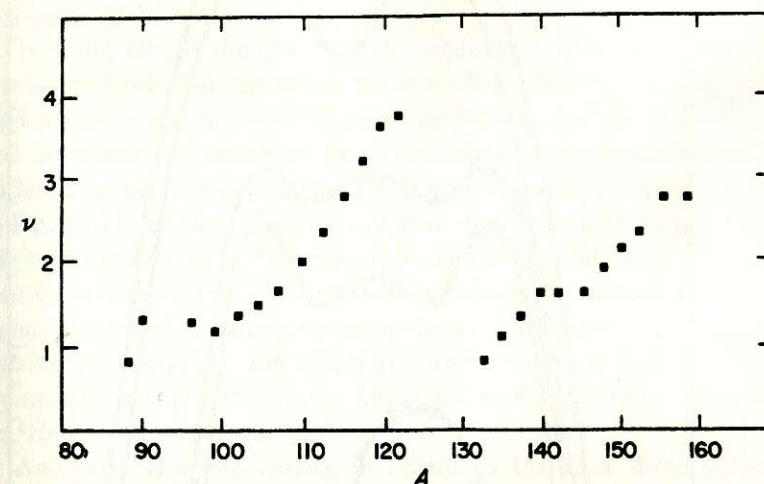


Fig. 12-14 Average neutron yield per fragment as a function of the fragment mass in the spontaneous fission of ^{252}Cf . (After Bowman et al. [23].)

of 10^{-22} s. During the time of scission, the nuclear shape is changing rapidly, and a neck connecting the two fragments is formed at this stage and snapped at scission. Shell effects in the fragments should show up in fission if the scission time (the time from when the nucleus is in the quasi-stationary state at the top of the barrier to the snapping of the neck) is long compared to $\sim 10^{-22}$ s, so that the nucleonic motion in each fragment can be regarded as being in a slowly changing average potential. The evidence that there are shell effects in the fragments points to the conclusion that the scission time may be long compared to 10^{-22} s. Further evidence of this is the near isotropy of the neutrons emitted from a fragment in its frame of reference, indicating that the neutrons are emitted after scission. If the snapping of the neck is very sudden, some neutrons would be expected to acquire enough excitation energy to escape at the point of scission. Fuller [24] has estimated that, if complete severance of the neck takes place within 2.5×10^{-22} s, it would result in the ejection of about 1.5 neutrons per fission in ^{252}Cf at the time of scission. Assuming that the angular distribution and energy of such neutrons would not by accident be such as to make them indistinguishable from evaporation neutrons, we conclude that the severance of the neck must be more gentle. We should point out that the

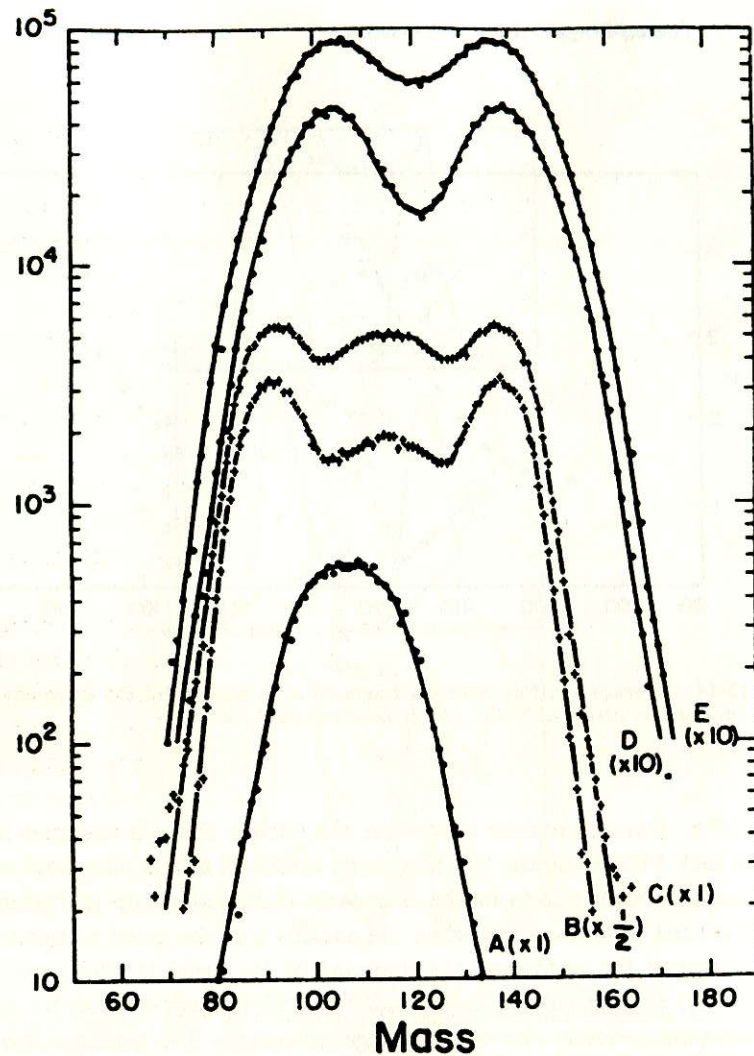


Fig. 12-15 Total initial mass yield distribution. For convenience of display, the number of events for each system has been multiplied by a scale factor given in parentheses. (A) ^{209}Bi (42.0-MeV α, f); (B) ^{226}Ra (30.8-MeV α, f); (C) ^{226}Ra (38.7-MeV α, f); (D) ^{238}U (29.4-MeV α, f); (E) ^{238}U (42.0-MeV α, f). (After J. P. Unik and J. R. Huizinga [29].)

experimental data are not completely consistent with isotropy of the emitted neutrons, and it is believed that about 10% of the emitted neutrons in ^{252}Cf originate from the fissioning nucleus rather than from the fragments [25].

Although the scission time may be longer than 10^{-22} s, as indicated here, it is doubtful whether a statistical equilibrium is established at scission, as claimed by Fong [26]. Up to the present time, there is no satisfactory *dynamical* theory of fission that describes the asymmetric mass split of the fissioning nucleus, but one may obtain some insight by plotting the static energy surfaces of the distorted nucleus, including the shell correc-

tion, as functions of the deformation parameters [27, 28], which we discuss in Section 12-5.

It is not always the case that the mode with asymmetric mass splitting is more probable than the symmetric one. When fission is induced by imparting enough excitation energy to target nuclei with $Z \leq 83$, the mass distribution in general is symmetric. Since the height of the fission barrier in these nuclei is rather large, considerable excitation energy has to be supplied. In Fig. 12-15, we show the fragment mass distribution obtained with 42-MeV ^4He ions incident on a ^{209}Bi target, leading to the fission of ^{213}At , and it is seen to be symmetric. When fission is induced in nuclides in the actinide region by imparting large excitation energy, the fine structures in the mass distribution disappear, and symmetric fission becomes nearly as frequent as asymmetric fission. This is also illustrated in Fig. 12-15 for ^{226}Ra and ^{238}U for ^4He -ion-induced fission [29].

Another interesting finding in regard to the mass distribution of the fragments has been reported by John et al. [15]. They find that thermal-neutron-induced fission of ^{257}Fm is strongly symmetric, as shown in Fig. 12-16. On the other hand, the spontaneous fission of ^{257}Fm still exhibits asymmetry, as shown in Fig. 12-17, although symmetric fission is also quite frequent. These mass distributions were derived from double energy measurements on coincident fission fragments by solid-state detectors, and the masses correspond to provisional masses (i.e., those with $\xi_1 = 0$ in Eq. 12-13). The most interesting point is that symmetric mass distribution in the low-energy fission of heavy actinides seems to appear abruptly at ^{257}Fm , since ^{256}Fm

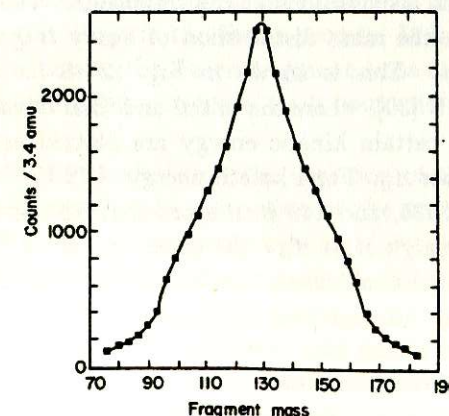


Fig. 12-16 Mass distribution for the thermal-neutron-induced fission of ^{257}Fm . (After John et al. [15].)

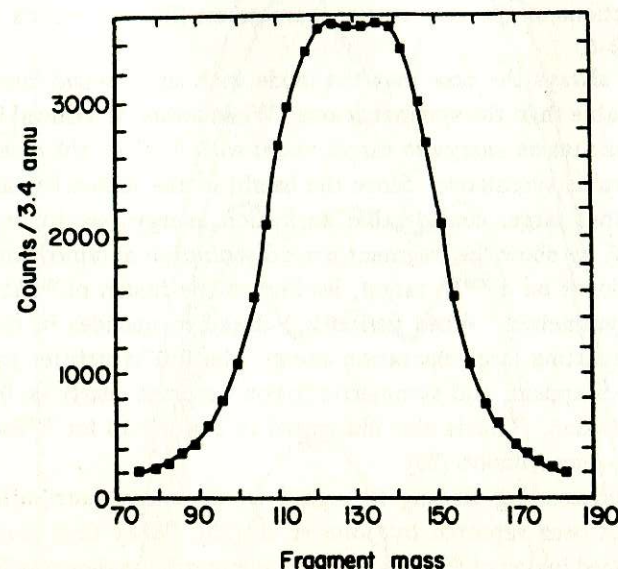


Fig. 12-17 Mass distribution for the spontaneous fission of ^{257}Fm . (After John et al. [15].)

fissions asymmetrically. This observation lends support to the occurrence of double-humped fission-barrier shapes due to shell effects and will be further discussed in Section 12-5.

We now make a few comments on the fine structure observed in the initial and final mass distributions of the fragments. The fine structure is more pronounced in the mass distribution of heavy fragments having the same kinetic energy. This is shown in Fig. 12-18 for thermal-neutron-induced fission of ^{235}U [30], where the initial and final fission yields of heavy fragments having a certain kinetic energy are plotted against the heavy-fragment mass number A_H . For a kinetic energy of 72 MeV there are distinct peaks at $A_H \approx 130$, 135, and 140 in the pre-neutron-emission distribution, while for a kinetic energy of 64 MeV the peaks appear at 140, 146, and 151. The distributions of the final masses are shifted somewhat to the left because of neutron emission. Thomas and Vandembosch [31] correlated the peaks in the fine structure to the fact that division into even-even fragments is energetically more favorable in fission, since these have more binding energy, because of the pairing effect, than odd-mass fragments. Furthermore, for a given charge of the even-even heavy fragment, the binding energy reaches

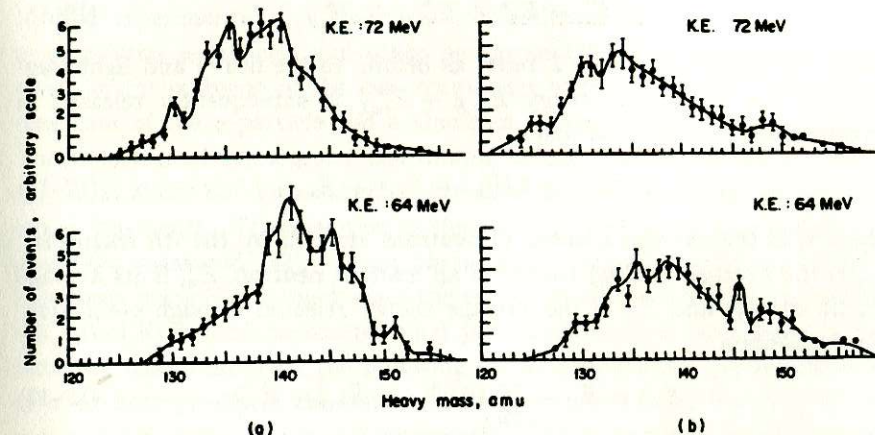


Fig. 12-18 The initial (a) and final (b) mass distributions for fixed kinetic energies in the thermal-neutron-induced fission of ^{235}U . Indicated errors are statistical ones. (After G. Andritsopoulos [30].)

a maximum for some value of A_H . For example, this maximum for $Z_H = 58$ comes near $A_H = 150$, for $Z_H = 56$ at $A_H \approx 145$, and for $Z_H = 54$ at $A_H \approx 140$ [31]. The peaks in the fine structure thus appear at the same values of A_H at which the even-even mass surface has peaks. Hence it appears that pairing and symmetry energy effects (which are the most rapidly varying terms in the mass formula when Z is fixed) are still operative at the scission point. Since both these effects are related to the concept of a Fermi surface, this lends credence to a description of the nucleus in terms of single-particle orbitals, even at this stage in the fission process. It is amusing that historically the fine structure in the fission-fragment mass distribution was better understood than the gross structure itself with its accompanying mass asymmetry.

Figures 12-9 to 12-11 also show the variation of the total pre-neutron-emission kinetic energy E_k^* as a function of the fragment mass for ^{252}Cf , $^{238}\text{U} + n$, and $^{235}\text{U} + n$. If we simply equated E_k^* to $e^2 Z_1 Z_2 / D$, where D is the separation of the charge centers at scission, E_k^* would be a maximum for symmetric fission with $Z_1 = Z_2$ (assuming that D is approximately constant and $Z_1/A_1 = Z_2/A_2$). We find from the experimental data, however, that E_k^* has a marked dip for symmetric fission and is maximum for $A_H \approx 132$. Milton and Fraser [18] correlated this behavior of E_k^* with the energy that goes into fragment excitation. If E_R is the energy release in fission, then

$$E_R = E_k^* + E_{ex,H}^* + E_{ex,L}^*, \quad (12-15)$$

where the subscripts H and L refer, as before, to the heavy and light fragments. The excitation energy $E_{ex,H}^* + E_{ex,L}^*$ is subsequently released in neutron and γ -emission, so that

$$E_{ex,i}^* = \bar{v}_i(\bar{B}_{ni} + \bar{E}_{ni}) + \bar{E}_{\gamma i}, \quad (12-16)$$

where \bar{v}_i is the average number of neutrons emitted by the i th fragments, \bar{B}_{ni} is the average binding energy of an emitted neutron, \bar{E}_{ni} is its average kinetic energy, and $\bar{E}_{\gamma i}$ is the average energy released through γ -emission. We thus obtain

$$E_k^* = E_R - \sum_{i=H,L} [\bar{v}_i(\bar{B}_{ni} + \bar{E}_{ni}) + \bar{E}_{\gamma i}]. \quad (12-17)$$

For given A_H , A_L , Milton and Fraser [18] took for E_R the maximum energy released, averaged over the various charge distributions Z_H , Z_L . The quantities \bar{E}_n and \bar{E}_γ were assumed to be independent of the fragment mass and were given values of 1.2 and 7.5 MeV, respectively, for ^{233}U as well as ^{235}U . By taking reasonable values of \bar{B}_n , Milton and Fraser could reproduce the variation of E_k^* with A_H . For symmetric fission, as will be seen from Fig. 12-14, ν is maximum, giving a dip in E_k^* . For $A_H \sim 132$, ν is minimum, and this gives rise to the peak in E_k^* . For this value of A_H , the heavy fragment is doubly magic ($N_H = 82$, $Z_H = 50$) and is not easily deformable; consequently it does not take up much excitation energy and the neutron emission is minimum.

In the preceding discussion, we arbitrarily assumed at one point that the charge division in the fragments is such that $Z_1/A_1 = Z_2/A_2 = Z/A$. Experimentally, this is found to be a good first approximation. More precisely, for a given fragment mass A_1 , the charge distribution of the fragment is found to be Gaussian, with its peak at $Z_1 = (Z/A) \cdot A_1$.

We end this section with a few comments about ternary fission, for which a fair number of experimental data exist [32]. According to Feather [2], ternary fission is a process in which three fragments appear within a time period of 10^{-18} s after scission. By far the most frequent third fragment is observed to be an α -particle, the other two being heavy fragments. The fractional yield of ternary fission in induced fission of the actinide nuclei is found to be about 2.1×10^{-3} for all of the species and is independent of the excitation energy between 6 and 40 MeV. This means that about 2 ternary fissions are observed, with one fragment an α -particle, in 1000 fission processes. The energy distribution of these emitted α -particles has been

studied experimentally, although the necessity of shielding the detectors from natural α -particles and other background effects has resulted, most often, in the omission of the low-energy part of the spectrum. The energy spectrum of the α -particle has a Gaussian shape, centered at ~ 16 MeV. Measurements of the angular distribution of the emitted α -particles reveal a peak at about 82° with respect to the direction of the lighter of the two heavy fragments. The variation of the α -energy with angle of emission has also been measured [33]. Using these input data, computer calculations have been made [33] to back-track the trajectory of the α -particle, obtaining the initial dynamical parameters that yield the observed distribution. The data are consistent with the following initial conditions: the α -particle is emitted isotropically at the instant of scission or within 10^{-21} s of it, in the region between the two heavy fragments, and has an initial kinetic energy of 2–3 MeV.

Clark and Kugler [34] have made a careful study of the energy spectrum of the α -particles emitted from $^{235}\text{U} + n$, including the low-energy part of the spectrum. In addition to the peak at ~ 16 MeV for the long-range α -particles, they find almost an equal number of short-range α -particles with energy < 8 MeV. This is a most puzzling phenomenon, since if an α -particle was initially in the Coulomb field of the two fragments, it should pick up appreciable kinetic energy at the detection point. It may be, as suggested by Kugler [35], that these α -particles are emitted at a very late stage of the scission, so that the distances between them and the fragment charge centers are much larger than the corresponding values for the long-range α -particles. More work on the low-energy distribution of the emitted α -particles may help to shed further light on this problem.

12-3 THE LIQUID-DROP MODEL

From a microscopic point of view, the phenomenon of fission is extremely complicated. As the fissioning nucleus is torn apart in a very short time, the motion of each individual nucleon is radically altered. The entire interval from the instant that some energy is imparted to the nucleus (e.g., by a neutron capture) to the time at which it is torn apart (scission) may be divided into two parts.

During the first interval of time, the imparted energy is redistributed among the nucleons over a comparatively large period ($\sim 10^{-15}$ s) involving many nucleonic collisions. During this time, the energy that goes into the collective degrees of freedom causes increased deformation of the nucleus, and this change in deformation takes place very slowly compared to the

time of individual nucleonic motion. If none of the individual nucleons attains enough energy to escape the nucleus (e.g., by neutron emission), the imparted energy may be nearly all spent in causing a large critical deformation, beyond which the system is unstable. This metastable state is reached at the saddle point, at the end of the first interval of time. Once the nucleus is over the saddle point, shape instability takes place, and the nucleus can distort very easily to reach the point of scission.

The second time interval, from the saddle point to scission, is very short ($\sim 10^{-21}$ s), and the separation of collective and intrinsic coordinates may not be meaningful at this stage, although there is evidence for the persistence of shell effects even here, as discussed in Section 12-2. (See the introduction of Chapter 9 for a discussion of the adiabatic approximation.)

In this section, we shall concentrate our attention on the collective motion of the nucleus up to the saddle point, where we can still meaningfully describe the motion in terms of collective variables. There are two aspects of the problem: the statics (i.e., the potential-energy surfaces of the nucleus with increasing deformation) and the dynamics—its equation of motion. In the absence of any complete theory, it is instructive to construct intuitive models of fission to see whether the salient experimentally observed characteristics can be extracted, and the liquid-drop model is an attempt in this direction. Immediately after the discovery of fission, Meitner and Frisch [36] emphasized the analogy of the process concerned with the division of a charged liquid drop into two smaller droplets due to deformation caused by an external impact. Bohr and Wheeler [37] gave an account of the mechanism of fission based on the statics of the model by calculating the potential-energy surfaces of a charged deformed liquid drop. A more ambitious project was undertaken by Nix and Swiatecki [38] and Nix [39], who traced out in detail both the static and the dynamic characteristics of the division of an idealized (nonviscous, irrotational) liquid drop whose size, surface tension, and charge are those of a nucleus, and compared the results with what is observed experimentally in the fission of real nuclei. This simple model is reasonably successful in describing the fission of nuclei lighter than radium, where the mass distribution of the fragments is symmetric, but fails for heavier nuclei. Despite its failure in the most interesting region of nuclei, the model has two important factors in its favor. The first is its conceptual simplicity, although the actual calculations (particularly the dynamics) are quite complicated. The second factor is that its failure in the heavy-mass region indicates the importance of the missing ingredients (e.g., single-particle effects like shell correction) in the simple model. Recent progress in the

understanding of fission phenomena has consisted mainly in the modification of the statics to account for shell effects, and has led to better agreement between the predictions of theory and the findings of experiment.

Before doing any calculation with the model, we should first inquire as to why a charged liquid drop should behave in any way like a nucleus [38]. We shall be particularly concerned with the variation of the potential energy with deformation. There are two important characteristics of the nucleus that we must keep in mind. First, it is reasonable to assume that the nucleus is incompressible, so that the total nuclear volume remains unaltered in fission, and the average nuclear density ρ is identical in the primary fragments and in the fissioning nucleus. Second, although the two-nucleon force is rather complicated, its range r_n is small compared to the nuclear radius R_0 of the heavy nuclei being considered. Consequently, the nuclear part of the potential energy can be expressed as the sum of a volume term proportional to A (independent of the shape of the nucleus), a surface term proportional to $A \cdot (r_n/R_0)$ (shape dependent), and terms containing higher powers of r_n/R_0 , which are smaller in magnitude (see Eq. 6-9). There are also the symmetry terms (see Eq. 6-21) proportional to $(N - Z)^2$. The volume part of the symmetry energy is shape independent, while the surface-symmetry term has the same shape dependence as the main surface term. The symmetry effects can be taken into account by replacing the coefficients a_v and a_s in Eq. 6-21 with C_v and C_s , as is done in Eq. 6-22. For a nucleus in the actinide region, the volume term is typically a few thousand MeV, the surface term (including the surface-symmetry energy) is several hundred MeV, and the volume-symmetry term is a few hundred MeV. Of these three, only the variation of the surface term with deformation need be considered, the other two remaining almost unchanged with deformation and through fission. The other large shape-dependent contribution is the Coulomb energy, which is of the order of 1000 MeV.

If we decide to neglect the finer corrections to the binding energy arising from pairing and shell effects (\sim a few MeV, but deformation dependent), we see that the *change* in the nuclear potential energy with deformation comes about through the variation of the surface and Coulomb terms only. Therefore, for considering the statics (i.e., the dependence of potential energy on deformation of the nucleus), a good first approximation should be just to consider the surface and Coulomb energies. Furthermore, although the nuclear force is rather complicated in nature, the surface term arises because a nucleon at the surface has fewer neighbors to interact with, and the proportionality constant C_s (see Eqs. 6-22 and 6-23) is accurately known.

The situation is completely analogous to that of a liquid drop. As the nucleus or the liquid drop is deformed, its surface area increases, resulting in an increase in the surface energy and a decrease in the Coulomb energy. Thus there is some cancellation of the two effects. For lighter elements this cancellation is only partial, but for elements of higher charge in the actinide region it is nearly complete, with the result that the neglected shell corrections of a few MeV can no longer be ignored. It is not surprising, then, that the simple liquid-drop model works reasonably well for the lighter nuclei but fails in the actinide region. A logical improvement to the model would be to incorporate the single-particle effects on the potential-energy surfaces of the liquid drop. In this section, we shall consider only the liquid-drop part of the energy, and examine the predictions of this simple model. In the next two sections shell correction will be treated in detail.

Let us now consider the potential energy of a charged drop as a function of the deformation parameters, with the size, surface tension, and charge of the drop the same as those of a nucleus. Let E_s and E_C be the surface and Coulomb energies of the deformed drop, and E_{s0} and E_{c0} the corresponding quantities for the undistorted spherical shape. Then

$$E_{s0} = 4\pi R_0^2 S = C_s A^{2/3}, \quad (12-18)$$

where S is the surface tension of the liquid, related to the coefficient C_s of the surface term in the mass formula 6-22, with $C_s = 18.56 [1 - 1.79(N - Z)^2/A^2]$ MeV. The Coulomb energy of a spherical drop is given by

$$E_{c0} = \frac{3}{5} \frac{Z^2 e^2}{R_0} = \frac{\kappa_c Z^2}{A^{1/3}}, \quad (12-19)$$

where $\kappa_c = 0.717$ MeV is the coefficient of the shape-dependent part of the Coulomb term in mass formula 6-22. For a deformed shape,

$$E_s = S\sigma \quad \text{and} \quad E_C = \frac{1}{2} \int \frac{\rho(\mathbf{r}_1)\rho(\mathbf{r}_2)}{|\mathbf{r}_1 - \mathbf{r}_2|} d\mathbf{r}_1 d\mathbf{r}_2, \quad (12-20)$$

where σ is the surface area of the drop, and $\rho(\mathbf{r})$ is the charge density at point \mathbf{r} . As the drop deforms, the surface energy increases ($E_s - E_{s0} > 0$) while the Coulomb energy decreases ($E_C - E_{c0} < 0$). If we take the spherical drop as the reference, the potential energy V of the drop up to second order in α is given by

$$V = (E_s - E_{s0}) + (E_C - E_{c0}) = \frac{1}{2} \sum_{\lambda,\mu} C_\lambda |\alpha_{\lambda\mu}|^2, \quad (12-21)$$

where C_λ is defined by Eqs. 9-9 to 9-11. A detailed derivation of this expression may be found in a book by Wilets [40].

We will consider, for simplicity, only small deformations of the type $\lambda = 2$. Using Eqs. 12-18 and 12-19, we find that

$$V = \frac{1}{2\pi} (E_{s0} - \frac{1}{2} E_{c0}) \sum_\mu |\alpha_{2\mu}|^2. \quad (12-22)$$

If V is positive, it means that there is an effective energy barrier for deformation and fission, while a negative or zero V indicates instability of the spherical drop toward deformation. From Eq. 12-22 we conclude that a charged spherical drop is unstable toward small deformations of the $\lambda = 2$ type if

$$E_{s0} \leq \frac{1}{2} E_{c0} \quad \text{or} \quad x = \frac{E_{c0}}{2E_{s0}} \geq 1. \quad (12-23)$$

The dimensionless quantity x is called the fissionability parameter, and, using Eqs. 12-18 and 12-19, we find

$$x = \frac{\kappa_c Z^2 / A^{1/3}}{2C_s A^{2/3}} = \frac{Z^2 / A}{51.77 [1 - 1.79(N - Z)^2 / A^2]}. \quad (12-24)$$

According to this formula, $x = 0.6991$ for ^{210}Po , increasing to the values 0.7597 for ^{235}U and 0.8274 for ^{254}Fm . As x approaches unity, we expect the height of the barrier to decrease. For $x < 1$, spontaneous fission is still possible through barrier penetration.

Although nuclei with $x < 1$ are stable with respect to small arbitrary deformations, a larger deformation will give the long-range repulsion more advantage over the short-range attraction, and it should be possible for a suitably deformed nucleus to divide spontaneously in this case. For this to happen, however, the nucleus will have to reach a critical stage of deformation, at which it will be on the verge of division. This will be a state of unstable equilibrium, and it can be found by plotting the potential-energy contours of the liquid drop as a function of the deformation parameters. For axially symmetric deformations, we can use the expansion

$$R(\theta) = \frac{R_0}{\xi} \left[1 + \sum_{\lambda=2}^{\infty} a_\lambda P_\lambda(\cos \theta) \right], \quad (12-25)$$

where $a_\lambda = [(2\lambda + 1)/4\pi]^{1/2} \alpha_{\lambda 0}$, and can then write down an expression for the deformation energy $V(x, a_2, a_3, \dots, a_\lambda, \dots)$, in a power series of the a_λ 's. Cohen and Swiatecki [41] have done this calculation, taking terms up to $\lambda = 18$.

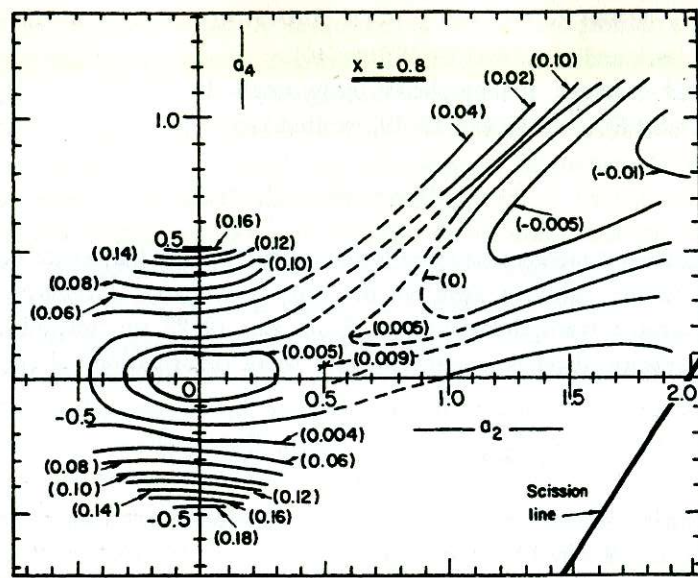


Fig. 12-19 Contour map of the potential-energy surfaces in the liquid-drop model as functions of a_2 and a_4 , all other a_λ 's being set equal to zero. The fissionability parameter x is fixed at 0.8. The labeled energies are in units of E_{s0} . The saddle point is shown by a cross. (After Wilets [40].)

For the purpose of orientation, let us consider only deformations of types a_2 and a_4 , putting all other $a_\lambda = 0$. The potential-energy contours for $x = 0.8$ are plotted in the a_2-a_4 plane in Fig. 12-19, each contour being a line of constant potential energy labeled by values of V/E_{s0} . For $x < 1$, as we have seen, the spherical shape with $a_2 = a_4 = 0$ is always a local minimum. We note from the figure that for large distortions there are other contours with potential energy equal to or less than that of the spherical configuration. In fact, these successive contours of lower and lower potential energy form a deep valley which favors more and more deformation of the nucleus, ultimately leading to scission. However, in order to go down this valley, starting from the spherical shape, the nucleus has to pass through some contours of higher potential energy.

The potential barrier that the nucleus must surmount will depend on the path that it follows in the a_2-a_4 plane. There is, of course, a particular path of least resistance leading to the potential hollow on the other side, given by the values of a_4 (in terms of a_2 and x) for which the potential is

minimal, that is, $\partial V/\partial a_4 = 0$ and $\partial^2 V/\partial a_4^2 > 0$. On this fission path, there will be a particular point in the a_2-a_4 plane where the potential energy is maximum, and this is the barrier height that the nucleus has to surmount to go down the valley of fission. This point is called the saddle point because the potential energy increases in the direction in the a_2-a_4 plane perpendicular to the fission path, and it is a configuration of unstable equilibrium for the nucleus. It is the low point or pass in the potential-energy ridge that separates the spherical drop from the valley leading to two-fragment division. In the general case, there may appear other passes leading to even deeper hollows in the potential that correspond to three- or many-fragment divisions of the drop, but these passes lie at considerably higher energy, hindering such divisions. In Fig. 12-19, where we have plotted the potential-energy contours, the position of the saddle point is shown by a cross.

It is thus possible in this simple model not only to obtain the height of the fission barrier but also to find the shape of the nucleus at the saddle point, since the deformation parameters at this point are known. In a more general treatment of the model, both even and odd a_λ 's may be considered, including the possibility of asymmetric mass division. It is found, however, that this gives rise to higher fission barriers, implying thereby that only symmetric division is favored in the liquid-drop model.

In Cohen and Swiatecki's work [41], all the even a_λ 's up to $\lambda = 18$ in expansion 12-25 were considered. As before, there is a fission path in the multidimensional a_λ -space leading to the saddle point. The shape of the liquid drop at the saddle point has been numerically computed for various values of the fissionability parameter x , and this is shown in Fig. 12-20. For $x = 1$, as we have seen, the spherical shape itself is an unstable equilibrium, while for the other extreme, $x = 0$, there is effectively no Coulomb repulsion—hence the saddle-point configuration consists of two touching spheres.

Calculation of the height of the fission barrier in the liquid-drop model gives a pronounced and smooth dependence of E_b on x , in contradiction with the experimental results. Since the barrier in the liquid-drop model for the actinide nuclides is only a few MeV, it is clear that the cancellation of the surface and Coulomb terms is nearly complete, and that the neglected shell effects (which show a rapid variation with the parameter x) can play a dominant role. To stress this point, we have plotted the fission barrier E_b against the mass number A in the liquid-drop model for nuclei along the stability line in Fig. 12-21, and the result is seen to be a smooth curve. The effect of including the shell correction (following the method of Myers

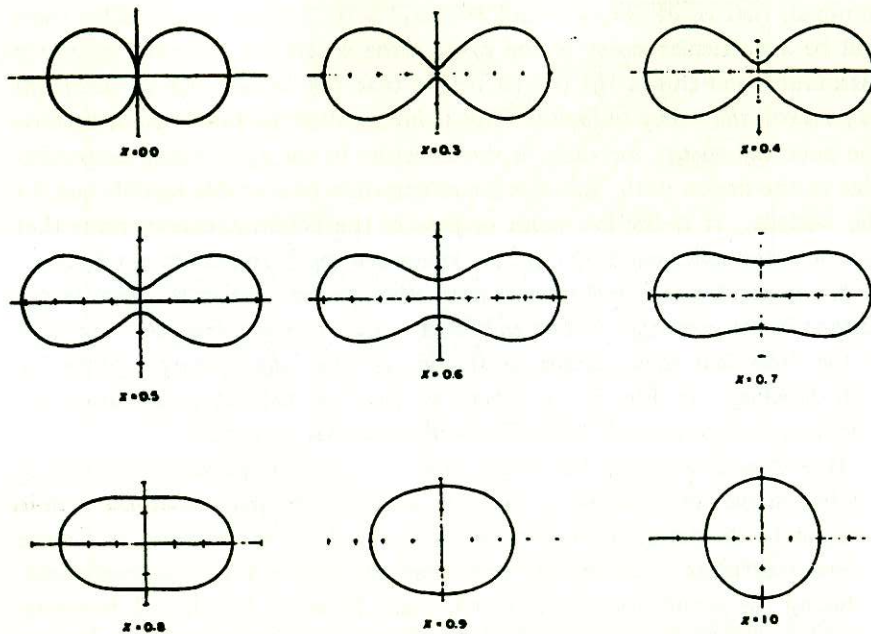


Fig. 12-20 Numerically computed saddle-point shapes of the liquid drop for various values of the fissionability parameter x . (After Cohen and Swiatecki [41].)

and Swiatecki [42]) is shown in the same figure by the dotted curve. It is clear that, although the liquid-drop model can be taken as a first approximation to describe the fission process, it is absolutely necessary to include shell effects in the theory. Moreover, the liquid-drop model predicts only a one-humped barrier, while shell effects, which are deformation dependent, may change the shape radically, introducing more than one hump, with important consequences. We shall devote the next section to an explanation of how the shell effect is evaluated in a single-particle picture.

We outlined some results of the dynamics of an oscillating liquid drop in Chapter 9. It was noted that for small deformations there are β -vibrations about the equilibrium shape which preserve the symmetry axis. The inertial parameter B associated with such oscillations is not given realistically in the hydrodynamical model. Without going into finer details, it is still instructive to obtain a crude estimate of the fission half-life of a nucleus from the simple ideas developed so far. In the multidimensional α -space, there is, as we have seen, a curve of least resistance to fission, which we call

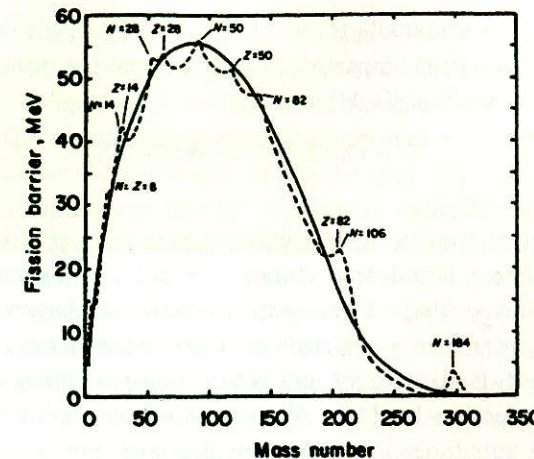


Fig. 12-21 The fission-barrier height E_b (in MeV) against the mass number A in the liquid-drop model is shown by the continuous curve. The effect of including the shell correction is shown by the dotted line. (After Myers and Swiatecki [42].)

the fission path. Along this fission path, the liquid-drop model predicts a single hump around the saddle point. We may imagine parameterizing this path by a single parameter α , which is a measure of the distortion of the nucleus along this path. If we denote the value of this parameter by α_s at the saddle point, the potential of the charged drop near this point along the fission path may be written as

$$V(\alpha) = V(\alpha_s) - C(\alpha - \alpha_s)^2 + \dots, \quad (12-26)$$

where C is a measure of the curvature of the barrier, and $V(\alpha_s) = E_b$, the height of the barrier. It is convenient to set $\alpha - \alpha_s = \alpha'$. The kinetic energy of the nucleus around the saddle point is $\frac{1}{2}B\dot{\alpha}'^2$, where B is the associated inertial parameter evaluated at the saddle point. When this model is applied to the nucleus, the Hamiltonian near the saddle point is

$$H(\alpha') = \frac{1}{2}B(\dot{\alpha}')^2 - C(\alpha')^2 + E_b. \quad (12-27)$$

To emphasize the resemblance of this Hamiltonian to that of an inverted harmonic oscillator, we can put $C = \frac{1}{2}B\omega_b^2$, where ω_b has the dimensions of frequency.

In order for fission to take place, the nucleus as a whole has to tunnel through this barrier. The problem of penetration through one-dimensional barriers in the WKB approximation is dealt with in detail in Appendix D.

For an inverted harmonic-oscillator barrier, the WKB result is exact. If an energy E ($< E_b$) has been imparted to the nucleus, the penetration probability is given by (see Eqs. D-11, D-12)

$$P = (1 + \exp 2K)^{-1} \approx \exp(-2K) \quad (12-28)$$

with $2K = 2\pi(E_b - E)/\hbar\omega_b$.

The curvature of the barrier along the fission path at the saddle point can be obtained from liquid-drop statics. In order to estimate $\hbar\omega_b$, it is also necessary to know $B(\alpha_s)$. Detailed microscopic calculations indicate that the inertial parameter B of a nucleus with large deformation (corresponding to the saddle point) is about ten times larger than the corresponding irrotational hydrodynamical value [43]. We can, however, estimate $\hbar\omega_b$ from a knowledge of the spontaneous half-lives of fissioning nuclei. The vibrating nucleus is making a certain number of assaults n on the barrier per second. This number is usually equated to the frequency of β -vibrations, setting $\hbar\omega_{\text{vib}} \approx 1$ MeV. This corresponds to $n = 10^{20.38}$ assaults per second on the barrier. The fission rate is then $n \cdot P$, and the half-life in seconds is

$$\tau_{1/2} = \frac{\ln 2}{n \cdot P} = 10^{-20.54} P^{-1} \text{ s}, \quad (12-29)$$

where P is given by Eq. 12-28. Empirical data give a value of E_b fluctuating in the range 4.5–6.5 MeV for A going from 230 to 250. Knowing the half-lives $\tau_{1/2}$ for various nuclei, we can deduce the value of $\hbar\omega_b$ from Eqs. 12-28 and 12-29; $\hbar\omega_b \approx 300$ –400 keV for these nuclei. It is to be noted that in the presence of a double-humped barrier the problem has to be reanalyzed, although the basic ideas are unaltered.

12-4 SHELL CORRECTION TO THE LIQUID-DROP MASS FORMULA

In Chapter 6, we found that the variation of the binding energy per nucleon with mass number A could be fairly well reproduced by the semiempirical mass formula. This formula yielded a smooth dependence of B/A on A for the most stable isobars. As was pointed out in Section 6-3, the experimental binding energies revealed small deviations from this smooth curve, and we could write (cf. Eq. 6-22)

$$B(A, Z) = B_{\text{dist}}^{LD}(A, Z) + \delta B(A, Z), \quad (12-30)$$

where $B(A, Z)$ is the experimental binding energy of a nucleus (A, Z) , B_{dist}^{LD} is its value predicted by the distorted liquid-drop mass formula 6-22,

and $\delta B(A, Z)$ arises because of shell correction. The important point to note is that, when δB is plotted against A , it has a structure which is *not* reproducible by adjusting the coefficients of the mass formula. In Chapter 6, the form of the semiempirical mass formula was obtained by considering a Fermi gas model of the nucleus, where the single-particle density of states was a smooth function of energy. Although terms like symmetry energy do have their origin in quantum effects (the Pauli principle), the specific effect of fluctuation of single-particle level density due to shell structure was ignored in the mass formula. Thus the mass formula may be regarded as a semiclassical approximation for the energy of the nucleus, where the single-particle levels, instead of being discrete and bunched together in shells, have somehow been smoothed to yield an average level density. This approximation, together with the assumption of the incompressibility of the nucleus, is sufficient to yield a smooth dependence of the energy on A .

It is important to realize that the semiempirical mass formula already contains the important two-body correlation terms (e.g., the volume, surface, Coulomb, and pairing terms all arise from some two-body effective interaction), but a correction of specific single-particle origin needs to be incorporated in it to obtain better agreement with experimental results. Although this correction is a small fraction of one per cent of the total binding, it is of great importance in determining the stability of superheavy nuclei and the shapes of fission barriers [44–46]. Because of the single-particle origin of the shell effect, we may attempt to extract it from a simple independent-particle model, and add this correction to B_{dist}^{LD} to obtain the shape of the fission barriers as well as to investigate the stability of superheavy nuclei.

Shell effects do not arise just from the discreteness of the levels but come about because of the degeneracy or of the bunching of states in the energy space. To appreciate this simple fact, consider one species of noninteracting fermions occupying singly the energy levels of a one-dimensional harmonic oscillator. The single-particle energies are

$$\epsilon_N = (N + \frac{1}{2})\hbar\omega, \quad N = 0, 1, 2, \dots, \quad (12-31)$$

and, considering A fermions, the Fermi energy is

$$\lambda = (A - \frac{1}{2})\hbar\omega. \quad (12-32)$$

The sum of the occupied single-particle energies E , is given by

$$\begin{aligned} E &= [\frac{1}{2} + \frac{3}{2} + \cdots + (A - \frac{1}{2})]\hbar\omega \\ &= \frac{A^2}{2}\hbar\omega. \end{aligned} \quad (12-33)$$

We shall presently show that it is the sum of the single-particle energies of the occupied orbitals that contains shell effects; if this quantity E is a smooth function of A , as in Eq. 12-33, no shell correction is present. For a more realistic three-dimensional isotropic harmonic oscillator, although the energies are equally spaced, there is a degeneracy $\frac{1}{2}(N+1)(N+2)$ in a given major shell N , and it is no longer possible to express E as a smooth function of A . Degeneracy, of course, is an extreme limit of bunching of states with respect to energy, and it may be thought that with increasing deformation of the potential well, as the levels become more uniformly distributed, the shell effects should disappear. That this is not so is illustrated in Fig. 12-22 by plotting the energy levels of an axially symmetric harmonic-oscillator potential (Eq. 9-147) against ϵ , for $\omega_1 = \omega_2 = \omega_{\perp} = \omega_0(1 + \epsilon/3)$ and $\omega_3 = \omega_0(1 - 2\epsilon/3)$. It will be seen that the shell structure persists even at large deformations, and regular energy gaps with large degeneracy appear for $\omega_3/\omega_{\perp} = \frac{2}{1}, \frac{1}{1}$ or $\frac{1}{2}$, that is, at $\epsilon = -0.75, 0$, and 0.6 , respectively.

In regard to the empirical mass formula 6-22, the liquid-drop part $B_{\text{dist}}^{\text{LD}}(A, Z)$ always prefers a spherical shape of the nucleus. It is the effect described by the shell-correction term δB which causes certain nuclei to have deformed shapes with extra stability. To see this in more detail, examine the Nilsson diagram (Fig. 9-32) of neutron levels for $N > 126$. The closed shells for spherical shapes in this region occur at $N = 126$ and 184 .

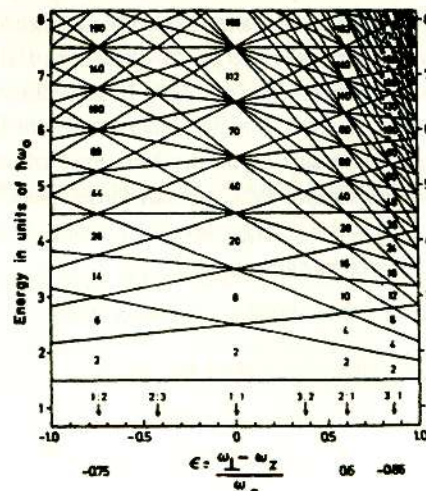


Fig. 12-22 Single-particle levels of an anisotropic harmonic oscillator (with $\omega_1 = \omega_2 = \omega_{\perp}$) as a function of $\epsilon = (\omega_{\perp} - \omega_3)/\omega_0$. [After R. K. Sheline, I. Ragnarsson, and S. G. Nilsson, *Phys. Lett.* 41B, 115 (1972).]

If we consider a nucleus with $N = 152$, then for a spherical shape the $g_{9/2}$ and $i_{11/2}$ levels are fully occupied and the $j_{15/2}$ levels partly so. Since the density of single-particle states near the Fermi energy is very large in this case, most of the valence nucleons are near this energy and the nucleus has less binding than in the situation (which occurs for $\epsilon \sim 0.05$) where the single-particle states are more uniform. The most favorable configuration is at $\epsilon \approx 0.25$, when the density of states near the Fermi level is very small, and most of the valence neutrons occupy deeper and more bound states. For such a deformation, we expect the shell correction δB to be positive, giving a deformed ground state. As is clear from Fig. 12-22, a closed shell may appear near $N \sim 140$ for $\epsilon \approx 0.6$, which is around the liquid-drop saddle point, thus completely altering the shape of the liquid-drop barrier.

Recognizing the point that shell correction is basically a single-particle effect and arises from the fluctuations in the single-particle level density, we shall now discuss a method of theoretically estimating δB . In Chapter 10, we saw that in the Hartree-Fock theory we can write the energy of a nucleus as

$$E_0 = \sum_m e_m^{(\text{HF})} - \frac{1}{2} \int \rho(\mathbf{r})\rho(\mathbf{r}')V(\mathbf{r}, \mathbf{r}') d^3r d^3r',$$

where $V(\mathbf{r}, \mathbf{r}')$ is the effective two-body interaction, the sum runs over the occupied HF orbitals m with self-consistent energies $e_m^{(\text{HF})}$, and the exchange term has been neglected. Strutinsky [47] has shown that E_0 can be approximated by the following expression:

$$E_0 \approx \sum_m e_m^{(\text{sm})} - \frac{1}{2} \int \tilde{\rho}(\mathbf{r})\tilde{\rho}(\mathbf{r}')V(\mathbf{r}, \mathbf{r}') d^3r d^3r',$$

where $\tilde{\rho}(\mathbf{r})$ is the "smooth" component of $\rho(\mathbf{r})$, and $e_m^{(\text{sm})}$ are the single-particle energies derived from the one-body potential $U = \int \tilde{\rho}(\mathbf{r}')V(\mathbf{r}, \mathbf{r}') d^3r'$, which we may identify as a phenomenological shell-model type of potential. Let us denote $\sum_m e_m^{(\text{sm})}$ by E ; this quantity contains the shell effects. Also, let us assume that there is a prescription for extracting the part of E that smoothly varies with nucleon number and deformation, and designate this as \tilde{E} . Then we may write

$$E_0 = (E - \tilde{E}) + \tilde{E} - \frac{1}{2} \int \tilde{\rho}(\mathbf{r})\tilde{\rho}(\mathbf{r}')V(\mathbf{r}, \mathbf{r}') d^3r d^3r'$$

The last two terms on the right side of the equation have no shell effects present, and we can identify these as the terms representing the liquid-drop

expression, E^{LD} . Hence we finally obtain

$$E_0 = E^{LD} + (E - \bar{E}). \quad (12-34)$$

According to Eq. 12-34, the liquid-drop energy should be "renormalized" by the shell-correction term $(E - \bar{E})$ to obtain the energy of the many-nucleon system. We shall now describe the method of Strutinsky for obtaining \bar{E} from a given shell-model potential (e.g., the Nilsson potential). The method works particularly well for a one-body potential in which all the levels are discrete, as in the Nilsson potential. There are some complications, however, for a finite U like the Woods-Saxon potential, where some bound-state levels are followed by a continuum; this we shall discuss later. In the following we shall also drop the superscript "sm" from the single-particle energies for simplicity.

The single-particle density of states is given by

$$g(e) = \sum_i \delta(e - e_i), \quad (12-35)$$

where the e_i 's are the eigenvalues of a properly chosen one-body potential, and the sum over i is taken over all states, taking account of the degeneracy of the levels. If we consider a nucleus with N neutrons, then, for the neutrons,

$$E = \sum_m e_m. \quad (12-36)$$

In this model, there is a similar expression for E for the protons. Equation 12-36 takes into account the quantum nature of the levels and their uneven fluctuations due to shell effects. In order to obtain the smooth part \bar{E} from E , we should either average it over a large number of nuclides, or smooth the quantum fluctuations of the level density $g(e)$ in a single nucleus. Strutinsky [47] chooses the latter procedure and gives a well-defined method for smoothing $g(e)$, from which \bar{E} can be obtained. To do this, it is necessary to smooth the individual delta functions occurring in Eq. 12-35 in such a manner that these overlap sufficiently with each other to yield a smooth $\tilde{g}(e)$. A simple way to do this is to replace $\delta(e - e_i)$ by a Gaussian centered about e_i , with appropriate normalization to preserve the strength of the level and a width γ which is at least of the same order as the shell spacings ($\sim \hbar\omega$ in the case of the harmonic oscillator). In other words, we could replace

$$\delta(e - e_i) \rightarrow \frac{1}{\gamma\sqrt{\pi}} \exp[-(e - e_i)^2/\gamma^2] \quad (12-37)$$

to obtain a smooth $\tilde{g}(e)$.

Even though this replacement preserves the normalization of each level (when the e -space extends from $-\infty$ to ∞), it does not reproduce the higher moments of the delta function. We can preserve all the moments of the delta function from 0 to $2S + 1$ by making the following replacement:

$$\delta(e - e_i) \rightarrow \frac{1}{\gamma\sqrt{\pi}} \exp(-u_i^2) L_{S+1/2}(u_i^2) \quad (12-38)$$

with $u_i = (e - e_i)/\gamma$. The function $L_n^{1/2}(x)$ is a polynomial of order n in x ,

$$L_n^{1/2}(x) = \sum_{m=0}^n \frac{1}{(n-m)!m!} \frac{\Gamma(n+\frac{3}{2})}{\Gamma(m+\frac{3}{2})} (-x)^m, \quad (12-39)$$

where $\Gamma(n)$ is the gamma function.

According to the Strutinsky prescription, then,

$$\tilde{g}(e) = \frac{1}{\gamma\sqrt{\pi}} \sum_i \exp(-u_i^2) L_{S+1/2}(u_i^2), \quad (12-40)$$

where u_i has been defined in Eq. 12-38. The function $L_{S+1/2}$ which modulates the Gaussian is often called the curvature function of the $(2S)$ th order. Note that, since each level is in principle being spread also into the negative ranges of e (even when the bottom of the well is at $e = 0$), $\tilde{\lambda}$ and \bar{E} are defined by

$$N = \int_{-\infty}^{\tilde{\lambda}} \tilde{g}(e) de, \quad \bar{E} = \int_{-\infty}^{\tilde{\lambda}} \tilde{g}(e)e de. \quad (12-41)$$

If the Strutinsky smoothing procedure is applied to an already smooth density distribution $\eta(e)$ [as can be done by replacing the sum \sum_i in Eq. 12-40 by an integral $\int \eta(e) de$], self-consistency demands that the same $\eta(e)$ be reproduced. This condition is satisfied with a $(2S)$ th-order curvature function if $\eta(e)$ is expressible in a polynomial of order $2S + 1$ or less. In order that the shell correction δE_{th} be unique for a given nuclear spectrum, one could require that the result be independent of γ over a wide range and not alter with increasing order, but less restrictive conditions have been given [62].

To illustrate the last two points about the uniqueness of δE for a discrete spectrum, we have calculated it for the 126 neutrons of ^{208}Pb . The single-particle spectrum of a modified oscillator type was taken following Krappe and Wille [48], and is given for completeness:

$$e_{-l+1/2} = (2n + l + \frac{3}{2}) - \kappa(N)l - \kappa(N)\mu_0[l(l+1) - \frac{1}{2}N(N+3)],$$

$$\epsilon_{i-l-1/2} = (2n + l + \frac{3}{2}) + \kappa(N)(l + 1) - \kappa(N)\mu_0[l(l + 1) - \frac{1}{2}N(N + 3)]. \quad (12-42)$$

Here the energy is expressed in units of $\hbar\omega$; n, l are the usual oscillator quantum numbers, with $N = 2n + l$. For a reasonable empirical fit of the neutron levels, the following values for the parameters occurring in Eq. 12-42 are chosen:

$$\mu_0 = 0.308, \quad \kappa(N) = 0.21[\frac{1}{2}(N + 1)(N + 2)]^{-1/3}. \quad (12-43)$$

Taking $\hbar\omega = 41/A^{1/3} \approx 6.92$ MeV, we show the results for $\delta E = (E - \tilde{E})$, using second- to tenth-order Strutinsky calculations, in Fig. 12-23 as a function of the smearing parameter γ . As $\gamma \rightarrow 0$, each Gaussian goes over to the delta-function limit, and $\tilde{E} \rightarrow E$. The second-order calculation does not yield a unique δE , because $\tilde{g}(e)$ is more complicated than a third-order polynomial. Note that calculations in all higher orders give the same result. As the order (2S) of the curvature function is increased, the value of γ for which δE becomes independent of γ also increases slightly. As $S \rightarrow \infty$, the Gaussian modulated by the curvature function again reproduces the delta function exactly for any finite γ , and $\delta E \rightarrow 0$. For any finite order, however, a unique δE can be found for a discrete spectrum provided that γ is chosen to be sufficiently large. We should mention that care must be taken to include the contribution to \tilde{E} coming from the negative regions of e in the

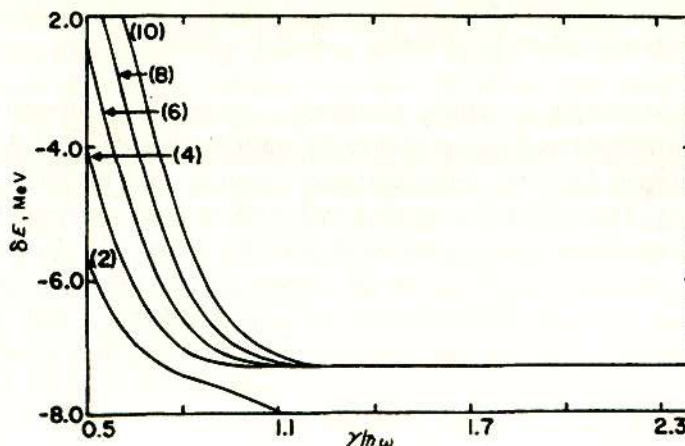


Fig. 12-23 Shell correction (in MeV) for the neutrons in ^{208}Pb as a function of γ for the discrete spectrum defined by Eq. 12-42. The smearing parameter γ is expressed in units of $\hbar\omega$ ($1 \hbar\omega = 6.92$ MeV), and the shell correction is shown for various curvature functions.

integrals of Eq. 12-41, where $\tilde{g}(e)$ is oscillatory in form. Furthermore, for a given γ , all states i in Eq. 12-40 must be included that may contribute finitely to $\tilde{g}(e)$ for $e < \lambda$. For $\gamma \approx 2.5 \hbar\omega$, this implies the inclusion of states as high as $N = 20$. In practice, $\gamma \approx 1.2 \hbar\omega$ yields the right shell correction.

The Strutinsky method of renormalizing the semiempirical mass formula has been used by Nilsson et al. [44] in an investigation of the stability of superheavy nuclei and also for the determination of the shapes of fission barriers. We saw in Section 9-9 that the same method has been used successfully to calculate the deformation of rare-earth nuclei. The form of the single-particle Hamiltonian chosen by Nilsson et al. for the calculation of shell corrections in actinide and superheavy nuclei is given by Eq. 9-171. The sum of the occupied single-particle energies, E , is replaced in the presence of pairing by the expression

$$E = \sum_v e_v V_v^2 - \frac{A^2}{G} - G(\sum_v V_v^4 - \sum' 1), \quad (12-44)$$

where e_v are the single-particle energies, and the other symbols were defined in Eq. 8-113. The sums are taken separately over neutrons and protons with pairing matrix elements G_n and G_p , respectively. The last term, with the summation \sum' over occupied energy levels, represents the subtraction of the diagonal pairing energy, so that only the correlation energy due to pairing remains. The theoretical estimate of the shell correction to binding energy, which we denote by $\delta B_{th}(A, Z)$, and by which the liquid-drop mass formula should be renormalized, is given by

$$\delta B_{th} = -\delta E_{th} = -(E - \tilde{E} - \langle E_{pair} \rangle), \quad (12-45)$$

where E is defined by Eq. 12-44, and \tilde{E} by Eq. 12-41, and $\langle E_{pair} \rangle$ is the average pairing energy, taken simply as -2.3 MeV for nuclei in this region.

An estimate of the binding energy of a nucleus (A, Z) as a function of the deformation parameters ϵ and ϵ_4 can now be made by adding this theoretical estimate of shell correction δB_{th} to the distorted liquid-drop part of the mass formula, $B_{dist}^{LD}(A, Z)$:

$$B_{th}(A, Z) = B_{dist}^{LD}(A, Z) + \delta B_{th}(A, Z). \quad (12-46)$$

Nilsson et al. [44] have compared the results of their calculation with experimental values for the rare-earth and actinide regions and extrapolated these estimates into the superheavy region. When Eq. 6-1 is used, the comparison can as well be made in terms of mass M rather than of the binding B of a nucleus. It is convenient, for this purpose, to make the

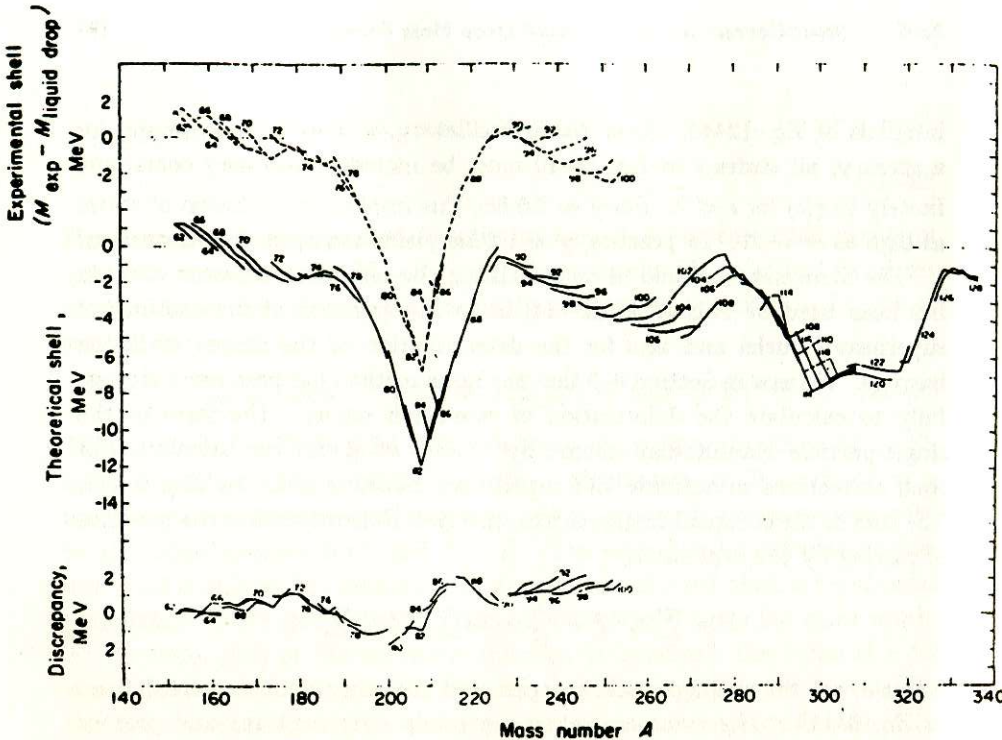


Fig. 12-24 Experimental and theoretical mass values (including shell correction) for $150 < A < 130$ plotted relative to the spherical liquid-drop mass. (After Nilsson et al. [44].)

comparisons with respect to the spherical liquid-drop mass, M_{LD} , defined in terms of $B_{\text{sph}}(A, Z)$ of Eq. 6-21. In Fig. 12-24 we plot the experimental and theoretical mass values, $(M_{\text{exp}} - M_{LD})$ and $(M_{\text{th}} - M_{LD})$, versus A , following Nilsson et al., and show the discrepancy in the known region in the lower scale. This discrepancy is within ± 2 MeV throughout the range shown, displaying excellent agreement with experiment. It should be noted that in deriving M_{th} the Myers-Swiatecki mass formula has been used, whose parameters (given in Eq. 6-24) were determined assuming a special form for δB_{th} . In principle, these parameters should be redetermined using δB_{th} estimated by the Strutinsky procedure.

It will be seen from Fig. 12-24 that the estimated masses for superheavy nuclei beyond the present experimental range show a broad shell structure at $Z = 114$ and $N = 184-196$. Although this is not as pronounced as the ^{208}Pb shell, it is the main reason for the hope that there may exist in this region an island of relative stability, which may be experimentally detectable.

We have seen that the Strutinsky method of calculating δB_{th} is unambiguous when applied to a single-particle spectrum with all discrete levels, as in a Nilsson-type potential. As pointed out by Lin [49], the method runs into difficulties, however, when applied to a finite potential well (e.g., the Woods-Saxon well) which has a single-particle spectrum of a finite number of discrete levels, followed by a continuum. If the continuum is completely ignored, and the Strutinsky prescription is applied to the bound levels only, δB_{th} turns out to depend both on the order and on γ . The results of such a calculation for the neutrons, using a Woods-Saxon potential well which fits the experimentally known top few single-particle levels of ^{208}Pb reasonably well, are shown in Fig. 12-25.

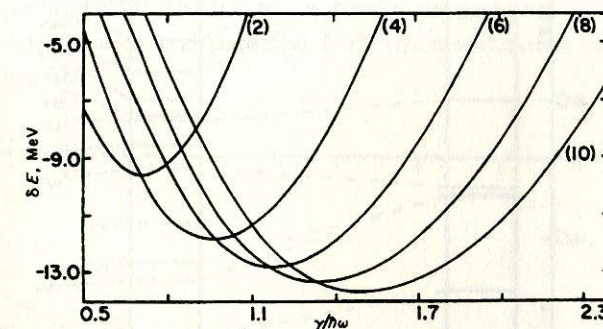


Fig. 12-25 Shell correction (in MeV) for the neutrons in ^{208}Pb as a function of γ for a Woods-Saxon spectrum, ignoring continuum effects. The smearing parameter γ is expressed in units of $\hbar\omega$ ($1 \hbar\omega = 6.92$ MeV), and the shell correction is shown for various curvature functions. (After Ross and Bhaduri [50].) The parameters of the Woods-Saxon potential are given by J. Blomquist and S. Wahlborn, *Ark. Fysik* **16**, 545 (1960).

The reason for this ambiguity is not hard to understand. The Strutinsky method is tailor-made for a spectrum with an infinite number of discrete levels. In the process of smoothing such a spectrum, individual level strengths are distributed in the entire e -space from $-\infty$ to $+\infty$. As the Gaussian level width γ is increased, the low-lying levels lose more and more of their strength. This loss, however, is compensated for by the higher-lying discrete levels, more and more of which begin to contribute to the low-lying energies as γ increases. Thus the single-particle smoothed level density $\tilde{g}(e)$ remains γ -independent, provided that γ is of the order of the shell spacing or

greater. When, however, only a finite number of discrete levels are being smoothed, this situation no longer exists, and the result becomes γ -dependent. To overcome this difficulty in applying the Strutinsky method to the spectrum of a finite well, one should consider not only the discrete bound states but also the modifications in the continuum-level density brought about by the potential.

This point is worth appreciating because it also clarifies the meaning of "resonances" in the continuum. For this purpose, we show in Fig. 12-26 the single-particle levels that are occupied by the neutrons in the topmost

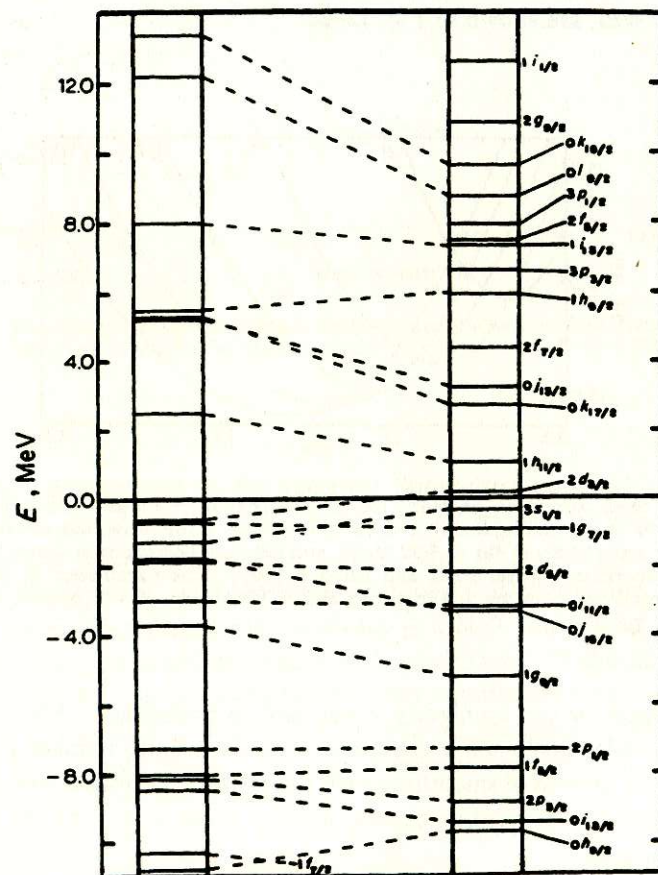


Fig. 12-26 Comparison of the single-particle spectra for the neutrons in ^{208}Pb , obtained using a Woods-Saxon potential (left) and an oscillator-type potential (right). The "levels" lying above zero energy in the Woods-Saxon spectrum correspond to peaks in the function $\Delta g(e)$ of Eq. 12-47 and are associated with continuum resonances. (The widths of these are not indicated.) (After Ross and Bhaduri [50].)

shell and the empty levels beyond $N = 126$, as generated by the Woods-Saxon potential and an appropriate spherical Nilsson potential. Although there are some differences in the level orderings in the two potentials, the few unoccupied bound levels in the Woods-Saxon potential are the same as those generated by the Nilsson potential. Comparing the two spectra in Fig. 12-26, we infer that the Woods-Saxon potential is only slightly too weak to bind the $1h_{11/2}$, $0k_{17/2}$, $0j_{13/2}$ levels. In the Strutinsky calculation with the Nilsson potential, these bound states do play a vital role, as is made evident by the fact that, if the spectrum is cut off at $2d_{3/2}$ (the last bound state of the Woods-Saxon), the results become quite γ -dependent. The bound states that are thus missed in the Woods-Saxon potential nevertheless appear as "bumps" in the continuum-level density (instead of delta functions) and are termed resonances. In the absence of any potential, the single-particle level density $g(e)$ is simply proportional to \sqrt{e} for $e > 0$. In the presence of a central potential $U(r)$, the modification to this density, $\Delta g(e)$, is given by

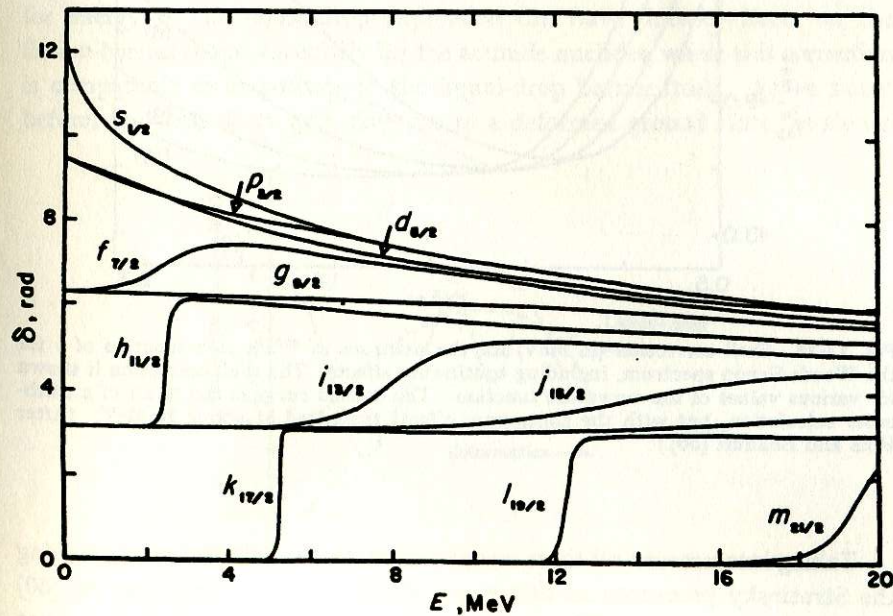


Fig. 12-27 Plot of some of the phase shifts generated by the Woods-Saxon potential for various l ($= j - \frac{1}{2}$) values against energy e . Note the steep rise in some of these through $\pi/2$ at certain energies corresponding to resonances. (After Ross and Bhaduri [50].)

$$\Delta g(e) = \frac{1}{\pi} \sum_l (2l+1) \frac{d}{de} \delta_l(e), \quad (12-47)$$

where $\delta_l(e)$ is the phase shift of the l th partial wave at energy e due to the potential $U(r)$ (see Problem 5-7). In the presence of a spin-orbit potential, the effective potential

$$U_{\text{eff}}(r) = U(r) + \frac{\hbar^2}{2M} \frac{l(l+1)}{r^2} \quad (12-48)$$

is different for the two possible values of $l = j \pm \frac{1}{2}$ for a given j , and the phases have to be calculated separately in these two channels. In Fig. 12-27, we plot some of the phases for $l = j - \frac{1}{2}$ as a function of e . At a resonance, $\delta(e)$ rises sharply, contributing a bump in the level density given by Eq. 12-47. We find that a level like $1h_{11/2}$, which was missed as a bound state, appears as a resonance at $e \approx 2.5$ MeV.

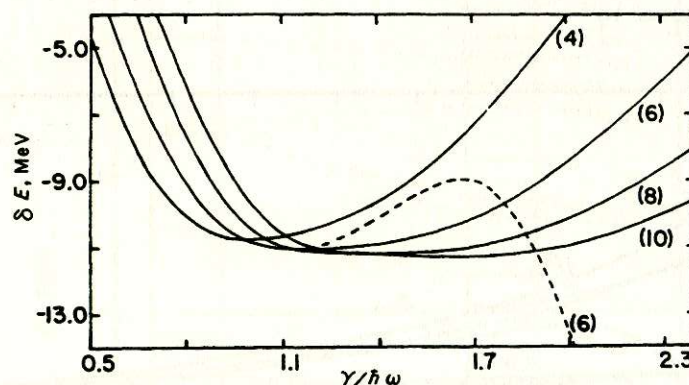


Fig. 12-28 Shell correction (in MeV) for the neutrons in ^{208}Pb as a function of γ for the Woods-Saxon spectrum, including continuum effects. The shell correction is shown for various values of the curvature function. The dashed curve is the result of a sixth-order calculation, but with the continuum effects truncated at about 20 MeV. (After Ross and Bhaduri [50].)

Taking into account all these resonances up to $e \approx 100$ MeV and applying the Strutinsky procedure as before, we obtain the shell correction δE [50] for the 126 neutrons in ^{208}Pb as shown in Fig. 12-28. It will be seen that fourth- to tenth-order calculations all yield a result of about -11 MeV, in contrast to the ambiguous results of Fig. 12-25, where only the bound levels of the finite well were smoothed. This calculation, although rather cum-

bersome for practical application (especially with deformed potentials), demonstrates the necessity to take into account the modifications in the continuum due to the finite potential.

Bolsterli et al. [51] have applied the Strutinsky method to finite potential wells. They diagonalize the deformed single-particle Hamiltonian in a large basis of deformed harmonic-oscillator states, and smooth the delta functions at not only the bound but also the artificial unbound eigenstates. With the optimum choice of the matrix size, this procedure ensures the overall smooth behavior of the density of states above the Fermi level. The method is practical and is widely used.

12-5 THE TRIUMPH OF THE DOUBLE HUMP

In this section we shall study how the shape of the fission barrier is affected by shell correction and the effect of this on various aspects of fission phenomena [46]. We noted before that the simple liquid-drop model energetically prefers a spherical ground state and gives rise to a one-humped barrier, as shown by the dotted curve in Fig. 12-29. Addition of the shell correction for energy to the liquid-drop expression can have drastic effects on the fission-barrier shape, especially for the actinide nuclides, where this correction is comparable in magnitude to the liquid-drop barrier itself. As we noted before, the shell effect may give rise to a deformed ground state, as shown

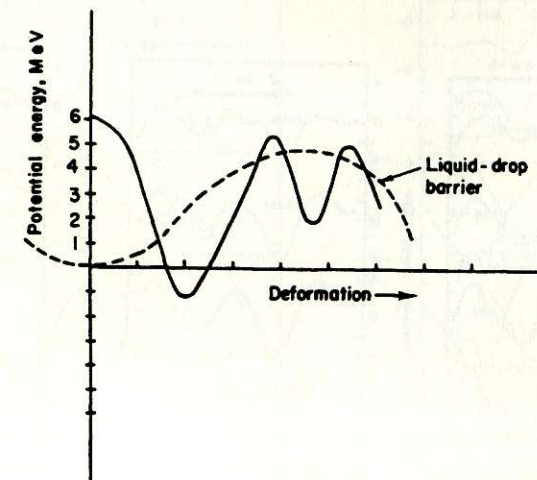


Fig. 12-29 A schematic diagram of the fission barrier after the inclusion of shell effects, for nuclides with neutron number $N \sim 142-148$. For a discussion of the relative heights of the barrier, see text. The liquid-drop barrier is shown by the dotted line.

in Fig. 12-29. One important characteristic of the shell correction is its modulation of the deformation energy as a function of deformation, due to the alternate compression and thinning out of single-particle levels near the Fermi surface with increasing deformation (Fig. 12-22). This may result in a second potential minimum at a much larger value of deformation, as shown in Fig. 12-29. For the modulation to be effective in giving rise to a second minimum, it should appear at a deformation close to that of the liquid-drop saddle point, where the liquid-drop profile of the potential energy

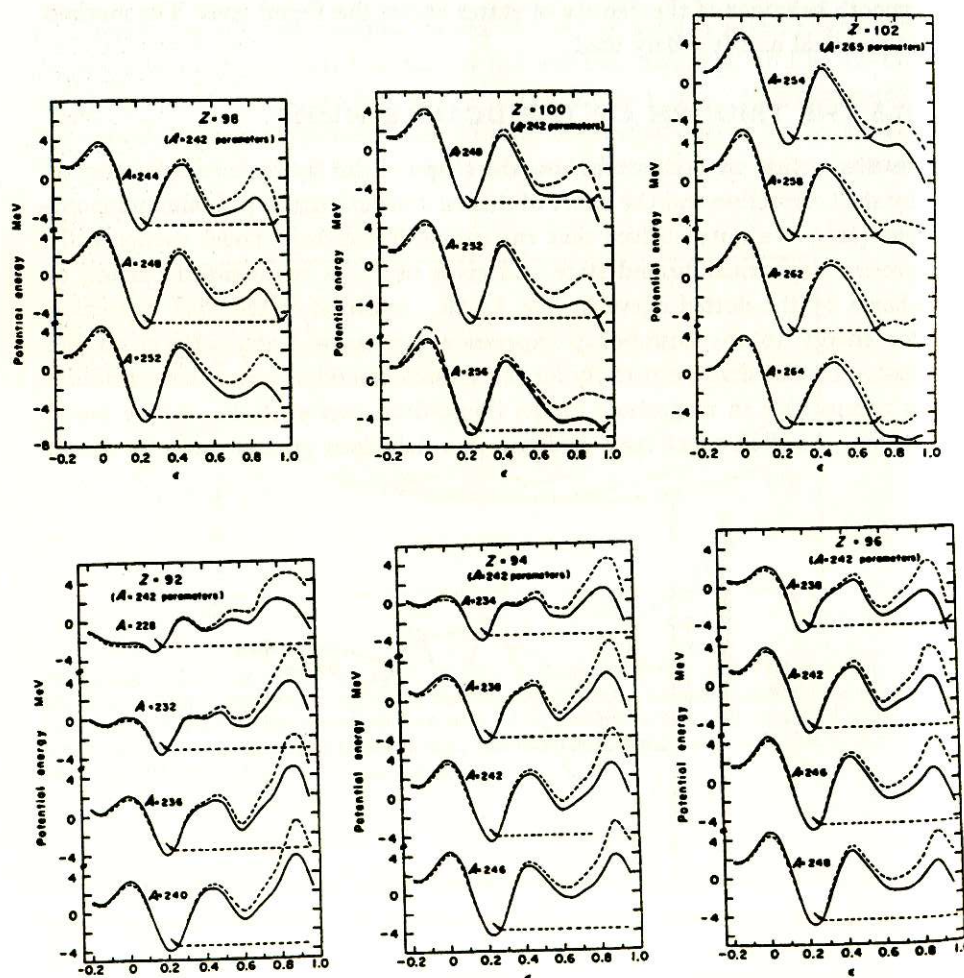


Fig. 12-30 Calculated fission barriers of some even-even nuclides, including shell correction. The calculations were done using a modified Nilsson-type potential. (After Nilsson et al. [44].)

is flat. This happens to be the case for nuclides with neutron numbers in the vicinity of 142–148, where theoretical calculations indeed predict a second minimum [44].

In Fig. 12-30, we show the fission barriers of some even-even nuclides as calculated by Nilsson et al. [44], using the deformed Nilsson-type potential to evaluate the shell correction. These and other calculations reveal a general trend toward a weak and shallow second minimum in Th nuclides and a greater height of the second barrier than of the first. In the U nuclides the second barrier height is still greater, with the second minimum increasing in depth, a trend that continues in Pu and Np, where the second barrier is only slightly higher. For Am and heavier nuclei ($Z \geq 95$) the second minimum is shallower again, and the height of the second barrier is less than the first. The second minimum of the fission barrier almost disappears for the isotopes of ^{100}Fm and is absent in the neighboring heavier nuclides. All the ground states are found to be prolate. We also show, in Fig. 12-31, the stabilizing effect of the shell correction on some nuclides in the superheavy region, this being particularly evident for the spherical ground state of the nuclide with $Z = 114$ and $N = 184$. A number of subsequent calculations performed by other authors [51] with more realistic finite wells have produced

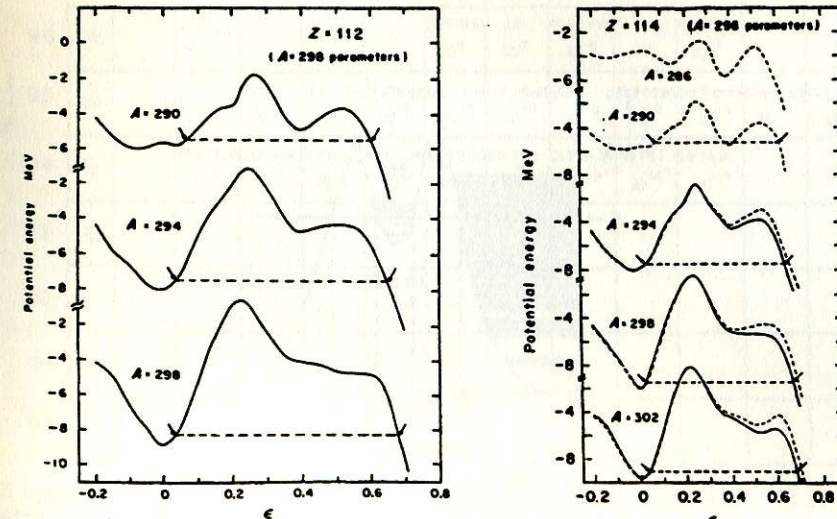


Fig. 12-31 Calculated fission barriers of some superheavy nuclides, including shell correction. (After Nilsson et al. [44].)

similar results. It is difficult to assess the significance of the quantitative differences obtained from these finite-well calculations, because of the uncertainty in shell-correction results mentioned in Section 12-4. It is found that in most cases the second minimum (when it exists) is about 2–3 MeV higher than the first one.

Before trying to correlate the results of experiments with these double humps along the fission path, we shall make a few relevant comments about the possible states in the two wells. As we mentioned before, when some excitation energy is given to a nuclide by the capture of a low-energy neutron, this energy is dissipated into many degrees of freedom by many nucleonic collisions and a compound nucleus is formed. Now, since there are two minima in potential energy, there are two possibilities for the compound-nucleus formation with different deformations. The level spacings between the compound nuclear states are very small, because the energy can be dissipated in very many degrees of freedom, not just in the fission degree of freedom along the fission path. At about 5-MeV excitation, for example, the compound nuclear levels of the first well (class I levels) may have a typical spacing of about 10 eV. The second compound nuclear configuration occurs at a greater deformation, where the energy available for distribution in the different degrees of freedom is about 3 MeV less (the difference between

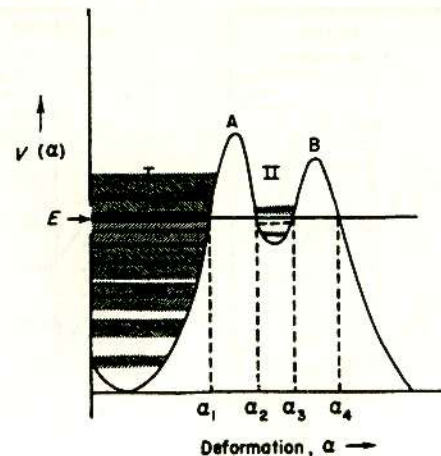


Fig. 12-32 Penetration through a two-humped fission barrier at an excitation energy E . The vibrational states of the two potential wells I and II are indicated by horizontal dashed lines. The widths of these levels are shown schematically by hatched lines. The class I states at this excitation energy form a continuum, while the class II states may be regarded as distinct.

the second and first minima). Consequently, the compound nuclear levels of the second well (class II levels) have a much greater spacing at the same excitation, of the order of a few hundred eV. At higher excitations, the class I and class II compound nuclear states can mix thoroughly. In addition to these compound nuclear levels, which arise basically because of the abundance of the nonfission degrees of freedom, there are certainly some vibrational levels in the two potential wells that correspond to vibrations in the fission degree of freedom. The vibrational states are really the respective bound states of the two potential wells shown in Fig. 12-32. The lowest vibrational states, especially in the second well, may be of narrow width, but the higher ones are very broad because of damping into the compound nuclear states. In analyzing the experimental results, which we now examine, we shall draw upon the above physical ideas.

As will be seen from Fig. 12-2, the spontaneous fission lifetimes display some systematic trends when plotted against Z^2/A . It was therefore a considerable surprise to discover an odd-odd isotope of americium ($A = 242$)

98	Cf											
97	Bk				(6.0±1.0)			(8.2±0.8)	2.0			
96	Cm					(1.55±0.8)	1.8	(4.2±0.6)		(1.92±0.8)		
95	Am			5±7 10^{-9}	6.6±7 10^{-5}	(1.6±0.4) 10^{-7}	(9.0±1.0) 10^{-4}	(1.5±0.6) 10^{-6}	(1.4±1.0) 10^{-2}	(8.0±1.0) 10^{-4}	(1.1±0.2) 10^{-3}	(6.4±0.8) 10^{-7}
94	Pu		(3.0±0.9) 10^{-8}	(3.4±0.8) 10^{-8}	(1.0±0.3) 10^{-7}	(6.5±1.5) 10^{-9}	(8.1±0.8) 10^{-8}	(9±4) 10^{-9}	(2.7±0.3) 10^{-8}	(5±3) 10^{-8}	(8±1.8) 10^{-8}	
93	Np											
92	U					(1.10±50)		(2.0±0.7)				
91	Pa											
90	Th											
		140	141	142	143	144	145	146	147	148	149	150

Fig. 12-33 A chart of the shape isomers. Half-life entries in seconds indicate nuclides for which these isomers have been observed.

decaying by a spontaneous fission lifetime of the order of milliseconds [52], shorter by a factor of 10^{20} than the lifetimes of more stable species. This fission isomer and some others were discovered before the existence of two-humped barriers had been realized. Subsequently, over 25 such short-lived isomers have been discovered, some with lifetimes of 10^{-8} s or less [53]. Figure 12-33 shows a table of these isomers.

In the conventional liquid-drop picture, such tremendous shortening of fission lifetimes requires the isomeric states in question to be excited by several MeV above the ground state. It is then difficult to explain the long lifetime of such a state against γ -decay, which is certainly not much stronger than spontaneous fission. The stability against γ -decay of these states would require them to have very high spins, which were experimentally not found to be present [54]. The mystery is easily solved by taking into account the modified two-humped fission-barrier shape, which is expected to prevail in the region of neutron numbers 142–148, just where the fission isomers are found. Such a two-humped fission barrier is shown in Fig. 12-32, where the lowest state in the second potential well is typically about 3 MeV above the normal ground state of the first well. We refer to the states of the first and second wells as class I and class II states, respectively. Obviously there will be some mixing between class I and class II states, particularly at higher excitations. Consider now the deformation of a nuclide to be such that it is in one of the *lowest vibrational* states of class II. It is easy for the nuclide to undergo spontaneous fission by tunneling to the right—much easier than if it were in a class I state at the same excitation. This accounts for the very short lifetimes of the fission isomers. Alternatively, the nucleus in the low vibrational class II state may de-excite by γ -decay, but then it has to decay to a lower state of class I. This implies tunneling to the left, thereby inhibiting γ -decay. The isomerism in this case is arising not because of high spins, but as a result of the peculiar shape of the potential barrier, and is therefore referred to as shape isomerism [55]. Since an excited class I state cannot easily decay by fission, it should have a small fission width but a large probability of neutron emission, whereas just the opposite is true for class II states.

We next consider the resonance-like structures observed in the induced-fission cross sections below the barrier energy, as discussed earlier in Section 12-1. In these experiments, the target nuclides have even numbers of neutrons (like $^{230}_{90}\text{Th}_{140}$ and $^{240}_{94}\text{Pu}_{146}$), so that the capture of a low-energy neutron results in a compound nuclear excitation energy which is below the fission-barrier height. Resonance structures are observed in two distinct

energy ranges. The grouping of the fission resonances is observed in a high-resolution experiment with neutrons having energies of a few hundred eV or a few keV energy incident on a ^{240}Pu target (see Fig. 12-5). This is an example of intermediate structure in fission cross section, with a fine spacing of about 15 eV within a group and an intermediate spacing of about 0.7 keV between them. On the other hand, the so-called vibrational resonances are observed with incident neutrons of a few hundred keV range, being captured by ^{230}Th and leading to subbarrier fission (see Fig. 12-7). Here the experimental resolution is a few tens of keV. We outline below, in a qualitative manner, how both these types of resonances can arise naturally in a double-humped barrier. The detailed quantitative theory is given in Lynn's article [56].

We first consider the phenomenon of vibrational resonances in subbarrier fission cross sections (Figs. 12-7 and 12-8). As we noted before, it is not possible to explain this in the liquid-drop picture, where the fission cross section should increase steeply with increasing excitation in the subbarrier region. We cannot postulate that this decrease in the fission cross section is due to the opening of channels leading to neutron emission, since in the (d, p) reactions the excitation energy imparted is less than the neutron binding energy. Consider Fig. 12-32, where the (compound) nucleus has been given an excitation energy E which is close in magnitude to one of the lowest vibrational class II states. Consider also the special situation in which the lowest one or two vibrational states have widths less than the spacing between the compound nuclear class II states at this excitation—a situation likely to occur if the second well is rather shallow with small zero-point energy (as in Th nuclei). At such excitations, the width of class I vibrational states is very large because of damping into the nearly continuous class I compound nuclear states, so that we can assume a continuous spectrum. The low-lying class II vibrational states at these excitations, on the other hand, can be considered to be discrete, and their decay to class I states is hindered by the potential barrier. The situation is thus analogous to the quantum-mechanical problem of penetration of a free particle (continuous spectrum) through a double-humped barrier. We briefly outline the treatment of Ignatyuk et al. [57] to demonstrate that under such conditions there will be resonances in the penetration function when the excitation energy E coincides with one of the well-defined bound states of the second well. These, in turn, will show up in the fission cross section.

Referring to Fig. 12-32, let P_A and P_B be the quasi-classical penetration probabilities of the separate barriers A and B at energy E . Then, by the WKB approximation (see Appendix D),

$$P_A = \exp \left[-2 \int_{\alpha_1}^{\alpha_2} |\kappa(\alpha)| d\alpha \right],$$

$$P_B = \exp \left[-2 \int_{\alpha_2}^{\alpha_3} |\kappa(\alpha)| d\alpha \right], \quad (12-49)$$

with $\kappa = \hbar^{-1}\{2B[E - V(\alpha)]\}^{1/2}$, where the α_i 's are shown in Fig. 12-32, and B is the inertial parameter of the nucleus. The phase associated with the second well is defined by

$$\phi(E) = \int_{\alpha_1}^{\alpha_3} \kappa(\alpha) d\alpha, \quad (12-50)$$

and the bound states of the second well are located at energies E_n , for which

$$\phi(E_n) = (n + \frac{1}{2})\pi. \quad (12-51)$$

Ignatyuk et al. [57] show that the penetration probability through the two barriers is given approximately by

$$P(E) = \frac{1}{4} P_A P_B \left(\frac{(P_A + P_B)^2}{16} \sin^2 \phi + \cos^2 \phi \right)^{-1}. \quad (12-52)$$

When E coincides with one of the bound states E_n of the second well, Eq. 12-51 is satisfied, and $\cos \phi = 0$. In this case, the penetrability is maximum:

$$P_{\max} = \frac{4P_A P_B}{(P_A + P_B)^2}. \quad (12-53)$$

This value is unity for a symmetrical two-humped barrier, where $P_A = P_B = \frac{1}{2}$. The minimum penetrability is given by the condition that $\sin \phi = 0$; then

$$P_{\min} = \frac{1}{4} P_A P_B, \quad (12-54)$$

which is just $\frac{1}{16}$ for the symmetric case. In any case,

$$\frac{P_{\max}}{P_{\min}} = \frac{16}{(P_A + P_B)^2} \gg 1, \quad (12-55)$$

thus showing a structure in the subbarrier penetration function for each bound state of the second well. Such a resonance, for example, is seen at a neutron excitation of 715 keV in the fission cross section of ^{230}Th and in the (d, p) reactions, as discussed earlier (see Figs. 12-7 and 12-8).

We next discuss briefly the intermediate structure in the subbarrier fission cross-section resonances as shown, for example, in Fig. 12-5. Let us

envise a situation in which the excitation is low enough for both the compound nuclear class I and class II states to be considered as discrete, but the vibrational states (in both the wells) to have widths greater than the spacing between the compound nuclear levels. For a given excitation, as mentioned before, the class I compound nuclear levels will be much more closely packed than the levels of the same nature in the second well. It is natural to expect a fine-grained resonance structure in the fission cross section due to the class I compound nuclear levels. Two distinct physical processes are taking place. First, the neutron is captured to form a compound nucleus, and then the compound nucleus undergoes fission. If the incident neutron excitation energy coincides with one of the class I compound nuclear levels, there is an enhancement in the cross section. Since these level spacings are of the order of 10–15 eV only, a group of them can have energy in the neighborhood of a class II compound nuclear level, whose width is typically a few tens of eV, with a level spacing of a few hundred eV. When this is the case, there is a strong coupling between class I and class II compound nuclear levels through the intermediate barrier. This will result in groups of finely grained resonances being strongly enhanced, as shown in Fig. 12-5, with a spacing between these groups corresponding to the level spacing between the class II compound nuclear states.

We now proceed to discuss, again in a qualitative manner, the effect of the double hump of the fission barrier on the angular distribution of the fission fragments. To do this, we shall first formulate the role of the "transition state" at the saddle point in the fission process, concentrating for simplicity on a single-humped barrier. We shall then point out what modifications may be expected in this picture because of the presence of a double barrier, and correlate these with the experimental observations.

Consider the situation in which the excitation energy imparted to the fissioning nucleus (by incident photons or neutron capture) is low enough to be near the threshold. In order to fission, the nucleus has to pass through the saddle point, where most of the excitation energy has been expended in deformation and the nucleus spends a relatively long time in a state of unstable equilibrium. These (decaying) states at the saddle point, called transition states, form a spectrum of excited states analogous to that near the ground state (Fig. 12-4). It is assumed that the nucleus has an axis of symmetry in its ground state and one in the transition state, although the orientation of these axes need not be the same, in general. Although the total angular momentum J and its projection M along a space-fixed axis must be conserved throughout the fission process, the projection K along

the symmetry axis may be different in the ground and transition states, depending on the orientation of the symmetry axis. Since the passage from the saddle to scission point is very fast, the assumption is that it is the direction of the symmetry axis at the transition state along which the fission fragments separate. Since J is fixed, this direction is determined by the quantum number K of the transition state through which the nucleus passes. The different transition states at the saddle point with well-defined values of energy, J and K are called the fission channels; at low excitation energies only a few of these are available.

These ideas are quite successful in the explanation of the observed angular distribution in a number of cases. For example, in the photofission of even-even nuclei like ^{232}Th and ^{238}U near threshold, there is a pronounced anisotropy of the fission fragments perpendicular to the direction of the photon beam [58]. In this case, all the nucleonic spins are paired off and $K = 0$ for both the ground and the lowest transition states. At low energies, it is the dipole absorption, which imparts an angular momentum of $1\hbar$ to the nucleus with negative parity, that is important. The fission channels at the saddle point must therefore have $J = 1^-$. The low-lying spectrum of the transition states corresponds (as for an even-even nucleus) to the $K = 0$ rotational band, with possibly only one 1^- low-lying octupole vibrational state (see Chapter 9). Thus the low-energy photofission has to go through this $K = 0$, $J = 1^-$ transition state, where the symmetry axis is perpendicular to the direction of angular momentum J . Since a photon beam carries angular momentum only along and against the beam direction, the symmetry axis of the transition state in this fission channel is perpendicular to the beam direction. From our previous considerations, it then follows that the fragments will fly perpendicularly to the beam direction. As the excitation energy is increased, many more 1^- fission channels will become available with other values of K , and the anisotropy should be less drastic, in accordance with observations.

Similar reasoning would lead us to expect pronounced anisotropy in the angular distribution of fragments in neutron-induced fission near the threshold. For the excitation energy imparted through neutron capture to be near threshold, it is necessary, as discussed before, for the target nucleus to have an even number of neutrons, so that the binding energy of the odd neutron added to form the fissioning compound nucleus is small. Anisotropies have been experimentally observed in many such cases, some of which are shown in Fig. 12-34. If $W(\theta)$ denotes the angular distribution of a fission fragment at an angle θ from the incident beam direction, a measure of the anisotropy

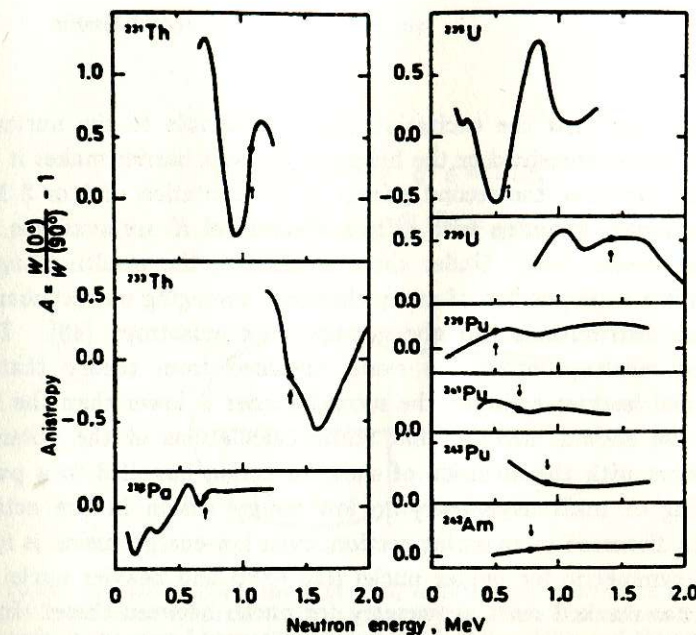


Fig. 12-34 Anisotropies in the angular distribution of a fission fragment in neutron-induced fission in the MeV region. The neutron energy corresponding to the fission barrier is shown by an arrow and a dot on each curve. Note that the structure in the anisotropy disappears in the heavier specimens. (After Bjornholm and Strutinsky [46].)

is $A = [W(0)/W(\pi/2)] - 1$. The approximate location of the fission barrier is shown by an arrow in these plots.

It will be seen from Fig. 12-34 that in the lighter actinides (up to ^{235}U) pronounced anisotropy appears in the angular distribution. Large (negative) dips in A near the threshold in these nuclides imply more fragments flying off in a direction perpendicular to the beam, as expected. However, the anisotropy is very weak or nearly absent in the heavier actinides, particularly in ^{243}Pu and ^{242}Am . This peculiarity cannot be explained by a one-humped barrier, but all these observations find a natural explanation on the basis of double fission barriers when we remember the relative variation of heights of the two barriers with increasing mass number. When two barriers are present, the threshold should be determined by the higher one. In the Th, Pa, and U nuclides, where the second barrier was estimated to be higher, the quantum numbers K of the few available transition states associated with this barrier should determine the angular distribution, resulting in anisotropy. However, in the nuclides ^{241}Pu , ^{243}Pu , and ^{242}Am , the first barrier is 1 or 2 MeV higher than the second, and therefore determines the threshold. The second well in these nuclides is still deep enough for the nucleus to spend a considerable time there, in the process "forgetting" the quantum numbers K associated with the transition states of the first barrier.

However, the fact that the excitation energy available to the nucleus is nearly equal to the threshold or the height of the first barrier makes it scan the transition states of the second barrier at an excitation of 1 or 2 MeV, where many fission channels with different values of K are available, and not just the lowest ones. Under these conditions, the resulting angular distribution is a superposition of many channels, averaging out peculiarities of individual distributions and giving only weak anisotropy [46]. These experimental results confirm the result obtained from theory that for americium and heavier actinides the second barrier is lower than the first.

Finally, we should mention that static calculations of the potential-energy surfaces with the inclusion of shell correction have led to a partial understanding of mass asymmetry in low-energy fission in the actinide nuclides. As discussed in an earlier section, even low-energy fission is found to be mass symmetric for lighter nuclei like ^{210}Po and heavier nuclei like ^{257}Fm , but has marked mass asymmetry for nuclei between these. In the liquid-drop model, one would expect this to imply the inclusion of P_3 , P_5 , and other odd Legendre polynomials in the angular dependence of the distortion, leading to a saddle-point shape that had no mirror symmetry about an axis perpendicular to the symmetry axis. As was pointed out earlier, however, the liquid-drop barrier was found to be stable against the inclusion of deformations of odd multipoles; this meant that such deformations only increased the barrier height. In the liquid-drop picture, therefore, the nucleus, on its path to fission, would deform in such a manner as to exclude these modes, and its shape at the saddle point would give rise to mass-symmetric fission only. As in the case of photofission of even-even nuclei near the threshold, exceptions would exist where the fission channel goes through the pear-shaped 1- octupole state, resulting in mass asymmetry (see Fig. 9-14). Nevertheless, for the vast majority of observed cases, mass asymmetry remained an outstanding puzzle which defied even qualitative explanation. Following a conjecture of Swiatecki, however, Möller and Nilsson [27] calculated the potential-energy surfaces of ^{210}Po , ^{236}U , ^{242}Pu , and ^{252}Fm , including the shell correction to energy, by using the Strutinsky procedure, and taking into account P_3 - and P_5 -modes of distortion in the modified Nilsson-type well. They found that, whereas in ^{210}Po the barrier remained stable against deformations of P_3 - and P_5 -types, in the other isotopes the height of the second barrier decreased when these deformations were included. This decrease was particularly large for ^{236}U , where there was a reduction in height of more than 2 MeV for the second barrier due to these modes, resulting in the saddle-point shape shown in Fig. 12-35.

Nuclear shape at $\epsilon = 0.85$,
 $\epsilon_3 = -0.16, \epsilon_4 = 0.12, \epsilon_5 = 0.08$

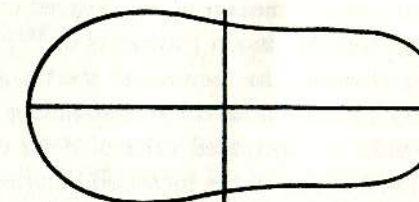


Fig. 12-35 The saddle-point shape of ^{236}U , including, in addition to the even modes, P_3 - and P_5 -modes of distortion in the nuclear shape. These odd modes actually decrease the height of the second barrier by about 2 MeV. (After Möller and Nilsson [27].)

One can expect unequal division of masses from such a shape. This instability of the second barrier against the inclusion of odd multipole distortions was much reduced in ^{252}Fm , where the decrease in height of the barrier peak was less than 0.5 MeV. This trend toward smaller asymmetry in going from uranium to fermium agrees with experimental observation. One would expect, on this basis, no asymmetry for the heavier isotopes of fermium (since the second barrier disappears), and this is found to be the case in the spontaneous fission of ^{257}Fm (see Fig. 12-16).

If a nuclear reaction leads to the formation of a nucleus in an excited state of the secondary minimum, this should result in electromagnetic transitions within the levels of the secondary well preceding isomeric fission. Specifically, in an even-even nucleus, the final decay in such a situation should proceed via $E2$ -transitions within the rotational band built on the isomeric level. The de-excitation of the nucleus via $E2$ -transitions may result either in the emission of γ -rays or in the emission of conversion electrons. The latter process, which is more important for nuclei with high Z and large deformation, is due to the sudden change during a transition in the electromagnetic field experienced by the atomic electrons, resulting in their acceleration and, in particular, the emission of some electrons on acquiring sufficient kinetic energy. The internal conversion process, as it is called, is thus the conversion of nuclear excitation energy to kinetic energy of the

electrons through the direct electromagnetic interaction between the nucleons and electrons. The conversion electrons have been measured preceding the spontaneous fission of the ^{240}Pu isomer, which has a half-life of about 4×10^{-9} s, by Specht et al. [59]. This resulted in the identification of the rotational band in the secondary minimum of ^{240}Pu , up to the 8^+ level. Specht et al. used an α -beam of 25 MeV in the reaction $^{238}\text{U}(\alpha, 2n)^{240}\text{Pu}$, and identified the rotational band by measuring the delayed coincidence between the conversion electrons and the fission fragments of ^{240}Pu . This rotational band may be fitted by choosing the moment of inertia \mathcal{J} so that $\hbar^2/2\mathcal{J} = 3.331$ keV, which is very different from the corresponding value of 7.156 keV for the ground-state band. The increased value of \mathcal{J} for the rotational band in the secondary minimum is due to the increased deformation. This experiment may be regarded as direct evidence for the existence of the secondary well in a fission isomer.

We may summarize this section by noting that diverse facets of fission phenomena find natural explanation in the existence of a fission barrier with a double hump, which comes about because of shell effects. More detailed treatment of the subject is given by Brack et al. [60] and by Swiatecki and Bjørnholm [61].

REFERENCES

1. O. Hahn and F. Strassmann, *Naturwissenschaften* **27**, 11 (1939); **27**, 89 (1939).
2. For a review on ternary fission, see I. Halpern, *Ann. Rev. Nucl. Sci.* **21**, 245 (1971) and N. Feather, in *Proceedings of the Second International Symposium on the Physics and Chemistry of Fission, Vienna, 1969*, International Atomic Energy Agency, Vienna, 1969, p. 83.
3. The time for prompt neutron emission was estimated to be less than 4×10^{-14} s from the instant of fission by J. S. Fraser and J. C. D. Milton, *Phys. Rev.* **93**, 818 (1954); J. E. Gindler and J. R. Huizenga quote a time range of 10^{-15} to 10^{-18} s for prompt neutron emission. See Fig. 1 in their article "Nuclear Fission," in *Nuclear Chemistry*, Vol. 2, edited by L. Yaffe, Academic Press, New York-London, 1968.
4. G. T. Seaborg, *Phys. Rev.* **88**, 1429 (1952).
5. R. A. Schmitt and R. B. Duffield, *Phys. Rev.* **105**, 1277 (1957).
6. J. A. Northrup, R. G. Stokes, and K. Boyer, *Phys. Rev.* **115**, 1277 (1959).
7. These figures are taken from E. K. Hyde, *The Nuclear Properties of the Heavy Elements*, Vol. III, Prentice-Hall, Englewood Cliffs, N.J., 1964. This book gives a detailed account of fission phenomena up to 1963.
8. A. Bohr, *Proceedings of the United Nations Conference on the Peaceful Uses of Atomic Energy, Geneva, 1955*, Vol. 2, United Nations, New York, 1956, p. 151.
9. P. E. Vorotnikov, S. M. Dubrovina, G. A. Otroschenko, and V. A. Shigin, *Sov. J. Nucl. Phys.* **5**, 210 (1967).

10. J. E. Lynn, *The Theory of Neutron Resonance Reactions*, Clarendon Press, Oxford, 1968, Chap. 8, Secs. 11 and 12.
11. J. Pedersen and B. P. Kuzminov, *Phys. Lett.* **29B**, 176 (1969).
12. H. W. Schmitt, J. H. Neiler, and F. J. Walter, *Phys. Rev.* **141**, 1146 (1966).
13. M. J. Bennet and W. E. Stein, *Phys. Rev.* **156**, 1277 (1967).
14. F. Pleasonton, *Phys. Rev.* **174**, 1500 (1968).
15. W. John, E. K. Hulet, R. W. Lougheed, and J. J. Wesolowski, *Phys. Rev. Lett.* **27**, 45 (1971).
16. W. E. Stein, *Phys. Rev.* **108**, 94 (1957).
17. J. C. D. Milton and J. S. Fraser, *Phys. Rev. Lett.* **7**, 67 (1961).
18. J. C. D. Milton and J. S. Fraser, *Can. J. Phys.* **40**, 1626 (1962).
19. S. L. Whetstone, Jr., *Phys. Rev.* **181**, 1232 (1963).
20. C. Signarbieux, M. Ribrag, and H. Nifenecker, *Nucl. Phys.* **A99**, 41 (1967).
21. See, for example, the review lecture by A. C. Pappas, J. Alstad, and E. Hageb, "Mass, Energy, and Charge Distribution in Fission," in *Proceedings of the Second International Symposium on the Physics and Chemistry of Fission, Vienna, 1969* (ref. 2).
22. V. F. Apalit, N. Yu. Gritsyuk, I. E. Kutikov, V. Lebedev, and L. A. Mikaelyan, in *Proceedings of the Symposium on the Physics and Chemistry of Fission, Salzburg, Austria, 1965*, Paper SM-60/92, International Atomic Energy Agency, Vienna, 1965.
23. H. R. Bowman, J. C. D. Milton, S. G. Thompson, and W. J. Swiatecki, *Phys. Rev.* **129**, 2133 (1963).
24. R. W. Fuller, *Phys. Rev.* **126**, 684 (1962).
25. See the article "Nuclear Fission" by J. E. Gindler and J. R. Huizenga (ref. 3), p. 155.
26. P. Fong, *Phys. Rev.* **135**, B1338 (1965).
27. P. Möller and S. G. Nilsson, *Phys. Lett.* **31B**, 283 (1970).
28. V. V. Pashkevich, *Nucl. Phys.* **A169**, 275 (1971).
29. J. P. Unik and J. R. Huizenga, *Phys. Rev.* **184**, B90 (1964).
30. G. Andritsopoulos, *Nucl. Phys.* **A94**, 537 (1967).
31. T. D. Thomas and R. Vandebosch, *Phys. Rev.* **183**, B976 (1964).
32. See the section on ternary fission in *Proceedings of the Second International Symposium on the Physics and Chemistry of Fission, Vienna, 1969* (ref. 2).
33. G. M. Raisbeck and J. D. Thomas, *Phys. Rev.* **172**, 1272 (1968).
34. G. Kugler and W. B. Clarke, *Phys. Rev.* **C5**, 551 (1972).
35. G. Kugler, unpublished thesis on "Ternary Fission Studies of ^{235}U ," McMaster University, Hamilton, 1970.
36. L. Meitner and O. R. Frisch, *Nature* **143**, 239 (1939).
37. N. Bohr and J. A. Wheeler, *Phys. Rev.* **56**, 426 (1939).
38. J. R. Nix and W. J. Swiatecki, *Nucl. Phys.* **71**, 1 (1965).
39. J. R. Nix, *Nucl. Phys.* **130**, 241 (1969).
40. L. Wilets, *Theories of Nuclear Fission*, Clarendon Press, Oxford, 1964, Chap. 2.
41. S. Cohen and W. J. Swiatecki, *Ann. Phys.* **22**, 406 (1963).
42. W. D. Myers and W. J. Swiatecki, *Nucl. Phys.* **81**, 1 (1966).
43. A. Sobiczewski, Z. Szymanski, S. Wycech, S. G. Nilsson, J. R. Nix, Chin Fu Tsang, C. Gustafson, P. Möller, and B. Nilsson, *Nucl. Phys.* **A181**, 67 (1969).
44. S. G. Nilsson, C. F. Tsang, A. Sobiczewski, Z. Szymanski, S. Wycech, C. Gustafson, I. Lamm, P. Möller, and B. Nilsson, *Nucl. Phys.* **A181**, 1 (1969).
45. T. Johansson, S. G. Nilsson, and Z. Szymanski, *Ann. Phys. (France)* **5**, 377 (1970).

46. S. Bjørnholm and V. M. Strutinsky, *Nucl. Phys.* **A136**, 1 (1969).
 47. V. M. Strutinsky, *Nucl. Phys.* **A95**, 420 (1967); **A122**, 1 (1968).
 48. H. J. Krappe and U. Wille, in *Proceedings of the Second International Symposium on the Physics and Chemistry of Fission, Vienna, 1969* (ref. 2), p. 197.
 49. W.-F. Lin, *Phys. Rev.* **C2**, 871 (1970).
 50. C. K. Ross and R. K. Bhaduri, *Nucl. Phys.* **A188**, 566 (1972).
 51. Y. A. Muzychka, V. V. Pashkevich, and V. M. Strutinsky, *Sov. J. Nucl. Phys.* **8**, 417 (1969); V. V. Pashkevich, *Nucl. Phys.* **A169**, 275 (1971); M. Bolsterli, E. O. Fiset, J. R. Nix, and J. L. Norton, *Phys. Rev. Lett.* **27**, 681 (1971); *Phys. Rev.* **C5**, 1050 (1972).
 52. S. M. Polikanov, V. A. Druin, V. A. Karnaukhov, V. L. Mikheev, A. A. Pleve, N. K. Skobelev, V. G. Subbotin, G. M. Ter-Akop'yan, and V. A. Fomichev, *Sov. Phys. JETP* **15**, 1016 (1962).
 53. J. Borggreen, Yu. P. Gangsksy, G. Sletten, and S. Bjørnholm, *Phys. Lett.* **25B**, 402 (1967); N. N. Lark, G. Sletten, J. Pedersen, and S. Bjørnholm, *Nucl. Phys.* **A189**, 481 (1969).
 54. G. N. Flerov, Yu. P. Gangsksy, B. N. Markov, A. A. Pleve, S. M. Polikanov, H. Jungclaussen, *Sov. J. Nucl. Phys.* **6**, 12 (1968).
 55. Two excellent nontechnical articles on this subject are the following: D. D. Clark, *Phys. Today*, December 1971, p. 23, and D. H. Wilkinson, *Comments Nucl. Particle Phys.* **2**, 131 (1968).
 56. J. E. Lynn, in *Proceedings of the Second International Symposium on the Physics and Chemistry of Fission, Vienna, 1969* (ref. 2), p. 249.
 57. E. B. Gai, A. B. Ignatyuk, N. C. Rabotnov, and G. N. Smyrenkin, in *Proceedings of the Second International Symposium on the Physics and Chemistry of Fission, Vienna, 1969* (ref. 2), p. 337.
 58. E. J. Winhold and I. Halpern, *Phys. Rev.* **108**, 990 (1956); A. P. Baerg, R. M. Bartholomew, F. Brown, L. Katz, and S. B. Kowalski, *Can. J. Phys.* **37**, 1418 (1959).
 59. H. J. Specht, J. Weber, E. Konecny, and D. Heunemann, *Phys. Lett.* **41B**, 43 (1972).
 60. M. Brack, J. Damgaard, A. S. Jensen, H. C. Pauli, V. M. Strutinsky, and C. Y. Wong, *Rev. Mod. Phys.* **44**, 320 (1972).
 61. W. J. Swiatecki and S. Bjørnholm, *Phys. Rept.* **4C**, No. 6 (1972).
 62. M. Brack and H. C. Pauli, *Nucl. Phys.* **A207**, 401 (1973).

PROBLEMS

12-1. Prompt neutron spectrum in fission. It is generally assumed that these neutrons are emitted from moving fission fragments after the fragments have attained their maximum velocities (see Section 10-1).

(a) Let a neutron be emitted from the fragment at a center-of-mass angle θ_{CM} , with energy in the *CM*-frame given by E_{CM} . Show that the energy E of the neutron in the laboratory frame is given by

$$E = E_f + E_{CM} + 2(E_f E_{CM})^{1/2} \cos \theta_{CM}, \quad (1)$$

where E_f is the fragment kinetic energy per nucleon, that is, the energy $\frac{1}{2}Mv_f^2$ of a neutron moving with the velocity of the fragment.

(b) Assume that the emission of neutrons in the *CM*-frame is (i) isotropic; (ii) anisotropic but symmetric about $\theta_{CM} = \pi/2$. In both situations, prove

that the average energies obey the relation

$$E = \bar{E}_f + \bar{E}_{CM}. \quad (2)$$

(c) Let the energy distribution of the emitted neutrons in the laboratory frame be $N(E)$, normalized, for convenience, to unity. For given E_f and E_{CM} , and assuming isotropic emission, show that

$$N(E) = \begin{cases} \frac{1}{4}(E_f E_{CM})^{-1/2}, & (\sqrt{E_{CM}} - \sqrt{E_f})^2 < E < (\sqrt{E_{CM}} + \sqrt{E_f})^2, \\ 0, & \text{otherwise.} \end{cases} \quad (3)$$

If the energy distribution of the neutrons in the *CM*-frame is given by $N'(E_{CM})$, it follows that the resulting $N(E)$ for a given E_f is

$$N(E) = \int_{(\sqrt{E}-\sqrt{E_f})^2}^{(\sqrt{E}+\sqrt{E_f})^2} \frac{N'(E_{CM}) dE_{CM}}{4(E_f E_{CM})^{1/2}}. \quad (4)$$

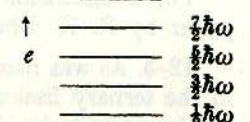
From Eq. 4 show that, for very low energies ($E \rightarrow 0$), $N(E) \propto \sqrt{E}$. If the distribution $N'(E_{CM})$ is taken to be Maxwellian, $N(E)$ can be obtained from Eq. 4. The resulting expression for $N(E)$, which can be written in a closed form, is known as the Watt formula. Empirically, however, the experimental data for thermal neutron capture of ^{233}U , ^{235}U , and ^{239}Pu are as well fitted by a Maxwellian form for $N(E)$:

$$N(E) \propto \sqrt{E} \exp\left(-\frac{E}{\tau}\right),$$

with $\tau \approx 1.3$ MeV. See, for more details, the paper by J. Terrell, *Phys. Rev.* **113**, 527 (1959).

12-2. Smoothed single-particle density of states and shell correction. (a) Consider the idealized single-particle spectrum given by Eq. 12-31, and assume that the lowest A states are each singly occupied by A fermions of one kind (we ignore the spin and i -spin degeneracy for simplicity here.) In the notation of the text, the single-particle density of states is given by

$$g(e) = \sum_{N=0}^{\infty} \delta(e - (N + \frac{1}{2})\hbar\omega).$$



Since, on the average, there is one state in the interval $\hbar\omega$, the smoothed density of states should simply be

$$\tilde{g}(e) = \begin{cases} 1/\hbar\omega, & e \geq 0, \\ 0, & e < 0. \end{cases}$$

Find the quantities λ and \bar{E} , using Eq. 12-41 for this case, and show that $\bar{E} = A^2/2\hbar\omega$; it thus follows from Eq. 12-33 that the shell correction to energy is zero.

(b) The smoothed density $\bar{g}(e)$ of the spectrum in (a) may also be found by the method outlined in Problem 6-6, which you should do before attempting this part. Using the notation of Problem 6-6, show that the single-particle partition function $Z(\beta)$ is given by

$$Z(\beta) = \frac{1}{2} \operatorname{cosech} \frac{\hbar\omega\beta}{2}.$$

Making the expansion in powers of \hbar (i.e., a semiclassical expansion), we obtain

$$Z(\beta) = \frac{1}{\hbar\omega\beta} - \frac{1}{24} \hbar\omega\beta + O(\beta^3) + \dots$$

Taking the Laplace inverse term by term, we get

$$g(e) = \frac{1}{\hbar\omega} - \frac{1}{24} \hbar\omega \delta'(e) + O[\delta'''(e)] + \dots$$

The first two terms in the series contribute smoothly to the energy.

Show that, if we include the δ' -term in the density of states, $\tilde{E} = (A^2/2)\hbar\omega + \frac{1}{24}\hbar\omega$, so that the shell correction $(E - \tilde{E}) = -\frac{1}{24}\hbar\omega$ for this case. An identical shell correction is found numerically when the Strutinsky method is applied to the single-particle spectrum given in (a).

(c) Consider the energy spectrum of an isotropic three-dimensional harmonic oscillator, for which

$$e_N = (N + \frac{3}{2})\hbar\omega, \quad N = 0, 1, 2, \dots,$$

with a degeneracy of $\frac{1}{2}(N + 1)(N + 2)$. We have again ignored the spin and i -spin degeneracy. Using the partition function method of (b), show that in this case the density of states contributing to the smoothed energy is

$$\bar{g}(e) = \frac{e^2}{2(\hbar\omega)^3} - \frac{1}{8} \frac{1}{\hbar\omega} + \frac{17}{1920} \hbar\omega \delta'(e).$$

For a discussion of this method and more solvable examples, see the paper by R. K. Bhaduri and C. K. Ross, *Phys. Rev. Lett.* 27, 606 (1971).

12-3. As was mentioned in Section 12-2, the most frequent third particle in the ternary fission of a spontaneously fissioning nucleus is an α -particle. Kugler and Clarke [34] used the stacked foil assembly shown in Fig. 12-36a of dimensions such that essentially all the emitted α -particles from fissioning ^{235}U were stopped in the foils. The number N_i of α -particles stopped in the i th foil from the source (see Fig. 12-36b) was measured by mass-spectrometric techniques; knowledge of the range-energy relation of the α -particles in lead then made it possible to determine the energy distribution of the emitted α -particles.

(a) Let p_i be the probability that an α -particle of energy E and range $r(E)$, emitted in an arbitrary direction, is stopped in the i th foil (Fig. 12-36b).

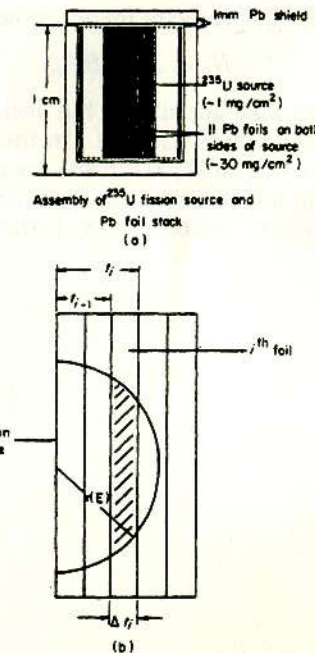


Fig. 12-36 (a) Assembly of ^{235}U fission source and lead foil stack. (b) The schematic geometry of fission source and foil stack. (After G. Kugler [35].)

Let Δt_i be the thickness of the i th foil, and t_i the total foil thickness up to and including the i th foil. Show that

$$\begin{aligned} p_i &= \frac{\Delta t_i}{r(E)}, \quad r(E) \geq t_i, \\ &= \frac{r(E) - t_{i-1}}{r(E)}, \quad t_{i-1} < r(E) < t_i, \\ &= 0, \quad r(E) \leq t_{i-1}. \end{aligned}$$

(b) Let the number of emitted α -particles between energies E and $E + dE$ be $n(E) dE$; then show that the total probability of finding a particle in the i th foil is

$$P_i = \Delta t_i \int_{E(t_i)}^{\infty} \frac{n(E) dE}{r(E)} + \int_{E(t_{i-1})}^{E(t_i)} \frac{r(E) - t_{i-1}}{r(E)} n(E) dE,$$

where $E(t_i)$ is the energy of an α -particle with range t_i .

The total number N_i of α -particles found in the i th foil is therefore

$$N_i = A + BP_i,$$

where A is a constant to take account of the background, and B is another constant depending on the source strength. In their experiment, Kugler and Clarke measured N_i for $i = 1$ to 11, and made use of the known range-energy function $r(E)$. Assuming a Gaussian form for $n(E)$, one could determine the parameters of the Gaussian, together with A and B , by a least-squares fit of the data.

Appendices

The appendices contain some mathematical details which may be of interest to the reader who wishes to understand the theory of nuclear fission better. They also contain some useful tables and figures. The appendices include the derivation of the basic equations of nuclear fission, and a detailed treatment of the theory of nuclear fission, including its applications to the field of nuclear energy.

The appendices also contain some useful tables and figures, including a table of the properties of the elements, and a table of the properties of the isotopes of the elements.

APPENDIX I. NUCLEAR FUSION

The appendices also contain some useful tables and figures, including a table of the properties of the elements, and a table of the properties of the isotopes of the elements.

The appendices also contain some useful tables and figures, including a table of the properties of the elements, and a table of the properties of the isotopes of the elements.

Angular Momentum, Spherical Tensors, and Dirac Matrices

The quantum theories of angular momentum and of the relativistic electron are notoriously plagued by a variety of notations and of different authors' personal choices of arbitrary phases. It therefore seems desirable to collect a number of important formulas in this appendix, to show the notation used in this book, and to provide a convenient single summary. The appendix is not an exposition of these parts of quantum mechanics, although it does contain most of the basic equations.

Throughout this appendix, angular momenta are measured in units of \hbar ; in other words, \hbar is set equal to 1.

A-1 ANGULAR MOMENTUM

(a) *Fundamental matrix elements.* Let any angular momentum \mathbf{J} have components J_x, J_y, J_z along spaced-fixed axes. Let

$$J_{\pm} = J_x \pm iJ_y. \quad (\text{A-1})$$

The fundamental relationships that identify the vector \mathbf{J} as an angular momentum are the commutators:

$$[J_x, J_y] = iJ_z \quad \text{and cyclic permutations,} \quad (\text{A-2})$$

$$[J_z, J_{\pm}] = \pm J_{\pm}, \quad (\text{A-3})$$

$$[J^2, J_z] = 0. \quad (\text{A-4})$$

Using the basic relationship $[x, p_x] = i$, we may prove these results for the

orbital angular momentum $\mathbf{l} = \mathbf{r} \times \mathbf{p}$ of a single particle and for any sum of orbital angular momenta. Equations A-2 are postulated to hold for spin angular momentum \mathbf{s} , for which there is no classical analog. It can then be proved that they hold for any angular momentum

$$\mathbf{J} = \sum_i (\mathbf{l}_i + \mathbf{s}_i).$$

From the commutation relations, it follows that J^2 and J_z are simultaneously observable, that is, we can specify states in which they both have given values. These values are $J(J+1)$ and M , respectively, where J is integral or half-integral and nonnegative and $-J \leq M \leq J$. In symbols, we denote the wave function of such a state by $|JM\rangle$, and

$$J^2|JM\rangle = J(J+1)|JM\rangle, \quad (\text{A-5})$$

$$J_z|JM\rangle = M|JM\rangle. \quad (\text{A-6})$$

Of course the states are orthogonal and normalized, that is,

$$\langle JM|J'M'\rangle = \delta_{JJ'}\delta_{MM'}. \quad (\text{A-7})$$

The components J_x and J_y cannot be given definite values simultaneously with J_z , but the combinations J_{\pm} have the important property of operating on the state $|JM\rangle$ and converting it into a state with an M -value one greater or one less:

$$J_{\pm}|JM\rangle = [J(J+1) - M(M \pm 1)]^{1/2}|JM \pm 1\rangle \quad (\text{A-8})$$

$$= [(J \mp M)(J \pm M + 1)]^{1/2}|JM \pm 1\rangle. \quad (\text{A-9})$$

Consequently,

$$\langle JM|J_{\pm}|J'M'\rangle = \delta_{JJ'}[(J \mp M)(J \pm M + 1)]^{1/2}\delta_{MM' \pm 1}. \quad (\text{A-10})$$

(b) *Orbital angular momentum.* In the Schrödinger picture of quantum mechanics, which uses differential operators, single-particle wave functions depend on the coordinates \mathbf{r} of a particle, and the momentum operator is $\mathbf{p} = -i\mathbf{\nabla}$. For the angular-momentum operators it is natural to use spherical polar coordinates, and from $\mathbf{L} = \mathbf{r} \times \mathbf{p}$ we find

$$L_{\pm} = e^{\pm i\phi} \left(\pm \frac{\partial}{\partial \theta} + i \cot \theta \frac{\partial}{\partial \phi} \right), \quad (\text{A-11a})$$

$$L_z = -i \frac{\partial}{\partial \phi}, \quad (\text{A-11b})$$

$$L^2 = -\frac{1}{\sin^2 \theta} \frac{\partial^2}{\partial \phi^2} - \frac{1}{\sin \theta} \frac{\partial}{\partial \theta} \left(\sin \theta \frac{\partial}{\partial \theta} \right). \quad (\text{A-11c})$$

The expression for L^2 is essentially the angular terms of the Laplacian. The eigenvalues of L^2 and L_z are $l(l+1)$ and m , respectively, where l takes on only nonnegative integral values and $m = -l, -l+1, \dots, l-1, l$. The eigenfunctions $|lm\rangle$ are given in this representation by the spherical harmonics

$$|lm\rangle = Y_l^m(\theta, \phi). \quad (\text{A-12})$$

The definition of spherical harmonics most widely used in nuclear physics is that given by Condon and Shortley [1]; it is the one adopted in this book:

$$Y_l^m = \Theta_l^m(\theta)(2\pi)^{-1/2}e^{im\phi}, \quad (\text{A-13a})$$

$$\Theta_l^m(\theta) = (-)^m \left[\frac{2l+1}{2} \frac{(l-m)!}{(l+m)!} \right]^{1/2} \sin^m \theta \frac{d^m}{(d \cos \theta)^m} P_l(\cos \theta), \quad m > 0, \quad (\text{A-13b})$$

$$\Theta_l^{-m}(\theta) = (-)^m \Theta_l^m(\theta), \quad m > 0, \quad (\text{A-13c})$$

$$P_l(\cos \theta) = \frac{(-)^l}{2^l l!} \frac{d^l}{(d \cos \theta)^l} \sin^{2l} \theta. \quad (\text{A-13d})$$

Another way of writing Θ_l^m , which is valid for either sign of m , is

$$\Theta_l^m = (-)^l \left[\frac{2l+1}{2} \frac{(l+m)!}{(l-m)!} \right]^{1/2} \frac{1}{2^l l!} \frac{1}{\sin^m \theta} \frac{d^{l-m}}{(d \cos \theta)^{l-m}} \sin^{2l} \theta. \quad (\text{A-14})$$

Useful explicit forms are as follows:

$$\Theta_0^0 = \sqrt{\frac{1}{2}};$$

$$\Theta_1^0 = \sqrt{\frac{3}{8}} \cos \theta, \quad \Theta_1^{\pm 1} = \mp \sqrt{\frac{3}{8}} \sin \theta;$$

$$\Theta_2^0 = \sqrt{\frac{15}{32}} (3 \cos^2 \theta - 1),$$

$$\Theta_2^{\pm 1} = \mp \sqrt{\frac{15}{16}} \cos \theta \sin \theta, \quad \Theta_2^{\pm 2} = \sqrt{\frac{15}{16}} \sin^2 \theta;$$

$$\Theta_3^0 = \sqrt{\frac{35}{192}} (5 \cos^3 \theta - 3 \cos \theta), \quad \Theta_3^{\pm 1} = \mp \sqrt{\frac{21}{32}} (5 \cos^2 \theta - 1) \sin \theta,$$

$$\Theta_3^{\pm 2} = \sqrt{\frac{105}{16}} \cos \theta \sin^2 \theta, \quad \Theta_3^{\pm 3} = \mp \sqrt{\frac{35}{32}} \sin^3 \theta.$$

(c) *Spin.* Since the spin of a fermion is a purely quantum-mechanical concept, there is no differential operator suitable to describe it, but an explicit representation of the operators \mathbf{s} is provided by any mathematical

entities that satisfy Eqs. A-2 to A-9. The standard procedure is to use the Pauli spin matrices σ , defined by

$$\mathbf{s} = \frac{1}{2}\boldsymbol{\sigma}, \quad (\text{A-15})$$

$$\sigma_x = \begin{pmatrix} 0 & 1 \\ 1 & 0 \end{pmatrix}, \quad \sigma_y = \begin{pmatrix} 0 & -i \\ i & 0 \end{pmatrix}, \quad \sigma_z = \begin{pmatrix} 1 & 0 \\ 0 & -1 \end{pmatrix}. \quad (\text{A-16})$$

The commutation relations A-2 through A-4 are satisfied in the form

$$[\sigma_x, \sigma_y] = 2i\sigma_z, \quad [\sigma_z, \sigma_{\pm}] = \pm 2\sigma_{\pm}. \quad (\text{A-17})$$

In addition, the operators anticommute, that is,

$$\sigma_i\sigma_j + \sigma_j\sigma_i = 2\delta_{ij}. \quad (\text{A-18})$$

In particular,

$$\sigma_x^2 = \sigma_y^2 = \sigma_z^2 = 1.$$

These results imply the cyclic relations typified by

$$\sigma_x\sigma_y = i\sigma_z. \quad (\text{A-19})$$

We see that $s^2 = \frac{1}{4}\sigma^2 = \frac{3}{4}$, which shows that these are appropriate operators to describe an angular momentum $J = \frac{1}{2}$.

The "wave functions" representing the eigenstates of s^2 and s_z are the two-component vectors

$$\alpha = \begin{pmatrix} 1 \\ 0 \end{pmatrix}, \quad \beta = \begin{pmatrix} 0 \\ 1 \end{pmatrix}. \quad (\text{A-20})$$

Since

$$\sigma_x\alpha = \alpha, \quad \sigma_z\beta = -\beta, \quad (\text{A-21})$$

we see that α describes a state with spin "up" and β a state with spin "down," that is, $m = \frac{1}{2}$ and $-\frac{1}{2}$, respectively. Also

$$\sigma_{-}\alpha = 2\beta, \quad \sigma_{+}\beta = 2\alpha. \quad (\text{A-22})$$

The wave function $\begin{pmatrix} a \\ b \end{pmatrix}$ represents a state with probability $|a|^2$ of finding the spin up and probability $|b|^2$ of finding it down. The state is normalized if $|a|^2 + |b|^2 = 1$.

The Hermitian adjoint of the vector

$$|\psi\rangle = \begin{pmatrix} a \\ b \end{pmatrix} \quad \text{is} \quad \langle\psi| = (a^*b^*),$$

and the product $\langle\psi_1|\psi_2\rangle$ is explicitly

$$(a_1^*b_1^*) \begin{pmatrix} a_2 \\ b_2 \end{pmatrix} = a_1^*a_2 + b_1^*b_2. \quad (\text{A-23})$$

The eigenstates α and β are of course orthogonal,

$$\langle\alpha|\beta\rangle = 0.$$

(d) *Isospin.* The essential feature of the three Pauli matrices and their associated eigenvectors is their ability to describe states distinguished from each other by the value of a quantity (like s_z) which has two possible values. It is therefore possible to use the same representation for the i -spin of nucleons. With

$$t_i = \frac{1}{2}\tau_i, \quad (\text{A-24})$$

$$\tau_1 = \begin{pmatrix} 0 & 1 \\ 1 & 0 \end{pmatrix}, \quad \tau_2 = \begin{pmatrix} 0 & -i \\ i & 0 \end{pmatrix}, \quad \tau_3 = \begin{pmatrix} 1 & 0 \\ 0 & -1 \end{pmatrix},$$

$$\gamma = \begin{pmatrix} 1 \\ 0 \end{pmatrix}, \quad \delta = \begin{pmatrix} 0 \\ 1 \end{pmatrix},$$

we have

$$(\frac{1}{2} + t_3)\gamma = \gamma, \quad (\frac{1}{2} + t_3)\delta = 0, \quad (\text{A-25})$$

$$t_{+}\delta = (t_1 + it_2)\delta = \gamma, \quad t_{-}\gamma = \delta. \quad (\text{A-26})$$

Equation A-25 shows that γ and δ provide representations for two charge states, γ being the proton and δ the neutron, with the operator for charge being $(\frac{1}{2} + t_3)e$. Equations A-26 show that t_{+} and t_{-} are operators which, respectively, convert neutron states into proton states and vice versa. They are therefore useful in describing β -decay.

(e) *Addition of two angular momenta.* Two angular momenta, \mathbf{J}_1 and \mathbf{J}_2 , may be added to form a resultant,

$$\mathbf{J} = \mathbf{J}_1 + \mathbf{J}_2.$$

The possible values of J are those that can be formed by a vector triangle, that is,

$$J = J_1 + J_2, J_1 + J_2 - 1, \dots, |J_1 - J_2| + 1, |J_1 - J_2|. \quad (\text{A-27})$$

The state in which J^2 and J_z have fixed values $J(J+1)$ and M is not, in general, a state in which J_{1z} and J_{2z} have fixed values, but is a combination of all the states for which

$$M_1 + M_2 = M. \quad (\text{A-28})$$

Specifically, if we denote the state with quantum numbers J_1, J_2, J , and M by $|J_1 J_2 JM\rangle$, we have

$$|J_1 J_2 JM\rangle = \sum_{M_1, M_2} (J_1 J_2 M_1 M_2 | JM) |J_1 M_1\rangle |J_2 M_2\rangle. \quad (\text{A-29})$$

In Eq. A-29, $|J_1 M_1\rangle |J_2 M_2\rangle$ is the state in which both angular momenta \mathbf{J}_1 and \mathbf{J}_2 have fixed magnitudes and z -components, and $(J_1 J_2 M_1 M_2 | JM)$ is the *Clebsch-Gordan vector-addition coefficient*.

These important coefficients have been given a wide variety of notations. There has also been some variation in the choice of phases, but most authors now use the conventions adopted by Condon and Shortley, namely, that all coefficients are real, those with $M = J$ are positive, and all angular-momentum states satisfy Eq. A-10. The Clebsch-Gordan coefficients are closely related to Wigner's *3-j symbols*, which refer to the addition of three angular momenta to a zero resultant. Precisely,

$$\begin{pmatrix} J_1 J_2 J \\ M_1 M_2 M \end{pmatrix} = \frac{(-)^{J_1 - J_2 - M}}{(2J + 1)^{1/2}} (J_1 J_2 M_1 M_2 | J - M). \quad (\text{A-30})$$

The Clebsch-Gordan coefficients satisfy the symmetry relations:

$$(J_1 J_2 M_1 M_2 | JM) = (-)^{J_1 + J_2 - J} (J_2 J_1 M_2 M_1 | JM), \quad (\text{A-31a})$$

$$= (-)^{J_1 - J + M_1} \left(\frac{2J + 1}{2J_1 + 1} \right)^{1/2} (J J_2 M - M_2 | J_1 M_1), \quad (\text{A-31b})$$

$$= (-)^{J_1 - J - M_1} \left(\frac{2J + 1}{2J_2 + 1} \right)^{1/2} (J_1 J - M_1 M | J_2 M_2), \quad (\text{A-31c})$$

$$= (-)^{J_1 + J_2 - J} (J_1 J_2 - M_1 - M_2 | J - M). \quad (\text{A-31d})$$

Also,

$$\sum_{M_1, M_2} (J_1 J_2 M_1 M_2 | JM) (J_1 J_2 M_1 M_2 | J' M') = \delta_{JJ'} \delta_{MM'}, \quad (\text{A-32a})$$

$$\sum_{JM} (J_1 J_2 M_1 M_2 | JM) (J_1 J_2 M_1' M_2' | JM) = \delta_{M_1 M_1'} \delta_{M_2 M_2'}. \quad (\text{A-32b})$$

A state of fixed M_1 and M_2 is not, in general, a state of fixed J , but a linear combination of states of all J from $|J_1 - J_2|$ to $J_1 + J_2$, namely,

$$|J_1 M_1\rangle |J_2 M_2\rangle = \sum_J (J_1 J_2 M_1 M_2 | JM_1 + M_2) |J_1 J_2 JM_1 + M_2\rangle. \quad (\text{A-33})$$

There is a closed form (due to Racah) for Clebsch-Gordan coefficients:

$$\begin{aligned} & (J_1 J_2 M_1 M_2 | JM) \\ &= \delta_{M_1 M_1 + M_2} [(2J + 1)(J_1 + J_2 - J)! (J + J_1 - J_2)! (J + J_2 - J_1)! \\ &\quad \times (J_1 + M_1)! (J_1 - M_1)! (J_2 + M_2)! (J_2 - M_2)! (J + M)! (J - M)!]^{1/2} \\ &\quad \times [(J + J_1 + J_2 + 1)!]^{-1/2} \\ &\quad \times \sum_s (-)^s [s! (J_1 + J_2 - J - s)! (J_1 - M_1 - s)! (J_2 + M_2 - s)! \\ &\quad \times (J - J_2 + M_1 + s)! (J - J_1 - M_2 + s)!]^{-1}. \end{aligned} \quad (\text{A-34})$$

The summation over s includes all values for which none of the factorials have negative arguments ($0! = 1$). This formula is cumbersome to use, and tables of Clebsch-Gordan coefficients have been prepared [1, 2, 3, 4, 5]. The coefficients are all square roots of rational fractions; some of the tables list the separate factors of these fractions, whereas others give simply numerical values. Some of the coefficients for low values of J_2 are given in Table A-1. It is also worth noting that

$$(J_1 J_2 J_1 J_2 | J_1 + J_2 J_1 + J_2) = 1, \quad (\text{A-35})$$

$$(J 0 M 0 | JM) = 1. \quad (\text{A-36})$$

TABLE A-1 Values of $\Phi(J_2, M_2, J)$ ^a.

$J_2 = 0$	$\Phi(0, 0, 0) = 1$
$J_2 = \frac{1}{2}$	$\Phi(\frac{1}{2}, \frac{1}{2}, J_1 + \frac{1}{2}) = 1$
$J_2 = 1$	$J = J_1$
$M_2 = 0$	$-2M_1$
$M_2 = 1$	$-\sqrt{2(J_1 - M_1)}$
	$J = J_1 + 1$
	$-\sqrt{2(J_1 - M_1 + 1)}$
$J_2 = \frac{3}{2}$	$J = J_1 + \frac{1}{2}$
$M_2 = \frac{1}{2}$	$J_1 - 3M_1$
$M_2 = \frac{3}{2}$	$-\sqrt{3(J_1 - M_1)}$
	$J = J_1 + \frac{3}{2}$
	$-\sqrt{3(J_1 - M_1 + 1)}$
$J_2 = 2$	$J = J_1$
$M_2 = 0$	$2[3M_1^2 - J_1(J_1 + 1)]$
$M_2 = 1$	$(2M_1 + 1)\sqrt{6(J_1 - M_1)}$
$M_2 = 2$	$\sqrt{6(J_1 - M_1)(J_1 - M_1 - 1)}$
	$J = J_1 + 1$
	$2M_1\sqrt{6(J_1 - M_1 + 1)}$
	$2(J_1 - 2M_1)$
	$-2\sqrt{J_1 - M_1 + 1}$
	$-\sqrt{6(J_1 - M_1 + 2)(J_1 - M_1 + 1)}$
	$2\sqrt{J_1 - M_1 - 1}$
	$-\sqrt{2(J_1 - M_1 + 1)}$
	1

^a Defined in Eq. A-37.

The quantities in Table A-1 are $\Phi(J_2, M_2, J)$, defined by

$$(J_1 J_2 M_1 M_2 | JM) = (-)^{M_1 - J_1} (2J + 1)^{1/2} \times \left[\frac{(J_1 + J - J_2)! (J + M)!}{(J_1 + J_2 + J + 1)! (J_1 + M_1)!} \right]^{1/2} \Phi(J_2, M_2, J). \quad (\text{A-37})$$

This equation holds only for $J \geq J_1$ and $M_2 \geq 0$. For $J < J_1$ and/or $M_2 < 0$, Eqs. A-31 must be used first to obtain a coefficient to which Eq. A-37 can be applied.

In particular, we may note the addition of orbital and spin angular momenta of a single nucleon:

$$\mathbf{j} = \mathbf{l} + \mathbf{s}.$$

The state $j = l + \frac{1}{2}, m$ is

$$(2l + 1)^{-1/2} [(l + m + \frac{1}{2})^{1/2} Y_l^{m-(1/2)} \alpha + (l - m + \frac{1}{2})^{1/2} Y_l^{m+(1/2)} \beta], \quad (\text{A-38a})$$

and the state $j = l - \frac{1}{2}, m$ is

$$(2l + 1)^{-1/2} [-(l - m + \frac{1}{2})^{1/2} Y_l^{m-(1/2)} \alpha + (l + m + \frac{1}{2})^{1/2} Y_l^{m+(1/2)} \beta]. \quad (\text{A-38b})$$

Another important case is the addition of the spins of two particles. The singlet state ($j = 0$) and the triplet states ($j = 1$) are given by

$$\begin{aligned} {}^1(\sigma)_0 &= (\frac{1}{2} \frac{1}{2} \frac{1}{2} - \frac{1}{2} | 0 0) \alpha(1) \beta(2) + (\frac{1}{2} \frac{1}{2} - \frac{1}{2} \frac{1}{2} | 0 0) \beta(1) \alpha(2) \\ &= (1/\sqrt{2})(\alpha(1) \beta(2) - \beta(1) \alpha(2)), \\ {}^3(\sigma)_1 &= (\frac{1}{2} \frac{1}{2} \frac{1}{2} \frac{1}{2} | 1 1) \alpha(1) \alpha(2) = \alpha(1) \alpha(2), \\ {}^3(\sigma)_{-1} &= (\frac{1}{2} \frac{1}{2} - \frac{1}{2} - \frac{1}{2} | 1 -1) \beta(1) \beta(2) = \beta(1) \beta(2), \\ {}^3(\sigma)_0 &= (\frac{1}{2} \frac{1}{2} \frac{1}{2} - \frac{1}{2} | 1 0) \alpha(1) \beta(2) + (\frac{1}{2} \frac{1}{2} - \frac{1}{2} \frac{1}{2} | 1 0) \alpha(2) \beta(1) \\ &= (1/\sqrt{2})(\alpha(1) \beta(2) + \alpha(2) \beta(1)). \end{aligned}$$

Also, the two-particle states with quantum numbers $SLJM$ are given by

$$\Psi_{JSL}^M = \sum_{M_S, M_L} (SLM_S M_L | JM)^{2S+1} (\sigma)_M Y_L^{M_L}.$$

For example,

$$\Psi_{112}^1 = \frac{1}{\sqrt{10}} {}^3(\sigma)_1 Y_2^0 - \sqrt{\frac{3}{10}} {}^3(\sigma)_0 Y_2^1 + \sqrt{\frac{3}{5}} {}^3(\sigma)_{-1} Y_2^2.$$

(f) *Addition of three angular momenta.* Suppose that $\mathbf{J} = \mathbf{J}_1 + \mathbf{J}_2 + \mathbf{J}_3$. We can form two kinds of states, for both of which the magnitude and orientation of \mathbf{J} are fixed. First, we can have states in which the magnitude of $\mathbf{J}_{12} = \mathbf{J}_1 + \mathbf{J}_2$ is fixed; these states are

$$|(J_1 J_2) J_{12}, J_3; JM\rangle = \sum_{M_3} (J_{12} J_3 M_{12} M_3 | JM) |J_{12} M_{12}\rangle |J_3 M_3\rangle. \quad (\text{A-39a})$$

Alternatively, we can take states in which $\mathbf{J}_{13} = \mathbf{J}_1 + \mathbf{J}_3$ has a definite magnitude:

$$|(J_1 J_3) J_{13}, J_2; JM\rangle = \sum_{M_2} (J_{13} J_2 M_{13} M_2 | JM) |J_{13} M_{13}\rangle |J_2 M_2\rangle. \quad (\text{A-39b})$$

Of course, the states $|J_{12} M_{12}\rangle$ and $|J_{13} M_{13}\rangle$ are themselves complex. For example,

$$|J_{12} M_{12}\rangle = \sum_{M_1} (J_1 J_2 M_1 M_2 | J_{12} M_{12}) |J_1 M_1\rangle |J_2 M_2\rangle.$$

One class of states, say with J_{12} fixed, can be expressed in terms of the other set with J_{13} fixed. The coefficients of the relationship are called Racah's *W*-functions:

$$\begin{aligned} &|(J_1 J_2) J_{12}, J_3; JM\rangle \\ &= \sum_{J_{11}} W(J_1 J_2 J_3 J; J_{12} J_{13}) [(2J_{12} + 1)(2J_{13} + 1)]^{1/2} |(J_1 J_3) J_{13}, J_2; JM\rangle. \end{aligned} \quad (\text{A-40})$$

The *W*-functions are essentially the same as Wigner's *6-j symbols*, defined by

$$\left\{ \begin{matrix} J_1 J_2 J_{12} \\ J_3 J_{13} \end{matrix} \right\} = (-)^{J_1 + J_2 + J_3 + J} W(J_1 J_2 J_3 J; J_{12} J_{13}). \quad (\text{A-41})$$

It is not surprising that *W*-functions arise in discussions of the individual-particle model, in angular correlations, and in differential-reaction cross sections involving three angular momenta. However, because we have not exhibited the mathematical details of such calculations in the text, we shall not summarize the various orthogonality relations of the *W*'s or all their connections with the Clebsch-Gordan coefficients. We shall simply quote one expression for *W* and give the definitions of the functions *Z* and *F*, which are referred to in some sections on angular correlations:

$$\begin{aligned} &W(J_1 J_2 J_3 J; J_{12} J_{13}) \\ &= \sum_{\text{all } M} (-)^S \times \end{aligned}$$

$$\begin{aligned} & \times \left(\begin{array}{c} J_1 J_2 J_{12} \\ M_1 M_2 - M_{12} \end{array} \right) \left(\begin{array}{c} J_1 J_3 J_{13} \\ M_1 M_3 - M_{13} \end{array} \right) \left(\begin{array}{c} J_2 J_{13} J \\ M_2 M_{13} - M \end{array} \right) \left(\begin{array}{c} J_3 J_{12} J \\ M_3 M_{12} - M \end{array} \right) \\ = & \sum_{\text{all } M} (-)^{S+T} \\ & \times [(2J_{12} + 1)(2J_{13} + 1)]^{-1/2} (2J + 1)^{-1} (J_1 J_2 M_1 M_2 | J_{12} M_{12}) \\ & \times (J_1 J_3 M_1 M_3 | J_{13} M_{13}) (J_2 J_{13} M_2 M_{13} | JM) (J_3 J_{12} M_3 M_{12} | JM), \quad (\text{A-42}) \end{aligned}$$

where $S = J_1 + J_2 - J_{12}$ and $T = J_{12} + M_{12} + J_{13} + M_{13}$. When L and L' are integral, we define

$$\begin{aligned} Z(LJL'J'; i\lambda) = & i^{L'-L+\lambda} [(2L + 1)(2L' + 1)(2J + 1)(2J' + 1)]^{1/2} \\ & \times (LL'00|\lambda 0) W(LL'JJ'; \lambda j). \quad (\text{A-43}) \end{aligned}$$

$$\begin{aligned} F_\lambda(LL'J_1J_2) = & (-)^{J_1-J_2+\lambda} [(2L + 1)(2L' + 1)(2J_2 + 1)]^{1/2} (LL'1 - 1|\lambda 0) \\ & \times W(LL'J_2J_2; \lambda J_1). \quad (\text{A-44}) \end{aligned}$$

A-2 SPHERICAL TENSORS

(a) *Rotation matrices* \mathcal{D} . It is important to be able to connect the wave function referred to one system of axes with the wave functions in a different frame obtained by a set of rotations of the original frame.

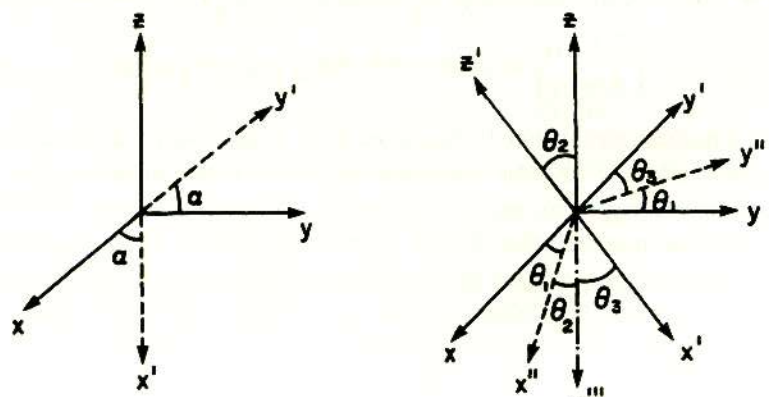


Fig. A-1 Rotations of Axes.

Consider the rotation of a right-handed frame of reference (x, y, z) about the z -axis by an angle α , as shown in Fig. A-1. Let P be a fixed point (x, y, z) in the old frame; then in the rotated frame the same point P is (x', y', z') . It is simpler to use polar coordinates (r, θ, ϕ) in the old frame, and (r', θ', ϕ') in the rotated frame. In the simple example shown in Fig. A-1, the rotation operation by α about the z -axis implies that $r' = r$, $\theta' = \theta$, and $\phi' = \phi - \alpha$. Thus the rotation operation $R_z(\alpha)$ on a function $f(r, \theta, \phi)$ gives

$$\begin{aligned} R_z(\alpha)f(r, \theta, \phi) &= f(r, \theta, \phi - \alpha) \\ &= f(r, \theta, \phi) - \alpha \frac{\partial}{\partial \phi} f(r, \theta, \phi) + \frac{\alpha^2}{2!} \frac{\partial^2}{\partial \phi^2} f(r, \theta, \phi) - \dots \\ &= \exp\left(-\alpha \frac{\partial}{\partial \phi}\right) f(r, \theta, \phi). \end{aligned}$$

Using Eq. A-11b, we can rewrite the above equation as ($\hbar = 1$),

$$R_z(\alpha)f(r, \theta, \phi) = \exp(-i\alpha L_z) f(r, \theta, \phi). \quad (\text{A-45})$$

Similarly, the rotation operator in the configuration space for rotation α about an arbitrary unit vector \mathbf{n} is given by $\exp[-i\alpha(\mathbf{n} \cdot \mathbf{L})]$. Generalizing the space to include both the configuration space and the spin space, we can write the rotation operator for a rotation α about the unit vector \mathbf{n} as

$$R_{\mathbf{n}}(\alpha) = \exp[-i\alpha(\mathbf{n} \cdot \mathbf{J})], \quad (\text{A-46})$$

where $\mathbf{J} = \mathbf{L} + \mathbf{S}$. Note that the operator $R_{\mathbf{n}}(\alpha)$ is unitary.

The rotations taking one coordinate system into another are conveniently specified by the Euler angles $(\theta_1, \theta_2, \theta_3)$, which denote three successive rotations: a rotation θ_1 about the z -axis, followed by a rotation θ_2 about the new y -axis y'' , followed by a rotation θ_3 about the final z -axis, z' . The ranges of values taken by the θ_i 's are $0 \leq \theta_1 \leq 2\pi$, $0 \leq \theta_2 \leq \pi$, and $0 \leq \theta_3 \leq 2\pi$. We can thus write the general rotation operator in terms of the Euler angles θ_i as

$$R(\theta_1, \theta_2, \theta_3) = \exp(-i\theta_3 J_{z'}) \exp(-i\theta_2 J_{y''}) \exp(-i\theta_1 J_z).$$

Using the relations

$$\exp(-i\theta_2 J_{y''}) = \exp(-i\theta_1 J_z) \exp(-i\theta_2 J_y) \exp(i\theta_1 J_z)$$

and

$$\exp(-i\theta_3 J_{z'}) = \exp(-i\theta_2 J_{y''}) \exp(-i\theta_3 J_z) \exp(i\theta_2 J_{y''}),$$

we finally obtain

$$R(\theta_i) = R(\theta_1, \theta_2, \theta_3) = \exp(-i\theta_1 J_z) \exp(-i\theta_2 J_y) \exp(-i\theta_3 J_z). \quad (\text{A-47})$$

Since, from the above definition, $[R(\theta_i), J^2] = 0$, it follows that

$$\begin{aligned} J^2 R(\theta_i) |JM\rangle &= R(\theta_i) J^2 |JM\rangle \\ &= J(J+1) R(\theta_i) |JM\rangle, \end{aligned}$$

so that rotations cannot change the total angular momentum of a state. However, unless the axis of rotation is along the z -axis, the z -component of angular momentum will change, so that

$$R(\theta_i) |JK\rangle = \sum_M \langle JM | R(\theta_i) | JK \rangle |JM\rangle. \quad (\text{A-48})$$

We define† the \mathcal{D} -functions as

$$[\mathcal{D}_{MK}^J(\theta_i)]^* = \langle JM | R(\theta_i) | JK \rangle \quad (\text{A-49})$$

to rewrite Eq. A-48:

$$R(\theta_i) |JK\rangle = \sum_M [\mathcal{D}_{MK}^J(\theta_i)]^* |JM\rangle. \quad (\text{A-50})$$

Thus, for the rotation operator $R(\theta_i)$, we can associate a $(2J+1) \times (2J+1)$ matrix $\mathcal{D}^J(\theta_i)$, whose elements are given by Eq. A-49. By combining Eqs. A-47 and A-49, we obtain

$$\begin{aligned} [\mathcal{D}_{M'M}^J(\theta_i)]^* &= \exp(-i\theta_1 M') \langle JM' | \exp(-i\theta_2 J_y) | JM \rangle \exp(-i\theta_3 M) \\ &= \exp(-i\theta_1 M') d_{M'M}^J(\theta_2) \exp(-i\theta_3 M), \end{aligned} \quad (\text{A-51})$$

with

$$d_{M'M}^J(\theta_2) = \langle JM' | \exp(-i\theta_2 J_y) | JM \rangle. \quad (\text{A-52})$$

We have chosen the representation in which J_z is diagonal and J_y pure imaginary; it can then be shown that $d_{M'M}^J(\theta_2)$ is real. It follows from Eq. A-51 that

$$\mathcal{D}_{M'M}^J(\theta_i) = \exp(i\theta_1 M') d_{M'M}^J(\theta_2) \exp(i\theta_3 M). \quad (\text{A-53})$$

We now list some useful properties of the rotation matrices. The unitarity relations are

† The reader must be warned that there are several different sets of conventions in the literature. There are different conventions for the definition of Euler angles, handedness of axes, and phases of the \mathcal{D} -functions. The phase used here is different from that in the earlier book by M. A. Preston. References 6, 7, and 8 differ from each other.

$$\sum_M [\mathcal{D}_{MK}^J(\theta_i)]^* \mathcal{D}_{MK}^J(\theta_i) = \delta_{KK} \quad (\text{A-54})$$

and

$$\sum_K [\mathcal{D}_{M'K}^J(\theta_i)]^* \mathcal{D}_{MK}^J(\theta_i) = \delta_{M'M}. \quad (\text{A-55})$$

The d -functions defined by Eq. A-52 obey the following relations:

$$d_{MK}^J(\theta_2) = (-)^{M-K} d_{-M,-K}^J(\theta_2), \quad (\text{A-56})$$

$$= (-)^{M-K} d_{KM}^J(\theta_2), \quad (\text{A-57})$$

$$= d_{KM}^J(-\theta_2); \quad (\text{A-58})$$

$$d_{MK}^J(\pi - \theta) = (-)^{J-M} d_{M,-K}^J(\theta), \quad (\text{A-59})$$

$$= (-)^{J+K} d_{-M,K}^J(\theta). \quad (\text{A-60})$$

Also,

$$d_{MK}^J(0) = \delta_{MK}, \quad d_{MK}^J(\pi) = (-)^{J-M} \delta_{M,-K}. \quad (\text{A-61})$$

Using Eqs. A-56 to A-58, we can easily prove that

$$[\mathcal{D}_{MK}^J(\theta_i)]^* = (-)^{M-K} \mathcal{D}_{-M,-K}^J(\theta_i), \quad (\text{A-62})$$

$$= (-)^{M-K} \mathcal{D}_{M,K}^J(-\theta_i), \quad (\text{A-63})$$

since

$$\mathcal{D}_{M,K}^J(-\theta_i) = \mathcal{D}_{-M,-K}^J(\theta_i). \quad (\text{A-64})$$

Using Eq. A-58 and definitions A-51 and A-53, it also follows that

$$[\mathcal{D}_{MK}^J(\theta_1, \theta_2, \theta_3)]^* = \mathcal{D}_{KM}^J(-\theta_3, -\theta_2, -\theta_1). \quad (\text{A-65})$$

Important special cases are the \mathcal{D} 's with a zero subscript; these are spherical harmonics:

$$\mathcal{D}_{M0}^J(\theta_1, \theta_2, \theta_3) = \left(\frac{4\pi}{2J+1} \right)^{1/2} Y_J^M(\theta_2, \theta_1), \quad (\text{A-66})$$

$$\mathcal{D}_{0K}^J(\theta_1, \theta_2, \theta_3) = (-)^K \left(\frac{4\pi}{2J+1} \right)^{1/2} Y_J^K(\theta_2, \theta_3), \quad (\text{A-67})$$

$$\mathcal{D}_{00}^J(\theta_1, \theta_2, \theta_3) = P_J(\cos \theta_2). \quad (\text{A-68})$$

The spherical-harmonic addition theorem follows from these results. If a certain vector \mathbf{r} has polar angles (θ, ϕ) with respect to the (x, y, z) -axes, and

(θ', ϕ') with respect to the (x', y', z') -axes obtained by the rotation operator $R(\theta_i)$, it follows from Eq. A-50 that

$$Y_l^m(\theta', \phi') = \sum_{m'} [\mathcal{D}_{m'm}^l(\theta_1, \theta_2, \theta_3)]^* Y_l^{m'}(\theta, \phi). \quad (\text{A-69})$$

For $m = 0$, since

$$Y_l^0(\theta', \phi') = \sqrt{\frac{2l+1}{4\pi}} P_l(\cos \theta'),$$

we obtain, using Eq. A-66,

$$P_l(\cos \theta') = \frac{4\pi}{2l+1} \sum_{m'} [Y_l^{m'}(\theta_2, \theta_1)]^* Y_l^{m'}(\theta, \phi). \quad (\text{A-70})$$

Since (θ_2, θ_1) are the polar angles of the z' -axis with respect to the (x, y, z) -axes and θ' is the angle between the z' -axis and \mathbf{r} , Eq. A-70 is the addition theorem for the Legendre polynomial of the angle between two vectors, namely, the ones we have called \mathbf{r} and the z' -axis.

Consider again a frame (x, y, z) and a rotated frame (x', y', z') , obtained as before by applying the rotation operator $R(\theta_i)$ on the (x, y, z) -axes. Let \mathbf{J} be an angular-momentum vector with z -component M and z' -component K . It can then be shown [6, 7, 8] that

$$\begin{aligned} J^2 \mathcal{D}_{MK}^J &= J(J+1) \mathcal{D}_{MK}^J, \\ J_x \mathcal{D}_{MK}^J &= M \mathcal{D}_{MK}^J, \\ J_z \mathcal{D}_{MK}^J &= K \mathcal{D}_{MK}^J, \end{aligned} \quad (\text{A-71})$$

and

$$J_{\pm} \mathcal{D}_{MK}^J = [(J \pm K)(J \mp K + 1)]^{1/2} \mathcal{D}_{M,K \mp 1}^J, \quad \text{with } J_{\pm} = J_x \pm iJ_y.$$

In the above situation, we can use Eq. A-50 to write

$$\langle x, y, z | R(\theta_i) | JK \rangle = \sum_M [\mathcal{D}_{MK}^J(\theta_i)]^* \langle x, y, z | JM \rangle$$

or

$$\langle x', y', z' | JK \rangle = \sum_M [\mathcal{D}_{MK}^J(\theta_i)]^* \langle x, y, z | JM \rangle$$

or

$$\Psi_{JK}(x', y', z') = \sum_M [\mathcal{D}_{MK}^J(\theta_i)]^* \Psi_{JM}(x, y, z). \quad (\text{A-72})$$

Using Eq. A-55, we can invert Eq. A-72 to obtain

$$\Psi_{JM}(x, y, z) = \sum_K \mathcal{D}_{MK}^J(\theta_i) \Psi_{JK}(x', y', z'). \quad (\text{A-73})$$

The following coupling relationships can then be derived, using Eqs. A-72 and A-73, where the \mathcal{D} 's have the same arguments $(\theta_1, \theta_2, \theta_3)$:

$$\mathcal{D}_{M_1 K_1}^{J_1} \mathcal{D}_{M_2 K_2}^{J_2} = \sum_J \mathcal{D}_{MK}^J (J_1 J_2 M_1 M_2 | JM) (J_1 J_2 K_1 K_2 | JK), \quad (\text{A-74})$$

$$\mathcal{D}_{MK}^J = \sum_{M_1 K_1} (J_1 J_2 M_1 M_2 | JM) (J_1 J_2 K_1 K_2 | JK) \mathcal{D}_{M_1 K_1}^{J_1} \mathcal{D}_{M_2 K_2}^{J_2}, \quad (\text{A-75})$$

$$\sum_{M_1 M_2} \mathcal{D}_{M_1 K_1}^{J_1} \mathcal{D}_{M_2 K_2}^{J_2} \mathcal{D}_{M_3 K_3}^{J_3 *} (J_1 J_2 M_1 M_2 | J_3 M_3) = (J_1 J_2 K_1 K_2 | J_3 K_3). \quad (\text{A-76})$$

The normalization factor for \mathcal{D}_{MK}^J is $[(2J+1)/8\pi^2]^{1/2}$:

$$\begin{aligned} &\frac{[(2J_1+1)(2J_2+1)]^{1/2}}{8\pi^2} \int_0^\pi \sin \theta_2 d\theta_2 \int_0^{2\pi} d\theta_1 \int_0^{2\pi} d\theta_3 \mathcal{D}_{M_1 K_1}^{J_1 *} \mathcal{D}_{M_2 K_2}^{J_2} \\ &= \delta_{M_1 M_2} \delta_{K_1 K_2} \delta_{J_1 J_2}. \end{aligned} \quad (\text{A-77})$$

Equations A-74 and A-77 yield

$$\begin{aligned} &\int \mathcal{D}_{M_1 K_1}^{J_1} \mathcal{D}_{M_2 K_2}^{J_2} \mathcal{D}_{M_3 K_3}^{J_3 *} \sin \theta_2 d\theta_2 d\theta_1 d\theta_3 \\ &= \frac{8\pi^2}{2J_3+1} (J_1 J_2 M_1 M_2 | J_3 M_3) (J_1 J_2 K_1 K_2 | J_3 K_3). \end{aligned} \quad (\text{A-78})$$

By using Eq. A-66, this result can be specialized to give

$$\begin{aligned} &\int Y_{l_1}^{m_1}(\theta_2, \theta_1) Y_{l_2}^{m_2}(\theta_2, \theta_1) Y_{l_3}^{m_3 *}(\theta_2, \theta_1) \sin \theta_2 d\theta_2 d\theta_1 \\ &= \left[\frac{(2l_1+1)(2l_2+1)}{4\pi(2l_3+1)} \right]^{1/2} (l_1 l_2 m_1 m_2 | l_3 m_3) (l_1 l_2 00 | l_3 0). \end{aligned} \quad (\text{A-79})$$

(b) *Spherical tensors.* A spherical tensor of rank n is defined as $2n+1$ quantities $T_n^{\mu}(\mu = -n, \dots, n)$ which transform in the same way as angular-momentum matrices under a rotation of axes. In symbols,

$$T_n^{\mu'}(c') = \sum_{\mu} T_n^{\mu}(c) \mathcal{D}_{\mu \mu'}^n(\Omega), \quad (\text{A-80})$$

where c and c' indicate two different coordinate systems to which quantities are referred, and the argument Ω of \mathcal{D}^n represents the Euler angles carrying c into c' .

Any vector operator A_x, A_y, A_z can be written as a spherical tensor of rank 1 by means of the definitions

$$T_1^{\pm 1} = \mp 2^{-1/2}(A_x \pm iA_y), \quad T_1^0 = A_z. \quad (\text{A-81})$$

A scalar invariant is a tensor of rank 0.

All tensor operators relevant to a given system have the same commutation relations with the total angular momentum of the system:

$$[J_{\pm}, T_n^{\mu}] = [n(n+1) - \mu(\mu+1)]^{1/2} T_n^{\mu \pm 1}, \quad (\text{A-82a})$$

$$[J_z, T_n^{\mu}] = \mu T_n^{\mu}. \quad (\text{A-82b})$$

A fundamental property of spherical tensors is expressed in the *Wigner-Eckart theorem*, which gives a simple relationship for matrix elements between states with different orientations:

$$\langle \tau' J' M' | T_n^{\mu} | \tau J M \rangle = (\tau' J' || T_n^{\mu} || \tau J) (J n M \mu | J' M'). \quad (\text{A-83})$$

The left side of this equation is the matrix element of T_n^{μ} between any two states; τ represents all quantum numbers other than J and M . As the notation indicates, the quantity $(\tau' J' || T_n^{\mu} || \tau J)$ does not depend on M , M' , or μ ; it is called the *reduced matrix element* and is defined by Eq. A-83.[†]

An immediate consequence of Eq. A-83 is the following important selection rule, which provides the basis for the angular-momentum selection rules in electromagnetic transitions and β -decay: a tensor of rank n has nonzero matrix elements between two states only if $\Delta J \leq n$ and $J + J' \geq n$.

A result which is often required is the reduced matrix element of the vector operator \mathbf{J} itself:

$$(\tau' J' || \mathbf{J} || \tau J) = \delta_{\tau\tau'} \delta_{JJ'} [J(J+1)]^{1/2}.$$

Spherical tensors of various ranks can be constructed from two tensors. Suppose that T_n^{μ} , U_k^{κ} are two tensors; their tensor product of rank N is

$$V_N^Q = \sum_{\mu, \kappa} (nk\mu\kappa | NQ) T_n^{\mu} U_k^{\kappa}. \quad (\text{A-84})$$

Examples of such product tensors are found in the theory of forbidden β -decay. If T_n and U_k both act on the same dynamical variable (e.g., if both are particle operators like \mathbf{r} and \mathbf{p} acting on the same particle), then

$$\begin{aligned} (\tau' J' || V_N^Q || \tau J) &= (-)^{J+J'+N} \sum_{\tau'' J''} \left\{ \begin{matrix} nkN \\ JJ' J'' \end{matrix} \right\} \\ &\times (\tau' J' || T_n^{\mu} || \tau'' J'') (\tau'' J'' || U_k^{\kappa} || \tau J) [(2N+1)(2J''+1)]^{1/2}. \end{aligned} \quad (\text{A-85})$$

[†] Defined by some authors to be $(-)^{2n}(2J'+1)^{1/2}$ times our value.

However, if T_n and U_k act on different spaces, the formula is more complicated and involves $9-j$ symbols; such cases arise when T_n acts on spatial and U_k on spin coordinates, or when T_n and U_k are particle operators acting on different particles.

We shall illustrate the application of Eq. A-85 by using it to derive the relationship employed in Eq. 5-2 to obtain a nuclear magnetic moment. If \mathbf{A} is any vector operator that acts in the same space as the angular momentum \mathbf{J} , then

$$\langle JM | A_z | JM \rangle = \frac{M}{J(J+1)} \langle JM | \mathbf{J} \cdot \mathbf{A} | JM \rangle. \quad (\text{A-86})$$

We begin the proof of this result by noting that the scalar product is

$$\mathbf{J} \cdot \mathbf{A} = -\sqrt{3} V_0^0,$$

where V_0^0 is the tensor product of rank 0, given by

$$V_0^0 = \sum_{\mu} (1 1 \mu - \mu 0 0) J_1^{\mu} A_1^{-\mu}.$$

Now

$$\begin{aligned} \langle JM | V_0^0 | JM \rangle &= (J 0 M 0 | JM) (J || V_0^0 || J) \\ &= (J || V_0^0 || J) \\ &= (-)^{2J} \sum_{J'} \left\{ \begin{matrix} 110 \\ JJJ' \end{matrix} \right\} (J || J_1 || J') (J' || A_1 || J) (2J'+1)^{1/2} \\ &= (-)^{2J} \left\{ \begin{matrix} 110 \\ JJJ \end{matrix} \right\} (J(J+1))^{1/2} (J || A_1 || J) (2J+1)^{1/2}. \end{aligned}$$

The 6- j symbol with a zero is a particularly simple one:

$$\left\{ \begin{matrix} J_1 J_1 0 \\ J_2 J_2 J \end{matrix} \right\} = \frac{(-)^{J+J_1+J_2}}{\sqrt{(2J_1+1)(2J_2+1)}}.$$

Therefore

$$\langle JM | \mathbf{J} \cdot \mathbf{A} | JM \rangle = \sqrt{J(J+1)} (J || A_1 || J).$$

But

$$\begin{aligned} \langle JM | A_z | JM \rangle &= \langle JM | A_1^0 | JM \rangle = (J 1 M 0 | JM) (J || A_1 || J) \\ &= \frac{M}{\sqrt{J(J+1)}} (J || A_1 || J), \end{aligned}$$

and Eq. A-86 follows immediately.

The tensor nature of various electromagnetic operators is important in the process of deducing transition rates in the collective model.

A-3 DIRAC EQUATION

We shall present a summary of the Dirac equation for relativistic fermions, without any detailed discussion of the physical background. As Dirac first suggested, a free relativistic particle of spin $\frac{1}{2}$ may be described by a wave function satisfying a wave equation linear in momentum. The Dirac equation can be written as

$$i \frac{\partial}{\partial t} \psi_p(\mathbf{r}, t) = H \psi_p(\mathbf{r}, t), \quad (\text{A-87})$$

where the Hamiltonian for the free particle is

$$H = \alpha \cdot \mathbf{p} + \beta m. \quad (\text{A-88})$$

The quantities α and β are Hermitian matrices; \mathbf{p} is the momentum operator. We have set $\hbar = c = 1$, but we keep the mass m explicit. The energy and momentum are related relativistically by

$$E^2 = m^2 + p^2. \quad (\text{A-89})$$

We assume a plane-wave solution of Eq. A-87,

$$\psi_p(\mathbf{r}, t) = \psi(\mathbf{p}) \exp[i(\mathbf{p} \cdot \mathbf{r} - Et)]; \quad (\text{A-90})$$

then, from Eqs. A-87 and A-88, we obtain

$$(\alpha \cdot \mathbf{p} + \beta m)\psi(\mathbf{p}) = E\psi(\mathbf{p}). \quad (\text{A-91})$$

For this equation to be consistent with

$$(p^2 + m^2)\psi(\mathbf{p}) = E^2\psi(\mathbf{p}),$$

β and each of the three components of α are required to have square unity and all four must anticommute:

$$\{\alpha_i, \alpha_j\} = 2\delta_{ij}, \quad (\text{A-92a})$$

$$\{\alpha_i, \beta\} = 0, \quad (\text{A-92b})$$

$$\alpha_1^2 = \alpha_2^2 = \alpha_3^2 = \beta^2 = 1, \quad (\text{A-92c})$$

where $\{A, B\} = AB + BA$.

In order that there be four matrices satisfying Eq. A-92, it is necessary that they be of order 4 at least. Many explicit representations are possible,

but we select

$$\alpha = \begin{pmatrix} 0 & \sigma \\ \sigma & 0 \end{pmatrix}, \quad \beta = \begin{pmatrix} 1 & 0 \\ 0 & -1 \end{pmatrix}, \quad (\text{A-93})$$

where σ represents the 2×2 Pauli spin matrices defined in Eq. A-16, and 1 is the 2×2 unit matrix. We also introduce the 4×4 spin matrices, denoted by Σ :

$$\Sigma = \begin{pmatrix} \sigma & 0 \\ 0 & \sigma \end{pmatrix}, \quad (\text{A-94})$$

which are to be interpreted as the spin operators in relativistic calculations.

The fact that the matrices are 4×4 implies that the wave function ψ must have four components. Just as the two components of the spin wave function

$$\alpha = \begin{pmatrix} 1 \\ 0 \end{pmatrix} \quad \text{and} \quad \beta = \begin{pmatrix} 0 \\ 1 \end{pmatrix}$$

are connected with the two spin states in nonrelativistic mechanics, the four components of ψ also have physical significance. In order to see this in more detail, let us write the four-component "spinor" $\psi(\mathbf{p})$ as

$$\psi = \begin{pmatrix} \phi \\ \chi \end{pmatrix}, \quad (\text{A-95})$$

where ϕ and χ are each two-component spinors. Then, writing out Eq. A-91 in detail by using A-93 and A-95, we obtain

$$(\alpha \cdot \mathbf{p})\chi + m\phi = E\phi, \quad (\text{A-96a})$$

$$(\alpha \cdot \mathbf{p})\phi - m\chi = E\chi, \quad (\text{A-96b})$$

where

$$E = \pm |E|, \quad |E| = \sqrt{m^2 + p^2}. \quad (\text{A-97})$$

From Eq. A-96, we see that

$$\chi = \frac{\sigma \cdot \mathbf{p}}{E + m} \phi \quad (\text{A-98})$$

and

$$\phi = \frac{\sigma \cdot \mathbf{p}}{E - m} \chi. \quad (\text{A-99})$$

From these equations, it is clear that, if E is positive, that is, $E = |E|$, then χ is very small compared to ϕ in the nonrelativistic limit, whereas for negative energies, $E = -|E|$, the opposite is true. Thus, for positive and negative energies, we can write the solutions ψ as

$$\begin{aligned}\psi_+ &= \begin{pmatrix} \phi \\ \frac{\sigma \cdot p \phi}{E+m} \end{pmatrix}, & E > 0, \\ \psi_- &= \begin{pmatrix} \chi \\ -\frac{(\sigma \cdot p) \chi}{|E|+m} \end{pmatrix}, & E < 0.\end{aligned}\quad (\text{A-100})$$

By choosing $\begin{pmatrix} 1 \\ 0 \end{pmatrix}$ and $\begin{pmatrix} 0 \\ 1 \end{pmatrix}$ for ϕ as well as χ , we thus find the four independent solutions of the free Dirac equation:

$$\begin{aligned}\psi_+^I &= \begin{pmatrix} 1 \\ 0 \\ \frac{p_z}{E+m} \\ \frac{p_x + ip_y}{E+m} \end{pmatrix}, & \psi_+^{II} &= \begin{pmatrix} 0 \\ 1 \\ \frac{p_x - ip_y}{E+m} \\ \frac{-p_z}{E+m} \end{pmatrix}, & E > 0, \\ \psi_-^I &= \begin{pmatrix} -p_z \\ |E|+m \\ -p_x - ip_y \\ 1 \end{pmatrix}, & \psi_-^{II} &= \begin{pmatrix} -p_x + ip_y \\ |E|+m \\ p_z \\ 0 \end{pmatrix}, & E < 0.\end{aligned}\quad (\text{A-101})$$

Note that the four solutions above are not eigenfunctions of the spin operator Σ_z unless p_x and p_y are set to zero. For the special case in which $p = p_z$,

$$\Sigma_z \psi_{\pm}^I = \psi_{\pm}^I, \quad \Sigma_z \psi_{\pm}^{II} = -\psi_{\pm}^{II}.$$

In this case (and also in the zero momentum limit) ψ_+^I is the positive-energy spin-up solution, ψ_-^{II} is the negative-energy spin-down solution, and so on. More precisely, although an arbitrary component of Σ is not a constant of motion in relativistic mechanics, the component of Σ in the direction of the motion is conserved. Formally, Σ_z does not commute with the Hamiltonian,

but $S(p) = \Sigma \cdot p / p$ does. This important component of the spin is called the "helicity." In the above example, ψ_{\pm}^I have helicity +1 and ψ_{\pm}^{II} have helicity -1. The spinors in Eq. A-101 are not normalized to unity in a unit volume. To do this, we should multiply each spinor by a normalizing factor N :

$$N = \left[1 + \frac{p^2}{(|E|+m)^2} \right]^{-1/2} = \left(\frac{|E|+m}{2|E|} \right)^{1/2}. \quad (\text{A-102})$$

Before proceeding, we point out that there is a simple interpretation for the matrices α_k ($k = 1, 2, 3$), for a free Dirac particle. Consider

$$\dot{x}_k = i[H, x_k] = i[\alpha_k p_j, x_k] = \alpha_k, \quad (\text{A-103})$$

which says that α is the velocity. Complications arise in the relativistic case, however, because α (and therefore the velocity) is not a constant of motion, even for a free particle. In the nonrelativistic limit, however, it is quite proper to treat α as p/m . Similarly, the nonrelativistic limit of β is +1.

For many purposes, it is convenient to write the Dirac equation in a more symmetric form. If we write the coordinates as x_1, x_2, x_3 , and $x_4 = it$, the time-dependent equation A-87 takes the form

$$\left[\frac{\partial}{\partial x_4} + \frac{1}{i} (\alpha \cdot \nabla) + \beta m \right] \Psi = 0.$$

Premultiplying the above equation by β , and putting

$$\begin{aligned}\gamma_k &= -i\beta\alpha_k, & k &= 1, 2, 3, \\ \gamma_4 &= \beta,\end{aligned}\quad (\text{A-104})$$

we obtain

$$\left(\sum_{\mu=1}^4 \gamma_{\mu} \frac{\partial}{\partial x_{\mu}} + m \right) \Psi = 0. \quad (\text{A-105})$$

Since β and α_k are Hermitian, γ_k is also Hermitian. It follows directly from the definition that the γ -matrices anticommute:

$$\{\gamma_{\mu}, \gamma_{\nu}\} = 2\delta_{\mu\nu}. \quad (\text{A-106})$$

We also define the important quantity

$$\gamma_5 = \gamma_1 \gamma_2 \gamma_3 \gamma_4 = i\alpha_1 \alpha_2 \alpha_3, \quad (\text{A-107})$$

which satisfies

$$\gamma_5^2 = 1, \quad \{\gamma_5, \gamma_{\mu}\} = 0, \quad [\gamma_5, \alpha_k] = 0. \quad (\text{A-108})$$

In this representation,

$$\gamma_k = -i \begin{pmatrix} 0 & \sigma_k \\ -\sigma_k & 0 \end{pmatrix} \quad (\text{A-109})$$

and

$$\gamma_5 = \begin{pmatrix} 0 & -1 \\ -1 & 0 \end{pmatrix}. \quad (\text{A-110})$$

Also,

$$\alpha = -\Sigma \gamma_5, \quad \Sigma = -\alpha \gamma_5, \quad (\text{A-111})$$

and

$$[\Sigma, \gamma_5] = 0. \quad (\text{A-112})$$

It must be pointed out that several notations are used for the γ 's. Our notations are the same as those of Rose [10] and Wu and Moszkowski [11]. Some arise naturally from keeping the coordinate x_4 real and distinguishing contravariant and covariant vectors; then Eq. A-105 may look slightly different. In all notations, however, the commutation relations are the same. In our notation, the γ 's are Hermitian, as are α , Σ , and β .

Let us briefly study the Dirac equation in the presence of a central one-body potential $V(r)$, which, for example, may be the Coulomb field produced by the nucleus at the site of the electron. In the relativistic case, even in a central potential, the orbital angular-momentum $\mathbf{l} = \mathbf{r} \times \mathbf{p}$ and Σ are not constants of motion, but \mathbf{j}^2 and j_z are, where $\mathbf{j} = (\mathbf{l} + \frac{1}{2}\Sigma)$ is the total angular momentum. There is another operator

$$K = \beta(\Sigma \cdot \mathbf{l} + 1), \quad (\text{A-113})$$

which also commutes with the Hamiltonian. From the definitions of K and \mathbf{j} , it follows that

$$K^2 = \mathbf{j}^2 + \frac{1}{4}. \quad (\text{A-114})$$

Let us denote the eigenvalues of \mathbf{j}^2 , j_z , and K by $j(j+1)$, μ , and $-\kappa$, respectively. It follows from Eq. A-114 that

$$\kappa = \pm (j + \frac{1}{2}). \quad (\text{A-115})$$

We write the equation $K\psi = -\kappa\psi$, using the two-component spinors ϕ and χ of Eq. A-95,

$$\begin{pmatrix} \sigma \cdot \mathbf{l} + 1 & 0 \\ 0 & -\sigma \cdot \mathbf{l} - 1 \end{pmatrix} \begin{pmatrix} \phi \\ \chi \end{pmatrix} = -\kappa \begin{pmatrix} \phi \\ \chi \end{pmatrix},$$

which can be written as

$$(\sigma \cdot \mathbf{l} + 1)\phi = -\kappa\phi, \quad (\sigma \cdot \mathbf{l} + 1)\chi = +\kappa\chi. \quad (\text{A-116})$$

Thus the two-component spinors ϕ and χ have opposite signs of κ . Note that ϕ and χ are separately eigenfunctions of $\sigma \cdot \mathbf{l}$, with different eigenvalues. Since

$$l^2 = \mathbf{j}^2 - \sigma \cdot \mathbf{l} - \frac{3}{4}, \quad (\text{A-117})$$

it follows that ϕ and χ are separately eigenfunctions of l^2 , although the four-component spinor ψ is not. For a fixed κ , the eigenvalues l_A of ϕ and l_B of χ are completely determined. For example, if $\kappa = j + \frac{1}{2}$, then $l_A = j + \frac{1}{2}$ and $l_B = j - \frac{1}{2}$. For $\kappa = -(j + \frac{1}{2})$, the above values of l_A and l_B become interchanged.

Noting this, let us define two-component spinors ψ_{jl}^μ which are eigenfunctions of \mathbf{j}^2 , j_z , and l^2 :

$$\begin{aligned} \psi_{jl}^\mu &= (l \frac{1}{2} \mu - \frac{1}{2} \frac{1}{2} | j \mu) Y_l^{\mu-(1/2)} \begin{pmatrix} 1 \\ 0 \end{pmatrix} \\ &\quad + (l \frac{1}{2} \mu + \frac{1}{2} - \frac{1}{2} | j \mu) Y_l^{\mu+(1/2)} \begin{pmatrix} 0 \\ 1 \end{pmatrix}. \end{aligned} \quad (\text{A-118})$$

Then we can write

$$\psi = \begin{pmatrix} \phi \\ \chi \end{pmatrix} = \begin{pmatrix} g_\kappa(r) \psi_{jl_A}^\mu \\ i f_\kappa(r) \psi_{jl_B}^\mu \end{pmatrix}, \quad (\text{A-119})$$

where $g_\kappa(r)$ and $f_\kappa(r)$ are radial wave functions to be determined. The factor i is introduced to make $f_\kappa(r)$ real.

If we substitute this form of ψ in the Dirac equation, we find

$$(\sigma \cdot \mathbf{p})\chi = [E - V(r) - m]\phi, \quad (\sigma \cdot \mathbf{p})\phi = [E - V(r) + m]\chi. \quad (\text{A-120})$$

To proceed, we have to know what $\sigma \cdot \mathbf{p}$ does operating on ϕ and χ . Using the identity

$$\sigma \cdot \mathbf{p} = \frac{\sigma \cdot \mathbf{r}}{r^2} \left(-ir \frac{\partial}{\partial r} + i\sigma \cdot \mathbf{l} \right) \quad (\text{A-121})$$

and the relation

$$\frac{\sigma \cdot r}{r} \mathcal{Y}_{jl=j\pm(1/2)}^{\mu} = - \mathcal{Y}_{jl=j\mp(1/2)}^{\mu}, \quad (\text{A-122})$$

we get

$$(\sigma \cdot p)\chi = - \frac{df}{dr} \mathcal{Y}_{jA}^{\mu} - \frac{1-\kappa}{r} f \mathcal{Y}_{jA}^{\mu}$$

and a similar expression for $(\sigma \cdot p)\phi$. Thus the radial form of the Dirac equation is

$$\begin{aligned} -\frac{df}{dr} - \frac{1-\kappa}{r} f &= (E - V - m)g, \\ \frac{dg}{dr} + \frac{1+\kappa}{r} g &= (E - V + m)f. \end{aligned} \quad (\text{A-123})$$

There are two linearly independent solutions to this system, one regular at the origin and one irregular. When V is the Coulomb potential $-Ze^2/r$ for an electron and a point nucleus, the calculation is straightforward. Rose [9] provides the regular solutions to these relativistic Coulomb functions, normalized thus:

$$\int r^2 dr \{f_{\kappa}(E')f_{\kappa}(E) + g_{\kappa}(E')g_{\kappa}(E)\} = \delta(E' - E), \quad (\text{A-124})$$

so that

$$\int dr \psi_{\tau}^H(E')\psi_{\tau}(E) = \delta_{\tau\tau}\delta(E' - E), \quad (\text{A-125})$$

where the superscript H represents the Hermitian adjoint, and τ stands for all quantum numbers, excluding energy. This normalization corresponds to one particle per unit energy interval in all space. Asymptotically,

$$\begin{aligned} f_{\kappa} &\sim -\frac{1}{r} \left(\frac{E-m}{\pi p} \right)^{1/2} \sin(pr + \delta_c), \\ g_{\kappa} &\sim \frac{1}{r} \left(\frac{E+m}{\pi p} \right)^{1/2} \cos(pr + \delta_c), \end{aligned} \quad (\text{A-126})$$

where p is the asymptotic momentum $(E^2 - m^2)^{1/2}$ and δ_c is the Coulomb phase shift:

$$\delta_c = \frac{\alpha Z E}{p} \ln 2pr - \arg \Gamma \left(\gamma + i \frac{\alpha Z E}{p} \right) + \eta - \frac{\pi}{2} \gamma, \quad (\text{A-127})$$

$$\gamma = \kappa^2 - \alpha^2 Z^2, \quad (\text{A-128})$$

and

$$\exp(2i\eta) = - \frac{\kappa - i\alpha Z/p}{\gamma + i\alpha Z E/p}. \quad (\text{A-129})$$

An irregular solution is formed by introducing any constant phase into the arguments of the trigonometric functions in Eq. A-126.

Inside a nucleus of nonzero radius, the solutions will not be Coulomb functions, but outside they will be linear combinations of regular and irregular functions, although the normalization will have changed.

The solution for $Z = 0$ yields the angular-momentum eigenstates of a free particle. This solution is

$$\begin{aligned} f_{\kappa} &= \frac{\kappa}{|\kappa|} \left(\frac{E-m}{\pi p} \right)^{1/2} p j_{l_B}(pr), \\ g_{\kappa} &= \left(\frac{E+m}{\pi p} \right)^{1/2} p j_{l_A}(pr), \end{aligned} \quad (\text{A-130})$$

where the j -functions are spherical Bessel functions. In β -decay, Eqs. A-130 are the low- Z approximation for the electron functions, and, with $E = p$, $m = 0$, they are the neutrino functions.

A-4 STRONG, ELECTROMAGNETIC, AND WEAK INTERACTION HAMILTONIANS

In relativistic mechanics, in going from one inertial frame to another, the velocity of light must be preserved. This is achieved by what is called a Lorentz transformation:

$$x_{\mu}' = \sum_{\nu=1}^4 a_{\mu\nu} x_{\nu}, \quad (\text{A-131})$$

such that

$$\sum_{\mu=1}^4 x_{\mu}^2 = \sum_{\mu=1}^4 x_{\mu}'^2,$$

which implies the orthogonality condition

$$\sum_{\nu} a_{\mu\nu} a_{\lambda\nu} = \delta_{\mu\lambda}.$$

Therefore

$$\det \alpha = \pm 1. \quad (\text{A-132})$$

When $\det \alpha = +1$, it is called a proper Lorentz transformation. This includes ordinary spatial rotations, but not space inversion or time reversal. Space inversion implies changing x_k to $-x_k$ ($k = 1, 2, 3$), while keeping x_4 the same. This changes the "handedness" of the spatial axes.

A quantity that remains invariant under a proper Lorentz transformation as well as space inversion is called a scalar. A pseudoscalar is one that changes sign when the axes change handedness, but is otherwise invariant. Quantities that transform as in Eq. A-131 and whose spatial components change sign under space inversion (like ordinary vectors) are vectors. A pseudovector (also called an axial vector) does not change sign under space inversion.

It turns out that $\psi^+ \psi$ is not invariant under Lorentz transformation, and hence we define an "adjoint" wave function

$$\bar{\psi} = \psi^+ \gamma_4, \quad (\text{A-133})$$

which has the property that $\bar{\psi} \psi$ is a scalar. By inserting appropriate γ 's between $\bar{\psi}$ and ψ , we can also construct other quantities that behave like pseudoscalars, vectors, axial vectors, or tensors under proper Lorentz transformation and space inversion. Both ψ and $\bar{\psi}$ are four-component spinors; hence sixteen bilinear combinations can be made out of them. These can be grouped into five different classes:

- $\bar{\psi} \psi$: scalar (S);
- $i\bar{\psi} \gamma_\mu \psi$: vector with four components (V);
- $\bar{\psi} \sigma_{\mu\nu} \psi$: antisymmetric tensor (T) containing six different components, where $\sigma_{\mu\nu} = (1/2i)(\gamma_\mu \gamma_\nu - \gamma_\nu \gamma_\mu)$;
- $i\bar{\psi} \gamma_\mu \gamma_5 \psi$: axial vector (A) with four components;
- $i\bar{\psi} \gamma_5 \psi$: pseudoscalar (P). (A-134)

The factor i has been introduced in the appropriate quantities to ensure hermiticity. Note that there is no pseudotensor form because the sixteen quantities $\gamma_\mu \gamma_\nu \gamma_5$ are the same sixteen as $\gamma_\mu \gamma_\nu$ but arranged in different order.

In many applications, it is necessary to construct matrix elements of the interaction Hamiltonian involving the above quantities. In the case of strong and electromagnetic interactions, since parity is conserved, the interaction Hamiltonian has to be a scalar. For weak interactions like β -decay, on the other hand, the Hamiltonian must have a pseudoscalar part which violates parity conservation. We now indicate briefly how such matrix elements may be constructed in each of the above cases.

For the electromagnetic case, the current operator of a Dirac particle is $ie\gamma_4 \gamma_\mu$, where e is the electric charge. In the nonrelativistic limit, the three spatial components give rise to the ordinary electric current \mathbf{j} and the fourth component is the charge. The interaction of this current with the electromagnetic field is $ie\gamma_4 \gamma_\mu A_\mu$, where A_μ is the four-potential of the electromagnetic field. The matrix element of this interaction therefore takes the form

$$ie(\psi^+ \gamma_4 \gamma_\mu A_\mu \psi_i) = ie(\bar{\psi} \gamma_\mu A_\mu \psi_i), \quad (\text{A-135})$$

where ψ , and ψ_i are the final and initial states, respectively, of the Dirac particle. For a free particle, expression A-135 contains the interaction of the normal magnetic moment and the charge of the Dirac particle with the electromagnetic potentials. The anomalous magnetic moment arises from an operator $\sigma_{\alpha\beta} q_\beta$, where q_β is the four-momentum transferred to the electromagnetic field.

For strong interactions, there are many ways of constructing the interaction matrix element. Consider the case of pions interacting with nucleons. Now, instead of the vector field A_μ of the electromagnetic case, we have the pionic field ϕ_π , which is a pseudoscalar. This is so since the pion has spin zero and negative intrinsic parity. In order to construct a scalar for the interaction energy of the pion field with nucleons, we recall that $i\bar{\psi} \gamma_5 \psi$ is a pseudoscalar, and therefore $i\bar{\psi} \gamma_5 \phi_\pi$ is an operator with scalar matrix elements between different states of the nucleon. The matrix element of the pseudoscalar interaction thus takes the form

$$i\sqrt{4\pi} g(\psi^+ \gamma_4 \gamma_5 \phi_\pi \psi_i) = i\sqrt{4\pi} g(\bar{\psi} \gamma_5 \phi_\pi \psi_i), \quad (\text{A-136})$$

where g is the pseudoscalar pion-nucleon coupling constant. There are other ways of coupling the pion field with the nucleonic "current." For example, we may use the "gradient coupling" with matrix elements

$$i\sqrt{4\pi} f \left(\bar{\psi} \gamma_\mu \gamma_5 \frac{\partial}{\partial x_\mu} \phi_\pi \psi_i \right), \quad (\text{A-137})$$

where f is the appropriate coupling constant.

For a vector meson with four components ϕ_μ , the interaction matrix elements take the same form as the electromagnetic case (cf. Eq. A-135):

$$i\sqrt{4\pi} g_v(\bar{\psi} \gamma_\mu \phi_\mu \psi_i), \quad (\text{A-138})$$

where g_v is the corresponding coupling constant. Finally, for a vector meson, there can be the gradient coupling also:

$$\sqrt{4\pi} f_v \left[\bar{\psi}_i \sigma_{\mu\nu} \left(\frac{\partial \phi_\nu}{\partial x_\mu} - \frac{\partial \phi_\mu}{\partial x_\nu} \right) \psi_i \right]. \quad (\text{A-139})$$

In the case of weak interactions, the important point is that the Hamiltonian must contain both scalar and pseudoscalar parts. In addition, we must distinguish between the wave functions of the baryons and the leptons. A general way of writing the interaction matrix element is

$$(\bar{\Psi}_f O \Psi_i)(\bar{\Psi}_i O_L \psi_i), \quad (\text{A-140})$$

where Ψ_f and Ψ_i are the final and initial baryonic states, while ψ_i and ψ_i are the corresponding leptonic ones. The operator O acts on the baryonic states, and O_L on the leptonic ones only. Different possible forms of O and O_L are used in β -decay theory. For example, we may take

$$O = C_V \gamma_\mu + C_A \gamma_\mu \gamma_5 \quad \text{and} \quad O_L = \gamma_\mu (1 + \gamma_5),$$

with C_V and C_A as constants to be determined by experiments.

REFERENCES

1. E. U. Condon and G. H. Shortley, *The Theory of Atomic Spectra*, Cambridge University Press, London, 1935; Formulas of Clebsch-Gordan coefficients for $J_3 = \frac{1}{2}, 1, \frac{3}{2}, 2$.
2. D. L. Falkoff, G. S. Holladay, and R. E. Sells, *Can. J. Phys.* **30**, 253 (1952). Formulas of Clebsch-Gordan coefficients for $J_3 = 3$.
3. M. A. Melvin and N. V. J. Swamy, *Phys. Rev.* **107**, 186 (1957). Formulas of Clebsch-Gordan coefficients for $J_3 = \frac{5}{2}$.
4. A. Simon, *Numerical Table of the Clebsch-Gordan Coefficient*, U.S.A.E.C. Rept. ORNL-1718, 1954. Given as decimal fractions for any $J \leq \frac{9}{2}$.
5. M. Rotenberg, R. Bivins, N. Metropolis, and J. K. Wooten, *The 3-j and 6-j Symbols*, The Technology Press, Massachusetts Institute of Technology, Cambridge, Mass. 1959. All Clebsch-Gordan coefficients with all three $J \leq 8$ are given as rational fractions.
6. A. R. Edmonds, *Angular Momentum in Quantum Mechanics*, Princeton University Press, Princeton, N.J., 1957.
7. M. E. Rose, *Elementary Theory of Angular Momentum*, John Wiley, New York, 1957.
8. E. P. Wigner, *Group Theory and Its Applications to Quantum Mechanics of Atomic Spectra*, Academic Press, New York, 1958.
9. M. E. Rose, *Phys. Rev.* **51**, 484 (1937).
10. M. E. Rose, *Relativistic Electron Theory*, John Wiley, New York, 1961.
11. C. S. Wu and S. A. Moszkowski, *Beta Decay*, John Wiley, New York, 1966.

Appendix B

Some Results Used in Scattering Theory

B-1 RADIAL WAVE FUNCTIONS

For the scattering of two particles, the radial wave equation outside the region of nuclear interaction is

$$\frac{d^2 u}{dp^2} + \left[1 - \frac{2\eta}{p} - \frac{l(l+1)}{p^2} \right] u = 0, \quad (\text{B-1})$$

where

$$\rho = kr, \quad k = \frac{mv}{\hbar}, \quad \eta = \frac{Z_1 Z_2 e^2}{\hbar v}, \quad (\text{B-2})$$

and the various quantities are the reduced mass, relative velocities, and so forth, appropriate to the center-of-mass system.

It is easy to check by differentiation that, for ρ large enough to ignore ρ^{-2} in comparison with unity, Eq. B-1 is satisfied by taking u as either the sine or the cosine of the argument $(\rho - \eta \ln \rho + \text{constant})$. The constant is selected to make the solution $\sin(\rho - \eta \ln \rho + \text{constant})$ become the asymptotic form of the solution of Eq. B-1, which is regular at $\rho = 0$. The equation is the confluent hypergeometric equation, which has been thoroughly studied; we shall merely quote results. If one particle is neutral, $\eta = 0$, and the equation is a form of Bessel's equation.

We shall denote the regular solution of Eq. B-1 by F_l ; it is defined by insisting that $F_l(0) = 0$ and that its asymptotic oscillations have unit amplitude. Then it can be shown that

$$F_l \sim \sin(\rho - \eta \ln 2\rho - \frac{1}{2}l\pi + \sigma_l), \quad (\text{B-3})$$

where

$$\sigma_l = \arg \Gamma(l+1+i\eta) = \sigma_0 + \sum_{s=1}^l \tan^{-1} \frac{\eta}{s}. \quad (\text{B-4})$$

For the other independent solution, we choose the one that is asymptotically out of phase by $\pi/2$:

$$G_l = \cos(\rho - \eta \ln 2\rho - \frac{1}{2}l\pi + \sigma_l). \quad (\text{B-5})$$

Then the Wronskian is

$$G_l \frac{dF_l}{d\rho} - F_l \frac{dG_l}{d\rho} = 1. \quad (\text{B-6})$$

Complete series expansions about $\rho = 0$ may be given, but we shall simply note that F_l is a series of ascending powers beginning with a term in ρ^{l+1} , and that G_l consists of two series, one beginning with a term in ρ^{-l} and the other starting with ρ^{l+1} and being multiplied by $\ln 2\rho$. For $l = 0$,

$$F_0(\rho) = C_0 \rho(1 + \eta\rho + \dots), \quad (\text{B-7a})$$

$$G_0(\rho) = \frac{1}{C_0} \{1 + 2\eta\rho[\ln 2\eta\rho + 2\gamma - 1 + h(\eta)] + \dots\}, \quad (\text{B-7b})$$

where

$$C_0^2 = 2\pi\eta[\exp(2\pi\eta) - 1]^{-1}, \quad (\text{B-8a})$$

γ = Euler's constant = 0.57722...,

$$h_0(\eta) = \eta^2 \sum_{n=1}^{\infty} \frac{1}{n(n^2 + \eta^2)} - \ln \eta - \gamma. \quad (\text{B-8b})$$

For $l > 0$, the behavior for small ρ is

$$F_l = C_l \rho^{l+1} \left(1 + \frac{\eta\rho}{l+1} + \dots\right), \quad (\text{B-9a})$$

$$G_l = \frac{1}{(2l+1)C_l} \rho^{-l} \left[1 + O\left(\frac{\eta\rho}{l}\right)\right], \quad (\text{B-9b})$$

where

$$C_l = C_0 \frac{1}{(2l+1)!!} \prod_{s=1}^l \left(1 + \frac{\eta^2}{s^2}\right)^{1/2}$$

$$= 2^l \exp(-\frac{1}{2}\pi\eta) \frac{|\Gamma(l+1+i\eta)|}{(2l+1)!}$$

and $(2l+1)!! = 1 \cdot 3 \cdot 5 \cdots (2l+1)$.

In a scattering experiment, the incoming and outgoing Coulomb waves are taken as

$$I_l = \exp(i\omega_l) (G_l - iF_l) \sim \exp[-i(\rho - \eta \ln 2\rho - \frac{1}{2}l\pi + \sigma_0)], \quad (\text{B-10a})$$

$$O_l = \exp(-i\omega_l) (G_l + iF_l) \sim \exp[i(\rho - \eta \ln 2\rho - \frac{1}{2}l\pi + \sigma_0)]. \quad (\text{B-10b})$$

For uncharged particles, the functions F_l and G_l are replaced by spherical Bessel functions, $j_l(\rho)$ and $n_l(\rho)$, according to

$$F_l \rightarrow \rho j_l(\rho), \quad G_l \rightarrow -\rho n_l(\rho). \quad (\text{B-11})$$

These Bessel functions in turn behave as follows:

$$j_l(\rho) \sim \rho^{-1} \sin(\rho - \frac{1}{2}l\pi), \quad (\text{B-12a})$$

$$n_l(\rho) \sim -\rho^{-1} \cos(\rho - \frac{1}{2}l\pi), \quad (\text{B-12b})$$

$$n_l \frac{dj_l}{d\rho} - j_l \frac{dn_l}{d\rho} = -\frac{1}{\rho^2}. \quad (\text{B-13})$$

At small ρ ,

$$j_l = \frac{\rho^l}{(2l+1)!!} \left[1 - \frac{\rho^2}{2(2l+3)} + \dots\right], \quad (\text{B-14a})$$

$$n_l = -\frac{(2l-1)!!}{\rho^{l+1}} \left[1 + \frac{\rho^2}{2(2l-1)} + \dots\right]. \quad (\text{B-14b})$$

The spherical Bessel functions are related to the Bessel functions by

$$j_l(\rho) = \left(\frac{\pi}{2\rho}\right)^{1/2} J_{l+(1/2)}(\rho), \quad (\text{B-15a})$$

$$n_l(\rho) = (-)^{l+1} \left(\frac{\pi}{2\rho}\right)^{1/2} J_{-l-(1/2)}(\rho). \quad (\text{B-15b})$$

The incoming wave is

$$I_l = -i\rho h_l^{(2)}(\rho) = -i\rho(j_l - in_l) \sim \exp[-i(\rho - \frac{1}{2}l\pi)], \quad (\text{B-16a})$$

and the outgoing wave is

$$O_l = i\rho h_l^{(1)}(\rho) = i\rho(j_l + in_l) \sim \exp[i(\rho - \frac{1}{2}l\pi)], \quad (\text{B-16b})$$

where we have introduced the spherical Hankel functions $h_l^{(1)}$ and $h_l^{(2)}$.

We also note the explicit forms

$$\begin{aligned} j_0(\rho) &= \frac{\sin \rho}{\rho}, & n_0(\rho) &= -\frac{\cos \rho}{\rho}; \\ j_1(\rho) &= \frac{\sin \rho}{\rho^2} - \frac{\cos \rho}{\rho}, & n_1(\rho) &= -\frac{\cos \rho}{\rho^2} - \frac{\sin \rho}{\rho}. \end{aligned} \quad (\text{B-17})$$

The functions F_l and ρj_l begin to increase at small ρ like ρ^{l+1} , then they increase more quickly, and after the point

$$\rho = \eta + [\eta^2 + l(l+1)]^{1/2}$$

they oscillate, the period and amplitude of the oscillations gradually tending to the asymptotic forms.

B-2 EFFECTIVE-RANGE FORMULA

Consider s-wave proton-proton scattering with the radial function in the center-of-mass system given by

$$\frac{d^2 u_1}{dr^2} - \left[\frac{1}{Rr} + V(r) \right] u_1 = -k_1^2 u_1, \quad (\text{B-18})$$

where $R = \eta_1/k_1 = \hbar^2/Mc^2$ as in Eq. 2-50, and $V(r)$ is the nuclear potential multiplied by M/\hbar^2 . We write the same equation for a different energy:

$$\frac{d^2 u_2}{dr^2} - \left[\frac{1}{Rr} + V(r) \right] u_2 = -k_2^2 u_2. \quad (\text{B-19})$$

If we multiply Eq. B-18 by u_2 , B-19 by u_1 , subtract, and integrate from r to r' , we obtain

$$\left(u_2 \frac{du_1}{dr} - u_1 \frac{du_2}{dr} \right) \Big|_r^{r'} = (k_2^2 - k_1^2) \int_r^{r'} u_1 u_2 dr. \quad (\text{B-20})$$

We denote the asymptotic form of u by ϕ ; then ϕ satisfies Eq. B-18 with $V(r)$ omitted, which is the Coulomb equation.

A similar procedure yields

$$\left(\phi_2 \frac{d\phi_1}{dr} - \phi_1 \frac{d\phi_2}{dr} \right) \Big|_r^{r'} = (k_2^2 - k_1^2) \int_r^{r'} \phi_1 \phi_2 dr. \quad (\text{B-21})$$

By subtracting Eq. B-20 from B-21, we obtain

$$\phi_2 \phi_1' - \phi_1 \phi_2' - u_2 u_1' + u_1 u_2' \Big|_r^{r'} = (k_2^2 - k_1^2) \int_r^{r'} (\phi_1 \phi_2 - u_1 u_2) dr. \quad (\text{B-22})$$

We now choose the limit r' so large that $u(r')$ has reached its asymptotic value. Consequently the upper limit on the left-hand side of Eq. B-22 is zero, and, since the integrand on the right vanishes for $r > r'$, we may write

$$(\phi_2 \phi_1' - \phi_1 \phi_2' - u_2 u_1' + u_1 u_2')_r = (k_2^2 - k_1^2) \int_r^\infty (\phi_1 \phi_2 - u_1 u_2) dr. \quad (\text{B-23})$$

Since u_1 and u_2 are solutions for the physical problem, they vanish at $r = 0$. Since the ϕ 's are solutions of the Coulomb equation and are the asymptotic forms of the u 's, we have

$$\phi \propto \sin(\rho - \eta \ln 2\rho + \sigma_0 + \delta)$$

when δ is the nuclear phase shift. The proportionality factor determines the wave-function normalization, but clearly divides through Eq. B-23. We therefore choose

$$\phi_i = C_{0i}[G_0(k_i r) + \cot \delta_i F_0(k_i r)].$$

Equations B-7 show that, as r tends to zero, the limit of ϕ is unity. There is therefore no problem of convergence in the integral in Eq. B-23 if we let r approach zero.

We still require the derivative of ϕ for small r . Again using Eq. B-7, we see that

$$\phi_i' = \frac{d\phi_i}{dr} = \frac{1}{R} \left(\ln \frac{r}{R} + 2\gamma \right) + \frac{1}{R} h(\eta_i) + C_{0i}^2 k_i \cot \delta_i.$$

Therefore, the limit of Eq. B-23 as r tends to zero is

$$\begin{aligned} &\frac{1}{R} [h(\eta_2) - h(\eta_1)] + C_{02}^2 k_2 \cot \delta_2 - C_{01}^2 k_1 \cot \delta_1 \\ &= (k_2^2 - k_1^2) \int_0^\infty (\phi_1 \phi_2 - u_1 u_2) dr. \end{aligned} \quad (\text{B-24})$$

We now let k_1 tend to zero and define

$$-a_p^{-1} \equiv \lim_{k_1 \rightarrow 0} C_{02}^2 k_2 \cot \delta_2 + \frac{1}{R} h(\eta), \quad (\text{B-25})$$

which is a generalization of Eq. 2-33.

We may now rewrite Eq. B-24 as

$$C_{02}^2 k_2 \cot \delta_2 + \frac{h(\eta)}{R} = -\frac{1}{a_p} + k^2 \int_0^\infty (\phi \phi_0 - uu_0) dr. \quad (\text{B-26})$$

This equation is exact; we obtain the effective-range expansion, Eq. 2-57, by defining

$$r_0 = 2 \int_0^\infty (\phi_0^2 - u_0^2) dr, \quad (B-27)$$

and by noting that at low energies

$$\phi(k; r) = \phi_0(r) + O(k^2).$$

The simpler derivation of the effective-range formula for neutron-proton scattering is left to the reader.

B-3 DERIVATION OF THE PROTON-PROTON SCATTERING CROSS SECTION

For particles incident along the z -axis, the total wave function is

$$\psi = \sum c_l r^{-1} u_l(r) P_l(\cos \theta), \quad (B-28)$$

where u_l satisfies

$$\frac{d^2 u_l}{dr^2} + \left[k^2 - \frac{1}{Rr} + V(r) - \frac{l(l+1)}{r^2} \right] u_l = 0.$$

Outside the nuclear potential, u_l is a linear combination of the Coulomb functions F_l and G_l , so that

$$u_l(r) \sim \sin(kr - \eta \ln 2kr - \frac{1}{2}l\pi + \sigma_l + \delta_l), \quad (B-29)$$

where δ_l is the change in the phase shift due to the potential $V(r)$. Note that δ_l is *not* the phase shift that $V(r)$ would produce in the absence of a Coulomb force.

Now the coefficients c_l in Eq. B-28 must be chosen so that the only incoming waves are those in the incident beam. The presence of the Coulomb force somewhat complicates the problem, since a plane wave $\exp(ikz)$ is not a solution of

$$\left(\nabla^2 + k^2 - \frac{1}{Rr} \right) \psi = 0,$$

even for large r . However, it can be verified by differentiating that $\exp\{i[kz + \eta \ln k(r-z)]\}$ is a solution for large r to order $1/r^2$; this expression is the Coulomb distorted plane wave, and it can be shown that

$$\begin{aligned} \exp\{i[kz + \eta \ln k(r-z)]\} &\sim \sum_{l=0}^{\infty} (2l+1)i^l (kr)^{-l} \\ &\times \sin(kr - \eta \ln 2kr - \frac{1}{2}l\pi) P_l(\cos \theta). \end{aligned}$$

Hence, if we set $c_l = (2l+1)k^{-1}i^l \exp[i(\delta_l + \sigma_l)]$ in Eq. B-28, we have

$$\psi = \exp\{i[kz + \eta \ln k(r-z)]\} - f(\theta) \frac{1}{r} \exp[i(kr - \eta \ln 2kr)], \quad (B-30)$$

where

$$f(\theta) = -\frac{1}{2ik} \sum_{l=0}^{\infty} (2l+1)\{\exp[2i(\delta_l + \sigma_l)] - 1\} P_l(\cos \theta). \quad (B-31)$$

For pure Coulomb scattering ($\delta_l = 0$), it can be shown from the properties of the Coulomb functions[†] that the amplitude $f(\theta)$ can be summed to give

$$f_c(\theta) = -\frac{1}{4k^2 R} \operatorname{cosec}^2 \frac{\theta}{2} \exp\left(-2i\eta \ln \sin \frac{\theta}{2} + i\pi + 2i\sigma_0\right). \quad (B-32)$$

Hence $f = f_c + f_N$, where, as in Eq. 5-27,

$$f_N = -\frac{1}{2ik} \sum (2l+1)e^{2i\sigma_l}(e^{2i\delta_l} - 1) P_l(\cos \theta).$$

To find the proton-proton cross section we must take account of the identity of the two particles. Interchange of their coordinates is equivalent to replacing θ by $\pi - \theta$. Hence the spatial wave function must be taken in singlet spin states as

$$\psi(r, \theta) + \psi(r, \pi - \theta),$$

and in triplet states as

$$\psi(r, \theta) - \psi(r, \pi - \theta).$$

Since $P_l(\cos \theta)$ has the parity of l , Eq. B-31 shows that these combinations automatically eliminate both singlet odd and triplet even states.

A wave function of form B-30 describes a unit incident proton flux and an outgoing flux through any large sphere of $|f(\theta)|^2$ particles per unit solid angle per second. In other words, $\sigma(\theta) = |f(\theta)|^2$. Therefore the scattering cross section is given in a singlet state as

$$|f(\theta) + f(\pi - \theta)|^2,$$

[†] For example, L. Schiff, *Quantum Mechanics*, 1st ed., McGraw-Hill, New York, 1949, p. 116.

and in a triplet state as

$$|f(\theta) - f(\pi - \theta)|^2.$$

In experiments with unpolarized beams, the relative weights of triplet and singlet states are 3 to 1; moreover, their contributions add incoherently. We thus obtain the final result,

$$\begin{aligned}\sigma(\theta) &= \frac{3}{4}|f(\theta) - f(\pi - \theta)|^2 + \frac{1}{4}|f(\theta) + f(\pi - \theta)|^2 \\ &= |f(\theta)|^2 + |f(\pi - \theta)|^2 - \operatorname{Re}[f^*(\theta)f(\pi - \theta)],\end{aligned}\quad (\text{B-33})$$

which is Eq. 5-36. The first term can be considered to describe direct scattering, the second exchange scattering, and the third the interference between the direct and exchange waves. By substituting the expression in Eq. B-32 for $f(\theta)$, we obtain by direct calculation from Eq. B-33 the Mott scattering due only to the Coulomb force:

$$\sigma_{\text{Mott}} = \left(\frac{e^2}{4E}\right)^2 \left[\operatorname{cosec}^4 \frac{\theta}{2} + \sec^4 \frac{\theta}{2} - \operatorname{cosec}^2 \frac{\theta}{2} \sec^2 \frac{\theta}{2} \cos\left(\eta \ln \tan \frac{\theta}{2}\right) \right], \quad (\text{B-34})$$

where all quantities are measured in the center-of-mass system.

When nuclear forces are present, it is easy to see that Eq. B-33 may be written as

$$\sigma(\theta) = \sigma_{\text{Mott}}(\theta) + \sigma_N(\theta) + \sigma_{NC}(\theta), \quad (\text{B-35})$$

where $\sigma_N(\theta)$, which involves only the nuclear phase shifts δ_i , and $\sigma_{NC}(\theta)$, which involves Coulomb-nuclear interference terms, are given by

$$\sigma_N(\theta) = |f_N(\theta)|^2 + |f_N(\pi - \theta)|^2 - \operatorname{Re}[f_N^*(\theta)f_N(\pi - \theta)], \quad (\text{B-36})$$

$$\begin{aligned}\sigma_{NC}(\theta) &= \operatorname{Re}\{f_C^*(\theta)[2f_N(\theta) - f_N(\pi - \theta)] \\ &\quad + f_C^*(\pi - \theta)[2f_N(\pi - \theta) - f_N(\theta)]\}.\end{aligned}\quad (\text{B-37})$$

It is left to the reader as a straightforward exercise to obtain the following result for the differential cross section when two protons scatter at an energy low enough so that the nuclear force is entirely in the S -state:

$$\begin{aligned}\sigma(\theta) &= \left(\frac{e^2}{4E}\right)^2 \left[\operatorname{cosec}^4 \frac{\theta}{2} + \sec^4 \frac{\theta}{2} - \operatorname{cosec}^2 \frac{\theta}{2} \sec^2 \frac{\theta}{2} \cos\left(\eta \ln \tan \frac{\theta}{2}\right) \right] \\ &\quad - \left(\frac{e^2}{4E}\right) \frac{1}{k} \sin \delta \left[\operatorname{cosec}^2 \frac{\theta}{2} \cos\left(\delta + \eta \ln \sin \frac{\theta}{2}\right) \right. \\ &\quad \left. + \sec^2 \frac{\theta}{2} \cos\left(\delta + \eta \ln \cos \frac{\theta}{2}\right) \right] + \left(\frac{1}{k^2}\right) \sin^2 \delta.\end{aligned}$$

B-4 COHERENT-SCATTERING LENGTH

The possibility of coherent scattering arises when a slow neutron is scattered by a target containing several scattering centers, such as a molecule or a crystal. For very slow neutrons, the neutron wavelength may be comparable to or greater than the relative distances between the individual scatterers. In this case, the incident neutron wave interacts with many scattering centers at the same time. The scattered waves from individual centers may have a phase relationship if the individual scatterers have similar scattering characteristics, thus giving rise to interference and coherent scattering. On the other hand, random phase differences between individual scatterers will give rise to incoherent scattering. In coherent scattering all the scattering centers participate in a collective way, whereas they act independently in incoherent scattering.

The simplest (and historically the most important) example is the scattering of slow neutrons ($\lambda \sim 7 \text{ \AA}$) from molecular hydrogen. The two protons in H_2 can have a total spin $S_H = 1$ (orthohydrogen) or 0 (parahydrogen). The interproton distance is less than 1 \AA , and the two scattering centers are very similar; hence the conditions for coherent scattering are satisfied. In coherent scattering, the amplitudes of the scattered waves should be added. The scattering amplitude f_k is given by Eq. 2-31; and in the limit $k \rightarrow 0$, using Eq. 2-33, $f_k = -a$, where a is the scattering length.

We denote the spin operator of the incident neutron by $s_n = \frac{1}{2}\sigma_n$ and, similarly, the spins of the two protons in H_2 by s_{p_1} and s_{p_2} . Then the general amplitude for the scattering of a neutron by a proton is

$$\hat{a} = \frac{1}{2}(3a_t + a_s) + (a_t - a_s)s_n \cdot s_p. \quad (\text{B-38})$$

In this equation, \hat{a} is to be regarded as an operator, which yields the correct scattering length when its expectation value is taken with respect to the appropriate wave function. This is so because, by using the equations immediately preceding Eq. 2-6, $\langle s_n \cdot s_p \rangle = -\frac{1}{4}$ for the singlet and $+\frac{1}{4}$ for the triplet state. The total amplitude for the scattering of the neutron from the two protons in H_2 is therefore

$$\hat{a}_H = \frac{1}{2}(3a_t + a_s) + (a_t - a_s)s_n \cdot S_H, \quad (\text{B-39})$$

where $S_H = s_{p_1} + s_{p_2}$.

The cross section of scattering from the hydrogen molecule with a given S_H and S_{zH} by an unpolarized neutron beam is

$$\sigma_{\text{mol}} = \frac{1}{2} \sum_{S_{zn}} \langle s_{zn} S_{zH} S_H^2 | 4\pi \hat{a}_H^2 | s_{zn} S_{zH} S_H^2 \rangle. \quad (\text{B-40})$$

Since

$$\sum_{S_{zn}} \langle S_n \cdot S_H \rangle = 0, \quad \frac{1}{2} \sum_{S_{zn}} \langle (S_n \cdot S_H)^2 \rangle = \frac{1}{4} S_H(S_H + 1), \quad (B-41)$$

Eq. B-40 yields,

$$\begin{aligned} \sigma_{\text{ortho}} &= \pi(3a_t + a_s)^2 + 2\pi(a_t - a_s)^2, \\ \sigma_{\text{para}} &= \pi(3a_t + a_s)^2. \end{aligned} \quad (B-42)$$

If the nuclear force were spin independent, then $a_t = a_s$, giving $\sigma_{\text{ortho}} = \sigma_{\text{para}}$. Early experiments showed that $\sigma_{\text{ortho}} \gg \sigma_{\text{para}}$. Since a_t has a positive sign, this indicates that a_s is large and negative. For parahydrogen, since $S_H = 0$, the coherent-scattering amplitude is

$$a_H = \frac{1}{2}(3a_t + a_s). \quad (B-46)$$

Interference between neutron waves scattered coherently by nuclei gives rise to optical phenomena like total reflection. Denote the wave number of the neutron wave by k in vacuum; then this is altered to some value k' inside the scattering medium because of interference between the waves. The refractive index of the medium is defined as

$$n = \frac{k'}{k}, \quad (B-43)$$

and if this is less than 1, there can be total reflection. The refractive index is simply related to the coherent-scattering amplitude of the scattering centers in the medium. If it is assumed for simplicity that there are N molecules per unit volume, all of the same kind with coherent-scattering amplitude A_{mol} ,

$$n = 1 - \frac{\lambda^2}{2\pi} N A_{\text{mol}}. \quad (B-44)$$

A simple derivation of this formula can be given, following Lord Rayleigh [1]. Let a plane neutron wave $\exp(ikz)$ be incident on a layer of thickness l of the medium, with $l \gg \lambda$, the wavelength of the neutron. When the wave emerges from the layer, it is given on the z -axis by

$$\begin{aligned} \exp[ik'l + ik(z - l)] &= \exp[ink l + ik(z - l)] \\ &= \exp(ikz) \exp[ikl(n - 1)]. \end{aligned} \quad (B-45)$$

The number of scattering centers in the elementary volume shown in Fig. B-1 is $(yl dy d\phi)N$; hence, when the transmitted beam is written as a sum of the incident plus the coherently scattered waves, it takes the form

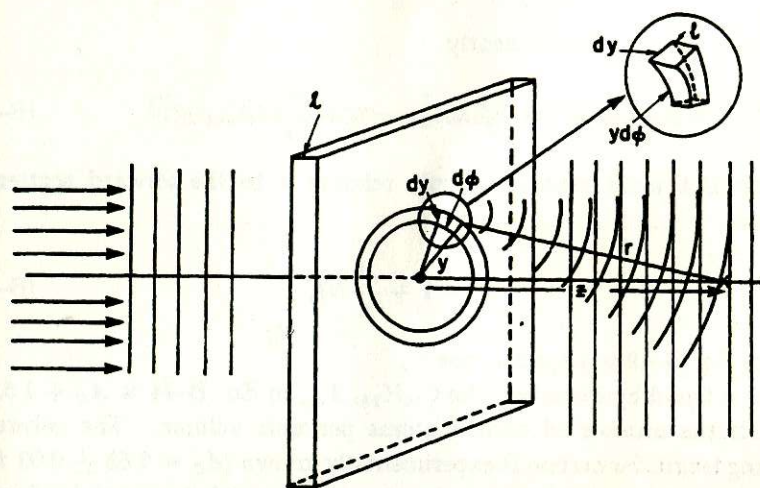


Fig. B-1 Neutron Refractive Index. The slab of scattering matter is of thickness $l \gg \lambda$. A neutron beam coming from the left parallel to the z -axis has plane wave fronts suggested by the perpendicular lines. Neutrons scattered in the indicated volume element constitute a spherical wave whose wave fronts are suggested by the arcs along the ray of length r .

$$e^{ikz} + 2\pi l N A_{\text{mol}} \int_0^\infty \frac{e^{ikr}}{r} y dy, \quad (B-46)$$

where $r = \sqrt{y^2 + z^2}$. Equation B-46 may be rewritten in the form

$$\exp(ikz) - 2\pi l N A_{\text{mol}} \int_z^\infty \exp(ikr) dr. \quad (B-47)$$

Using the relation

$$\int_z^\infty e^{ikr} dr = \lim_{p \rightarrow 0} \int_z^\infty e^{ikr} e^{-pr} dr = -\frac{\exp(ikz)}{ik},$$

the transmitted wave on the z -axis is given by

$$e^{ikz} \left(1 - i \frac{2\pi l N A_{\text{mol}}}{k} \right). \quad (B-48)$$

Equating this with the alternative form B-45, we can write

$$\exp[ikl(n-1)] \approx 1 + ikl(n-1) = 1 - \frac{i2\pi l N A_{\text{mol}}}{k},$$

since $k(n-1) \ll 1$. Consequently,

$$n = 1 - \frac{2\pi}{k^2} N A_{\text{mol}} = 1 - \frac{\lambda^2}{2\pi} N A_{\text{mol}}. \quad (\text{B-49})$$

There is a more general formula relating n to the forward scattering amplitude,

$$n^2 = 1 + \frac{\lambda^2}{\pi} N f_k. \quad (\text{B-50})$$

of which Eq. B-49 is a special case.

With a liquid hydrocarbon like $\text{C}_{12}\text{H}_{18}$, A_{mol} in Eq. B-44 is $A_C + 1.5A_H$, and N is the number of carbon atoms per unit volume. The coherent-scattering length for carbon is experimentally known ($A_C = 6.63 \pm 0.03$ fm). This compound has n slightly less than 1, so it is possible to do total reflection experiments. For the grazing angle θ_c for total reflection, using Snell's law, we can write

$$\cos \theta_c = 1 - \frac{\theta_c^2}{2} = n = 1 - \frac{\lambda^2}{2\pi} N(A_C + 1.5A_H)$$

and

$$\theta_c = \lambda \left[\frac{N(A_C + 1.5A_H)}{\pi} \right]^{1/2}. \quad (\text{B-51})$$

Accurate determination of θ_c therefore determines A_H , since A_C is known from other sources.

Fermi and Marshall [2] first used this method to determine the coherent-scattering lengths of various elements. More recent extensive work was done by Koester [3], who measured the critical angle θ_c for the total reflection of neutrons from the "mirror" surface of various hydrocarbons.

REFERENCES

1. Lord Rayleigh, *Phil. Mag.* **47**, 375 (1899).
2. E. Fermi and L. Marshall, *Phys. Rev.* **71**, 666 (1947); **72**, 408 (1947).
3. L. Koester, *Z. Phys.* **198**, 187 (1967); **203**, 515 (E) (1967).

Appendix C

The Notation of Second Quantization

C-1 THE WAVE FUNCTION OF A MANY-FERMION SYSTEM

For a system of identical fermions in the independent-particle model, the Slater determinantal wave function ensures the indistinguishability of the particles and the antisymmetry under the exchange of any two particle coordinates. Since it is not meaningful, however, to determine which particle is in which single-particle state, the particle indices are really superfluous. This suggests the adoption of an occupation number representation, in which only the state labels are used, and one requires to know only which states are occupied. Since what is being exploited is the indistinguishability of the particles, this method is quite general and can be used for bosons as well, provided that one indicates in some way the number of particles in each state.

In the so-called occupation number representation, also called second quantization, algebraic manipulations are easily done in a systematic and concise manner. In what follows, we shall explain this notation, concentrating specifically on fermions.

Let us denote a complete set of single-particle states by $\{\alpha\}$: $\alpha_1, \alpha_2, \alpha_A$, etc. Here α stands for a whole set of quantum numbers which uniquely defines a single-particle state. Then an A -fermion determinantal wave function is denoted by

$$\frac{1}{\sqrt{A!}} \begin{vmatrix} \phi_{\alpha_1}(1) & \cdots & \phi_{\alpha_1}(A) \\ \vdots & & \vdots \\ \phi_{\alpha_A}(1) & \cdots & \phi_{\alpha_A}(A) \end{vmatrix} \equiv \frac{1}{\sqrt{A!}} \det \{\alpha_1 \cdots \alpha_A\}. \quad (\text{C-1})$$

In this equation, $(1) \cdots (A)$ are particle indices. In the second quantized notation, we define a set of operators a_α^+ and a vacuum state $|0\rangle$, such that

$$a_{\alpha_1}^+ a_{\alpha_2}^+ \cdots a_{\alpha_A}^+ |0\rangle \quad (C-2)$$

is identical to C-1 and represents a many-body state in which $\alpha_1, \alpha_2, \dots, \alpha_A$ are singly occupied by particles. For the equivalence between C-1 and C-2 to hold, the operators a_α^+ have to obey certain algebraic relations. Since

$$\begin{aligned} a_{\alpha_1}^+ a_{\alpha_2}^+ \cdots a_{\alpha_A}^+ |0\rangle &\equiv \frac{1}{\sqrt{A!}} \det \{\alpha_1 \alpha_2 \cdots \alpha_A\} \\ &= -\frac{1}{\sqrt{A!}} \det \{\alpha_2 \alpha_1 \cdots \alpha_A\} \\ &= -a_{\alpha_1}^+ a_{\alpha_2}^+ \cdots a_{\alpha_A}^+ |0\rangle, \end{aligned}$$

it follows that

$$a_{\alpha_1}^+ a_{\alpha_2}^+ = -a_{\alpha_2}^+ a_{\alpha_1}^+$$

or

$$\{a_{\alpha_1}^+, a_{\alpha_2}^+\} = a_{\alpha_1}^+ a_{\alpha_2}^+ + a_{\alpha_2}^+ a_{\alpha_1}^+ = 0. \quad (C-3)$$

Similarly, defining the Hermitian conjugate of these operators, we obtain

$$\{a_{\alpha_1}, a_{\alpha_2}\} = 0. \quad (C-4)$$

Furthermore, we know that the overlap of two determinantal wave functions

$$\frac{1}{A!} \int \det^* \{\alpha_1 \cdots \alpha_A\} \det \{\beta_1 \cdots \beta_A\} d^3 r_1 \cdots d^3 r_A \quad (C-5)$$

- = 0 unless the sets $\{\alpha\}$ and $\{\beta\}$ are the same,
- = +1 if the sets are the same but differ by an even number of permutations,
- = -1 if the sets differ by an odd number of permutations.

Writing C-5 in the new notation, we obtain

$$\langle 0 | a_{\alpha_A} a_{\alpha_{A-1}} \cdots a_{\alpha_1} a_{\beta_1}^+ a_{\beta_2}^+ \cdots a_{\beta_A}^+ | 0 \rangle. \quad (C-6)$$

To satisfy the above conditions with C-6, we must have

$$\langle 0 | 0 \rangle = 1, \quad (C-7)$$

$$a_\alpha | 0 \rangle = 0 \quad \text{for all } \alpha, \quad (C-8)$$

and

$$\{a_\alpha, a_\beta^+\} = \delta_{\alpha\beta}. \quad (C-9)$$

Using Eqs. C-7 to C-9, one can prove that the two-particle wave function $a_{\alpha_1}^+ a_{\alpha_2}^+ |0\rangle$ is normalized to 1, that is,

$$\langle 0 | a_{\alpha_2} a_{\alpha_1} a_{\alpha_2}^+ a_{\alpha_1}^+ | 0 \rangle = 1.$$

The operators a_α^+ and a_α can be interpreted as the creation and annihilation operators for a particle in state α . To see this, consider a state

$$\begin{aligned} |\psi\rangle &= a_{\alpha_1}^+ a_{\alpha_2}^+ a_{\alpha_3}^+ |0\rangle \\ &= |1, 1, 1, 0, 0, \dots\rangle. \end{aligned} \quad (C-10)$$

This means that in $|\psi\rangle$ there is one particle each in states $\alpha_1, \alpha_2, \alpha_3$, while all other states are empty. If a_{α_1} is an annihilation operator, its application to $|\psi\rangle$ should result in a state $|0, 1, 1, 0, 0, \dots\rangle$. Using Eq. C-9, one finds that

$$\begin{aligned} a_{\alpha_1} |\psi\rangle &= a_{\alpha_1} a_{\alpha_2}^+ a_{\alpha_3}^+ a_{\alpha_1}^+ |0\rangle \\ &= (1 - a_{\alpha_1}^+ a_{\alpha_1}) a_{\alpha_2}^+ a_{\alpha_3}^+ |0\rangle \\ &= a_{\alpha_2}^+ a_{\alpha_3}^+ |0\rangle - a_{\alpha_1}^+ a_{\alpha_2}^+ a_{\alpha_3}^+ a_{\alpha_1}^+ |0\rangle \\ &= a_{\alpha_2}^+ a_{\alpha_3}^+ |0\rangle, \text{ using Eq. C-8} \\ &= |0, 1, 1, 0, 0, \dots\rangle. \end{aligned} \quad (C-11)$$

A similar operation by a_{α_2} on $|\psi\rangle$ reveals a difference:

$$\begin{aligned} a_{\alpha_2} |\psi\rangle &= a_{\alpha_2} a_{\alpha_1}^+ a_{\alpha_3}^+ a_{\alpha_2}^+ |0\rangle \\ &= -a_{\alpha_1}^+ a_{\alpha_2}^+ |0\rangle \\ &= -|1, 0, 1, 0, 0, \dots\rangle. \end{aligned} \quad (C-12)$$

Thus there is an overall minus sign in Eq. C-12, although a_{α_2} still behaves like an annihilation operator. The minus sign appears because there is an odd number of operators (here just $a_{\alpha_1}^+$) between a_{α_2} and $a_{\alpha_2}^+$. More generally,

$$\begin{aligned} a_\alpha | \dots, n_\alpha, \dots \rangle &= (-)^p \sqrt{n_\alpha} | \dots, 1 - n_\alpha, \dots \rangle, \\ a_\alpha^+ | \dots, n_\alpha, \dots \rangle &= (-)^p \sqrt{1 - n_\alpha} | \dots, 1 + n_\alpha, \dots \rangle, \end{aligned} \quad (C-13)$$

where any occupation number n_γ in a state γ is either 0 or 1, and

$$p = \sum_{\gamma=1}^{\alpha-1} n_\gamma.$$

It can also be shown that the operator

$$\hat{n} = \sum_{\alpha} a_{\alpha}^+ a_{\alpha} \quad (\text{C-14})$$

behaves like a number operator on a many-body state $|\psi\rangle$, so that

$$\hat{n}|\psi\rangle = \sum_{\gamma} n_{\gamma} |\psi\rangle = A|\psi\rangle. \quad (\text{C-15})$$

C-2 THE OPERATORS

We now formulate the procedure for writing down operators in this notation. For simplicity, we consider first a one-body operator, such as kinetic energy,

$$T = \sum_{i=1}^A t(i), \quad (\text{C-16})$$

where the index i refers to a particle. A standard result with the determinantal wave function C-1 for the following diagonal matrix element is

$$\begin{aligned} & \frac{1}{A!} \int \det^* \{\alpha_1 \cdots \alpha_A\} T \det \{\alpha_1 \cdots \alpha_A\} d^3 r_1 \cdots d^3 r_A \\ &= \sum_{\alpha_i=1}^A \int \phi_{\alpha_i}^*(\mathbf{r}_i) t(\mathbf{r}_i) \phi_{\alpha_i}(\mathbf{r}_i) d^3 r_i = \sum_{\alpha_i=1}^A \langle \alpha_i | t | \alpha_i \rangle, \end{aligned} \quad (\text{C-17})$$

where the sum on α_i is over occupied states only, and the subscript on t is irrelevant. Similarly, the matrix element between two determinantal states in which all the single-particle states except one are identical is given by

$$\begin{aligned} & \frac{1}{A!} \int \det \{\alpha_1 \alpha_2 \cdots \alpha_A\}^* T \det \{\alpha_M \alpha_2 \cdots \alpha_A\} d^3 r_1 \cdots d^3 r_A \\ &= \langle \alpha_1 | t | \alpha_M \rangle, \quad M > A. \end{aligned} \quad (\text{C-18})$$

If the single-particle states in the two determinants differ by more than one, then the matrix element is zero.

The above results in the occupation number notation are as follows:

$$\underbrace{\langle 1 1 1 \cdots 1}_{A} \underbrace{0 0 \cdots | T | \underbrace{1 1 1 \cdots 1}_{A} 0 0 \cdots \rangle} = \sum_{j=1}^A \langle \alpha_j | t | \alpha_j \rangle \quad (\text{C-19})$$

and

$$\underbrace{\langle 1 1 1 \cdots 1}_{A} \underbrace{0 0 \cdots | T | \underbrace{0 1 1 \cdots 1}_{A} 0 \cdots n_M = 1, 0 \cdots \rangle} = \langle \alpha_1 | t | \alpha_M \rangle. \quad (\text{C-20})$$

These equations follow if we define the one-body operator as

$$T = \sum_{\beta \alpha} \langle \beta | t | \alpha \rangle a_{\beta}^+ a_{\alpha}, \quad (\text{C-21})$$

where the indices β, α run over the complete set.

Next we consider the two-body operator,

$$v = \sum_{i < j} v(i, j), \quad (\text{C-22})$$

where i and j refer to particles. Again all the usual matrix elements of v can be obtained by working with the second-quantized wave function C-2 and writing the operator v as

$$v = \frac{1}{2} \sum_{\alpha \beta \gamma \delta} \langle \alpha \beta | v | \gamma \delta \rangle a_{\alpha}^+ a_{\beta}^+ a_{\delta} a_{\gamma}, \quad (\text{C-23})$$

where the sums run over the complete set, with $\alpha \neq \beta$ and $\gamma \neq \delta$. Note the order of the two annihilation operators.

As a simple example, assume that two fermions occupy the two states η and ζ with wave function

$$\Psi = \frac{1}{\sqrt{2}} \det \{\eta, \zeta\} = \frac{1}{\sqrt{2}} [\phi_{\eta}(\mathbf{r}_1) \phi_{\zeta}(\mathbf{r}_2) - \phi_{\eta}(\mathbf{r}_2) \phi_{\zeta}(\mathbf{r}_1)]. \quad (\text{C-24})$$

The diagonal matrix element of an operator $v(1, 2)$ with this wave function is simply

$$\langle \eta \zeta | v | \eta \zeta \rangle - \langle \eta \zeta | v | \zeta \eta \rangle, \quad (\text{C-25})$$

where, for a local $v(1, 2)$,

$$\langle \alpha \beta | v | \gamma \delta \rangle = \int \phi_{\alpha}^*(\mathbf{r}_1) \phi_{\beta}^*(\mathbf{r}_2) v(\mathbf{r}_1, \mathbf{r}_2) \phi_{\gamma}(\mathbf{r}_1) \phi_{\delta}(\mathbf{r}_2) d^3 r_1 d^3 r_2. \quad (\text{C-26})$$

In the second-quantized notation, using the forms C-2 and C-23, the diagonal matrix element $\langle \Psi | v | \Psi \rangle$ is

$$\frac{1}{2} \sum_{\alpha \beta \gamma \delta} \langle \alpha \beta | v | \gamma \delta \rangle \langle 0 | a_{\alpha} a_{\beta} a_{\gamma}^+ a_{\delta}^+ + a_{\alpha}^+ a_{\beta}^+ a_{\gamma} a_{\delta} | 0 \rangle. \quad (\text{C-27})$$

The reader should verify that this expression reduces to C-25 on using the properties of the creation and annihilation operators given in Section C-1.

Now we can write down a Hamiltonian

$$H = \sum_{i=1}^A t(i) + \sum_{i < j} v(i, j), \quad (\text{C-28})$$

where the second term on the right has $\frac{1}{2}A(A-1)$ terms, A being the number of particles. In the second-quantized version, we write this as

$$H = \sum_{\alpha\beta} \langle \alpha|\beta\rangle a_\alpha^+ a_\beta + \frac{1}{2} \sum_{\alpha\beta\gamma\delta} \langle \alpha\beta|v|\gamma\delta\rangle a_\alpha^+ a_\beta^+ a_\delta a_\gamma, \quad (\text{C-29})$$

where there is no reference to the particle number A . The two expressions C-28 and C-29 are equivalent in the sense that their matrix elements with respect to many-body wave functions are identical.

In the independent-particle model, the ground state of a nucleus is described by a state $|c\rangle$ in which all states $\alpha_1, \alpha_2, \dots, \alpha_A$ are occupied by nucleons and all others are empty. In our notation,

$$|c\rangle = a_{\alpha_1}^+ a_{\alpha_2}^+ \cdots a_{\alpha_A}^+ |0\rangle, \quad (\text{C-30})$$

where α_A defines the Fermi level of the system. Note that

$$a_\beta |c\rangle = 0 \quad \text{if } \beta > \alpha_A$$

and

$$a_\beta^+ |c\rangle = 0 \quad \text{if } \beta \leq \alpha_A. \quad (\text{C-31})$$

It is often convenient to make a transformation such that $|c\rangle$ behaves like a vacuum state:

$$a_\beta^+ = b_\beta, \quad a_\beta = b_\beta^+, \quad \text{for } \beta \leq \alpha_A. \quad (\text{C-32})$$

The operator b^+ is called a "hole"-creation operator, while for $\beta > \alpha_A$ the a 's are the usual particle operators. Now we obtain

$$\begin{aligned} a_\beta |c\rangle &= 0, \quad \beta > \alpha_A, \\ b_\beta |c\rangle &= 0, \quad \beta \leq \alpha_A, \end{aligned} \quad (\text{C-33})$$

so that $|c\rangle$ behaves like the vacuum state with respect to particle and hole operators.

In order to evaluate the matrix elements of operators in a systematic manner, we now introduce a few definitions.

1. *The normal order of a product of operators* is such that all creation operators (of particles as well as holes) stand to the left of the annihilation operators. The sign is determined by whether an odd or an even number of permutations is required to obtain the normal ordering. For example,

$$N(a_{\alpha_1} a_{\alpha_2}^+ a_{\alpha_3}) = -a_{\alpha_2}^+ a_{\alpha_1} a_{\alpha_3} \quad \text{when } \alpha_1, \alpha_2, \alpha_3 > \alpha_A$$

$$\begin{aligned} N(a_{\alpha_1} a_{\alpha_2}^+ a_{\alpha_3}) &= N(a_{\alpha_1} a_{\alpha_2}^+ b_{\alpha_3}^+) \quad \text{when } \alpha_1, \alpha_2 > \alpha_A, \alpha_3 < \alpha_A \\ &= a_{\alpha_2}^+ b_{\alpha_3}^+ a_{\alpha_1}. \end{aligned}$$

Note that the normal ordered product, operating on $|c\rangle$, gives zero identically.

2. *A contracted product of any two (creation or annihilation) operators A and B* is defined by

$$AB = AB - N(AB). \quad (\text{C-34})$$

Because of the commutation relations C-3 and C-4, the contracted product is simply a c -number, namely,

$$\begin{aligned} a_\alpha a_{\alpha'}^+ &= \delta_{\alpha\alpha'}, & \alpha, \alpha' > \alpha_A, \\ a_\alpha^+ a_{\alpha'} &= b_\alpha b_{\alpha'}^+ = \delta_{\alpha\alpha'}, & \alpha, \alpha' \leq \alpha_A. \end{aligned} \quad (\text{C-35})$$

All other contractions are identically zero. Note that, because of definition 1,

$$\langle c|AB|c\rangle = \langle c|AB|c\rangle = AB. \quad (\text{C-36})$$

3. *Wick's theorem*: Often we encounter a product of many creation and annihilation operators whose expectation value is required with respect to $|c\rangle$. Wick's theorem states that, if the total number of creation plus annihilation operators is odd, the expectation value of their product with respect to $|c\rangle$ vanishes. If, on the other hand, the total number is even, so that all of these operators can be contracted, the expectation value is just the sum of all possible fully contracted combinations. For example,

$$\begin{aligned} \langle c|a_{\alpha_1} a_{\alpha_2}^+ b_{\alpha_3}^+ b_{\alpha_4}|c\rangle &= 0, \\ \langle c|a_{\alpha_1} a_{\alpha_2}^+ b_{\alpha_3} b_{\alpha_4}^+|c\rangle &= a_{\alpha_1}^+ a_{\alpha_2}^+ b_{\alpha_3} b_{\alpha_4}^+ = \delta_{\alpha_1\alpha_2} \delta_{\alpha_3\alpha_4}, \end{aligned}$$

since all other contractions are zero, with $\alpha_1, \alpha_2 > \alpha_A$ and $\alpha_3, \alpha_4 \leq \alpha_A$.

C-3 EVALUATION OF MATRIX ELEMENTS

We can now apply the methods developed in Sections C-1 and C-2 to the calculation of matrix elements. A first-order change in Eq. 10-4 implies that

$$\langle c|H|\delta c\rangle + \langle \delta c|H|c\rangle = 0,$$

where $|c\rangle$ and $|\delta c\rangle$ are defined by Eqs. 10-5 and 10-6. In the above equation, the first term is simply the complex conjugate of the second. We thus get the minimal condition

$$\langle c|H a_b^+ a_m|c\rangle = 0,$$

with $b > A$ and $m \leq A$. Substituting for H from Eq. C-29, we can write

$$\sum_{\alpha,\beta} \langle \alpha|\beta\rangle \langle c|a_\alpha^+ a_\beta a_b^+ a_m|c\rangle + \frac{1}{2} \sum_{\alpha,\beta,\gamma,\delta} \langle \alpha\beta|v|\gamma\delta\rangle \langle c|a_\alpha^+ a_\beta^+ a_\delta a_\gamma a_b^+ a_m|c\rangle = 0. \quad (\text{C-36})$$

We consider first the matrix element $\langle c|a_\alpha^+a_\beta a_\delta a_\gamma^+a_m|c\rangle$. Since $m \leq A$, $a_m = b_m^+$, from Eq. C-32. Also, for the matrix element to be nonzero, $\alpha \leq A$; consequently $a_\alpha^+ = b_\alpha$. Thus

$$\begin{aligned}\langle c|a_\alpha^+a_\beta a_\delta a_\gamma^+a_m|c\rangle &= \langle c|b_\alpha a_\beta a_\delta + b_m^+|c\rangle \\ &= b_\alpha b_m^+ a_\beta a_\delta = \delta_{\alpha m} \delta_{\beta \delta}.\end{aligned}$$

$$\therefore \sum_{\alpha, \beta} \langle \alpha|\beta\rangle \langle c|a_\alpha^+a_\beta a_\delta a_\gamma^+a_m|c\rangle = \langle m|\delta|b\rangle.$$

Next, we evaluate the matrix element

$$\langle c|a_\alpha^+a_\beta^+a_\delta a_\gamma a_\delta^+a_m|c\rangle, \text{ with } \alpha \neq \beta, \gamma \neq \delta.$$

Obviously, for a nonzero value, α, β , and $m \leq A$, so that

$$\langle c|a_\alpha^+a_\beta^+a_\delta a_\gamma a_\delta^+a_m|c\rangle = \langle c|b_\alpha b_\beta a_\delta a_\gamma a_\delta^+b_m^+|c\rangle.$$

(i) $\delta \leq A, \gamma > A$: We obtain

$$\langle c|b_\alpha b_\beta b_\delta^+ a_\delta a_\gamma a_\delta^+ b_m^+|c\rangle = b_\alpha b_m^+ b_\beta b_\delta^+ a_\gamma a_\delta^+ - b_\alpha b_\delta^+ b_\beta b_m^+ a_\gamma a_\delta^+.$$

When substituted into the second term in Eq. C-36, this yields

$$\frac{1}{2} \left[\sum_{\delta=1}^A (\langle m\delta|v|b\delta\rangle - \langle \delta m|v|b\delta\rangle) \right].$$

(ii) $\delta > A, \gamma \leq A$: This case yields two more terms, identical to the above expression, except that now the dummy index is γ , going from 1 to A .

Summing (i) and (ii) and denoting the dummy index by n , we obtain the minimal condition given by Eq. 10-7.

Using these techniques, it is also straightforward to evaluate the quantity

$$\langle c|a_m^+a_\delta a_\alpha^+a_\beta a_\alpha a_\delta a_n|c\rangle$$

occurring in the particle-hole matrix element $\langle bm^{-1}|v|an^{-1}\rangle$ of Eq. 10-62. We consider the nondiagonal matrix element when $b \neq a, m \neq n$, and we remember that, in our notation, $m, n \leq A$ while $a, b > A$. We then have

$$\langle c|b_m a_\delta a_\alpha^+a_\beta a_\alpha a_\delta^+ b_n^+|c\rangle. \quad (C-37)$$

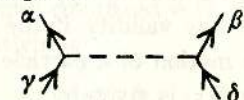
Using Wick's theorem, we can reduce expression C-37 to the following sum of contracted pairs (noting that b_m can only be contracted with a_δ or a_α):

$$\begin{aligned}&b_m a_\delta a_\alpha^+a_\beta^+ a_\delta a_\alpha a_\delta^+ b_n^+ + b_m a_\delta a_\alpha^+a_\beta^+ a_\delta a_\alpha a_\delta^+ b_n^+ \\ &+ b_m a_\delta a_\alpha^+a_\beta^+ a_\delta a_\alpha a_\delta^+ b_n^+ + b_m a_\delta a_\alpha^+a_\beta^+ a_\delta a_\alpha a_\delta^+ b_n^+ \\ &= -\delta_{ab} \delta_{\beta n} \delta_{\gamma a} \delta_{\delta m} + \delta_{\alpha n} \delta_{\beta b} \delta_{\gamma a} \delta_{\delta m} \\ &+ \delta_{ab} \delta_{\beta n} \delta_{\gamma m} \delta_{\delta a} - \delta_{\alpha n} \delta_{\beta b} \delta_{\gamma m} \delta_{\delta a}.\end{aligned}$$

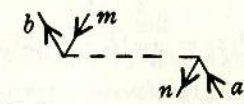
Substituting this value for expression C-37 in Eq. 10-62, we get

$$\begin{aligned}\langle bm^{-1}|v|an^{-1}\rangle &= \frac{1}{2} (-\langle bn|v|am\rangle + \langle nb|v|am\rangle) \\ &\quad + \langle bn|v|ma\rangle - \langle nb|v|ma\rangle \\ &= \langle bn|v|ma\rangle - \langle bn|v|am\rangle, \quad (C-38)\end{aligned}$$

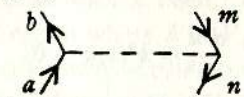
which is Eq. 10-63 of the text. Furthermore, since we denote the matrix element $\langle \alpha\beta|v|\gamma\delta\rangle$ by the diagram



it follows that $\langle bn|v|ma\rangle$ becomes



while $\langle bn|v|am\rangle$ is equivalent to



We consider now a multipole operator of order J ,

$$O_J = \sum_{\alpha, \beta} \langle \alpha|r^J Y_J M|\beta\rangle a_\alpha^+ a_\beta.$$

Then, we define

$$\begin{aligned}D_{bm}^J &= \langle bm^{-1}|O_J|c\rangle \\ &= \sum_{\alpha, \beta} \langle bm^{-1}|a_\alpha^+ a_\beta|c\rangle \langle \alpha|r^J Y_J M|\beta\rangle \\ &= \sum_{\alpha, \beta} \langle c|a_m^+ a_\delta a_\alpha^+ a_\beta|c\rangle \langle \alpha|r^J Y_J M|\beta\rangle\end{aligned}$$

or

$$D_{bm}^J = \langle b|r^J Y_J M|m\rangle. \quad (C-39)$$

Note that, if $|c\rangle$ has zero angular momentum, only the component of $|bm^{-1}\rangle$ that has angular momentum J contributes to D_{bm}^J .

Appendix D

The WKB Approximation

The WKB (Wentzel-Kramers-Brillouin) approximation is a solution to the Schrödinger equation which has validity if the local wave number varies sufficiently slowly. For the motion of a particle of energy E in a potential $V(x)$, the local wave number $k(x)$ is given by

$$k^2(x) = \frac{2m}{\hbar^2} [E - V(x)],$$

and the wave equation is simply

$$\frac{d^2u}{dx^2} + k^2(x)u = 0.$$

However, the considerations which follow are of a mathematical nature and apply equally well if the independent variable is the radial coordinate r , the coordinate β of the collective model, or any other coordinate for which the wave function can be separated. To emphasize this, we denote the variable by α and remark that, whatever the explicit form of the kinetic-energy operator, so long as the problem is separable, we can by transformation of variables put the wave equation into the form

$$\frac{d^2u}{d\alpha^2} + k^2(\alpha)u = 0 \quad (\text{D-1a})$$

or

$$\frac{d^2u}{d\alpha^2} - \kappa^2(\alpha)u = 0, \quad (\text{D-1b})$$

where k and κ are real functions given by

$$k^2 = C[E - V_e(\alpha)], \quad E > V_e, \quad (\text{D-2a})$$

$$\kappa^2 = C[V_e(\alpha) - E], \quad E < V_e, \quad (\text{D-2b})$$

where E is the energy of the system, $V_e(\alpha)$ is the effective potential energy, and C is a proportionality constant. When k is constant, the solutions of Eq. D-1 are exponentials $\exp(\pm ik\alpha)$, $\exp(\pm \kappa\alpha)$. Hence, if k is slowly varying, we might expect that the solutions

$$u_0 = \exp \left[\pm i \int^\alpha k(\alpha) d\alpha \right]$$

might have some validity. Indeed, we find that

$$\frac{d^2u_0}{d\alpha^2} + k^2 u_0 = \pm \frac{1}{2} i \frac{dk}{d\alpha} u_0,$$

showing that, if $dk/d\alpha$ is small compared with k^2 , the approximation is valid. This condition may be written as

$$\left(\frac{dk}{d\alpha} \right) \frac{1}{k} \ll k. \quad (\text{D-3})$$

Since $1/k$ is the "local wavelength," this expression states that the result is valid if the change in k over a wavelength or, indeed, over several wavelengths is negligible compared with k itself. One situation in which this would arise would be in a region where $E \gg V_e(\alpha)$. It could also occur when $V_e \gg E$, provided that V_e is a slowly varying function. The one region where the condition certainly fails is that in which $V_e \approx E$, for there k is very small but $dk/d\alpha$ is large, being proportional to $k^{-1}(dV/d\alpha)$.

We can attempt to improve on the expression u_0 by finding the next approximation in the form $f(\alpha)u_0(\alpha)$, where $f(\alpha)$ remains near unity. It is easy to see, ignoring the second derivative of $f(\alpha)$, that $f(\alpha) = k^{-1/2}$. This second approximation is the one usually called the WKB solution,

$$u = A k^{-1/2} \exp(\pm i\omega), \quad (\text{D-4a})$$

or

$$u = B \kappa^{-1/2} \exp(\pm \omega), \quad (\text{D-4b})$$

where

$$\omega = \int^\alpha k d\alpha \quad \text{or} \quad - \int^\alpha \kappa d\alpha, \quad (\text{D-4c})$$

as the case may be.

The most common application of the WKB approximation in nuclear physics is to problems of barrier penetration. In considering a potential that goes to zero at large values of α , but rises well above the energy E for certain other values, as shown in Fig. D-1, it is seen that there are two regions where the WKB solution would be useful. In region 1, the solution of form D-4a

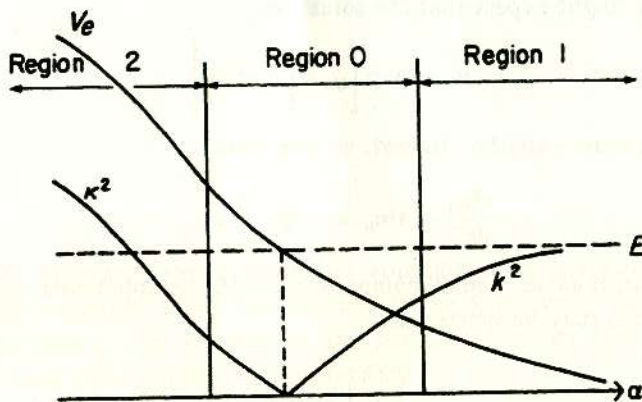


Fig. D-1 A potential $V_e(\alpha)$ that goes to zero for large α , but is greater than E for small α . In regions 1 and 2, where k^2 and κ^2 are not small, simple WKB solutions for the wave function can be found (see text).

with an imaginary exponential would be valid; in region 2, that of form D-4b. However, in the intermediate region, labeled region 0 in the figure, the approximation is not valid since k^2 is small, vanishing at the point where $E = V_e$. To obtain expressions for the penetration of particles in region 1 into region 2, it is necessary to make use of the wave function in region 0 only in order to connect the expressions in the other two regions. Explicitly, using an obvious notation, we can write the wave functions in regions 1 and 2, respectively, as

$$\psi(1) = A_- u_-(1) + A_+ u_+(1) \quad (\text{D-5a})$$

and

$$\psi(2) = B_- u_-(2) + B_+ u_+(2). \quad (\text{D-5b})$$

It is necessary to find the relationship between the B 's and the A 's in order to determine the relationship between the particle densities in the two asymptotic regions.

In the immediate vicinity of the point where $E = V_e$, we can treat k^2 as a linear function of α ; that is, if we shift the origin of α to this turning point,

$$\frac{d^2u}{d\alpha^2} + \alpha \omega u = 0. \quad (\text{D-6})$$

In this case,[†] if we take the hitherto unspecified lower limit on the integral D-4c defining ω to be $\alpha = 0$,

$$\omega = \frac{2}{3} \alpha^{1/2} |\alpha|^{3/2},$$

and exact solutions[‡] of Eq. D-6 are

$$u_{\pm} = \omega^{1/2} |k|^{-1/2} Z_{\pm 1/3}(\omega), \quad (\text{D-7})$$

where $Z_p(\omega)$ is a Bessel function and

$$\begin{aligned} Z_p(\omega) &= J_p(\omega), & \alpha > 0 \\ &= I_p(\omega) = i^{-p} J_p(i\omega), & \alpha < 0. \end{aligned}$$

For small ω , $J_p(\omega) = I_p(\omega) = (\frac{1}{2}\omega)^p (p!)^{-1}$, and we can readily see that

$$u_+(\alpha \rightarrow 0^+) = u_+(\alpha \rightarrow 0^-) = 0,$$

$$u_-(\alpha \rightarrow 0^+) = u_-(\alpha \rightarrow 0^-) = \text{a nonzero number},$$

$$\frac{du_+}{d\alpha}(\alpha \rightarrow 0^+) = - \frac{du_+}{d\alpha}(\alpha \rightarrow 0^-) = \text{a nonzero number},$$

$$\frac{du_-}{d\alpha}(\alpha \rightarrow 0^+) = \frac{du_-}{d\alpha}(\alpha \rightarrow 0^-) = 0.$$

[†] We see the advantage of the minus sign in the definition D-4c of ω ; ω increases with $|\alpha|$. If regions 1 and 2 are reversed so that region 2 lies to the right of region 1, the signs in Eq. D-4c are to be reversed.

[‡] More generally, Eq. D-1 can be written, with $v = k^{1/2}u$, as

$$\frac{d^2v}{d\omega^2} + \left[1 + \frac{1}{4} \frac{1}{k^2} \left(\frac{dk}{d\omega} \right)^2 - \frac{1}{2} \frac{1}{k} \frac{d^2k}{d\omega^2} \right] v = 0,$$

and, if k is proportional to a power of ω , say ω^β , the solutions are $\omega^{1/2} Z_p(\omega)$, with $p = \frac{1}{2}(\beta - 1)$.

Hence, since the wave function and its derivative must be continuous at $\alpha = 0$, it follows that, if a solution for $\alpha > 0$ is

$$\psi = \omega^{1/2} k^{-1/2} [A J_{1/3}(\omega) + B J_{-1/3}(\omega)],$$

its value for $\alpha < 0$ must be

$$\psi = \omega^{1/2} \kappa^{-1/2} [-A I_{1/3}(\omega) + B I_{-1/3}(\omega)].$$

Now, for large ω ,

$$J_p(\omega) \sim (\frac{1}{2}\pi\omega)^{-1/2} \cos \left[\omega - \left(p + \frac{1}{2} \right) \frac{\pi}{2} \right] \quad (D-8a)$$

and

$$I_p(\omega) \sim (2\pi\omega)^{-1/2} \{e^\omega + e^{-\omega} \exp[-\pi i(\frac{1}{2} + p)]\}. \quad (D-8b)$$

Of course, in the asymptotic expression D-8b, the term with the decreasing exponential can be written only when the solution taken is $u_+ - u_-$, for which the positive exponential vanishes.

The solutions valid for k small are thus seen to have asymptotic forms D-8 similar to the WKB solutions D-4. Hence, if in region 1 our solution is an outgoing wave, $u_+(1) = A_+ k^{-1/2} e^{i\omega}$, we need to take in region 0 the solution with the same asymptotic form, namely,

$$A_+ k^{-1/2} i \exp \left(i \frac{\pi}{4} \right) \operatorname{cosec} p\pi (\frac{1}{2}\pi\omega)^{1/2} \left[\exp \left(-ip \frac{\pi}{2} \right) J_p - \exp \left(ip \frac{\pi}{2} \right) J_{-p} \right].$$

To assure continuity at $\alpha = 0$, the solution for $\alpha < 0$ must, therefore, be

$$A_+ \kappa^{-1/2} i \exp \left(i \frac{\pi}{4} \right) \operatorname{cosec} p\pi (\frac{1}{2}\pi\omega)^{1/2} \left[-\exp \left(-ip \frac{\pi}{2} \right) I_p - \exp \left(ip \frac{\pi}{2} \right) I_{-p} \right].$$

For large ω , this becomes $\exp(-i\pi/4) A_+ \kappa^{-1/2} e^\omega$.

Thus we have seen that a solution in region 1 given by $A k^{-1/2} e^{i\omega}$ is connected to a solution in region 2 given by $\exp(-i\pi/4) A \kappa^{-1/2} e^\omega$. However, this formula cannot be used in reverse. In other words, if we know that the wave function in region 2 is closely approximated by $\kappa^{-1/2} e^\omega$, we cannot deduce that the wave in region 1 is simply an outgoing wave, since the phase of the oscillating wave in region 1 is determined by the mixture of the increasing and decreasing exponentials in region 2, and, when the region-2 wave function contains the increasing exponential, our approximate solution, of course, tells us nothing about the amount of decreasing exponential present. However, it is possible in a similar way to establish the connection giving the

amplitude and phase of the wave in region 1 if region 2 is known to contain only the decreasing exponential. This connection is

$$\kappa^{-1/2} e^{-\omega} \rightarrow 2k^{-1/2} \cos \left(\omega - \frac{\pi}{4} \right). \quad (D-9a)$$

Also, for a wave of general phase γ in region 1, the connection giving the magnitude in region 2 is

$$k^{-1/2} \cos \left(\omega + \gamma - \frac{\pi}{4} \right) \rightarrow \sin \gamma \kappa^{-1/2} e^\omega. \quad (D-9b)$$

We can see how to use these formulas to calculate transmission through a reasonably wide barrier as shown in Fig. D-2. Let us consider a wave incident from the left, so that region III contains both a wave moving in the positive α -direction and a reflected wave moving in the negative sense. The wave is transmitted through the classically forbidden zone of region II, and in region III there is only an "outgoing" wave, that is, one moving toward positive α . In short, the asymptotic form in region I is simply

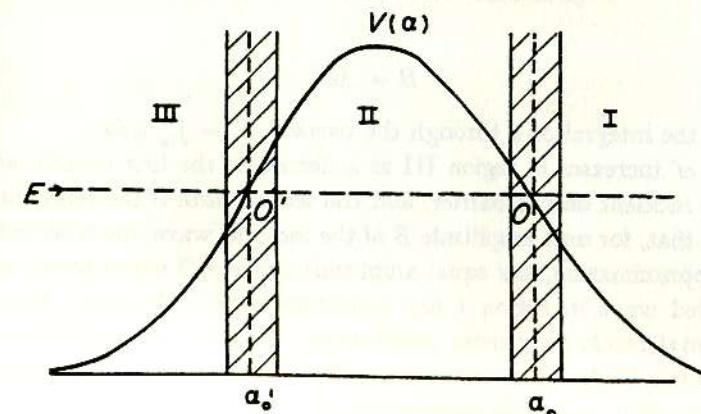


Fig. D-2 Transmission of a wave of incident energy E through a barrier $V(\alpha)$. The shaded regions are in the vicinity of the classical turning points O and O' .

$$u(I) \sim Ak^{-1/2}e^{i\omega}.$$

We know, therefore, from the above discussion that in region II, when we are sufficiently far from the turning point O' ,

$$u(II) \sim A \exp(-i\pi/4) \kappa^{-1/2} e^{\omega}.$$

It is necessary that the barrier be sufficiently broad that the term in $e^{-\omega}$ will be negligible at points within region II near O' . This expression refers, of course, to an ω defined to vanish at the right-hand turning point. To make the connection between regions II and III, we must use relations in which we define our origin at the left-hand turning point. If we use primes to denote such quantities, we have for region II

$$\omega' = \int_0^{\alpha'} \kappa d\alpha' = \int_{\alpha'_*}^{\alpha} \kappa d\alpha = \int_{\alpha'_*}^{\alpha_*} \kappa d\alpha - \int_{\alpha_*}^{\alpha} \kappa d\alpha = \int_{\alpha'_*}^{\alpha_*} \kappa d\alpha - \omega.$$

Hence near the left side of region II we can write

$$u(II) \sim A \exp(-i\pi/4) \kappa^{-1/2} \exp\left(\int_{\alpha'_*}^{\alpha_*} \kappa d\alpha\right) e^{-\omega'},$$

and Eq. D-9a shows that the wave function in region III is

$$\begin{aligned} u(III) &\sim 2A \exp(-i\pi/4) k^{-1/2} \exp\left(\int_{\alpha'_*}^{\alpha_*} \kappa d\alpha\right) \cos\left(\omega' - \frac{\pi}{4}\right) \\ &= Bk^{-1/2}(e^{-i\omega'} + ie^{i\omega'}), \end{aligned}$$

where

$$B = Ae^K \quad (\text{D-10})$$

and K is the integral of κ through the barrier: $K = \int_{\alpha'_*}^{\alpha_*} \kappa d\alpha$.

Since ω' increases in region III as α decreases, the first term in $u(III)$ is the wave incident on the barrier, and the second term is the reflected wave. It is seen that, for unit amplitude B of the incident wave, the reflected wave, to this approximation, has equal amplitude and is $\pi/2$ out of phase, and the transmitted wave in region I has amplitude $\exp(-\int_{\alpha'_*}^{\alpha_*} \kappa d\alpha)$. This is the fundamental result for barrier penetration. It can be phrased in terms of flux. If α is a Cartesian coordinate, the flux in the α -direction is proportional to $\text{Im}[u^*(du/d\alpha)]$; if α is the radial coordinate r , the flux is $\text{Im}[(1/r^2)u^*(du/dr)]$; and in general the flux is $g(\alpha) \text{Im}[u^*(du/d\alpha)]$, where $g(\alpha)$ is some "geometrical" factor. Hence the flux at a point α_1 in region I, compared to that at a point α_3 in region III, is

$$\frac{\text{Flux in I}}{\text{Flux in III}} = \left[\frac{g(\alpha_1)}{g(\alpha_3)} \right] \exp(-2K). \quad (\text{D-11a})$$

Equation D-10 gives the barrier transmission, that is, the intensity ratio $(A/B)^2$,

$$T = \exp(-2K). \quad (\text{D-11b})$$

If the barrier is so thin that the term $e^{-\omega}$ is not negligible near O' , it can be shown[†] that a better approximation is

$$T \approx \frac{1}{1 + \exp(2K)}, \quad (\text{D-12a})$$

$$R \approx \frac{\exp(2K)}{1 + \exp(2K)}, \quad (\text{D-12b})$$

where R is the intensity of the reflected wave in region III. Notice that $R + T = 1$, as it should. The approximation that we have developed is, of course, the limit of Eq. D-12 for $K \gg 1$, and is valid when the turning points are well separated.

We may note that for one particular case, namely, a parabolic barrier, Eq. D-12 is exact.

Equation D-11 is valid if the points α_1 and α_3 are sufficiently remote from the barrier that $dk/d\alpha$ is small and satisfies Eq. D-3. If this is not the case, an extra factor must be introduced into Eq. D-11a, namely, the ratio of the value of $1 - (1/2k^2)(dk/d\alpha)$ at α_1 to its value at α_3 .

[†] See, for example, N. Fröman and P. O. Fröman, *JWKB Approximation*, North-Holland, Amsterdam, 1965.

Appendix E

Electromagnetic Transitions

E-1 MULTIPOLE EXPANSION OF THE ELECTROMAGNETIC FIELD

We stated in Chapter 3 that the interaction energy of a system of charged particles with the electromagnetic field can be expanded in a series of multipole moments. The usefulness of Eq. 3-1 is subject to the provisos that the field changes only slightly over the nuclear volume, and that the nucleons move nonrelativistically. The first condition is equivalent to requiring that the wavelength of the radiation be large compared to nuclear dimensions, or that

$$R \ll \lambda, \text{ i.e., } \omega R \ll c,$$

where ω is the angular frequency of the radiation and R is the radius of the nucleus. This condition may be rewritten in terms of the energy of the corresponding photon as

$$\hbar\omega \ll \frac{\hbar c}{R} \approx \frac{197}{1.2 A^{1/3}} \approx 165 A^{-1/3} \text{ MeV.}$$

In other words, for energies of 25 MeV or more, the convergence of the series is much slower, and different approaches may be preferable.

The various multipole moments are tensors. In studying nuclei, it is more useful to employ spherical tensors than Cartesian tensors, because spherical tensors have special properties in connection with angular momentum. A summary of the properties of spherical tensors is given in Appendix A.

Of special usefulness in this connection is the Wigner-Eckart theorem, given by Eq. A-83.

Let us first write the electromagnetic field in free space in terms of spherical tensors. For a pure radiation field, we may put the electrostatic potential $\phi = 0$ and express the electric and magnetic fields \mathcal{E} and \mathcal{H} in terms of the vector potential \mathcal{A} by

$$\mathcal{E} = -\frac{1}{c} \frac{\partial \mathcal{A}}{\partial t}, \quad (\text{E-1a})$$

$$\mathcal{H} = \text{curl } \mathcal{A}. \quad (\text{E-1b})$$

Maxwell's equations are satisfied if

$$\left(\nabla^2 - \frac{1}{c^2} \frac{\partial^2}{\partial t^2} \right) \mathcal{A} = 0, \quad (\text{E-2a})$$

$$\text{div } \mathcal{A} = 0. \quad (\text{E-2b})$$

A general field \mathcal{A} can be expressed in terms of any complete orthogonal set of solutions of (E-2). If we put

$$\mathcal{A} = q_k e^{-i\omega t} \mathbf{A}_k(\mathbf{r}), \quad (\text{E-3})$$

with $k = \omega/c$, Eqs. (E-2) are equivalent to

$$\text{curl curl } \mathbf{A}_k - k^2 \mathbf{A}_k = 0. \quad (\text{E-4})$$

It is found that the following two expressions both satisfy this last equation for integral values of λ and μ :

$$\mathbf{A}_{\lambda\mu}^E = \left(\frac{-i}{k} \right) \text{curl} [\mathbf{r} \times \text{grad} (j_\lambda(kr) Y_{\lambda\mu}(\theta, \phi))], \quad (\text{E-5a})$$

$$\mathbf{A}_{\lambda\mu}^M = \mathbf{r} \times \text{grad} (j_\lambda(kr) Y_{\lambda\mu}), \quad (\text{E-5b})$$

where j_λ denotes the spherical Bessel functions. By allowing λ , μ , and k to take on all possible values, these solutions are made to span a complete orthogonal set, and consequently any \mathcal{A} can be written as a series of them:

$$\mathcal{A} = \sum_{\lambda,\mu,\sigma} \int dk q_k^{\lambda\mu\sigma} e^{-i\omega t} \mathbf{A}_{\lambda\mu}^\sigma(k, \mathbf{r}). \quad (\text{E-6})$$

The individual solutions are of considerable interest in themselves.

We define

$$\mathbf{E}_{\lambda\mu}^\sigma = ik \mathbf{A}_{\lambda\mu}^\sigma, \quad (\text{E-7a})$$

$$\mathbf{H}_{\lambda\mu}^\sigma = \text{curl } \mathbf{A}_{\lambda\mu}^\sigma, \quad (\text{E-7b})$$

and, using Eq. (E-4), we note that

$$\mathbf{H}^M = \mathbf{E}^E, \quad \mathbf{H}^E = -\mathbf{E}^M.$$

Consequently,

$$\mathbf{r} \cdot \mathbf{E}^M = \mathbf{r} \cdot \mathbf{H}^E = 0, \quad (\text{E-8})$$

which means that the electric field is transverse in the M -mode and the magnetic field is transverse in the E -mode. These are the properties of the fields of oscillating magnetic and electric multipoles, respectively. The fields with superscript M and E are therefore called magnetic and electric radiations. The energy in the field for one of these solutions is

$$\text{energy} = \frac{1}{4\pi} \int [|\mathbf{E}_{\lambda\mu}^\sigma|^2 + |\mathbf{H}_{\lambda\mu}^\sigma|^2] dV. \quad (\text{E-9})$$

The energy flow density is given by Poynting's vector, and the momentum density in the field is just $1/c^2$ of this quantity: $(1/4\pi c) \mathbf{E} \times \mathbf{H}$. Consequently the angular momentum carried by the field is:

$$\text{angular momentum of field} = \frac{1}{4\pi c} \int \mathbf{r} \times \text{Re}(\mathbf{E}_{\lambda\mu}^* \times \mathbf{H}_{\lambda\mu}) dV. \quad (\text{E-10})$$

For the classical field, it is just a matter of juggling with vector relationships and integral theorems to show that the z -component of the angular momentum is (μ/ω) times the energy. If we introduce quantization simply by saying that the energy of the field is $\hbar\omega$ times the number of photons, we have demonstrated that the photons associated with a field of the type $\mathbf{A}_{\lambda\mu}^\sigma$ each have an angular-momentum z -component equal to $\mu\hbar$. More satisfactorily, we can introduce a quantized field by treating the quantities $q_k^{\lambda\mu\sigma}$ in Eq. E-6 as quantum-mechanical operators, which create and destroy photons of type λ, μ, k . Then Eqs. E-9 and E-10 are operator equations, and the eigenvalues of energy and angular momentum are readily determined, since $q^* q$ is the operator whose eigenvalues are the numbers of photons present. In this way, the same result is obtained, together with the fact that the square of the angular momentum carried by one photon is $\lambda(\lambda+1)\hbar^2$.

There are, of course, other sets of solutions of Eq. E-4, of which the simplest are sets of plane waves of various polarizations. These lead to a quantized description with photons of definite linear momentum, and fixed directions of \mathbf{E} and \mathbf{H} . Such photons are suitable for discussing some problems, but for most nuclear problems photons of definite angular momentum are more convenient. Which of these two alternatives we use is merely a

matter of convenience, since an arbitrary state can be expressed as a linear combination of the states of any complete set.

The interaction energy between a charged system and the electromagnetic field is

$$-\int \left[\frac{1}{c} \mathbf{j}(\mathbf{r}) \cdot \mathcal{A}(\mathbf{r}) + \mathbf{M}(\mathbf{r}) \cdot \mathcal{H}(\mathbf{r}) \right] d^3r, \quad (\text{E-11})$$

where $\mathbf{j}(\mathbf{r})$ is the current density and $\mathbf{M}(\mathbf{r})$ is the dipole moment per unit volume due to a distribution of spins. If we take the more fundamental viewpoint from which \mathbf{j} and \mathbf{M} are attributed to A particles, this energy becomes

$$H_{\text{int}} = - \sum_{i=1}^A \left[\frac{e_i}{m_i c} \mathbf{p}_i \cdot \mathcal{A}(\mathbf{r}_i) + \mu_i \mathbf{s}_i \cdot \mathcal{H}(\mathbf{r}_i) \right], \quad (\text{E-12})$$

where μ_i is the intrinsic magnetic moment of the i th particle, μ_0 is the nuclear magneton, and the remaining notation is evident.

The transition probability per second for a process due to this interaction which takes the charged system and the field from a state I to a state F is

$$T = \frac{2\pi}{\hbar} |\langle F | H_{\text{int}} | I \rangle|^2 \rho_E, \quad (\text{E-13})$$

where ρ_E is the number of final states per unit energy interval. The coefficients $q_k^{\lambda\mu\sigma}$ and $q_k^{\lambda\mu\sigma*}$, treated as annihilation and creation operators for the quantized field, have nonzero matrix elements between states which differ by precisely one photon of type k, λ, μ, σ . For example, radiation may be discussed by taking an initial state with no photons and a final state with one photon, or absorption may be handled by reversing these states. In either case, it is clear that, in addition to the matrix element of q , an essential role is played by the matrix element $\langle f | H' | i \rangle$, where f and i refer only to the states of the charged system and

$$H' = - \sum_i \left[\frac{e_i}{m_i c} \mathbf{p}_i \cdot \mathbf{A}_{\lambda\mu}^\sigma(k, \mathbf{r}) + \mu_i \mathbf{s}_i \cdot \mathbf{H}_{\lambda\mu}^\sigma(k, \mathbf{r}) \right]. \quad (\text{E-14})$$

Of course, $|E_i - E_f| = \hbar\omega = \hbar ck$, since $E_I = E_F$. In the special case of $kR \ll 1$, the Bessel functions satisfy

$$j_\lambda(kr) \simeq \frac{(kr)^\lambda}{(2\lambda+1)!!}.$$

where $(2\lambda + 1)!! = 1 \cdot 3 \cdot 5 \cdots (2\lambda + 1)$. With this approximation, it can be seen by straightforward calculation that

$$\langle f|H'|i\rangle \text{ is proportional to } \langle f|M_{\lambda\mu}|i\rangle \text{ or } \langle f|Q_{\lambda\mu}|i\rangle$$

for $\sigma = M$ or E , respectively, where $M_{\lambda\mu}$ and $Q_{\lambda\mu}$ are magnetic and electric multipole operators,

$$Q_{\lambda\mu} = \sum_i [e_s r_i^\lambda Y_\lambda^{\mu*}(\Omega_i) - ig_{si}\mu_0 k(\lambda + 1)^{-1} \mathbf{s}_i \times \mathbf{r}_i \cdot \nabla (r^\lambda Y_\lambda^{\mu*})_i], \quad (\text{E-15})$$

$$M_{\lambda\mu} = \mu_0 \sum_i \left(g_{si} s_i + \frac{2}{\lambda + 1} g_{ti} l_i \right) \cdot \nabla (r^\lambda Y_\lambda^{\mu*})_i, \quad (\text{E-16})$$

μ_0 is the nuclear magneton, and the g 's are the gyromagnetic ratios.

These operators are closely related to the multipoles introduced in Chapter 3; apart from a normalizing factor, $M_{\lambda 0}$ is the magnetic 2^λ -pole moment of Eq. 3-20, and the first term of $Q_{\lambda 0}$ is the Q_λ of Eq. 3-6. (The matrix element of the second term of $Q_{\lambda\mu}$ is of the same order of magnitude as that of $M_{\lambda+1}$ and is usually ignored.) Thus the static electromagnetic moments are the diagonal matrix elements of the same operators that are involved in transitions.

When all the expressions are properly normalized (our expressions for A are not), the transition probability for emission of a photon of energy $\hbar\omega$, angular momentum λ , μ , and of electric or magnetic type, with the nucleus going from a state i to a state f , is

$$T_{if}(\sigma\lambda\mu) = \frac{8\pi(\lambda + 1)}{\lambda[(2\lambda + 1)!!]^2} \frac{k^{2\lambda+1}}{\hbar} |\langle f|\mathcal{O}_{\lambda\mu}|i\rangle|^2, \quad (\text{E-17})$$

where $\mathcal{O}_{\lambda\mu}$ stands for $Q_{\lambda\mu}$ or $M_{\lambda\mu}$. Usually we are not interested in the orientation of either the initial or the final nucleus, so we sum over M , and average over M_i . We define the so-called reduced matrix element:

$$B(\sigma\lambda, J_i \rightarrow J_f) = (2J_i + 1)^{-1} \sum_{M_i, M_f} |\langle f|\mathcal{O}_{\lambda\mu}|i\rangle|^2, \quad (\text{E-18a})$$

$$T(\sigma\lambda) = \frac{8\pi(\lambda + 1)}{\lambda[(2\lambda + 1)!!]^2} \frac{k^{2\lambda+1}}{\hbar} B(\sigma\lambda). \quad (\text{E-18b})$$

Of course, only one value of μ , that is, $\mu = M_f - M_i$, contributes to each term.

We can make a very rough estimate of the matrix elements by replacing spherical harmonics and angular momentum vectors by unity, and noting that the initial and final wave functions vanish outside the nuclear radius R :

$$\langle f|\mathcal{O}_{\lambda\mu}|i\rangle \sim ZeR^\lambda, \quad (\text{E-19a})$$

$$\langle f|M_{\lambda\mu}|i\rangle \sim A \left(\frac{e\hbar}{2Mc} \right) R^{\lambda-1}. \quad (\text{E-19b})$$

We note that the ratio of the magnetic and electric moments of the same order is approximately $(\hbar/Mc)/R$, which varies from about 0.2 to 0.03. Since the square appears in Eq. E-17, the relative transition probabilities vary from 0.04 to 0.001, but in view of the crudity of the approximations, these last numbers might be in error by a factor of nearly ten. On the same basis of approximation, the second term in $Q_{\lambda\mu}$ contributes about $kA(e\hbar/2Mc)R^\lambda$ to $\langle f|Q|i\rangle$. Its ratio to the contribution E-19a is thus of the order of $\hbar\omega/Mc^2$, and this term can be neglected except in unusual circumstances.

The estimates E-19 substituted in Eq. E-17 show that the ratio of transition rates of successive multipoles λ and $\lambda + 1$ is of order $(kR)^2/(2\lambda + 3)^2$. So long as we are dealing with $kR \ll 1$ for which our theory has been developed, we may therefore consider only the lowest multipole which contributes to a given transition.

The selection rules are important. The parity of $Q_{\lambda\mu}$ is that of Y_λ^μ , namely $(-)^{\lambda}$, but $M_{\lambda\mu}$ has parity $-(-)^{\lambda}$, since in addition to Y_λ^μ it contains a vector in the gradient operator and pseudo vectors s and l . Also, since $Q_{\lambda\mu}$ and $M_{\lambda\mu}$ are spherical tensors, the selection rule $J_i + J_f \geq \lambda \geq |J_i - J_f|$ applies. The lowest multipoles arising in specified γ -transitions are therefore as shown in Table E-1. (The square brackets indicate that these multipoles do not contribute to cases in which either J_i or J_f is zero.) If our estimates of the matrix elements are reliable, some of these transi-

TABLE E-1

ΔJ	$\Pi_i \Pi_f$	Multipoles
$0 \rightarrow 0$		(E0) special case
$\frac{1}{2} \rightarrow \frac{1}{2}$	+ 1	(E0) M1
$\frac{1}{2} \rightarrow \frac{1}{2}$	- 1	E1
0	+ 1	(E0) M1 E2
0	- 1	E1 M2
1	+ 1	M1 [E2]
1	- 1	E1 [M2]
2	+ 1	E2 [M3]
2	- 1	M2 [E3]
3	+ 1	M3 [E4]
3	- 1	E3 [M4]

tions will emit pure multipole radiation. For example, a $\Delta J = 0$ transition with parity change may proceed by either $E1$ - or $M2$ -radiation. The relative intensities are expected to be in the ratio $(Mc^2/\hbar\omega)^2$, which is at least 10^4 or 10^5 , and pure $E1$ -radiation will result. However, when the lower-order radiation is magnetic, the situation is not so clear-cut. For $\Delta J = 0$ or $\Delta J = 1$ with no parity change, $M1$ and $E2$ may mix with relative intensity $[(\hbar/Mc)/R]^4(Mc^2/\hbar\omega)^2$. This ratio is still considerably greater than unity in most cases, but the first factor may be as small as 10^{-4} . Since quadrupole moments are considerably enhanced in distorted nuclei, we may expect to find appreciable $M1 - E2$ mixtures in their spectra.

The multipole $E0$ occurs in brackets in Table E-1. As a glance at Eqs. E-5 shows, there is no radiation field for $\lambda = 0$. This vanishing of the field is the mathematical form of the physical statement that each photon carries off at least one unit of angular momentum. Consequently, although the matrix element of Q_{00} may not vanish, there is no term $\lambda = 0$ in the expansion of the radiation field, and the $E0$ -multipoles do not contribute to γ -transitions. In particular, $0 \rightarrow 0$ γ -transitions are completely forbidden.

How, then, does an excited state of spin zero decay, if there are no other states between it and a zero-spin ground state? It might go by β -decay, forming a different nuclide, but this is a very slow process and, although the excited state cannot emit a single photon, it can decay more quickly through the electromagnetic interaction between the nucleus and its atomic electrons. The excess nuclear energy is given to one of the electrons which is thereby expelled from the atom. This form of energy transfer is called *internal conversion*, and the emitted electron is a *conversion electron*. A $0 \rightarrow 0$ transition can also go by higher-order electromagnetic processes such as the emission of two photons, or one photon and a conversion electron, but for most nuclear states these processes would have a probability at least two orders of magnitude smaller than internal conversion. If a state has excitation energy greater than two electron masses, it can decay also by the electromagnetic creation of a positron-negatron pair. At high energies, this *internal pair creation* is more important than internal conversion. Besides providing a mechanism for $0 \rightarrow 0$ decays, internal conversion and internal pair creation often compete significantly with γ -emission for transitions of higher multipolarity.

E-2 SINGLE-PARTICLE TRANSITION RATES

In view of the sensitivity of the static moments to configuration mixing and collective effects, it is not surprising that the extreme single particle model

does not yield realistic values of γ -decay probabilities. The formulas for lifetimes in this model are particularly simple, however, and are often used as reference values for comparing experimental data.

We shall first estimate the transition probability E-17 for electric λ -pole transition of a single proton in this model. For simplicity, we assume that the orbital angular momentum of the proton is l in the initial state, and zero in the final state. Let the initial intrinsic spin of the proton be spin up, i.e., parallel to l , and remain so after the transition. Clearly, the electric multipole radiation emitted is of order $\lambda = l$. The initial and final wavefunctions of the proton may be written as

$$\phi_i = u_i(r) Y_l^m(\theta, \phi) \alpha, \quad \text{and} \quad \phi_f = u_f(r) (4\pi)^{-1/2} \alpha,$$

where α is the spin-up wave function, and u_i, u_f are functions of $r = |\mathbf{r}|$ only. In evaluating the matrix-element $\langle f | Q_{\lambda\mu} | i \rangle$, we shall ignore the second term in Eq. E-15. We then obtain ($\lambda = l$),

$$\langle f | Q_{\lambda\mu} | i \rangle = (4\pi)^{-1/2} e \int_0^\infty r^\lambda u_f(r) u_i(r) r^2 dr.$$

For an order of magnitude estimate, we shall replace the radial integral by a rough approximation. Taking the u 's constant over the nuclear radius R , we obtain

$$\int_0^\infty r^\lambda u_f(r) u_i(r) r^2 dr \approx \frac{3R^\lambda}{(\lambda + 3)},$$

so that

$$|\langle f | Q_{\lambda\mu} | i \rangle|^2 \approx \frac{e^2}{4\pi} R^{2\lambda} \left(\frac{3}{\lambda + 3} \right)^2. \quad (\text{E-20})$$

Substituting this in Eq. E-17, we have the estimate for the single-proton transition probability, which is also called the Weisskopf unit,

$$T_W(E, \lambda \rightarrow 0) = \frac{2(\lambda + 1)}{\lambda [(2\lambda + 1)!!]^2} \left(\frac{3}{\lambda + 3} \right)^2 \frac{e^2}{\hbar c} \left(\frac{\omega R}{c} \right)^{2\lambda} \omega \text{ sec}^{-1}. \quad (\text{E-21a})$$

In a similar manner, by taking the expression E-16 for $M_{\lambda\mu}$, we may obtain the corresponding single-particle estimate for the λ -pole magnetic transition, called the Moszkowski unit,

$$T_M(M, \lambda \rightarrow 0) = \frac{2(\lambda + 1)}{\lambda [(2\lambda + 1)!!]^2} \left(\frac{3}{\lambda + 2} \right)^2 \frac{e^2}{\hbar c} \left(\frac{\hbar/Mc}{R} \right)^2 \\ \times \left(\mu_p \lambda - \frac{\lambda}{\lambda + 1} \right)^2 \left(\frac{\omega R}{c} \right)^{2\lambda} \omega \text{ sec}^{-1}. \quad (\text{E-21b})$$

There is also a Weisskopf unit for magnetic transition; it is

$$T_w(M, \lambda \rightarrow 0) = 10 \left(\frac{\lambda + 2}{\lambda + 3} \right)^2 \left(\mu_p \lambda - \frac{\lambda}{\lambda + 1} \right)^{-2} T_M(M, \lambda \rightarrow 0). \quad (\text{E-21c})$$

These units are often used for all experimental transitions, without distinguishing neutron or proton, and regardless of any model of the states involved. In obtaining numerical values of these units, the nuclear radius R is taken to be $1.2A^{1/3}$ fm. It is of interest to quote these numerical results in the form of the width for γ -decay, defined as

$$\Gamma_\gamma = \hbar T. \quad (\text{E-22})$$

If E_γ is the γ -ray energy, $\Gamma_{w\gamma}(E\lambda)$ is proportional to $A^{2\lambda/3}E_\gamma^{2\lambda+1}$, and $\Gamma_{w\gamma}(M\lambda)$ to $A^{2(\lambda-1)/3}E_\gamma^{2\lambda+1}$. For E_γ in MeV, the numerical coefficients for $\Gamma_{w\gamma}$ are given in Table E-2. Of course, in comparison with experiment, it is the

TABLE E-2 Coefficients for $\Gamma_{w\gamma}$ in sec⁻¹.

λ	$E\lambda$	$M\lambda$
1	6.8×10^{-2}	2.1×10^{-2}
2	4.9×10^{-6}	1.5×10^{-6}
3	2.3×10^{-14}	6.8×10^{-15}
4	6.8×10^{-21}	2.1×10^{-21}
5	1.6×10^{-27}	4.9×10^{-28}

partial γ -ray width which must be used after corrections are made for competing processes such as internal conversion. The single-particle estimate for $B(\sigma\lambda)$ may be easily obtained from Eqs. E-18 and E-20. For example,

$$\begin{aligned} B(E2, 0 \rightarrow 2) &= \sum_{M_f} |\langle f | Q_{2\mu} | i \rangle|^2 = 5 |\langle f | Q_{2\mu} | i \rangle|^2 \\ &= \frac{5}{4\pi} \left(\frac{3}{5} \right)^2 R^4 e^2 \\ &\approx 2.95 \times 10^{-5} A^{4/3} e^2 b^2. \end{aligned} \quad (\text{E-23})$$

This is the unit used in Eq. 9-93 of the text; the value for the downward transition $2 \rightarrow 0$ is, of course, reduced by a factor of 5.

Author Index

Author Index

- Abramowitz, M., 210
Adler, R. J., 134
Afnan, I. R., 294
Ajzenberg-Selove, F., 56, 503
Alburger, D. E., 22
Alder, K., 390, 429
Alexander, T. K., 471
Alistad, J., 556
Andrews, H. R., 437
Andritsopoulos, G., 564
Apalit, V. F., 559
Arndt, R. A., 154, 155, 178
Ashkin, J., 118
Assimakopoulos, P., 22
Aston, F. W., 190
Azuma, R. E., 502

Bacher, R. F., 202
Baerg, A. P., 598
Bamberger, A., 468, 471
Bander, M., 50
Bando, H., 313
Banerjee, B., 497
Banerjee, M. K., 474
Banerjee, P. K., 289, 307, 457
Baranger, M., 355, 385, 390, 396, 400, 422,
 457
Baranov, S. A., 532, 537
Barber, R. C., 189
Bardeen, J., 318
Bargmann, V., 62
Bartholomew, G. A., 431
Bartholomew, R. M., 598
Bartlett, J. H., 26
Bar-Touv, J., 467ff
Bassichis, W. H., 472, 477
Batchelor, R., 431
Baym, G., 193
Beardsworth, E., 22
Becker, R. L., 274
Beil, H., 493
Beiner, M., 460
Bellicard, J. B., 93
Belyaev, S. T., 498
Bencze, Gy., 522
Bennet, M. J., 554
Benson, H. G., 481
Bergère, R., 493
Berkelman, K., 107
Berman, S. M., 134
Bernstein, A. M., 239

Bernthal, F. M., 368
Bertozzi, W., 94, 110
Bertrand, F. E., 493
Bertsch, G. F., 424
Bes, D. R., 325, 328, 422, 499
Bethe, H. A., 92, 100, 118, 168, 193, 202,
 247, 255, 266, 267, 282, 289, 297,
 331, 336
Bhaduri, R. K., 284, 306, 585ff, 606
Bhargava, P. C. 497
Birbrair, B. L., 385
Bishop, R. L., 189
Bivins, R., 617
Bizzeti, P. G., 468, 471
Bjornholm, S., 577, 589, 594, 600, 602
Blair, J. M., 42
Blankenbecler, R., 134
Bleckwenn, J., 108
Bleuler, K., 178
Blin-Stoyle, R. J., 79
Blomquist, J., 447, 585
Bogolyubov, N. N., 318
Bohr, A., 324, 342, 346, 358, 493, 548
Bohr, N., 568
Bolsterli, M., 486, 589, 591
Borggreen, J., 594
Bottino, A., 103, 481
Bounin, P., 93
Bouten, M., 98
Bouten, M. C., 98
Bowman, C. D., 45
Bowman, H. R., 559
Boyd, D. P., 22
Boyer, K., 546
Brack, M., 581, 602
Brandow, B. H., 247, 267, 274, 282, 309,
 331, 336
Breit, G., 155, 162, 179
Brennan, M. H., 239
Brink, D. M., 21, 239, 458
Brody, T. A., 336
Bromley, D. A., 429, 431, 438
Brown, F., 598
Brown, G. E., 16, 141, 297, 374, 474, 486
Brueckner, K. A., 160, 271, 282, 306, 453,
 457
Bryan, R., 178
Buchanan, C. D., 132
Buchler, J. R., 300
Buck, Brian, 372, 375
Burniller, F., 107

Burbidge, E. M., 207
 Burbidge, G. R., 207
 Burcham, W. E., 189
 Cambey, L. A., 189
 Campi, X., 308, 461
 Carazza, B., 481
 Carlos, P., 493
 Carter, E. B., 471
 Case, K. M., 153
 Cerny, J., 58, 206
 Chaban, A. A., 371, 386
 Chadwick, J., 5
 Chamberlain, O., 145
 Charlesworth, A. M., 502
 Chasman, R. R., 528
 Chaudhury, M. L., 522
 Chen, K. W., 107
 Chong, K. F., 36
 Christy, A., 353
 Clark, B. C., 94
 Clark, D. D., 594
 Clark, J. W., 300
 Clarke, W. B., 567, 606
 Clayton, D., 206
 Clement, D. M., 294
 Cline, D., 393, 394
 Cohen, B. L., 328, 447
 Cohen, S., 571ff
 Cohen, V. W., 17
 Cologero, F., 166, 293
 Condon, E. U., 512, 617
 Cone, A. A., 107
 Cooper, L. N., 310, 318
 Corngold, N. R., 17
 Cosper, S. W., 206
 Cottingham, W. N., 170
 Crannel, H., 98
 Croissiaux, M., 107
 Curie, M., 5
 Czirr, J. B., 47
 Dahlblom, T. K., 269, 294, 296
 Dalitz, R. H., 85
 Dally, E., 107
 Damgaard, J., 602
 Das, T. K., 378
 Das Gupta, S., 368, 390, 403, 422, 471, 474
 Davies, K. T. R., 302ff, 331, 457
 Davies, R., 471
 Davydov, A. S., 371, 386ff
 Day, B. D., 256, 269, 294

de Boer, J., 342, 354
 De Pagter, J. K., 98, 132
 De Shalit, A., 238
 de Takacsy, N., 445, 474
 de Tourreil, R., 164, 179
 Dickinson, W. C., 45
 DoDang, G., 355
 Donaldson, R., 145
 Donnelly, I. J., 306
 Donnelly, T. W., 96
 Donovan, P. F., 22
 Dreizler, R. M., 355, 378
 Drell, S. D., 78, 104, 134
 Druin, V. A., 594
 Dubrovina, S. M., 551
 Duckworth, H. E., 189
 Duffield, R. B., 546
 Duhm, H. H., 424, 427
 Dunning, J. R., 107
 Edmonds, A. R., 235, 638
 Ehrenfest, P., 5
 Ehrlich, R. D., 94
 Ehrman, J. B., 55
 Eichler, J., 342, 354
 Eisenberg, J. M., 492
 Eisenbud, L., 159
 Elias, J. E., 98, 132
 Elliott, J. P., 236, 482, 486
 Ellis, P. J., 474
 Elsasser, W., 219
 Elton, L. R. B., 92, 95
 Elze, W., 379
 Engeland, T., 444, 474
 Engelbertink, G. A. P., 468, 471
 Erkelenz, K., 178
 Erwin, A. R., 171
 Evans, H. C., 471
 Faddeev, L. D., 266
 Faessler, A., 363, 371, 385, 389
 Falkoff, D. L., 617
 Feather, N., 541, 566
 Feldman, M., 107
 Ferguson, A. J., 431
 Fermi, E., 219, 650
 Feshbach, H., 85, 165, 179
 Feynman, R. P., 21
 Filippov, G. F., 371, 386ff
 Fiset, E. O., 589, 591
 Fitch, V. L., 113, 119
 Flerov, G. N., 539, 594

Flocard, H., 460
 Flowers, B. H., 235, 486
 Fogel, K. G., 269, 294
 Foldy, L. L., 110
 Fomichev, V. A., 594
 Fong, P., 562
 Ford, K. W., 119
 Fowler, W. A., 206
 Frank, S. G. T., 107
 Fraser, J. S., 542, 556, 565
 Fraser, W. R., 46
 Freeman, J. M., 189
 Freier, G., 42
 Friar, F., 94, 110
 Friar, J. L., 92
 Friedman, J. I., 98, 132
 Friedman, K. A., 155
 Frisch, O. R., 568
 Fröman, N., 667
 Fröman, P. O., 527, 530, 667
 Frosch, R. F., 93, 98
 Fryberger, D., 94
 Fukuda, S., 493
 Fuller, R. W., 561
 Funke, L., 406
 Gai, E. B., 595
 Galster, S., 108
 Gammel, J. L., 160, 271, 282, 306
 Gamow, G., 512, 533
 Gangsksy, Yu. P., 594
 Garvey, G. T., 206, 212
 Geiger, H., 82, 509, 511, 533
 Geiger, J. S., 437
 Gelli-Mann, M., 21, 104
 Gerace, W. J., 206, 212
 Gertzman, H. S., 394
 Geschwind, S., 189
 Ghiorso, A., 509, 516, 533
 Gibson, B. F., 98
 Giltinan, D. A., 161
 Gindler, J. E., 542, 562
 Giraud, B., 477
 Glendenning, N. K., 130, 424, 427
 Götz, U., 390, 429
 Goldberg, A., 98
 Goldenberg, J., 103
 Goldhaber, M., 492
 Goldman, D. T., 453
 Goldstein, H., 29, 52, 358
 Goldstone, J., 255
 Gomes, L. C., 253

Goodman, A. L., 468
 Goswami, A., 468
 Gottfried, K., 167
 Gove, H. E., 394, 429, 431, 438
 Graber, J., 189
 Graham, R. L., 437
 Grange, P., 179, 287, 292, 303
 Green, A. E. S., 178, 180
 Green, A. M., 16, 166, 296, 474
 Greiner, W., 363, 371, 385, 389, 492
 Griffin, J. J., 494, 498
 Griffy, T. A., 97, 108
 Gritsyuk, N. Yu., 559
 Grodzins, L., 382
 Gross, E. E., 50, 51
 Grove, N. B., 189
 Gunion, J. F., 134
 Gunye, M. R., 403, 468, 482
 Gurney, R. W., 512
 Gustafson, C., 427, 576, 577, 583, 590

Haddock, R. P., 47, 50
 Haftel, M. I., 280
 Hageb, E., 556
 Hahn, B., 89, 541
 Halpern, I., 541, 566, 598
 Hamada, T., 130, 162, 179
 Hamilton, D., 21
 Hansen, E. R., 527
 Haracz, R. D., 155
 Hargrove, C. K., 94
 Harris, S. M., 496
 Harting, D., 58
 Hartmann, G. C., 98, 132
 Hartzler, A. J., 145
 Harvey, B. G., 58, 424, 427
 Harvey, M., 471
 Hausser, O., 353, 471
 Haxel, O., 219
 Hayward, J., 474
 Heisenberg, J., 93, 94, 103, 110
 Heisenberg, W., 26, 190
 Heitler, H., 5
 Heller, L., 43, 44, 51
 Hendrie, D. L., 424, 427
 Henley, E. M., 50, 51, 53, 59
 Herman, R., 94
 Herzberg, G., 5
 Hess, W. N., 145
 Heunemann, D., 602
 Hill, D. L., 119, 475
 Hjorth, S. A., 370, 373

Author Index

- Hoffman, F. de., 168
 Hofstader, R., 85, 89, 94, 100, 107, 108
 Holinde, K., 178
 Holladay, G. S., 617
 Hollander, J. M., 368
 Holt, J. M., 155
 Hooton, B. W., 471
 Hoshizaki, N., 154, 155
 Houk, T. L., 37
 Hoyle, F., 207
 Hughes, E., 107, 108
 Huizenga, J. R., 379, 542, 562, 563
 Hukai, Y., 189
 Hulet, E. K., 554, 563
 Hull, M. H., Jr., 162, 179
 Hungerford, E. V., 50
 Hyde, E. K., 206, 548
 Hyuga, H., 16
 Ichimura, M., 16
 Ignatyuk, A. B., 595
 Igo, G., 514
 Immele, J. D., 379
 Ingber, L., 178, 300
 Inglis, D., 496
 Irvine, J. M., 449, 481
 Isabelle, D. B., 103
 Jackson, A. D., 297, 482
 Jaffe, R. L., 206, 212
 Jägare, S., 373
 Jakeman, E., 313
 Jankus, V. Z., 108
 Janout, Z., 155
 Janssens, T., 107
 Jarvis, O. N., 424, 427
 Jastrow, R., 152
 Jenkin, J. G., 189
 Jensen, A. S., 602
 Jensen, D. A., 94
 Jensen, J. H. D., 219, 235
 Johansson, T., 577
 John, W., 554, 563
 Johnson, A., 369, 373
 Johnston, I. D., 130, 162, 179
 Joliot-Curie, F., 5
 Jungclaussen, H., 594
 Junker, K., 390, 429
 Källén, G., 9
 Kahana, S., 443
 Kallio, A., 337
 Kanellopoulos, T. V., 141
 Kaplan, I., 520
 Karnaughov, V. A., 594
 Katz, L., 598
 Kaun, K. H., 406
 Kazarinov, Yu. M., 155
 Kellogg, J. B., 123
 Kelson, I., 206, 212, 463ff, 467ff
 Kemnitz, P., 406
 Kendall, H. W., 98, 132
 Kerman, A. K., 324, 385, 410, 456
 Khadkikar, S. B., 468, 482
 Kiang, D., 385
 Kirk, P. N., 98, 132
 Kisslinger, L. S., 324ff, 397, 499
 Klein, A., 355, 378
 Klein, H., 108
 Kluyver, J. C., 58
 Koester, L., 37, 650
 Kohman, T. P., 509
 Kolsky, H. G., 123
 Konecny, E., 602
 Kouki, T., 296
 Kowalski, S. B., 598
 Kramer, G., 130
 Krane, K. S., 22
 Krappe, H. J., 581
 Kugler, G., 567, 606
 Kulakov, V. M., 537
 Kumar, K., 355, 385, 390, 395, 400, 422,
 453
 Kuo, T. T. S., 297, 457
 Kusunegi, A., 58
 Kutikov, I. E., 559
 Kuzminov, B. P., 552
 Lamm, I.-L., 427, 577, 583, 590
 Lampi, E. E., 42
 Landau, L. D., 360
 Lane, A. M., 236, 324
 Langenberg, D. N., 17
 Lark, N. N., 594
 Lassila, K. E., 162, 179
 Lauritsen, T., 56
 Law, J., 324
 Lawson, R. D., 220, 324
 Lebedev, V., 559
 Lehmann, P., 107
 Lehar, F., 155
 Leprêtre, A., 493
 Lesser, P. M. S., 394
 Le Tourneau, J., 470

Author Index

- Leung, J. S., 53
 Levinson, C. A., 271, 282, 467
 Lewis, M. B., 493
 Lifshitz, E. M., 360
 Lin, E. D., 328
 Lin, W.-F., 585
 Lin, Y. C., 92
 Lindgren, I., 123
 Lipinski, H. M., 38, 51
 Litherland, A. E., 429, 431, 438
 Littauer, R. M., 107
 Lockett, A. M., 457
 Loiseau, B. A., 296, 457
 Lomon, E. L., 165, 170, 179, 180, 300
 Lougheed, R. W., 554, 563
 Love, W. A., 145
 Lumpkin, A. H., 378
 Lynn, J. E., 551, 595
 McCarthy, J. S., 93, 96, 98, 103
 McCarthy, R. J., 302ff, 331
 McDonald, F. A., 162, 179
 Macdougall, J. D., 189
 Macfarlane, M. H., 324, 477ff
 Macfarlane, R. D., 509
 McGowan, F. K., 396
 Macgregor, M. H., 154, 155, 157, 178
 McKellar, B. H. J., 21, 296
 McKeown, M., 378
 McKinley, W. A., 85
 McLatchie, W., 189
 McManus, H., 429, 438
 McVoy, K. W., 46, 50
 Mahoney, J., 424, 427
 Majorana, E., 26
 Mang, H. J., 497, 531, 534, 535
 Manify, J. J., 50
 March, R., 171
 Margolis, B., 445
 Mariscotti, K. A. J., 372, 375
 Mark, H., 220
 Markov, B. N., 594
 Marsden, E., 82
 Marsh, B., 22
 Marshak, R. E., 159, 160
 Marshalek, E. R., 385
 Marshall, L., 650
 Masterson, K. A., 457
 Mathews, P. T., 213
 Matsumoto, M., 136
 Mavromatis, H. A., 482
 Mayer, M. G., 219, 235
 Meitner, L., 568
 Meldner, H., 462
 Melvin, M. A., 617
 Metropolis, N., 143, 157, 617
 Meyers, W. D., 197, 202ff
 Michael, C., 130, 294
 Michel, F. C., 21
 Migneco, E., 550
 Mikaelyan, L. A., 559
 Mikhiev, V. L., 594
 Miller, M. D., 155, 300
 Milner, W. T., 396
 Milton, J. C. D., 542, 556, 559, 565
 Mitchell, G., 471
 Mitra, A. N., 165
 Miyazawa, A., 78
 Möller, P., 427ff, 576, 577, 583, 590, 600
 Mongan, T. R., 165
 Moravcsik, M. J., 50
 Mortiz, J., 108
 Moshinsky, M., 336, 504
 Moszkowski, S. A., 176, 178, 313, 334, 459,
 632
 Mott, N. F., 85
 Mottelson, B. R., 324, 342, 374, 415, 417ff,
 429, 493, 497
 Mukherjee, P., 447
 Murray, G., 189
 Muzychka, Y. A., 591
 Myers, W. D., 573
 Nagata, S., 313
 Nakamura, Y., 163
 Nathan, O., 353
 Neeman, Y., 104
 Negele, J. W., 92, 94, 110, 300, 306ff, 457,
 460
 Neiler, J. H., 554ff
 Nemeth, J., 300, 457
 Newton, T. D., 410
 Nifenecker, H., 556
 Nilsson, B., 427, 576, 583, 590
 Nilsson, S. G., 342, 353, 410, 412, 413,
 415ff, 427ff, 498, 576, 578, 583,
 590, 600
 Nissim-Sabat, C., 94
 Nix, J. R., 428, 568, 576, 589, 591
 Nogami, Y., 36, 53, 296, 324, 457
 Nöideke, G. K., 94
 Nordheim, L., 239
 Northrup, J. A., 546
 Norton, J. L., 589, 591

Author Index

- Noyes, H. P., 38, 51
 Nuttall, J. M., 511, 533
 Nygren, D. R., 47, 50
- Ohubo, S., 159
 Olness, J. W., 468, 471
 Olsen, C. E., 22
 Oppenheimer, J. R., 5
 Ormrod, J. H., 189
 Orphan, V. J., 189
 Otroschenko, G. A., 551
- Pais, A., 153
 Pal, M. K., 456
 Pandharipande, V. R., 300
 Pappas, A. C., 556
 Parikh, J. C., 478
 Parker, W. H., 17
 Partovi, M. H., 170, 180
 Pashkevich, V. V., 562, 591
 Paul, E. B., 429, 431, 438
 Pauli, H. C., 390, 429, 581, 602
 Peaslee, D. C., 197
 Pedersen, J., 552, 594
 Pehl, R. H., 58
 Peierls, R. E., 166, 475
 Peker, L. K., 385
 Pelte, D., 471
 Pennington, E. M., 529
 Perlman, I., 516, 517, 526
 Perring, J. K., 155
 Pethick, C. J., 193
 Petschek, A. G., 267, 282, 331, 336
 Phipps, T. E., 123
 Piel, W. F., Jr., 378
 Pines, D., 324
 Pitthan, R., 493
 Pleasonton, F., 554, 557
 Pleve, A. A., 594
 Poggenburg, J. K., 531, 535
 Polikanov, S. M., 594
 Poskanzer, A. M., 206
 Povh, B., 468, 471
 Powers, R. J., 94
 Pradhan, H. C., 324
 Prakash, A., 155
 Pratt, R. H., 97
 Preston, M. A., 179, 284, 287, 292, 303,
 385, 390, 403, 422, 520, 522, 526,
 529
 Prior, O., 498
 Pryor, R. J., 394
- Quang-Hoc, N., 470
 Quentin, P., 460
 Qvist, B., 269, 294
- Rabi, I. I., 123
 Rabotnov, N. C., 595
 Ragnarsson, I., 578
 Rainwater, J., 113, 119, 342
 Raisbeck, G. M., 567
 Rajaraman, R., 266, 296
 Ramsey, N. F., 17, 65, 107, 123
 Rand, R. E., 98
 Rarita, W., 128
 Rasetti, F., 5
 Rasmussen, J. O., 323, 368, 509, 517, 523,
 526, 528, 531, 533, 535
 Rasmussen, N. C., 189
 Rassey, A. J., 419, 431
 Ravenhall, D. G., 88, 89, 91, 94
 Rayleigh, Third Baron, 343, 648
 Rees, J. R., 107
 Reid, R. V., 123, 130, 163, 292, 303
 Rho, M., 323, 498
 Ribrag, M., 556
 Rich, M., 494
 Rigopoulos, R., 58
 Ring, P., 497
 Ripka, C., 457, 471, 472, 477
 Rivet, E., 58
 Robinson, R. L., 396
 Rockmore, R. M., 374
 Rolfs, C., 502
 Rose, M. E., 235, 632, 634, 638
 Rosenblum, S., 509, 533
 Rosenbluth, M. N., 107
 Ross, A., 220
 Ross, C. K., 296, 375, 457, 585ff, 606
 Ross, M., 78
 Rostovsky, V. S., 371, 390
 Rotenberg, M., 457, 617
 Rouse, G., 107
 Rowe, D. J., 324, 456, 497
 Royds, T., 509
 Ruppel, H. M., 162, 179
 Russek, A., 78
 Rutherford, E., First Baron, 4, 5, 82, 509
 Ryde, H., 369, 373
- Sachs, A. M., 58
 Sachs, R. G., 78, 81
 Saethre, Ø., 373
 Sakai, M., 392

Author Index

- Sakurai, J. J., 103
 Saladin, J. X., 394
 Samaranayake, V. K., 178
 Sanderson, E. A., 482
 Sandulescu, A., 522
 Saudinos, J., 424, 427
 Sauer, P. U., 303, 331
 Saunier, G., 470
 Sayer, R. O., 396
 Scharff-Goldhaber, G., 372, 375
 Scharff-Goldhaber, S., 378
 Scherk, L., 522
 Schiff, L. I., 82, 108, 645
 Schlenker, S. L., 300
 Schmidt, K. H., 108
 Schmidt, T., 75
 Schmitt, H. W., 554ff
 Schmitt, R. A., 546
 Schrieffer, J. R., 313, 318
 Schwalm, D., 468, 471
 Schwartz, C., 75, 238
 Schweber, S. S., 168
 Schwinger, J., 128
 Scott, B. L., 178, 334
 Seaborg, G. T., 516, 545
 Seamon, R. E., 155
 Seeger, P. A., 208
 Segré, E., 145
 Sells, R. E., 617
 Serduke, F. J. D., 294
 Shambroom, D., 37
 Sharpey-Schafer, J. F., 437
 Shatinsky, V. M., 537
 Sheline, R. K., 363, 371, 385, 389, 431, 578
 Sher, M. S., 43, 51
 Shigin, V. A., 551
 Shlaer, W., 107
 Shortley, G. H., 617
 Shucan, T. H., 16
 Shukla, A. P., 477ff
 Sick, I., 93, 96, 98, 103
 Siegel, R. T., 145
 Siemens, P. J., 100, 284ff, 299, 306
 Signarbieux, C., 556
 Signell, P. S., 43, 51, 155, 160, 163, 170,
 178
 Silsbee, H. B., 123
 Simon, A., 617
 Simonov, Yu. A., 166, 293
 Singh, B., 482
 Sites, J. R., 22
 Skobelev, N. K., 594
- Skyrme, T. H. R., 459
 Slater, R. M., Jr., 47
 Sleator, W., 42
 Sletten, G., 594
 Sliv, L. A., 385
 Smyrenkin, G. N., 595
 Sobczewski, A., 427, 576, 577, 583, 590
 Sodan, H., 406
 Sogard, M. R., 98, 132
 Sorenson, R. A., 324, 325, 327, 397, 499
 Specht, H. J., 602
 Spruch, L., 78
 Sprung, D. W. L., 164, 179, 247, 289, 292,
 294, 300, 307, 457, 461
 Srivastava, M. K., 164
 Stapp, H. P., 143, 157
 Stegun, I. A., 210
 Stein, N., 449
 Stein, W. E., 554, 556
 Stelson, P. H., 382, 396
 Stephens, W. E., 206
 Stephenson, G. J., Jr., 474
 Steyert, W. A., 22
 Stokes, R. G., 546
 Stovall, T., 103
 Strassmann, F., 541
 Struble, G. L., 379, 468
 Strutinsky, V. M., 206, 577, 579, 591, 600,
 602
 Stuart, R. N., 45
 Subbotin, V. G., 594
 Suelzle, L. R., 98
 Suess, H. E., 219
 Swamy, N. V. J., 617
 Swant, J. A., 189
 Swiatecki, W. J., 197, 202ff, 559, 568,
 571ff, 573, 602
 Symon, K. R., 82
 Szymanski, Z., 373, 422, 427, 576, 577,
 583, 590
- Tabakin, F., 165, 179, 280
 Talmi, I., 206, 212
 Tamagaki, R., 163
 Tamura, T., 355
 Tarbutton, R. M., 457
 Taylor, B. N., 17
 Taylor, R., 107
 Teleghi, V. L., 94
 Teller, E., 492
 Ter-Akopyan, G. M., 594
 TerLouw, W. J., 300

- Terrell, J., 605
 Thaler, R. M., 160, 161
 Theobald, J. P., 550
 Thomas, J. D., 567
 Thomas, R. G., 55
 Thomas, T. D., 564
 Thompson, S. G., 204, 509, 533, 559
 Thomson, J. J., 4
 Thouless, D. J., 497
 Tibell, G., 58
 Tomusiak, E. L., 443
 Torizuka, Y., 493
 Törn, A., 269, 294
 Tripp, R., 145
 Tsang, C. F., 204, 427, 576, 577, 583, 590
 Überall, H., 85, 99, 103
 Ueda, T., 178, 180
 Uehling, E. A., 43
 Ugadawa, T., 355
 Uher, R. A., 499
 Uhrhane, F. J., 93
 Unik, J. P., 563
 Vaida, M. L., 123, 129
 Valatin, J. G., 318, 374, 497
 Vandenbosch, R., 564
 Vanderhaeger, G., 58
 van Leuven, P., 98
 van Oostrum, K. J., 94
 van Rookhuyzen, P., 189
 van Speybroeck, L. P., 98, 132
 Vautherin, D., 300, 458, 460, 462
 Verhaar, B. J., 477
 Verondini, E., 50
 Veyssi  re, A., 493
 Villars, F., 134
 Vinciguerra, D., 103
 Vinh Mau, R., 170
 Viola, V. E., Jr., 189
 Vogt, E., 522
 Volkov, A. B., 368, 377
 Von Weizs  cker, C. F., 202
 Vorotnikov, P. E., 551
 Wahlborn, S., 447, 585
 Walcher, Th., 493
 Walecka, J. D., 78, 97, 239, 253
 Walker, G. E., 96
 Walker, J. K., 107
 Walter, F. J., 554
 Walter, W. D., 171
 Wapstra, A. H., 188, 189
 Warburton, E. K., 468, 471
 Ward, D., 437
 Warke, C. S., 306, 468
 Watari, W., 136
 Watson, K. M., 45
 Webb, S. J., 95
 Weber, G., 58
 Weber, J., 602
 Wegener, D., 108
 Weiss, M. S., 98
 Weisskopf, V. F., 253, 675
 Weitzner, H., 306
 Wesolowski, J. J., 554, 563
 West, E., 171
 Wheeler, J. A., 475, 568
 Whetstone, S. L., 556
 Whitney, R. R., 98
 Wiegand, C. E., 100, 145
 Wigner, E. P., 26, 62, 159, 202, 638
 Wilets, L., 112, 571, 572
 Wilkin, C., 130, 294
 Wilkinson, D. H., 22, 594
 Wille, U., 581
 Williams, J. H., 42
 Wilson, R., 37, 38, 51, 107
 Wilson, R. N., 88
 Wilson, R. R., 107
 Winhold, E. J., 598
 Winslow, G. H., 516
 Winter, G., 406
 Wolfenstein, L., 139
 Wong, C. Y., 602
 Wong, S. K. M., 470
 Woo, C. W., 300
 Woolcock, W. W., 178
 Wooten, J. K., 617
 Wright, R. M., 154, 155, 163, 178
 Wu, C. S., 112, 355, 632
 Wycech, S., 427, 576, 577, 583, 590
 Yamaguchi, Y., 165
 Yearian, M. R., 94, 98, 103, 107, 108, 132
 Yennie, D. R., 88
 Yoccoz, J., 475, 477
 Yoder, N. R., 45, 155, 163
 Ypsilantis, T., 143, 145, 157
 Yukawa, H., 134
 Zacharias, J. R., 123
 Zachariassen, F., 104
 Zamick, L., 504
 Zeller, M., 47

Subject Index

Subject Index

- Alpha-decay, 509ff
and angular momentum, 522, 533
distribution of α -particles on nuclear
surface, 525ff
experimental data, 509ff
formation factor, 516, 531ff
Geiger-Nuttall law, 511
hindrance factor, 510
lifetimes, 510
nuclear radius, 520
optical potential, 514, 521
and pairing force, 535
quadrupole moment, 526
reduced width, 523
and collective model, 533, 534
selection rules, 533
theory
barrier penetration, 517
and non-central field, 526
"traditional," 515, 520
- Alpha-particle, 509
radius, 521
- Angular momentum 611ff; *see also*
 D -functions, W -functions, Collective
model, Single-particle model
in alpha-decay, 522, 533
Clebsch-Gordan coefficients, 616ff
commutation relations, 360, 611
in electromagnetic field, 670
in gamma ray emission, 673
and impact parameter, 28, 136
 λ , pseudo-, 413
and multipole order, 673
of nucleons in nuclei, 223, 235
operators for, 612, 614, 623
projected in Hartree-Fock calculations,
474
reduced matrix element, 626
relative to moving principal axes, 360
in special relativity, 632
total nuclear, 66ff
in collective model, 368, 407
of odd- A and even- A nuclei, 67
of odd-odd nuclei, 237
in single-particle model, 223, 235
tables, 224ff, 242
of two nucleons in same shell, 234
vector addition of, 615ff
- Annihilation operator, 653
- Asymptotic quantum numbers, 413, 533
- Asymptotic scattering wave function, 31,
644ff
- Atom, 4, 12
characteristics of electronic atom, 111
muonic, 85, 111ff
- Atomic abundances, 207
- Atomic mass, 188ff
- Barrier; *see also* Transmission coefficient,
Penetration factor
in α -decay, 515ff
Coulomb, general discussion, 40ff
in fission, 589ff
Bartlett forces, 26
- Bessel functions, spherical, 641
- β (collective parameter) 356, 383
- β -decay, 6, 208
 $B(E2)$, 382, 672, 676
- Bethe-Goldstone equation, 252ff, 263
- Binding Energy, 188ff; *see also* Coulomb
energy; Deuteron; Kinetic energy;
Separation energy; Saturation;
Surface energy; Symmetry energy;
Shell effects
and α - and β -decay energetics, 189
of atomic electrons, 188
average per nucleon, 189, 190, 247
calculated for finite nuclei, 300ff
closed shell nuclei calculated, 456ff
defined, 188
of deuteron, 51
and exchange forces, 195ff
and exclusion principle, 199, 214, 247ff
and Fermi gas model, 191ff
Garvey-Kelson formula, 211ff
isobaric parabolas, 198, 199
of A -particle in hypernuclei, 213
of nuclear matter, 247
semi-empirical formula, 202, 577
shell effects in, 203, 204, 578
and stability of nuclei, 204, 206, 300
Strutinsky method, 579ff
in superheavy elements, 583
- Born approximation, 153
in nucleon scattering, 153, 157
- Boson resonances, 170ff
experimental data, 172
and nucleon form factors, 111
- Brueckner theory, 271ff
- Center-of-mass, in collective motion, 344
coordinates, 29, 503
in E -1 transitions, 491
in model calculations, 219
- Charge density, *see* Density

Charge independence of nuclear forces, 50ff
 experimental evidence, 53ff
 violation by electromagnetic forces, 53
 selection rules, 57
Charge multiplet, 9, 55
Charge parity, 58
Charge symmetry, 51
 experimental evidence, 54
 Thomas-Ehrman effect, 55
 charge parity, 58
Clebsch-Gordan coefficients, 616ff
Clusters, 298, 514
Clusters, many-body, 263, 294, 301
Coherent scattering, 37, 647
Collective model, 340ff; *see also Eulerian angles; Symmetry properties; Single particle model for nonspherical nuclei; Distortion of nuclear shape; Distortion parameters; Moment of inertia; Alpha-decay*
 and α -decay, 532ff
 and angular momentum, 347, 350, 360, 368, 372, 379, 386, 392, 405, 438
 β defined, 356, 383
 β - γ plots, of potential energy, 357, 360, 400ff
 of wave function, 400ff
 β -vibrations, 361ff, 368, 378ff, 385, 398, 393
Bohr Hamiltonian, 361, 396, 397
 collective variables, 341, 397
 coupling to particle motion, 403ff, 410
 couplings with vibrations, 362ff, 370, 371
 decoupling parameter, 408, 431
 electric quadrupole moment, 351, 353, 354, 382ff, 393ff, 527
 equilibrium shape, 420ff, 468, 470
 preference for prolate shape, 422
 γ defined, 356
 γ -vibrations, 361ff, 378ff, 385, 390, 393
 irrotational flow, 343, 348, 493
 K , possible values, 367, 368, 379, 386, 409
 K -mixing of states, 386, 407, 598
 K selection rules, 384, 532
 level sequence, 350, 369, 378, 386, 388, 392, 409, 440, 583
 liquid drop model, 343ff, 569ff
 moment of inertia, 359, 362, 371ff, 386, 493ff

back-bending, 372-4; VMI, 374ff
 nonaxial shape, 357, 386ff, 393, 402, 467ff
 octupole vibrations, 347, 368, 379, 380, 446
 odd-odd nuclide, 440
 and optical model, 424
 phonons, 346ff
 β -type, 361
 γ -type, 361
 polarization of the core, 342, 444
 quadrupole vibrations, 346ff
 quasi-rotational bands, 392, 393
 rotational bands, 368-9, 378ff, 385, 388, 392, 409, 430, 437, 532, 601
 from projection of HF intrinsic state, 474ff
 rotational model and $BE(2)$, 381ff
 rotational wave functions, 363, 367, 386, 397, 401, 407, 408
 symmetries of, 364ff, 406
 rotation-particle coupling, 403ff, 410
 rotation-vibration coupling, 362ff, 370, 371
 spin-orbit force, 410, 413
 symmetry restrictions, 364ff
 transition nuclei, 390ff
 energy levels, 391-3
 quadrupole moments, 394-5
 Kumar-Baranger calculations, 396ff
 vibrational excitations, 343ff, 358, 361, 362, 380, 385, 391, 437
 vibrational model and quadrupole moments, 352, 354
 vibrational parameters, 345, 437, 498
 vibrational wave function, 349
Collective dipole state, 490ff
Compressibility, *see Incompressibility*
Configuration mixing, 233, 239ff, 448, 473
Conservation laws, 21, 126
Constituents of nuclei, 14ff
Core excitation, 445
Coriolis force, 374, 405, 408ff, 430
Correlations of nucleons in nuclei and nuclear matter, 244ff, 304ff; *see also Nuclear matter; G-matrix; Finite nucleus calculations; Healing distance; Wound integral*
Coulomb energy, 197, 199, 203, 303
Coulomb force, 9, 20, 83, 234
Coulomb potential in nucleus, 83, 89
Coulomb scattering, 41, 82

penetration factor, 41
 distance of closest approach, 83
Coulomb wave functions, 39ff, 639
Cranking formula, 496
Creation operator, 653
Cross section for scattering, in S-state, 32
 for zero energy, 33
 for low energy, 38
 for Coulomb scattering, 41, 82, 644ff
 differential, 82

 \mathcal{D} -functions, 622ff
 Δ -resonances, 13
 $\Delta(1236)$, 14, 295
Depolarization, 141
Density operator, 453
Density of nuclei, 85ff, 100, 247, 292ff, 306, 461
 analysis of experiments, 87, 91ff
 central depression in, 93, 461
 effect of nucleon size, 95
 for deformed nuclei, 102
 for gold, 91
 for lead, 93
 for oxygen, 96
 from shell model, 95, 461
 functional forms, 91, 119
 two-parameter Fermi, 87
 three-parameter Fermi, 90
 oscillations in, 93
 table of, 99
Density of states, 196, 210; *see also Strutinsky method*
 surface effects, 210
Detectors, resolution of, 15, 113
Deuteron, 20, 35, 46, 123ff
 binding energy, 51
 D -state admixture, 129, 130
 exchange currents, 130ff
 quadrupole moment, 123
 magnetic moment, 123
 radius, 125
 relation to n - p scattering, 36
 scattering with π^+ , 131
 and tensor force, 123
 and various potentials, 129
 wave function, 129
Dineutron, 21, 37
Dipole moment, *see Electric dipole moment; Magnetic moment*
Dirac equation and matrices, 628ff
Distortion of nuclear shape, 73, 127, 202, 420ff, 463ff; *see also Collective model*
 parameters $\sigma, \beta, \epsilon, \eta$ defined, 70, 356, 414
Double scattering and polarization, 137ff
Effective charge, 309, 444
Effective force, in nuclei, 306ff, 443, 457, 460
Effective mass, 281
Effective range, 34, 36, 41
 for Bargmann potential, 62
 for hard-core, 62
 n - n , 50, 51
 n - p , 38, 51
 p - p , 45, 51
 theory, 34, 41, 642
Electric dipole moment, 65, 69, 491ff, 598
Electric moment, $l = 4$, 423ff
Electric monopole, 674
Electric potential, 44
Electric quadrupole moment, 64, 65, 68ff, 382ff, 672; *see also Collective model* and $B(E2)$, 384
 defined, 68, 351, 672
 of deuteron, 123
 of excited states, 353, 354
 giant resonance, 493
 intrinsic, 70, 382
 intrinsic and static, 393
 measured values, 73, 224ff
 and nuclear ellipticity, 70, 383
 and pairing force, 422
 and shell effects, 74, 422
 of a single particle, 72
 in transitions, 444
 table, 224-231
Electromagnetic current, 105ff, 671
Electromagnetic interaction, 106, 483, 637, 671
Electromagnetic radiation, 668ff
Electron scattering, 85ff, 105ff
 analysis of, 91ff
 correction for bremsstrahlung, 118
 on gold, 90
 on lead, 91
 on nucleon, 104
 recoil effects, 118
Energy gap above correlated state, 322, 324, 397, 466
Energy production in stars, 207
Eulerian angles, 355, 621

Exchange currents, 17, 134
 Exchange forces, 24ff; *see also* Neutron-proton scattering; Nucleon forces; Saturation; Bartlett, Heisenberg, Majorana, Serber forces
 definition, 24
 and high-energy scattering, 149, 153
 matrix elements, 236
 and saturation, 195, 291
 and spin of odd-odd nuclides, 237

Fermi gas model, 191ff
 zero temperature, 192
 Pauli principle correlations, 248ff
 Fermi momentum, 193, 210
 of nuclear matter, 194, 248
 of finite nucleus, 252, 272
 and pairing, 322ff
 Fermions, 7
 Final state interactions, in three-body decays, 46
 in two-pion resonances, 171
 Finite nucleus, Brueckner calculation, 252ff
 effective interaction, 306ff
 Hartree-Fock calculations, 449ff
 local density approximation, 305
 ^{20}Ne and ^{24}Mg , 465ff
 partial occupancy of states, 273, 300
 particle-hole calculations, 482ff
 results in ^{16}O , ^{40}Ca , ^{208}Pb , 303, 304, 444ff, 448, 461, 471, 483, 486
 self-consistency, 271ff
 shell model calculations, 441ff
 single-particle spectrum, 301ff

Fission, 541ff
 angular distribution, 597ff
 barrier, 545ff, 573, 575
 double-humped, 552, 589ff
 charge distribution, 566
 delayed neutrons, 542
 energetics, 541ff, 553ff, 566
 fissionability parameter, 571
 fragment masses, 553ff
 asymmetry, 560, 600
 fine structure, 559, 564
 symmetric, 563
 fragment velocities, 555ff
 isomers, 594, 601
 liquid drop model, 569ff, 600
 neutron-induced, 546, 548ff, 598
 thermal, 557ff

301

pairing effects, 583
 photofission, 546, 598
 prompt neutrons, 542, 559, 561, 604
 resonances, 548, 588, 595, 597
 saddle point, 568, 573
 scission, 541
 shell effects, 573, 576ff
 spontaneous, 558ff, 563, 593
 Strutinsky method, 579ff, 585
 ternary, 541, 544, 566, 606
 transition state, 549, 597

Forces, *see* Nucleon forces, Exchange forces, Potential, etc.

Form factor, electromagnetic, of nuclei, 86, 121
 diffraction minima, 96, 121
 for carbon, 97
 for deuteron, 98
 for helium, 98
 for lithium, 98
 for oxygen, 96
 from projected HF wave functions, 98
 oscillations in, 88

Form factors of nucleons, 103ff
 and boson resonances, 111
 definitions, 106
 non-relativistic limits, 110
 neutron, 108, 109
 proton, 107

γ (collective parameter), 356
 γ -decay, *see* Radiative transitions
 γ -matrices, 631
 Geiger-Nuttall rule, 511
 G-matrix in nuclear matter and finite nuclei,
 and Bethe-Goldstone equation, 252ff
 BBP theorem, 267
 calculation, 279ff, 282, 335
 effective interaction from, 306ff, 357ff
 in Hartree-Fock calculations, 457
 identities involving, 330ff
 local-density approximation, 305, 457
 many-body approach, 259
 pair approximation, 257
 partial-wave decomposition, 277ff
 reference spectrum, 282, 335
 renormalized BHF calculation, 271, 300
 self-consistency, 270, 271
 separation method, 333
 single particle potential and, 266ff, 289,

S-state matrix elements, 284
 Gyromagnetic ratio, *see* Magnetic moment
 Harmonic oscillator, density distribution, 95, 250
 form factor, 96, 121
 Kallio's approximation, 337
 Moshinsky brackets, 336
 Nilsson transformation, 412
 oscillator parameter, 95, 303, 304, 414
 potential, 96, 411
 wave functions, 120
 Hartree-Fock method, 449ff
 density-dependent, 452, 460
 in deformed nuclei, 463ff
 intrinsic state, 463, 479
 matrix elements, 451
 and pairing, 481
 projection of angular momentum, 474ff, 505
 rotational bands, 477
 Heiling distance, 257, 285
 Heisenberg force, 26
 Helicity, 631
 Hole states, 656
 Hypercharge, 10
 Hypernuclei, 213

Impact parameter, 28, 136
 Incompressibility of nuclear matter, 299, 331, 504
 and breathing mode, 332
 Inertial parameter B_2 , for β - and γ -vibrations, 385
 in hydrodynamic model, 345
 in Kumar-Baranger theory, 396ff
 microscopic calculation, 498
 relation to $B(E2)$, 352, 437
 relation to moment of inertia, 359

Internal conversion, 674
 Intrinsic state in Hartree-Fock, 463, 479
 Isobars, binding energy of, 199
 Isomers, shape, 593ff
 Isotopes, 4, 5
 Isotope shift in X-rays, 121
 I-spin (or Isospin), 7, 615
 conservation, 52, 55, 59
 multiplets, 9, 55
 and nuclear force, 59
 of nuclei, 233
 raising and lowering operators, 8, 615

Kinetic energy, and Fermi gas model, 194
 average per nucleon, 193
 surface effects, 196

Lambda (Λ) particle, 63, 213
 interaction with nucleon, 59
 Legendre polynomial, 613, 623
 Lippman-Schwinger equation, 167
 Liquid-drop model, *see* Binding energy, Collective Model, Fission

Magic numbers, 204ff, 218ff
 Magnetic dipole moments, 75ff, 627, 671
 and collective model, 78

deuteron, 123, 132ff

exchange, 17

exchange currents, 130

g -factor, 75, 671, 673

isoscalar and isovector, 80

nucleons, 17, 106

of odd-neutron nuclides, 77, 224

of odd-proton nuclides, 76, 228

orbital, 66

quenching, 78

Sachs' theorem, 81

Schmidt limits and groups, 75ff

and shell model, 75

table, 224-231

Majorana force, 26

Many-body forces, 19, 294ff

Mass, atomic. *See* Binding Energy

determinations, 188, 189

standards, 188

tables, 189

Mass-energy parabolas, 198, 199

Mass-excess, 188

Mass formulae, 202, 211, 577

Mass number, 5

Mass spectroscopy, 188

Mesons, 10, 14, 106, 130ff, 166ff; *see also* Muons, Pions

Mixing parameter ϵ_1 , 143, 156, 178-9

Moment of inertia, 359

back-bending, 372-4

and classical stretching, 376

forking, 378

in hydrodynamic model, 359, 362, 386ff

microscopic calculation, 493ff

variable moment model (VMI), 374-8

Momentum-dependent potentials, 165, 179, 246

Moszkowski unit, 676

Mott cross-section, 41, 85
 Multipole expansion, 64, 668
 Multipole moments, 64, 65, 68
 of nuclear interaction, 488–9
 Multipole operators, 659, 672
 Muons, 84
 Muonic atoms, 84, 111ff
 nuclear size effects, 112ff
 Neutron, 5, 6, 17, 108, 109
 Neutron optics, 36, 37, 648
 Neutron-neutron interaction, 45ff, 166ff;
 see also Nucleon force, Potential
 final state interaction, 46
 scattering length, 47, 51
 effective range, 50, 51
 Neutron-proton scattering, 20, 28, 36, 146,
 154; *see also* Nucleon force, Potential
 angular distribution, 146
 chemical binding in, 36
 cross section at low energy, 33, 36, 38
 at high energy, 146
 with tensor forces, 141
 effective range, 34, 51
 exchange forces, 149
 phase-shift analyses, 30, 154ff
 scattering length, 33, 37, 51
 Neutron star, 193, 210, 300
 Nilsson diagrams, 415–419
 Non-local potentials, 135, 246, 451, 522
 Nordheim's rules, 239, 241
 Nuclear magneton, 17
 Nuclear matter, 244ff; *see also* G-matrix
 angle-averaged Pauli operator, 276
 Bethe-Goldstone equation, 252ff, 263
 binding energy, 247
 and central-to-tensor ratio, 293
 and contribution of higher order
 clusters, 264, 269
 and contribution of two-body clus-
 ters, 292, 294
 and contribution of three-body forces,
 296
 results of calculations, 297
 Brueckner self-consistency, 270
 correlations due to Pauli principle, 249
 defect wave function, 256, 285, 290
 density, 247
 Fermi momentum, 248
 healing distance, 192, 256, 263, 285
 incompressibility, 299
 independent pair model, 253ff, 269
 many-body clusters, 263, 265, 269
 momentum-dependent potential, 245
 occupancy of states, 272, 273
 off-shell effects, 283
 pairing gap in, 313
 Pauli operator in, 255, 256, 301
 wound, 257; *see* Wound integral
 Nucleons, 6, 17
 excited states, 13
 Nucleon forces, 19ff, 123ff; *see also* Poten-
 tial, Polarization, Tensor force
 Bartlett, 26
 boundary-condition description, 165
 central potentials, 21, 27
 charge exchange, 26
 charge independence, 50ff
 charge symmetry, 51
 exchange forces, 25
 Heisenberg, 26
 magnetic interactions, 44
 Majorana, 26
 many-body, 19, 294
 neutron-neutron, 45
 neutron-proton, 36
 non-central potentials, 123, 156, 159
 parity dependence, 21–2
 phase parameters, 156
 and pion field, 59, 128, 166, 173
 proton-proton, 39
 range, 22, 128, 135
 repulsive core, 23, 152, 161, 163, 164
 Serber exchange, 149
 spin dependence, 24, 35, 36, 137
 spin-orbit, 153, 157, 159, 177, 180
 and superfluid nucleus, 313, 315ff
 tensor-central ratio, 179
 two-body scattering data, 51, 145, 154
 Wigner, 26
 Nucleosynthesis in stars, 206ff
 Occupation number representation, 652ff
 Octupole vibrations, 349, 379, 598
 Packing fraction, 188
 Pairing correlations, 309ff
 and alpha-decay, 535
 BCS Hamiltonian, 316
 BCS wave function, 318
 binding energy of pair, 312
 Cooper pair, 310
 delta-function interaction, 316

energy gap 313, 322, 325
 in equi-spaced model, 338
 even-odd mass difference, 326
 and fission, 583
 gap equation, 321
 and Hartree-Fock-Bogolubov theory,
 481
 limitation of BCS theory, 323
 and moment of inertia, 497ff
 neutron-proton pairing, 324
 and number operator, 322
 occupation numbers U and V , 318, 327
 pairing interaction, 314ff, 339
 quasiparticle, 318
 quasiparticle energies, 322
 Pairing energy, 202, 322
 Parity, 21, 26, 673
 Partial waves, 28, 30, 277
 Particle-hole calculations, 455, 471, 482ff
 operators defined, 484
 Pauli exclusion principle, 7
 and antisymmetry in shell model, 234
 correlations in nuclear matter due to,
 248ff
 and statistics, 7
 and healing of two-nucleon wave func-
 tion, 192, 256, 301
 and occupied states in shell model, 221,
 224, 272, 301
 projection operator Q , 255, 256, 259,
 272, 276
 and proton-proton scattering, 150
 and symmetry energy, 199ff
 Penetration factor, 41, 662ff
 in alpha-decay, 517ff, 539ff
 in fission, 576, 596
 WKB approximation, 660ff
 Phase-equivalent potentials, 185
 Phase shifts, 31, 141
 analysis of, from experiment, 154ff, 158
 bar, 143
 in Born approximation, 153
 for Coulomb scattering, 40
 and effective range expansion, 34, 41
 in electron scattering, 89
 for hard-core, 62
 in nuclear matter, 192
 for nucleon-nucleon scattering, 156, 293
 and resonances, 186
 and S -matrix, 31, 143
 for square well, 61
 Phonons, 346ff
 Photons, 11, 12, 670
 virtual, 120
 Photonuclear reactions, 483
 Pick-up and stripping reactions, 327
 Pions, 10
 Bohr orbit, 46
 capture in deuteron, 45ff
 and nuclear force, 11, 135, 166, 170, 173,
 294
 pion-nucleon coupling constant, 178
 pion-nucleon resonances, 13
 pion-nucleon scattering, 13
 properties, 9, 10
 virtual, 11
 Polarization of nucleons, 137ff
 defined, 137
 depolarization, 141
 differential cross section, 140
 double scattering, 138
 experimental values, 162
 polarized beam, 141
 and spin-flip, 138
 and tensor force, 138
 triple scattering, 141
 Potential, two-nucleon, 22ff, 158ff, 166ff
 Bargmann, 62
 Brueckner, Gammel, Thaler, 160
 and deuteron, 129
 from field theory, 166ff
 Hamada-Johnston, 162
 non-local, 135
 one-boson-exchange, 173ff, 177ff, 292,
 297, 303
 one-pion-exchange, 135
 phase equivalence, 185
 Reid, 163, 292, 297, 303
 and repulsive core, 152
 separable, 165, 184
 Signell-Marshak, 160
 spin-orbit, 153
 Sprung-de Tourreil, 164
 symmetry properties, 159
 Tabakin, 165
 two-pion exchange, 169
 velocity-dependent, 165, 179
 Yale, 162
 Protons, 5, 6, 13, 17, 110
 Proton-proton scattering, 39, 147, 644ff;
 see also Nucleon force, Potential
 Coulomb penetration factor, 41
 Coulomb phase shift, 40
 differential cross section, 147, 150

effective range, 41, 45
 electric potential, 44
 high energy, 150ff
 low energy, 39ff
 Mott cross section, 41, 646
 phase shift analysis, 154
 scattering length, 45
 total cross section, 147
 vacuum polarization, 43
 Prout's hypothesis, 3
 Pseudoscalar and pseudovector, 636

Quadrupole moment, *see* Electric quadrupole moment
Quarks, 104
Quasiparticle, 318

Racah coefficients, 619
Radiative transitions, 444, 671ff
Radioactive decay constant, 510
 and complex energy, 513, 519
 partial, 510
Radius nuclear, 82ff, 303, 461; *see also*
 Density
 accuracy, 115
 in Ca isotopes, 94, 461
 calculated for closed shell nuclei, 461
 equivalent radius, 100
 half-fall-off, 87, 100, 101
 mean-square, 86, 100ff, 303, 304, 461
 of neutron and proton, 110
 table, 99
Rearrangement energy, 301, 453, 457
Reduced i -spin, 235
Reduced matrix element, 626, 672
Reference spectrum, 335
Refractive index for neutrons, 648ff
Relativistic wave functions, 629ff
Repulsive core, *see* Nuclear forces
Resonances, electromagnetic, 491ff
Rotational motion, *see* Collective model;
 Hartree-Fock method
Rotations of axes, 355ff, 360, 365, 621;
see also \mathcal{D} -functions
Rutherford-Bohr atom, 4, 82

Saturation of binding energy, 190, 194,
 288ff
Scalar, 636
Scattering; *see also* Cross section; Coulomb
 scattering; Nucleon forces; Neu-

tron-proton scattering; Proton-
 proton scattering; Pion
 angular distribution in laboratory, 29
 coherent, 37, 647
 Coulomb, 40ff, 82
 coupled states, 141ff
 of electrons by nuclei; *see* Density of
 nuclei
 hard sphere, 62
 impact parameter, 28, 136
 at low energy, 30
 Mott, 41, 85, 646
 nucleon-nucleon, 27ff, 141ff
 parameters, 145
 scattering amplitude, 32, 144, 167, 187
 for identical particles, 150
 scattering length, 33, 37, 45, 50, 51, 62
 virtual scattering, 192
Schmidt limits, 75ff
Second quantization, 651ff
Semiempirical mass formulae, 202ff, 211,
 577
Seniority, 235
Separation energy, 471
Shape of nucleus, 68ff, 420ff, 468ff
 co-existence, 473, 480
 in fission, 573, 584
Shape parameter, P , 41, 44
Shell model, 442ff, 577
Single-particle model, 217ff; *see also*
 Collective model, Correlation of
 nucleons, Magic numbers, Alpha-
 decay, Fission
 level density, 580ff, 605
 level order, 220, 222ff, 447, 453, 586
 magnetic dipole moment, 75ff
 quadrupole moment, 72, 675
 and spin-orbit forces, 221
 for non-spherical nuclei, 410ff
 angular momentum, 403, 408
 Coriolis effect, 405, 408, 430
 decoupling parameter, 408, 431
 equilibrium shape, 420ff
 and Hartree-Fock calculations, 463ff
 one-body potential, 411, 427, 428
 magic numbers, 433
 Nilsson states, 410ff, 429ff
 quantum numbers, 406, 407, 413, 416
 wave functions, 404, 406, 410, 413,
 438, 440
 for spherical nuclei, 218ff, 442ff
 corrections to, 455

and Hartree-Fock theory, 449ff
 magic numbers, 221, 223
 and spin, 223ff
 table of configurations 224–231
Sizes of nuclei, 82ff, 303, 461
 table, 99
S-matrix, 31, 142
 unitarity, 62
 for Bargmann potential, 62
Softness parameter, σ , 376
Spectroscopic factor, 327, 449
Spherical harmonics, 613, 623
 addition theorem for, 623
 integral of three, 625
Spherical tensors, 620, 625ff
Spin, 613; *see also* Angular momentum
Spinor, 629
Spin-orbit force, 153, 157, 159, 177, 180,
 221ff, 410, 413, 470
Stability regions, 204, 584
Statistics of particles, 7
Strange particles, 14
Strong interaction, 10, 637; *see also*
 Nucleon forces, Pion
Strutinsky method, 579ff
Superheavy elements, 206, 583
Surface, nucleus; effects on density of
 states, 196, 210
 energy, 196, 197, 202, 570
 neutron excess in, 100
 surface symmetry energy, 202
 thickness, 88, 103, 115
Symmetry energy, 199ff
 surface, 202
 from nuclear matter calculations, 299
Symmetry properties
 and multiphonon states, 350
 and possible shell-model states, 234
 and rotational wave functions, 364–8,
 406–8
 and two-nucleon potential, 159
Tamm-Dancoff method, *see* Particle-hole
 calculations
Tensor force, 123ff
 classical analogue, 127
 component in effective interaction, 308
 and D -state in deuteron, 128–132
 and magnetic moment of deuteron, 124
 matrix elements, 127, 182, 183
 in OBEP, 178
 in OPEP, 128, 176
X-rays, muonic, 84, 111ff
Z-function, 620
Zitterbewegung, 103

phase shifts due to, 157
 and quadrupole moment of deuteron,
 125
 saturation in nuclear matter due to, 288
 and scattering matrix, 141ff
 tensor-central ratio, 179
Thomas-Ehrman effect, 55
Three-body force, 19, 294
Three-body effective interaction, 459
Three-three resonance, *see* $\Delta(1236)$
T-Matrix for two-body scattering, 167ff
 half off-shell, 167, 187, 283
Transformation brackets of Brody-
 Moshinsky, 336
Transition probability, 671
Transmission coefficient; *see* Penetration
 factor
Triple scattering; *see* Polarization
U, Hartree-Fock field, 450ff, 463ff
Uncertainty principle, 11
Vacuum polarization, 43, 116
Valence nucleons, 233, 403, 443
Variational principle, 451ff
Vector addition; *see* Angular momentum
Velocity-dependent forces; *see* Momen-
 tum-dependent potentials
Vibrational states; *see* Collective model
W-function, 619
Wave functions
 angular momentum, 618, 633
 Bessel, 641
 Coulomb, 640
 relativistic, 632
 for scattering, 639ff
Weak interaction, 638
Weisskopf units, 675, 676
Wick's theorem, 657
Wigner-Eckart theorem, 626
Wigner force, 26
Wigner symbols, $3j$, 616
 $6j$, 619
WKB formalism; *see* Penetration factor
Woods-Saxon potential, 97
 energy levels of, 447, 587
Wound integral, 257, 263, 273, 286ff